DEVELOPMENT OF MEASUREMENT PROCEDURES FOR RAPID ANALYSIS OF MAJOR, RARE EARTH AND PLATINUM GROUP ELEMENTS IN GEOLOGICAL MATERIALS

Syed Nadeem Hussain Bokhari

Ph.D. THESIS

Supervised by

Univ. Prof. Ao. Univ. Prof. Mag. rer. nat. Dr.mont. Thomas Meisel

Chair of General and Analytical Chemistry

MONTANUNIVERSITÄT LEOBEN

August 2016

Abstract

Rapid and effective measurement procedures are required in geological, industrial and environmental science to obtain reliable information on the chemical composition of the unknown samples. Sample preparation is arguably the most important and the primary step in whole-rock geochemical analysis. Geological materials comprising complex matrices and refractory minerals such as zircon and chromite pose problems in complete digestion and recovery. For the release of critical analytes contained in these mineral phases into the solutions, acid digestions combined with hazardous HF or alkali fusions are often used. The use of HF has safety concerns and alkali fusions can result in high salt contents, which are problematic when analysed with a ICP-MS. A classical sample digestion technique, namely sodium peroxide sintering was developed in this study and optimised for whole-rock analysis, including rare earth elements (REE) and platinum group elements (PGE) in geological materials. Sintering was shown to ensure the complete release of all the critical analytes into the solution and thus can be combined with various techniques.

The complexity of the matrix elements to form spectral overlaps in the ICP-MS spectrum for the determination of the mass fractions of the analytes is a well-known problem. New methods for the determination of major, trace and PGE including Ag and Au are developed using a new collision/reaction cell in combination with MS/MS technology in geological materials. Sintering was combined with isotope dilution mass spectrometry and tellurium co-precipitation and an improved method was developed for trace PGE determination. Sintering was combined with isotope dilution mass spectrometry and anion-exchange chromatography and discrepancies in mass fractions of Ru and Re in basalts were addressed. The method developed eliminates the use of HF for the determination of Ru and Re in basalts. The sintering method releases ruthenium into the solution, which is hosted in the silicate phases of the rock. The measurement principle for ruthenium sparging is applied to the sinter solutions. In addition, two new methods for ruthenium distillation were applied to the sinter solution using (phosphoric acid/$K_2Cr_2O_7$ + concentrated HCl trap) and ($KBrO_3$/chilled sulphuric acid trap) were developed. Ruthenium sparging and distillation were applied to the quantification of ruthenium mass fractions using an isotope dilution method to two new reference materials (MUH-1 and OKUM).

The capabilities of cloud point extraction were evaluated on sinter solutions for matrix removal and pre-concentration of PGE. This combination did not produce a good method for the determination of PGE mass fractions. The capabilities of two new resins Diphonix® and CL for removal of matrix elements was tested on sinter solutions. Although Diphonix® offers good analyte/matrix separation, it could not be applied to the sinter solution due to the complex chemistry of PGE ions. Retention abilities of PGE ions on Ag-loaded CL resin were excellent, but elution from the resin was problematic.

The method developed for sample digestion was applied to industrial and geological samples in collaboration with the University Of Isfahan, Iran and the University Of Bologna Italy for major and trace element determinations. The method developed with the collision/reaction cell was applied to environmental samples for trace PGE mass fraction determination in collaboration with the University Of Oulu, Finland.

Kurzfassung

Um zuverlässige Informationen über die chemische Zusammensetzung von unbekannten Proben in den Bereichen Geologie, Industrie und Umwelt zu erhalten sind schnelle und effiziente Messverfahren sind erforderlich. Die Probenvorbereitung ist wohl der wichtigste und grundlegende Schritt bei der Untersuchung der Gesamtgesteinschemie in der geochemischen Analyse. Geologische Materialien mit ihren komplexen Matrizes und der refraktäre Charakter von Mineralien wie Zirkon und Chromit erschweren einen vollständigen Aufschluss. Um kritische Analyten aus diesen Mineralphasen in Lösung zu bringen sind Säureaufschlüsse unter Verwendung der gefährlichen Flusssäure oder alkalische Schmelzaufschlüsse erforderlich. Die Verwendung von Flusssäure stellt ein Sicherheitsrisiko dar, während alkalische Schmelzaufschlüsse durch hohe Salzgehalte Probleme bei der Analyse mittels ICP-MS verursachen. Eine klassische Probenaufschlusstechnik, die Natrium peroxide sinterung, wird für die Untersuchung der Gesamtgesteinschemie, einschließlich der Seltenerdelemente (REE) und Elemente der Platingruppe (PGE), in geologischen Referenzmaterialien entwickelt und optimiert. Die Sinterung stellt sicher, dass alle kritischen Analyten vollständig in Lösung gehen, und kann daher mit verschiedenen Techniken kombiniert werden. Spektrale Überlagerungen durch Matrixelemente im ICP-Massenspektrum, die die Gehaltsbestimmung der Analyten verkomplizieren, sind ein bekanntes Problem. Neue Methoden für die Bestimmung der Massenanteile von Haupt- und Spurenelementen und der PGE, einschließlich Ag und Au, in geologischen Referenzmaterialien werden entwickelt, für die eine neuartige Kollisions-/Reaktionszelle in Kombination mit der MS/MS-Technologie verwendet wird. Durch Kombination der Sinterung mit Isotopenverdünnungs-Massenspektrometrie und Tellur-Copräzipitation wird ein verbessertes Verfahren zur Bestimmung von PGE-Gehalten im Spurenbereich entwickelt.

Durch Kombination der Sinterung mit Isotopenverdünnungs-Massenspektrometrie und Anionenaustauschchromatographie werden bekannte Diskrepanzen in den Massenanteilen von Ru und Re in Basalten untersucht. Das entwickelte Verfahren vermeidet die Verwendung von Flusssäure für die Bestimmung Ru und Re-Massenanteilen in Basalten. Das Sintern ermöglicht die Freisetzung von Ruthenium aus silikatischen Bestandteilen des Gesteins in die Lösung. Als neuartige Methode zur Abtrennung von Ruthenium aus den Sinterlösungen wurde das Prinzip des Sparging adaptiert. Darüber hinaus wurden zwei neue Verfahren zur Destillation von Ruthenium aus den Sinterlösungen (kondensierte Phosphorsäure + $K_2Cr_2O_7$ / Absorption in konz HCl) und ($KBrO_3$ / Absorption in gekühlter Schwefelsäure) entwickelt. Ruthenium-Sparging und Destillation werden zur Quantifizierung von Ruthenium in zwei neuen Referenzmaterialien (MUH-1 und OkUM) eingesetzt.

Die Eignung der Cloud Point Extraction für die Matrixabtrennung und Anreicherung der PGE aus den Sinterlösungen wird untersucht. Diese Kombination bietet keine gute Basis für die Bestimmung der Massenanteil der PGE. Die Fähigkeiten von zwei neuen Harzen, Diphonix® und CL, zur Entfernung von Matrixelementen aus Sinterlösungen wurden getestet. Obwohl Diphonix® eine gute Trennung von Analyten und Matrix erlaubt, kann es aufgrund der Chemie der PGE-Ionen nicht für die Sinterlösungen verwendet werden. Das Retentionsvermögen von PGE-Ionen auf Ag-beladenem CL-Harz ist ausgezeichnet, aber die Elution ist nach wie vor problematisch.

Das entwickelte Verfahren zum Probenaufschluss wurde in Zusammenarbeit mit der Universität Isfahan (Iran) und der Universität Bologna (Italien) für Haupt- und Spurenelementbestimmungen in industriellen und geologischen Proben angewendet. Das entwickelte Messverfahren unter Verwendung der Kollisions-/reaktionszelle wurde in Zusammenarbeit mit der Universität von Oulu (Finnland) für die Bestimmung von PGE-Massenanteilen im Spurenbereich in Umweltproben eingesetzt.

Declaration

I declare that this thesis, which I submit for the award of Doctor of Philosophy at the Montanuniversität, Leoben, Austria, represent my own research work, except where due acknowledgements are made in terms of references, and the work has not been published by any other university.

Syed Nadeem Hussain Bokhari

Acknowledgement

I would like to thank my advisor, Professor Thomas Meisel, at the Chair of General and Analytical Chemistry for his encouragement, support and supervision from the first day at Montanuniversität Leoben till the last word of this thesis and for ongoing guidance. I salute Professor Thomas Meisel for the wisdom and knowledge I learned from him. I believe I am trained to face any challenges in life after working with him.

I would like to thank Professor Wolfhard Wegscheider, Chairman, Department of General and Analytical Chemistry, for the provision of moral and financial support to carry out this research.

I would also like to pay special regard to my colleague, Dr Christoph Walkner at General and Analytical Chemistry for teamwork on working with ICP-MS/MS.

Special thanks to Professor Henry Longerich, Memorial University, Canada for his valuable comments and suggestions that significantly improved the English and quality of the thesis.

Special gratitude to Professor Paavo Perämäki University of Oulu, Finland and his student Terhi Suoranta for collaboration in the application of our research methods for PGE mass fraction determination in environmental samples.

Gratitude to Professor Roberto Braga, University of Bologna, Italy and his student Valerio Funari for collaboration in the application of our research methods for major and trace element determination in industrial samples.

I would like to thank Professor Ramin Samadi, University of Isfahan, Iran and his student Narges Shirdashtzadeh for collaboration in the application of our research methods for major and trace element determination in geological samples.

At the end, I would thank all my colleagues at the institute who had made this venture very pleasant.

Dedications

This thesis is dedicated to all my teachers, especially Imam Hussain (A.S), my parents and family members for their unconditional love and efforts in bringing me up to the vision of life.

Publications/conference abstracts

1. Method development and optimisation of sodium peroxide sintering for geological samples. (submitted: Geostandards and geoanalytical research). (Syed Nadeem Hussain Bokhari, Thomas Meisel)
2. Multi-element analysis of crude oils using ICP-QQQ-MS. (submitted: Organic geochemistry). (Christoph Walkner, Thomas Meisel, Reinhard Gratzer, Syed Nadeem Hussain Bokhari)
3. Active biomonitoring of palladium, platinum and rhodium emissions from road traffic using transplanted moss. (accepted in print: Environmental Science and Pollution Research). (Suoranta T, Niemelä M, Poikolainen J, Piispanen J, Bokhari SNH, Meisel T, Perämäki P)
4. Elimination of interferences in the determination of palladium, platinum and rhodium mass fractions in moss samples using ICP-MS/MS. (DOI: 10.1111/ggr.12116). (Terhi Suoranta, Syed N. H. Bokhari, Thomas Meisel, Matti Niemelä and Paavo Perämäki)
5. The Rare Earth Elements in Municipal Solid Waste Incinerators ash and promising tools for their prospecting. (DOI: 10.1016/j.jhazmat.2015.09.015). (Funari V, Bokhari SNH, Vigliotti L, Meisel T, Braga R)
6. Petrography, thermobarometry and geochemistry of Darreh Dehpicrites (East of Nain Ophiolitic mélange). http gs-journal.ir/en/journal/chapter view/0/139/156/5576. (Nargess Shirdashtzadeh, Ghodrat Torabi, Ramin Samadi, Thomas Meisel, Bokhari SNH)
7. Solid residues from Italian municipal solid waste incinerators: A source for "critical" raw materials. (DOI: 10.1016/j.wasman.2014.11.005). (Valerio Funari, Roberto Braga, Bokhari SNH, Thomas Meisel, Enrico Dinelli)
8. Depositional environment of oil shale within the Eocene Jijuntun Formation in the Fushun Basin (NE China). (DOI: 10.1016/j.marpetgeo.2014.04.011). (Susanne Strobl, Reinhard Sachsenhofer, Achim Bechtel, Reinhard Gratzer, Doris Gross, Syed N.H. Bokhari, Rong Liu, Zhaojun Liu, Qingtao Meng, Pingchang Sun)
9. Origin and evolution of metamorphosed mantle peridotites of Darreh Deh (Nain Ophiolite, Central Iran): Implications for the Eastern Neo-Tethys evolution. (DOI: 10.1127/0077-7749/2014/0418). (Shirdashtzadeh Nargess, Torabi Ghodrat, Meisel Thomas, Arai, Shoji; Bokhari, Syed Nadeem Hussain; Samadi Ramin, Gazel Esteban)
10. The determination of homogeneity of geochemical reference material at 9. ASAC JunganalytikerInnen Forum June 2013; Vienna (Austria).[1]
11. The determination of homogeneity of geochemical reference material at Goldschmidt 2013; Florence Italy.[1]
12. Improved analyte recovery of refractory material through optimisation of sintering at Technical University of Graz CHEMIETAGE October 2013.[1]
13. Osmium isotope and PGE reference materials OKUM and MUH-1 at Goldschmidt 2013; Florence Italy.[2]
14. Accurate determination of Sc and Eu in Zr and Ba-rich matrix in geological reference materials with ICP-MS. KKCV Belgium Feb 2014.[1]
15. Development and characterisation of matrix-matched REE reference material RM for mining. KKCV Belgium Feb 2014.[1]
16. Complete zircon and chromite digestion by sintering in granite, rhyolite, andesite and harzburgite rock reference materials for geochronological purposes. European Geosciences Union Vienna Austria May 2014.[1]
17. Accurate rhenium determination in basaltic geological reference material. Goldschmidt 2014. CA USA.[1]
18. Stability of geological reference materials Goldschmidt June 2014. CA USA.[1]

19. Interference removals on Sc and Eu in Zr and Ba-rich matrix in geological reference material with ICP-QQQ-MS at 24th ICP-MS conference at Helmholtz Zentrum Geesthact Hamburg Germany September 2014.[1]
20. Interference removals on Pd and Gold in PGE RM at European winter plasma conference Munster Germany February 2015.[1]
21. Interference removals on Pd and Gold and Ruthenium in PGE RM European Geosciences Union Vienna Austria April 2015.[1]
22. Determination of Rh, Ir and Ag in Platinum Group Elements (PGE) reference materials (RM) for industrial analytics at Anakon Conference Graz Austria March 2015.[1]
23. Testing for impurities in pure rare earth element oxides and metals with a ICP-QQQ-M at EWCPS Munster Germany February 2015.[2]
24. Trace element quantification in crude oils using ICP-QQQ-M at EWCPS Munster Germany February March 2015.[2]
25. Determination of trace elements in Upper Austrian crude oils using ICP-QQQ-MS at Anakon Graz Austria March 2015.[2]
26. Method development for PGE determination in reference material BIR-1 at Prague Goldschmidt August 2015.[1]
27. Removal of Interferences on platinum in Platinum Group Elements (PGE) reference materials (RM). Geoanalysis Leoben Austria July 2015.[1]
28. Determination of Ru, Pd, Rh and Au in MUH-1 reference material with sintering-Te-co-precipitation with ID-ICP-MS Geoanalysis Leoben Austria July 2015.[1]
29. Determination of Ru in OKUM and BIR-1 with sintering-anion exchange Geoanalysis Leoben Austria July 2015.[1]
30. Study of interferences on Os isotopes. ASAC Innsbruck Austria June 2015. [1]
31. Data for Ru, Pd, Ir, Au and Rh for OKUM reference material with sintering-Te-Co-precipitation. Euroanalysis Bordeaux France September 2015. [1]
32. Plasma chemistry of rare earth elements in NH_3 and O_2 gases Innsbruck Austria Chemietage September 2015.[1]
33. Solid residues from Italian municipal solid waste incinerators: A source for "critical" raw materials. Bergamo Italy May 2014.[2]
34. THE REE POTENTIAL IN "URBAN" ORE DEPOSITS: an evaluation of contents and prospecting tools from Italian municipal solid waste incinerators. ERES Greece September 2014.[2]
35. Major and trace elements analysis of industrial wastes with sintering. ASAC-Junganalytikerinnenforum Tulln Austria June 2015.[2]
36. MSWI residues as an unconventional source of critical raw materials: understanding possible easy ways to evaluate their occurrence and added-value products. SUM Milan Italy September 2014.[2]
37. Recent development in PGE analysis. 4th international highly siderophile element geochemistry workshop Durham University, UK July 2016.[2]
38. Determination of palladium in environmental samples by ICP-MS techniques. 8th Nordic Conference on Plasma Spectrochemistry Leon, Norway June 2016.[2]

[1] (First author) [2] (Co-author)

Table of Contents

List of Tables

List of Figures

List of abbreviations

AMFC	Agilent mass flow controller
STS	Shield Torch System
HMI	High Matrix Introduction
ISTD	Internal standard
ORS	Octopole Reaction System
RF	Radiofrequency
m/z	Mass-to-charge
AAS	Atomic absorption spectrometry
ICP-AES	Inductively coupled plasma-atomic emission spectrometry
INAA	Instrumental neutron activation analysis
HPA	High-Pressure Asher
FA	Fire assay
HSE	Highly siderophile elements
HPLC	High-performance liquid chromatography
HPIC	High-performance ion chromatography
REEOs	Rare earth elements-oxide
HREE	Heavy rare earth elements
LREE	Light rare earth elements
XRF	X-ray fluorescence spectrometry
NAA	Neutron activation analysis
INAA	Instrumental neutron activation analysis
RNAA	Radiochemical neutron activation analysis
IDMS	Isotope dilution mass spectrometry
I.E	Ionisation energies
eV	Electron volt
AAS	Atomic absorption spectrometry
DDEM	Discrete dynode electron multiplier
TRA	Time-resolved analysis
PP	Polypropylene
FTMS	Fourier-transform mass spectrometry
TIMS	Thermal ionisation mass spectrometry
PGE	Platinum group elements
ICP-SFMS	Inductively coupled plasma-sector-field mass spectrometry
HR-ICP-SFMS	High resolution-inductively coupled plasma-sector-field mass spectrometry
PFA	Perfluoroalkoxy
PTFE	Polytetrafluoroethylene
IDMS	Isotope dilution mass spectrometry
RM	Reference material
2-MBT	2-mercaptobenzothiazole

1. Introduction and thesis objectives

Sample decomposition is the primary step after pulverisation of the rocks in the measurement procedures for geo-analytical chemistry. The main aim of the transformation of rock portion into a solution is so that the total elemental mass fractions can be determined with advanced instrumental methods. Some methods of analysis do not require this transformation i.e. laser ablation, but with an additional complication of unsatisfactory stastics. The chemical composition, the degree of crystallinity of the mineral phases, and the complexity of the geological material make it necessary to choose a suitable sample digestion technique which is commensurate with the specific objective of the analysis (Chao and Sanzolone 1992).

One of the important needs for geochemical analysis is high sample/analyte throughput, i.e. to measure as many samples and analytes as feasible in a short amount of time. Advances in inductively coupled plasma-mass spectrometry, especially in sampling, have increased the sample throughput to hundreds of elemental determinations per hour. Conventional sample decomposition methods such as acid digestions, alkali fusions and similar methods, which require laborious procedures, are not on equal footing with rapid measurement systems (Chao and Sanzolone 1992).

Recent advancements using the high-pressure-asher, Carius tube and microwave digestions had made measurement procedures faster through the use of automated technology but the complete sample digestion for highly siderophile elements (HSE) and analytes in silicate phases of rocks is still a question mark (Meisel and Horan 2016). Successful attempts have been made with the use of HF which can attack silicates and release HSE i.e. Re and Ru (Dale *et al.* 2012, Ishikawa *et al.* 2014, Meisel *et al.* 2009). HF readily dissolves silica to form SiF_6^{2-} and is a hazardous mineral acid which is used in the laboratory (Potts 1987b). HF attacks Ca in the body and form complexes with bones and may even lead to serious conditions including death. On the other hand, recent debate by Day *et al.* (2015) suggests that the use of HF is only applicable for young lavas but when Re-Pt-Os chronological information is desired, the ratios Re/Os and Pt/Os may not correspond with measured $^{187}Os/^{188}Os$ or $^{186}Os/^{188}Os$ ratios. Thus, this study points out a drawback of HF-assisted HPA or Carius tube digestions for geochronology of the rock, and may only be applicable to young basalts. When acid digestions combined with HF are used for sample digestion, the insoluble fluorides of REE may remain in the precipitates and undermine the REE quantification, and precipitates can need to be treated with NaOH or $K_2S_2O_7$ (Gupta 1981, Walsh *et al.* 1981). Main aims of this thesis are: -

1. Method development for sample digestion.

The first objective of this thesis is to present an improved and optimised sample digestion method i.e. sodium peroxide sintering that does not involve HF and can easily attack the silicate phases of the rock for the release of HSE. This method also enables complete digestion of refractory minerals i.e. zircon and chromite. Thus, sodium peroxide sintering has been developed and optimised for the determination of rare earth and PGE mass fractions in geological materials in this thesis. Chapter 5 describes the details of the developed sample digestion method. The homogeneity in test portions has been tested with the method developed in reference materials MTA-1, MRH-1 and uncertified USGS G-3 as described in chapter 6.

2. Method development for mass fraction determination of major, trace and PGE-Ag and Au using collision/reaction cell.

Secondly, the rapid sodium peroxide sintering sample digestion method has been combined with a fast system of measurement i.e. ICP-MS. Inductively coupled plasma mass spectrometry is arguably the most versatile trace elemental analysis technique available today that enables analysis at pg/ml level for a variety of matrices (Nelms 2005). The importance of spectral overlaps on the analytes of interest was soon recognised since the the first ICP-MS reports were published in 1983. Magnetic field based resolution of the analytes from interferences was introduced in the late 1980's. This technology resolved most of the polyatomic interferences but was not able to resolve isobaric interferences of mono-elemental species, i.e. ^{87}Rb and ^{87}Sr. Then the advent of collision/reaction cell in ICP-QMS in the late 1990's took a new step in reduction of interferences forward. Through collision and reaction with gases placed in a cell before the analyser quadrupole, interferences such as $^{40}Ar_2^+$ on $^{80}Se^+$ were removed (Nelms 2005). More recently, a triple quadrupole ICP-QQQ-MS instrument was introduced which has an octopole collision cell, located between two quadrupole mass filters, which is the traditional configuration of tandem mass spectrometers, which has been used, in organic mass spectrometry for some years. A tandem mass spectrometer is the combination of two spectrometers with a collision/reaction cell in between. The first cell acts as a mass filter and only allows the selection of ions of one m/z ratios to enter the reaction cell. A reactive gas is injected in the cell with a controlled flow rate, which reacts with either interferences and/or analytes. When the interference reacts with cell gas, new product ions are formed which are not selected by the second mass analyser and interferences are removed. On the other hand, if interference does not react with the cell gas, the analyte may react and form a new polyatomic product ion. The knowledge of the m/z of the product ions is thus needed for method development. The second mass analyser is set to the m/z of the product ion of the analyte formed in the reaction with the cell gas. This allows an excellent way of removing spectral overlaps. The second aim of this thesis is to utilise collision/reaction cell technology of the QQQ Agilent 8800 to remove interferences especially on rare earth and platinum group elements including some major elements and to develop a superior analytical method for their determination. The details of the method developed will be described in chapter 7, 8 and 9.

3. Method development with sintering and Te-co-precipitation for PGE mass fraction determination.

Sodium peroxide sintering has been combined with isotope dilution and tellurium co-precipitation for optimisation and method development for PGE mass fraction determination using glassy carbon crucibles as a third objective of this thesis. In addition, the developed method has been combined with collision/reaction cell technology for minimisation of interferences in the analysis of PGE mass fractions of two new geological reference materials OKUM and MUH-1 with ICP-MS/MS. The method will be described in chapter 10.

4. Method development with sintering and anion-exchange chromatography for addressing Ru and Re discrepancies in basaltic reference materials.

Sodium peroxide sintering has been combined with anion-exchange chromatography to address the discrepancies of Ru and Re in basaltic reference materials TDB-1 and BIR-1 as the fourth objective of this study. The literature data for TDB-1 and BIR-1 basaltic reference materials present discrepancies as reflected in a large data scatter. The data for PGE mass fractions of OKUM and MUH-1 has also been presented with the same technique used. The method will be described in chapter 11.

5. Development of a new rapid analytical method for ruthenium mass fraction determination with sparging and distillation.

A novel analytical method for ruthenium determination in geological reference materials with sparging and distillation will be described in this thesis as fifth objective. Osmium contents can also be determined in geological reference material digested with sodium peroxide sintering. The digested samples do not need to be pre-concentrated; rather sinter solutions can be directly sparged into the instrument for ruthenium determination. The Ru mass fractions have been determined in OKUM and MUH-1 using this method. Two new methods of ruthenium determinations with distillation of sinter solution have been developed for geological reference materials. Chapters 12 and 13 will describe the details of the sparging and distillation which were developed in this study.

6. Evaluation of cloud point extraction (CPE) for the extraction/pre-concentration of PGE from sinter solution.

Capabilities of cloud point extraction (CPE) for the extraction/pre-concentration of PGE have been evaluated by combination with sodium peroxide sintering using thiourea and the 2-MBT (2-mercaptobenzoothiazole) complexing agent. It is shown through the study that cloud point extraction does not form a good basis for PGE determination from the samples digested with sodium peroxide sintering. The details of the tests performed will be given in chapter 14.

7. Evaluation of new resins Diphonix® and CL for pre-concentration of PGE from sinter solution and matrix removal with a sintering solution.

Capabilities of two new resins Diphonix® and CL have been evaluated in the procedure for the PGE determination in geological materials digested with sodium peroxide sintering. Due to the formation of hydroxy chloro-complexes in sinter solutions, PGE retention ability was found to be very low on CL resin, however, with Ag-loaded resin, PGE retention ability was significantly enhanced. Further work is needed for complete elution of PGE ions using other sample digestion techniques. Diphonix® has a remarkable ability to remove matrix elements e.g. complete removal of rare earth elements. However, due to the presence of hydroxy chloro-complexes in sinter solution and retention of Ru and Pd etc. on Diphonix, this does not form a good basis for PGE separation from matrix elements. The details of the tests performed will be given in chapter 15.

Method developed for PGE determination with collision/reaction cell was carried out on environmental samples in collaboration with the University of Oulu Finland (online publication). The sample digestion procedure was applied to geological samples in collaboration with the University of Tehran (online publication). The sample digestion procedure was also applied to industrial samples in collaboration with the University of Bologna Italy (online publication).

Thesis overview

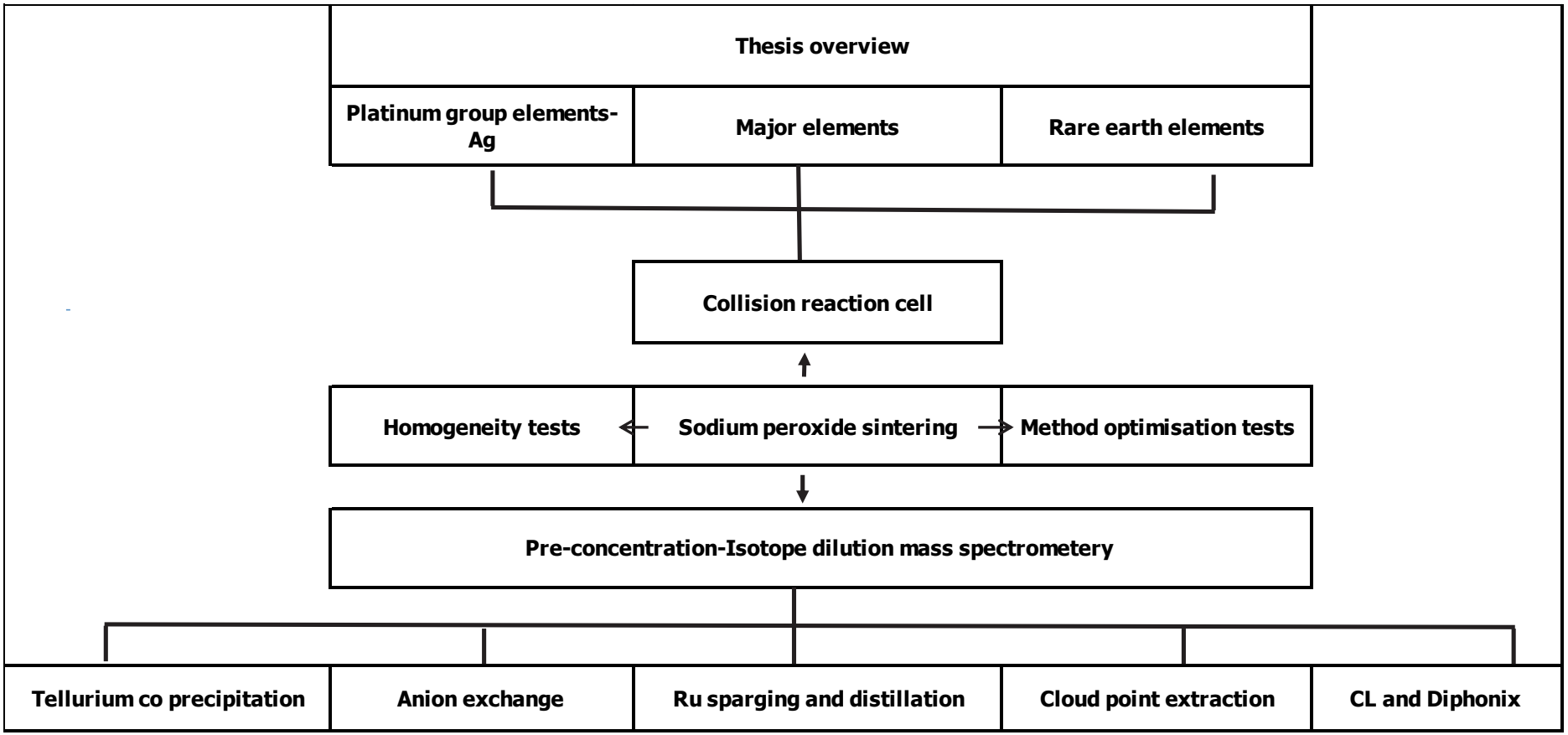

2. Introduction to the Rare Earth Elements (REE)

The term 'REE' rare earth element is mostly employed in geology as a synonym of the lanthanide series. They range from proton number La (57) to Lu (71): lanthanum (La), cerium (Ce), praseodymium (Pr), neodymium (Nd), promethium (Pm), samarium (Sm), europium (Eu), gadolinium (Gd), terbium (Tb), dysprosium (Dy), holmium (Ho), erbium (Er), thulium (Tm), ytterbium (Yb), and lutetium (Lu). Yttrium (39) and Sc (21) are generally included with the REE as they occur with them in natural minerals and have similar geo-chemical properties.

Johann Gadolin in 1794 suggested the term 'rare earth' because early REE discovered were thought to be present in trace amounts in the earth's crust as oxides with earthy appearance (Evan 1997). REE are widely dispersed, as they are found in the Earth's crust and mantle in appreciable amounts, hence the term "rare" in rare earth elements is conventional. Due to similarities in their chemical properties, it took more than a century to completely isolate, characterise and classify REE (Evan 1997). The REE have between 2 to 7 stable naturally occurring isotopes, with the exception of Sc, Y, Pr, Tb, Ho and Tm, which are mono-isotopic.

2.1 Occurrence and abundances of the REE

REE occur in different mineral classes and structural types, but only a few are recovered for the production of rare earth oxides (REEOs). The important mineral species for recovery are Xenotime [YPO_4], monazite [(Ce, La, Nd, Th)(PO_4)][(REE)PO_4], Bastnäsite [(Ce, La)(CO_3)F], and rare earth bearing clay. Generally, the REE from Sm to Lu are less abundant compared to other REE and hence are the most expensive among the REE. The rare-earth elements are not rare in nature as the term suggests. Their concentrations in the earth's crust are often equal to or higher than some significant elements, such as iodine, cobalt, silver, gold, platinum and selenium (Evan 1997). Cerium (68 mg/kg) and lanthanum (32 mg/kg) are the most abundant. Lutetium and thulium are the rarest (about 0.5 mg/kg) while the concentrations of the remainder are from 1 to 9 mg/kg. Promethium is an element with no stable isotopes.

China is the world's largest producer of REE (97%) as it has a some of the largest deposits of REE and ore sites. China and the United States have the largest Bastnäsite deposits and the second largest segment of deposits contain monazite. Australia, Brazil, India, Malaysia, South Africa, Sri Lanka, Thailand and Vietnam are also the key producers of rare earth elements (Gambogi 2015).

Table 2.1: Estimates of the crustal abundances of the rare earth elements

Analyte	Mason and Moore	Jackson and Christiansen	Sabot and Maestro	Wedephol	Lide
Year	**1982**	**1953**	**1995**	**1995**	**1997**
La	30	29	18	30	39
Ce	60	70	46	60	66.5
Pr	8.2	9	5.5	6.7	9.2
Nd	28	37	24	27	41.5
Sm	6	8	6.5	5.3	7.05
Eu	1.2	1.3	0.5	1.3	2

Gd	5.4	8	6.4	4	6.2
Tb	0.9	2.5	0.9	0.65	1.2
Dy	3	5	5	3.8	5.2
Ho	1.2	1.7	1.2	0.8	1.3
Er	2.8	3.3	4	2.1	3.5
Tm	0.5	0.27	0.4	0.3	0.52
Yb	3.4	0.33	2.7	2	3.2
Lu	0.5	0.8	0.8	0.35	0.8
Y	33	29	28	24	33
Sc	22		10	16	22

All concentrations in (mg/kg)

(Long *et al.* 2012)

2.2 Chemistry and classification of the REE

The REE have similar physical and chemical properties, which change periodically with the proton number. The REE are usually divided into two groups:

Light REE (LREE)

LREE consist of Sc and the Lanthanides from La to Gd. The LREE have larger ionic (+3) radii compared to the HREE and consecutively larger coordination number, typically 8 or 9 (Letcher and Scott 2012) https://en.wikipedia.org/wiki/Scandium.

Heavy REE (HREE)

HREE consist of the lanthanides from Tb to Lu. The HREE have smaller ionic radii compared to the LREE and their coordination number is typically 8 (Aspinall 2012). Yttrium is usually grouped with the heavier lanthanides. Although it is the 2nd lightest among the REE in terms of atomic number. Y^{3+} has many similar properties as the HREE in their (+3) oxidation state, due to the similarities of the radii of Y^{3+} (104 pm) and Ho^{3+} (104.1 pm).

Electronic configuration of the rare earth elements

The lanthanides are also known as f-block elements as their f orbitals are filled as the atomic number increases, which explains their similarities. In addition, their chemical properties are determined by the 3d-shells. With increasing atomic number, from La to Lu, a consecutive filling of the lower-energy *4f*-orbitals takes place instead of the *5d*-orbital while their oxidation states remain unchanged. This phenomenon is very important for the understanding of the chemistry of REE, as many properties result from the shielding of the inner *4f*-orbitals. Shielding offered by electrons of higher orbitals to the *4f*-electrons keeps their behaviour minimally affected by ionisation or complexation/bonding. Thus, their magnetic and spectroscopic properties are conserved upon binding. The electronic configuration of rare earth elements is given in Table 2.2.

REE generally favour tri-positive oxidation state and exhibit ionic bonding in their compounds. Besides, stable +3 oxidation state, only cerium, terbium and praseodymium with an oxidation number of +4 and samarium, europium and ytterbium with the oxidation number of +2 form stable compounds. The existence of further oxidation states beyond 3+ is due to the loss of an electron from *4f* orbital $4f^0$ (Ce^{4+}) which has *f*-shell with an unpaired

Table 2.2: Electronic configuration of the REE

REE in ground state electronic configuration							
Element	**Z**	***4d***	***4f***	***5s***	***5p***	***5d***	***6s***
La	57	10		2	6	1	2
Ce	58	10	2	2	6		2
Pr	59	10	3	2	6		2
Nd	60	10	4	2	6		2
Pm	61	10	5	2	6		2
Sm	62	10	6	2	6		2
Eu	63	10	7	2	6		2
Gd	64	10	8	2	6	1	2
Tb	65	10	9	2	6		2
Dy	66	10	10	2	6		2
Ho	67	10	11	2	6		2
Er	68	10	12	2	6		2
Tm	69	10	13	2	6		2
Yb	70	10	14	2	6		2
Lu	71	10	14	2	6	1	2
Y	39	1		2			

Table 2.3: Electronic configuration of the REE in the +3 state

REE in (+3) oxidation state electronic configuration							
IOn	**Z**	***4d***	***4f***	***5s***	***5p***	***5d***	***6s***
La	57	10		2	6	1-	2-
Ce	58	10	1	2	6		2-
Pr	59	10	2	2	6		2-
Nd	60	10	3	2	6		2-
Pm	61	10	4	2	6		2-
Sm	62	10	5	2	6		2-
Eu	63	10	6	2	6		2-
Gd	64	10	7	2	6	1	2-
Tb	65	10	8	2	6		2-
Dy	66	10	9	2	6		2-
Ho	67	10	10	2	6		2-
Er	68	10	11	2	6		2-
Tm	69	10	12	2	6		2-
Yb	70	10	13	2	6		2-
Lu	71	10	14	2	6	1-	2-
Y	39	1-		2-			

electron in +3 state as shown in Table 2.3. (Eu^{2+}) will be $4f^7$ (Eu^{2+}) half-filled with a stable configuration (Cotton *et al.* 2000).

Ionic radii of the REE

Atomic volume and ionic radii are determined by their effective nuclear charge. Effective nuclear charge increases with increasing atomic number causing a decrease in atomic size, which is called as the lanthanide contraction. It is due to shielding effect on inner 4*f* electrons. Thus, a decrease in ionic radii (La 1.06 Å to Lu 0.85 Å) is observed as the atomic number increases (Topp 1965). Ionic radii of REE and Y are shown in Figure 2.1.

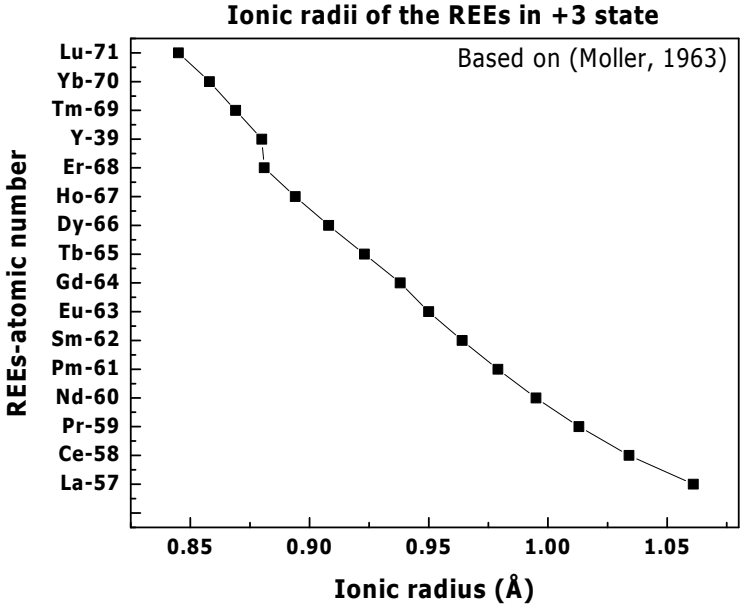

Figure 2.1: Ionic radii of REE

Ionisation energies of the REE

The ionisation energy of an atom depends on its atomic number and electronic configuration. Successive ionisation energies increase with increasing charge on the cation. Ionisation potential is the electric potential (commonly measured in volts) required to separate an electron from the orbital system into free space with the kinetic energy remaining unchanged. Ionisation energy is the work done in removing the electron at zero temperature and is measured conveniently in electron volts, where 1 eV = 1.6022×10^{-19} J. The molar ionisation energy, or change in molar internal energy, is N_A eV = 96.485 kJ/mol where N_A is the Avogadro constant (Lang and Smith 2010). The first ionisation energies are shown in Table 2.4.

Table 2.4: The first ionisation energies of the REE

REE	Y	La	Ce	Pr	Nd	Pm	Sm	Eu	Gd	Tb	Dy	Ho	Er	Tm	Yb	Lu
Atomic number	39	57	58	59	60	61	62	63	64	65	66	67	68	69	70	71
First ionisation energy (kJ/mol)	600	538	534	527	533	540	545	547	593	566	573	581	589	597	603	524

The ionisation energies of first four oxidation states of the REE are given in Table 2.5.

Table 2.5: The ionisation of first four oxidation states

	Ionisation energies/eV				
	Z	**M^{+}**	**M^{2+}**	**M^{3+}**	**M^{4+}**
La	57	5.58	11.1	19.2	50.0
Ce	58	5.5	10.9	20.2	36.8
Pr	59	5.5	10.6	21.6	39.0
Nd	60	5.5	10.7	22.1	40.0
Pm	61	5.6	10.9	22.3	41.1
Sm	62	5.6	11.1	23.4	41.4
Eu	63	5.7	11.2	24.9	42.7
Gd	64	6.2	12.1	20.6	44.0
Tb	65	5.9	11.5	21.9	39.4
Dy	66	5.9	11.7	22.8	41.4
Ho	67	6.0	11.8	22.8	42.5
Er	68	6.1	11.9	22.7	42.7
Tm	69	6.2	12.1	23.7	42.7
Yb	70	6.3	12.2	25.1	43.6
Lu	71	5.4	13.9	21.0	45.3

Ionisation energies from (Martin *et al.* 1978)

Bonding in rare earth elements

REE being typical metals can make bonds with non-metals. Some REE of low valence can form chemical bonds in organometallic or atom cluster compounds. REE lack sufficient electrons and show strong repulsive forces towards a positive charge. REE tend to make chemical bonds with atoms that belong to a hard acid group as REE themselves are hard bases. Oxygen and REE tend to make REE-O bonds. REE also tend to make bonds with nitrogen group atoms. The nature of chemical bonding in REE complexes and whether 4 *f* electrons contribute to bonding in these complexes has been long a controversy. It is now believed that chemical bonds in REE complexes are based on quantum chemistry exhibiting polar covalent bond properties. Electrons from *f* orbitals do not involve in bonding while electrons of 5*d* and 6*s* are contributing in bonding (Huang 2011). REE cations have a high affinity for bonding to fluorides, hydroxides and other oxygen-containing ligands. The order of preference for donor atoms follows the sequence: O > N > S and F > Cl, showing that REE have an overwhelming affinity to oxygen donor atoms (Bulman 2003).

2.3 Graphical plots of the REE

Graphical plots of REE in various rocks and minerals are often normalised to chondritic meteorite concentrations. Normalisation is done to eliminate the effects of the Oddo-Harkins rule (even atomic numbered elements are more abundant than those with an odd atomic

number) and to allow a graphical comparison to a known standards (Evan 1997). When the absolute concentration of REE is plotted against atomic number; a saw-tooth pattern is developed as shown in Figure 2.2. These patterns make it difficult to differentiate the effects of the chemical and physical fractionation processes. These oscillating patterns arise from the variations in the stability of a nucleus being dependent on whether the neutron number (N) and the atomic number (Z) are odd or even. Those nuclei with both N and Z even exhibit an enhanced stability while those with both N and Z odd are the least stable (Henderson 2013). In order to eliminate these patterns, REE mass fractions of a sample of interest are often by dividing by the mass fractions of known chondrite material (Wasson and Kallemeyn 1988). A logarithmic plot of normalised REE versus atomic number is shown in Figure 2.3. The data for chondritic meteorites is given in Table 2.6.

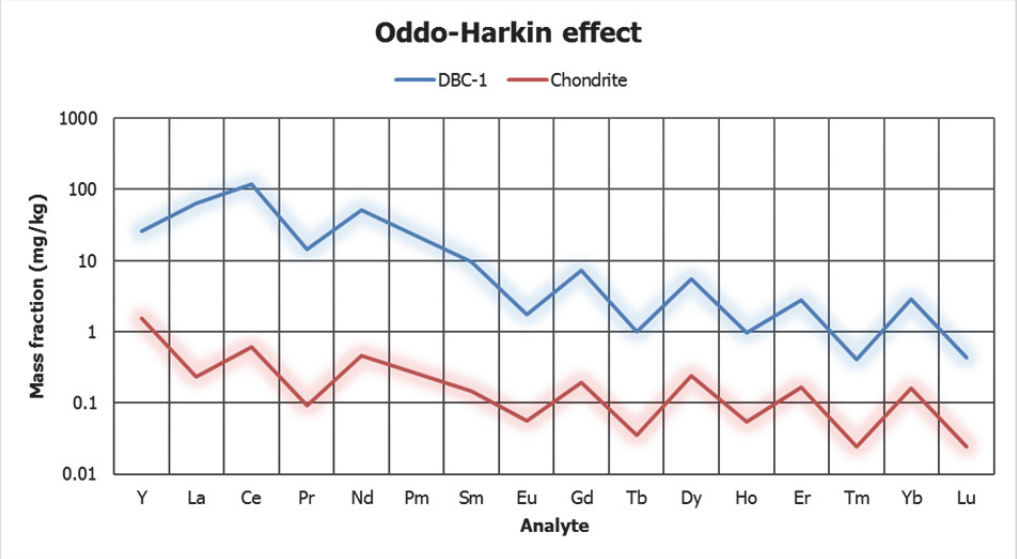

Figure 2.2: Relative abundances of REE vs atomic number

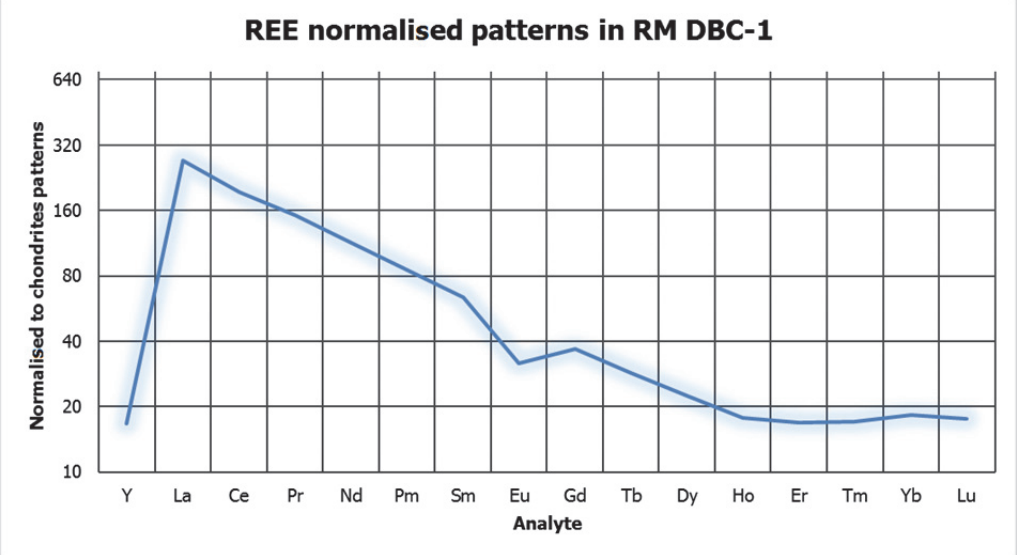

Figure 2.3: REE normalised patterns in RM DBC-1

2.4 Importance of the REE studies

The study of rare earth elements is significant for science, research and industry. The geochemical processes can be understood by studying the behaviour and degree of

fractionation in geological materials. The knowledge of REE abundances helps in understanding their distribution patterns and the radioactive scheme of decay of their isotopes. From distribution patterns, the nature and source of rocks and minerals can be evaluated; since REE mobilisation during processes of magma and rock formation can be predicted regarding their geochemical properties (ionic radius, ionic charge and nature of bonding in geologic systems) (Potts 1992). From the radioactive decay scheme of REE, the ages of rocks and minerals are determined i.e. decays of ^{138}La to ^{138}Ce, ^{147}Sm to ^{143}Nd, and ^{176}Lu to ^{176}Hf (Lipin *et al.* 1989). The current developments in analytical methods that are rapid in generating wide datasets on several trace elements in short time allow geochemists to consider the REE abundances when conducting petro genetic studies. Moreover, REE are of economic interest because these have many important conventional and high-technology applications which are outlined below: -

2.4.1 Uses of Rare Earth Elements

Important uses of rare earth element as in (http://www.namibiarareearths.com) are described below

Lanthanum: Camera lenses, battery-electrodes and hydrogen storage.

Cerium: Catalytic converters, coloured glass and steel production.

Praseodymium: Super-strong magnets, welding goggles and lasers.

Neodymium: Extremely strong permanent magnets, microphones, electric motors of hybrid automobiles and lasers.

Samarium: Cancer treatment, nuclear reactor control rods and X-ray lasers.

Europium: Colour TV screens, fluorescent glass and genetic screening tests

Gadolinium: Shielding in nuclear reactors, nuclear marine propulsion and to increase the durability of alloys.

Terbium: TV sets, fuel cells and sonar systems.

Dysprosium: Commercial lighting, hard disk devices and transducers.

Holmium: Lasers, glass colouring and high-strength magnets.

Erbium: Glass colorant, signal amplification for fibre optic cables and metallurgical uses.

Thulium: High-efficiency lasers and portable x-ray machines, high-temperature superconductors.

Ytterbium: Improved stainless steel, lasers and ground monitoring devices.

Lutetium: Refining petroleum, LED bulbs and integrated circuit manufacturing.

Yttrium: TV sets, cancer treatment drugs and to enhance the strength of alloys.

Table 2.6: Chondrite REE data in the literature

Chondrite mass fractions in mg/kg															
Author	**Y**	**La**	**Ce**	**Pr**	**Nd**	**Sm**	**Eu**	**Gd**	**Tb**	**Dy**	**Ho**	**Er**	**Tm**	**Yb**	**Lu**
(Haskin *et al.* 1968)	1.96	0.332	0.876	0.112	0.6	0.183	0.0685	0.252	0.047	0.317	0.07	0.201	0.03	0.207	0.0325
(Wakita *et al.* 1971)		0.34	0.91	0.121	0.64	0.195	0.073	0.26	0.047	0.3	0.078	0.2	0.032	0.22	0.034
(Masuda *et al.* 1973)		0.378	0.976		0.716	0.23	0.0866	0.311		0.39		0.255		0.249	0.0387
(Nakamura 1974)		0.329	0.865		0.63	0.203	0.077	0.276		0.343		0.225		0.22	0.0339
(Evensen *et al.* 1978)		0.2446	0.6379	0.0964	0.4738	0.154	0.058	0.2043	0.0375	0.2541	0.0567	0.166	0.0256	0.1651	0.0254
(Laul 1979)		0.34	0.85	0.12	0.64	0.195	0.073	0.26	0.047	0.3	0.078	0.2	0.032	0.22	0.034
(Anders and Ebihara 1982)	1.44	0.236	0.616	0.0929	0.457	0.149	0.056	0.197	0.0355	0.245	0.0547	0.16	0.0247	0.159	0.0245
(Boynton 1985)		0.31	0.808	0.122	0.6	0.195	0.0735	0.259	0.0474	0.322	0.0718	0.21	0.0324	0.209	0.0322
(Taylor and McLennan 1985)	2.1	0.367	0.957	0.137	0.711	0.231	0.087	0.306	0.058	0.381	0.0851	0.249	0.0356	0.248	0.0381
(Wasson and Kallemeyn 1988)	1.8	0.29	0.763	0.117	0.572	0.183	0.069	0.249	0.043	0.302	0.0693	0.198	0.03	0.2	0.03
(Anders and Grevesse 1989)	1.56	0.2347	0.6032	0.0891	0.4524	0.1471	0.056	0.1966	0.0363	0.2427	0.0556	0.1589	0.0242	0.1625	0.0243
(Korotev 1996)	2.12	0.319	0.82	0.121	0.615	0.2	0.0761	0.267	0.0493	0.33	0.0755	0.216	0.0329	0.221	0.033
(Palme 1988)	1.57	0.245	0.638	0.096	0.474	0.154	0.058	0.204	0.037	0.254	0.057	0.166	0.026	0.165	0.025
(McDonough and Sun 1995)	1.57	0.237	0.613	0.0928	0.457	0.148	0.0563	0.199	0.0361	0.246	0.0546	0.16	0.0247	0.161	0.0246

Data source from http://meteorites.wustl.edu/goodstuff/ree-chon.htm by (Randy L. Korotev)

REE normalisation in this study has been done with data from Anders et al (1982).

2.5 Methods of determination of rare earth elements

There is an increasing demand for high purity rare earth compounds for industry, medicines, technology, environment and for method validation of analytical procedures. Therefore, development of new precise, reliable, rapid, cost effective and accurate analytical methods are required for routine determination of REE in environmental and geological matrices.

This paragraph gives an overview of the advances in REE's analytical chemistry. The commonly employed methods are as follows,

1. Neutron activation analysis (NAA), instrumental neutron activation analysis (INAA), and radiochemical neutron activation analysis (RNAA).
2. Inductively coupled plasma atomic emission spectrometry (ICP-AES).
3. Inductively coupled plasma mass spectrometry (ICP-MS) including isotope dilution mass spectrometry (IDMS).
4. High-performance liquid chromatography (HPLC) and ion chromatography (HPIC).
5. X-ray fluorescence spectrometry (XRF).

Each method has its own pros and cons with regard to its ability to determine the individual REE effectively, instrumental detection limits and the difficulties of operation and sample preparation.

2.5.1 Neutron activation analysis (NAA)

Hevesy and Levi (1938) described that samples containing REE become radioactive after exposure to a source of neutrons and hence leads to the innovation of NAA (Gschneidner *et al.* 2002). It is a highly sensitive and accurate technique for both qualitative and quantitative detection of rare earth elements, especially at low concentrations. NAA is modified depending upon the need of interest of research to radiochemical neutron activation analysis (RNAA) and instrumental neutron activation analysis (INAA). Radiochemical neutron activation analysis (RNAA) involves irradiation after the chemical separation of interfering matrices. No chemical separation is used in INAA.

Advantages

1. NAA has the advantage that it is a non-destructive technique.
2. High sensitivity and capability of the simultaneous determination of many trace elements even at ng/g levels.
3. No need for analytical blanks.

Disadvantages

1. Very expensive instruments are required i.e. nuclear reactor that requires long cooling time before analysis (time-consuming).
2. Weak emissions of gamma rays are not suitable for the determination of Pr, Er, Dy, Gd and Ho.
3. Handling of radioactive materials (Dybczyński *et al.* 2010, Henderson 2013, Revel and Ayrault 2000).

2.5.2 Inductively coupled plasma atomic emission spectrometry (ICP-AES)

ICP-AES offers rapid multi-element detection over a wide concentration range, but its detection limit is in the µg/g range, which is insufficient for the determination of REE as trace impurities in high-purity materials.

Advantages

1. The most effective multi-element technique for the quantitative determination of many trace elements with widely varying matrices, and are often used in the determination of the REE.
2. High sensitivity and are capable of the simultaneous determination of many trace elements even at (ng/g) levels.
3. Instrumental detection limits are approximately 50.0 µg/l (Djingova and Ivanova 2002).

Disadvantages

1. The large costs of infrastructure maintenance and operating expenses.
2. The presence of several emission lines and spectral interferences.
3. The necessity of having samples dissolved.
4. The determination of REE by ICP-AES requires prior separation of matrix elements i.e. Ba, Na, Ca, Cu, Fe and Ni etc. and their pre-concentration for accurate results.

2.5.3 X-ray fluorescence spectrometry (XRF)

XRF is capable of multi-element quantification of trace elements in various sample types, but the detection limits for elements from medium atomic numbers is typically in the µg/g range. The detection limits offered by XRF for many metals are inadequate (Balaram 2005).

2.5.4 Inductively coupled plasma mass spectrometry (ICP-MS)

The inductively coupled plasma mass spectroscopy (ICP-MS) technique is a powerful method for the direct determination of REE (Pedreira *et al.* 2002). ICP-MS provides rapid analysis time, high sensitivity, multi-element determination capability, wide linear dynamic range and high detection power compared to the previously mentioned techniques.

2.5.4.1 Types of ICP-MS

There are three main types of commercially available ICP-MS.

1. ICP-QMS
2. ICP-SFMS or HR-ICP-SFMS
3. ICP-MS/MS

Quadrupole ICP-MS

Inductively coupled plasma-mass spectrometry (ICP-MS) is accepted as the most powerful elemental analytical technique available today, capable of true multi-elemental determinations in short analysis times. The ICP-MS is most often equipped with quadrupole (Q) mass analysers. Quadrupole mass analysers represent approximately 85 % of all ICP-MS systems installed worldwide.

ICP-SFMS

This ICP-MS usually comes with a high-resolution (HR) analyser based on a double-focusing magnetic sector design. A ICP-SFMS usually offers up to 10,000 resolving power. The HR-ICP-SFMS has the capability of resolving a large number of spectral interferences, but the transmission of ions decreases approximately inversely to resolution as the resolving power increases, which results in increased detection limits. However, HR-ICP-MS is reported to offer higher detection power than the ICP-QMS when it is operated at a similar resolving power as a ICP-QMS. Other benefits of the ICP-SFMS include high sensitivity combined with low background levels (Thomas 2013).

ICP-QQQ-MS

It is also called as ICP-MS/MS and will be dealt with detail in chapter 4.

2.6 Interferences in the ICP-MS spectrum

After the first publications in 1980 describing plasma source mass spectrometry as an analytical technique for trace element analysis in Houk *et al.* (1980), a rapid increase in the number of articles describing instrumental developments, fundamental studies and applications occurred, which have also been covered in a number of reviews and books (Evans and Giglio 1993). Despite the early claims that inductively coupled plasma mass spectrometry (ICP-MS) utilising continuum sampling, was relatively free from interferences a prominent feature in many of the 500 or so publications in the field has been the problem of interferences; either in general or in conjunction with a particular application (Evans and Giglio 1993).

ICP-MS is a sensitive technique and effect of interferences in multi-elemental analysis has loomed large. Thus, ICP-MS does suffer from severe interferences of concern to particular elements. Interferences can be divided into two categories although there is a overlap and both share the same cause (Evans and Giglio 1993).

1. Spectroscopic interferences
2. Nonspectroscopic interferences

2.6.1 Spectroscopic interferences

Spectroscopic interferences form the largest and most intractable problems in ICP-MS. These are caused by atomic or molecular ions having the same nominal mass as the analyte of interest, thereby causing an erroneously large signal at the m/z of interest. Spectroscopic interferences can be divided into two categories, depending on the origin of the interferences (Evans and Giglio 1993).

1. Monoatomic interferences
2. Polyatomic interferences

Monoatomic interferences

These interferences are caused by equal m/z overlapping isotopes of different elements in the sample. These interferences are easy to predict and well documented, so they can sometimes be overcome by utilising alternative isotopes or elemental correction equations.

Polyatomic interferences

Polyatomic ion interferences are caused by ions formed from precursors in the plasma gas, entrained atmospheric gases, water, acids used for dissolution and the sample matrix. The polyatomic ions so formed, may then result in interferences on analytes with the same nominal m/z. The polyatomic ions are usually formed in the cool regions of the plasma due to the highly concentrated element. The polyatomic ions, such as hydrides and oxides of the matrix element, can cause mass overlaps on analytes of interest.

Important spectral interferences in ICP-MS analysis are from the LREE on the HREE. Polyatomic interferences arise when REE combine with oxygen and form oxides ($REEO^+$) and hydroxides ($REEOH^+$) (Houk and Praphairaksit 2001). Barium forms polyatomic ions BaO^+ and $BaOH^+$, which interfere REE importantly with the two Eu isotopes.

There are three sources of polyatomic interferences. Polyatomic interferences could originate from condensation reactions in the expansion region in accordance with molecular beam theory (Gray 1986). However less ion-molecule chemistry is reported to occur in the expansion region as in Douglas and French (1988). Collisional reactions occur in the boundary layer around the outside surface of the sampler (Vaughan and Horlick 1990). And the third source of polyatomic interferences is its survival through the plasma itself, particularly with respect to refractory metal oxide ions (Olivares and Houk 1985).

2.6.2 Non-spectral interferences

Non-spectroscopic interferences, better called matrix effects form the second major group of problems in ICP-MS. These matrix effects affect the formation of analyte ions. Non-spectral interferences that occur are often signal suppression effects on the analytes when the ICP is optimised in the absence of these components. Highly concentrated matrix element can suppress the signal intensity of the REE, reducing the sensitivity for the analytes (Thomas 2013, Zhang *et al.* 2006).

2.7 Methods to reduce spectral and non-spectral interferences

Spectral interferences have been corrected using several different methods, which are discussed, in this section.

Measuring double charged REE at their half masses

This method determines REE at their half masses in more concentrated REE sample solutions, e.g. to measure $^{154}Sm^{2+}$ at m/z 77 but results have shown that the sensitivity of the analytes was greatly reduced and certain analytes were not quantifiable at half their masses (Kawabata *et al.* 1991).

Solvent extraction and chromatographic separation

Separation of the matrix element from the spectral interfered analytes by solvent extraction and chromatography prior to the quantification of trace impurities of REE with ICP-MS has proven to be more successful. Several studies have determined the purity of high purity REEOs, such as La_2O_3, Pr_2O_3, Nd_2O_3 and Gd_2O_3, by chromatographic separation of the rare earth matrix element from the analytes prior to quantification with ICP-MS in order to eliminate spectral interferences. Purities of the different REEOs were determined to be > 99.9 % (Pedreira *et al.* 2002). In other studies, solvent extraction was used for separating a Ce matrix element from the analytes prior to quantification with ICP-MS, but

the total analysis time per sample was 30 minutes, which is relatively high for routine analyses (Li *et al.* 1997).

Algebraic corrections

The oxide and hydroxide interferences on REE have been reported to be corrected using an algebraic/statistical correction scheme. This requires no additional laboratory exercise. However, the mathematical corrections are sometimes erroneous (e.g. correction of the interference of barium on europium) due to the low stability of barium oxide, and when Ba/Eu ratios are high, negative results can be obtained (Aries *et al.* 2000, Cao *et al.* 2001). In principle, any isobaric overlap can be corrected by calculating the relative contribution of the interfering analyte, based on the signal of another isotope at an interference free m/z. However, mathematical correction is subject to error, particularly when multiple steps are required. The magnitude of this error depends on the absolute signals and the contributions from interferences are subtracted (Linge and Jarvis 2009). The non-spectral interferences in the form of signal suppression of analytes are often handled by diluting the sample solution to an appropriate concentration (Zhang *et al.* 2006).

ID-TIMS

REE analysis with ID-TIMS is the most precise and accurate, but not applicable to the determination of the monoisotopic REE (Pr, Tb, Ho and Tm) (Ishikawa *et al.* 2003).

HPLC and HPIC

The separation of individual members of the REE group employing both, HPLC or HPIC, techniques have proved to be satisfactory and have been applied for their quantification using online detection systems (i.e. UV–VIS, ICP-AES and ICP-MS). The selectivity, low amount of sample needed and simultaneous analysis of several elements in a relatively short time are some advantages of these techniques. However, chemical dissolution of the sample is required, as well as the previous separation of REE from most of the major rock components to prevent overloading and precipitation of interfering elements in the column (Kumar 1994, Sialer 2010, Verma and Santoyo 2007).

Table 2.7: Common spectral interferences on the rare earth elements

Analyte	Hydride interference		Oxide interference		Hydroxide interference	
	amu+1	MH	amu+16	MO	amu+17	MOH
^{139}La	138+1	BaH	123+16	SbO, TeO	122+17	SbOH,TeOH
^{140}Ce	139+1	LaH	124+16	SnO, TeO	123+17	SnOH, TeOH
^{141}Pr	140+1	CeH	125+16	TeO	124+17	TeOH
^{146} Nd	145+1	NdH	129+16	TeO	129+17	XeOH
^{147}Sm	146+1	NdH	128+16	NdO	128+17	NdOH
^{153}Eu	152+1	SmH, GdH	136+16	BaO, CeO	135+17	BaOH
^{157}Gd	156+1	GdH	141+16	PrO	140+17	CeOH
^{159}Tb	158+1	GdH, DyH	143+16	NdO	142+17	CeOH, NdOH
^{163}Dy	162+1	DyH, ErH	147+16	SmO	146+17	NdOH
^{165}Ho	164+1	DyH, ErH	149+16	SmO	148+17	SmOH
^{166}Er	165+1	HoH	150+16	SmO	149+17	SmOH
^{169}Tm	168+1	ErH, YbH	153+16	EuO	152+17	SmOH, GdOH
^{172}Yb	171+1	YbH	156+16	GdO	155+17	GdOH
^{175}Lu	174+1	YbH, HfH	159+16	TbO	158+17	TbOH

Metal hydride, metal oxide and metal hydroxide interferences on rare earth elements

3. Introduction to platinum group elements

3.1 Introduction

Platinum group elements are the part of (HSE) (highly siderophile elements). They are also called as noble metals and include ruthenium (Ru), rhodium (Rh), palladium (Pd), rhenium (Re), osmium (Os), iridium (Ir), platinum (Pt) and gold (Au). They are termed as siderophile due to strong affinity towards iron and as chalcophile because of strong affinity towards sulphur. The fractionation during geological processes divides PGE into the Ir-sub group (IPGE: including Os, Ir and Ru and have the highest melting points) and the Pd-sub group (PPGE: including Pt, Pd and Rh and have the lower melting points) (Barnes *et al.* 1985). HSE abundances in geological materials vary significantly, ranging from ~1 mg/g in ore materials to a few pg/g in basalts (Meisel and Horan 2016).

PGE are widely used as catalysts in various chemical processes, as catalytic converters in automobiles, also in electrical industry and jewellery. Besides these applications, PGE are important indicators for the understanding of petro genesis of mantle-derived rocks. The Re/Os isotope system is a geochronometer for understanding the evolutionary processes of the earth (Markey *et al.* 1998).

IPGE being refractory are more compatible during silicate fractionation than PPGE and associate with spinel, chromite, and alloys (Qi 2007). Rhenium is moderately incompatible during partial melting of the mantle but osmium is more compatible thus all crustal rocks have low Os concentration and high Re concentration relative to the mantle (Martin 1990). The Re-Os system is a useful tracer of melt-crust interaction (Shirey and Walker 1998). Silicates, olivine and spinel are the refractory phases that host IPGE within the mantle during partial melting (Ross and Keays 1979). Spinels and chromite-bearing spinels may retain IPGE and Ir is compatible in chromite (Peach and Mathez 1996). Ruthenium and Ir are partitioned in spinal and Pd is insoluble in chromium spinels (Capobianco *et al.* 1994). PGE are also reported to be present as microscopic inclusions of metal alloys within chromite (Peach and Mathez 1996). lridium, Os, Re and Pt have been reported to exist in magmatic liquids i.e. sulphide and silicate (Ballhaus *et al.* 2006). The Osmium, Ir and Ru are traditionally associated with the mineral phases i.e. olivine, pyroxene, chromite and sulphides (Woodland 1999). During melting, silicate becomes saturated with sulphur and sulphur droplets act as PGE collectors and if sulphide phases are absent, the PGE will remain in the silicate magma, increasing in concentration as silicate crystallisation proceeds (Woodland 1999).

Platinum and Pd are mobile as chloride, hydroxide or bisulfide complexes depending upon pH, temperature, oxygen fugacity and ligand concentrations. PGE-chloro-complexes are formed under strong oxidising, acidic or alkaline conditions, hydroxy complexes are formed at neutral and basic pHs and bi-sulphide complexes are formed under reducing conditions and low temperatures (Fleet and Wu 1993).

3.2 Analytical methods for PGE mass fraction determination

The analytical procedure for PGE determination in geological samples consists of three steps i.e. sample digestion, pre-concentration/separation of matrix elements and measurement (Enzweiler and Potts 1995). Fire assay and acid digestions are the two dissolution procedures that dominate the scientific literature for the determination of bulk HSE abundances and isotopic compositions of geologic samples (Meisel and Horan 2016).

3.2.1 Fire assay

Fire assay (FA) is the most often applied method for PGE and Au separation/pre-concentration from base metals and silicates. There are two main types of fire assays i.e. lead and Ni-S fire assays. The main advantage of FA is the larger test portion size of up to 100 g, which is necessary to minimise nugget effects.

The fluxes for lead fire assay comprise sodium carbonate, borax, litharge and reducing agents such as flour or charcoal. Some silver or gold is usually added to the flux as a powder or as a solution to increase the recoveries of PGE (Juvonen *et al.* 2002, Suominen *et al.* 2004). Osmium is completely lost during the cupellation procedure as a volatile oxide, Ru and Ir are partially lost as oxides into the cupel (Hall and Pelchat 1994, Qi 2007, Ravizza and Pyle 1997, Van Loon and Barefoot 1991). The analysis of Ag or Au prills can be performed by INAA or by dissolution with acids for measurement with AAS, ICP-AES or ICP-MS.

NiS-fire assay combined with tellurium co-precipitation is used for bulk analysis of ores and samples with high abundances of HSE for exploration and mining industries (Meisel and Horan 2016). High blanks are of concern due to the usage of large quantities of Ni metal and alkali salts (Na_2CO_3, Na_2O_2, $Li_2B_4O_7$) and Re and Au are partially volatilised during processing (Savard *et al.* 2010). Incomplete spike-sample equilibrium has also been reported in Reisberg and Meisel (2002). The NiS button can be analysed by laser ablation and the use of larger test portions can reduce the problems of heterogeneity.

3.2.2 Acid digestions

Acid digestion at elevated temperature and pressure is more frequently used for dissolution of samples with normal crustal or mantle abundances (Meisel and Horan 2016). Sample digestion by using acids have proved to be more rapid and economical in comparison to fire assay but may not result in complete recovery of the HSE (Qi 2007).

Acid/aqua regia cannot reach PGE occurring as inclusions in chromite and/or silicate minerals (Meisel and Horan 2016, Qi 2007). Carius tubes based acid digestions are best suited for attacking PGE inclusions in chromite and/or silicates at elevated temperatures (> 200 °C) and under high-pressure conditions (> 50 bars) (Shirey and Walker 1995). Low blanks and trace concentrations of Re and Os can be determined with Carius tubes digestions. The danger of explosions of Carius tubes exists and special handling skills are required (Meisel and Horan 2016). High-pressure asher based acid digestions are effective for low HSE blanks (Meisel *et al.* 2001a). The use of HF was reported to be essential when using Carius tubes or HPA digestions for some basalts to obtain complete digestion and recovery of HSE (Dale *et al.* 2012, Ishikawa *et al.* 2014, Meisel *et al.* 2009). However, the use of HF is beneficial for young lava, but Re/Os and Pt/Os ratios can be altered when using HF, and chronological studies may not be possible on old basalts as discussed by Day *et al.* (2015). Expensive apparatus and maintenance costs are also the drawbacks for HPA digestions.

3.2.3 Pre-concentration techniques for PGE

Matrix separation is usually carried out using anion or cation exchange chromatography. In the case of cation exchange pre-concentration techniques, chloro-complexes of PGE and Au in HCl solution are allowed to pass through the exchange column directly and cationic matrix species are retained on the resin. The solutions obtained can be analysed online or offline with ICP-MS (Meisel et al. 2003). Anion-exchange chromatography removes the matrix elements while chloro-complexes of PGE are retained on the resins. PGE are eluted with strong acids for the measurement with ICP-MS (Enzweiler and Potts 1995). Tellurium

co-precipitation is another pre-concentration technique which has been combined with alkali fusion and NiS-fire assay for PGE pre-concentration (Enzweiler and Potts 1995, Qi 2007, Savard *et al.* 2010). Use of cationic surfactant septonex combined with modified silica gel separon for sorption of Au and the PGE from the samples of air born particulate was reported in Vlašánková *et al.* (1999). Cloud point extraction techniques for PGE in geological samples have been reported in various reports such as like Bezerra *et al.* (2005), da Silva *et al.* (1998), Meeravali and Jiang (2008). The use of activated carbon for adsorption and pre-concentration of Au, Pd and Pt and subsequent analysis with the spectrographic technique was used by Bouberlová-Kosinová (1970). Thiourea solutions were used for the adsorption of gold on activated carbon of ore samples and analysis with EDXRF (Peräniemi et al. 1992). Pre-concentration by organic solvent extraction has been reported by Meier (1980).

3.2.4 Instrumental techniques

Atomic absorption spectrometry (AAS) and inductively coupled plasma atomic emission spectrometry (ICP-AES) are not the method of choice for PGE measurement because of the trace abundances of PGE and severe interferences (Qi 2007). Instrumental neutron activation analysis (INAA) has been combined with NiS-FA for low background and better detection limits (Li and Ebihara 2003, Parry *et al.* 1988). Quantification of HSE with ICP-QMS, ICP-SFMS, magnetic sector multi-collector ICP-MS and MC-ICP-MS has been reported in a variety of reports due to its versatility, high sensitivity and nearly interference-free analysis (Meisel and Horan 2016). Most recently ICP-QQQ-MS instrument have been installed and new methods for PGE analysis using the collision/reaction cell have been reported in Bokhari *et al.* (2015a), Bokhari *et al.* (2015c), Bokhari *et al.* (2015d), Bokhari *et al.* (2015e), Sugiyama and Shikamori (2015), Suoranta *et al.* (2016). As ICP-QQQ-MS is the method used for PGE determination in this thesis, the detailed discussion using this technology is covered in chapter 4.

4. Analytical techniques used in the study

4.1 Tandem mass spectrometry (ICP-MS/MS)

Quadrupole-based inductively coupled plasma–mass spectrometry (ICP-QMS) was introduced commercially in 1983. The low detection limits and multi-element capability of ICP-MS made it an attractive option in a wide range of environmental, medical, biological, industrial and archaeological applications, amongst others (Bayon *et al.* 2009). The basic principle of ICP-MS was elemental differentiation based on atomic mass. While atoms of a given element may have different atomic masses, or isotopes, the isotopic composition of each element is well known (Coplen T.B. *et al.* 2003). Interferences in ICP-MS are classed as either spectroscopic or non-spectroscopic (Evans and Giglio 1993). Later sector-field ICP-MS with the higher mass resolution was introduced which had the capability of resolving some of the spectral interferences. Sector-field instrumentation is, however, substantially more expensive, and higher mass resolution comes at the cost of reduced ion transmission and thus, higher detection limits due to the lower signal intensity. The gap between sector-field ICP-MS and ICP-QMS was reduced by the introduction of the cool plasma and multipole collision/reaction cells. These collision/reaction cells provide a versatile means for removing spectral overlaps, as interferences can be reduced either through differences in reaction chemistry (with a reactive cell gas) or by kinetic energy discrimination using a bias voltage (when an inert cell gas is used). Later a Triple Quadrupole ICP-MS (ICP-QQQ-MS) instrument was introduced, which is equipped with an octopole collision cell located between two quadrupole mass filters a shown in Figure 4.1 and Figure 4.2. The tandem mass spectrometer configuration provides two separate mass selection steps, which provides additional control over the ion/molecule chemistry that occurs in the cell. A tandem mass spectrometer can be considered as two spectrometers connected in series by a chamber called the collision cell. The sample enters the first spectrometer, then it is treated with gases in the collision cell and output of the reaction in collision cell is input to the second spectrometer. The first quadrupole allows only the ions of a given m/z ratio into the gas-pressurized octopole cell, rejecting all the ions having other m/z ratios. The second quadrupole then selects only the ion of interest emerging from the cell and rejects the ions at all other m/z ratios. This configuration permits the operation of this ICP-MS instrument in MS/MS mode (Fernández, *et al.* 2012; Balcaen, *et al.* 2013) which in principle offers a superior capability to deal with spectral overlaps. This configuration is used as an alternative to reduce background signals at analyte oxide m/z and also to improve the accuracy of its determination. Different from the conventional collision/reaction cell interfaces, in a tandem mass spectrometer configuration there is full control of the ions that enter the cell and consequently the reactions with the gas introduced into the cell are more efficient. The shift mass mode restricts the ions that enter the ORS (Octopole reaction system) cell to a single mass-to-charge ratio (m/z). Therefore, only selected ions react with the gas inside the cell allowing better control of the reactions and more efficient collision and reaction interactions inside the ORS. In addition, all ions that present the same m/z as the analyte oxide are rejected at the first quadrupole. The second quadrupole is then set to a specific mass unit (Agilent publications).

4.2 Principles of ICP-MS/MS

As in regular ICP-QMS, the test sample in a highly diluted solution form is transported with a sample introduction system i.e. a peristaltic pump forces the solution into the nebuliser where it is converted into an aerosol in argon gas. The spray chamber separates the fine aerosol from larger droplets (Thomas 2013).

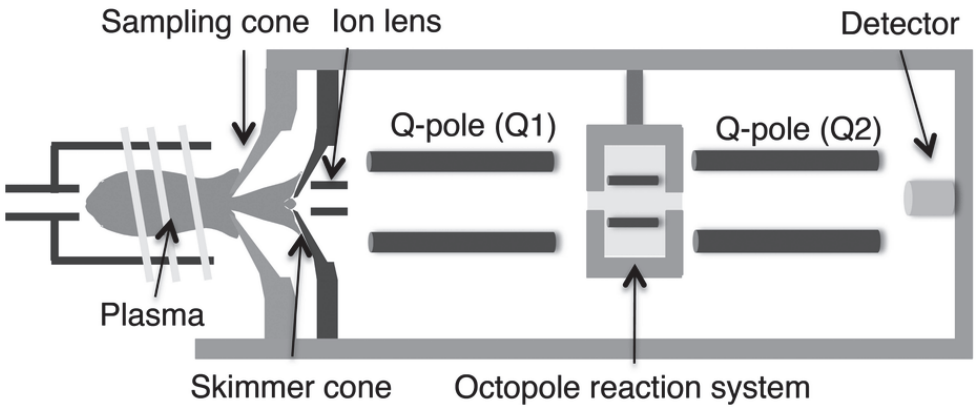

Figure 4.1: MS/MS system in Agilent 8800 (Agilent publications)

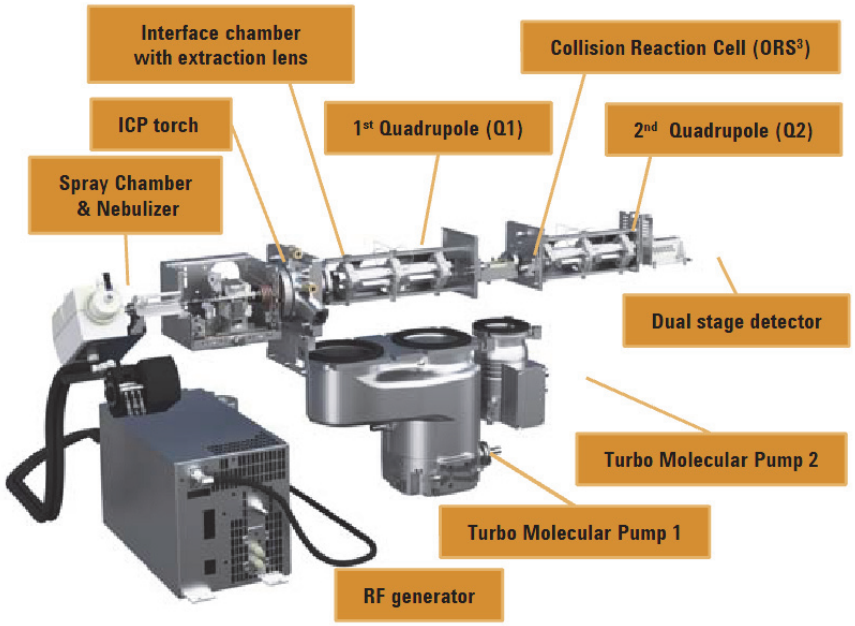

Figure 4.2: Complete setup for Agilent 8800 (Agilent publications)

The aerosol is then vaporised, converted to atoms and finally ionised after it has been introduced into the inductively coupled plasma (ICP). This whole process is achieved by utilising a ICP operating at a temperature range of 7000 – 10000 K. By applying a radio-frequency (RF) signal through a copper coil, an intense magnetic field is produced. The magnetic field interacts with an argon gas that is flowing through a concentric quartz tube, a torch, which ionises the gas. By applying electrons from a high-voltage spark, a high-temperature plasma is generated, where the temperature reaches up to 10000 K. Ions produced in the plasma are directed into the mass spectrometer through an interface region. The interface region consists of two metallic cones, a sampler cone and a skimmer cone, which allows the ions to pass through to the ion optics. The ions are guided by the ion optics into the mass filter Q1, which separates ions of interest from the unwanted ions by their mass-to-charge ratio (m/z) and leads them to the collision/reaction cell. The collision/reaction cell can be supplied with reactive gases that react with the ions. After CRC events (collision/reaction cell chemistry) with the ions in the cell, ions are received by a second mass filter Q2 and finally reach the detector. The tandem mass spectrometer configuration of the 8800 is based on two high-frequency, hyperbolic profile quadrupoles,

and a Octopole Reaction System (ORS) collision/reaction cell. Two working principles of this technology can be developed using the mass hunter workstation acquisition software.

1. Setting On-mass method on the mass hunter workstation
2. Setting Mass-shift method on the mass hunter workstation

4.2.1 Setting On-mass method on the mass hunter workstation

For setting the on-mass method on the mass hunter workstation, the same m/z is chosen on both the quadrupole Q1 and Q2 e.g. $^{151}Eu^{+}$ m/z 151 as shown in Figure 4.3. All the ions of m/z 151 enter the Q1 that includes $^{135}Ba^{16}O^{+}$ m/z 151 also. In the collision/reaction cell, $^{135}Ba^{16}O^{+}$ reacts with NH_3 gas and makes a new product of higher mass, which is not selected by Q2. $^{151}Eu^{+}$ thus can be measured interference free on Q2 as presented in Bokhari and Meisel (2014a), Bokhari *et al.* (2015b).

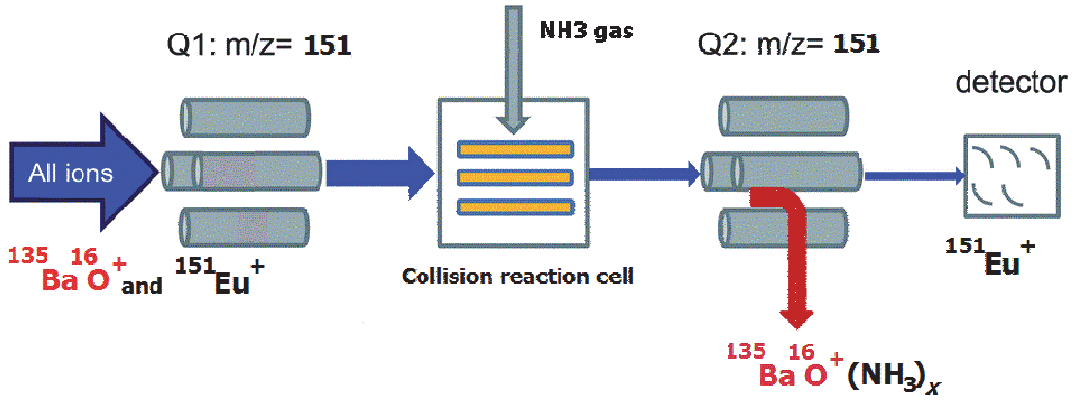

Figure 4.3: On-mass method for Eu measurement

4.2.2 Setting Mass-shift method on the mass hunter workstation

In the case of the mass-shift method, a different m/z is set on each quadrupole i.e. for the measurement of $^{45}Sc^{+}$, Q1 is set at m/z 45 and Q2 is set at m/z 130. All the ions of m/z of 45 enter the mass filter Q1. In collision/reaction cell, the interfering ions remain unreacted or do not make a product ion of m/z of 130 and are rejected out of the reaction cell. This is shown in Figure 4.4 as presented in Bokhari and Meisel (2014a), Bokhari *et al.* (2015b).

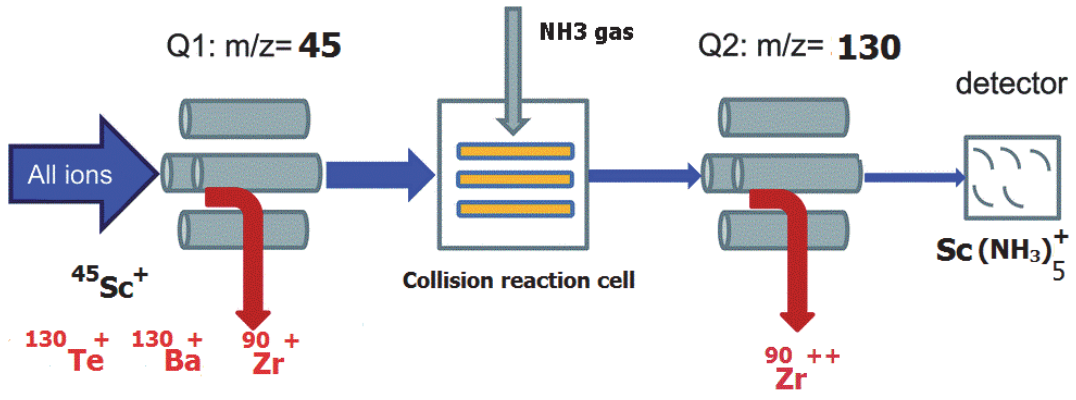

Figure 4.4: Mass-shift method for Sc measurement

4.3 Instrumentation of the ICP-MS/MS Agilent 8800 (Source-Agilent notes)

Sample introduction

The standard sample introduction system is composed of:

1. Low-flow concentric nebuliser
2. Peltier cooled spray chamber
3. Peristaltic pump

Nebuliser

It is a concentric nebuliser made from glass with a low sample flow rate of ~0.2 ml/min.

Spray chamber

A quartz, low-volume, Scott-type double-pass spray chamber provides an improved removal of larger aerosol droplets, compared to cyclonic or impact-bead designs. Peltier cooling eliminates the need for a separate external cooling water supply. Controlled temperature ranges from -5 °C to +20 °C (with instrument cooling water at 15–30 °C). The standard setting of temperature was 2 °C for analysis in this study.

Peristaltic pump

Low-pulsation, 10-roller peristaltic pump has three separate channels for the delivery of sample, internal standard (ISTD) and spray chamber drain. The low-flow rate sample introduction system and Peltier cooled spray chamber deliver a stable and consistent operation.

Plasma RF generator

The RF generator is a high power-transfer efficiency and maintenance-free solid state digital drive of 27.12 MHz with variable frequency matching. It provides significantly improved matrix tolerance for changes in the sample matrix. Typical RF power ranges from 500 W to 1600 W and with step size of 10 W.

Torch

The torch is a one-piece quartz unit with a 2.5 mm internal diameter (i.d) injector. The exceptionally wide torch injector supports the robust plasma to efficiently decompose the sample matrix providing the narrow ion energy spread required for effective interference minimisation. This also minimises matrix deposition on the interface and ion lens, signal drift and routine maintenance. The torch self-aligns in x and y-directions within the mounting bracket which ensures consistent repositioning after routine maintenance or when switching the torches.

Shield Torch system

The Shield Torch System (STS) reduces plasma potential and thereby precisely controls the ion energy which is essential for tuning stability, optimum cell performance and for effective cool plasma operation.

Interface-Sampling cone

The sampler cone is a one mm diameter orifice, with a Cu base and a Ni or Pt tip. Access to the interface region for routine maintenance is easy and no tools are required for removal/refitting of the sampling cone. The sampling cone-retaining ring ensures reliable thermal contact and reproducible fitting, even with different operators, giving a dependable long-term performance.

Skimmer cone

The skimmer cone has 0.4 mm diameter orifice and is made of Ni or Pt with a Cu base. Precisely controlled skimmer tip temperature ensures minimal matrix condensation and provides good tolerance to high matrix samples. The small skimmer orifice reduces matrix contamination of the high vacuum region and thus reduces maintenance procedures.

Plasma gas control

The gas control consists of a four channel Agilent mass flow controller (AMFC) for precise and stable control of gas flows i.e. plasma (cool) gas, auxiliary gas, nebuliser gas, and make-up or dilution (HMI) gas.

Torch position

The torch position is stepper motor controlled in three axes (horizontal, vertical and sampling depth), with a step size of 0.1 mm. Expert auto tuning delivers quick and reliable auto alignment following maintenance.

• Horizontal and vertical position: ±2 mm

• Sampling depth: 5 to 8 mm was is used in this study

Ion lens

The off-axis ion lens provides high ion transmission and low backgrounds, combined with a uniform mass response. The lens is in front of the gate valve outside the high vacuum region, and so can be accessed easily for scheduled cleaning, without venting the vacuum system. The conical extraction and off-axis Omega lens provide continuous focusing of all ions across the mass range, ensuring high ion transmission and the lowest mass bias. The location of ion lens is easy to access for routine maintenance.

Extraction lens

The extraction lens is positioned behind the skimmer cone and focuses the ions as they enter the intermediate vacuum stage, providing high ion transmission across the mass range. The lens operates at a fixed voltage for simple, reliable tuning and superior matrix tolerance.

Off-axis Omega lens

The omega lens protects the first quadrupole (Q1), ORS^3 octopole reaction system, and high vacuum region from the contaminations, by rejecting neutral species from the ion

beam. The low voltage of this deflector lens contributes to the minimal mass bias and low background noise characteristics of the instrument.

Octopole reaction system

A new, 3rd generation collision/reaction cell, the ORS^3, provides exceptional interference removal. The ORS^3 is longer and narrower than the previous ORS cell used on other ICP-QMS instruments, and operates at a higher frequency, at higher cell gas pressure and at a higher kinetic energy discrimination (KED) bias voltage. This delivers improved performance in the He mode, ensuring the instrument can perform well in collision mode as well as reaction mode. The octopole ion guide is temperature-controlled with four cell gas lines fitted as standard, for maximum flexibility in collision and reaction modes. A small internal volume cell ensures rapid cell gas switching and high ion transmission.

Octopole

The octopole comprises a thermally-stabilised cell with 12 MHz ion guide operated with fixed RF amplitude for the full mass range. It permits fast analysis with uniform conditions, for stability and consistent interference removal. An octopole ion guide minimises ion scattering at high cell pressures providing high ion transmission and good sensitivity.

Cell gas control

The 8800 ICP-QQQ has four cell gas flow controllers as standard:

- Maximum flow rate of 12 ml per minute (typically used for He cell gas)
- Maximum flow of 10 ml/min (typically used for H_2)
- Maximum flow of 10 ml/min, corrosive gas resistant (typically used for NH_3 in He)
- Maximum flow of 1 ml/min (typically used for heavier reaction gases such as O_2)

The different cell gas modes can easily be implemented sequentially in one visit to the sample, enabling easy comparison of data from different modes. Cell gas changes occur under software control and with minimal switching time (~5 s), due to the low internal volume of the octopole-based cell.

Mass analysers

The 8800 ICP-QQQ-MS tandem mass spectrometer configuration incorporates two Agilent-manufactured quadrupole mass analysers, each with an optimum hyperbolic rod profile and both operate at high (3 MHz) frequency. A hyperbolic profile quadrupole provides superior ion transmission, resolution and abundance sensitivity at standard settings, so eliminating the need for multiple resolution settings to separate adjacent peaks. A higher operating frequency allows ions travelling down the axis of the quadrupole to be subjected to more RF cycles and therefore non-target (off-mass) ions are rejected more efficiently. The first quadrupole mass filter (Q1) is located after the off-axis ion lens and filters the ions arriving from the plasma, selecting the mass, which is allowed to enter the ORS^3. The second quadrupole mass filter (Q2) is located after the ORS^3 and filters the ions that emerge from the collision/reaction cell, selecting only the masses which are passed to the detector. The primary function of Q1 is to control the ions that are permitted to enter the collision/reaction cell. Pre-filter and post-filter rods control fringing fields and improve rejection of non-target ions. Each of the two quadrupoles of the 8800 ICP-QQQ-MS has the following performance specifications:

• Mass range: 2–260 m/z

• Mass scan speed:

Slew rate (Li to U, no intervening peaks): 56.6 million m/z/s

Scan speed (Li to U, plus data collection at 40 intervening masses): >3000 a.m.u/s

• Abundance sensitivity in Single Quad mode (measured at Cs):

• Low Mass side: 5 x 10^{-7}

• High Mass side: 1 x 10^{-7}

In MS/MS mode, the overall abundance sensitivity (AS) of the ICP-QQQ-MS system is derived from the product of Q1 AS x Q2 AS (so 10^{-7} x 10^{-7} = 10^{-14}). However, this is impossible to measure in practice, as the signal difference exceeds the dynamic range of the detector.

First quadrupole (Q1)

The first high-frequency hyperbolic quadrupole is positioned in front of the ORS, to control the ions that are passed to the collision/reaction cell and enable MS/MS operation.

Second quadrupole (Q2)

The second high-frequency hyperbolic quadrupole filters the ions that emerge from the cell exit, passing only the target analyte/product ions to the detector. MS/MS operation delivers highest peak separation as the resolution performance is the product of the two mass spectrometers.

Electron multiplier detector

Auto-switching, dual-mode discrete dynode electron multiplier (DDEM) detector provides a full nine orders dynamic range with standard hardware and operating conditions. Fast measurement of transient signals is provided (with a 3 ms TRA sweep time, as used for single nanoparticle analysis), due to the use of a proprietary analogue amplifier, which operates at the same short integration time (100 µs) in both pulse and analogue mode.

• Minimum dwell time: 100 µs

• Dynamic range: 9 orders

Vacuum system

A four-stage differential vacuum system using one split flow turbomolecular pump, a second turbo pump for the ORS^3 chamber, and a single external rotary pump. The vacuum pumping efficiency contributes to the high ion transmission and high sensitivity. Auto Recover mode returns the 8800 ICP-QQQ-MS to standby (pumping) state when electrical power is resumed after a power failure, saving valuable time. No need to manually start the vacuum system following an overnight power failure. The rotary pump is external to the cabinet and so can be located conveniently in the laboratory, or in an external service corridor (may require an extended 3 m vacuum hose option). The rotary pump hose on the Agilent 8800 ICP-QQQ-MS is chemically inert for resistance to corrosive acids.

4.4 Ion-molecule reactions chemistry in collision/reaction cells

Using a collision/reaction cell is an elegant way to minimise isobaric interferences, especially for heavy isotopes. For that purposes, the cell placed just before the second mass filter is filled with a low-pressure gas chosen for its chemical reactivity and selectivity towards the interfering ions.

4.4.1 Collision/reaction cell

A collision/reaction cell consists of RF multipole ion guides enclosed in a cell that can be pressurized with a gas (Balcaen *et al.* 2010). The length of the rods in multipoles ranges from ~5 to 15 cm. The Agilent 7500c, 7700, and 8800 utilise octopole ion guides. The efficiency of ion transmission in octopole ion guides is considered good with reduced scattering losses (Tonietto *et al.* 2010). The ions occupy a large volume in the wider potential well in an octopole, and can travel further while passing through the cell. A higher-order multipole ion guide provides a greater gas thickness (at appropriate pressures) as compared to a lower order multipole. The increased gas thickness has a profound effect on a number of collisions leading to a chemical reaction and hence the efficiency of the cell.

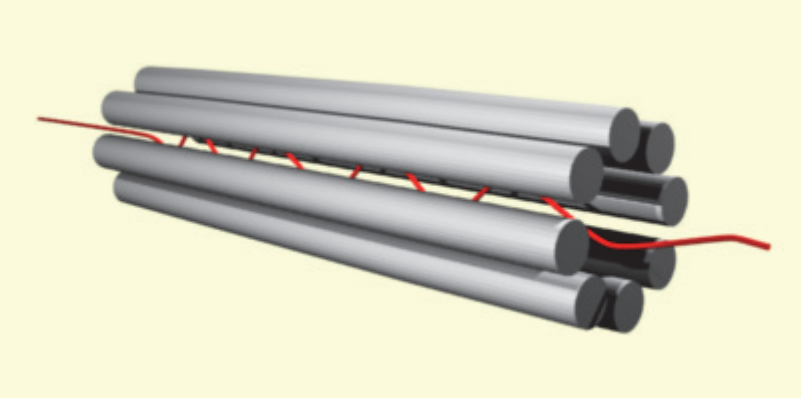

Figure 4.5: Source - https://commons.wikimedia.org/wiki

4.4.2 Mechanism of collisions in collision/reaction cell

Ions entering the collision/reaction cell move radially and collide with the gas atoms. During the collisions, analyte ions lose energy and a potential difference in the reaction cell causes the ions to move along the potential field and confine them in this region. Collisional focusing can physically confine the ions into a narrow ion beam (Isnard *et al.* 2006, Tanner *et al.* 2002).

Collisional processes include energy transfer and collisional fragmentation. In case of an elastic collision when analyte ion of mass m_1 and kinetic energy E_1 collides with gas species of mass m_2 and energy E_2=0,

the energy E'_1 after collision is given below as in Tanner *et al.* (2002)

$$E'_1 = E_1\left[\frac{m_1^2+m_2^2}{(m_1+m_2)^2}\right] \quad \text{---------- (A)}$$

$$E'_2 = E_1 - E'_1 \quad \text{---------- (B)}$$

As m2 $\longrightarrow$ 0, E'1 $\longrightarrow$ E1 and no energy transfer takes place and the analyte ion will have the same energy before and after the collision. If m2 = m1, the collision partners exit with

equal energy, so that the incident ion loses half of its initial energy. Multiple collisions of the ion result in a sequential loss of kinetic energy and results in energy damping (a reduction in the width and magnitude of the kinetic energy distribution). Thus, the ion loses energy according to the reduced mass of the collision partners: a larger neutral/ion mass ratio increases the rate of energy damping of the ion. Complete damping to the thermal condition, if possible, means that the ion simply executes an essentially 'random walk' through the cell. Large ion energy at the entrance to the cell (source potential plus expansion energy minus cell-offset potential) requires more collisions for energy damping. For a given cell pressure, a higher initial energy also results in a efficiency reduction because the ion progresses farther into the cell before the energy is damped, and hence the number of collisions is reduced. Further, higher energy lowers the probability of a reaction during the collision, compromising the specificity of the thermal chemistry, and increasing the potential for sputtering cell materials (Tanner et al. 2002).

Collisional fragmentation

An inelastic collision is defined by internal degrees of freedom during a collision (rotational, vibrational or electronic). For a polyatomic ion, these include rotational, vibrational and electronic degrees of freedom. Subsequent collisions can transfer (relax) this energy to translation (kinetic energy or heat). The chemical bond may dissociate if the energy is more than the bond energy and a polyatomic ion may fragment. Fragmentation may be successful in a single collision; in this case relatively high collision energy is required to account for the distribution of the energy into the various degrees of freedom. Fragmentation can also occur through multiple collisions, in which the internal energy is accumulated by sequential energy pumping to the dissociation limit (Tanner *et al.* 2002).

Kinetic energy discrimination

Ions from the ICP retain a significant portion of their original kinetic energy and trajectory, whereas ions formed inside the cell are typically formed at lower kinetic energy and/or with an off-axis trajectory. The lower energy ions formed in the cell are unable to overcome the potential barrier and are thus prevented from passing into the analysing quadrupole and onto the ion detector. Kinetic energy discrimination (KED) refers to the use of a potential barrier between the cell and mass analyser, typically by operating the cell at a dc offset potential somewhat lower than that of the analysing quadrupole (Tanner *et al.* 2002).

4.5 Ion-molecule reactions

The reactions taking place inside collision/reaction cells are referred as ion-molecule reactions. Although many different types of gas-phase, ion–molecule reactions exist, only a relative few have thus far been shown to play important roles in interference reduction in ICP-MS [http://www.chem.yorku.ca/profs/bohme/research/research.html], (Amr *et al.* 2010).

Thermochemistry of reactions

Thermodynamic and kinetic aspects should be considered when developing reaction chemistry strategies. More fundamental aspects of ion thermochemistry can be found in Lias (1988). Studies by Tanner and colleagues may be reviewed for a complete discussion of reaction thermodynamics and kinetics considerations in ICP-MS (Koyanagi *et al.* 2000). In brief, reactions must be thermodynamically allowed under the reaction conditions used, i.e., they must be experimentally exothermic, and the reaction rates must be analytically useful.

Compilations of thermodynamic data and reaction rates are available in Koyanagi *et al.* (2000) and should be consulted as a guide for experiments, but empirical testing and verification under actual instrumental conditions is nonetheless advised.

Enthalpy of reactions

Enthalpy is a state property, and it is defined for the set of thermodynamic properties of a system (which include temperature, pressure, composition etc.).

Enthalpy of formation

The enthalpy of formation (commonly called the heat of formation) of species X, is $\Delta H_{f,T}(X)$, the amount of heat required to produce X from its standard state components at temperature T. The 'standard state' of an element is the normal state of aggregation at atmospheric pressure at the specified temperature. Accordingly, at room temperature the standard state of H is H_2, that of O is O_2, and that of Ar is Ar. The heats of formation of standard states at 298 K are defined as zero.

Enthalpy of reaction

The change of enthalpy in a reaction is (the sum of the heats of formation of the products) minus (the sum of the heats of formation of the reactants):

$$\mathbf{A^+ + B^+ \longrightarrow C^+ + D^+} \qquad \text{(A)}$$

$$\mathbf{\Delta H_r = \Delta H_f(C^+) + \Delta H_f(D^+) - \Delta H_f(A^+) - \Delta H_f(B^+)} \qquad \text{(B)}$$

If the enthalpy of reaction is negative, the reaction is exothermic and might proceed. If the enthalpy of the reaction is positive, the reaction is endothermic and will not take place unless additional energy is supplied to the process (by excess axial kinetic energy before relaxation in a collision/reaction cell or by the r.f). In reality, the reaction energy is given by the free energy of reaction:

$$\mathbf{\Delta G_r = \Delta H_r - T\Delta S_r} \qquad \text{(C)}$$

where T is the temperature (in K) and ΔS is the entropy change of the reaction (defined the same as for enthalpy).

Kinetics

The enthalpy of a reaction determines the thermodynamic viability of a proposed reaction. The actual value of the reaction for analytical purposes is dependent on the kinetics (rate of the reaction). The density of a reactant or product ion, which is proportional to the ion signal observed, is exponentially dependent on the rate constant, the density of the neutral reactant, and the reaction time. In addition, the product ion distribution (the identity of the product ions and their branching ratio, for multiple products or reaction channels) is of critical importance. Rate constants of ion–molecule reactions have been measured using a variety of techniques, including high-pressure ion sources, ion traps, ion cyclotron resonance, flowing afterglows (FAS) and SIFTs. In many instances, the reported values are remarkably consistent, while in others there is substantial variation (Tanner *et al.* 2002).

4.6 Types of ion-molecule reactions

Several reaction mechanisms have been reported that occur in collision/reaction cell, which categorises ion-molecule reactions into following types.

1. Charge transfer reactions
2. Proton transfer reactions
3. Hydrogen atom transfer
4. Atom transfer reactions
5. Oxidation reactions
6. Clustering

Charge transfer reactions

It is generally understood that, in ICP-MS applications, the most important, useful and abundant types of reactions are charge transfer reaction as shown below,

$$A^+ + B \longrightarrow B^+ + A \qquad (A)$$

$$Ar^+ + NH_3 \longrightarrow NH_3^+ + Ar \qquad (B)$$

In early applications, interferences caused by argide ions (Ar^+ and ArX^+, where X may be Ar, O, Cl, C, Na and so on) were studied. The corresponding neutral argides have high ionisation potentials and their charge transfer reactions often proceed with high efficiency near the collision rate (Nelms 2005, Tanner *et al.* 2002).

Reactions involving hydrogen-containing substances

Another three types of reactions i.e. proton transfer reactions, hydrogen atom transfer and atom transfer reaction involves hydrogen-containing substances (Nelms 2005, Tanner *et al.* 2002).

Proton transfer reactions

Such reactions involve the transfer of a proton (H^+).

$$AH^+ + B \longrightarrow BH^+ + A \qquad (A)$$

$$ArH^+ + H_2 \longrightarrow H_3^+ + Ar \qquad (B)$$

Hydrogen atom transfer

Such reactions involve the transfer of a hydrogen atom (H).

$$A^+ + BH_2 \longrightarrow AH^+ + B \qquad (A)$$

$$Ar^+ + H_2 \longrightarrow ArH^+ + H \qquad (B)$$

Hydride ion transfer reaction

Such reactions involve the transfer of a hydride ion (H^-).

$$A^+ + BH \longrightarrow B^+ + AH \qquad (A)$$

Oxidation reactions

Oxidation reactions have apparent selectivity and speed and are therefore very promising.

$$A^+ + BO \longrightarrow AO^+ + B \qquad (A)$$

$$Ce^+ + N_2O \longrightarrow CeO^+ + N_2 \qquad (B)$$

The leaving group as in equation (B) i.e. N_2 with thermodynamic stability are attractive in ion-molecule reactions. The molecule CO_2 is also a promising reactant due to the thermodynamic stability of CO as a leaving group. This is important as O_2 has a different application because a very strong A^+– O bond is required for this reaction to proceed. However, as a result, some reactions with oxygen have very high specificity (Nelms 2005, Tanner *et al.* 2002).

Clustering

It is a common reaction between many electron donor molecules and ions, which can be rationalized in terms of the ligand–ion mutual electron donation. Association or clustering reactions are of the type:

$$A^+ + B \longrightarrow AB^+ \qquad (A)$$

$$Ni^+ + NH_3 \longrightarrow Ni^{+\cdot}\, NH_3 \qquad (B)$$

Clustering generally, plays a negative role in reaction cell ion chemistry when applied to the ICP-MS. Ammonia is a good clustering ligand, meaning that it forms adducts readily and hence can be an analytical complication unless steps are taken to control the appearance of cluster ions (Nelms 2005, Tanner *et al.* 2002).

The most useful reagent gases for ICP-MS can be classified as charge-exchange reagent gases (e.g., H_2, NH_3, Xe, CH_4, and N_2), oxidation gas reagents (e.g., O_2, N_2O, NO, and CO_2), a relatively few adduction gases (e.g., H_2 and CO), and other reagent gases (e.g., CH_4, C_2H_6, C_2H_4, CH_3F, SF_6, and CH_3OH). Gas ions with a low mass have the advantage of being converted to low m/z products, and they are easily swept away or ejected from the reaction cell. In general, heavier gases are both more reactive, due to their higher cross-sections and better damping characteristics, and less specific (Koppenaal *et al.* 2004). The more appropriate reagent gases mostly react at high rates, are highly selective, and provide significant resolution efficiency from the interfering isobars. Therefore, the primary product ions are created rapidly and (preferably) nearly completely. The secondary products are easily removed or minimally re-react, which results in minimal spectral complexities (Koppenaal *et al.* 2004).

5. Method development and optimisation of sodium peroxide sintering

5.1 Introduction and background

Sample decomposition is one of the fundamental and integral steps a geochemical analysis. The complex nature of the geochemical matrices makes it necessary to choose a suitable sample decomposition technique that is compatible with the specific objective of analysis (Sulcek and Povondra 1989). According to Sulcek and Povondra (1989) the selection of the sample decomposition procedure should be based upon the chemical and mineralogical characteristics of the sample, analytes to be determined, precision and accuracy requirements, sample throughput, manpower and time and cost constraints. Despite considerable developments in solid sample introduction techniques such as laser ablation sampling, solution nebulisation remains the preferred method for many ICP-MS applications (Hu *et al.* 2010). However, the introduction of sample material via a nebulisation system requires the complete dissolution of the test portion of the rock, therefore, the sample preparation step is often the main constraint in terms of time of analysis and accuracy of results (Cotta and Enzweiler 2012). Inductively coupled plasma mass spectrometry (ICP-MS) has been widely used to determine trace elements in geological samples and has been found to provide reliable analytical results at relatively low concentration levels (Djingova and Ivanova 2002, Meisel and Horan 2016, Thomas 2013, Völlkopf *et al.* 1999). In the case of geological sample analysis, dissolution is often the limiting factor to obtain accurate results, which is particularly true when applied to coarse-grained granitic rocks, which contain significant quantities of resistant minerals such as zircons (Sulcek and Povondra 1989, Totland *et al.* 1992). There is no single technique capable of dissolving all elements in all kind of geochemical samples, but satisfactory methods can be developed for given type of the sample and selected group of elements (Sulcek and Povondra 1989).

The complete dissolution of some rock matrices is difficult when resistant minerals are present, such as garnet, sphene, spinel, zircon, rutile and chromite (Cotta and Enzweiler 2012). The digestion of garnet, sphene, spinel, zircon, rutile and chromite has been performed with acid attacks in sealed polytetrafluoroethylene (PTFE) bombs at high temperatures (>160 °C) which require several days (Révillon and Hureau-Mazaudier 2009, Yu *et al.* 2001). Acid mixtures of different combinations have been reported for digestion of refractory phases, such as HF/HNO_3 in Eggins *et al.* (1997), Robinson *et al.* (1999), HF/$HClO_4$ in Dulski (2001), Totland *et al.* (1992), HF/H_2SO_4 by Chao and Sanzolone (1992), Totland *et al.* (1992), HF/HBr/HNO_3 in Makishima *et al.* (2002), Makishima and Nakamura (2001). The dissolution of granitic samples was achieved by NH_4F and HNO_3 that minimises the use of HF (Hu *et al.* 2010). Sulphuric acid tends to form the precipitates of (Sr, Ba, Pb)-SO_4 and Th, Ta and Nb are hydrolysed (Münker 1998, Yu *et al.* 2001). Mixtures of HF/HNO_3/$HClO_4$ were said to be effective for dissolution of granitoid and sediment samples (Pretorius *et al.* 2006, Révillon and Hureau-Mazaudier 2009). Digestions of refractory minerals using $HClO_4$ were effective and for fluorides removal as in Robinson *et al.* (1999), Yokoyama *et al.* (1999). However, the acid digestions suffered precipitation of insoluble fluorides i.e. CaF_2, MgF_2 and AlF_3 despite their effectiveness in the dissolution of refractory minerals of rocks (Cotta and Enzweiler 2012). The preferred sample preparation technique is wet chemical digestion with HF (Meisel *et al.* 2002). Acid blanks can be controlled and silicon can be removed easily by volatilisation that makes this technique attractive (Meisel *et al.* 2002). However, the dissolutions are often incomplete in the presence of zircon ($ZrSiO_4$), tourmaline etc. (Fan and Kerrich 1997a, Hall and Plant 1992, Longerich *et al.* 1990, Zuleger and Erzinger 1988). Acid digestions of geologic samples are very successful when applied to

fine-grained mafic samples, but digestions are often incomplete when applied to coarse-grained granitic rocks, especially those containing significant quantities of zircons (especially zircons which are large grained, young and contain low concentrations of U) (Taylor *et al.* 2002). The natural ratio of zirconium to hafnium is 30-40 Claiborne *et al.* (2006) in rhyolite and acid digestion often fails to recover the corresponding amount of hafnium and zirconium.

Microwave-assisted digestions of geological samples are not effective for refractory phases and results in incomplete recoveries of associated trace elements (Makishima *et al.* 2002, Sengupta *et al.* 1996, Totland *et al.* 1992). HPA digestions have been used effectively for dissolution of mineral phase (Paliulionyte *et al.* 2006).

Fusion techniques with alkali salts such as $LiBO_2$, Na_2CO_3, NaOH, Na_2O_2 etc. on the other hand are known to be reliable, but high blanks levels and high total dissolved solids (TDS) contents of the resultant solutions are of concern (Meisel *et al.* 2002). Fusion of silicate rocks with fluxes of $LiBO_2$ / $Li_2B_4O_7$ results into suspensions that can be dissolved in dilute nitric and hydrochloric acids (Cremer and Schlocker 1976, Feldman 1983). Silica, boron and a large amount of flux in the resulting solutions require a high dilution factor to meet ICP-MS requirements (Cotta and Enzweiler 2012). Volatilisation of Si and B has been done by a heating/evaporation step with HF as SiF_4 and HBF_4 (Panteeva *et al.* 2003, Yu *et al.* 2001). Matrix-matched calibrations using reference materials have been used to minimise the matrix effect (de Madinabeitia *et al.* 2008, Meisel and Kane 2011). Polyatomic interferences are generated on several analytes due to the matrix effects of the solutions produced with fluxes of $LiBO_2$/$Li_2B_4O_7$ (Cotta and Enzweiler 2012, Münker 1998).

Certain minerals (spinels, beryl, tourmalines, chromite, zircon, monazite, niobates, tungstates, topaz, cassiterite) are resistant to acid digestions and must be subjected to sintering or fusion and subsequent acid digestions to bring them into solution (Lapakko 2002). Fusion with sodium peroxide or sintering with sodium peroxide is preferred over $LiBO_2$/$Li_2B_4O_7$ fusions (Cotta and Enzweiler 2012, Meisel *et al.* 2002). Meisel *et al.* (2002) favour sintering over fusions as the losses of analytes with lower temperatures are minimised and decomposition of Na_2O_2 results into NaOH and H_2O_2, which do not cause memory effects like that of Li and B etc. The sinter dissolves in water and Ti and Fe are precipitated as hydroxides along with the co-precipitation of the lanthanides and the trace elements. High sodium and silica contents are separated by this method (Robinson *et al.* 1986, Yu *et al.* 2001). This method works well for the lanthanides, Sc and Y, but the HFSE are not completely co-precipitated (Yu *et al.* 2001). The addition of small amounts of Ti and Fe to the sample before fusion can completely co-precipitate Ti and Fe hydroxides and HFSE (Taicheng *et al.* 2002). Niobium and Ta recoveries were reported lowered by this method (Bayon *et al.* 2009). Mixing residue and supernatant leads to complete recovery of analytes by Meisel *et al.* (2002). Cotta and Enzweiler (2012) used the residue and the discarded supernatant for high recovery of analytes with low salt contents (Cotta and Enzweiler 2012). Further optimisation steps were carried out in this thesis using sodium peroxide sintering and were applied to the determination of analytes in different matrices i.e. geological and industrial (incinerators material) (Funari *et al.* 2016, Funari *et al.* 2015, Shirdashtzadeh *et al.* 2014).

5.1.1 Method requirements for sample digestion

Robust, accurate and precise analytical methods are required for the identification, batch analysis, in certification, to increase the value of test results, to prove what we claim is true, for quality assurance, regulations and quality standards of laboratories and for reliability and consistency of analytical measurements, which is an integral part of any good

analytical practice. Many factors are of concern in the chemistry of sample dissolution of geological materials i.e. the measurement quality objectives, nature of sample, effectiveness of dissolution technique, analyte recovery, interferences during analysis and safety issues etc. Method validation has received significant focus from industrial and regulatory agencies. A complete method validation process involves a series of measures and steps that lead to development of an optimised analytical method that can meet the demands of the clients. Analytical procedures need to be validated, verified, or revalidated before initial use in routine testing, in a different laboratory, or when conditions for which the method has been changing e.g. different instrument or samples with a different matrix and the change is outside the original scope of the method. The power of any experimental test depends on upon the extent to which the applied analytical method is significantly precise for the determination of analytes. The selection of chemical methods is based upon the chemical judgment of a protocol which gives data with the lowest uncertainties for an analyte, the cost of the analysis, the availability of analysts, equipment and its chemical independence.

Complete sample digestion is important for recovery of refractory minerals and for the determination of rare earth elements and platinum group elements by inductively coupled plasma mass spectrometry (ICP-MS) in geological materials. From the viewpoint of different decomposition procedures, it is evident that acid digestions have limitations of incomplete digestions of refractory phases. Alkaline fusions offer complete digestions but are limited due to some analyte losses at high temperatures, high total dissolved solids and memory effects. Thus a universal method for sample digestion is needed which,

1. Can completely digest the sample,
2. Can completely decompose refractory minerals,
3. Provides low blanks,
4. Is safe and inexpensive,
5. Gives maximum analyte recovery,
6. Has capacity to include larger test portions to avoid problems of nuggets and inhomogeneity,
7. Produces stable resulting solutions,
8. Can be used in certification and the method validation.

5.1.2 Selection of the protocol for sample digestion

Rhyolite (MRH-1), is a new reference material certified by the International Association of Geo-analysts and has a significant amount of zirconium (471 mg/kg) (Potts *et al.* 2015a). In a recent inter-laboratory comparison (ILC-2015) different analytical procedures were evaluated for digestion including the recovery of zirconium. Zirconium mass fractions in MRH-1 were compared with results determined by independent analytical procedure i.e. WD-XRF, acid digestions, fusions, and sintering as shown in Figure 5.1. The diagram shows problems related to the accurate determination of Zr in the silicate-bearing reference material MRH-1. The results of acid digestion range from low to high recovery for Zr. The WD-XRF analytical procedure shows dispersed data for zirconium contents. However, fusion melts and sodium peroxide sintering data including our lab and some other labs show a complete recovery of zirconium. Thus sodium peroxide sintering appears to have the potential for the digestion of refractory minerals i.e. zircon. Total recovery of the Zr in reference materials (RM) is, thus, a measure of good REE results because zircon is one of the refractory minerals that contain significant amounts of REE, especially the heavy REE (i.e., Dy-Lu) and special care must be taken in sample preparation of these materials (Fan and Kerrich 1997b, Hall and Plant 1992, Longerich *et al.* 1990). Hence, to ensure accurate REE values, a universal digestion method, that is one that successfully dissolves all

mineralogical matrices, needs to be employed and this is the goal of this work. With the data on zircon-rich geological reference materials i.e. MRH-1,

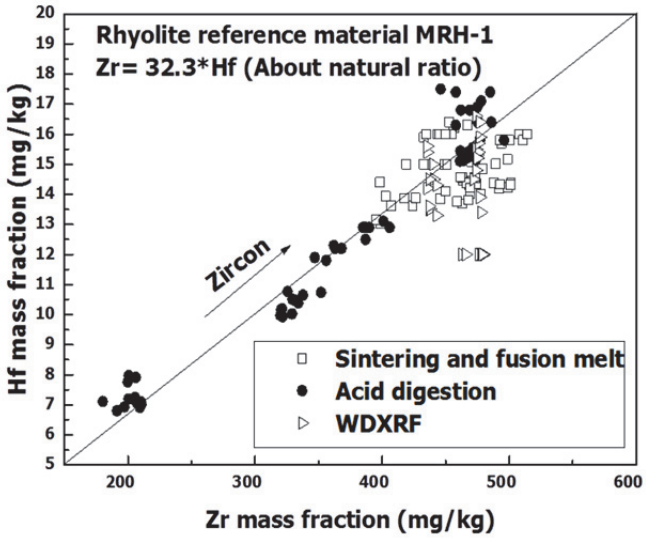

Figure 5.1: Problems of different digestion techniques in the recovery of zircon in rhyolite MRH-1 reference material.

high Zr contents can be reliably characterised. As before data on well-characterised zircon-poor geological reference materials, BCR-1, RGM-1, AGV-1, BHVO-1 etc. was used to demonstrate the validity of an analytical procedure for zircon-rich rocks e.g. (Gao *et al.* 1999).

The results of an inter-laboratory comparison shown in Figure 5.2 for Zr-Hf mass fractions demonstrate highest recovery with sintering and fusion techniques in comparison to the other methods i.e. acid digestion, WD-XRF and other methods. INAA is less frequently used in inter-laboratory comparison nowadays.

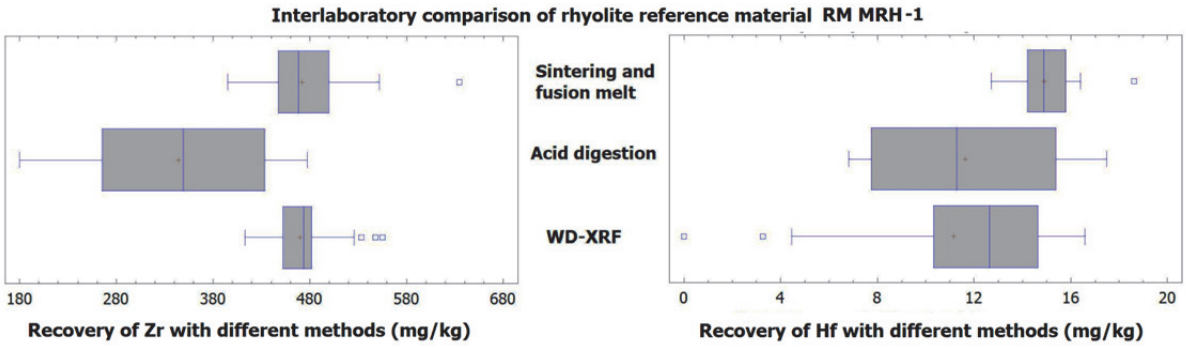

Figure 5.2: Recovery of Hf and Zr with current methods applied on rhyolite (MRH-1) reference material. Data is taken from ILC of different labs

Figure 5.2 shows that WD-XRF is not sufficiently precise at low concentrations and acid digestions end up with incomplete sample digestion and sintering remains a suitable choice of sample digestion.

The main aim of this chapter is to optimise sodium peroxide sintering and use it throughout the study for sample digestion of major, trace and platinum group elements and combine it with different techniques i.e. collision/reaction cell for interference removal on major and trace elements, rare earth elements and platinum group elements. The optimised method will be used in combination with different pre-concentration techniques i.e. tellurium co-precipitation, ion exchange chromatography, cloud point extraction technique and for sparging in ruthenium and osmium determination.

5.1.3 Advantages of sodium peroxide sintering

Some advantages of sintering over other techniques are described as follows,

1. It is highly effective in attacking minerals.
2. The resulting sinter residue is easily dissolved (Cotta and Enzweiler 2012).
3. It does not introduce elements that cause significant memory effects in ICP-MS (Meisel *et al.* 2002).
4. Sample decomposition can be achieved in only thirty minutes and the measurement can be performed instantaneously.
5. Sample with different matrices can appear in the same analytical batch.
6. Refractory minerals such as zircon, tourmaline, chromite, rutile, garnet, spinel and corundum, ilmenite, bauxite, beryl, titanite and cassiterotantalite can be completely dissolved (Chao and Sanzolone 1992).
7. It is effective for the decomposition of sulphides, arsenides (partly due to its oxidising properties), rare earth phosphates, W, Nb, Ta minerals, zirconium oxide and vanadates (Chao and Sanzolone 1992, Johnson and Maxwell 1981).
8. It is a destructive technique and the resultant solution can be analysed by one or several techniques (Chao and Sanzolone 1992).
9. The benefits of sodium peroxide sintering over fusion are that it decomposes zircon, does not attack the graphite crucibles and can be more effectively removed from the crucible (Lapakko 2002).
10. Sodium peroxide sintering is the only reliable method of solubilizing rare earth elements (Lichte *et al.* 1987).
11. Silicate remains in solutions and can be quantified.
12. The procedure is simple and inexpensive.
13. Highly reproducible results can be obtained.
14. The technique is easy to learn by inexperienced analysts.
15. Higher total dissolved solids compared to the acid digestion techniques and higher blanks do not affect the quality of the results (Meisel *et al.* 2002).
16. The sodium peroxide sinter method is the current practice for dissolving resistant mineral phases. As the granitic materials have higher analyte concentrations (especially the lanthanides), additional reagent contaminations from the flux are of less importance (Taylor *et al.* 2002).

5.1.4 Aims of the chapter

From the above review of the literature, it is shown that sodium peroxide sintering is a suitable method of sample digestion. Sodium peroxide sintering is better than fusion, because it decomposes zircon completely and does not attack the graphite crucible as much as fusion and the sample can be more easily removed from the crucible than a fusion melt (Lapakko 2002). Prior to its proper usage and application, sodium peroxide sintering was thoroughly studied and optimised as it needed further attention to make it more attractive and reliable for recovery and accurate determination of targeted analytes of interest. Following are the important steps that are addressed in this chapter: -

1. Determination of amount of sodium peroxide that can be used with a minimum amount of the sample for whole-rock chemistry evaluation as no study exists which shows systematically, the amount of sodium peroxide used for recovery of the analytes.
2. Determination of the amount of sodium peroxide that is needed for complete digestion and recovery of refractory minerals i.e. Zr.
3. Determination of the heating time for sinter for the complete recovery of refractory minerals i.e. Zr.
4. Determination of the effect of the amount of sodium peroxide that is needed for the complete digestion and recovery of all rare earth elements.
5. Determination of the effect of the amount of sodium peroxide on the digestion of chromite (Cr) and Nickel (Ni) in harzburgite i.e. MUH-1.
6. Evaluation of the presence analytes in the supernatant and residue phases of the sinter solution.
7. Addressing nuggets effects with sodium peroxide sintering and the need of the larger test portions for sample digestion.
8. Study of stability conditions under which sinter solutions precipitate.
9. Consideration of important factors prior to sample digestions i.e. sampling and impurities etc.
10. Design for the measurement protocol that uses, matrix-matched calibration, one or fewer measurements, the sequence of run during measurement and drift corrections.
11. The evaluation of the procedural blanks etc.

5.2 Experimental

5.2.1 Instrumentation and Reagents

Analytical reagent-grade sodium peroxide ACS, ISO Merck KGaA Darmstadt, Germany was used for sample digestion. Hydrochloric acid: 37 g/100 g p.a., Roth Karlsruhe, Germany was sub-boiled for experimental purposes. HNO_3: 65 g/100 g p.a., Roth Karlsruhe, Germany (sub-boiled) was used for dilutions. An ultra-clear unit for ultra-pure water (Siemens water technologies) with conductivity: 0.055 µS/cm, TOC content: < 1 ng/g, (for diluting acids and samples). Glassy carbon crucibles (Sigradur® 25 x 25 mm Hochtemperatur-Werkstoffe GmbH, Germany) were used for sample digestion. Glassy carbon is preferred over Ni or Zr crucibles as they consist of pure carbon with very low blanks. were used for the sample digestion. The samples were stored in centrifuge vials (50 ml, Sarstedt). Small magnetic bars (2 mm diameter and 7 mm length) for stirring the sinter solution were used in the glassy carbon crucibles. Agilent 7500cx ICP-MS was used for sample analysis.

5.2.2 Literature of variable amounts of sample: sodium peroxide

The solution chemistry involved in many dissolution procedures is poorly understood and refinements and the understanding of these techniques have not kept pace with the rapid development of modern analytical instrumentation (Potts 1987c). As XRF was used for REE, Sc and Y and the method modified by Robinson (1986) aimed to determine Y, Sc and REE and HFSE in different types of geological materials (Yu *et al.* 2001). These studies suggested that a sodium peroxide sinter method at 480 °C has the potential for the rapid determination of Y, Sc and REE in different types of geological materials.

Literature exists that utilises different amounts of sodium peroxide for recovery of analytes of interest. The aims of sodium peroxide sintering are to render the sample soluble in aqueous solution with a minimum salt content (Potts 1987c). The sample is thus, mixed with sodium peroxide (Na_2O_2) at a low ratio. It has been reported that the minimum ratio of

the sample to sodium peroxide (Na_2O_2) is 1:1. The mixture is heated at a temperature below the melting point of sodium peroxide (Na_2O_2) with an aim to heat the mixture until it can attack the rock matrix and makes the analytes soluble in an acidic medium. Jeffery (1975) recommended fusing 0.5 g sample with 1 g sodium peroxide (Na_2O_2) at 500 °C for 10 minutes. Van Loon (1980) described a similar procedure and reported that many minerals will decompose at 430 °C but 480 °C is required for 2 hours to decompose the most resistant minerals. The melt is normally extracted in cold water and any insoluble hydroxide is dissolved by adding 5 mol/l HCl, excess HCl being added to a final concentration of 0.3 to 0.4 mol/l HCl. A finely powdered sample of 100 mg and 600 mg fine-grained sodium peroxide Na_2O_2 were sintered at 480 ± 10 °C in a muffle furnace for 0.5 hours in glassy carbon crucibles (Meisel *et al.* 2002). For sintering, 100 mg of sample and 500 mg of pulverised Na_2O_2 were weighed in glassy carbon crucibles (Cotta and Enzweiler 2012). Robinson *et al.* (1999) reports as Na_2O_2 (0.4 g) was weighed into a clean platinum crucible, followed by 100 mg of finely ground sample and an additional 0.6 g of Na_2O_2 for magnetite, chromite and sulphides. According to Longerich *et al.* (1990) La, Ce, Pr, Nd, Sm, Eu, Gd, Tb, Dy, Ho, Er, Tm, Yb, Lu, Y, Nb, Zr, Ta and Hf were determined by sintering 0.2 g of milled rock with 0.8 g of sodium peroxide (Na_2O_2) for 1 hour at 480°C in a covered nickel crucible. For the determination of trace elemental contents using sodium peroxide sintering, highly purified reagents are required. Crock *et al.* (1999) cite disadvantages of these methods as elevated salt concentrations in the digestate, greater dilution requirements, and contributions of elements in the sintering and fusion reagents to the digestate. They are generally more appropriate for the determination of whole-rock components than trace elements. Following problems with the solutions of high salt contents are mentioned in (Potts 1987c)

1. Erratic performance of nebulisers,
2. Memory effects,
3. Clogging of the cones,
4. High background signals and scattered light effects in optical emission measurements.

During measurement, the signal intensities could drop suddenly because of clogging of cones and there are memory effects which can be observed when a blank solution with the same matrix is analysed. Therefore, the sintering method of sample digestion needed further attention to make it more attractive and reliable for recovery and accurate determination of targeted analytes of interest. The method needed to be optimised and validated before it could be used for regulatory purposes, certification and homogeneity testing. Following are the steps listed below for the method development of sample digestion.

5.2.3 Method development for sodium peroxide sintering

The protocol for method development was based on Meisel *et al.* (2002). The reference materials, MTA-1 trachyandesite, MRH-1 rhyolite and MUH-1 were selected for optimisation studies.

Sampling

All geochemical measurements are based on sampling (Ramsey 1997). Sample preparation is very important in the whole of the protocol as the results of analysis depend on careful steps being taken. The grain size of the sample during sampling is of major concern. The finest sample powder should represent the homogeneous sample. Glass bottles were used to store the RM because sample does not stick to its side walls. The sample should never be shaken but must be rolled so as not to lead to sample segregation

based upon particle size and density. The test portions of 100 mg were weighed with a highly accurate digital balance.

Wash protocol for apparatus

The purity of the reagents and cleanliness of glassware used is important in the sample preparation protocol. Special care was taken in cleaning and drying of the apparatus i.e. PTFE beakers, carbon crucibles, spatulas, volumetric flasks, small magnetic bars used in stirring the mixture of sample and Na_2O_2, and plastic tweezers. Teflon (PTFE) beakers and volumetric flasks were filled with 1% solution of HNO_3 and left overnight to minimise any impurities from the previous sample. The rest of the lab ware used in the sintering process was cleaned with a 1 % solution of HNO_3. Glassy carbon crucibles were cleaned by the addition of solid NaOH and heating at 380°C and the followed by a further rinsing with ultra-pure water. The plastic spatulas were carefully cleaned and wiped during sampling to remove any dust or previously taken samples. Sample preparation areas were not free from dust to avoid contaminations from the surroundings, as class 100 clean rooms were not used in this study.

Grinding of granular sodium peroxide

Commercially available Na_2O_2 was supplied in granular form that has a longer shelve life and for security reasons. For sintering, a very fine powdered form is required and therefore it was ground using a special agate mill or agate mortar and pestle. The material of the agate mill or agate mortar and pestle were Si so it should not add additional impurities to the concentration of the analytes. The agate mortar and pestle were cleaned with sand and concentrated HCl and rinsed several times with ultra-pure water. The complete digestion of a sample depends on a number of factors e.g. the fineness of the Na_2O_2 and proper mixing of sodium peroxide with the sample (a thin glass rod was used and then sidewise rotation (by hand) of the carbon crucibles, heating duration, the complete reaction with water etc.

Procedure for sample digestion

For early experiments, the sample size was kept constant at 0.1 g and sodium peroxide was variable in different digestions. The amounts of sodium peroxide used were 200 mg, 300 mg, 400 mg, 500 mg and 600 mg. Each sample to sodium peroxide combination i.e. 1:2, 1:3, 1:4, 1:5 and 1:6 was digested in 4 replicates on the same day. The sampling was done from the same bottle. Samples were dried at 110 °C and weighed directly into the dry glassy carbon crucibles. A thorough mixing of the sample and sodium peroxide was done using a glass rod or the mixing was performed by rotating the glassy carbon crucibles by hand. Sodium peroxide was commercially available in a granular bead form and was converted to a fine powder with an agate mortar. These samples were heated at 480 ± 10 °C in a muffle furnace for 30-45 minutes. Samples were cooled and the outer side walls were rinsed carefully with ultra-pure water to remove any contaminants from the oven. The crucibles were then transferred to clean Teflon/plastic beakers with the addition of small magnetic bars. The Teflon beakers were placed on hot magnetic plates and heated at 90 °C with a magnetic rotation of 250 rpm. The beakers were covered with watch glass lids. Ultra-pure water was added dropwise to the glassy carbon crucibles until the reaction was completed as evidenced from no more fizzing from the crucibles. The fizzing occurs because of the following reaction which produces oxygen.

$$2Na_2O_{2\,(s)} + 2H_2O_{\,(l)} \longrightarrow 4\,NaOH_{\,(aq)} + O_{2\,(g)}$$

The process of the chemical reaction was completed in 30 minutes. The contents of the crucible were then transferred to 50 ml PP vials. The un-dissolved precipitates of hydroxide were collected by centrifugation at the base of plastic vials. The supernatant was poured into the beakers while the precipitates of hydroxides were dissolved by addition of 3 ml of 3 mol/l HCl in the PP (polypropylene) vials. The addition of 2 ml of concentrated HCl into the carbon crucible dissolved the remaining sample if present, and the resulting solution was transferred into the beaker containing supernatant. Although chloride molecular interferences (MCl^+) in the MS spectrum are known to be problematic, HCl was preferred since, in some cases, magnetite (Fe_3O_4) remained un-dissolved after converting the hydroxides (Meisel *et al.* 2002), although it is well known that oxalic acid could have been used in place of the HCl. Warming the residue with concentrated HCl dissolved the magnetites. The rinsing solution was added to the volumetric flask. The dissolved residue and the acidified supernatant were combined and made up to the mark (100 ml) in volumetric flasks. To store the sinter solution, half of the contents of the volumetric flask were poured back into the rinsed PP vials (50 ml, Sarstedt) while discarding the rest. The clear solution was then analysed with Agilent 7500cx ICP-MS for the determination of the effect of sodium peroxide on analyte recovery. The measurement protocol using the ICP-MS is given in the next sections.

5.2.4 Measurement protocol

The measurement protocol was designed on the basis of Ellison and Williams (2013) for the identification of influencing quantities on the measurement. The measurement protocol involved the defining of matrices, measurand and analytes, instrumental tuning conditions, selection of matrix-matched certified reference materials for calibration, drift corrections after analysis, internal standards, sequencing of the sample and number of measurements etc.

Defining matrices, measurand and analytes

The matrices of the geological reference material were silicates. The measurands were the concentrations in mg/kg of the analytes, which reflects the distribution patterns of the analytes in the geological reference materials. Analytes were the major and trace elements in the geological reference materials.

Tuning conditions

Instrument tuning conditions are important for an accurate measurement. The best instrumental conditions i.e. tuning etc. were achieved to reduce the potential interferences with an acceptably low oxide formation rate as monitored by CeO^+/Ce^+. The typical operating conditions of the Agilent 7500 cx ICP-MS are shown in Table 5.1.

Table 5.1: Typical operating conditions of the ICP-MS

Model:	7500cx (Agilent)
RF power:	1500 W
Spray chamber temperature	2 °C
Oxide ratio CeO^+/Ce^+:	1.0-1.2 %
Doubly charged Ce^{2+}/Ce^+:	1.0-1.2 %
Carrier gas flow:	0.85 l/min (variable)

Makeup gas:	0.25 l/min (variable)
Interface cones:	Ni sample and skimmer cones

Selection of matrix-matched certified reference materials for the calibrations

External calibration is an often used paradigm for quantitative ICP-MS analysis (Potts 1987c). Kane (2005) cites that reference materials have a critical role in geo-analytical laboratories, as quality control materials for instrumental techniques and can be used for calibration in some situations. There are several factors that need to be considered in order to use a matrix-matched RM. These include sample size, inhomogeneity (a major problem), grain size, stability (not usually a problem with geological RMs), measurement uncertainty of certified values (usually not well-established), information about the certification process and availability in suitable quantities (Meisel and Moser 2004a). Two other essential factors are the concentration range and the matrix, which should match that of the sample so as to produce similar potential interferences (Meisel and Moser 2004a) and similar matrix effects. Most results of chemical analytical measurements are directly related to reference materials which are used for the calibration. In this study 11 procedural calibrants were chosen, most of which were certified by IAG protocol (Kane et al. 2001). These included procedural blanks, USGS RM BCR-2, IAG reference materials microgranite OU-3, pegmatite OU-9, nephelinite NKT-1, enriched stream sediment SdAR-1 which were characterised in Geo*PT* 6, Geo*PT* 23, Geo*PT*29 and Geo*PT*31 respectively, IAG certified reference materials Penrhyn slate OU-6, harzburgite MUH-1, shale SBC-1 (USGS-IAG also Geo*PT*28), rhyolite MRH-1 and basalt BRP-1 (Cotta and Enzweiler (2008) and also distributed as Geo*PT* 25 under the name HTB-1). The signal intensities of all analytic isotopes were measured in a blank as well as in calibrants with different, known analyte concentrations that covered the concentration range of interest. Indium, Re and Ge were added to each calibrant as internal standards. All uncertainty in the calibration process was incorporated to observable quantities through the addition of internal standards. The linear relationship between the blank-corrected standards on a diagram of signal intensity vs. concentrations was used to establish a calibration curve that was used to calculate the concentrations of the analytes in samples of unknown compositions. Sample solutions for the optimisation experiments and reference materials were prepared following the same protocol for digestion with a 1:6 sample/Na_2O_2 ratio.

Drift Corrections

Although the modern ICP-MS instruments generally provide relatively stable signals for extended periods, the instrument drift (i.e. temporal variations, most commonly a decrease, of signal intensity with time) does occur and has to be corrected for, in order to ensure high precision quantitative analysis. The drop in intensity of the instrument over a longer running time is due to changes in background noise, matrix effects and accumulation of deposits on cones. Two methods used for drift corrections are internal standardisation and external drift corrections (Linge and Jarvis 2009). The problem of the instrumental drift in conventional ICP-MS can only be solved by the use of internal standardisation using several elements that are spaced across the mass spectrum and by frequent recalibration (Dulski 2001, Longerich *et al.* 1990, Willbold and Jochum 2005). This drift correction using internal standardisation would ideally be done by the normalisation of all data to a non-analyte isotope present in the same or known concentrations in all the samples and the standards. Ideally, internal standards should be un-interfered species absent from the samples and calibration solutions.

An alternative to internal standardisation is an external drift correction. Here signal drift is monitored by analysing a specific drift monitor solution, normally a mid-range calibration solution, regularly throughout the run. Therefore, the drift behaviour of each

element is measured and corrected individually and no internal standards are added to the samples. The major assumption of external drift correction is that signal drift is linear with time, although non-linear correction has also been applied (Cheatham *et al.* 1993). Sharp changes in the signal, which may be caused by matrix changes, for example, will not be corrected. In most cases, however, instrumental drift can be approximated as a linear change if the drift monitor is measured frequently, normally every 5-10 samples (Linge and Jarvis 2009). In this study for more precise and accurate measurements, standard test samples of OU-6 and BCR-2 were measured after every 12 vials including the rinses samples. The measurement of standard test samples provided the basis for linear regression for drift correction of data.

One measurement or less to avoid larger variances

The digested samples were analysed at ambient temperature with an Agilent 7500cx ICP-MS. Repeated measurements on the same samples solutions expanded the total combined uncertainty and its impact was so large that it is not possible to identify whether the large variance in the results is due to inhomogeneity, incomplete digestion or the measurement itself. The results of the measurements needed to rely mainly on one measurement in order to demonstrate the effect of particular constraint under observation i.e. test portion size and amount of sodium peroxide in sintering optimisation experiments. It is suggested in designing experiments for validation and homogeneity that measurements should be independent and as under nearly identical conditions.

Sequence of a sample solution in measurement run

To achieve a measurement with the lowest uncertainties, it is better to measure only one type of rock (sample solutions) to minimise the memory effect of the analytes of another rock type e.g. higher concentration should be measured with the high concentration sample solution and vice versa. If two different rock sample solutions of low and high concentration have to be measured in the same run, then it is suggested that the sample solution with the lower concentrations be measured first.

5.3 Results and discussion

It was noted that no two measurements were identical and variances in relative standard deviations were due to different calibration/measurements. Thus, the results mainly rely on one measurement as it is less affected by day to day instrumental drifts etc.

5.3.1 Blanks, BECs and detection limits

The measurements were made in no gas and helium mode with the Agilent 7500 cx ICP-QMS. The integration time for rare earth elements was kept 2 seconds while for the other elements the integration time ranged from 0.1 to 0.5 s. A linear calibration curve (the slope of the calibration curve is the sensitivity or the signal per unit concentration) was obtained with matrix-matched calibration using certified reference materials as mentioned earlier in this section. A total of 4 replicates were measured for each analyte. Instrument drift was monitored with Ge, In and Re (internal standard). The blanks and detection limits are given in Table 5.2. (b) indicates a procedural blank. DL indicates the detection limits DL= (3 times the standard deviations of blank signal/slope of the calibration curve). BECs refer to background equivalent concentrations of the analytes BEC= (Blank concentrations/slope of the curve). R is Pearson Correlation coefficient of the linear regression obtained from the curve of matrix-matched calibrations with reference materials.

Detection limits are influenced by the background equivalent concentrations, contaminations, and interferences. The detection limits for Li, V, Cr and Nb were higher than those for other analytes. BECs were higher for Li, Ca, V, Cr, Ni, Ba, Nb, Zr and Pb and these are assumed to be from a combination of factors i.e. argide and chloride interferences and memory effects. Procedural blank was significantly higher for Mg, V, Cr, Ca, Fe, Sr and Pb. The blanks for rare earth elements were less than 10 pg/ml except for the most abundant La and Ce.

Table 5.2: Blanks, detection limits and BECs

Blanks, detection limits and BECs						
Tune Step	**m/z**	**Analyte**	**R**	**b (blank)**	**DL**	**BEC**
				pg/ml	pg/ml	pg/ml
No gas	7	Li	1.00	42	384	8695
No gas	24	Mg	1.00	425	1	5
No gas	27	Al	0.99	189	3	25
No gas	43	Ca	1.00	995	42	408
He	43	Ca	1.00	134	25	391
He	45	Sc	0.99	4	74	41
No gas	47	Ti	0.99	105	1	2
No gas	51	V	1.00	158	997	5969
He	51	V	1.00	194	187	1270
No gas	52	Cr	1.00	1046	252	3899
He	52	Cr	1.00	581	489	2821
He	53	Cr	1.00	88	1810	3337
No gas	55	Mn	0.99	113	0	1
He	56	Fe	0.98	993	0	11
He	57	Fe	0.98	238	2	10
No gas	59	Co	1.00	40	13	137
He	59	Co	1.00	19	19	65
No gas	60	Ni	1.00	262	207	2664
No gas	69	Ga	1.00	60	27	154
He	75	As	1.00	7	154	262
No gas	85	Rb	1.00	83	23	385
No gas	88	Sr	0.99	664	246	255
No gas	89	Y	1.00	19	13	43
No gas	90	Zr	1.00	135	231	610
No gas	93	Nb	0.99	254	418	772
No gas	111	Cd	1.00	2	13	20
No gas	133	Cs	1.00	3	2	8
No gas	137	Ba	0.99	491	107	5829
No gas	139	La	0.98	32	13	51
No gas	140	Ce	0.98	72	9	123
No gas	141	Pr	0.97	9	2	12
No gas	145	Nd	0.96	4	20	52
No gas	146	Nd	0.96	9	28	60
No gas	147	Sm	0.97	2	3	14
No gas	149	Sm	0.97	2	14	18
No gas	151	Eu	0.95	2	3	6
No gas	153	Eu	0.95	3	6	8
No gas	157	Gd	0.97	3	5	19
No gas	159	Tb	0.99	3	1	2
No gas	160	Gd	0.98	3	7	12
No gas	161	Dy	0.99	2	4	9
No gas	163	Dy	0.99	2	4	7
No gas	165	Ho	1.00	2	1	2
No gas	166	Er	1.00	2	1	5

No gas	167	Er	1.00	2	1	6
No gas	169	Tm	1.00	2	1	1
No gas	172	Yb	1.00	2	3	7
No gas	173	Yb	1.00	2	4	9
No gas	175	Lu	1.00	1	1	1
No gas	178	Hf	1.00	31	13	70
No gas	181	Ta	1.00	6	2	5
No gas	205	Tl	1.00	3	1	3
No gas	206	Pb	0.99	297	140	922
No gas	207	Pb	0.99	268	74	998
No gas	208	Pb	0.99	1209	141	959
No gas	232	Th	1.00	56	18	40
No gas	238	U	0.99	5	3	4

5.3.2 Estimation of the analyte concentrations in the sinter supernatant and the residue phases

For the estimation of the extent to which the analytes are present in both the supernatant and the residual phases of the sinter, a 500 mg test portion of the reference material, MUH-1 was digested with a ratio of 1: 6 sample to sodium peroxide. After the centrifugation, the un-dissolved hydroxide residual phase was separated from the supernatant phase. The residual phase was dissolved in 15 ml of 3 mol/l and 1 ml concentrated HCl which formed a nearly clear solution. 1 ml of the solution from both the phases were taken and diluted to 5 ml with 0.1 mol/l HNO_3 and were analysed with the ICP-MS. The contents determined in the two phases are given in Table 5.3.

Table 5.3: The distribution of analytes in the sinter supernatant and residue phases

Table of the distribution of the analytes in the sinter supernatant and residue phases					
Relative intensity of analyte ($A_{supernatant}/A_{residue}$)					
B	1.91	Zn	0.02	Nd	0.002
Cr	1.69	Be	0.02	Yb	0.002
V	1.58	Cu	0.01	Er	0.002
Rb	1.57	Ga	0.01	Dy	0.002
As	0.65	Sr	0.01	Gd	0.002
Mo	0.62	Sm	0.01	Ho	0.002
Bi	0.53	Nd	0.01	Er	0.002
Se	0.39	Sm	0.01	Ca	0.001
Li	0.12	Eu	0.004	Dy	0.001
Cd	0.12	Lu	0.004	Mn	0.001
U	0.10	Pr	0.003	Ce	0.001
Tl	0.088	Tb	0.003	Y	0.0001
Pb	0.078	Tm	0.003	Ni	0.0001
Ba	0.071	Yb	0.003	Fe	0.0
Th	0.034	La	0.003	Al	0.0

The table shows that B, Cr, V, Rb, As, Mo, Bi, Se, Li, Cd, U, Tl, Pb, Ba, Th, Zn, Be, Cu and Ga are present in significant amounts in the supernatant, while presence of the remaining elements were less than 1 % of their concentration in the residual phase. Al, Fe and Ni were present in the residual phase. This indicates that hydroxides especially Al, Fe and Ca were present in residual phase and were dissolved with 3 mol/l HCl as insignificant precipitates were observed. From this test, it was decided to combine the supernatant and residual phase unlike the method proposed in Cotta and Enzweiler (2012) in order to obtain a more complete recovery of all of the analytes from the rock sample.

5.3.3 The effect of decomposition time

For the determination of the effect of heating time of the sintering and the effect of test portion mass on the recovery and precision of the zirconium mass fractions in reference material MRH-1 which has a high zirconium content was digested with a 1:6 sample to Na_2O_2 ratio. Other reference materials MTA-1 and MUH-1 were also tested in the same way. The test portions were also varied from 100 to 500 mg. From the results in Figure 5.3 it is demonstrated that zirconium cannot be completely digested when using a heating time of 30-45 minutes for a 50 mg sample. The minimum decomposition time for decomposition of the refractory mineral, zircon, was found to be 120 minutes. This length of time was not required for the reference materials MTA-1 and MUH-1 where 30-45 minutes was sufficient for decomposition of zircons. Chao and Sanzolone (1992) also noted a similar effect that in that only the most resistant minerals required a longer time for decomposition. Figure 5.3 also shows the precision of the results with increasing test portion size as the precision of the results is a function of the precision of the instrument and the material's homogeneity. Therefore, it must be determined whether or not the inhomogeneity that was detected increased as a function of test portion mass in the manner predicted by the sampling theory Ingamells and Pitard (1986).

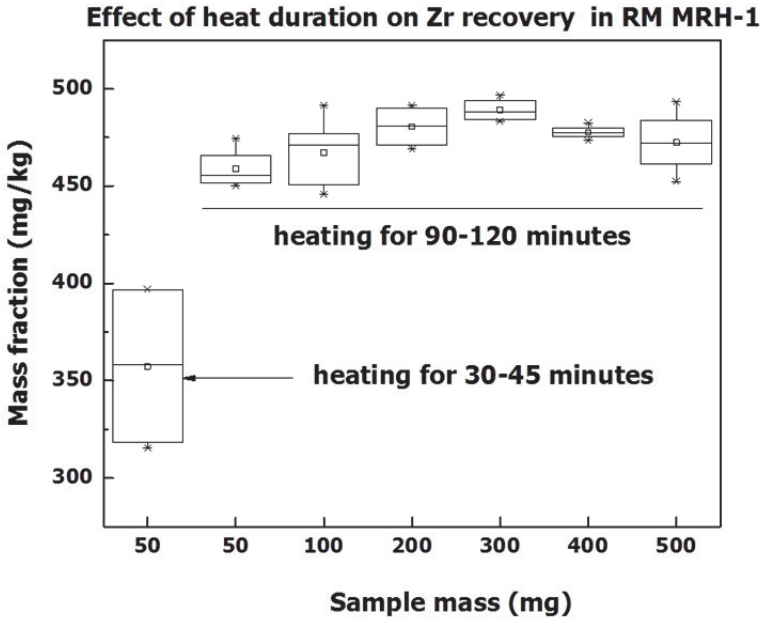

Figure 5.3: Effect of heating duration on recovery of zirconium in RM MRH-1

It is suggested that for similar rock types i.e. zircon-bearing rocks such as of MRH-1 and G-3, the sinter should be heated for 120 minutes to recover all the analytes and to

monitor the existing heterogeneities in a smaller test portion mass. For the RM, MTA-1, only 30-45 minutes heating was required to completely digest the sample.

5.3.4 Stability and precipitation of the sample solution

Solutions prepared after sample digestion were thought to undergo deterioration with time due to loss by precipitation effect of some analytes. Monitoring of the stability of the sinter solution was important because the measurements were performed several times with the ICP-MS. The stability of sinter solutions has not been discussed in the literature. Therefore, a general procedure was adapted to measure representative ICP-MS based sample solutions of a particular test portion at intervals of time in terms of days, weeks and months. The stability of the sample solutions, prepared with test portions of 50-500 mg was evaluated by measuring all of the analytes several times over approximately 300 days.

All the test portion sizes, 100-500 mg sample of the rhyolite RM (MRH-1), were measured after different days show a relative standard deviation of less than 5% and hence they were statistically stable as shown in Figure 5.4. All the analytical mean data obtained were in the range of the uncertainties of the certified values. No significant statistical variation or abnormal phenomena were observed. Therefore, the ICP-MS based samples solution with test portions 50-500 mg for RM MRH-1 was considered to be stable under the storage conditions used.

An exception was some of 500 mg sample solutions which demonstrated some loss by precipitation. The addition of one-two drops of concentrated hydrofluoric acid did not dissolve these precipitates. One of the sample solutions, when measured 157 days after its preparation, showed a 55% relative standard deviation demonstrating that it was not stable with time. RM MTA-1 solutions (100 mg) test portion when measured after one year were found to be stable, but after two years zirconium and hafnium, in particular, precipitated with less recovery in comparison to other analytes (Figure 5.5-Figure 5.8).

It can be generalised from this stability study that,

a. 100 mg test portions sample solutions were stable for a period of one year under room temperature and ambient pressure conditions. Sample solutions high in zirconium contents may precipitate after this period of time.
b. Sample solutions with more than 100 mg test portion size (1:6 sample to Na_2O_2 ratio) are more prone to the chemical changes i.e. precipitation, chemical reaction and complex formation etc.
c. Sample solutions with less zircon contents did not change with time and hence could be regarded as stable (e.g. MUH-1).

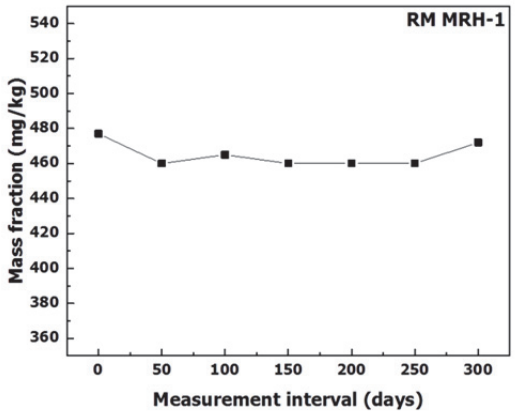

Figure 5.4: Stability of sintering solution determined on analyte Zr in RM MRH-1

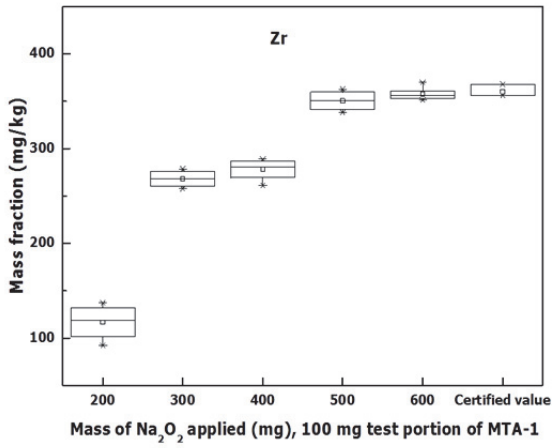

Figure 5.5: Zr measured after 7 days of preparation in RM MTA-1

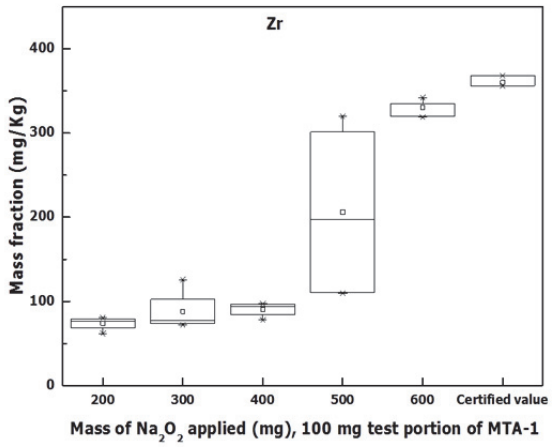

Figure 5.6: Zr measured after 2 years of preparation in RM MTA-1

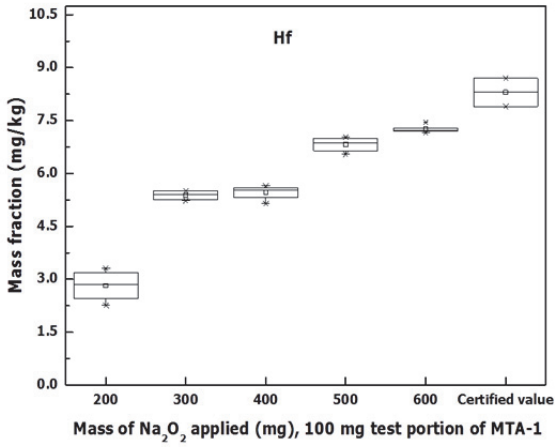

Figure 5.7: Hf measured after 7 days of preparation in MTA-1

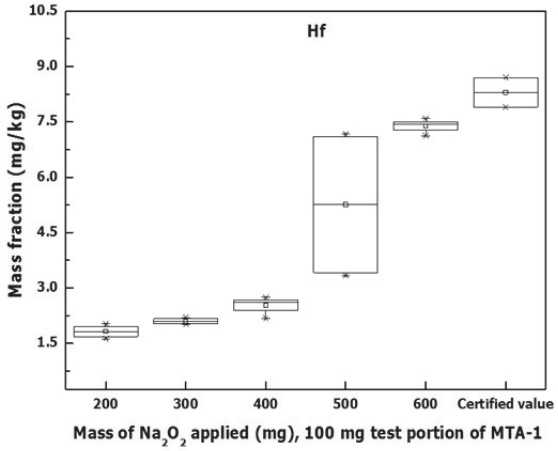

Figure 5.8: Hf measured after 2 years of preparation in MTA-1

5.3.5 Effect of the amount of sodium peroxide on recovery of 50 analytes

The measurements were designed in such a way so as to measure all the sample solutions in the same run and in the same batch, as the impact of two or more different measurements on the precision of results was larger than the impact of any other constraints i.e. effect of the amount of Na_2O_2, inhomogeneity etc. The recovery of the analytes showing only the effect of the amount of sodium peroxide cannot be predicted due to varying instrumental parameters i.e. tuning conditions and the intensity etc. For the determination of one particular constraint on the recovery of the analyte, the measurement has to be one or two or more measurements with identical results. Thus, in order to show the effect of sodium peroxide on the recovery of the analyte due to sample digestion problem, data from only one measurement was chosen.

The results showing the effect of the amount of sodium peroxide on the recovery of 50 analytes in RM MTA-1 are shown in Figure 5.9. The means were determined with relative standard deviations for each of four replicate digestions with 200 mg, 300 mg, 400 mg, 500 mg and 600 mg of sodium peroxide (Na_2O_2) for 100 mg test portion of RM MTA-1. The

means of the analytes were divided by the certified values to obtain unity values for comparison purposes.

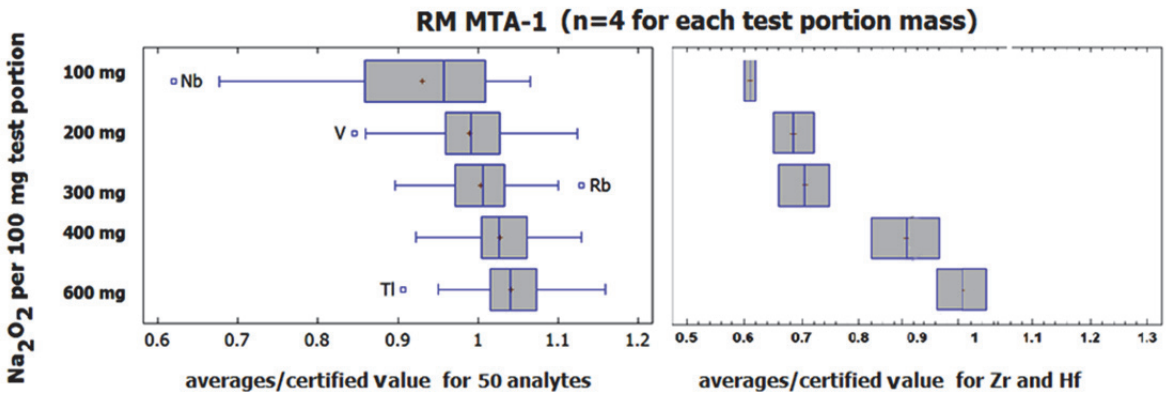

Figure 5.9: Analyte recovery vs amount of Na_2O_2 and Zr & Hf recovery vs amount of Na_2O_2

Figure 5.9 shows that the recovery of the analytes was increasing with increasing amount of sodium peroxide used in the sample digestion. The maximum recovery for 50 analytes was achieved with at least a ratio of 1:5 sample to sodium peroxide. Niobium was an outlier for 1:1 sample: Na_2O_2 ratio suggesting it cannot be digested with that sample to sodium peroxide ratio. Vanadium was an outlier for 1:2 sample: Na_2O_2 ratio, Rb for 1:3 sample: Na_2O_2 ratio and Tl for 1:6. In general, for all the analytes recovery increases with an increasing amount of Na_2O_2. The recovery of Zr and Hf is also shown in Figure 5.9 and which indicates that a 1:6 sample to sodium peroxide ratio is needed for the complete digestion and the recovery of these refractory analytes. The same results were shown in Figure 5.5 and Figure 5.7. Figure 5.10 shows the recovery of Nb with an increasing amount of sodium peroxide in RM MTA-1. A minimum of a 1:4 sample to sodium peroxide was required for the complete recovery of Nb.

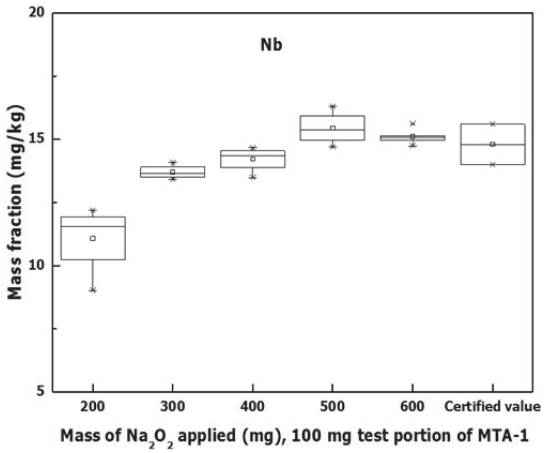

Figure 5.10: Effect of the amount of Na_2O_2 on Nb

5.3.6 The effect of the amount of sodium peroxide on the recovery of the HREE

The heavy rare earth elements (HREE) are Y, Eu, Gd, Tb, Dy, Ho, Er, Tm, Yb and Lu. Zircon is one of the refractory minerals that contain significant amounts of REE, especially

the heavy REE (i.e., Dy-Lu). A similar fact has been reported by Peter *et al.* (2012) in which Zr has been reported to host REE. Zircon ($ZrSiO_4$) is a common accessory mineral, occurring in a wide variety of sedimentary, igneous, and metamorphic rocks. Known to incorporate an assortment of minor and trace elements, zircon has the ability to retain substantial chemical and isotopic information, leading to its use in a wide range of geochemical investigations, including studies on the evolution of Earth's crust and mantle as well as age dating. The chemical and physical properties of zircon and its ability to incorporate and retain trace elements are largely determined by its crystal structure (Finch and Hanchar 2003).

In general, for HREE (Y, Eu, Gd, Tb, Dy, Ho, Er, Tm, Yb and Lu), optimisation tests indicated that the digestion recovery increased with an increase in the amount of sodium peroxide used. The plots of the recovery of heavy rare earth elements are shown all in Figure 5.11. At least a 1:5 sample to sodium peroxide ratio is required for the complete recovery of HREE.

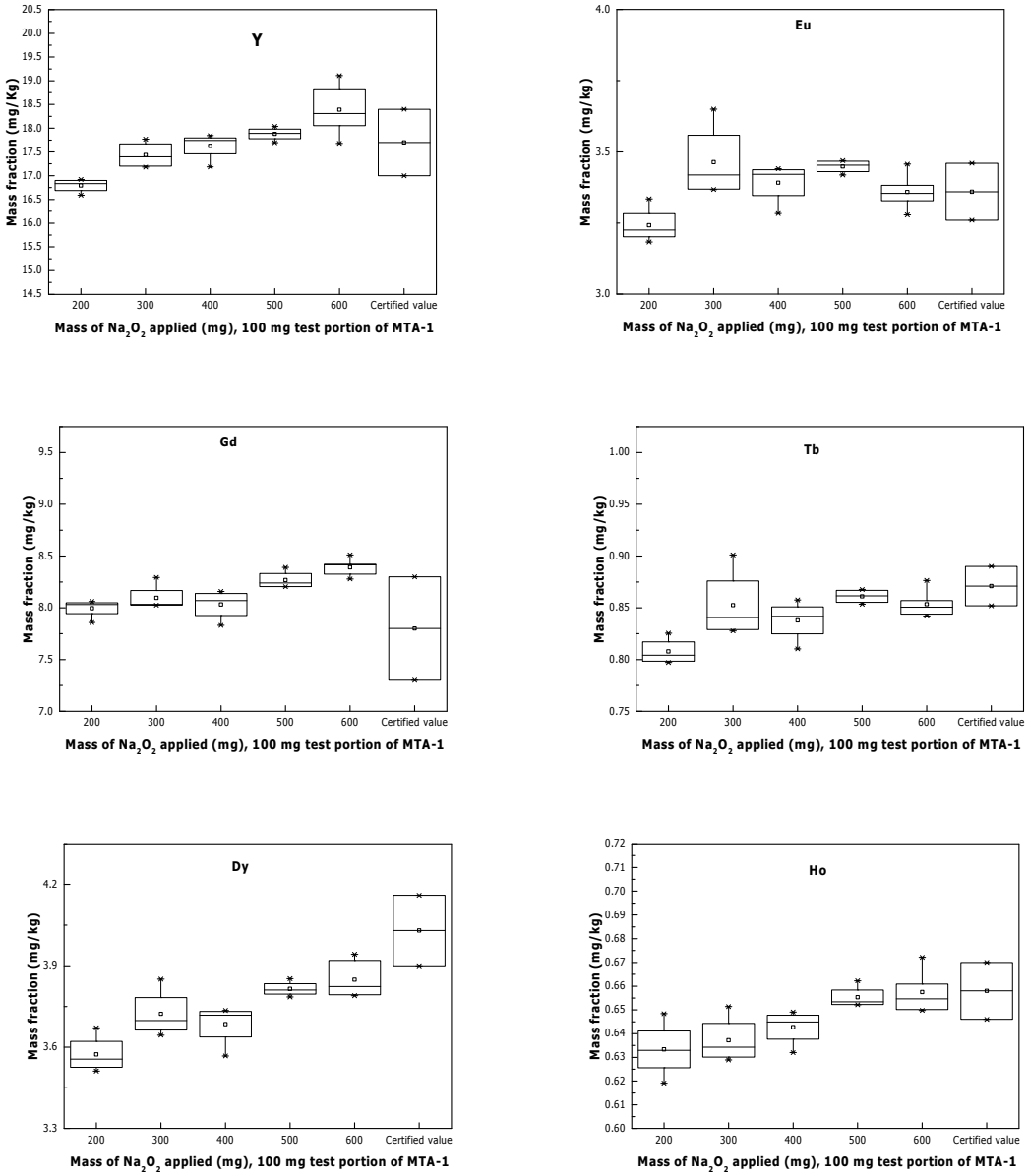

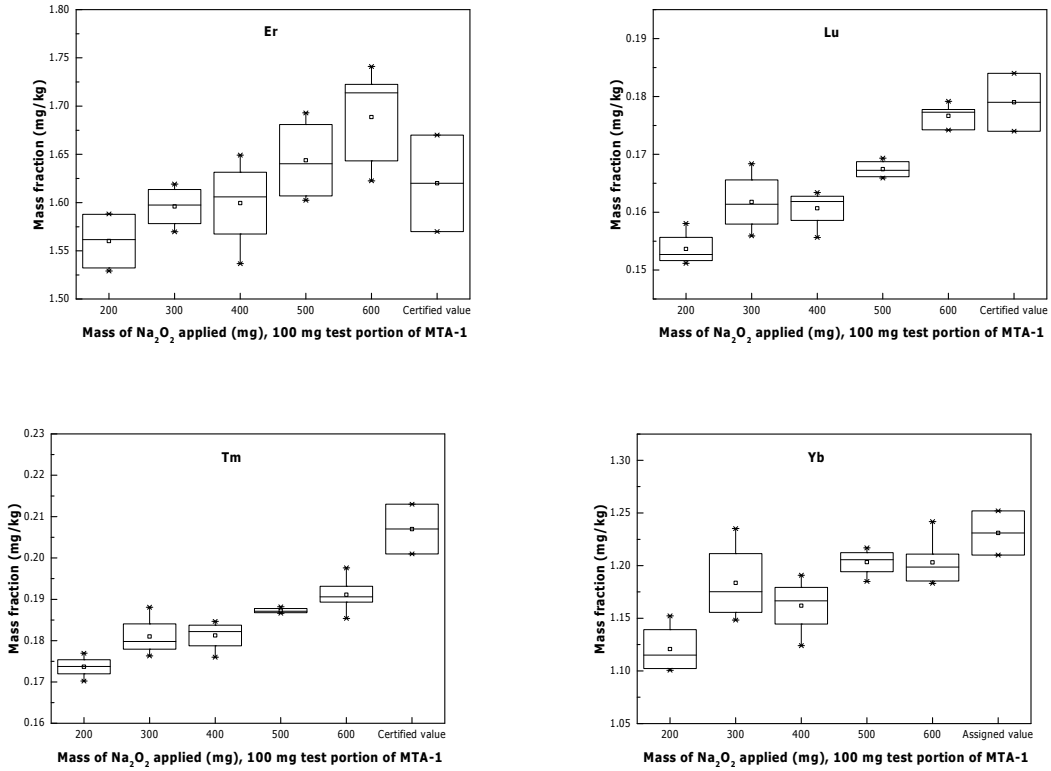

Figure 5.11: Effect of the amount of Na_2O_2 on HREE

5.3.7 The effect of the amount of sodium peroxide on the recovery of the LREE

The lighter REE are La, Ce, Pr, Nd etc. Contrary to simple generalisations about their behaviour, light rare-earth elements (LREE) do not act as incompatible elements in very felsic magmas. In fact, LREE concentrations typically decrease, often drastically, during differentiation of such magmas. The simplest explanation for this depletion involves the separation of minute, easily overlooked quantities of extremely LREE-rich accessory minerals, either monazite or allanite. The data from Miller and Mittlefehldt et al (1982) shows that felsic liquids with < 50 mg/kg LREE may be saturated in either of these accessory elements and that the concentration required for saturation decreases in more felsic liquids. This accounts for the incompatible behaviour of LREE even at high concentrations in mafic magmas in comparison to compatible their behaviour at low concentrations in felsic magmas (Miller and Mittlefehldt 1982).

The effect of sample: Na_2O_2 ratio on the recovery of LREE is shown in Figure 5.12. The amount of sodium peroxide seems to have the least effect on their recovery as 1:2 sample: Na_2O_2 produced the same results as a 1:6 ratio. Thus, they may not be contained in zircon minerals, but rather in monazite or allanite in this rock type and good recovery can be accomplished with a minimum sample to sodium peroxide ratio of 1:2.

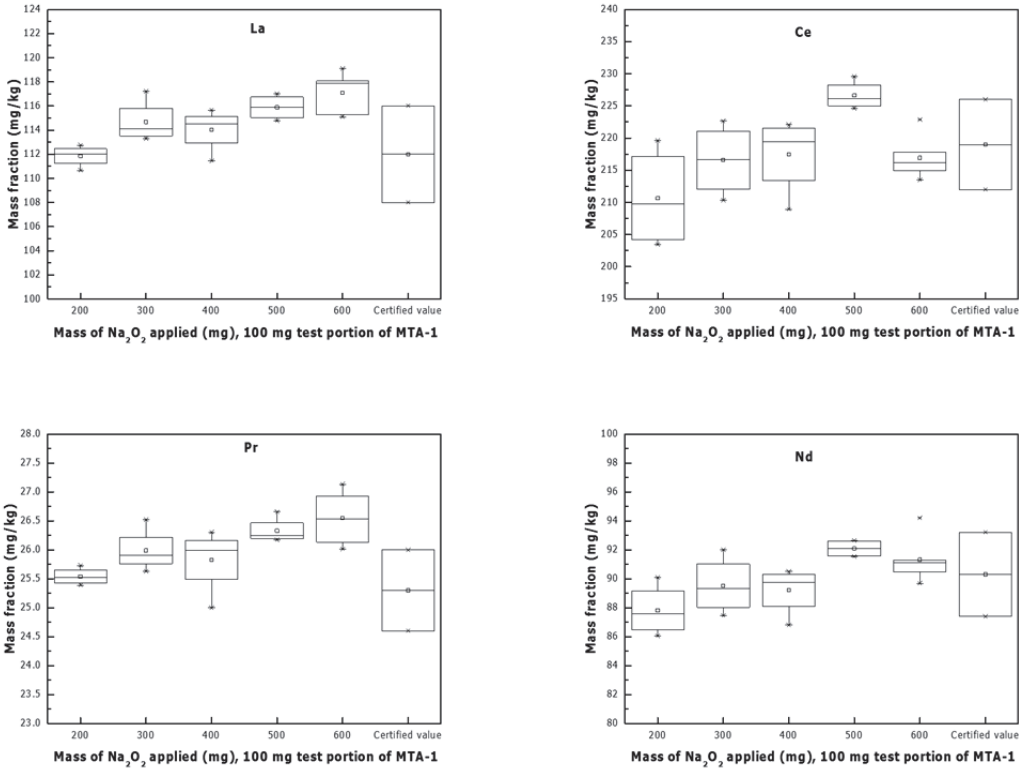

Figure 5.12: Effect of the amount of Na_2O_2 on LREE

5.3.8 Nugget effect (Bi, Nb, and Ta)

Bismuth is a native metal that can be found in its metallic form, either pure or as an alloy. Nuggets of bismuth metal have been found in one digestion which used a 1:4 sample to sodium peroxide ratio and is shown in Figure 5.13. This demonstrates that a 1:4 sample to sodium peroxide ratio is not sufficient to digest a Bi nugget. Also, the same sample of MTA-1 had nuggets of Nb and Ta in one of the digestions of a 400 mg test portion.

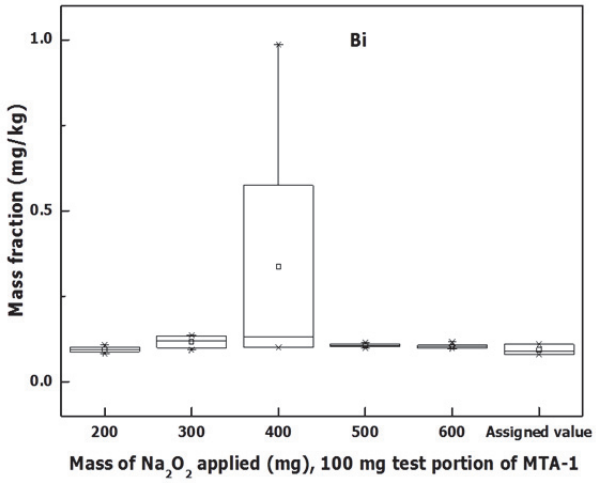

Figure 5.13: Nugget of Bi in RM MTA-1

5.3.9 SiO_2 measurement with ICP-MS

Potts (1987a) describes several methods for SiO_2 determination i.e. XRF, chemical (gravimetric, calorimetric, volumetric), AES, AA, etc. According to Madsen *et al.* (1995) methods for determining silica are gravimetric, chemical, microscopic, atomic absorption, XRD, IR, calorimetry and for the bulk material are thermal analysis and magnetic resonance. Madsen *et al.* (1995) cites that XRD and IR would dominate in the future and the analyst would develop new techniques such as gas chromatography, mass spectroscopy, and inductively coupled plasma mass spectrometry for the detection of silica measurements in bulk. Heinrichs and Herrmann (2011) describes gravimetric, volumetric and spectrophotometric methods of SiO_2 determination. In this study, different reference materials i.e. MGL-AND, G-3, MTA-1, MRH-1, MUH-1, OU-6 and SBC-1 were evaluated for SiO_2 measurement with a ICP-MS and data was compared with ILC, certified or XRF values. In this study 4 replicates were digested and measured. Table 5.4 shows averages of each of four replicates of RM with their RSDs. At least 300 mg Na_2O_2 was needed to totally recover SiO_2 in these reference materials.

Table 5.4: Measurement of SiO_2 with ICP-MS

Measurement results for SiO_2 in (g/100g) (n =4)				
Reference material	Determined	RSDs	*Certified or Ref	Rel *u*
MGL-AND	59.4	1.3%	*59.2	0.96%
G-3	68.1	1.8%	68.7	0.07%
MTA-1	60.3	1.8%	*58.7	0.34%
MRH-1	76.2	2.0%	*76.4	0.25%
MUH-1	40.9	0.7%	*40.4	0.42%
OU-6	57.1	0.3%	*57.3	0.52%
SBC-1	47.4	0.6%	47.6	0.17%

5.3.10 Effect of the amount Na_2O_2 on the digestion of chromite in MUH-1

That the term chromite refers to the mineral and was recommended by Thayer *et al.* (1956). He distinguishes the mineral chromite from ore and describes the ore as a chrome ore. Chromite is an oxide mineral composed of chromium, iron and oxygen ($FeCr_2O_4$). It is dark grey to black in colour with a metallic to the submetallic lustre and a high specific gravity. It occurs in the basic and the ultrabasic igneous rocks and in the metamorphic and sedimentary rocks that are produced when chromite-bearing rocks are altered by heat or weathering. Chromite is important because it is the only economic ore of chromium, an essential element for a wide variety of metal, chemical and manufactured products. Many other minerals contain chromium, but none of them have been found in deposits that can be economically mined to produce chromium.

Problems of incomplete digestion of chromite with mineral acids and HF have been long reported (Rodgers 1972). Dinnin (1959) described a rapid method of chromite digestion with a Na_2O_2 fusion in zirconium crucibles and its measurement with a volumetric titration using ferrous ammonium sulphate dichromate.

Harzburgite MUH-1 has a high mass fraction of Ni and Cr. Sodium peroxide sintering can effectively dissolve and recover both the analytes. It is shown in Figure 5.14 and Figure 5.15 that the recovery of chromium and Ni in the geological samples increases with increase

in the amount of sodium peroxide. This difference in recovery is 30-40% in the case of chromium where 1:6 ratio of sample to sodium peroxide is required for sample digestion. For recovery of Ni at least a 1:5 sample: Na_2O_2 ratio is needed as shown in Figure 5.14.

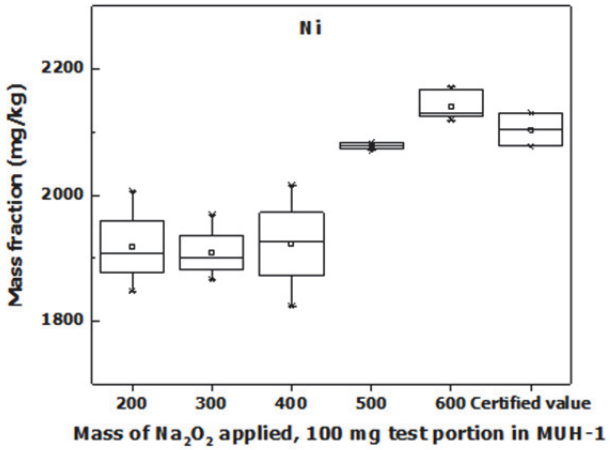

Figure 5.14: Effect of the amount of Na_2O_2 on recovery of Ni in MUH-1

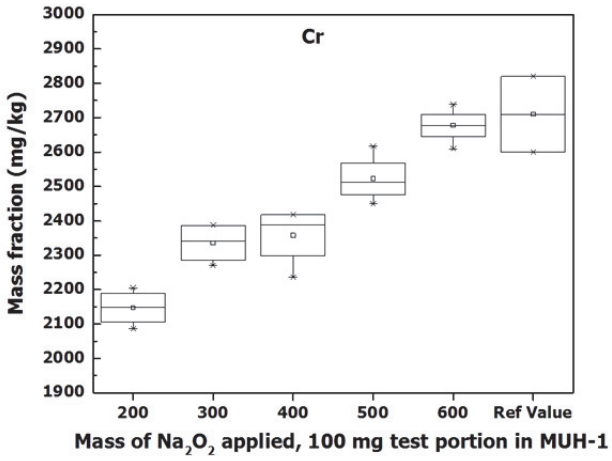

Figure 5.15: Effect of the amount of Na_2O_2 on recovery of Cr in MUH-1

5.3.11 Contribution of procedural blanks

Another serious issue in determining the elemental mass fractions in unknown samples is the contribution from the reagent blanks. Blanks have a small impact on the final uncertainty unless the concentrations are near the detection limit. The procedural blanks were processed following the same chemistry as that of sample preparation of RMs. The assumption is that the procedural blank represents a constant background signal that affects standards and samples identically. A procedural blank is the background signal check that is not due to the analyte in the material of interest. The blanks significantly greater than zero (according to chemical significance, not necessarily statistical significance), were rejected along with samples prepared in the same batch. Another way could have been to subtract their mean from the total analyte found in each sample to add the variance of the mean blanks in the total uncertainty. Therefore, in order to correct for the procedural blank, one must subtract the intensities of the procedural blank. This was done after all intensities were

drift corrected. An increased amount of sodium peroxide (Na_2O_2) was prone to blank contribution for some analytes for example Cd was observed in Figure 5.16.

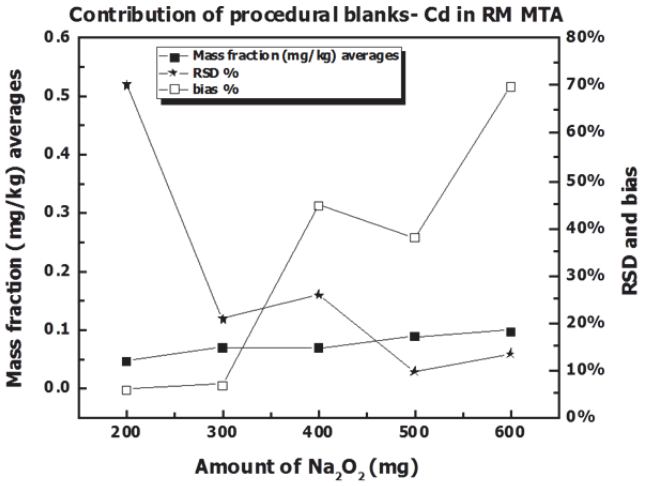

Figure 5.16: RSDs, bias and means of Cd in MTA-1 RM

5.3.12 Recovery of other elements based on recovery of Zr

The mineral zircon is the host for the significant fractions of the whole-rock abundance of U, Th, Hf and the heavy REE (Bea 1996, O'Hara 2001, Sawka and Chappell 1988). Complete dissolution of refractory minerals (such as garnet and zircon) is a prerequisite for accurate and the precise isotopic and elemental analysis of the terrestrial and meteoritic materials with solution-based ICP-MS (Pourmand *et al.* 2012). As they form highly charged cations, Zr, Hf, Th and U belong to the class of so-called incompatible elements, that is those elements that do not readily enter crystalline phases from the Earth's mantle, but instead concentrate in silicate liquids during partial melting and fractional crystallisation processes (Le Fèvre and Pin 2002). Zirconium (Zr) and hafnium (Hf) display only one oxidation state (4+) in natural samples, and have a very similar ionic radius. As a result, their chemical properties are almost identical, and they behave as "geochemical twins" in most circumstances. Indeed, Zr/Hf ratios significantly higher than the values typical for silicate rocks (35-40) are documented only in rocks interpreted to reflect interactions with carbonatitic melts (Le Fèvre and Pin 2002). Therefore, a larger test portion required for the determination the homogeneity of these elements. These elements are important geochemically as process indicators or parent isotopes for the age determinations of the rocks (Hoskin and Schaltegger 2003). Based on this assumption if zircon is not digested and recovered all the hosted analytes in the mineral zircon will follow the incomplete digestion and recoveries. This can be seen in Figure 5.17 that shows the mass fractions of Zr, Hf and Th plotted against the amount of Na_2O_2 used. The decrease in the concentrations of Th in one of the outliers (incomplete digestion) is due to the fact that Th is hosted by mineral zircon, therefore, a decreased recovery of Zr eventually lead to a decrease in the recovery of the analyte for which it acts as a host. This is regarded as the mineralogical effect of the mineral zircon on Hf and Th.

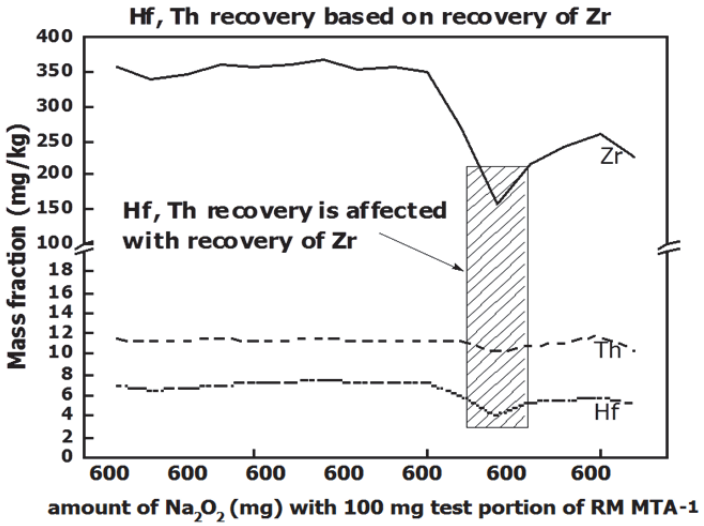

Figure 5.17: Recovery of analytes in an incomplete digestion

5.4 Summary

Sodium peroxide sintering combined with ICP-MS is a rapid and reliable analytical method that can be used for method validation, homogeneity testing and quality control purposes for reference material of diverse geological origin.

The supernatant and the residue are the essential components of the sinter solutions and the supernatant cannot be discarded when the whole-rock chemistry of the analyte is required. From the tests on the analyte contents of the supernatant, it is obvious that certain analytes i.e. B, Cr, V, Rb, As, Mo, Bi, Se, Li, Cd, U, Tl, Pb, Ba, Th and Zn etc. are also significantly present in the supernatant. Thus combining supernatant and residue allows the measurement of the whole-rock chemistry. This supports the work by Meisel *et al.* (2002).

The effect of amount of sodium peroxide on the completeness of the sample digestion and the recovery of analyte is demonstrated and it is emphasised that for the complete digestion of geological materials which are rich in zircons (e.g. granite or rhyolite) and for geological materials which are rich in chromite (peridotites) e.g. MUH-1, a 1:6 sample to Na_2O_2 ratio was required. A 1:5 sample to Na_2O_2 ratio is the minimum amount that can be used for sample digestion but a 1:6 sample to Na_2O_2 ratio is safer and ensures that samples are completely digested.

Sample decomposition time has profound effect on the completeness of digestion and the recovery of zircon-rich samples. It has been shown that refractory materials need a longer time for complete digestion i.e. 120 minutes, whereas samples not containing refractory phases can be digested in 30-45 minutes.

Through the study of the stability of sinter solutions, it was shown that sample solutions prepared by this method can be stored for several months but freshly prepared solutions are required for zircon-rich materials which tend to form the precipitates.

Sodium peroxide digestions can handle the problems of nuggets as well. Nuggets are often contained in the geological materials. Nugget effects for example of Bi, Ta, and Nb can be avoided if larger test portions of the sample are digested with a 1:6 sample to Na_2O_2 ratio. With the availability of large sized glassy carbon crucibles which can accommodate 5-10 g sample, nuggets problems can be easily accommodated.

Lighter rare earth elements are the least affected by low sodium peroxide to sample ratios. A ratio of sample to Na_2O_2 of 1:2 to 1:3 was shown to be sufficient for their digestion. However, heavy rare earth elements are seriously affected by the amount of sodium peroxide because they are primarily hosted in the mineral zircon. If the zirconium is not completely digested, the heavy rare earth elements will be not completely recovered as well.

If the supernatant which contain mainly the silicon is not removed, it is possible to determine precisely the Si contents of the geological materials. It is shown that SiO_2 mass fraction can be measured with acceptable precision with ICP-MS.

The highest recovery of all the critical 50 analytes has been achieved and conditions for application of the method have been improved and optimised as shown in the results for selected reference materials.

Table 5.5: Results for optimisation experiments using different amount of Na_2O_2 with 100 mg RM MTA-1 (mg/kg)

Sample ID	Mass of Na_2O_2(g)	Li	MgO	Al_2O_3	SiO_2	P_2O_5	K_2O	CaO	TiO_2	V	Cr	MnO	Fe_2O_3T	Co	Ni	Cu	Zn
1	0.2	23.6	1.67	15.2	43.8	0.950	4.39	3.76	1.14	70	27.2	0.040	4.56	11.4	21.4	25.0	118
2	0.2	22.9	1.67	14.9	52.2	0.940	4.28	3.66	1.08	69	27.1	0.040	4.42	11.1	22.3	20.1	105
3	0.2	22.9	1.69	15.0	53.5	0.940	4.40	3.73	1.12	71	27.3	0.040	4.49	11.5	21.5	21.5	85.9
4	0.2	22.8	1.67	14.8	51.7	0.930	4.36	3.68	1.08	69	27.7	0.044	4.41	11.2	23.0	20.8	104
5	0.3	23.5	1.72	15.8	56.9	0.940	4.62	3.84	1.26	87	29.1	0.044	5.28	12.4	24.3	20.3	90.2
6	0.3	23.1	1.73	16.0	57.2	0.960	4.65	3.85	1.26	87	31.2	0.042	5.27	12.5	26.5	20.6	104
7	0.3	22.7	1.76	16.0	57.8	0.970	4.72	3.94	1.24	87	30.3	0.045	5.07	12.5	24.4	24.7	111
8	0.3	24.1	1.81	16.5	58.9	1.000	4.91	4.00	1.29	89	33.0	0.046	5.37	12.9	29.1	21.8	120
9	0.4	23.5	1.78	16.5	59.2	0.980	4.89	4.03	1.34	102	38.9	0.041	5.92	13.8	33.3	21.2	146
10	0.4	22.4	1.7	15.6	55.6	0.940	4.59	3.79	1.24	86	29.6	0.046	5.16	12.4	24.7	20.5	110
11	0.4	23.7	1.79	16.4	58.9	0.990	4.85	4.14	1.34	100	37.2	0.045	5.88	13.7	29.0	21.6	108
12	0.4	23.3	1.78	16.5	59.5	1.010	4.93	4.07	1.34	100	32.3	0.047	5.85	13.7	27.9	22.4	88.6
13	0.5	25.0	1.76	16.2	59.3	1.000	4.80	4.00	1.35	101	31.4	0.046	5.89	13.7	26.2	22.2	132
14	0.5	23.8	1.77	16.4	60.1	0.990	4.85	3.99	1.36	102	31.1	0.046	5.89	13.5	26.8	22.5	98.7
15	0.5	24.3	1.78	16.8	60.9	0.990	5.01	4.02	1.34	104	33.4	0.048	5.98	13.8	28.5	22.4	122
16	0.5	23.4	1.78	16.2	60.0	1.030	4.94	4.09	1.40	104	32.4	0.050	5.94	13.9	28.8	22.0	86.7
17	0.6	24.0	1.87	17.4	63.1	1.080	5.33	4.41	1.43	110	34.1	0.048	6.19	14.3	32.7	26.9	107
18	0.6	22.6	1.78	16.3	59.0	1.010	4.88	4.00	1.36	103	31.6	0.052	5.88	13.6	27.6	22.7	93.5
19	0.6	25.3	1.77	16.2	58.9	1.000	4.80	4.04	1.36	102	31.6	0.049	5.88	13.5	26.2	23.5	95.6
20	0.6	23.4	1.76	16.4	59.2	1.000	4.92	4.01	1.36	102	31.4	0.048	5.85	13.5	29.5	22.4	86.9
21	0.6	23.4	1.82	16.9	59.3	1.050	5.17	4.20	1.39	107	32.9	0.050	6.01	13.8	31.8	24.8	110
Certified		22.7	1.74	16.0	58.64	1.002	4.85	3.85	1.395	102	35	0.0469	5.91	13.4	27.0	21.6	89

Sample ID	Mass of Na_2O_2(g)	Ga	As	Rb	Sr	Y	Zr	Nb	Cd	Sn	Sb	Cs	Ba	La	Ce	Pr	Nd	Sm
1	0.2	22.5	6.19	111	2429	16.6	62.0	6.31	0.012	0.88	5.16	11.6	2842	112	229	25.5	94.9	13.5
2	0.2	22.0	6.23	111	2409	16.9	74.8	9.93	0.023	1.18	7.81	11.8	2784	112	229	25.6	94.2	13.5
3	0.2	22.4	6.46	112	2450	16.9	78.5	10.7	0.031	1.21	8.01	11.9	2824	113	231	25.7	95.0	13.6
4	0.2	22.1	6.47	111	2426	16.8	80.6	10.4	0.025	1.08	7.81	11.7	2737	111	223	25.4	93.4	13.3
5	0.3	23.1	6.76	117	2539	17.2	72.0	13.0	0.067	1.31	8.62	12.0	2914	114	230	25.9	95.9	13.7
6	0.3	23.2	6.81	116	2543	17.2	75.7	12.5	0.066	1.23	8.36	11.8	2871	113	229	25.6	95.3	13.6
7	0.3	23.3	7.06	118	2603	17.6	126	13.2	0.081	1.58	8.79	12.0	2939	114	232	25.9	95.8	13.8
8	0.3	24.0	6.65	120	2618	17.8	79.1	13.1	0.082	1.22	8.88	12.4	2992	117	235	26.5	98.7	14.0
9	0.4	23.9	7.08	119	2579	17.8	91.2	13.8	0.065	1.37	9.07	12.0	2973	114	231	26.0	96.1	13.6
10	0.4	22.9	6.48	116	2545	17.2	78.0	12.4	0.056	1.18	8.36	11.8	2831	111	223	25.0	91.8	13.1
11	0.4	23.8	7.07	120	2618	17.8	97.3	14.1	0.076	1.46	9.18	12.2	2989	116	232	26.3	97.2	13.8
12	0.4	23.9	7.20	119	2607	17.7	96.1	13.9	0.082	1.33	9.19	12.1	2950	115	229	26.0	94.7	13.6
13	0.5	23.9	6.77	116	2530	17.7	283	14.5	0.093	1.43	8.95	12.2	2975	117	235	26.7	97.9	14.3
14	0.5	23.9	6.99	118	2571	17.9	110	14.6	0.090	1.65	9.15	12.0	2943	115	231	26.3	96.3	13.7
15	0.5	24.1	7.14	119	2555	17.9	112	14.0	0.087	1.44	9.31	12.1	2907	115	232	26.2	97.1	13.8
16	0.5	24.1	7.03	121	2644	18.0	320	16.0	0.091	1.58	9.31	12.1	2970	116	234	26.2	96.0	13.9
17	0.6	24.8	9.31	127	2743	19.1	342	15.8	0.111	1.09	9.55	12.6	3062	119	241	27.1	99.5	14.6
18	0.6	23.4	6.76	120	2648	18.3	335	15.3	0.102	0.95	9.06	11.9	2970	115	233	26.0	95.7	13.9
19	0.6	23.6	6.92	115	2531	17.7	319	14.6	0.103	0.94	8.82	12.2	3027	118	237	26.9	98.5	14.4
20	0.6	23.6	6.69	120	2616	18.1	320	15.0	0.101	0.98	8.95	12.1	2924	115	231	26.1	95.8	13.9
21	0.6	24.2	6.70	125	2719	18.8	334	15.5	0.097	1.06	9.49	12.5	2987	118	236	26.5	97.3	14.1
Certified		21.7	6.5	104	2692	17.7	368	14.8		1.8	8.5	11.7	2828	112	219	25.3	90.7	13.2

Sample ID	Mass of Na_2O_2(g)	Eu	Gd	Tb	Dy	Ho	Er	Tm	Yb	Lu	Hf	Ta	W	Tl	Pb	Bi	Th	U
1	0.2	3.65	8.04	0.800	4.00	0.569	1.59	0.197	1.199	0.151	1.62	0.576	0.100	0.390	34.7	0.071	11.4	1.60
2	0.2	3.53	8.06	0.809	4.11	0.574	1.59	0.180	1.189	0.153	1.74	0.656	0.079	0.393	33.1	0.062	11.2	1.56

3	0.2	3.55	8.03	0.826	4.09	0.589	1.53	0.198	1.201	0.158	1.90	0.671	0.106	0.395	33.7	0.068	11.4	1.58
4	0.2	3.54	7.86	0.797	4.06	0.563	1.54	0.200	1.214	0.152	2.02	0.642	0.097	0.364	33.2	0.060	10.6	1.51
5	0.3	3.67	8.02	0.830	4.11	0.591	1.57	0.191	1.203	0.160	2.03	0.714	0.356	0.405	34.3	0.126	11.1	1.54
6	0.3	3.61	8.04	0.828	4.12	0.587	1.59	0.197	1.212	0.156	2.14	0.729	0.254	0.409	34.1	0.065	10.8	1.56
7	0.3	3.68	8.03	0.851	4.21	0.594	1.61	0.201	1.206	0.163	2.02	0.698	0.260	0.419	34.2	0.110	11.6	1.54
8	0.3	3.75	8.29	0.901	4.23	0.617	1.62	0.210	1.248	0.168	2.20	0.784	0.291	0.432	34.6	0.065	11.1	1.57
9	0.4	3.69	8.02	0.844	4.14	0.600	1.61	0.202	1.247	0.163	2.61	0.715	0.711	0.410	33.7	0.057	10.9	1.58
10	0.4	3.56	7.83	0.810	4.02	0.580	1.54	0.186	1.187	0.156	2.18	0.688	0.255	0.402	32.7	0.061	10.5	1.46
11	0.4	3.70	8.12	0.839	4.03	0.602	1.65	0.211	1.243	0.162	2.75	0.718	0.658	0.415	34.3	0.682	11.0	1.59
12	0.4	3.67	8.16	0.858	4.22	0.609	1.60	0.210	1.204	0.162	2.61	0.723	0.579	0.407	34.0	0.096	10.9	1.58
13	0.5	3.69	8.39	0.857	4.39	0.654	1.69	0.200	1.297	0.166	7.04	0.775	0.794	0.419	34.3	0.064	12.0	1.84
14	0.5	3.67	8.27	0.866	4.21	0.662	1.67	0.213	1.275	0.166	3.33	0.757	0.951	0.420	34.1	0.246	11.5	1.79
15	0.5	3.70	8.20	0.853	4.27	0.652	1.60	0.206	1.246	0.168	3.49	0.749	0.776	0.417	34.1	0.069	11.2	1.81
16	0.5	3.69	8.20	0.868	4.29	0.652	1.61	0.208	1.236	0.169	7.17	0.774	0.775	0.415	33.4	0.070	11.8	1.72
17	0.6	3.84	8.51	0.854	4.34	0.672	1.74	0.206	1.264	0.177	7.50	0.775	0.868	0.415	34.1	0.084	11.4	1.76
18	0.6	3.71	8.28	0.857	4.19	0.650	1.62	0.203	1.222	0.179	7.44	0.739	0.775	0.410	32.3	0.063	11.1	1.64
19	0.6	3.81	8.42	0.876	4.33	0.661	1.71	0.207	1.301	0.174	7.59	0.800	0.802	0.428	34.7	0.057	11.6	1.69
20	0.6	3.69	8.33	0.844	4.32	0.655	1.64	0.205	1.260	0.177	7.12	0.769	0.794	0.400	32.7	0.050	11.1	1.62
21	0.6	3.74	8.42	0.847	4.38	0.650	1.72	0.209	1.259	0.178	7.27	0.758	0.775	0.398	33.5	0.089	11.4	1.80
Certified		3.36	7.8	0.871	4.03	0.658	1.62	0.207	1.231	0.179	8.3	0.74	0.93	0.45	34.1	0.10	11.4	1.72

*Sc values were higher in RM due to the doubly charged interference effects of higher Zr contents. The removal of Zr interferences on Sc are shown in detail in chapter 9.

6. Homogeneity tests of RM MRH-1, MTA-1 and G-3

6.1 Introduction

Reference materials (RMs) are required in chemical metrology to assure reliable analytical results. Reference Materials are well-characterised materials produced in quantity and can be certified for one or more physical or chemical properties. They play a pivotal role during the development of the new analytical techniques, methodologies and new sample preparation procedures; for assessing short and long term stability of instrumentation; for the detection of random and/or systematic errors during routine analysis; for cross-calibration of different analytical techniques and methodologies and in inter-laboratory calibrations (Ingamells and Pitard 1986). They are used to assure the accuracy and compatibility of the measurements in the interpretation of data. Certified reference materials are used as primary standards in many diverse fields of the science, industry, and technology. They are also used extensively in the fields of the environmental and clinical analysis. In many applications, the traceability of quality control and the measurement procedures to the national measurement system are carried out through the use of RMs. Homogeneity testing is of the highest importance for the certification of the reference materials, as it should demonstrate the validity of the certified values and their uncertainties in the analysis of individual units or portions thereof (Pauwels *et al.* 1998). A reference material is said to be homogeneous with respect to a specified property if the property value, as determined by tests on samples of specified size is found to lie within the specified uncertainty limits. According to Kane (2001) it is a critical goal of certifications to achieve reference values with confidence limits that do not exceed one-third of the uncertainty of routine laboratory measurements, taking particular account of the high specification for precision and trueness in some geo-analytical applications. Almost all geological samples are inhomogeneous if a small enough test portion is taken for analysis. Arguably, inhomogeneity can be avoided if non-mineralised samples (such as glasses) or un-zoned crystals (such as synthetic silicates) are chosen for certification. Whereas, in metamorphic rocks many minerals can withstand acid attack, among others kyanite, fluorite and tourmaline (the last two being also present in many granites), as well as zircon present in basic, intermediate and acidic igneous rocks, and equivalent metamorphic types, and in addition baddeleyite and chromite in basic rocks (Navarro *et al.* 2008). Zircon, the most important Zr-phase in most of these rocks, is also a carrier of other trace elements, including the REE, U, Th and Hf. These minerals contain a large number of coordination sites which host a variety of REE elements and if undigested pose inhomogeneity problems to an analyst. Meisel *et al.* (2001b) states that the sample inhomogeneity is an important reason for irreproducible results and this factor can dominate the uncertainty. To study homogeneity a series of experiments must be performed which involves a variation of the amount of processed sample by a factor of 10 or more. To an analyst a result that apparently reflects heterogeneity may not be true, instead, heterogeneity is one of the influence quantities of the uncertainty budget and its contribution can only be assessed when all the other influence quantities are small. Previous homogeneity tests have been demonstrated to yield "false" heterogeneities in samples which are truly homogeneous, as they fail to recognise the uncertainties which might be statistically significant, but negligible for inter-comparison and calibration tests, where more significant sources of uncertainty, not necessary related to the sample itself, are considered (Thompson and Wood 1993).

The experimental determination of element specific homogeneity factors is tedious and time-consuming. In many cases, it is assumed from an exemplary survey analysis of one or two elements (with sometimes inadequate methods and/or irrelevant sample mass) that all the certified elements behave in the same way. In order to be on the safe side, RM

producers generally quote the homogeneity of their materials to be satisfactory only at high to very large (100–500 mg) sample masses (Rossbach *et al.* 1998). In using RMs correctly, it is important to understand that homogeneity is a property of specific analytes in an RM, measured under specific conditions, and can be extrapolated only to results obtained under less stringent conditions, not to more stringent ones. For example, if a sample is homogeneous for a given constituent measured with 5% repeatability on a sample test portion of 500 mg it will also be homogeneous for test portions less than 500 mg measured with poorer repeatability (S. Kane 2001). Ingamells and Pitard (1986) provided an extensive discussion of inhomogeneity as applied to the geological samples. At some level in every sample, inhomogeneity exists. With the exception of liquid reference materials, all reference materials will display a degree of heterogeneity. This is especially true for geological reference materials, where multi-mineralic powders are heterogeneous at a sufficiently small scale. Glasses are least inhomogeneous, and coarse-grained poly-mineralic rocks are most inhomogeneous, but none can be considered entirely homogeneous as one progressively reduces the sample size, until in the extreme, the atomic scale is reached. This can present problems for the analyst, who needs to be able to achieve repeatability of measurement between different aliquots of the same sample. These examples suggest that inhomogeneity in geological samples caused by mineralogy is more likely to occur within the units rather than between the units. If micro analytical sample sizes are taken, unacceptably large uncertainties due to sampling error are expected and have been experimentally demonstrated for these elements (Kane 1997a, Kane and Xu 1993). The key consideration is that conclusions regarding homogeneity testing apply only to the test portion mass at which the testing was done or to larger test portion masses. The certified value itself should not change as a function of the test portion mass, but the contribution of inhomogeneity to the uncertainty of that value is quite likely to increase with decreasing test portion mass (Kane *et al.* 2003). The goal of any RM certification is to inform the user the "right" answer (i.e., the true concentration) and how well it is known. In the absence of systematic errors, material heterogeneity, or sources of uncertainty determined by non-statistical means, this information is summarised by a confidence interval for each certified value. If the material is heterogeneous, there is no single "right" answer, but rather there is a statistical population of "right" answers (i.e., true concentrations) corresponding to each unit (or sample) of the RM. In this case, a statistical prediction interval or a tolerance interval is an appropriate summary of the population of "right" answers in the batch of material. Systematic error and uncertainties based on experience rather than data, introduce additional wrinkles into assessing the final uncertainty. A reference material property value with lower uncertainty is important in chemical characterisation. The data with lower uncertainty for an RM can be achieved by testing homogeneity in larger test portions. The larger the test portion taken for analysis, the more likely that a sample will appear homogeneous; conversely, the smaller the test portion mass, the more easily inhomogeneity will be detected. The idea of using larger test portions in testing homogeneity needs the correct use of the method and or method development, identification and eradication of sources of uncertainties such as nuggets, interferences, stability, and calibration, contamination that influence the homogeneity and make the effect of test portion size ambiguous.

A reference material is said to be homogeneous with respect to a specified property if the property value, as determined by tests on samples of specified size is found to lie within the specified uncertainty limits. From the ISO definition,

1. Homogeneity is a fundamental property of the materials; it assures uniformity in structure or composition.
2. Homogeneity is not an overall or general quality factor but is related to one or more specified properties of the material.
3. Homogeneity assessment is done with statistical tests giving uncertainty limits.

4. Homogeneity is always related to a specified sample mass size.
5. Homogeneity does not depend on the source (supply unit) of the sample analysed.

The ability to detect inhomogeneity is dependent on many factors. Kane *et al.* (2003) describe these factors as

a) The mineralogy of the bulk sample.
b) Grain size distribution and shape characteristics of individual minerals.
c) Mass of test portion taken for analysis.
d) Repeatability of the measurement technique used for the homogeneity test.
e) The number of degrees of freedom for both "within" and "between" sample variances (Kane *et al.* 2003).

6.1.1 Aims of this chapter

Chapter 5 describes the optimisation of a sample digestion method i.e. sodium peroxide sintering. For the purpose of homogeneity testing in test portions, here the testing was applied to the reference materials; trachyandesite MTA, rhyolite MRH and USGS granite G-3. The method aimed to determine precise and accurate analyte mass fractions in the given test portions of the samples. If the precision and accuracy ere not obtained, the tests are extended by taking larger test portions of the materials. The purpose of this chapter is to present the results of a homogeneity tests on the Mongolian reference material; trachyandesite: MTA-1, rhyolite MRH-1 and USGS uncertified reference material granite G-3. The following are the main aims of the chapter;

1. Method development and application based on the optimisation experiments performed in chapter 5.
2. Selection of samples from between the bottles and within the bottles.
3. Selection of test portions for the sample digestion.
4. Design for the measurement protocol i.e. matrix-matched calibrations etc.
5. Problems related to the determination of Sc and Eu in RM MRH-1, MTA-1 and G-3.
6. Problems related to the addition of HF and accompanying decreased recovery of Nb, Ta and Zr due to hydrolysis.
7. Testing reproducibility of the results.
8. Effect of the test portion on the precision of the results.
9. Confining the measurement uncertainty on the test portion by reducing the effect of the influencing quantities.

6.2 Experimental

6.2.1 Materials and reagents

The material and reagents used in this section were the same as described in chapter 5. The Agilent 7500 cx ICP-MS was used for the measurement and it was tuned for maximum intensities. The typical instrumental operating conditions are the same as in chapter 5.

6.2.2 Selection (sampling) of from between and within bottles

According to Van der Veen *et al.* (2001), a homogeneity test involves an evaluation of both between and within-bottle homogeneity. The determination of analyte concentrations within the bottle is based on a minimum sample intake from one single bottle and the between-bottle homogeneity deals with the bottle-to-bottle variations of the analyte concentrations. But in the determination of the analyte concentrations for homogeneity testing in both within and between-bottle units, the effect of measurement variability must be quantified. If the effect of the variability of two or more measurements is larger, than, the effect of homogeneity due to a well-established and optimised sample digestion method cannot be quantified. Thus for within-bottle homogeneity study, a small portion of each bottle when digested can differentiate heterogeneity between bottles. The heterogeneity is usually caused by mineralised particles and it is the fate of the bottle how many particles a bottle receives. These examples suggest strongly that inhomogeneity in geological samples caused by mineralogy is more likely to occur within units rather than between units Kane *et al.* (2003).

The reference materials MTA-1 and MRH-1 were supplied in three packets each while G-3 was available in bottles. Through the participation in inter-laboratory comparison which was based on selection of test portions from each packet (i.e. four digestions for one packet and total of 12 digestions), and through participation of several labs each providing results from similar arrangements, it was established that the between-bottle variances for candidate RM MTA-1 and MRH-1 were negligible as observed in ILC. Thus, further tests were performed by selection of test portions from single specified packets.

6.2.3 Sample preparation and the estimation of the test portions

Cotta *et al.* (2007) reports that when prepared for bulk analysis, geochemical RMs are rarely studied to determine the minimum mass required for analysis and most RM producers recommend a sample mass between 100 mg to 500 mg, except for gold, platinum-group elements and other specific analytes. RM producers recommend a minimum mass for proper investigations of homogeneity (Kempenaers *et al.* 2000). Meisel *et al.*, (2004) emphasises Ingamells sampling theory that states that sampling a test portion from the container of the sample powder is indeed part of the method and hence should be validated to estimate the degree of heterogeneity. This task may involve many repeated measurements with different test portion sizes (Ingamells and Switzer 1973, Meisel and Moser 2004a). Heterogeneity is always a concern for geological samples because of their multi-mineralic nature (Ingamells and Pitard 1986, Kane 1997a, Kane and Potts 2007) and past certification was performed at a certain mass. Materials may be inhomogeneous within units of an issue as well as between units, especially if the rock consists of a minor crystalline phase that contains high concentrations of an analyte (Ingamells and Pitard 1986). According to Kane (1997a) in the real world of geoanalysis, many samples that are analysed will exhibit some degree of inhomogeneity. If a small test portion size is chosen for analysis, then all the geological samples are inhomogeneous. Arguably, inhomogeneity can be avoided if non-mineralised samples (such as glasses) or un-zoned crystals (such as synthetic silicates) are chosen for certification (Kane *et al.* 2007). In the Geo*PT*™ programme, the procedure of Thompson and Wood (1993) considers materials to be sufficiently homogeneous for the use when the inhomogeneity contributes less than 40% of the target uncertainty (Kane *et al.* 2003). In the ideal situation, homogeneity will be assessed for every element that is to be certified. This is not always practical; however, it may be possible to group elements according to their similarities in geochemical behaviour, and to perform the homogeneity test for just a few elements that are representative of each larger group (Kane *et al.* 2003). Because the determination of trace concentration e.g. PGE, is tedious, experimental designs with

different conditions (e.g. sample mass) and even simple replicate measurement with constant sample mass are often avoided (Meisel *et al.* 2001b). Both element and analytical test portion masses contribute to the homogeneity (Kane 2002). In bulk analysis, a large number of these building blocks are involved and potential heterogeneities are reduced through the averaging effect (Mattiuzz and Markowicz 2000).

In the view point of Ingamells and Pitard (1986), Kane (2002) and Meisel *et al.* (2001) and references therein in this study, ranges of test portions of the candidate RM rhyolite (MRH-1) and trachyandesite (MTA-1) and uncertified USGS granite (G-3) were chosen. Therefore, different test portions 50-500 mg were selected for within-bottle homogeneity study. The selected test portions were digested following the optimised protocol and validated method of sodium peroxide sintering described in chapter 5 (at least four replicates of each reference material were digested). The ratio of quantities of sample: Na_2O_2 were kept at 1:6 for complete digestion of important minerals i.e. Zircon. Supernatant and residue were combined for whole-rock chemistry. Two drops of HF were added to avoid precipitation in the larger test portions. Necessary dilutions were made where sample handling was difficult for the larger test portions.

6.2.4 Measurement protocol

The measurements were performed with the Agilent 7500 cx ICP-MS in no gas and helium mode. The Ge, In, and Re internal standards were added to solutions. The integration times for rare earth elements were 2 seconds, while for other elements the time ranged from 0.1 seconds to 0.3 seconds. Matrix-matched calibrations were achieved through the use of certified reference materials mentioned in chapter 5. Drift corrections were made using linear regressions.

6.3 Control on reduction of the influencing quantities on homogeneity

According to Meisel *et al.* (2001b), uncertainty caused by the poor reproducibility of the measurement result can make a significant contribution to the heterogeneity of a rock powder. It is very difficult to determine whether the lack of accuracy is caused by inadequate methods, proximity to the determination limit, sample preparation, or sample inhomogeneity. Some of the most important influencing quantities which can affect the results of homogeneity of RM are discussed in next paragraphs.

Sampling

As the samples were taken from the same units, between bottles heterogeneity can be ignored. A clean and dry apparatus was used for sampling i.e. a spatula etc. The spatula was wiped thoroughly before taking another sample of the material. As the samples were weighed directly into glassy carbon crucibles, cricibles were also washed and dried with a defined washing protocol after usage. Glassy carbon crucibles were rinsed with concentrated HCl. A few beads of NaOH were added and heated at 380 °C. When the NaOH was melted, the crucibles were kept in deionized water over night. The crucibles were washed carefully and dried in a clean drying place. For evaluation of between crucible blanks, an estimate of the blanks was made on several occasions and negligible contributions were found. Sample preparation areas were cleaned to minimise contamination. Sub-boiled HCl and HNO_3 were used in sample preparation. Analytical grade granular sodium peroxide was ground using an agate mortar and pestle. The agate mortar and pestle was cleaned several times with sand after each use. The contribution of the blanks from the agate mortar and pestle was negligible.

Influencing quantities affecting sample preparation factors

In order to determine the effect of the test portion size on the homogeneity, several other factors were maintained constant. The sample to sodium peroxide ratio has a profound effect on complete sample digestion. A ratio of 1:6 was used for sample digestion with proper mixing of the sample and sodium peroxide, thus this factor does not contribute to sample heterogeneity. Another factor involved was the precipitation effect of larger test portion size. The sample solutions which were precipitated were not used in the estimation of the homogeneity.

Influencing quantities affecting the ICP-MS preparations

The preparation of ICP-MS involves preparation of diluted solutions for the measurement, cleaning of the interface and skimmer cones, the maximum signal intensity with lowest RSDs, the addition of internal standard to the diluted solution, drift corrections after the measurement, matrix effects, integration times and the tune modes etc.

The preparation of the diluted solutions involved the use of micropipettes. Micropipettes were calibrated prior to use; thus negligible effects were observed in pipetting of the solutions. The interface and skimmer cones were cleaned each day. Low oxide profile was obtained when with maximum signal was obtained. Drift corrections were made with a linear regression. Helium gas was used to minimise interferences. However, interferences on Eu from BaO and Sc from Zr were minimised using collision/reaction cell technology of the Agilent 8800 ICP-MS/MS which will be discussed in chapter 7.

Influencing quantities affecting final results

The data obtained after the measurement was influenced by the calibration, internal standard, sensitivity, matrix effects, nugget effects, precision, repeatability, test portion size and heterogeneity of the zirconium. Biases from the certified values were affected by blanks contributions, nuggets, Zr heterogeneity, test portion size and interferences. A great care was taken in establishing the final property values of RM demonstrating the effect of only the test portion size on recovery and homogeneity of the analyte. However, because of the time restriction a quantitative evaluation of each factor was not performed. Future studies on homogeneity should demonstrate the quantitative effect of each constraint.

6.4 Results and discussion

6.4.1 Nuggets of Ta and Bi in RM MTA

Nuggets are discrete mineral phases mainly of alloys, sulphides, arsenides, etc. which are often characteristic of the platinum group elements (Ru, Rh, Pd, Os, Ir, and Pt) and Au in geological materials (Meisel *et al.* 2001b). Nuggets contains metals and sulphides and hardly partition into the silicates. Nugget effect are important in exploration studies of PGE because this is a natural way of pre-concentration of the PGE and Au. The identification of the reasons for the nugget effects facilitates the understanding of the geochemical history and the formation of the rock samples described (Meisel *et al.* 2001b). Homogeneity is an attribute of a sample which assures that analysis of all subsamples taken for measurement will produce the same analytical result within measurement uncertainty. This challenges the analytical chemist when selecting representative samples (Meisel *et al.* 2001b). The segregation effects and nugget effects cannot be discounted even after thorough grinding and blending (Kane *et al.* 2003). In reality, all geological samples are heterogeneous to

some degree for some constituent elements. The nugget effects for gold and the platinum group elements are the most obvious example (Kane 1997a).

Nuggets of Tantalum and Bi was observed in RM trachyandesite (MTA-1) when several test portion sizes of 400 mg were digested Other elements which were associated with this type of nuggets showing high concentrations were Th, Ce, Nb and Y. Nuggets seen in MTA-1 are shown in Figure 6.1. Thus care must be taken with sample digestion when nuggets are present in sample. Larger test portion must then be taken for the dissolution.

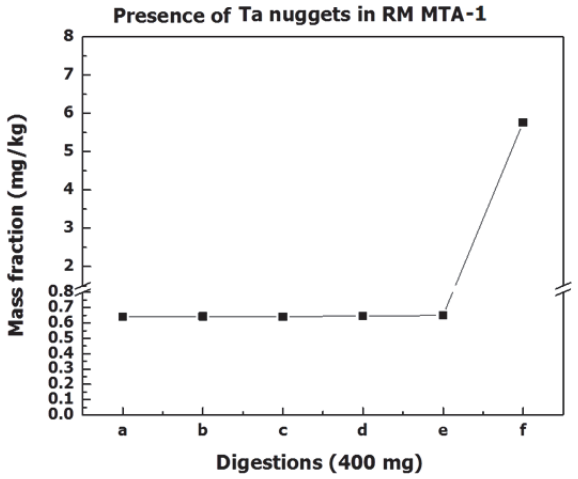

Figure 6.1: Nugget effect in RM MTA-1 in 400 mg digestions

6.4.2 Recovery of Zr, Nb, Ta and Hf upon dilution

When larger test portions were taken for digestions with sodium peroxide, it was found that the use of more sodium peroxide in small glassy carbon crucibles was required. Due to the aggressive nature of sodium peroxide, the addition of water was made drop by drop to avoid bumping and loss of solution from the crucible which would could result into analyte losses. To ensure that all analytes were transferred into the solution, the crucibles were thoroughly rinsed after the reaction was completed, followed by the addition of concentrated HCl. The dilutions of the larger test portions to 100 ml may result in the formation of precipitates. One or two drops of HF can prevent the formation of precipitates.

However, solutions containing one or two drops of HF, when diluted to 500 ml volume, can lead to decreased recovery of Zr, Nb, Ta and Hf. Münker (1998) has reported that addition of sulphuric acid for sample digestion tends to form the precipitates of (Sr, Ba, Pb)-SO_4 and Th, Ta and Nb were hydrolysed. The low recovery of Zr, Nb, Ta and Hf in our study might be due to hydrolysis because larger volume of water i.e. 500 ml for dilution, was used. This was observed in both materials MRH-1 and MTA-1. However, the mechanism is not certain. This effect due to possible hydrolysis of Zr, Nb, Ta and Hf is shown in Figure 6.2 - Figure 6.5. To avoid this situation, HF was not added to larger volume/larger test portion and recovery of analyte was not affected, in doing so.

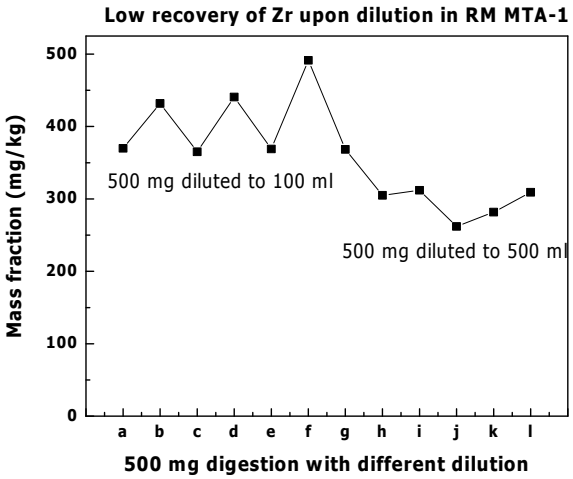

Figure 6.2: Low recovery of Zr in MTA-1

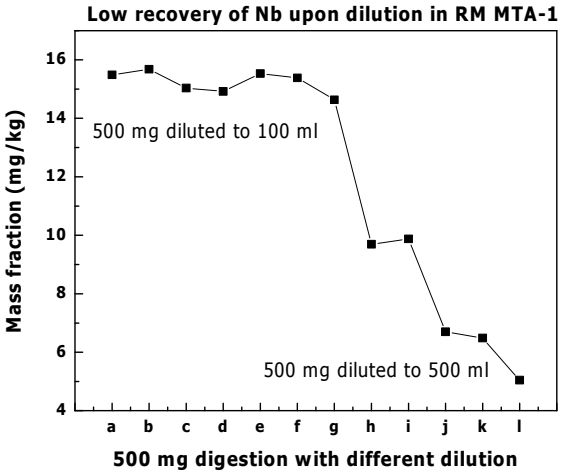

Figure 6.3: Low recovery of Nb in MTA-1

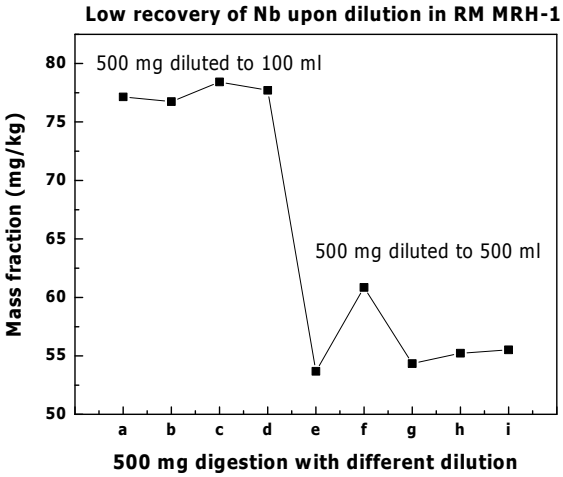

Figure 6.4: Low recovery of Nb in MRH-1

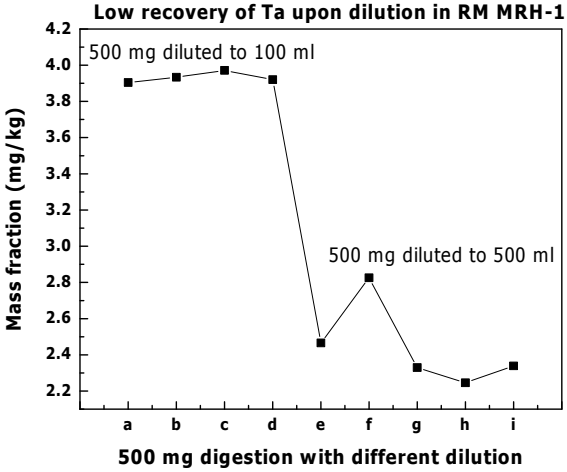

Figure 6.5: Low recovery of Ta in MRH-1

6.4.3 Estimation of the minimum test portion for sufficient homogeneity

If a larger test portion of the sample is taken for analysis, the sample is more likely to appear homogeneous, on the other hand, in smaller test portions, the inhomogeneity will be more readily found (Ingamells 1973, Ingamells and Pitard 1986). An extensive discussion of inhomogeneity in geological samples is given in Ingamells and Pitard (1986). According to this report, inhomogeneity exists in every sample at some level i.e. smaller test portion. Glasses are least inhomogeneous and coarse-grained poly-mineralic rocks are most inhomogeneous. No sample can be entirely homogeneous on the atomic scale. This effect is more apparent in different aliquots of the same sample i.e. smaller to larger test portion. Thus, estimation of the minimum mass is recommended in the certification of reference material as it meets the wide range of user needs (Kane *et al.* 2003, Paliulionyte *et al.* 2006).

The key consideration is that conclusions regarding homogeneity testing apply only to the test portion mass at which the testing was done or to larger test portion masses. The certified value itself should not change as a function of test portion mass, but the contribution of inhomogeneity to the uncertainty of that value is quite likely to increase with decreasing test portion mass (Kane *et al.* 2003).

In many cases, homogeneity fails to give sufficient quantitative information on homogeneity mainly because of a lack of measurement repeatability and an insufficient number of replicates (Meisel *et al.* 2001b). The influencing quantities such as calibration, interferences, the effect of dilution, the effect of temperature, instruments optimised conditions, nuggets, contaminations, had a greater effect on the interpretation of data in determining homogeneity. Therefore, to make the effect of test portion on homogeneity more apparent, experimental conditions were made confined to one calibration, one sample volume, measurement of one kind of rock sample in a batch, measurement sequence run of samples and tuning conditions etc. Within the same test portion size, relative standard deviations should be independent if measured in different calibrations.

The scatter graphs for granite (G-3) for different masses show that precision increases with test portion size. Each analyte has a different minimum sample mass in which it is homogeneous. This was demonstrated by Kane (1997a) and Potts (1987) that actual analytical sample mass in determining homogeneity varies from element to element.

When the data points aggregate well with each other, they are said to be more precise. The plots show the precision of the mass fractions of analytes in granite G-3. For example, in granite G-3 for analytes Ga, Ba, Rb, Cs, W, La and Ce the highest precision was achieved when the minimum test portion taken, was at least 500 mg as shown in Figure 6.6 - Figure 6.11. For the analyte Zr the highest precision was achieved when the minimum test portion was at least 400-500 mg as shown in Figure 6.12.

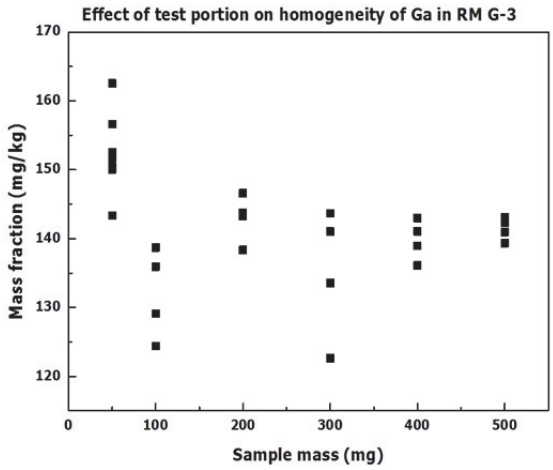

Figure 6.6: Effect of test portion on Ga in G-3

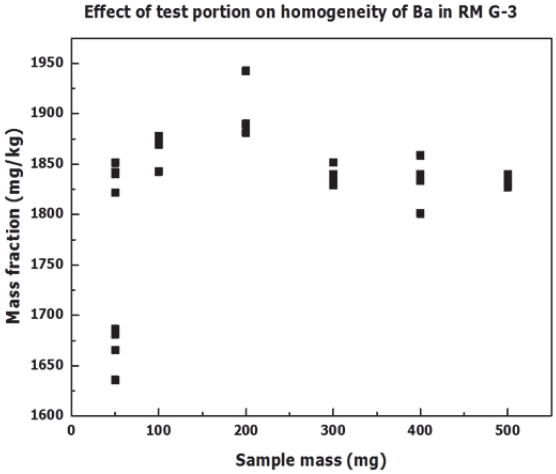

Figure 6.7: Effect of test portion on Ba in G-3

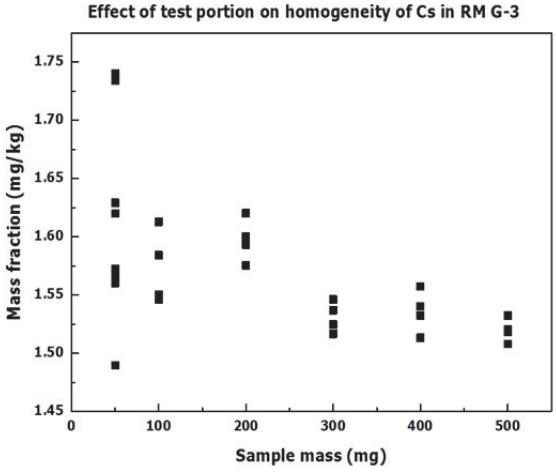

Figure 6.8: Effect of test portion on Cs in G-3

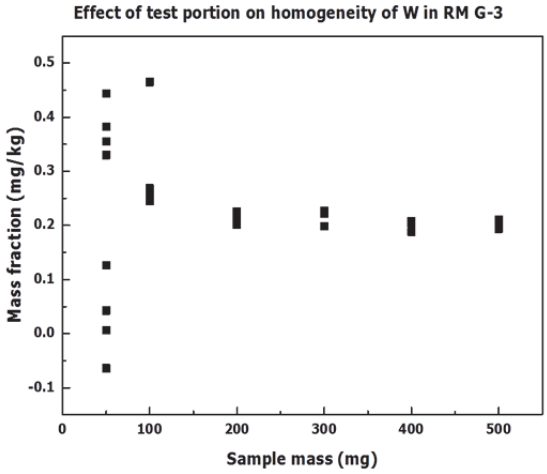

Figure 6.9: Effect of test portion on W in G-3

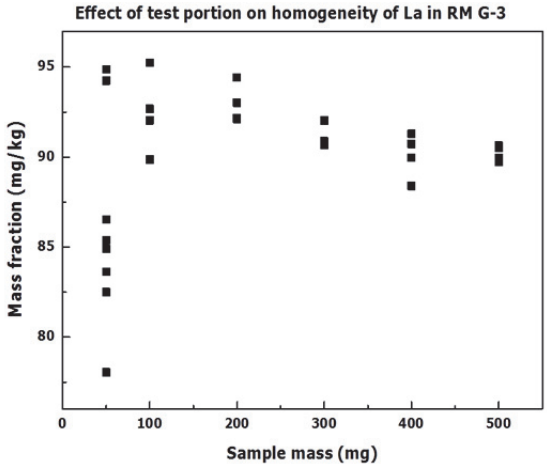

Figure 6.10: Effect of test portion on La in G-3

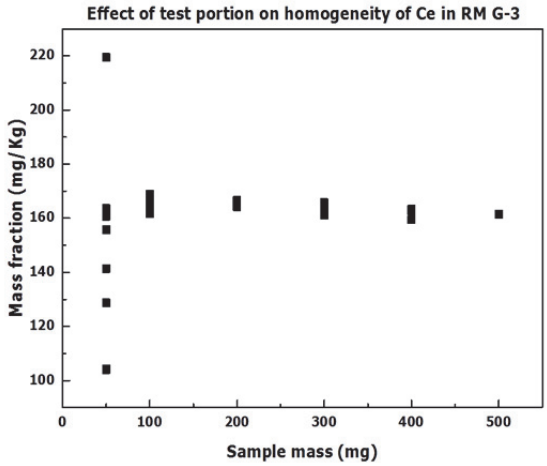

Figure 6.11: Effect of test portion on Ce in G-3

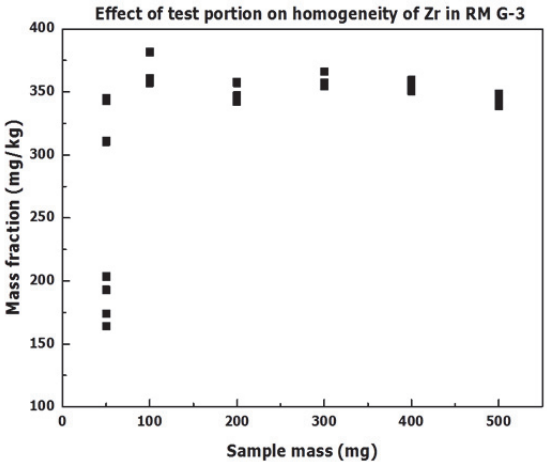

Figure 6.12: Effect of test portion on Zr in G-3

6.4.4 Effect of the test portion size on RSDs of analytes concentration

Data reliability is the most important aspect of a good measurement. Reliable data results for materials need to have sufficiently lower uncertainties compared to the results obtained in routine analysis. The lowest uncertainties for a property value of material can be achieved by carefully controlling all those factors, which cause large RSDs. Experiments on test portions of sample needed to involve a careful attention to and the study needs to be thorough and eliminate those factors for a property value of analyte, which affect possible uncertainties. The comparisons of the means of relative standard deviations of all the analytes in different test portions in this study involved one calibration.

RSDs of analytes in RM MTA-1 (trachyandesite)

It is well-known that the relative variance of the sample concentration decreases with increasing sample mass (Geelhoed and Glass 2001). Figure 6.13 shows the relative standard deviations for the analytes for RM trachyandesite MTA-1. A 50 mg test portion had relative standard deviations in a range of 2-7%. The lowest RSDs were achieved in either of the test

portions of 300 mg or 400 mg. A higher relative standard deviation for Tantalum and Nb was due to nugget effects in 400 mg test portion.

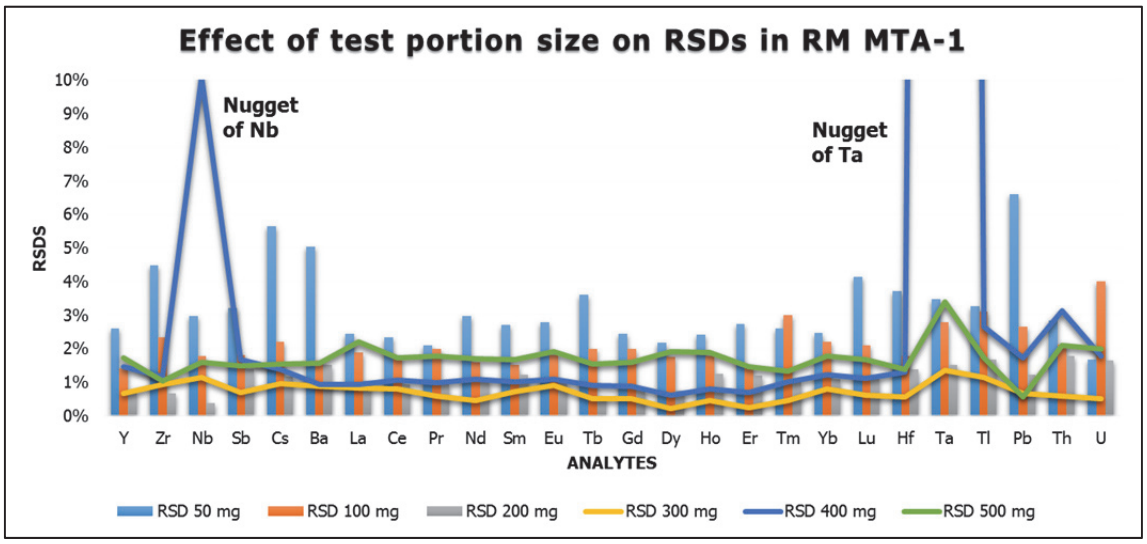

Figure 6.13: RSDs of analytes in different test portions in RM MTA-1

RSDs of analytes in RM MRH-1 (rhyolite)

Figure 6.14 shows relative standard deviations for the analytes for RM MRH-1. A 50 mg test portion had relative standard deviations in the range of 2-8%. Low RSDs were achieved in all the test portion sizes except for the 50 mg sample. The higher relative standard deviation for Ta was due to a nugget effects which is most often found in smaller test portions. A sample of 100 mg is the minimum test portion size recommended to determine the homogeneity in RM MRH-1.

RSDs of analytes in granite RM G-3

Figure 6.15 shows relative standard deviation for the analytes for uncertified USGS G-3. A 50 mg and 100 mg test portion had relative standard deviations in a range of 1.5-4%.

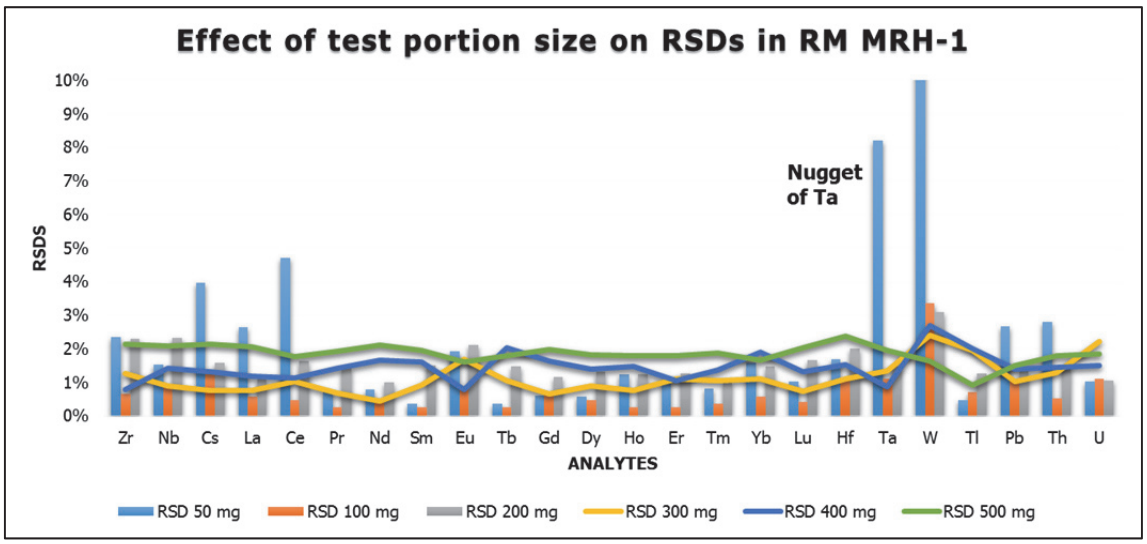

Figure 6.14: RSDs of analytes in different test portions in MRH-1

The lowest RSDs were achieved in either 200 mg or 300 mg test portions. Granite G-3 is a plutonic rock in which chemical changes during crystallisation have taken place slowly and incompatible minerals such as zircon do not readily enter crystalline phases from the Earth's mantle but instead concentrate in silicate liquids during partial melting and fractional crystallisation processes (Le Fèvre and Pin 2002). Therefore, a larger test portion is required for good sampling of such material when the mineral zircon and associated analytes occur.

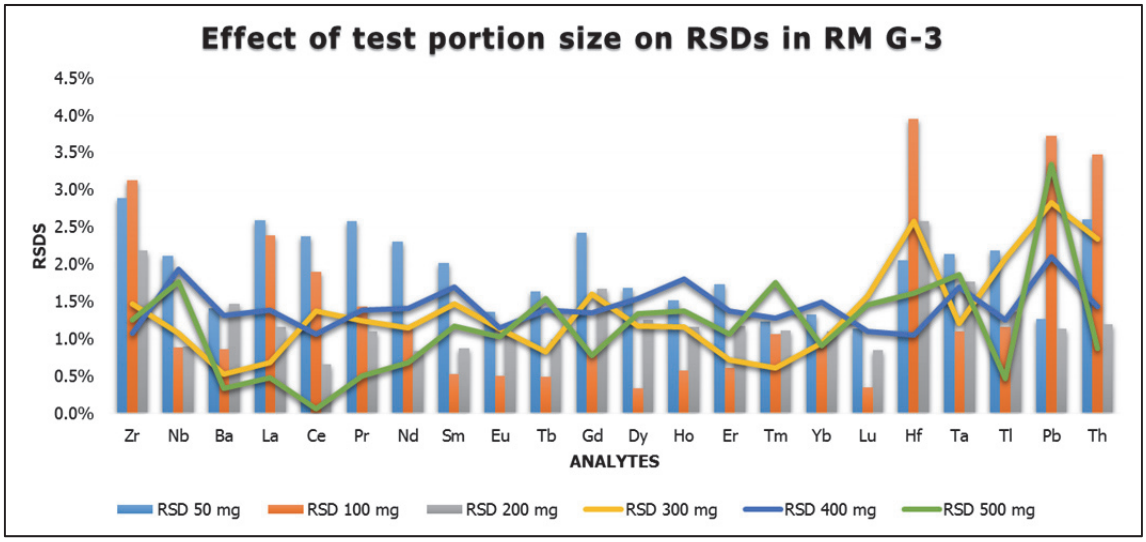

Figure 6.15: RSDs of analytes in different test portions in G-3

6.4.5 Intermediate precision vs. test portion size

Good precision is the most important figure of the merit of an analytical technique to allow it to be used in homogeneity testing of candidate RMs (Moreira *et al.* 2012). The extent to which intermediate precision may be established depends on the circumstances under which the procedure is intended to be used. For the estimation of the minimum sample intake, the relative standard deviations (RSDs) obtained for the various test portions were compared to the relative standard deviation for RMs and the intermediate precision were assessed which are shown in Figure 6.16 - Figure 6.18. As predicted by Ingamells (1973) between sample relative standard deviation decreases when the sample size is increased (Ingamells 1973). This can be seen as the intermediate precision increases with increasing test portion size in granite (G-3) and trachyandesite (MTA-1). For RM MRH-1 100 mg test portion was the minimum test portion for establishing good precision of the analytes.

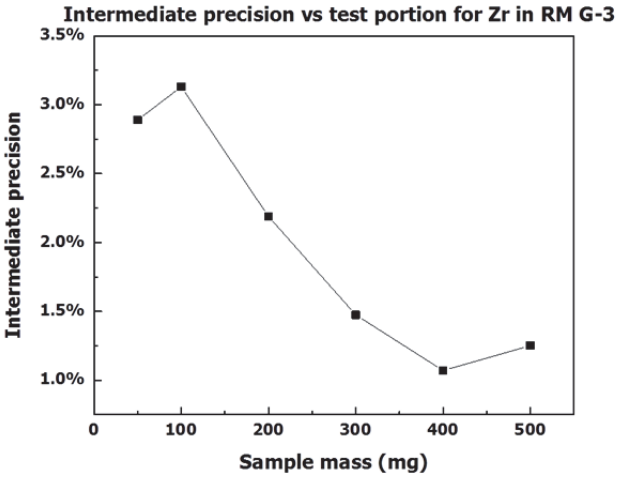

Figure 6.16: Intermediate precision of Zr vs test portion size in G-3

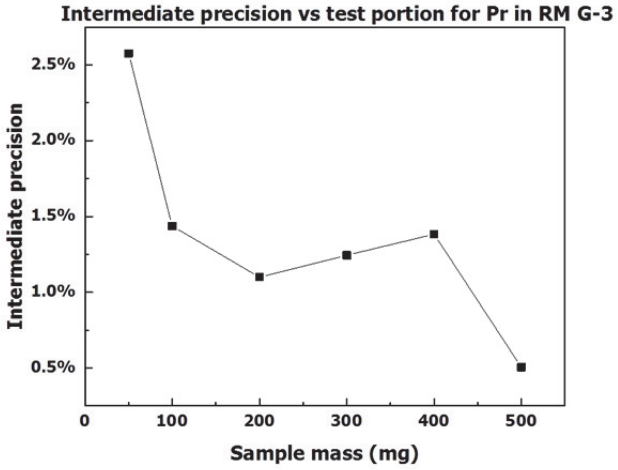

Figure 6.17: Intermediate precision of Pr vs test portion size in G-3

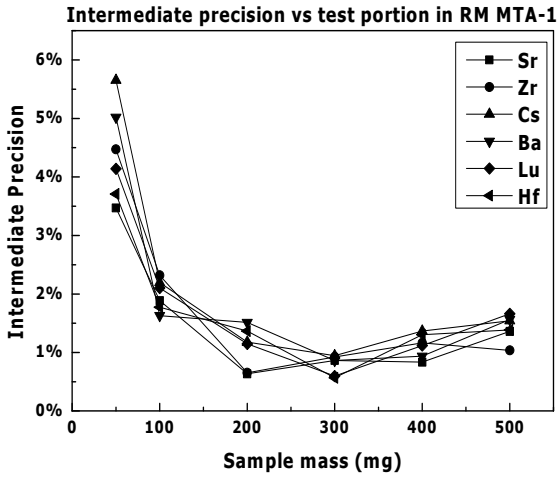

Figure 6.18: Intermediate precision of analytes vs test portion size in MTA-1

6.4.6 Table for Results

MTA-1

Table 6.1: Mass fractions determination for the analytes in RM MTA-1

The mass fractions determined are based on the mean of the mass fractions determined in all test portions. The mass fractions are shown in Table 6.1.

Mass fractions of analytes determined in MTA-1 (mg/Kg)														
Analyte	**50 mg**		**100 mg**		**200 mg**		**300 mg**		**400 mg**		**500 mg**			
	Ave	RSD	Ave	RSD	Ave	RSD	Ave	RSD	Ave	RSD	Ave	RSD	Certified	Precision
Li	23	4%	23	3%	16	4%	17	0%	18	4%	19	3%	23	5%
Be	2.30	2%	2.25	3%	1.67	4%	1.76	2%	1.85	3%	1.95	4%	2.22	5%
Mg	1.68	2%	1.65	2%	1.50	2%	1.49	1%	1.54	2%	1.58	2%	1.74	2%
Al	16.1	2%	15.5	2%	14.9	1%	14.8	1%	14.2	17%	15.6	2%	16.0	4%
Ca	4.37	4%	4.21	2%	4.30	1%	4.25	1%	4.38	2%	4.46	2%	3.85	1%
Ti	1.35	3%	1.32	2%	1.34	0.3%	1.32	1%	1.33	1%	1.35	2%	1.40	1%
V	105	5%	98	3%	99	0.3%	98	1%	101	3%	100	1%	102	3%
Cr	34	9%	30	4%	27	1%	27	1%	27	4%	27	1%	35	6%
Mn	0.048	5%	0.048	2%	0.047	0.5%	0.047	1%	0.047	2%	0.047	2%	0.047	2%
Fe	5.67	2%	5.56	3%	5.39	1%	5.36	1%	5.47	3%	5.43	1%	5.91	1%
Co	13.5	3%	13.3	3%	12.6	1%	12.5	1%	12.7	2%	12.7	2%	13.4	3%
Ni	32.5	2%	32.6	7%	25.2	3%	24.2	1%	24.5	3%	24.1	2%	27.0	5%
Cu	18.8	5%	20.1	7%	17.4	2%	16.9	2%	17.4	7%	16.6	1%	21.6	5%
As	7.06	5%	7.15	18%	6.37	3%	6.28	2%	7.36	8%	7.08	10%	6.50	12%
Rb	114	6%	116	2%	108	1%	107	1%	107	2%	105	1%	104	3%
Sr	2599	3%	2529	2%	2703	1%	2685	1%	2651	3%	2698	1%	2692	2%
Y	18.5	3%	18.6	1%	17.4	1%	17.3	1%	15.5	28%	17.4	2%	17.7	4%
Zr	343	4%	342	2%	374	1%	368	1%	364	1%	367	1%	368	3%
Nb	13.7	3%	14.1	2%	15.5	0.4%	15.4	1%	15.9	10%	15.2	2%	14.8	5%
Sb	9.0	3%	8.4	2%	9.0	1%	9.1	1%	9.1	4%	8.9	1%	8.5	13%
Cs	11.7	6%	12.2	2%	11.4	1%	11.3	1%	11.3	2%	11.2	2%	11.7	4%
Ba	2633	5%	2711	2%	2774	2%	2761	1%	2721	1%	2720	2%	2828	2%
La	110	2%	113	2%	122	1%	121	1%	111	22%	120	2%	112	4%
Ce	214	2%	216	2%	223	1%	222	1%	208	15%	221	2%	219	3%
Pr	24.3	2%	24.8	2%	25.9	1%	25.7	1%	23.6	21%	25.5	2%	25.3	3%
Nd	91.3	3%	92.5	2%	96.5	1%	95.6	0.5%	87.3	21%	94.4	2%	90.7	3%
Sm	13.2	3%	13.3	2%	13.8	1%	13.8	1%	12.5	24%	13.6	2%	13.2	2%
Eu	3.50	3%	3.50	2%	3.48	1%	3.47	1%	3.19	21%	3.46	2%	3.36	3%
Tb	0.871	4%	0.863	2%	0.883	1%	0.871	1%	0.819	18%	0.882	2%	0.871	2%
Gd	8.24	2%	8.13	2%	8.28	1%	8.23	1%	7.63	22%	8.35	2%	7.80	6%
Dy	3.90	2%	3.92	2%	4.07	1%	4.04	0.2%	3.80	15%	4.01	2%	4.03	3%
Ho	0.644	2%	0.644	2%	0.674	1%	0.667	0.4%	0.631	12%	0.661	2%	0.658	2%
Er	1.506	3%	1.516	1%	1.570	1%	1.565	0.2%	1.490	11%	1.557	1%	1.620	3%
Tm	0.196	2%	0.197	3%	0.206	1%	0.205	1%	0.197	9%	0.203	1%	0.207	3%
Yb	1.26	2%	1.24	2%	1.28	1%	1.279	1%	1.228	9%	1.268	2%	1.231	2%
Lu	0.176	4%	0.17	2%	0.179	1%	0.178	1%	0.17	9%	0.176	2%	0.179	3%
Hf	7.29	4%	7.32	2%	8.33	1%	8.18	1%	8.03	1%	7.99	1%	8.30	5%
Ta	0.796	3%	0.782	3%	0.685	1%	0.662	1%	1.522	138%	0.719	3%	0.740	7%
W	0.54	9%	0.52	8%	0.49	6%	0.48	4%	0.51	11%	0.49	5%	0.93	15%
Tl	0.42	3%	0.44	3%	0.45	2%	0.46	1%	0.46	3%	0.46	2%	0.45	7%
Pb	34	7%	34	3%	34	1%	34	1%	34	3%	34	1%	34	4%
Bi	0.60	63%	0.11	3%	0.04	23%	0.03	3%	0.04	17%	0.03	6%	0.10	20%
Th	11.3	3%	11.5	2%	12.0	2%	12.2	1%	10.5	36%	12.1	2%	11.40	4%
U	1.70	2%	1.71	4%	1.80	2%	1.82	0.5%	1.84	3%	1.83	2%	1.72	9%

*The higher RSDs in 400 mg test portion are due to the Ta nugget found in one of the digestion.

MRH-1

The mass fractions determined for MRH-1 are obtained through means of the mass fractions determined in all the test portions. The mass fractions are shown in Table 6.2.

Table 6.2: Mass fractions determination of the analytes in RM MRH-1

Mass fractions of analytes determined in MRH-1 (mg/kg)												
Analyte	**100 mg**		**200 mg**		**300 mg**		**400 mg**		**500 mg**			
	Ave	RSD	Ave	RSD	Ave	RSD	Ave	RSD	Ave	RSD	Certified	Rel *u*
Li	42	3.0%	42	1.0%	41	2.0%	39	2.0%	39	1.0%	47	6.0%
Be	6.74	1.0%	6.69	1.0%	6.68	2.0%	6.48	1.0%	6.57	2.0%	7.1	6.0%
Mg	0.084	2.0%	0.082	4.0%	0.082	8.0%	0.076	1.0%	0.076	4.0%	0.094	11.0%
Al	12.3	1.0%	11.9	1.0%	11.9	1.0%	11.6	0.3%	11.8	2.0%	11.86	1.0%
Ca	0.227	41.0%	0.247	37.0%	0.193	33.0%	0.177	23.0%	0.174	26.0%	0.048	8.0%
Ti	0.192	1.0%	0.189	2.0%	0.19	1.0%	0.184	0.0%	0.187	1.0%	0.199	5.0%
V	2.209	6.0%	2.121	7.0%	1.848	9.0%	1.745	19.0%	1.657	12.0%	3.4	29.0%
Cr	36	3.0%	36	2.0%	36	1.0%	35	2.0%	36	1.0%	41	5.0%
Mn	0.075	2.0%	0.0743	1.0%	0.0743	1.0%	0.0725	1.0%	0.0733	2.0%	0.0713	1.0%
Fe	1.74	1.0%	1.74	3.0%	1.74	1.0%	1.71	2.0%	1.7	1.0%	1.81	3.0%
Zn	175	2.0%	173	5.0%	168	2.0%	164	2.0%	165	2.0%	161	4.0%
Rb	283	1.0%	284	1.0%	285	1.0%	278	1.0%	281	2.0%	274	1.0%
Sr	4.4	10.0%	3.4	5.0%	3.4	7.0%	2.8	14.0%	3.5	14.0%	4.5	13.0%
Y	45.8	1.0%	45.3	1.0%	45.8	1.0%	44.7	1.0%	45	1.0%	44.7	4.0%
Zr	475	1.0%	481	2.0%	489	1.0%	478	1.0%	472	4.0%	471	2.0%
Nb	79.5	1.0%	79.3	2.0%	79.8	1.0%	78.3	1.0%	75.7	6.0%	75	4.0%
Mo	1.09	12.0%	1	3.0%	1.17	15.0%	1.36	35.0%	0.96	3.0%		
Cd	0.18	12.0%	0.187	14.0%	0.172	4.0%	0.168	5.0%	0.181	5.0%	0.09	78.0%
Sb	0.151	6.0%	0.128	7.0%	0.126	5.0%	0.108	6.0%	0.099	6.0%	0.16	13.0%
Cs	4.23	1.0%	4.2	2.0%	4.22	1.0%	4.1	1.0%	4.12	2.0%	4.3	5.0%
La	68.9	1.0%	68.6	1.0%	68.9	1.0%	66.7	1.0%	67.2	2.0%	68	3.0%
Ce	131	0.30%	131	2.0%	132	1.0%	128	1.0%	129	2.0%	127	2.0%
Pr	18.4	0.40%	18.4	1.0%	18.5	1.0%	17.9	1.0%	18	2.0%	18.5	2.0%
Nd	68.4	0.40%	68.4	1.0%	69	0.0%	66.5	2.0%	66.8	2.0%	67.5	3.0%
Sm	15	0.50%	15.0	2.0%	15.1	1.0%	14.6	2.0%	14.6	2.0%	14.8	2.0%
Eu	0.452	1.0%	0.45	2.0%	0.45	2.0%	0.436	1.0%	0.44	2.0%	0.471	4.0%
Tb	1.7	0.3%	1.70	1.0%	1.7	1.0%	1.65	2.0%	1.66	2.0%	1.7	2.0%
Gd	11.49	1.0%	11.46	1.0%	11.53	1.0%	11.22	2.0%	11.29	2.0%	11.4	2.0%
Dy	9.05	0.5%	9.02	1.0%	9.07	1.0%	8.77	1.0%	8.82	2.0%	9.1	2.0%
Ho	1.67	0.2%	1.66	1.0%	1.68	1.0%	1.63	1.0%	1.63	2.0%	1.62	2.0%
Er	4.36	0.3%	4.33	1.0%	4.37	1.0%	4.25	1.0%	4.25	2.0%	4.4	2.0%
Tm	0.64	0.4%	0.63	1.0%	0.64	1.0%	0.62	1.0%	0.62	2.0%	0.63	3.0%
Yb	4.09	1.0%	4.08	1.0%	4.11	1.0%	3.97	2.0%	4.00	2.0%	4	3.0%
Lu	0.58	0.4%	0.58	2.0%	0.59	1.0%	0.57	1.0%	0.57	2.0%	0.58	3.0%
Hf	14.9	1.0%	14.9	2.0%	15.3	1.0%	14.8	2.0%	14.5	4.0%	14.6	6.0%
Ta	3.99	1.0%	4.01	1.0%	4.05	1.0%	3.95	1.0%	3.99	2.0%	4.2	7.0%
W	1.49	3.0%	1.52	3.0%	1.52	2.0%	1.48	3.0%	1.49	2.0%	1.8	17.0%
Tl	1.11	1.0%	1.11	1.0%	1.13	2.0%	1.1	2.0%	1.11	1.0%	1.14	6.0%
Pb	45.9	1.0%	45.0	1.0%	45.1	1.0%	44	1.0%	44.4	1.0%	47	4.0%
Th	30.2	1.0%	30.1	1.0%	30.4	1.0%	29.6	1.0%	29.8	2.0%	28.9	5.0%

G-3

The mass fractions determined for G-3 are based on means of the mass fractions determined in all the test portions. The mass fractions for G-3 are shown in Table 6.3.

Table 6.3: Mass fractions determination of the analytes in RM G-3

	Mass fractions of analytes determined in G-3 (mg/kg)															
Analyte	**50 mg**		**100 mg**		**200 mg**		**300 mg**		**400 mg**		**500 mg**					
	Ave	RSD	Ave	RSD	Ave	RSD	Ave	RSD	Ave	RSD	Ave	RSD	1*	2*	3*	4*
Li	22.47	2%	24.28	2%	24.70	2%	25.22	5%	26.02	2%	25.70	0.3%		32		34.00
Be	4.23	7%	3.92	4%	3.75	3%	3.93	2%	3.96	4%	3.95	4%		3.9		2.50
Mg	0.726	1%	0.715	1%	0.704	1%	0.702	2%	0.708	2%	0.705	1%				0.750
Al	16.6	1%	16.4	1%	16.6	2%	16.3	1%	16.4	1%	16.3	1%				15.4
Ca	2.06	4%	2.02	3%	1.95	2%	1.95	3%	1.92	5%	1.78	1%				1.96
Ti	0.500	1%	0.513	2%	0.519	2%	0.504	2%	0.502	2%	0.497	1%				0.480
V	40.8	3%	37.4	2%	39.0	2%	34.5	9%	33.1	1%	34.3	3%		34		36.0
Cr	18.02	6%	14.76	7%	13.40	2%	13.68	7%	13.41	2%	13.48	4%		19.00		8.70
Mn	0.039	2%	0.039	1%	0.039	1%	0.038	3%	0.038	1%	0.037	1%				0.030
Fe	2.92	1%	2.93	2%	2.93	1%	2.88	2%	2.90	1%	2.87	1%				2.66
Co	4.48	1%	4.37	1%	4.41	1%	4.38	3%	4.39	1%	4.34	2%		4.5		4.60
Ni	12.69	21%	6.98	10%	5.50	4%	5.81	13%	5.29	3%	5.70	10%		8		5.00
Cu	17.8	11%	19.6	39%	13.9	4%	14.2	7%	14.8	4%	14.0	3%		16		11.0
Zn	133	18%	99	13%	100	8%	94	16%	90	9%	83	4%		81		86
Ga	151	1%	132	5%	143	2%	135	7%	140	2%	141	1%		24		23
As	2.61	33%	2.88	28%	2.42	3%	1.93	7%	1.87	3%	2.36	11%				0.24
Rb	176	1%	166	1%	170	1%	163	1%	163	1%	163	0.5%				170
Sr	458	0.3%	468	1%	474	2%	459	1%	457	1%	455	1%				478
Y	10.0	1%	9.81	1%	10.0	1%	9.71	1%	9.68	1%	9.60	1%	8.79		10.3	11.0
Zr	327	6%	365	3%	351	2%	358	1%	354	1%	345	1%		361	321	309
Nb	12.4	3%	13.1	1%	13.2	1%	13.0	1%	12.5	5%	12.2	2%		12.3	14.0	12.0
Mo	2.04	15%	2.17	11%	2.54	27%	2.39	24%	2.13	3%	2.14	9%				
Cd	0.128	11%	0.154	10%	0.135	4%	0.147	5%	0.150	9%	0.140	6%		0.130		0.016
Sb	0.576	57%	0.146	9%	0.125	3%	0.133	12%	0.134	6%	0.132	16%		0.170		0.070
Cs	1.68	4%	1.57	2%	1.60	1%	1.53	1%	1.54	1%	1.52	1%		1.50		1.34
Ba	1839	1%	1866	1%	1901	1%	1839	1%	1833	1%	1833	0.5%		1991		1880
La	90	6%	92	2%	93	1%	91	1%	90	1%	90	0.3%	88	92	92	89
Ce	155	6%	165	2%	165	1%	164	1%	162	1%	161	0.3%	164	168	171	160
Pr	15.9	5%	16.5	1%	16.6	1%	16.2	1%	16.2	1%	16.1	1%	16.4	16.9	17.4	18.0
Nd	53.0	4%	54.5	1%	54.8	1%	53.5	1%	53.2	1%	53.1	1%	53.3	54.0	56.8	55.0
Sm	7.21	3%	7.29	1%	7.35	1%	7.17	1%	7.13	2%	7.07	1%	7.00	7.40	7.69	7.20
Eu	1.55	1%	1.59	1%	1.64	1%	1.57	1%	1.57	1%	1.57	1%	1.31	1.40	1.50	1.40
Tb	0.465	1%	0.480	0.5%	0.495	1%	0.475	1%	0.478	1%	0.473	1%	0.451	0.460	0.470	0.480
Gd	4.37	1%	4.66	1%	4.88	2%	4.58	2%	4.64	1%	4.63	1%		3.97	4.07	4.30
Dy	2.11	2%	2.11	0.3%	2.17	1%	2.09	1%	2.09	2%	2.07	1%	2.06	2.13	2.23	2.40
Ho	0.353	1%	0.343	1%	0.348	1%	0.343	1%	0.340	2%	0.335	2%	0.338	0.356	0.370	0.400
Er	0.845	2%	0.865	1%	0.878	1%	0.855	1%	0.855	1%	0.845	1%	0.859	0.88		0.920

Tm	0.118	4%	0.115	5%	0.118	4%	0.110	0.5%	0.113	4%	0.113	4%	0.114	0.122	0.123	0.180
Yb	0.765	2%	0.768	1%	0.775	1%	0.745	1%	0.743	1%	0.733	1%	0.716	0.730		0.800
Lu	0.108	5%	0.110	0.5%	0.110	0.5%	0.105	5%	0.103	5%	0.100	0.3%	0.101	0.106	0.11	0.110
Hf	7.67	5%	8.57	4%	8.24	3%	8.51	3%	8.34	1%	8.21	2%		9.00	9	7.90
Ta	0.968	2%	0.858	1%	0.873	1%	0.840	2%	0.830	3%	0.808	4%		0.910	0.890	0.880
W	0.030	262%	0.313	34%	0.215	6%	0.218	6%	0.203	5%	0.198	5%		0.300		0.200
Tl	0.785	2%	0.830	1%	0.825	2%	0.818	2%	0.810	1%	0.805	1%				0.910
Pb	31.3	10%	28.7	4%	28.6	1%	28.1	3%	28.1	2%	28.5	3%		31		30.0
Bi	0.168	56%	0.038	13%	0.043	30%	0.043	12%	0.035	16%	0.04	0.4%				0.04
Th	21.2	11%	24.61	3%	24.3	1%	24.73	2%	24.17	1%	23.93	1%		24	24.2	24.7
U	2.008	17%	1.923	10%	2.323	9%	2.275	18%	2.21	8%	2.03	8%		2.3		2.07

1* Pourmand *et al.* 2011 2*Cotta *et al.* 2011 3*Meisel *et al.* 2002 4* Robin *et al* .1986

6.5 Summary

This chapter describes the method validation of sodium peroxide sintering and homogeneity in test portions of three reference materials MTA-1, MRH-1 and G-3. This chapter has shown the importance of several influencing quantities that may affect the homogeneity of a reference material. In order to study the effect of only test portion size on the homogeneity, the influencing quantities i.e. purity of reagents, calibration, tune condition, ICP-MS settings, the sample to sodium peroxide ratio, incomplete digestions, replicate measurements and nugget effects were minimised.

The test portion size has an important role in determining the homogeneity of the material. Smaller test portions e.g. 50 mg show larger deviations in RSDs and show heterogeneity of most analytes especially in rock types, which have significant amounts of the refractory mineral zircon. It was demonstrated that at least 300 mg is the minimum test portion size for trachyandesite RM MTA-1 and RM USGS granite G-3 and 100 mg test portion for Rhyolite MRH-1 to assure the acceptable precision of less than 3% with a 1:6 sample: Na_2O_2 ratio.

Trachyandesite rock sample (MTA-1) has nuggets as shown in 400 mg test portion and care must be taken to use larger test portions.

ICP-MS is a more sophisticated tool for homogeneity testing compared to XRF where a larger test portion is typically analysed with lower detection limits along with better relative precision.

7. Method development for interference removal on the rare earth elements and Sc in geological materials

7.1 Objectives of this study

The advances in the analytical chemistry of the rare earth elements was discussed in section 2.5 where the problems related to the REE measurements were mentioned. The main goal of this work was to explore the capabilities of a ICP-QQQ-MS instrument and to develop an analytical method that is both sensitive and selective to allow for the accurate determination of rare earth elements in geological materials. Limited literature is available for the study of the rare earth elements using this collision/reaction cell technology, which has recently emerged. The outline of this work revolves around the collision/reaction cell and gases used in it to minimise interferences which were a problem in earlier studies. Following were the main features of this study:

1. The development of new precise, reliable, rapid, cost effective and accurate analytical method for the routine determination of the REE.
2. Interference removal with the collision/reaction cell technology of the Agilent 8800 ICP-MS/MS.
3. The identification of the interferences on rare earth elements in the collision/reaction cell.
4. Study of the behaviour/reactivity of all rare earth elements and corresponding interferences with cell gases.
5. To explore and provide understanding for all the possible adduct ions of rare earth elements with O_2 and NH_3 gas using collision/reaction cell of the ICP-MS/MS as limited literature is available on REE chemistry with this technology.
6. The proposal of a method for interference removal.
7. Method development and the optimisation.
8. Testing the proposed method on the standard solution of rare earth elements and finding the effect of removal of interferences.
9. The suggestion of different REE products ions (for mass filter and detectors) for each element i.e. on-mass and mass-shift method.
10. Method validation of proposed method with reference materials.
11. A major aim of this method for the determination of the REE at the trace level is the elimination of barium oxide interference on Eu isotopes.
12. Interference removal of doubly charged ions of Zr on Sc in Zr-rich reference materials.

7.2 Experimental

7.2.1 Reagents and materials

HCl 37 g/100 g p.a., Roth, Karlsruhe, Germany, HNO_3 65 g/100 g p.a., Roth, Karlsruhe, Germany were used for sample preparation. An ultra-clear unit for ultra-pure water (Siemens water technologies) with conductivity: 0.055 µS/cm, TOC content: < 1 ng/g, (for diluting acids and samples). Sodium peroxide (Na_2O_2) (purity > 95 g/100g, Merck, Darmstadt, Germany) for digestion of geological reference materials. Glassy carbon crucibles (25 x 25 mm, HTW) were used for sample digestion. Single elements standard solutions (1000 µg/l) of Ce, La, Gd, Tb, Pr, Nd, Er, Dy, Ho, Yb, Tm, Lu, Sm and Eu for initial testing of interferences were obtained from Merck KGaA Darmstadt, Germany. The solutions were diluted to 10 ng/ml with 1 g/100 g HNO_3. Solutions after preparation were stored in PP vials (50 ml, Sarstedt). All acids (HCl and HNO_3) used for the preparation of samples were sub-

boiled. All the standard solutions used for initial testing were diluted to 5 ml with a final concentration of 1 ng/ml. For testing the product ions 10 ng/ml solutions were used.

Several geological reference materials (DBC-1, BIR-1, BCR-2, MTA-1, OU-9, NKT-1, G-3, SdAR-1, OU-3, BCR-176-R (incineration RM), MRH-1 and MUH-1) were digested with sodium peroxide sintering using 1:6 sample to sodium peroxide ratio for the method validation. Single element pure solutions were used for finding the effect of interferences of LREE on heavier HREE only. For measurement of REE in geological reference material 10 reference materials were used for establishing a calibration. 1 μg/g solutions of indium (In) and germanium (Ge) were used as internal standard to control the instrument drift during measurement. Linear regression was used for drift correction.

7.2.2 Instrumentation

A ICP-MS/MS Agilent 8800 (Agilent Technologies, Tokyo, Japan) was used for the measurements in this study. The detailed descriptions of the instrument are given in chapter 4. Standard instrument configuration as given in Table 7.1 was used with Ni sampler and interface cones, standard ion lens and micro-mist glass concentric nebuliser (for sample introduction system), a Peltier cooled glass quartz double-pass Scott- type spray chamber, and a quartz torch with 2.5 mm injector. A composite diagram of the instrument is shown in Figure 4.2 and Figure 7.1.

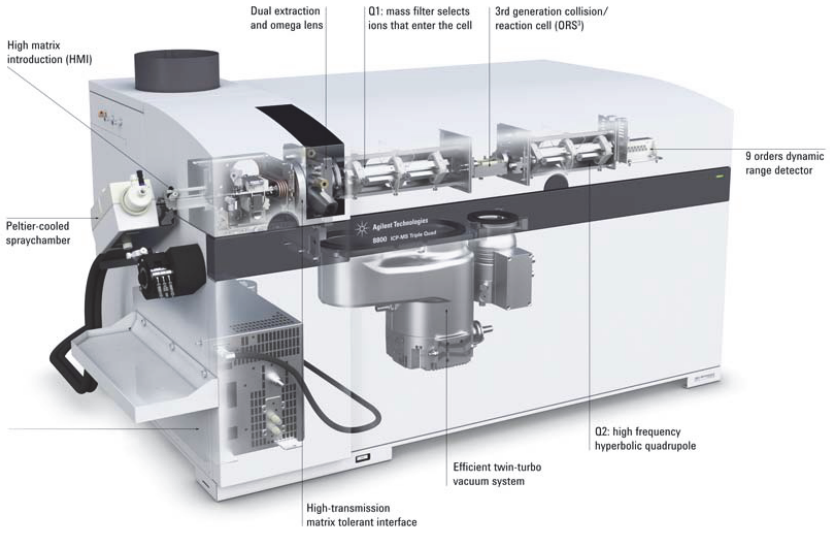

Figure 7.1: Agilent 8800 ICP-MS/MS (Source-Agilent website)

Sample introduction system consisted of an ESI autosampler (SC-2, Elemental service and Instruments GmBH, Mainz, Germany), 3 ml sample loop and a six-port valve system as shown in Figure 7.2. The solution was loaded to 3 ml loop by means of carrier solution (1% HNO_3) conveyed by the peristaltic pump of ICP-MS/MS. Additionally, seventh-port setup supplies continuously a 1 μg/l In and Ge internal standard solution that mixes with sample solution before being sprayed through the torch into the ICP-MS/MS system.

The CRC (collision/reaction cell) gases were He (99.99%), O_2 (99.99%), and 10% NH_3 in helium (supplied by Linde, Gas GmBH, Stadl-Paura Austria). The flow rates of 10% NH_3 gas in Helium were 2 ml/min, 3 ml/min and 5 ml/min denoted as NH_3-L, NH_3-M, NH_3-H which are low, medium and high. The O_2 flow rate was maintained at 0.3 ml/min. An additional helium gas was added to ammonia gas at 1 ml/min flow rate. The instrument was tuned with (1 μg/l) tune solution of Li, Co, Y, Ce and Tl for the best intensities with the lowest oxide formation.

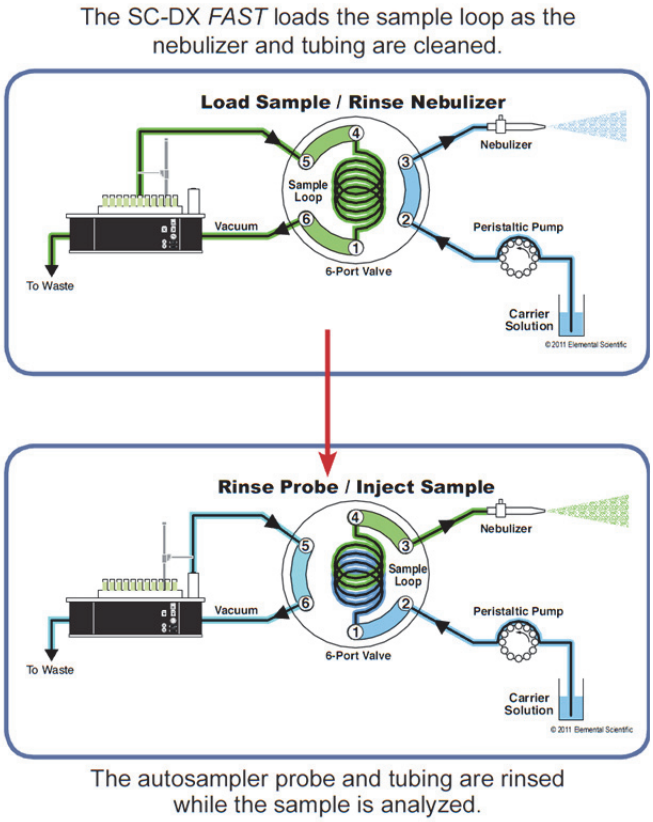

Figure 7.2: SC-2 auto sampler setting – Source- ESI 2014 info brochure

Instruments operating conditions are given Table 7.1.

Table 7.1: Typical instrumental operating conditions

Parameters	No gas	O_2	NH_3		
			Low	Medium	High
Scan type	Single Quad	MS/MS	MS/MS	MS/MS	MS/MS
RF Power (W)	1550				
sample depth (mm)	5.9	5	5.5		
Gas flow rate (ml/min)	-	0.3	2	3	5
He (ml/min)	-	-	1	1	1
Oxide formation	1.03				
Doubly charged ions	1.1				
Carrier gas flow rate (l/min)	0.71				
Makeup gas flow rate (l/min)	0.33				
Energy Discrimination (mV)	5	-7	-7		
OctP Bias (V)	-8	-5			
Q1 Bias (V)	0	-2	-2	-2	-3
Integration time (sec)	0.3	0.75			
Replicates	4				

Sweeps	60				
Q1 axis offset	-0.04				
Q2 axis offset	0				
Q1 Axis Gain	1.0014	1.0014	1.0004		
Q2 Axis Gain	1.0005	1.0014	1.001	1.0005	1.0004

7.3 Interferences on the rare earth elements

The ICP-MS is the most frequently employed analytical technique to quantify REE in geological samples in trace concentrations. However, the dissolution of silicate rocks and the occurrence of spectral interferences in the ICP-MS mass spectrum hamper the reliable quantification of REE. Spectral overlaps of polyatomic ions (MO^+, MOH^+ etc.) of light REE on heavy REE are of particular concern for ICP quadrupole mass spectrometers. Also, matrix-induced polyatomic ions of BaO^+ and $BaOH^+$ on REE from m/z 146 (Nd) through to m/z 155 (Gd), including ^{151}Eu and ^{153}Eu, are known to plague the reliable quantification of these elements (Inagaki and Haraguchi 2000).

The hydride interferences of the analytes adjacent to the REE are (amu+1) e.g. $^{139}La^1H^+$ on $^{140}Ce^+$, $^{140}Ce^1H^+$ on $^{141}Pr^+$, $^{146}Nd^1H^+$ on $^{147}Sm^+$, $^{158}Gd^1H^+$ on $^{159}Tb^+$ etc. Similarly, $^{138}Ba^1H^+$ is a non-REE interference on REE. Oxides and hydroxides of non-REE elements cause interferences in detection as well e.g. $^{122}Sb^{16}O^+$ and $^{121}Sb^{16}O^1H^+$ on $^{139}La^+$. REE-oxide and hydroxide interferences are e.g. $^{156}Gd^{16}O^+$ and $^{155}Gd^{16}O^1H^+$ interference on $^{172}Yb^+$. These interferences are given in Table 2.7 in chapter 2.

7.4 Reactivity of REE singly charged cations with ammonia and oxygen gas

Using a ICP-MS equipped with a collision/reaction cell, it is intended here to investigate the chemical reactivity of REE with the cell gases (O_2 and NH_3) in order to provide a way of eliminating isobaric interferences and to get an efficient method applicable for the separation of REE in the gas-phase. Only single mono-ionisations of REE (noted hereafter REE^+) are usually obtained in ICP-MS. In order to investigate the behaviour/reactivity of rare earth elements, NH_3 and O_2 gases were used in reaction collision cell of ICP-MS/MS.

1. Reactivity of rare earth elements with NH_3 gas
2. Reactivity of rare earth elements with O_2 gas

7.4.1 Reactivity of REE with NH_3 gas

The gas-phase reactions of REE cations with small molecules are important in understanding the atomic ion reactivity in relation to their electronic configurations (Gross and Caprioli 2003). Reactions of REE cations with ammonia gas are also important in studies of the influence of irradiation by fast neutron bombardment. Study of the gas-phase reactions of REE cations is reported from the 1980s with various techniques i.e. Fourier-transform mass spectrometry, ion beam technologies, laser ablation etc. Studies over 20 years on REE cation gas-phase reactions with different techniques and different molecules i.e. hydrogen, oxygen and nitrous oxide, nitric oxide, carbon dioxide and carbon disulfide, heavy water, methane, alkanes and cycloalkanes, alkenes, alcohols, benzene and substituted benzenes, phenol, orthoformates, ferrocene and Fe pentacarbonyl, methyl fluoride and methyl chloride, and sulphur hexafluoride present enormous data with variation in reactivity and product ions. These variations arise from the accessibility of the excited electronic configuration that makes available two unpaired non *f* electrons for chemical

bonding (Koyanagi *et al.* 2009). Literature that reports the gas-phase reaction of REE cations using NH_3 gas is limited (Koyanagi *et al.* 2009). For the purpose of understanding the fundamental aspects of the ion-molecule reactions of rare earth elements in reaction collision cell and their application to removal of interferences in pure and real matrices, experimental tests/results of rare earth elements with ammonia molecules are presented in this study.

The ICP-MS/MS is a cost effective way of doing reactivity measurements. In this study all the REE cations were formed within the same source of argon plasma at 10000 K. Typical instrument configurations are given in Table 7.1. The ions of rare earth elements were generated using standard test solutions (1 ng/ml for reactivity testing using on-mass method) and (10 ng/ml for product ion testing and interference removal capability using on-mass and mass-shift method) described earlier in chapter 4. In the case of reactivity testing, ions emerging from plasma were led to the first quadrupole mass filter for selection of particular REE of interest. The second quadrupole, a second mass filter was kept on the same m/z. Filtered ions of particular REE of interest e.g. $^{139}La^{+}$ were led to collision/reaction cell where the 10% ammonia/He gas was supplied at 2, 3 and 5 ml/min with stabilisation time of 25 seconds. For Eu, in particular, a flow rate 5 ml/min was maintained presented in earlier studies Bokhari *et al.* (2015b). The stabilisation time was 25 seconds for the gas chamber to switch in between low, medium and high flow rates. The flow rate 2 ml/min of NH_3 gas could only initiate product formation to a minimum as shown in Figure 7.3. The original intensity of REE decreased only to 30-50% ensuring less formation of REE ammonia products ions. The black shaded box line indicates decrease in original intensity relative to the intensity in no gas mode and the grey unshaded box line shows the intensity of product ions formed relative to intensity in no gas mode. When the flow rate was increased to 3 ml/min, cluster formation for reactive elements increased and its original intensity of the ions decreased to a maximum relative to the intensity in no gas mode as shown in Figure 7.4.

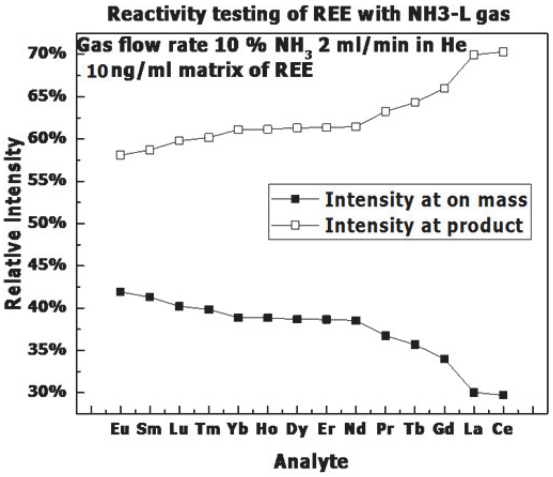

Figure 7.3: Reactivity of REE with NH_3 at 2 ml/min flow rate

The order of reactivity of REE with NH_3 gas with a flow rate of 3 ml/min in the collision/reaction cell is given below.

La>Gd>Ce>Tb>Lu>Pr>Sm>Nd>Dy>Er>Ho>Eu>Yb>Tm

On the basis of this reactivity testing with NH_3 gas, REE can be classified into three groups.

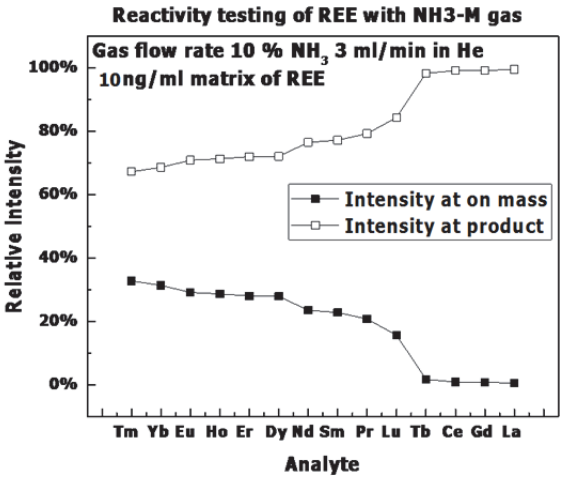

Figure 7.4: Reactivity of REE with NH3 at 3 ml/min flow rate

1. Most reactive REE
2. Intermediate reactive REE
3. Least reactive REE

7.4.1.1 Most reactive REE

The experimental results of the reaction of REE^+ with NH_3 are described here. *Lanthanum, Gd, Ce, Tb* can be grouped into REE which react efficiently with NH_3 gas in collision/reaction cell. They confirm the order of reactivity $La^+ \approx Gd^+$ $Sm^+ > Eu^+$, already observed by other researchers with different experiments in Koyanagi *et al.* (2009). La and Ce have 4+ oxidation states and are most reactive of rare earth elements. The reactivity of an element is determined by a number of oxidation states in which an ion exists in hot plasma. In considering reaction probabilities, other thermodynamic factors, such as ionisation energies and bond energies, must be included and are reaction specific (Armentrout 2004). Not all exothermic reactions are efficient to occur, as some reactions require a spin change on the way to products which inhibits the reaction. As for any exothermic process, increasing the amount of energy available will decrease the probability of the reaction (Armentrout 2004). In simpler terms, the intensities of the product ions will be more depending upon binding energy in an exothermic reaction. If the reaction is favoured at low temperatures, it will release more energy that will inhibit the formation of product ion. For the reaction that requires a spin change in the pathway leading to product ions, the energy released could be utilised in that spin change with more efficient reaction (Armentrout 2004).

7.4.1.2 Intermediate reactive REE

Lu, Pr, Sm and *Nd* have an intermediate reactivity towards NH_3 gas.

7.4.1.3 Least reactive REE

Dysprosium, Er, Ho, Eu, Yb and *Tm* react less efficiently at given a flow rate (medium) of NH_3 gas. Similar reactivity trends have been reported by Sugiyama (2012) and has given the same order but at a higher flow rate 8 ml/min of NH_3. The scan of intensities in on-mass and mass-shift modes of product ions is given in Figure 7.5.

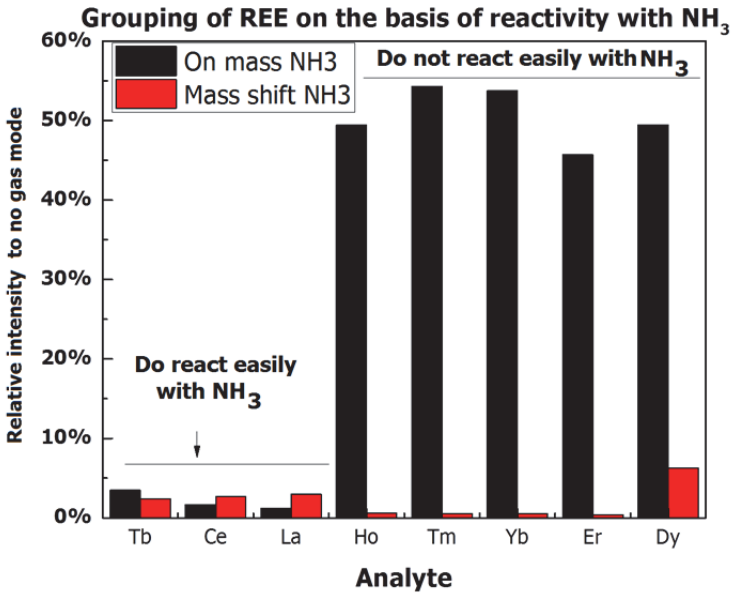

Figure 7.5: Grouping of REE on the basis of reactivity with NH_3-M

7.4.2 Explanation of reaction efficiencies

Reactions of REE^+ ions have been evidenced with several gases suggesting that REE^+ strongly reacts when it has two non-*f* unpaired valence electrons. The reactivity and electronic promotion energy (PE) are correlated. PE is the energy needed for the promotion of one electron from the fundamental electronic configuration $4f^n5d^06s^1$ to the reactive configuration $4f^{n-1}5d^16s^1$, where n is the number of 4*f*-electrons in the REE^+ ground state. Gibson (2003) has proposed a quantitative correlation between the bonding energies and the electronic promotion energies for oxide ions and molecules of the f-block elements in the gas-phase. Reactions with H_2O are slightly more selective, giving $REEO^+$ with relatively high reaction rate coefficients for La^+, Ce^+, Gd^+, Tb^+ and Lu^+, and with low reaction rate coefficients for Pr^+, Nd^+ and Sm^+ (Cheng *et al.* 2006, Gibson 2003).

Nitrogen donor gases such as N_2O and NH_3 are more selective across the REE^+ series. The primary reactions with N_2O generally proceed via the O-atom transfer to the bare atomic cation for all the REE^+ ions;

$$REE^+ + N_2O \rightarrow REEO^+ + N_2 \text{ (Koyanagi and Bohme 2001)}$$

Nitrogen atom transfer leading to the $REEN^+$ cations were observed for La^+ and Ce^+;

$$REE^+ + N_2O \rightarrow REEN^+ + NO$$

while $REENH^+$ was not found for the other REE^+ ions as suggested by Koyanagi *et al.* (2009), Tanner *et al.* (2002). Product ions with more NH_3 cluster could not be observed, because of the limitations of the m/z for ICP-MS/MS 8800 instrument which goes up to 260 m/z.

Based on experimental tests on the reactivity of REE^+ with NH_3 in collision/reaction cell, 1 ng/ml of REE were tested to make all possible adduct ion until m/z 260 with ammonia gas. All REE cations show some reactivity with ammonia. La, Ce, Gd and Tb form the most reactive group of REE towards ammonia. A similar trend has been reported in Koyanagi *et al.* (2009) on rare earth chemistry using inductively coupled plasma /selected-ion flow tube (ICP/SIFT) tandem mass spectrometer. If the La, Ce, Gd and Tb are more reactive, it would

be wise enough to see what product ions are formed in order to differentiate the mechanism of the reaction.

Primary reaction channel

Koyanagi *et al.* (2009) propose two primary reaction channels with NH_3 that result in the formation of the protonated REE nitride $REENH^+$ and $REE(NH_3)$ as shown in the equation below (Koyanagi *et al.* 2009);

$$(REE^+ + NH_3 \rightarrow REENH^+ + H_2) \text{ ----------1a}$$

$$\rightarrow REE^+(NH_3) \text{ ---------1b}$$

(1a) correspond to the formation of the $REE(NH^+)$ adduct ion with the elimination of H_2. (1b) is related to the addition of NH_3 as $REE^+(NH_3)$. Looking at the peak scan profile of the adduct ions it can be established that only La, Ce, Gd and Tb make protonated REE nitride $REENH^+$ as shown in Figure 7.6, Figure 7.7, Figure 7.8 and Figure 7.9. The results of this study confirm generalisation from Koyanagi *et al.* (2009). Koyanagi *et al.* (2009) propose the structure of $REENH^+$ as $^+REE{=}N\text{-}H$ where the positive charge is on the metal centre and the oxidation number is in stable (+3) state. He further states that H atom transfer reaction does not take place because of low affinities of H atom with REE^+ cation. The hydrogen affinities of NH_2 are 108.6 kcal/mol and hydrogen affinities of La^+, for example, are 57.2 kcal/mol and for Lu^+ are 48.6 kcal/mol. The hydrogen affinities of REE^+ are much smaller than hydrogen affinities of NH_2.

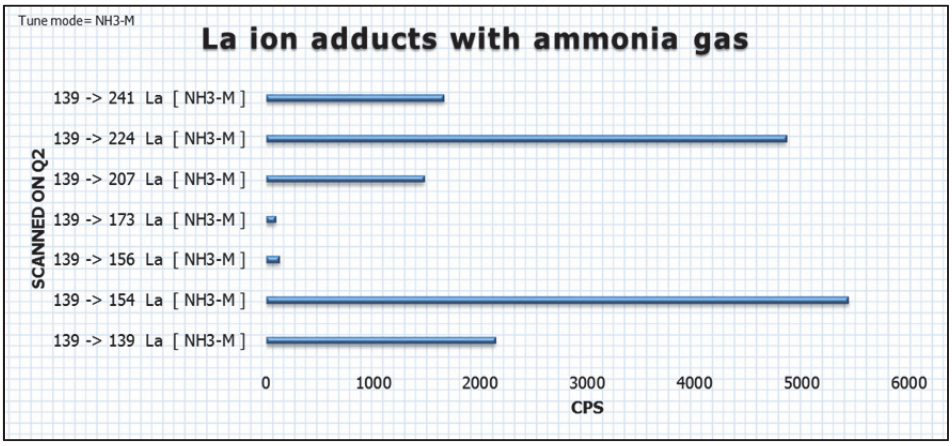

Figure 7.6: Scan of product ions of La

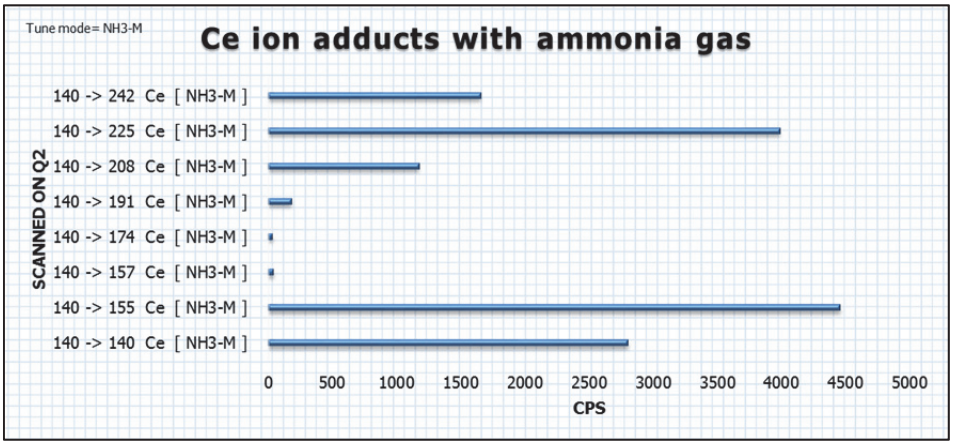

Figure 7.7: Scan of product ions of Ce

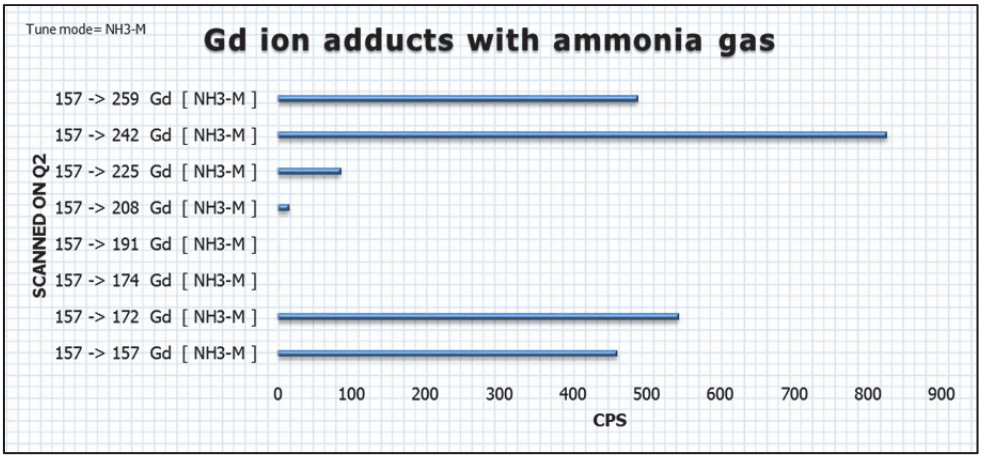

Figure 7.8: Scan of product ions of Gd

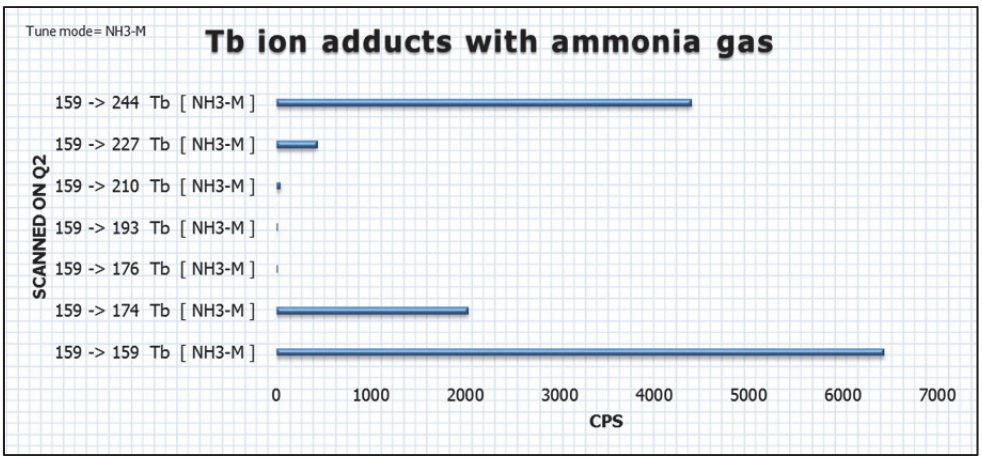

Figure 7.9: Scan of product ions of Tb

The first ionisation energies of REE are lower than 6.3 eV and for ammonia are 10.072 ± 0.010 (Locht *et al.* 1991), therefore electron transfer reactions are not expected with ammonia and NH_3 addition occurs more likely. The reaction channel (Ib) is the addition of ammonia to form $REE^+(NH_3)$ and it takes place in Pr^+, Nd^+, Sm^+, Eu^+, Dy^+, Ho^+, Er^+, Tm^+, Yb^+ and Lu although the product ion intensities were so small. This makes the basis for classification of REE into intermediate and less reactive groups. These reactions are likely to be termolecular with He acting as the third body (Koyanagi *et al.* 2009). Better intensities were obtained using 10 ng/ml solutions to identify such product ions which are reported later. These results are in accordance with Koyanagi *et al.* (2009) as shown in Figure 7.10 - Figure 7.19.

Koyanagi *et al.* (2009) demonstrate that the efficiency of formation of $REENH^+$ decreases as the energy required to promote an electron to make two non *f* electrons available for bonding increases. The periodic trend in reaction efficiency along REE is similar in a match with the periodic trend in electron promotion energy needed to achieve a d^1, s^1 or d^2 excited electronic configuration in REE cations. In case of most reactive REE i.e. La^+, Ce^+, Gd^+ and Tb^+ the electrostatic attraction between the atomic REE cation and ammonia is sufficiently strong to provide enough energy to achieve electron promotion and to overcome any barrier to subsequent N-H bond insertion and H_2 loss, but in case of other REE cations Pr, Nd, Sm, Eu, Dy, Ho, Er, Tm, Yb and Lu with which the collisional stabilisation of intermediate adduct ion predominates. The higher-order sequential addition of up to 6 NH_3 molecules was observed with the REE^+ that is given in Figure 7.6 - Figure 7.19. As the

interest of this study was to find a product ion with maximum intensity avoiding the overlap of interferences, therefore in coming sections, the focus will be more on interference removal capability.

The promotional energy (PE) of rare earth elements for first $5d^16s^1$ is given in Table 7.2. The PE of La, Ce, Gd and Tb to acquire $5d^16s^1$ electronic configuration is much lower than other REE^+. This explains the overall reactivity of rare earth elements with ammonia gas. Moreover, the electrostatic attraction between REE^+ and ammonia is relatively strong to provide the energy to achieve electron promotional energy for La^+, Ce^+, Gd^+ and Tb^+ with subsequent N-H bond insertion and H_2 elimination but this is not the case with other REE^+.

Table 7.2: Promotional energies (PE) of REE in kcal/mol

REE	Ground state E configuration	PE to first $5d^16s^1$ configuration
La^+	$5d^2$	4.5 ± 3.0
Ce^+	$4f^15d^2$	4.6 ± 5.7
Pr^+	$4f^36s^1$	22.3 ± 0.8
Nd^+	$4f^46s^1$	34.8± 8.3
Sm^+	$4f^66s^1$	62.1± 5.8
Eu^+	$4f^76s^1$	92.8 ± 5.0
Gd^+	$4f^75d^16s^1$	0
Tb^+	$4f^96s^1$	9.3 ± 8.1
Dy^+	$4f^{10}6s^1$	36.0± 6.1
Ho^+	$4f^{11}6s^1$	37.8± 5.4
Er^+	$4f^{12}6s^1$	34.5± 3.1
Tm^+	$4f^{13}6s^1$	55.5± 7.4
Yb^+	$4f^{14}6s^1$	79.4± 4.0
Lu^+	$4f^{14}6s^1$	36.6± 3.6

PE values from (Koyanagi and Bohme 2001)

The Figure 7.4 illustrates and confirms this experimental fact. NH_3 addition to other REE at flow rate 2 and 3 ml/min are given in Figure 7.3 and Figure 7.4. The PE for Eu is the highest 92.8 ± 5.0 and it presents lowest of reactivity at flow rate 2 ml/min somewhat similar conditions to the experiments of Koyanagi *et al.* (2009). Nevertheless, at a higher flow rate of 3 ml/min Tm, Yb, and Eu present the least reactivity.

So within the framework of Koyanagi, *et al*. (2009) scheme which shows Tm, Yb and Eu follow the least addition reaction in which bonding is relatively weak so as this study suggests from the evidence of the product ions. The other REE^+ show reactivity lesser than the reactivity of La, Ce, Gd and Tb and hence are categorised as intermediate to least reactive. For 3 ml/min gas flow rate of ammonia, Tm presents as the most unreactive analyte, which is probably due to the collisional stabilisation of, adduct ions at a higher flow rate.

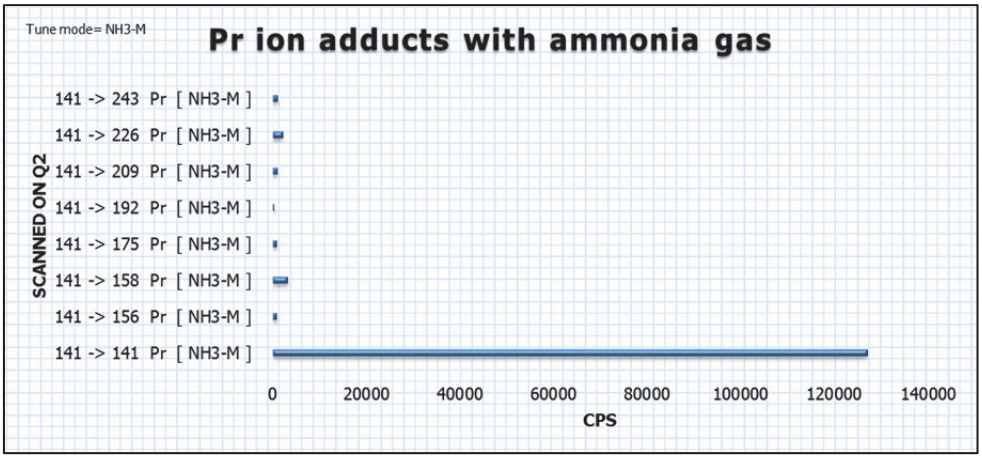

Figure 7.10: Scan of product ions of Pr

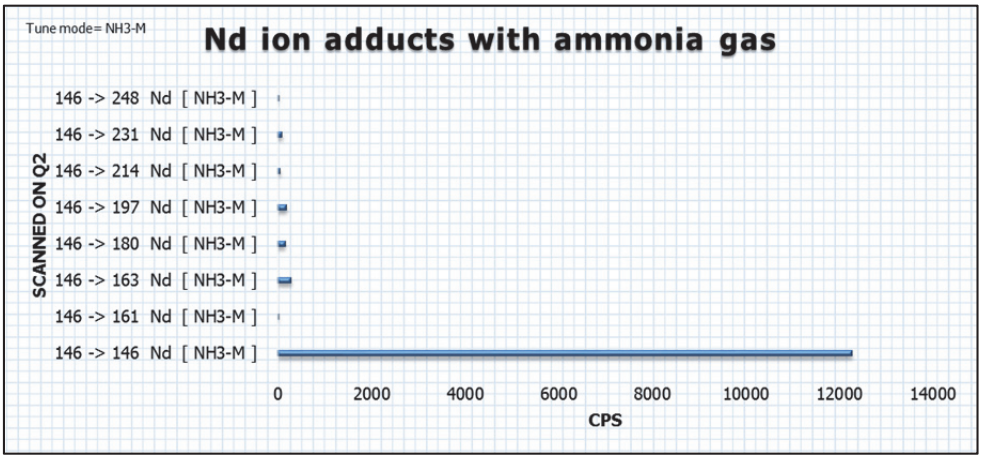

Figure 7.11: Scan of product ions of Nd

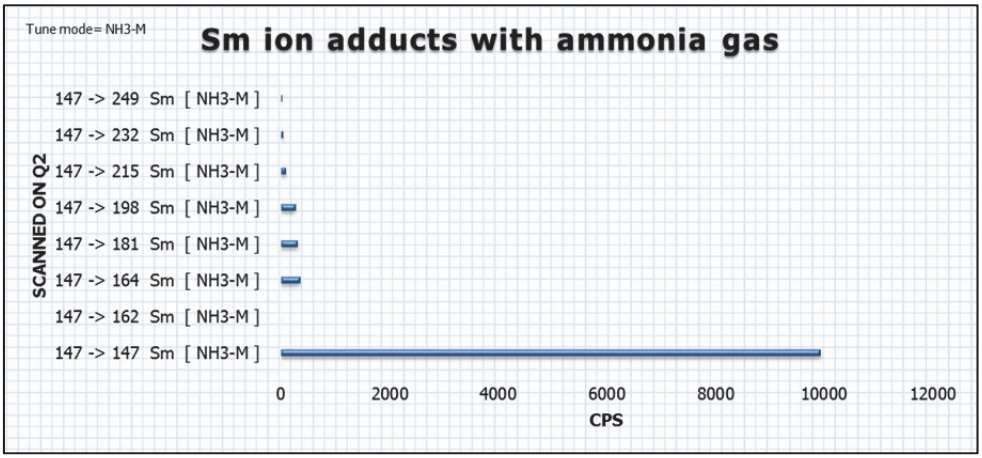

Figure 7.12: Scan of product ions of Sm

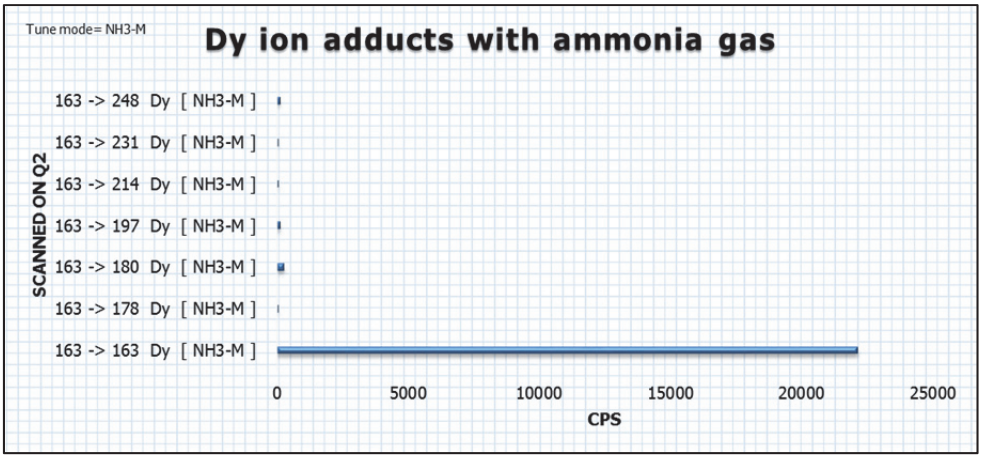

Figure 7.13: Scan of product ions of Dy

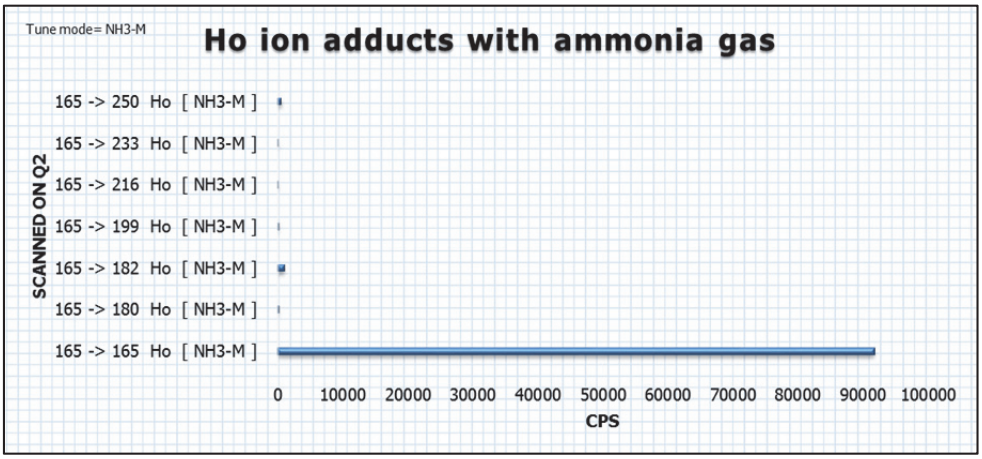

Figure 7.14: Scan of product ions of Ho

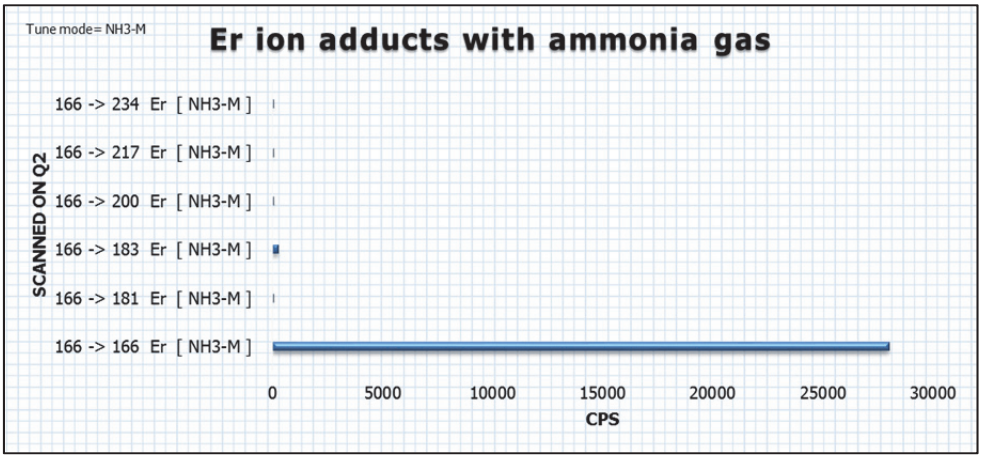

Figure 7.15: Scan of product ions of Er

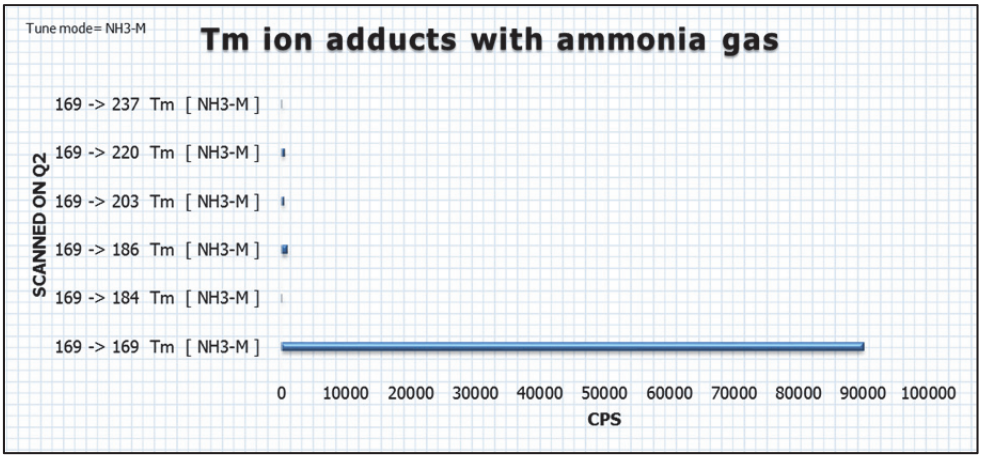

Figure 7.16: Scan of product ions of Tm

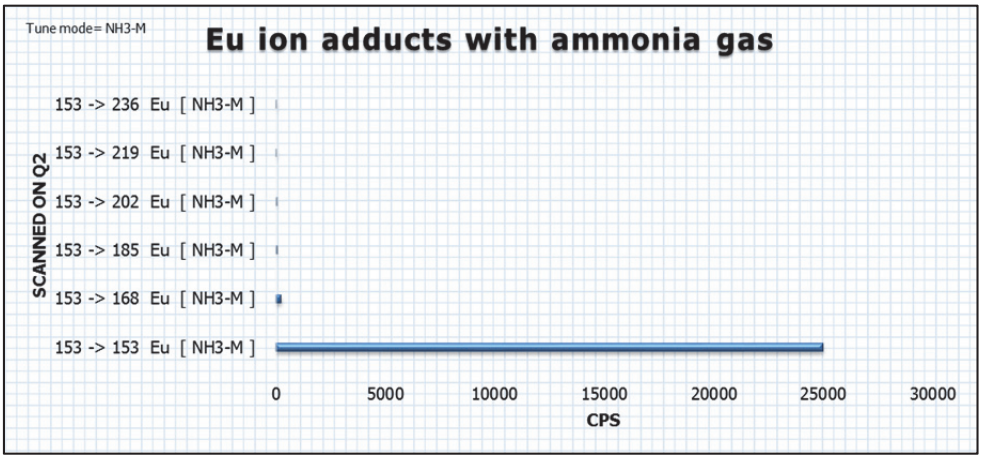

Figure 7.17: Scan of product ions of Eu

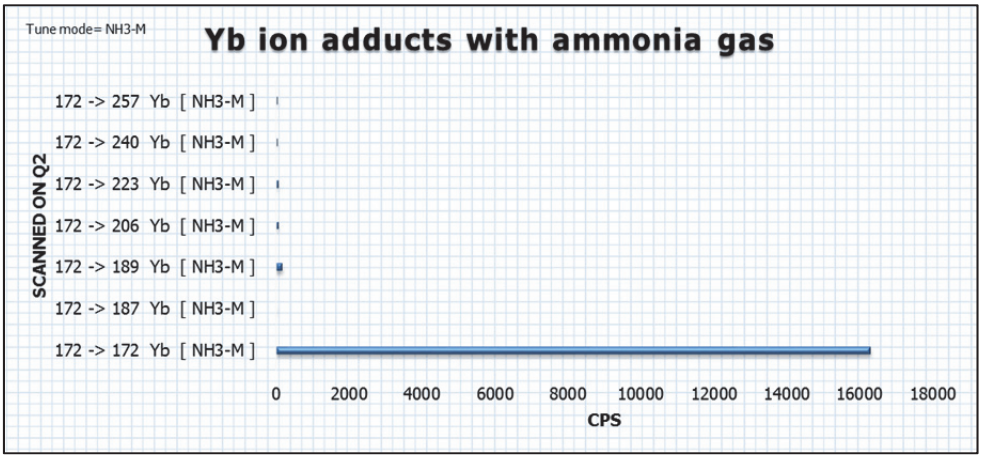

Figure 7.18: Scan of product ions of Yb

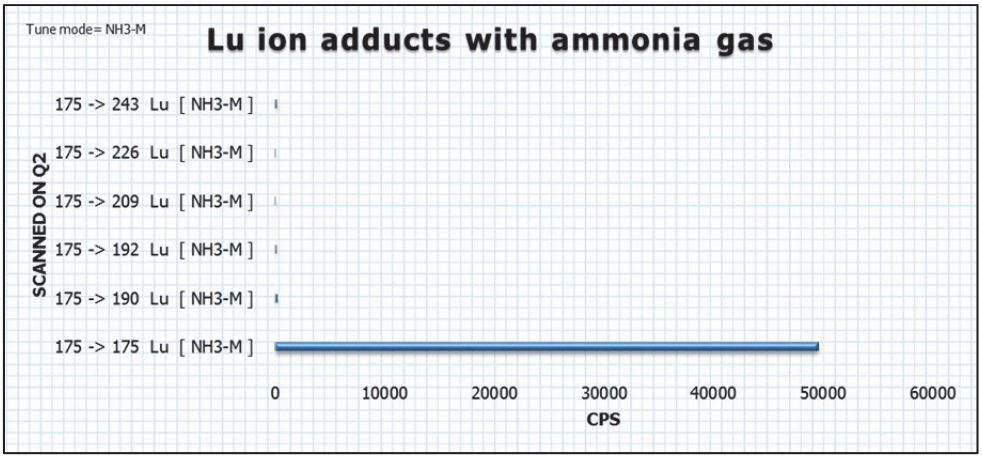

Figure 7.19: Scan of product ions of Lu

7.5 Reactivity of rare earth elements with O_2 gas

In this section, REE ion chemistry has been experimentally explored for periodic oxidation of REE cations using ICP-MS/MS collision/reaction cell technology. The formation of $REEO^+$ was achieved using O_2 gas to understand the periodic behaviour in reactivity and the influence of promotion energies on ease of reactions. The oxide formation requires a transition of an electron from $f^n d^0$ to $f^{n-1}d^1$. The main aim of these measurements was to remove spectral interferences on rare earth elements. 10 ng/ml final dilutions of standard REE solution were prepared with 1% HNO_3. REE^+ cations were produced with argon plasma and were allowed in an on-mass configuration of mass hunter workstation to pass through Q1 and CRC and then Q2. Oxygen gas was supplied at 0.3 ml/min flow rate. The purpose of keeping the on-mass configuration on mass hunter workstation was to check the behaviour of REE^+ cations in terms of increase or decrease in signal intensities. The results of this test are shown in Figure 7.20. The relative signal intensity refers to the ratio of intensity in on-mass oxygen mode to the intensity in no gas mode.

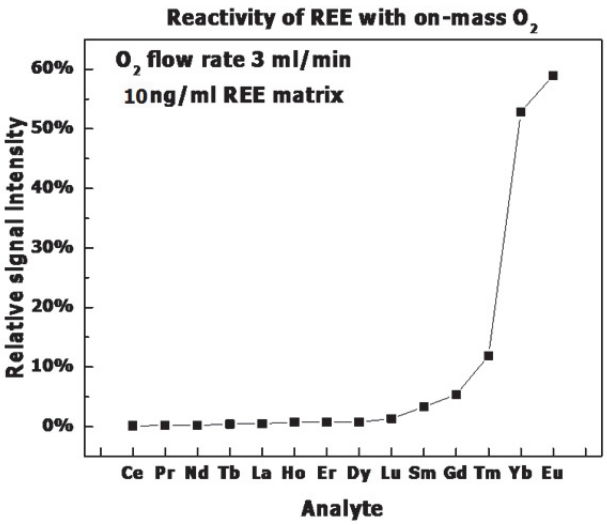

Figure 7.20: Reactivity of REE with O_2

Signal intensities of rare earth elements in on-mass O_2 mode relative to intensities in no gas mode are plotted in Figure 7.20. The reduced intensities of rare earth elements

reflect that most of the ions have reacted and converted to oxides, whereas the intensities of Eu and Yb in about 50-60% which show that conversion to oxides has not been so efficient. This is because enthalpy of reaction of Yb and Eu are higher than the rest of rare earth elements. ΔH_r for Ce is the lowest and therefore its oxide formation is the highest.

7.5.1 Explanation of reaction efficiencies

In an earlier study, reactivity of Ce^+ and Nd^+ with N_2O and O_2 has been measured Cornehl *et al.* (1997). Campbell (1999) has reported temperature-dependent rate coefficients for the gas-phase reactions of neutral lanthanide atoms with N_2O. A very comprehensive study of Koyanagi and Bohme (2001) has reported the oxidation reactions of REE^+ cations with N_2O and O_2. Gases with O donor atoms, as O_2 and H_2O, have often been found reactive towards REE^+ ions, but less selective than gases based on the softer N-donor atoms. A recent bonding configuration analysis by Gibson (2003) suggests that two unpaired 5d valence electrons bring about the bonding between the metal centre and oxygen atom ($REEO^+$) instead of 5d and 6s. There are two main reaction mechanisms associated with the use of oxygen in the collision/reaction cell:

O-atom transfer or oxygen atom abstraction

In this case, oxygen is abstracted by analyte ion leading to formation of an oxide ion which can be symbolised by equation below;

$$\mathbf{X^+ + O_2 \rightarrow XO^+ + O, \quad \Delta H_r = D\,(O_2) - D\,(X^+ - O)} \qquad \mathbf{(A)}$$

- X^+ is the analyte ion,
- XO^+ is the oxide ion formed,
- ΔH_r is the enthalpy of reaction,
- $D(O_2)$ is the bond dissociation energy of O_2,
- $D(X^+\text{-}O)$ is the bonding energy of the product ion (O_2).

Charge transfer or electron transfer

In the case of charge transfer reactions, one of the electrons of the O_2 molecule is transferred to the reactant ion X^+, resulting in its reduction and formation of neutral X as shown in the equation below.

$$\mathbf{X^+ + O_2 \rightarrow X + O_2^+, \Delta H_r = IE\,(O_2) - IE(X)} \qquad \mathbf{(B)}$$

- $IE(O_2)$ = ionisation energy of oxygen molecule,
- IE(X) = ionisation energy of analyte atom,
- ΔH_r is the enthalpy of reaction.

The reactions of REE^+ with O_2 generally exhibited with O-atom transfer or oxygen atom abstraction reactions as suggested in Koyanagi and Bohme (2001) as given in equation (A). For knowing the thermodynamic properties of these reactions it is important to consider oxygen affinity to REE. The oxygen affinities based on literature are given in Table 7.3. Most of the O-atom-transfer reactions of the REE^+ cations with O_2 are thermodynamically allowed as higher the oxygen atom affinities higher is the chances for the formation of an oxide. These range from 88.1 ± 5.9 for Yb^+ to 206.6 ± 3.4 for La^+. The oxygen atom affinity for oxygen is 119.1± 0.1 kcal/mol (Koyanagi and Bohme 2001). This relates to the enthalpy of reaction. All REE^+ have positive affinities for O atoms and are summarised in Table 7.3.

Table 7.3: Oxygen atom affinities with REE

REE	Ground state E config	Oxygen Atom Affinities (kcal/mol)
La^+	$5d^2$	206.6 ± 3.4
Ce^+	$4f^15d^2$	203.6 ± 5.9
Pr^+	$4f^36s^1$	189.6 ± 4.3
Nd^+	$4f^46s^1$	180.8 ± 4.3
Sm^+	$4f^66s^1$	139.6 ± 4.3
Eu^+	$4f^76s^1$	93.2 ± 4.3
Gd^+	$4f^75d^16s^1$	180.0 ± 4.3
Tb^+	$4f^96s^1$	171.0 ± 5.9
Dy^+	$4f^{10}6s^1$	143.4 ± 5.9
Ho^+	$4f^{11}6s^1$	141.3 ± 5.9
Er^+	$4f^{12}6s^1$	140.3 ± 5.9
Tm^+	$4f^{13}6s^1$	116.6 ± 5.9
Yb^+	$4f^{14}6s^1$	88.1 ± 5.9
Lu^+	$4f^{14}6s^1$	128.0 ± 5.9

*Data for oxygen atom affinities with REE from Koyanagi and Bohme (2001), Lias (1988), Murad and Hildenbrand (1980).

The chemistry of ion-molecule reactions in collision/reaction cell is based on properties of both reactants and products. As there is no activation energy barrier in such reactions, therefore ΔH_r is the deciding factor for a reaction to proceed and for its efficiency. Enthalpy of reaction ΔH_r is the heat absorbed or evolved during the reaction. For an exothermic reaction ΔH_r is negative and for endothermic it is positive. Exothermic reactions are spontaneous with the release of energy and occur more rapidly than endothermic reactions where heat has to be absorbed to cross the energy barrier for activation and which may not occur at all. ΔH_r can be calculated from the bond energies and ionisation energies of reactants and products. For the O-atom transfer reaction, ΔH_r is the difference between the bond (binding) energy of the O_2 molecule and that of the product ion XO^+, which are expressed as $D(O_2)$ and $D(X^+\text{-}O)$ respectively.

For example, bond dissociation energy of O_2 molecule is 5.1 eV. During a collision with X^+ ion, if electron affinity of O_2 is more towards X^+ ion, a new bond is formed as X-O. If bond dissociation energy of the new bond (endothermic) is more than the bond formation (exothermic) then the reaction would proceed rapidly (Agilent-Notes. 2012). Efficient oxide ion formation is expected in the O_2 mode for the ions that go through exothermic O-atom transfer reactions. Enthalpy of the reaction of rare earth elements with their oxides are shown in Table 7.4.

Table 7.4: Enthalpy of reaction of rare earth elements (from Agilent-notes 2012)

Analyte	Mass number	Product ion	Bond dissociation energy (X-O)	Enthalpy of reaction (ΔHr)
X^+	amu	(X-O)	(eV)	(eV)
Ce^+	140	CeO^+	8.30	-3.20
La^+	139	LaO^+	8.23	-3.13
Pr^+	141	PrO^+	8.23	-3.13
Nd^+	146	NdO^+	7.76	-2.66
Gd^+	157	GdO^+	7.47	-2.37
Tb^+	159	TbO^+	7.33	-2.33
Ho^+	165	HoO^+	6.24	-1.14
Dy^+	163	DyO^+	6.11	-1.01
Er^+	166	ErO^+	5.96	-0.86
Sm^+	147	SmO^+	5.80	-0.70
Lu^+	175	LuO^+	5.34	-0.24
Tm^+	169	TmO^+	4.92	0.18
Eu^+	153	EuO^+	4.00	1.10
Yb^+	172	YbO^+	3.87	1.23

The order of reactivity based on collision/reaction cell and as from Figure 7.20 is given as

Ce>Pr>Nd>Tb>Ce>Ho>Er>Dy>Lu>Sm>Gd>Tm>Yb>Eu

All rare earth elements tend to make oxides efficiently except Yb and Eu where the oxide formation is 10-15% as shown in Figure 7.21. Figure 7.21 shows the intensities of product ions (oxides) which reflect that the lower the enthalpy of reaction, the higher is the formation of oxides and vice versa. Namely, most REE^+ ions (Ce^+, Ce^+, Pr^+, Nd^+, Sm^+, Gd^+, Tb^+, Dy^+, Ho^+, Er^+ and Lu^+) are very reactive with O_2 (giving $REEO^+$) except for three of them: Eu^+, Tm^+ and Yb^+ as suggested also in Koyanagi and Bohme (2001).

For Eu^+, Tm^+ and Yb^+ the enthalpies of reactions are 1.10, 0.18, 1.23 eV respectively which are endothermic so a slow reaction is expected. But for the rest of other REE fast reactions are expected as they are exothermic as shown in Table 7.4.

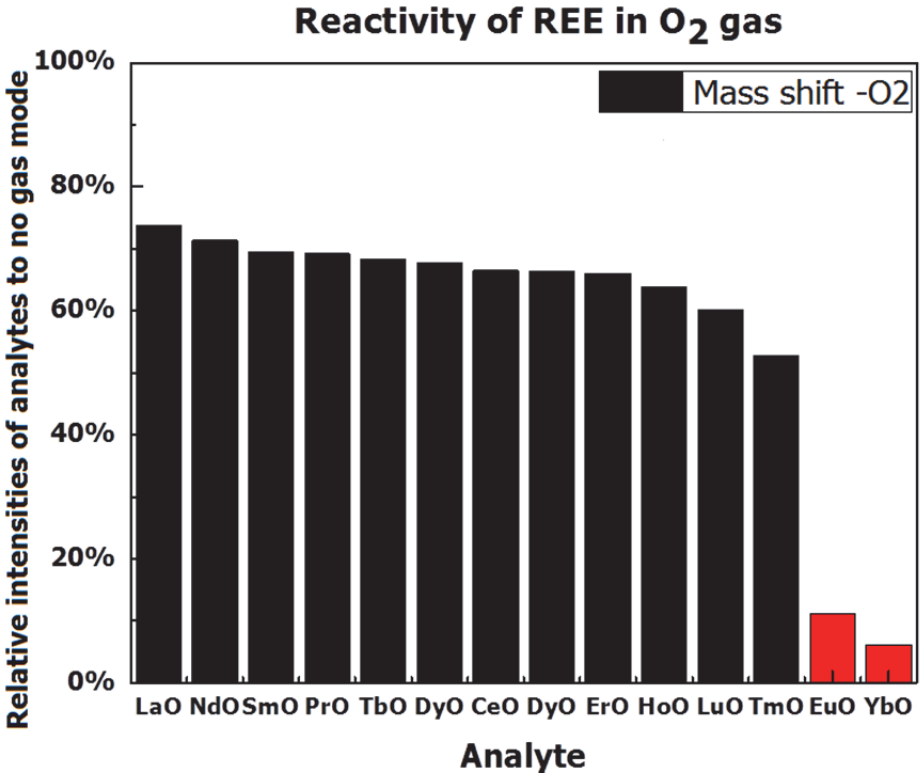

Figure 7.21: Relative intensity of oxide ion, all REE make oxides. Eu and Yb show better intensities in on-mass O_2 mode

7.6 Method development based on reactivity with NH_3 and O_2

Based on reactivity data of rare earth elements with NH_3 and O_2, a method can be developed with the underlying principle that some REE do not react efficiently with NH_3 / O_2 while others do. Interference removal capability with mass-shift O_2 may not be very successful because all REE with the exception of Eu and Yb are reacting efficiently and corresponding oxide shift will still be interference on HREE. However, following methods can be applied to see the effect on interferences for removal which are given as follows:

1. Mass-shift O_2 method
2. On-mass NH_3 and mass-shift NH_3 method
3. Mass-shift NH_3 and mass-shift O_2 method

4. On-mass NH_3 and mass-shift O_2 method

7.6.1 Mass-shift O_2 method

All the REE react with cell gas O_2 to form REE-O. In O_2 mass-shift mode, all 13 REE can be detected as their REE-O^+ reaction product ions at 16 a.m.u higher than the original elemental mass (M+16). This reaction chemistry can be applied to CRC of conventional quadrupole ICP-MS (ICP-QMS), but in practice, the reaction chemistry is not consistent enough for routine analysis of real samples.

In ICP-QMS, all of the ions produced in the plasma are able to enter the reaction cell, so the other analyte ions or cell-formed reaction product ions may overlap with the analyte ion of interest. For example, in the case of Dy measured as $^{163}Dy^{16}O^+$ using O_2 mass-shift mode, $^{146}Nd^+$ also reacts with the O_2 cell gas to form $^{146}Nd^{16}O_2{}^1H^+$ that would overlap the $^{163}Dy^{16}O^+$ product ion at m/z 179. Furthermore, hafnium has a natural isotope at m/z 179 which could also overlap the target product ion (Juane *et al.* 2015).

To avoid the formation of the overlapping $NdOH^+$ product ion, the precursor ion $^{146}Nd^+$ (and any native ions such as Hf^+ that would appear at the analyte product ion mass) must be removed before they enter the reaction cell; this can only be achieved with MS/MS mode on the ICP-QQQ-MS. In MS/MS mode, the first quadrupole (Q1) operates as a single a.m.u. mass filter so that only ions with the targeted m/z enter the reaction cell and can react with the cell gas. All other masses are rejected by Q1, so they are not able to pass through the cell or undergo the reactions that would lead to interfering product ions. When REE-oxides have to be measured with the other analytes for routine analysis following setup should be created in mass hunter workstation for the accurate determination of analytes (See Table 7.5). The shaded are restricted masses which should not be allowed to enter through Q1.

Table 7.5: Setup for REE-oxide measurement

Table showing the possible overlaps on the product ions

Analyte	Q1 (m/z)	Q2 (m/z)	Must be rejected at Q1
Eu	151	167	No overlap
Eu	153	169	No overlap
Gd	157	173	No overlap
Tb	159	175	^{175}Lu overlap
Dy	163	179	^{179}Hf overlap
Ho	165	181	^{181}Ta overlap
Tm	166	182	^{182}W overlap
Yb	172	188	^{188}Os overlap
Lu	175	191	^{191}Ir overlap
Hf	179		overlap on DyO^+
Ta	181		overlap on HoO^+
W	182		overlap on TmO^+
Os	188		overlap on YbO^+
Ir	191		overlap on DyO^+

7.6.1.1 Study of interference removal with mass-shift oxide formation in O_2

Pure standard solutions of REE were prepared with final dilution to contain 10 ng/ml matrix in 1% HNO_3. Each solution of REE was then measured in such a way that Q1 was set to original mass (m/z) of REE and Q2 was set to the new mass of an oxide (amu+16) e.g. $^{139}La^+$ at Q1 and $^{139}La^{16}O^+$ at Q2. The spray chamber etc. was rinsed with 1% HNO_3 prior to analysis. Following oxide shifts were tested and listed below in Table 7.6.

Table 7.6: Mass-shift oxygen product ions

	Scan mode	
	Single quad	**MS/MS**
Gas mode	**No gas**	**Mass-shift O_2**
Mass filter	**Q1**	**Q2**
m/z	**amu**	**amu+16**
La	139	139 -> 155 La [O_2]
Ce	140	140 -> 156 Ce [O_2]
Pr	141	141 -> 157 Pr [O_2]
Nd	146	146 -> 162 Nd [O_2]
Sm	147	147 -> 163 Sm [O_2]
Eu	151	151 -> 167 Eu [O_2]
Eu	153	153 -> 169 Eu [O_2]
Gd	157	157 -> 173 Gd [O_2]
Tb	159	159 -> 175 Tb [O_2]
Dy	160	160-> 176 Dy [O_2]
Dy	163	163 -> 179 Dy [O_2]
Ho	165	165 -> 181 Ho [O_2]
Er	166	166 -> 182 Er [O_2]
Tm	169	169 -> 181 Tm [O_2]
Yb	172	172 -> 188 Yb [O_2]
Lu	175	175 -> 191 Lu [O_2]

The relative intensities (%) of interferences i.e. $^{140}Ce^{16}OH^+$ on $^{157}Gd^+$, $^{148\text{-}149\text{-}150}Sm^{16}O^+$ on $^{165}Ho^+$, $^{163}Dy^+$ and $^{166}Er^+$, $^{139}LaH^+$ on $^{140}Ce^+$, $^{143\text{-}150}Nd^{16}O^+$ on $^{153}Tb^+$ and $^{166}Er^+$, $^{141}Pr^{16}O^+$ on $^{157}Gd^+$ and $^{157}Gd^{16}O^+$ on $^{173}Yb^+$ are plotted in no gas mode and oxide shift modes in Figure 7.22. Background equivalent concentrations (BEC) refer to the ratio intensity of interference on particular m/z of the analyte to the intensity of the analyte of interest at its m/z in no gas mode.

In no gas mode 10 ng/ml solution of $^{157}Gd^+$ creates the highest background equivalent concentrations (BEC) on $^{173}Yb^+$ which is 3.5-4%. In mass-shift oxygen mode of 172 -> 188 Yb [O2] the interference of $^{157}Gd^{16}O^+$ is reduced to 0.04% but not completely. Same is the case for $^{139}LaH^+$ and $^{140}Ce^{16}OH^+$ where the interferences still exist on product ion of REE in shift mode. This can be problematic when a higher concentration of REE has to be measured and oxide shift would carry an additional intensity of the interferences. This can be due to the fact that some REE tend to make oxide in plasma and enter in Q1 as an oxide e.g. $^{157}Gd^+$ in plasma is oxidised and enters the Q1 as GdO^+ equivalent to the m/z of $^{173}Yb^+$. $^{157}Gd^{16}O^+$ is further oxidised to $^{157}Gd^{16}O_2^+$ although there is extreme drop in its intensity at m/z of $^{173}Yb^{16}O^+$. A similar phenomenon has been reported for Ti measurement in blood

serum where O_2 shift was not helpful in removing the interferences on Ti (Balcaen *et al.* 2014). However, other interferences i.e. $^{148\text{-}149\text{-}150}Sm^{16}O^+$, $^{141}Pr^{16}O^+$, $^{143\text{-}150}Nd^{16}O^+$ and $^{159}Tb^{16}O^+$ etc. are minimised. In general, with O_2 shift mode the interfering REE ions are reduced to less than 0.02% except $^{139}LaH^+$ on $^{140}Ce^+$, $^{157}Gd^{16}O^+$ on Yb^+ and $^{140}Ce^{16}OH^+$ on $^{173}Yb^+$.

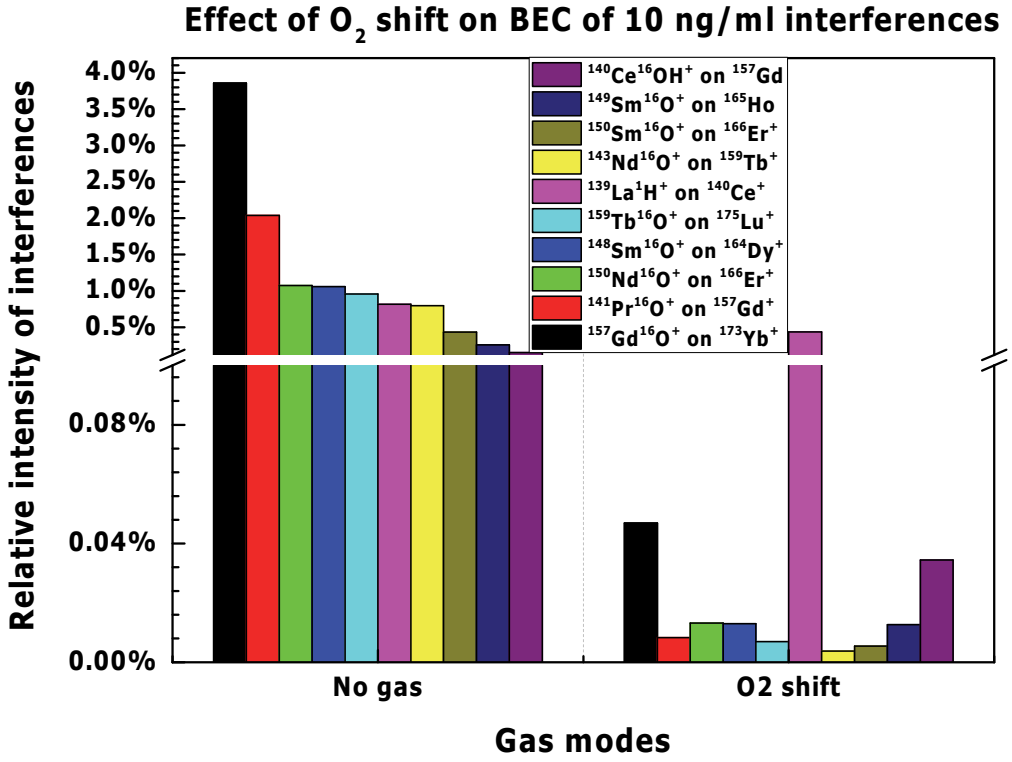

Figure 7.22: BEC created by 10 ng/ml interferences on analytes and effect of O_2 shift mode

7.6.2 Study of interference removal with on-mass and mass-shift NH_3

As shown in the earlier section of the chapter, REE were classified into three categories based on their reactivity with NH_3 i.e. most reactive (Ce, La, Gd and Tb) intermediate (Lu, Pr, Sm and Nd) and least reactive REE (Dy, Er, Ho, Eu, Yb and Tm). For the investigation of the effect of the ammonia gas in removal of oxides and hydride interferences, different flow rates i.e. 2, 3 and 5 ml/min were tested with on-mass and different mass-shift modes of REE as shown in Figure 7.23.

It was not possible to show all the on-mass and mass-shift modes with ammonia gas in Figure 7.23, thus the label in the plot (on-mass and mass-shift mode NH_3 gas modes) is used to represent on-mass and mass-shifts of all kind which will be discussed later with individual interference removal of REE.

Figure 7.23 shows that NH_3 gas (on-mass and mass-shifts of all kind applied) is effective in eliminating the interferences e.g. $^{157}Gd^{16}O^+$, $^{141}Pr^{16}O^+$, $^{150}Nd^{16}O^+$, $^{150}Sm^{16}O^+$, $^{139}LaH^+$, $^{140}Ce^{16}OH^+$ and $^{159}Tb^{16}O^+$ etc. All these interferences are removed or turned down to a minimum value with either of on-mass or mass-shift modes of ammonia. For the reactive REE with NH_3 gas, all the possible product ions were tested for removal of interferences. Only the significant mass-shifts NH_3 with better intensities are discussed in this section.

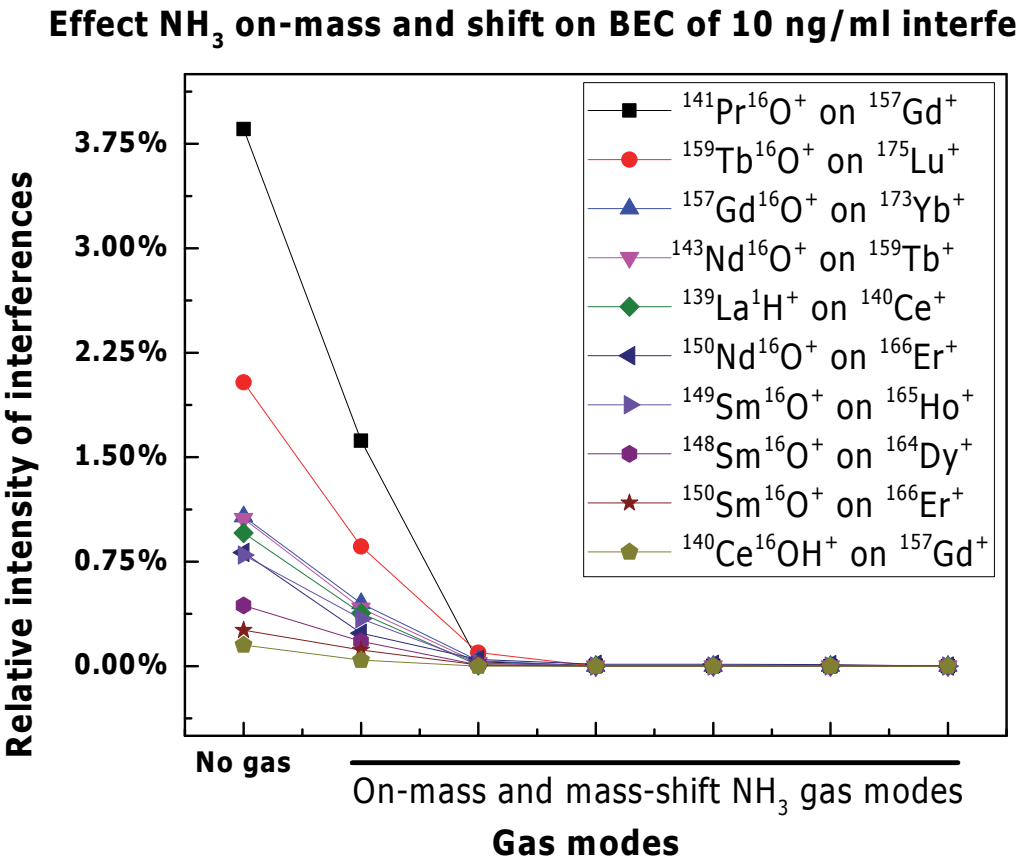

Figure 7.23: BEC created by 10 ng/ml interferences on analytes and effect of NH_3 modes

7.6.3 Mass-shift-NH_3 and mass-shift O_2 method

For the REE that react efficiently with NH_3 gas (*La, Ce, Gd, Tb, Pr* and *Nd*), NH_3 cell gas can be used with a mass-shift mode, where the target REE element is measured as its reaction product ion.

Removal of REE interferences with mass-shift NH_3 and mass-shift O_2

1. Interference of $^{139}LaH^+$ on $^{140}Ce^+$
2. Interference of $^{141}Pr^{16}O^+$ and $^{140}Ce^{16}OH^+$ on $^{157}Gd^+$
3. Interference of $^{142}Ce^{16}OH^+$, $^{143}Nd^{16}O^+$, $^{142}Nd^{16}OH^+$, and $^{158}GdH^+$ on $^{159}Tb^+$
4. Interference of $^{157}Gd^{16}O^+$ on $^{173}Yb^+$

$^{139}La^1H$ interferences on ^{140}Ce

$^{139}La^+$ produces $^{139}La^1H^+$ at m/z=140 which is the m/z of $^{140}Ce^+$. Figure 7.22 and Figure 7.23 show the false background equivalent concentrations of $^{140}Ce^+$ induced by La^+ in no gas mode. As La^+ and Ce^+ are both reactive to NH_3 gas, with on mass-NH_3 in flow rate of 2-3 ml/min interference is not removed although Ce intensity is significantly decreased as shown in Table 7.7. Oxygen mass-shift does not remove the interference at all. 140 -> 155 Ce [NH3-M] and 140 -> 225 Ce [NH3-M] can be the best compromise for measurement.

Table 7.7: Selection of gas modes for removal LaH^+ interference on Ce^+

Product ions	$^{140}Ce^+$ (intensity)	$^{139}LaH^+$ (intensity)
140 Ce [No Gas]	409771	3345
140 -> 140 Ce [NH3-L]	121738	968
140 -> 140 Ce [NH3-M]	3628	42
140 -> 155 Ce [NH3-L]	24121	198
140 -> 155 Ce [NH3-M]	5977	54
140 -> 156 Ce [O2]	227525	1789
140 -> 225 Ce [NH3-L]	148	1
140 -> 225 Ce [NH3-M]	7000	58

The suggested gas mode for removal of $^{139}LaH^+$ interference on $^{140}Ce^+$ (although there was no improvement in the ratio of the intensity of the interferences to analytes) are

140 -> 155 Ce [NH3-L] and 140 -> 225 Ce [NH3-M].

Interferences of $^{141}Pr^{16}O^+$ and $^{140}Ce^{16}O^1H^+$ on $^{157}Gd^+$

$^{157}Gd^+$ is expected to have $^{141}Pr^{16}O^+$ and $^{140}Ce^{16}O^1H^+$ interferences in the ICP-MS spectra. The intensities of each interference at Q1 on m/z=157 and mass-shifts with NH_3 are given in Table 7.8.

Table 7.8: Selection of gas modes for removal of $^{157}Pr^{16}O^+$ and $^{140}Ce^{16}OH^+$ interference on $^{157}Gd^+$

Product ions	$^{157}Gd^+$ (intensity)	$^{141}Pr^{16}O^+$ (intensity)	$^{140}Ce^{16}O^1H^+$ (intensity)
157 Gd [No Gas]	392068	7990	596
157 -> 173 Gd [O2]	223971	33	135
157 -> 157 Gd [NH3-L]	133280	3366	170
157 -> 172 Gd [NH3-L]	15217	0	3
157 -> 242 Gd [NH3-M]	7364	0	3
157 -> 172 Gd [NH3-M]	4175	0	0
157 -> 157 Gd [NH3-M]	3366	381	0
157 -> 242 Gd [NH3-L]	154	0	0

$^{141}Pr^+$ forms an oxide $^{141}Pr^{16}O^+$ in the ICP-MS spectrum, which overlaps with the original intensities of $^{157}Gd^+$, as a result, the intensities of Gd^+ are enhanced on its m/z giving a false estimation of its concentration. The plot for the interference of $^{141}Pr^{16}O^+$ on $^{157}Gd^+$ is given in Figure 7.22 and Figure 7.23. There is a difference in reactivity of both the analyte and the interference with NH_3 cell gas which can be of an advantage in removing $^{141}Pr^{16}O^+$ on $^{157}Gd^+$. $^{141}Pr^{16}O^+$ interference is removed with mass-shift NH_3 method by making a cluster of Gd(NH). A second approach is to apply mass-shift-O_2 method which is better than mass-shift NH_3 method due to the intensities. By shifting the product ion of Gd^+ at Q2 at m/z 173 ($^{157}Gd^{16}O^+$), the interference from $^{141}Pr^{16}O^+$ can be significantly removed relative

to the intensities of $^{157}Gd^{+}$ as shown in Figure 7.24. $^{140}Ce^{16}O^{1}H^{+}$ interference is best removed with the mass-shift ammonia mode because in O_2 mass-shift mode $^{140}Ce^{16}O^{1}H^{+}$ formation is favoured.

The intensities in O_2 shift mode are up to 60% relative to intensity in no gas mode as indicated by point 2 in Figure 7.24. The on-mass measurement with oxygen is creating 45% more interference which is an evidence that $^{141}Pr^{+}$ is oxidised to $^{141}Pr^{16}O^{+}$ creating an interference on $^{157}Gd^{+}$. The best removal of interferences are at point 2, 3 and 4 as shown in Figure 7.24. The suggested gas modes for removal $^{141}Pr^{16}O^{+}$ and $^{140}Ce^{16}O^{1}H^{+}$ interferences on $^{157}Gd^{+}$ are

157 -> 172 Gd [NH3-L] and 157 -> 173 Gd [O2].

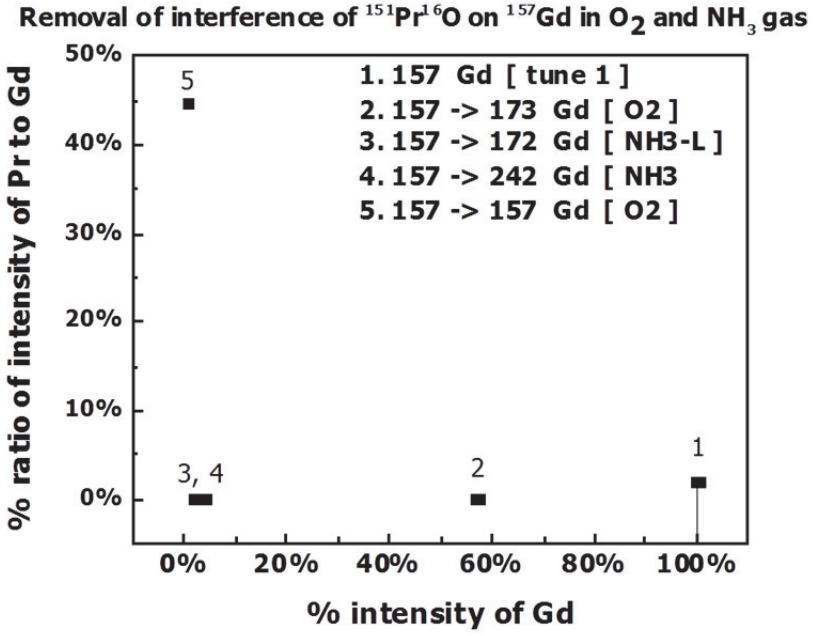

Figure 7.24: Removal of PrO^{+} interference on Gd^{+}

Interferences of $^{143}Nd^{16}O^{+}$ on $^{159}Tb^{+}$

The interference of Nd^{+} in terms of intensities of $^{143}Nd^{16}O^{+}$ are given below in Table 7.9.

Table 7.9: Selection of gas modes for removal of $^{143}Nd^{16}O^{+}$ interferences on $^{159}Tb^{+}$

Product ions	$^{159}Tb^{+}$ (intensity)	$^{143}Nd^{16}O^{+}$ (intensity)
159 Tb [No Gas]	538249	4293
159 -> 175 Tb [O2]	305373	20
159 -> 159 Tb [NH3-L]	192107	1830
159 -> 174 Tb [NH3-L]	15941	0
159 -> 159 Tb [NH3-M]	9485	122
159 -> 244 Tb [NH3-M]	9142	0
159 -> 174 Tb [NH3-M]	3116	0
159 -> 244 Tb [NH3-L]	178	0

$^{143}Nd^{+}$, $^{142}Nd^{+}$ forms $^{143}Nd^{16}O^{+}$ and $^{142}Nd^{16}O^{1}H^{+}$ on $^{159}Tb^{+}$. The % interferences of Nd^{+} are shown in Figure 7.22 and Figure 7.23. Tb^{+} is more reactive to NH_3 and less reactive to O_2 than Nd^{+}. Based on better reactivity of Tb than Nd, it is possible to remove interference of Nd^{+} by shifting its m/z to a m/z of new product ion on Q2 which lets the Nd^{+} out of the mass filter. Terbium makes a cluster of ions with NH_3 as $TbNH^{+}$ (Q1 + 15 m/z) 159 -> 174 Tb [NH3-L] and at (Q1 + 85 m/z) 159 -> 244 Tb [NH_3-M]. The intensity of $TbNH^{+}$ is better than the 159 -> 244 Tb. Therefore, $TbNH^{+}$ (at Q1 + 15 m/z) i.e. 159 -> 174 Tb [NH3-L] is the best options for complete removal of interference.

On the other hand, the reactivity of Tb^{+} towards O_2 is lesser than Nd^{+}. Keeping on-mass Tb^{+} measurement in O_2 does not help Nd removal and the situation gets worse. The only possibility is by shifting the Tb^{+} mass to a new product ion mass at Q2 as TbO^{+}. Few counts of Nd are still present but the intensity of TbO^{+} relative to interference is about 60-70% than the intensity of Tb^{+} ammonia clusters as shown in Figure 7.25.

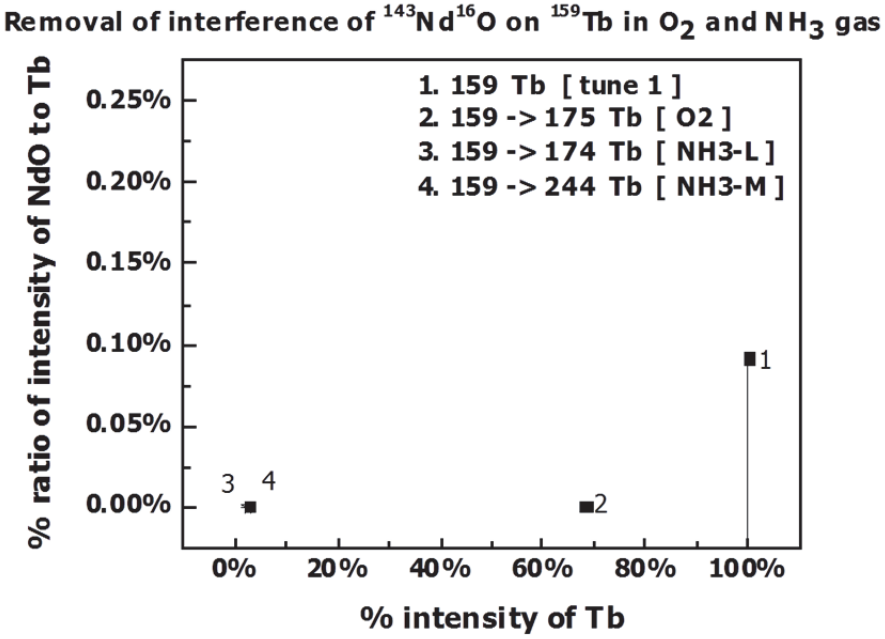

Figure 7.25: Removal of Nd interferences on Tb

It is important to note that some oxidised ions = 159 can also enter Q1 that can further oxidise at Q2 in O_2 shift mode creating some interferences on Tb^{+} even on the new mass of the product ion and O_2 shift mode may or may not be good depending upon the amount of interfering species oxidising at Q1. However, the suggested modes are given as under;

159 -> 174 Tb [NH3-L] and 159 -> 175 Tb [O2]

7.6.4 Product ion scan of $^{159}Tb^{+}$ at Q2

To find the suitable ammonia cluster product ion for Tb^{+}, a 10 ng/ml solution of Tb was introduced into ICP-MS/MS and a product ion scan was performed. Q1 was set to m/z 159 that would allow only ions of Tb^{+} to enter the cell. Q2 was scanned for over a selected range of masses to find the product ion formed in the cell with NH_3 cell gas in the collision/reaction cell. An additional scan of $^{159}Tb^{16}O^{+}$ is also presented to compare the intensities. The scan of the product is shown in Figure 7.26. The scan shows that 159 -> 174 Tb [NH3-L] and 159 -> 244 Tb [NH3-M] clusters have better intensities as well the

lowest interferences. Similar facts have been reported in Juane *et al.* (2015). A similar strategy was applied for selection of appropriate shift modes with better intensities and lowest interferences for all the other REE.

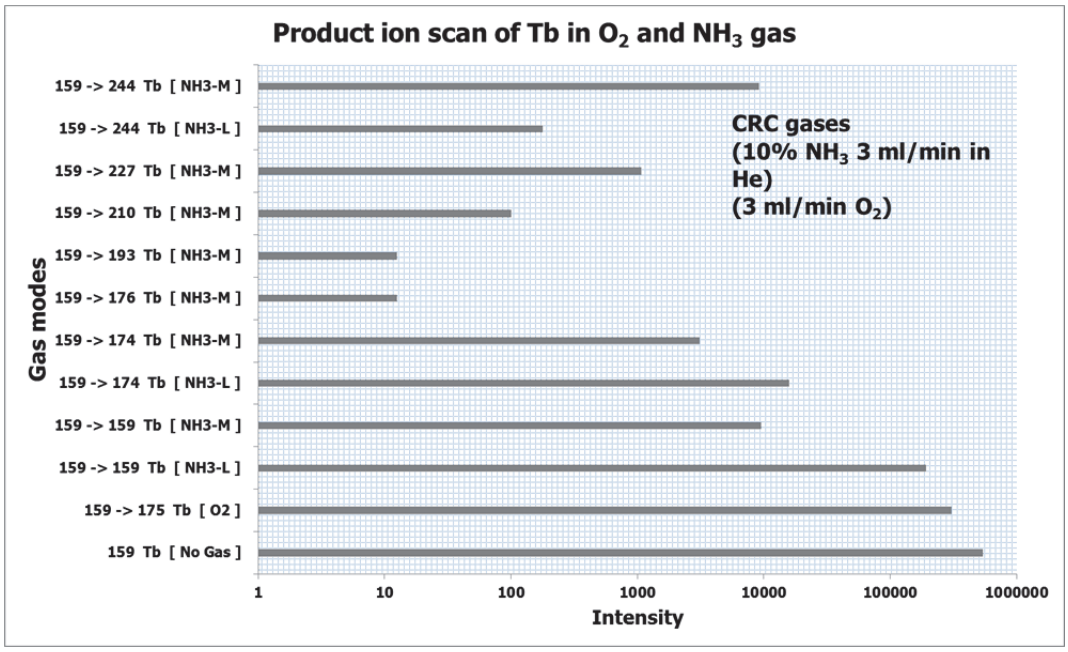

Figure 7.26: Product ion scan of Tb on Q2

Interference of $^{157}Gd^{16}O^+$ on $^{173}Yb^+$

The intensities at m/z=173 of $^{173}Yb^+$ and intensities of interference of $^{157}Gd^{16}O^+$ at m/z=173 are given in Table 7.10.

Table 7.10: Selection of gas modes for removal of $^{157}Gd^{16}O^+$ interference on $^{173}Yb^+$

Product ions	$^{173}Yb^+$ intensity	$^{157}Gd^{16}O^+$ intensity
172 Yb [No Gas]	392068	4452
172 -> 172 Yb [NH3-L]	133280	1869
172 -> 188 Yb [O2]	223971	54
172 -> 172 Yb [NH3-M]	3366	38
172 -> 257 Yb [NH3-M]	7364	3
172 -> 257 Yb [NH3-L]	154	2
172 -> 187 Yb [NH3-L]	15217	0
172 -> 187 Yb [NH3-M]	4175	0

Gd^+ is more reactive than Yb^+ to NH_3 gas and Yb^+ is less reactive to O_2 than Gd^+. Apparently on-mass NH_3 method should remove all $^{157}Gd^{16}O^+$ interferences but the intensity with on-mass NH_3 method is very low with the flow rate of 2-3 ml/min of NH_3 gas. The intensity for 172 -> 187 Yb [NH3-L] is much better than on-mass NH_3 method with the lowest BECs of $^{157}Gd^{16}O^+$ interferences as shown in the Table 7.10. 172 -> 188 Yb [O2] is also better with excellent intensities and lowest BECs of $^{157}Gd^{16}O^+$.

Therefore, the suggested product ions are as under;

172 -> 188 Yb [O2] and 172 -> 187 Yb [NH3-L]

7.6.5 On-mass NH_3 and mass-shift O_2 method

Lanthanum, Ce, Gd, Tb, are more reactive group of rare earth elements to the NH_3 gas and *Er, Dy, Ho, Yb, Tm, Lu, Sm, Eu* are less reactive to NH_3 gas. The interferences of *La, Ce, Gd, Tb, Pr, Nd* on *Er, Dy, Ho, Yb, Tm, Lu, Sm, Eu* (oxide interferences) can be removed at a constant flow rate of NH_3 gas in reaction cell and letting *La, Ce, Gd, Tb, Pr* and *Nd* to react with NH_3 with the on-mass NH_3 mode. *La, Ce, Gd, Tb, Pr and Nd* make new product ions and interference free quantification of REE will be possible in an on mass-NH_3 method.

1. $^{147}Sm^{16}O^+$ interference on $^{163}Dy^+$
2. $^{149}Sm^{16}O^+$ interference on $^{165}Ho^+$
3. $^{150}Nd^{16}O^+$ and $^{150}Sm^{16}O^+$ interference on $^{165}Er^+$
4. $^{159}Tb^{16}O^+$ interference on $^{175}Lu^+$

$^{147}Sm^{16}O^+$ interference on $^{163}Dy^+$

The intensities at m/z=163 of $^{163}Dy^+$ and intensities of interference of $^{147}Sm^{16}O^+$ at m/z=163 are given Table 7.11.

Table 7.11: Selection of gases for removal of $^{147}Sm^{16}O^+$ interference on $^{163}Dy^+$

Product ions	$^{163}Dy^+$ intensity	$^{147}Sm^{16}O^+$ intensity
163 Dy [No Gas]	128576	1359
163 -> 163 Dy [NH3-L]	49740	533
163 -> 163 Dy [NH3-M]	35915	30
163 -> 178 Dy [NH3-L]	1010	0
163 -> 178 Dy [NH3-M]	61	0
163 -> 179 Dy [O2]	77661	17
163 -> 248 Dy [NH3-L]	3	0
163 -> 248 Dy [NH3-M]	218	0

Samarium reacts more efficiently with NH_3 than $^{163}Dy^+$. The intensities of $^{163}Dy^+$ product ions with NH_3 gas are very low although BECs of Sm is zero but it cannot be applied for reliable measurement for low concentration of Dy in geological samples. Here $^{147}Sm^{16}O^+$ interference on $^{163}Dy^+$ can be removed by reacting Sm^+ with ammonia and keeping the Dy^+ measurement in on-mass NH_3 mode. Mass-shift of oxygen is also applicable with quite good intensities for removal of $^{147}Sm^{16}O^+$ interference on $^{163}Dy^+$and lowest BECs of $^{147}Sm^{16}O^+$.

The relative intensities of $^{163}Dy^+$ and $^{147}Sm^{16}O^+$ are plotted in Figure 7.27 as below. The relative intensities i.e. approximately 60% with very low relative interferences of $^{147}Sm^{16}O^+$ as shown by point 2 in Figure 7.27. The relative intensities of on-mass Dy with ammonia gas are approximately 30% and lowest relative BECs of $^{147}Sm^{16}O^+$ as shown with point 3 in Figure 7.27.

Therefore, the suggested product ions are given as under;

163 -> 163 Dy [NH3-M] and 163 -> 179 Dy [O2]

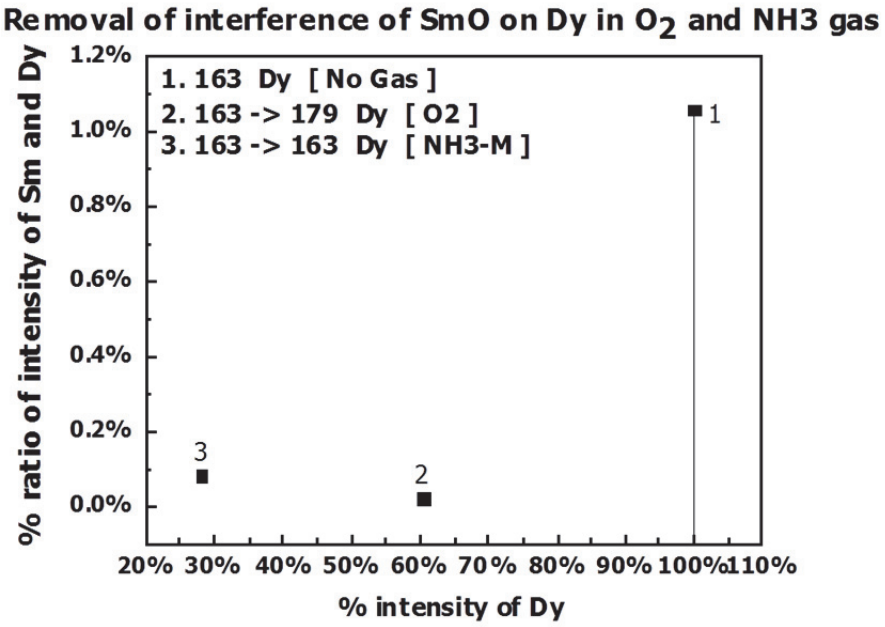

Figure 7.27: Removal of Sm interferences on Dy

$^{149}Sm^{16}O^{+}$ interference on $^{165}Ho^{+}$

The intensities at m/z=165 of $^{165}Ho^{+}$ and intensities of interference of $^{149}Sm^{16}O^{+}$ at m/z=165 are given Table 7.12.

Table 7.12 Selection of gas modes for removal of $^{149}Sm^{16}O^{+}$ interference on $^{165}Ho^{+}$

Product ions	$^{165}Ho^{+}$ intensity	$^{149}Sm^{16}O^{+}$ intensity
165 Ho [No Gas]	546814	1413
165 -> 165 Ho [NH3-L]	212443	629
165 -> 165 Ho [NH3-M]	156948	52
165 -> 180 Ho [NH3-L]	6380	1
165 -> 180 Ho [NH3-M]	375	0
165 -> 181 Ho [O2]	324907	69
165 -> 250 Ho [NH3-L]	23	0
165 -> 250 Ho [NH3-M]	1135	0

Samarium shows more reactivity with NH_3 than Ho^{+}. The intensities of Ho^{+} product ions with NH_3 gas are very low although BECs created by SmO^{+} is zero but it cannot be applied for reliable measurement for low concentration geological samples. Here $^{149}Sm^{16}O^{+}$ interference on $^{165}Ho^{+}$ can be removed by reacting Sm with ammonia and keeping the $^{165}Ho^{+}$ measurement in an on-mass NH_3 mode. The mass-shift of oxygen is also applicable with quite good intensities for removal of $^{149}Sm^{16}O^{+}$ interference on $^{165}Ho^{+}$ and lowest BECs of $^{149}Sm^{16}O^{+}$.

The relative intensities of $^{165}Ho^{+}$ and $^{149}Sm^{16}O^{+}$ are plotted in Figure 7.28 as below. The relative intensities approximately 60% with very low relative interferences of $^{149}Sm^{16}O^{+}$

as shown by point 2 in Figure 7.28. The relative intensities of on-mass $^{165}Ho^{+}$ with ammonia gas are approximately 30% and the lowest BECs of $^{149}Sm^{16}O^{+}$ as shown by point 3 in Figure 7.28.

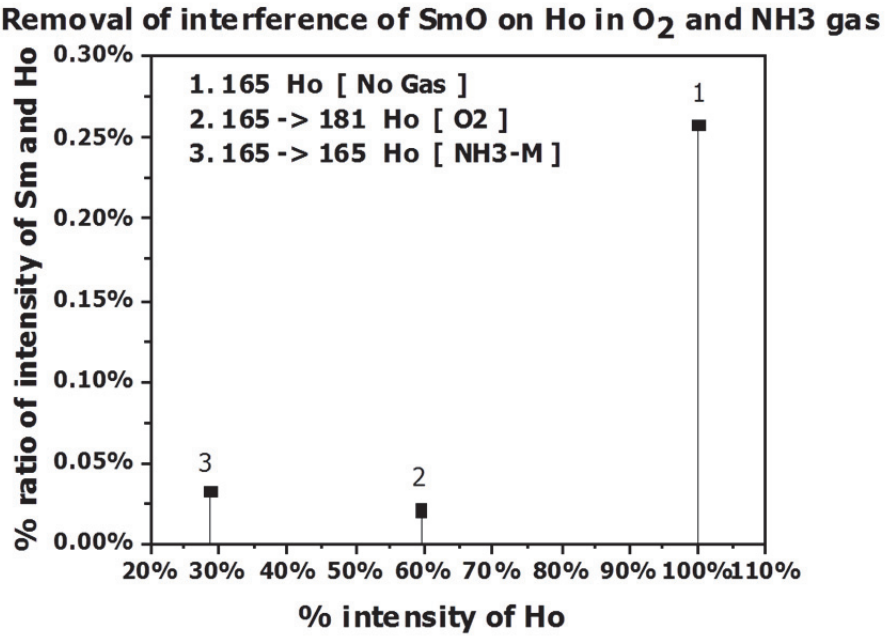

Figure 7.28: Removal of Sm interferences on Ho

Therefore, the suggested product ions are as under;

165 -> 165 Ho [NH3-M] and 165 -> 181 Ho [O2]

$^{150}Nd^{16}O^{+}$ and $^{150}Sm^{16}O^{+}$ interference on $^{166}Er^{+}$

Both of the Sm^{+} and Nd^{+} produce oxides i.e. $^{150}Nd^{16}O^{+}$ and $^{150}Sm^{16}O^{+}$at m/z=166 of Er in no gas mode. The intensities at m/z=166 of Er and intensities of interferences of $^{150}Nd^{16}O^{+}$ and $^{150}Sm^{16}O^{+}$ are given Table 7.13.

Table 7.13: Selection of gas modes for removal of $^{150}Nd^{16}O^{+}$ and $^{150}Sm^{16}O^{+}$ interferences on Er^{+}

Product ions	$^{166}Er^{+}$ intensity	$^{150}Nd^{16}O^{+}$ intensity	$^{150}Sm^{16}O^{+}$ intensity
166 Er [No Gas]	183260	1969	798
166 -> 166 Er [NH3-L]	70847	825	324
166 -> 166 Er [NH3-M]	51358	71	18
166 -> 181 Er [NH3-L]	2168	0	0
166 -> 181 Er [NH3-M]	105	0	0
166 -> 182 Er [O2]	108418	24	10
166 -> 251 Er [NH3-L]	12	0	0
166 -> 251 Er [NH3-M]	438	0	0

Nd^+ and Sm^+ are both more reactive to the cell gas ammonia than Er^+. $^{150}Nd^{16}O^+$ and $^{150}Sm^{16}O^+$ interferences can be eradicated by reacting them with cell gas i.e. ammonia, while keeping the Q2 at m/z=166 in an on-mass NH_3 mode. Some Er^+ also reacts with ammonia to form 166 -> 181 Er [NH3-L] and 166 -> 251 Er [NH3-M] as seen in the product ion scan in Figure 7.15 on Q2 but the intensities of these product ions are very little.

Thus, it is better to use on-mass 166 -> 166 Er [NH3-M] with better intensities and lowest BEC of Sm and Er oxides. Oxide mode with 166 -> 182 Er [O2] is better than all other modes because of excellent intensities and relatively low background equivalent concentrations of Sm and Nd oxides. The interference removal efficiency of NH_3 and O_2 gas for Er^+ are shown in Figure 7.29 and Figure 7.30. The loss in intensity is up to 40% with O_2-shift mode and maximum interferences are wiped out while intensity loss is about 70% with NH_3 gas with the maximum removal of Nd and Sm oxides. The intensities in terms of counts are given in the Table 7.13 above.

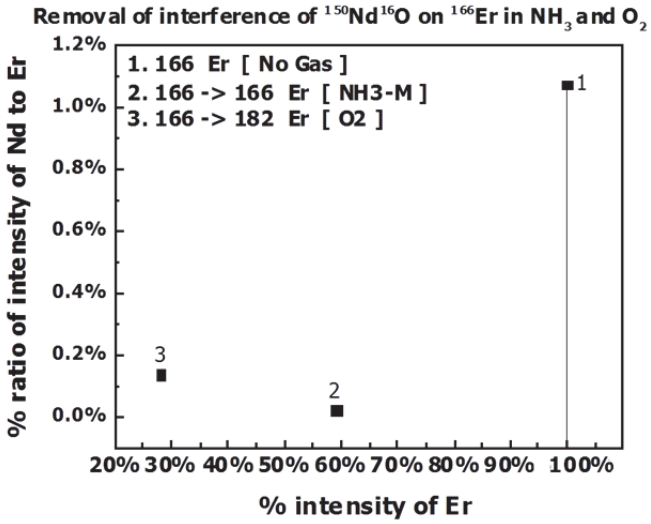

Figure 7.29: Removal of interference of Nd on Er

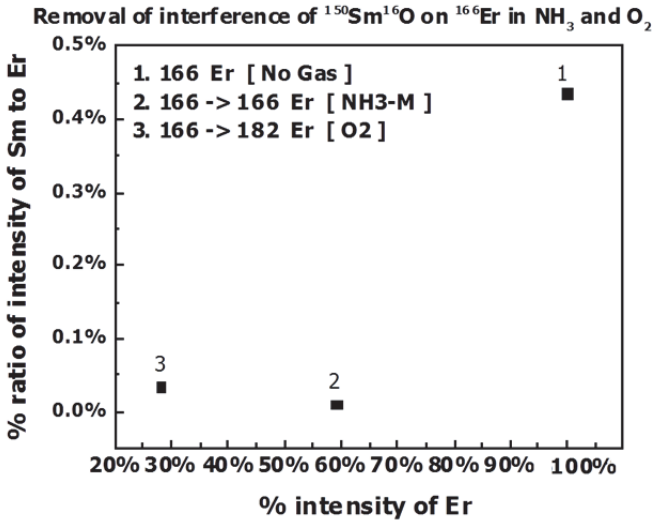

Figure 7.30: Removal of interference of Sm on Er

Therefore, the suggested product ions for Er measurement are as under;

166 -> 166 Er [NH3-M] and 166 -> 182 Er [O2]

$^{159}Tb^{16}O^{+}$ and $^{158}Gd^{16}O^{16}H^{+}$ interferences on $^{175}Lu^{+}$

$^{159}Tb^{+}$ and $^{158}Gd^{+}$ make an oxide $^{159}Tb^{16}O^{+}$ and $^{158}Gd^{16}O^{1}H^{+}$ in spectra overlapping with $^{175}Lu^{+}$. The actual interferences caused by 10 ng/ml matrix of ^{159}Tb on ^{175}Lu are shown Figure 7.22 and Figure 7.23. Table 7.14 shows the intensities of 10 ng/ml Tb and Gd solutions on Lu.

Table 7.14: Selection of gas modes for removal of $^{159}Tb^{16}O^{+}$ and $^{158}Gd^{16}O^{16}H^{+}$ interferences on $^{175}Lu^{+}$

Product ions	$^{175}Lu^{+}$ intensity	$^{159}Tb^{16}O^{+}$ intensity	$^{158}Gd^{16}O^{16}H^{+}$ intensity
175 Lu [No Gas]	491991	4703	498
175 -> 175 Lu [NH3-L]	197864	1874	199
175 -> 175 Lu [NH3-M]	77275	26	4
175 -> 190 Lu [NH3-L]	8886	0	0
175 -> 190 Lu [NH3-M]	345	0	0
175 -> 191 Lu [O2]	304643	34	7
175 -> 260 Lu [NH3-L]	62	0	0
175 -> 260 Lu [NH3-M]	5001	6	5

Gd^{+} and Tb^{+} are more reactive to cell gas NH_3 than Lu^{+}. Therefore, Gd^{+} and Tb^{+} are reacted with excess NH_3 gas while keeping Q2 filter mass at 175. Other possible mass-shifts of Lu^{+} are also presented i.e. 175 -> 190 Lu [NH3-L] and 175 -> 260 Lu [NH3-M] but these are with lower intensities although BEC of Gd and Tb are turned down to zero. On mass–NH_3 mode can be good a compromise with sufficiently lowest BEC of $^{158}Gd^{16}O^{16}H^{+}$and $^{159}Tb^{16}O^{+}$. The O_2-shift mode is always better than ammonia as far as intensities are concerned, relative to intensities of interferences.

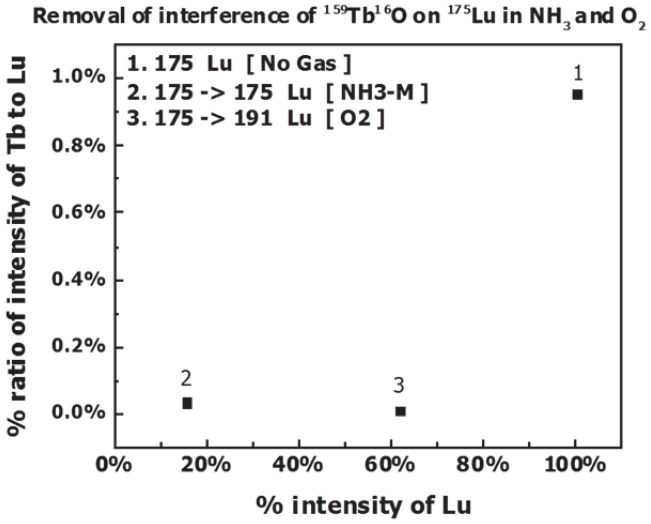

Figure 7.31: Removal of Tb interference on Lu

Oxide shift mode 175 -> 191 Lu [O2] and 175 -> 175 Lu [NH3-M] are presented in Figure 7.31. For O_2 shift mode drop in intensity is approximately 40% and for on-mass NH_3 mode it is 80% with lowest BEC of Gd and Tb.

Thus the suggested product ions for Lu measurement are as under;

175 -> 175 Lu [NH3-M] and 175 -> 191 Lu [O2]

7.7 Optimisation of gas flow rates

The CRC gas flow rates for 10% NH_3/He has been shown to play an important role in product ion formation and interference removals. These were adjusted for minimal BECs (background equivalent concentrations) and highest intensities i.e. sensitivity. The gas flow rate in mass hunter workstation of the Agilent 8800 for a third gas line can only be set in %. The valve if fully open would set 100% NH_3 gas in helium. The gas flow rates as 20%, 30%, and 50% mean a flow rate of 2 ml/min, 3 ml/min, and 5 ml/min. 0 to 5 ml/min suffice the optimal conditions for the lowest BECs and maximum sensitivity. Moreover, the Agilent applications notes also recommends similar setting Juane *et al.* (2015), Sugiyama (2012).

7.7.1 Optimised method recommended for REE measurements

The optimised gas modes after a thorough study of interference removal with CRC gases are presented in Table 7.15.

Table 7.15: Optimised gas modes and product ions recommended for REE measurements

Analyte	m/z	Gas mode		
		Mass-shift O_2	Mass-shift NH_3	On-mass NH_3
La	139	139 -> 155 La [O2]	139 -> 224 La [NH3-M]	
La	139		139 -> 154 La [NH3-L]	
Ce	140	140 -> 156 Ce [O2]	140 -> 225 Ce [NH3-M]	
Pr	141	141 -> 157 Pr [O2]	141 -> 156 Pr [NH3-L]	141 -> 141 Pr [NH3-M]
Nd	146	146 -> 162 Nd [O2]		146 -> 146 Nd [NH3-M]
Sm	147	147 -> 163 Sm [O2]		147 -> 147 Sm [NH3-L & M]
Eu	151	151 -> 167 Eu [O2]		151 -> 151 Eu [NH3-H]
Eu	153	153 -> 169 Eu [O2]		153 -> 153 Eu [NH3-H]
Gd	157	157 -> 173 Gd [O2]	157 -> 172 Gd [NH3-L]	
Gd	157		157 -> 242 Gd [NH3-M]	
Tb	159	159 -> 175 Tb [O2]	159 -> 174 Tb [NH3-L]	
Tb	159		159 -> 244 Tb [NH3-M]	
Dy	160	160-> 176 Dy [O2]		1630-> 160 Dy [NH3-M]
Dy	163	163 -> 179 Dy [O2]		163 -> 163 Dy [NH3-M]
Ho	165	165 -> 181 Ho [O2]	165 -> 180 Ho [NH3-L]	165 -> 165 Ho [NH3-M]
Er	166	166 -> 182 Er [O2]		166 -> 166 Er [NH3-M]
Tm	169	169 -> 181 Tm [O2]		169 -> 169 Tm [NH3-M]
Yb	172	172 -> 188 Yb [O2]	172 -> 187 Yb [NH3-L]	
Lu	175	175 -> 191 Lu [O2]	175 -> 190 Lu [NH3-L]	175 -> 175 Lu [NH3-M]

7.8 Method validation with geological reference material

For the validation of analytical method developed, several geological reference materials for chosen i.e. DBC-1, BCR-2, MTA-1, OU-9 and ML-2. Reference materials were digested with optimised method developed sodium peroxide sintering as mentioned in chapter 5. The ratio of sample to sodium peroxide was 1:6. Final make up volume was 100 ml. 1 ml of the sample solution was taken and diluted with 1% HNO_3 to 5 ml for the measurement with the Agilent 8800 ICP-MS/MS. Four replicates of each sample were analysed in gas modes and product ions mentioned in optimised method. Blanks were digested similar to the method of sample digestion. The instrument was run on several 1%HNO_3 rinses to monitor any background of the rare earth elements. 1 mg/l solution of Ge and In were used as an internal standard which were continuously supplied with automated fast SC-2X auto-sampler system coupled with ICP-MS/MS. Indium and Ge intensities were monitored with the cell gases. Indium behaviour was not much affected by CRC gases. Ge intensities were affected as it made some adduct ions with NH_3 gas. The best product ions of Ge were scanned i.e. 74 -> 90 Ge [NH3-L], 74 -> 90 Ge [NH3-M] and 74 -> 90 Ge [NH3-H] in mass-shift NH_3 mode with flow rates 2, 3 and 5 ml/min.

7.8.1 BECs, blanks and detection limits

The results of all the rare earth elements in suggested gas modes (i.e. on-mass and mass-shift O_2 and NH_3/He) were evaluated in comparison with background equivalent concentrations (BECs) and detection limits of analytes in no gas mode. Detection limits and BECs were based on sodium peroxide procedural blank solutions which were prepared in the same batch as that of reference materials. (b) refers to the procedural blank. DL are the detection limits DL= (3 times the standard deviations of blank concentration/slope of the curve). BECs refer to background equivalent concentrations of the analytes BEC= (Blank concentrations/slope of the curve). R is the coefficient of linear regression obtained from the curve of matrix-matched calibrations with reference materials. The background equivalent concentrations were calculated by dividing procedural blank concentrations with a slope of the calibration curve. Blanks, detection limits, and BECs for all the REE determined in O_2 and NH_3/He mode were considerably lower than in no gas as shown in Table 7.16.

Table 7.16: Blanks, DL and BECs

Gas modes	Scan Type	Q1	Q2	Name	R	b (blank)	DL	BEC
Gases	**Mode**	**m/z**	**m/z**			**pg/ml**	**pg/ml**	**pg/ml**
No gas	No gas		140	Ce	0.999	0.80	489	560
O_2	MS/MS	140	155	Ce	0.999	0.01	134	91
NH_3-M	MS/MS	140	156	Ce	0.999	0.21	14	133
No gas	No gas		160	Dy	0.998	0.02	36	45
No gas	No gas		163	Dy	0.999	0.02	74	64
NH_3-M	MS/MS	160	160	Dy	0.979	0.07	28	5
O_2	MS/MS	160	176	Dy	0.999	0.00	4	2
NH_3-M	MS/MS	163	163	Dy	0.992	0.27	3	3
O_2	MS/MS	163	179	Dy	1.000	0.00	2	1
No gas	No gas		166	Er	0.999	0.00	3	5
NH_3-M	MS/MS	166	166	Er	0.982	0.85	5	5
O_2	MS/MS	166	182	Er	1.000	0.00	3	3

No gas	No gas		151	Eu	0.999	0.00	1	3
No gas	No gas		153	Eu	0.997	0.00	1	5
NH_3-M	MS/MS	151	151	Eu	0.984	0.21	3	1
NH_3-H	MS/MS	151	151	Eu	0.998	0.00	10	3
O_2	MS/MS	151	167	Eu	1.000	0.00	6	2
NH_3-M	MS/MS	153	153	Eu	0.983	0.31	1	1
NH_3-H	MS/MS	153	153	Eu	1.000	0.00	3	1
O_2	MS/MS	153	169	Eu	0.999	0.00	7	3
No gas	No gas		157	Gd	0.997	0.01	41	27
NH_3-L	MS/MS	157	172	Gd	0.995	0.00	26	7
NH_3-M	MS/MS	157	172	Gd	0.988	0.00	0	0
O_2	MS/MS	157	173	Gd	0.998	0.00	2	2
No gas	No gas		165	Ho	0.999	0.02	4	14
NH_3-M	MS/MS	165	165	Ho	0.978	5.06	5	10
O_2	MS/MS	165	181	Ho	1.000	0.03	3	12
No gas	No gas		139	La	0.998	0.15	83	107
O_2	MS/MS	139	154	La	0.993	0.00	40	35
NH_3-M	MS/MS	139	155	La	1.000	0.04	4	24
No gas	No gas		175	Lu	0.998	0.10	9	74
NH_3-M	MS/MS	175	175	Lu	0.981	12.18	13	56
O_2	MS/MS	175	191	Lu	1.000	0.14	5	69
No gas	No gas		146	Nd	0.993	4.04	639	550
NH_3-M	MS/MS	146	146	Nd	0.994	5.22	37	73
NH_3-M	MS/MS	146	161	Nd	0.999	0.00	0	0
O_2	MS/MS	146	162	Nd	1.000	0.01	13	23
No gas	No gas		141	Pr	0.999	0.87	639	550
NH_3-M	MS/MS	141	141	Pr	0.996	1.92	9	5
O_2	MS/MS	141	157	Pr	1.000	0.01	3	4
No gas	No gas		147	Sm	0.999	0.03	98	136
NH_3-M	MS/MS	147	147	Sm	0.981	0.76	5	14
NH_3-L	MS/MS	147	147	Sm	0.997	0.01	19	24
NH_3-M	MS/MS	147	162	Sm	0.825	0.00	0	0
O_2	MS/MS	147	163	Sm	0.999	0.01	10	20
No gas	No gas		159	Tb	0.999	0.01	6	9
O_2	MS/MS	159	175	Tb	0.997	0.00	2	1
NH_3-M	MS/MS	159	175	Tb	1.000	0.00	0	0
NH_3-M	MS/MS	159	175	Tb	0.978	0.00	0	0
NH_3-M	MS/MS	159	244	Tb	0.999	0.07	8	1
No gas	No gas		169	Tm	0.997	0.00	3	0
NH_3-M	MS/MS	169	169	Tm	0.987	0.10	1	0
O_2	MS/MS	169	185	Tm	1.000	0.00	0	0
No gas	No gas		89	Y	1.000	0.33	3	42
NH_3-L	MS/MS	89	191	Y	1.000	0.12	16	15
NH_3-M	MS/MS	89	191	Y	1.000	0.89	50	27
No gas	No gas		172	Yb	0.997	0.00	6	5
NH_3-M	MS/MS	172	172	Yb	0.983	0.42	4	3
O_2	MS/MS	172	188	Yb	1.000	0.00	9	58

7.8.2 REE analysis in geological materials with developed method

DBC-1

The ball clay test material, IAG RM DBC-1, was circulated as *GeoPT*33. Ball clay is a water-lain deposit comprising the products of weathering and residual minerals, such as monazite (Potts *et al.* 2013). Four replicates (n=4) of the sample were analysed using collision/reaction cell of Agilent 8800 ICP-MS/MS. REE normalised with chondrite patterns from Anders and Ebihara (1982) for DBC-1 are shown in Figure 7.32. The mean of four values is taken for comparison of each gas mode.

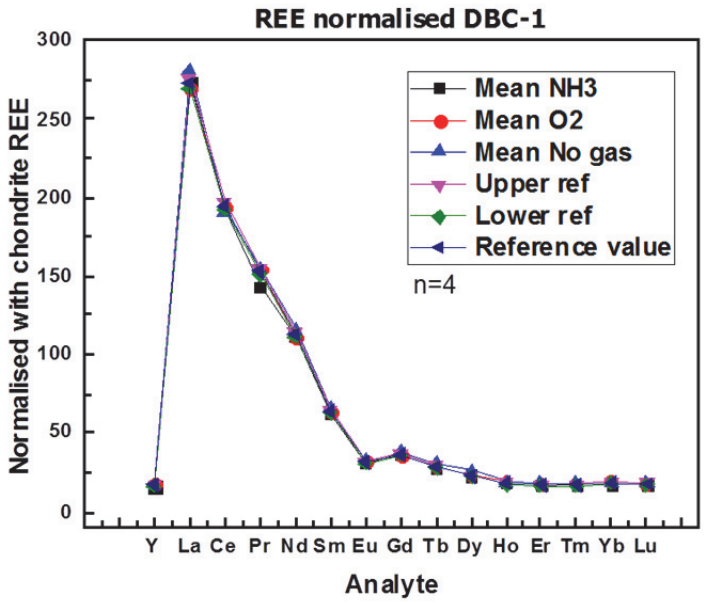

Figure 7.32: REE normalised data for DBC-1 in different gas modes

Chondrite plots use a larger scale and effect of each gas mode in interference removal may not be clear. Therefore, the mean value of each gas mode is divided with assigned or reference value. Upper and lower level of uncertainty of reference value are also plotted in Figure 7.33.

In Figure 7.33 the mean of no gas mode values are presented with red line. This indicates that no gas values are out of boundaries of uncertainty of the reference data. This is because, no gas mode utilises single quadrupole where all the ions are allowed to enter the collision/reaction cell. As there is no gas in the cell, the formation of oxides of lighter REE in plasma is enhanced and that create interferences on heavier REE. Interferences are very clear in particular for Tb, Dy, Er, Tm and Lu. The efficiency of oxygen gas with the mass-shift is not good either for Ho, Er, Tm, Yb and Lu. A possible explanation can be given, that oxides are still being formed in plasma and enter the first mass filter Q1. For the case of Gd interference on Yb, when Q1 is set to m/z of Yb=172, some of Gd^+ ions enter as GdO^+ through Q1. They further react with oxygen in collision/reaction cell and form a product GdO_2^+ at m/z of 188 which is the shifted mass of Yb. Ammonia gas mode is better than oxygen gas and no gas mode as it can be seen in Figure 7.33. The data obtained for DBC-1 is shown in the Table 7.17. The RSDs for NH_3 gas mode can be further improved by increasing the integration time. The data obtained with ammonia gas mode is in good agreement with reference values.

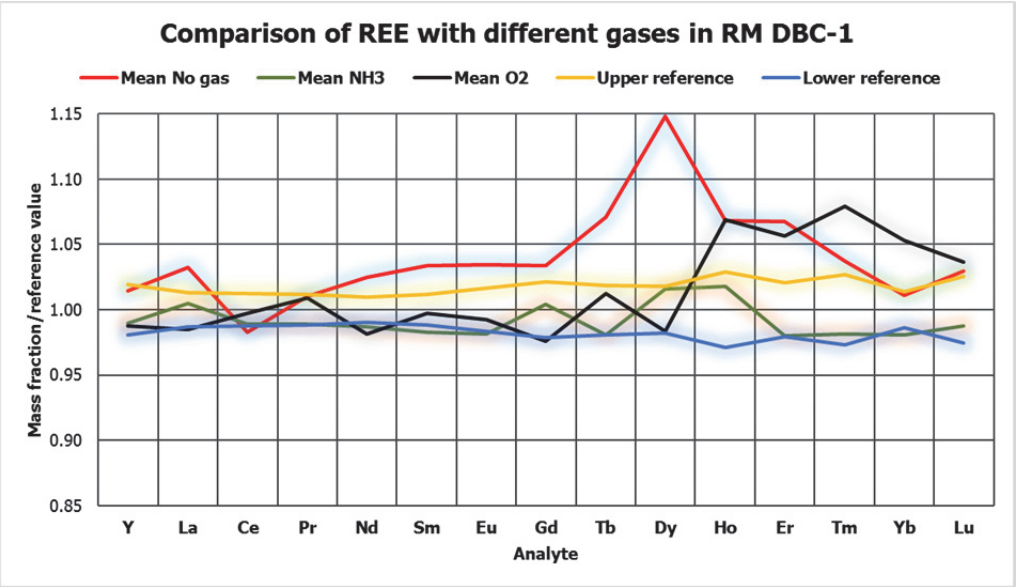

Figure 7.33: REE data with CRC gases in RM DBC-1

BCR-2

USGS RM BCR-2 (Basalt, Columbia River), was collected in 1996, from the Bridal Veil Flow Quarry. The quarry, located approximately 29 miles east of Portland, Oregon is the same collection site used to provide material for BCR-1. Four replicates of BCR-2 were measured in different gas modes using CRC gases. Chondrite normalised REE patterns are given in Figure 7.34.

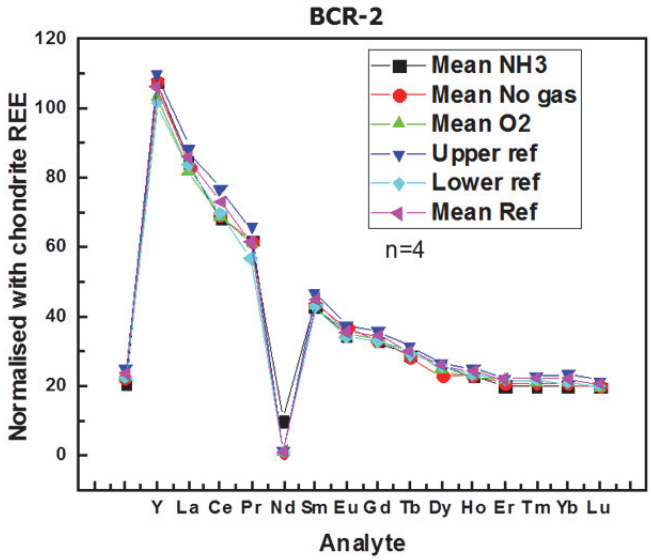

Figure 7.34: REE normalised data for BCR-2 in different gas modes

Comparison of different CRC gases for accurate determination of REE is given in Figure 7.35. Effect of interferences of LREE on HREE seems to be less and therefore all the gases even no gas mode is effective in determining the accurate value of REE in BCR-2. This is because of the fact that BCR-2 has lesser concentration of LREE in comparison with DBC-1. The data obtained in such gas modes is given in Table 7.18.

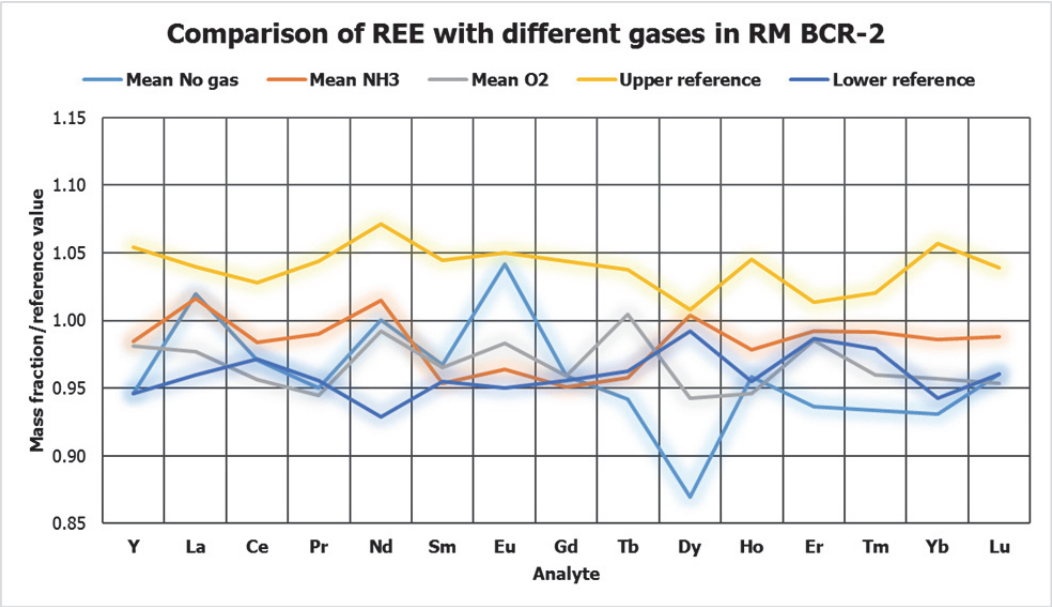

Figure 7.35: REE data with CRC gases in RM BCR-2

MTA-1

IAG RM MTA-1 trachyandesite was collected from trachyte-latite occurrence at Durvan durt located in Mongolia and was certified by International Association of Geoanalysts. REE normalised with chondrite patterns are shown in Figure 7.36, which have been processed through CRC gases of collision/reaction cell. Four replicates have been analysed with different gas modes.

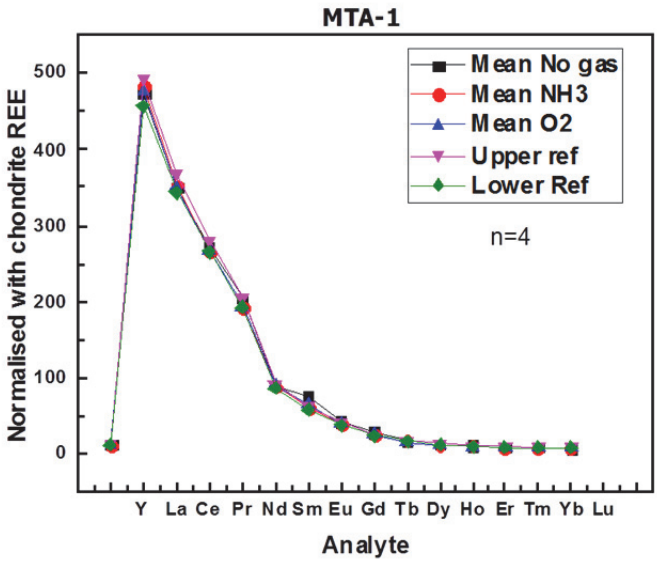

Figure 7.36: REE normalised data for MTA-1 in different gas modes

Table 7.17: REE data for DBC-1

Gas modes	Y	La	Ce	Pr	Nd	Sm	Eu	Gd	Tb	Dy	Ho	Er	Tm	Yb	Lu
Mean No gas	26.74	66.5	117.81	14.35	52.97	9.85	1.83	7.47	1.08	6.34	1.04	2.99	0.43	2.94	0.44
RSD	0.90%	0.90%	0.90%	1.00%	1.10%	0.70%	0.70%	1.10%	1.50%	0.70%	1.40%	0.90%	0.40%	1.40%	1.60%
Mean NH_3 gas	25.76	64.73	118.58	14.34	51.02	9.27	1.74	7.26	0.99	5.61	0.99	2.72	0.4	2.89	0.43
RSD	2.80%	1.40%	1.00%	1.00%	4.20%	1.20%	1.30%	1.20%	4.90%	1.80%	0.80%	1.20%	2.70%	2.90%	3.70%
Mean O_2 gas	28.33	63.41	119.54	14.34	50.73	9.51	1.76	7.06	1.02	5.43	1.04	2.96	0.44	3.06	0.45
RSD	0.50%	0.40%	0.40%	0.30%	0.30%	0.20%	1.30%	0.90%	0.30%	0.30%	1.10%	0.70%	1.30%	1.80%	1.10%
Reference value	26.35	64.4	119.9	14.21	51.69	9.53	1.77	7.23	1.01	5.52	0.97	2.8	0.41	2.91	0.43
Rel *u*	1.9%	1.3%	1.3%	1.2%	1.0%	1.2%	1.7%	2.1%	2.0%	1.8%	3.1%	2.1%	2.4%	1.4%	2.3%

Comparison of REE data in gas modes for geological reference material DBC-1 (n=4 unit =mg/kg)

Table 7.18: REE data for BCR-2

Gas modes	Y	La	Ce	Pr	Nd	Sm	Eu	Gd	Tb	Dy	Ho	Er	Tm	Yb	Lu
Mean No gas	35.84	26.25	52.95	6.60	28.74	6.61	2.12	6.50	1.03	6.04	1.31	3.50	0.52	3.35	0.50
RSD	0.8%	0.7%	0.5%	0.8%	0.8%	0.6%	1.5%	1.8%	1.2%	1.0%	0.6%	0.8%	1.6%	1.1%	1.7%
Mean NH3 gas	34.16	26.48	53.70	6.48	28.98	6.58	1.99	6.64	1.06	6.44	1.27	3.53	0.52	3.34	0.50
RSD	0.6%	1.6%	2.6%	2.1%	1.3%	1.5%	1.0%	2.7%	0.6%	1.5%	0.7%	1.5%	0.7%	3.4%	2.4%
Mean O2 gas	34.05	24.99	51.92	6.56	28.39	6.60	2.00	6.66	1.09	6.16	1.28	3.66	0.53	3.41	0.49
RSD	0.8%	1.0%	0.9%	1.0%	0.8%	1.2%	2.5%	0.8%	0.9%	1.4%	1.9%	1.5%	0.8%	2.3%	1.7%
Reference value	37.00	25.00	53.00	6.80	28.00	6.70	2.00	6.80	1.07	6.41	1.33	3.66	0.54	3.50	0.51
Rel *u*	5.4%	4.0%	2.8%	4.4%	7.1%	4.5%	5.0%	4.4%	3.7%	0.8%	4.5%	1.4%	1.9%	5.7%	3.9%

Comparison of REE data in gas modes for geological reference material BCR-2 (n=4 unit mg/kg)

Table 7.19: REE data for ML-2

Gas modes	Y	La	Ce	Pr	Nd	Sm	Eu	Gd	Tb	Dy	Ho	Er	Tm	Yb	Lu
Mean No gas	2.18	1.88	2.72	0.40	1.79	0.34	0.08	0.33	0.05	0.28	0.07	0.17	0.02	0.15	0.03
RSD	1.8%	1.1%	1.9%	1.5%	2.0%	0.5%	7.5%	5.6%	2.9%	4.1%	4.5%	2.8%	4.2%	3.4%	2.9%
Mean NH3 gas	2.13	1.85	2.82	0.39	1.58	0.33	0.07	0.33	0.05	0.28	0.06	0.16	0.02	0.14	0.02
RSD	0.2%	2.3%	2.0%	2.6%	3.5%	2.7%	2.4%	1.5%	4.8%	1.5%	2.7%	5.2%	13.9%	1.1%	0.5%
Mean O2 gas	2.28	1.71	2.77	0.39	1.56	0.31	0.07	0.31	0.05	0.27	0.06	0.16	0.02	0.13	0.02
RSD	4.9%	1.8%	1.1%	1.6%	0.5%	0.4%	4.1%	0.4%	1.7%	1.0%	1.7%	4.4%	1.6%	12.4%	9.0%
Reference value	2.11	1.80	2.74	0.40	1.59	0.33	0.07	0.32	0.05	0.28	0.06	0.16	0.02	0.14	0.02
Rel *u*	2.4%	2.2%	2.2%	2.5%	1.9%	3.0%	0.06%	3.1%	0.06%	3.6%	0.03%	0.06%	0.04%	0.08%	0.07%

Comparison of REE data in gas modes for geological reference material ML-2 (n=4 unit mg/kg)

Table 7.20: REE data for MTA-1

Gas modes	Y	La	Ce	Pr	Nd	Sm	Eu	Gd	Tb	Dy	Ho	Er	Tm	Yb	Lu
Mean No gas	17.45	111.89	215.36	25.17	93.57	13.40	4.21	8.29	1.02	3.93	0.63	1.75	0.19	1.19	0.17
RSD	0.7%	0.7%	0.7%	0.6%	0.5%	0.8%	1.1%	1.1%	1.2%	0.9%	1.2%	1.8%	2.6%	3.1%	1.6%
Mean NH3 gas	16.22	113.99	217.68	24.58	88.05	12.94	3.30	7.49	0.88	3.94	0.62	1.53	0.20	1.15	0.17
RSD	1.7%	2.1%	1.0%	0.9%	1.6%	1.5%	1.2%	3.0%	9.9%	1.6%	1.3%	0.9%	2.2%	1.5%	2.6%
Mean O2 gas	20.15	112.66	215.26	24.84	88.58	13.44	3.58	7.79	0.87	3.70	0.62	1.52	0.20	1.17	0.17
RSD	5.8%	0.3%	0.3%	0.4%	0.4%	0.6%	0.7%	0.6%	0.7%	0.6%	0.6%	1.1%	1.9%	5.8%	1.7%
Reference value	17.70	112.00	219.00	25.30	90.70	13.20	3.36	7.80	0.87	4.03	0.66	1.62	0.21	1.23	0.18
Rel *u*	1.6%	3.6%	3.2%	2.8%	3.2%	2.3%	3.0%	6.4%	2.3%	3.2%	1.5%	3.1%	4.8%	1.6%	5.6%

Comparison of REE data in gas modes for geological reference material MTA-1 (n=4 unit mg/kg)

Table 7.21: REE data for OU-9

Gas modes	Y	La	Ce	Pr	Nd	Sm	Eu	Gd	Tb	Dy	Ho	Er	Tm	Yb	Lu
Mean No gas	8.77	2.04	8.24	1.19	5.05	3.38	0.04	2.65	0.49	1.84	0.20	0.37	0.05	0.39	0.05
RSD	0.3%	1.4%	0.7%	0.7%	2.4%	0.1%	32.6%	1.1%	11.0%	0.5%	34.3%	10.9%	14.9%	14.3%	1.8%
Mean NH3 gas	8.38	2.00	8.86	1.20	4.74	3.35	0.05	2.71	0.43	1.80	0.14	0.33	0.05	0.35	0.04
RSD	0.1%	4.2%	0.8%	0.6%	17.0%	0.5%	1.5%	3.3%	10.8%	2.9%	1.1%	1.0%	3.0%	0.1%	0.4%
Mean O2 gas	8.30	2.03	8.82	1.18	4.95	3.45	0.05	2.88	0.56	1.91	0.18	0.36	0.05	0.34	0.05
RSD	1.4%	0.8%	0.7%	3.8%	0.3%	5.3%	17.5%	5.1%	7.5%	5.3%	8.3%	7.1%	108.7%	29.9%	6.7%
Reference value	8.14	2.03	8.75	1.24	5.07	3.15	0.05	2.53	0.46	1.70	0.15	0.30	0.05	0.40	0.04
Rel *u*	5.9%	7.4%	5.8%	8.1%	6.3%	6.7%	20.0%	7.1%	8.7%	7.6%	13.3%	10.0%	20.0%	10.0%	25.0%

Comparison of REE data in gas modes for geological reference material OU-9 (n=4 unit mg/kg)

The comparative plot for REE data obtained using different gases in collision/reaction cell is shown in Figure 7.37. The most obvious interferences on rare earth elements are the interferences induced by Ba as BaO on Eu isotopes. Tb and Er are also shown to be affected by LREE interferences in no gas modes. The interferences were better removed with ammonia gas using on-mass and mass-shift modes. O_2 gas does not seem to be good for Eu as the points lie out of the limits of certified values. The lower intensities can pose a problem when REE are in trace concentrations. The overall performance of NH_3 is better than O_2 and no gas mode. The data is presented in Table 7.20.

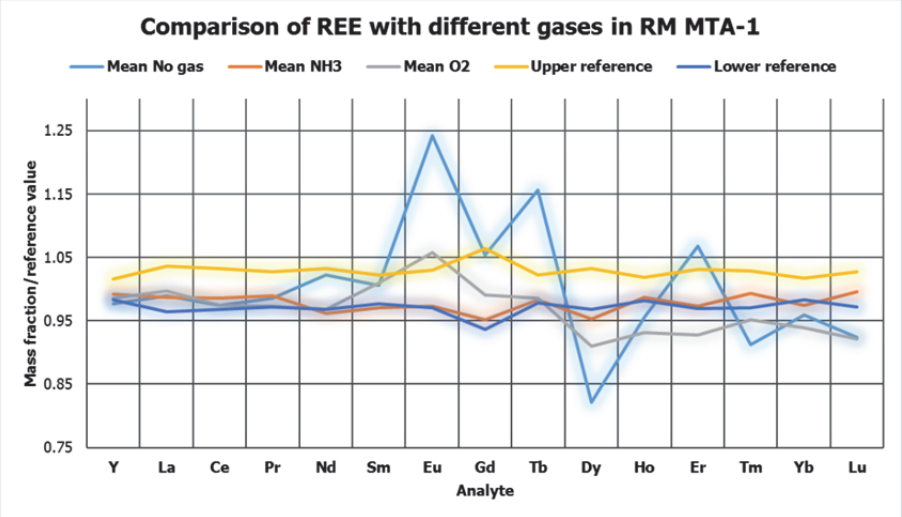

Figure 7.37: REE data with CRC gases in RM MTA-1

OU-9

OU-9, a pegmatite, prepared at the Open University from material supplied by F. Breaks of the Ontario Geological Survey, Canada and was circulated as *GeoPT* 23. REE normalised with chondrite patterns are shown in Figure 7.38 using collision/reaction cell gases. Four replicates have been analysed with different gas modes.

The comparative plot for REE data obtained using different gases in collision/reaction cell is shown in Figure 7.39. The most obvious interferences on rare earth elements are the interferences induced by Ba as BaO on Eu isotopes but as Ba contents of OU-9 are very small therefore Eu values are not affected. Gd, Tb and Er and Lu are also shown to be effected by LREE interferences in no gas modes (red line). The interferences were better removed with ammonia gas mode using on-mass and mass-shift modes. O_2 does not seem to be good for HREE. The overall performance of NH_3 is better than O_2 and no gas mode. The data is presented in Table 7.21.

ML-2

ML-2, a limestone, was supplied by Dr. B. Batjargal of the Central Geological Laboratory, Mongolia and circulated as *GeoPT* 30A. REE normalised with chondrite patterns is shown in Figure 7.40 which have been processed through CRC gases of collision/reaction cell. Four replicates have been analysed with different gas modes.

The comparative plot for REE data obtained using different gases in collision/reaction cell is shown in Figure 7.41. NH_3 gas mode shows better results compared to other gases i.e. no gas and O_2 gas. Nd, Eu, Gd, Ho and Lu seem to be problematic with no gas mode. O_2

gas shows similar results as that of no gas mode. The overall performance of NH_3 is better than O_2 and no gas mode. The data for ML-2 is presented in Table 7.19.

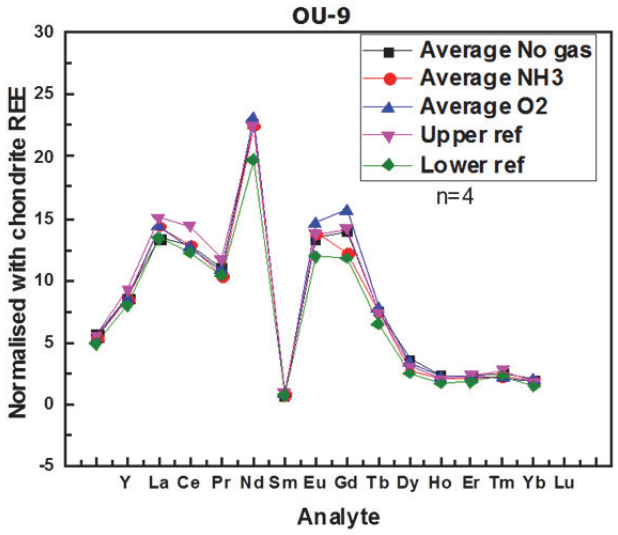

Figure 7.38: REE normalised data for OU-9 in different gas modes

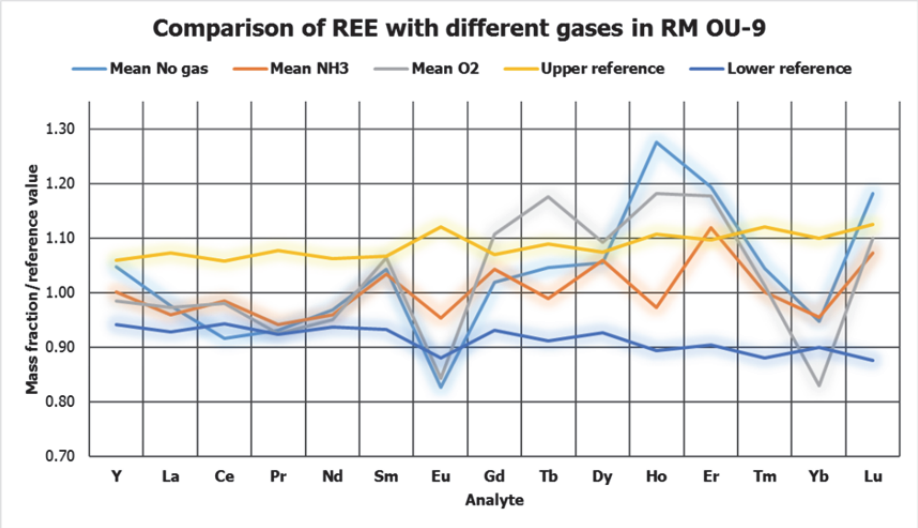

Figure 7.39: REE data with CRC gases in RM OU-9

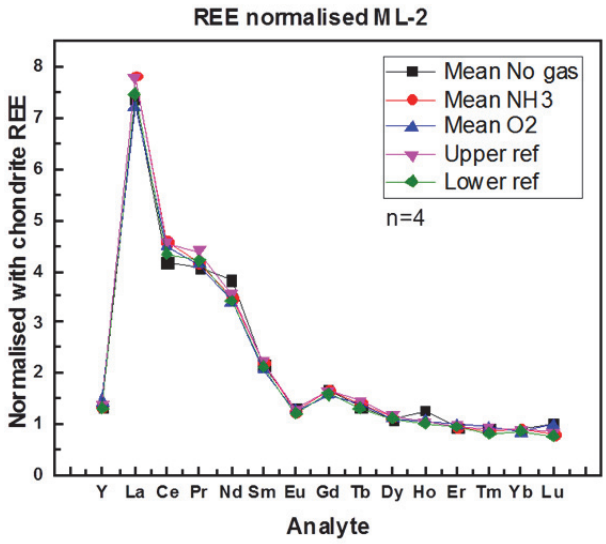

Figure 7.40: REE normalised data for ML-2 in different gas modes

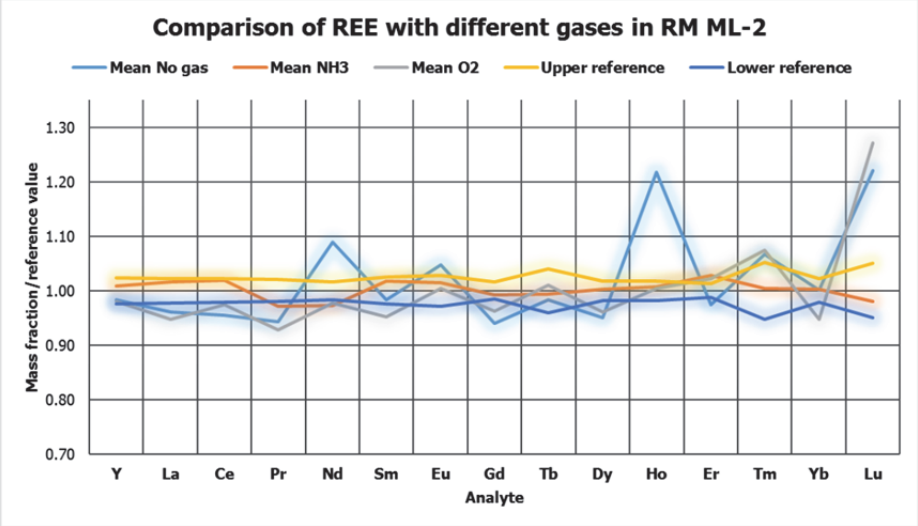

Figure 7.41: REE data with CRC gases in RM ML-2

7.9 Addressing the special case of the interferences of BaO on Eu

Eu exists as two isotopes in the nature ^{51}Eu (47.81) and ^{153}Eu (52.19) whereas Ba has 7 isotopes of which ^{135}Ba (6.59) and ^{137}Ba (11.23) are crucial as they make oxide interferences on ^{151}Eu and ^{153}Eu. Barium and the Lanthanides e.g. $^{136}Ce^{+}$ and $^{135\text{-}137}Ba^{+}$ react with oxygen in the plasma to form small portions of $^{135\text{-}137}Ba^{16}O^{+}$ and $^{136}Ce^{16}OH^{+}$ which add to signal intensity giving higher intensities for $^{151}Eu^{+}$ and $^{153}Eu^{+}$. The effect of $^{137}Ba^{16}O^{+}$ on $^{153}Eu^{+}$ is higher than $^{135}Ba^{16}O^{+}$ on $^{151}Eu^{+}$ due to the higher isotopic abundance of ^{137}Ba. These interferences are critical when accurate reference values have to be determined. When the Ba contents are higher in reference material, the signal intensities are enhanced with additional interferences on Eu. The matrix-induced polyatomic ions of BaO^{+} and $BaOH^{+}$ can interfere with some middle REE from ^{146}Nd through to ^{155}Gd as given in Table 7.22. This is often observed in the geological and the environmental samples. Moreover, the formation of BaO^{+} results into significant interferences on both the isotopes of ^{151}Eu and ^{153}Eu when Ba/Eu ratio is more than 200:1 thus leaving no isotope free from interferences (Cao *et al.* 2001).

Table 7.22: Interferences caused by Ba isotopes

Ba isotopes	BaO interference	Analyte	BaOH interferences	Analyte
^{130}Ba	$^{130}Ba^{16}O$	^{146}Nd	$^{130}Ba^{16}O^{1}H$	^{148}Sm
^{132}Ba	$^{132}Ba^{16}O$	^{148}Sm	$^{132}Ba^{16}O^{1}H$	^{149}Sm
^{134}Ba	$^{134}Ba^{16}O$	^{150}Nd, ^{150}Sm	$^{134}Ba^{16}O^{1}H$	^{151}Eu
^{135}Ba	$^{135}Ba^{16}O$	^{151}Eu	$^{135}Ba^{16}O^{1}H$	^{152}Gd, ^{152}Sm
^{136}Ba	$^{136}Ba^{16}O$	^{152}Gd, ^{152}Sm	$^{136}Ba^{16}O^{1}H$	^{153}Eu
^{137}Ba	$^{137}Ba^{16}O$	^{153}Eu	$^{137}Ba^{16}O^{1}H$	^{154}Gd, ^{154}Sm
^{138}Ba	$^{138}Ba^{16}O$	^{154}Gd, ^{154}Sm	$^{138}Ba^{16}O^{1}H$	^{155}Gd

To overcome these interferences a number of steps have been taken as reported in the literature. The algebraic correction scheme is one approach to correct for the oxide and hydroxide overlap of the lighter REE on the MREE and HREE (Jarvis 1989). This approach has been used in spark source mass spectrometry as well as ICP-MS. The major advantages of these corrections are speed and ease of application and no additional experimental work (Cao *et al.* 2001).

Larger errors can be caused by the correction of Ba interference on Eu due to the instability of BaO and negative results are obtained when the ratio of Ba/Eu is too high. Jarvis (1989) reports the measurement of the doubly charged ions of Eu to overcome this problem which depends on the optimum instrument conditions to acquire the maximum signal intensities. But it becomes useless when the Eu concentration is too trace in the sample due to significant loss of intensity.

The spectroscopic overlaps of BaO and BaOH interferences on Eu and other middle REE are generally removed with chromatographic separation of Ba with resins. Most effective method is to remove Ba from matrix through resin chromatography. Shabani *et al.* (1990) reported removal of Ba through the solvent extraction, but the REE recoveries were mainly affected. Jarvis *et al.* (1997a) used ion exchange chromatography for the removal of

Ba matrix but during the elution of REE , Ba is also eluted as evident from higher Ba/Eu ratios.

Two step separations with anion and cation exchange resins were employed to remove Ba in Crock *et al.* (1984) which yielded good results but it is time-consuming and laborious process. Resins exchange was combined with an algebraic correction to overcome spectral interferences (Cao *et al.* 2001). Single quad ICP-MS cannot resolve the spectral interference of Ba on Eu and therefore its use is limited in interference removals. Sample pre-treatment with resins, laser ablation, flow injection on-line solid phase extractions are successful for Ba removal on Eu prior to the ICP-MS detection. But all these procedures are cumbersome and require complex instrumental configurations.

REE conversion to $REEO^+$ using dynamic cell reaction pressurized with oxygen to explore their determination at m/z +16 by ICP-MS was employed by Ardini *et al.* (2010). He reported >96% quantitative conversion of the REE to their oxides except Tm, Eu and Yb for which the formation of oxides was only 10%. Measurement of Eu in the marine sample was carried out with algebraic correction without formation of oxides.

Measurement of Eu is much more challenging when a matrix has more than 1000 mg/kg barium contents. Therefore, a new and robust method is required which is simple and is able to produce desirable accurate results. The aim of this study is to remove the Ba interferences on REE especially on Eu in several geological reference materials. The Agilent 8800 ICP-MS/MS has been proposed with its efficiency for the removal of interferences in collision reaction cell as several elements including S, P and Ti in different matrices were measured with this robust technique with high sensitivity.

7.9.1 Experimental

Initial tests and results

The pure solutions of Eu and Ba with higher concentrations of 1 mg/ml and 10 mg/ml respectively were prepared using 1% HNO_3 and were tested to see the magnitude of interferences on Eu.

7.9.2 Reactivity of Ba with NH_3, O_2 and H_2

The Figure 7.42 shows the effect of reactivity of Ba with the different cell gases. It can be seen that the intensity of Ba decreases with increasing the flow rate of NH_3 gas i.e. at flow rate 5 ml/min. There is a significant decrease in intensity of Ba up to 80%. The decrease in intensity with the on-mass NH_3 corresponds to the with the formation of some $Ba(NH_3)_x$ clusters. This effect can be helpful in shifting the m/z of Ba to higher m/z for removal of Ba interferences on Eu or an on-mass ammonia method with high flow rate can be applied. This gas flow rate i.e. 5 ml/min can be applied while doing Eu measurement at m/z 151 and 153 in method development for BaO interference removal on Eu isotopes.

The intensity of Ba increases with H_2 due to hydride formation with its own isotopes on m/z 135 i.e. ^{134}BaH. The intensity of Ba increase with on-mass O_2 mode. The increase in the intensity of Ba with O_2 can be due to the formation of argide oxides.

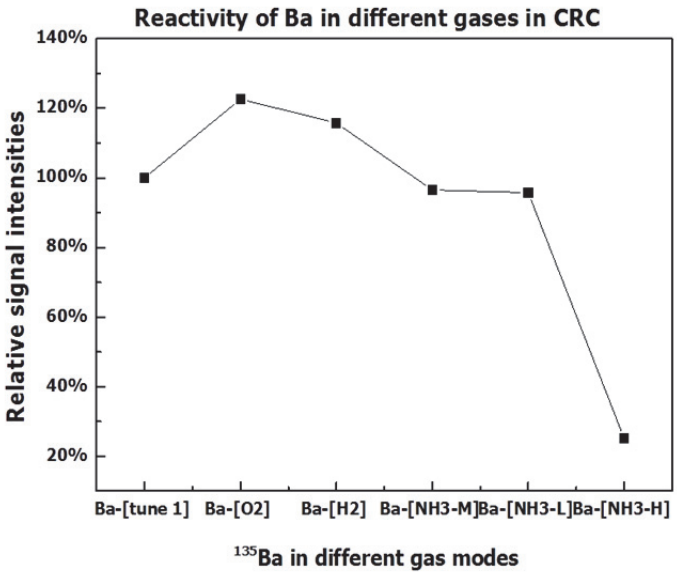

Figure 7.42: Reactivity of Ba in different gas modes

7.9.3 Testing BaO removal in O_2 gas mode

Europium does not react frequently with NH_3 cell gas and oxide formation of Eu is also very less i.e.10-20% as shown earlier in Figure 7.21. Figure 7.43 shows the relative intensities of Eu and %ratio of Ba intensity to Eu intensity. The intensities of Eu increase in on-mass Eu mode because of Ba being oxidised to BaO and have the highest amount of interference. Therefore, on-mass O_2 mode cannot be applied. The ratio of Ba/Eu decreases significantly when the mass-shift mode is applied shifting the mass of Eu from 151 to 167 (EuO^+) and 183 (EuO_2^+) respectively. Point 3 in Figure 7.43 is better compromised because of good intensities of Eu with less interferences of Ba.

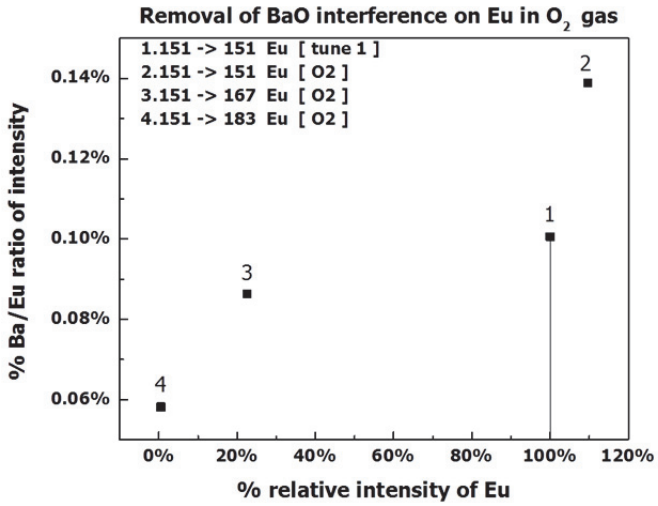

Figure 7.43: Test for interference removal of BaO on Eu in O_2 gas mode

7.9.4 Testing BaO removal in H_2 gas mode

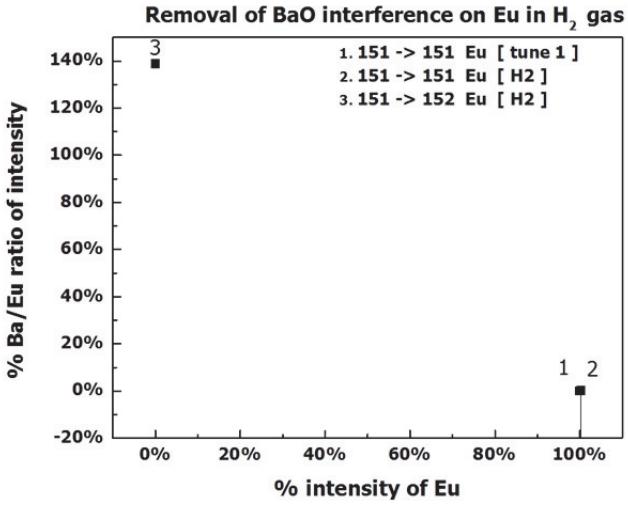

Figure 7.44: Test for interference removal of BaO on Eu in H_2 gas mode

The capacity of hydrogen gas in interference removal of BaO is not good as shown in Figure 7.44. Points 1 and 2 show the presence of 100% interferences and when hydride shift is applied i.e. 151-152, the corresponding interference of Ba increases to 138% while the intensity of Eu decreases to less than 1% as shown in point 3 of Figure 7.44.

7.9.5 Testing BaO removal in NH_3 gas mode and the method development

Different product ions were scanned for ammonia with varied intensities and discussion relates with ion-molecule chemistry of formation of these product ions. The focus of this section is to explore the possibilities of interference removals of BaO produced by Ba. However, following products ions were found to exist in ICP-MS/MS spectra i.e. 151 -> 168 Eu, 151 -> 185 Eu, 151 -> 202 Eu, 151 -> 219 Eu, 151 -> 236 Eu, 151 -> 253 Eu. The intensities of the product ions were variable in different flow rates of ammonia. Here, only the on-mass modes which are effective in interference removal with better intensities are shown in Figure 7.45.

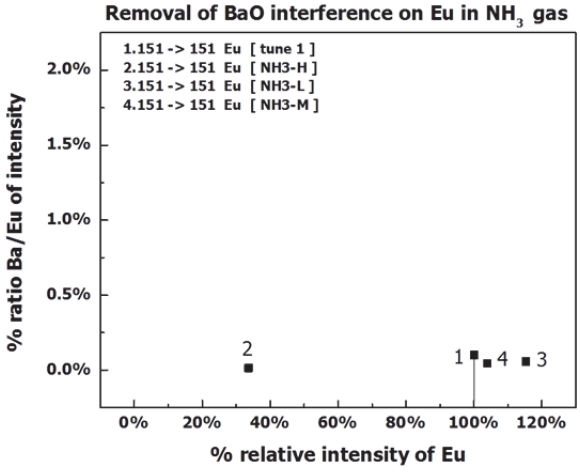

Figure 7.45: Test for interference removal of BaO on Eu in NH_3 gas mode

BaO interference is considerably decreased with a high flow rate of ammonia i.e. 5 ml/min and drop in intensities of Eu are up to 40% as shown by point 2 in Figure 7.45. This is in accordance with initial tests on Ba reactivity with ammonia where Ba intensity was found to decrease with high flow rate, ensuring a formation of another product $Ba(NH_3)_x$ shifted away from the m/z of Eu as shown in Figure 7.42.

Based on Figure 7.43 and Figure 7.45 a method was developed using oxygen gas with mass-shift 151 -> 167 Eu [O2] and ammonia gas with on-mass measurement 151 -> 151 Eu [NH3-H] where BaO can be easily minimised. These steps were applied on the geological reference materials for method validation.

7.9.6 Method validation on reference materials

Several reference materials were chosen for method validation, which are having variable mass fraction of Ba ranging from i.e. 4650 to 3.79 mg/kg as shown in the Table 7.23. To ensure complete sample digestion, a method developed in chapter 5 with sodium peroxide sintering was applied for digestion of these reference materials. Four replicates of each sample were digested and measured with different gas modes and product ions. Calibration was achieved with matrix-matched reference materials instead of pure standard solutions. Germanium and In were used as internal standards with conditions described earlier. The linear drift correction was applied for controlling instrument drift during measurement. The results are discussed in the later section for each gas modes separately to evaluate their capability for BaO removal.

Table 7.23: Reference materials chosen for method validation

*Certified values and other are reference values. MTA-1, MRH-1 and MUH-1 are IAG certified and certificates available at http://www.geoanalyst.org. The reference values are taken from *GeoPT* reports, which are also available at http://www.geoanalyst.org.

Ba-reference or *certified values in reference materials (mg/kg)								
NKT-1	MTA-1	DBC-1	G-3	SdAR-1	OU-3	BCR-176-R	MRH-1	MUH-1
741	*2842	476	1942	749	29	4650	*3.79	*4.98

7.9.7 Detection limits, blanks and BECs

The detection limits, blanks and BECs are given in the Table 7.24 below. The detections limits, blanks and BECs are based on sodium peroxide procedural blank digested along with reference material for method validation purposes. The instrument was configured for best tuning condition mentioned elsewhere in section 10 and will not be further discussed. The on-mass and mass-shift modes for respective gases O_2 and NH_3 were applied for measurement. (b) refers to the procedural blank. DL are the detection limits DL= (3 times the standard deviations of blank concentration/slope of the curve). BECs refer to background equivalent concentrations of the analytes BEC= (Blank concentrations/slope of the curve). R is the coefficient of linear regression obtained from the curve of matrix-matched calibrations with reference materials. The background equivalent concentrations were calculated by dividing procedural blank concentrations with a slope of the calibration curve. The table for detection limits, blanks and BECs show that detection limits, blanks and

BECs were particularly high for O_2 mode but as far as ammonia gas with high flow rate is concerned it has lower detection limits, blanks and BECs. The use of ammonia gas is the method of choice and test for validation of method proposed for the measurement. For no gas mode, MS/MS mode was applied instead of single quadrupole configuration to achieve lowest possible blanks, DLs and BECs.

Table 7.24: Detection limits, blanks and BECs

Gas modes	Scan Type	Q1	Q2	Name	R	b (blank)	DL	BEC
Gases	**Mode**	**m/z**	**m/z**			**pg/ml**	**pg/ml**	**pg/ml**
No gas	MS/MS	151	151	Eu	0.998	0.007	1.43	0.43
O_2	MS/MS	151	151	Eu	0.999	0.057	1.69	1.18
O_2	MS/MS	151	167	Eu	1.000	0.003	0.95	0.27
NH_3-L	MS/MS	151	151	Eu	0.999	0.004	1.23	0.53
NH_3-M	MS/MS	151	151	Eu	0.999	0.013	0.94	0.83
NH_3-H	MS/MS	151	151	Eu	0.998	0.025	1.36	0.35
No gas	MS/MS	153	153	Eu	0.999	0.007	0.56	0.35
O_2	MS/MS	153	169	Eu	0.999	0.005	2.13	0.50
O_2	MS/MS	153	153	Eu	1.000	0.076	2.21	1.38
NH_3-L	MS/MS	153	153	Eu	0.998	0.005	1.11	0.56
NH_3-M	MS/MS	153	153	Eu	0.999	0.006	0.87	0.36
NH_3-H	MS/MS	153	153	Eu	0.999	0.020	0.56	0.25

7.9.8 Matrix-matched calibration

The matrix-matched calibrations are important for the robust measurement. The calibration was achieved with certified reference material i.e. BCR-2. MUH-1, OU-6, BRP-1, OU-9 and OU-3 etc. instead of pure standard solutions. Calibrants were digested with a similar procedure which was applied to the reference materials i.e. sodium peroxide sintering. The calibration plots are shown as block diagram for all as shown in Figure 7.46. Re was chosen for internal standardisation of these calibration plots. The concentrations in ng/g are plotted horizontally while ratio of the intensities of internal standard and analytes are plotted vertically.

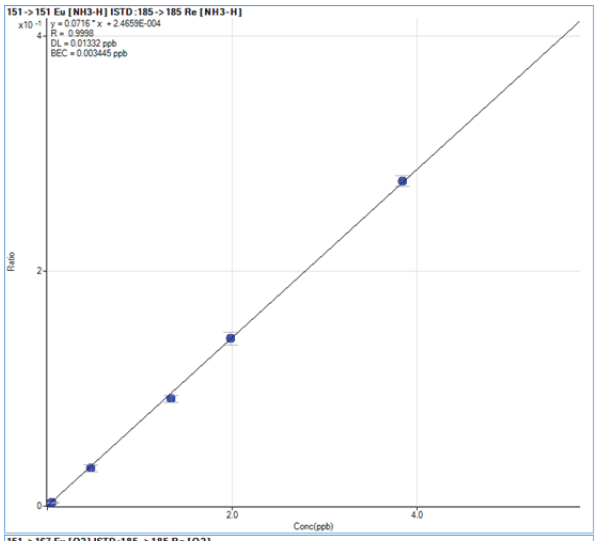
151-> 151 Eu [NH3-H] ISTD:185-> 185 Re [NH3-H]
x10 -1
y = 0.0716 * x + 2.4659E-004
R = 0.9998
DL = 0.01332 ppb
BEC = 0.003445 ppb
Ratio
Conc(ppb)

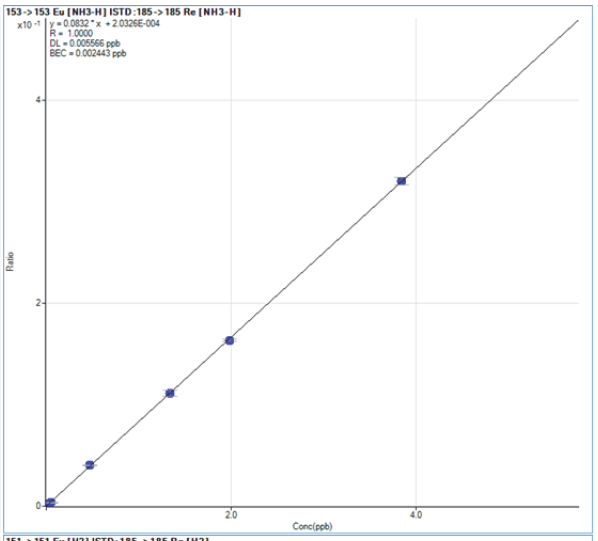
153-> 153 Eu [NH3-H] ISTD:185-> 185 Re [NH3-H]
x10 -1
y = 0.0832 * x + 2.0326E-004
R = 1.0000
DL = 0.005566 ppb
BEC = 0.002443 ppb
Ratio
Conc(ppb)

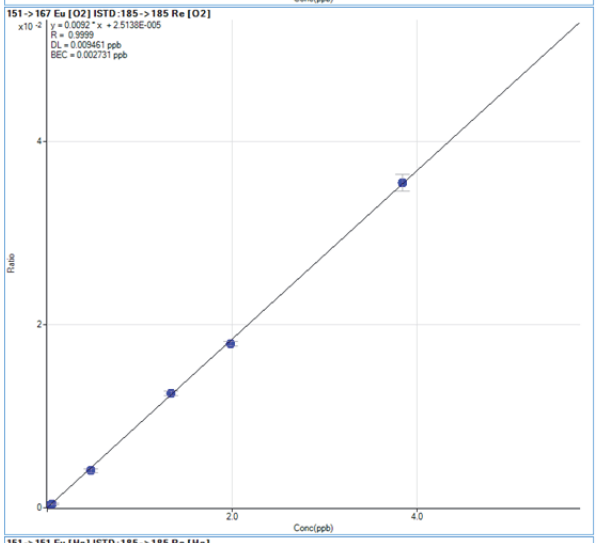
151-> 167 Eu [O2] ISTD:185-> 185 Re [O2]
x10 -2
y = 0.0092 * x + 2.5138E-005
R = 0.9999
DL = 0.009461 ppb
BEC = 0.002731 ppb
Ratio
Conc(ppb)

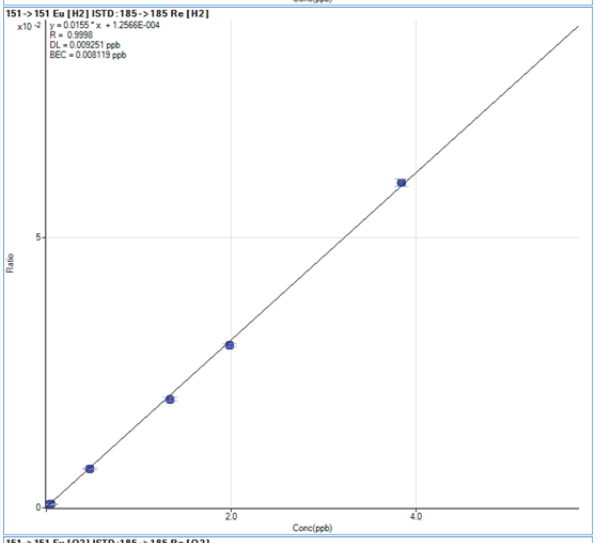
151-> 151 Eu [H2] ISTD:185-> 185 Re [H2]
x10 -2
y = 0.0155 * x + 1.2566E-004
R = 0.9998
DL = 0.009251 ppb
BEC = 0.008119 ppb
Ratio
Conc(ppb)

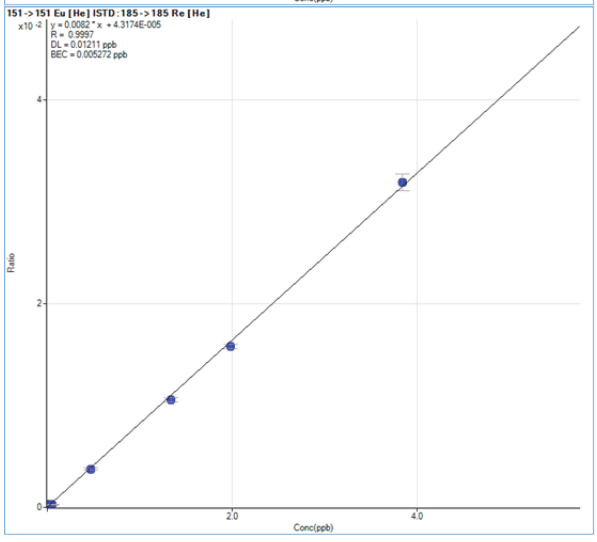
151-> 151 Eu [He] ISTD:185-> 185 Re [He]
x10 -2
y = 0.0082 * x + 4.3174E-005
R = 0.9997
DL = 0.01211 ppb
BEC = 0.005272 ppb
Ratio
Conc(ppb)

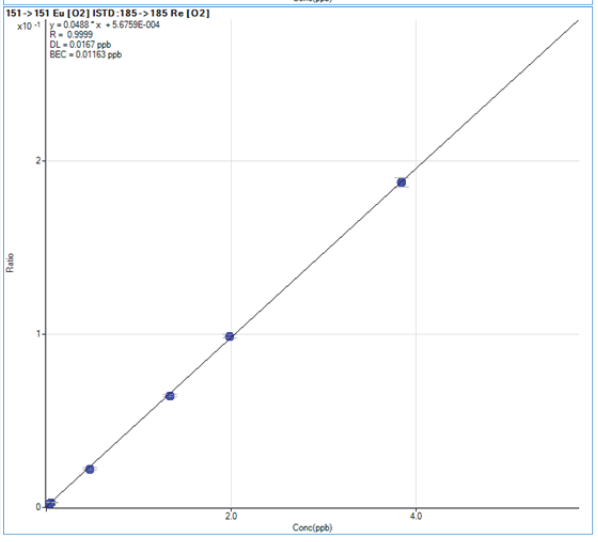
151-> 151 Eu [O2] ISTD:185-> 185 Re [O2]
x10 -1
y = 0.0488 * x + 5.6759E-004
R = 0.9999
DL = 0.0167 ppb
BEC = 0.011163 ppb
Ratio
Conc(ppb)

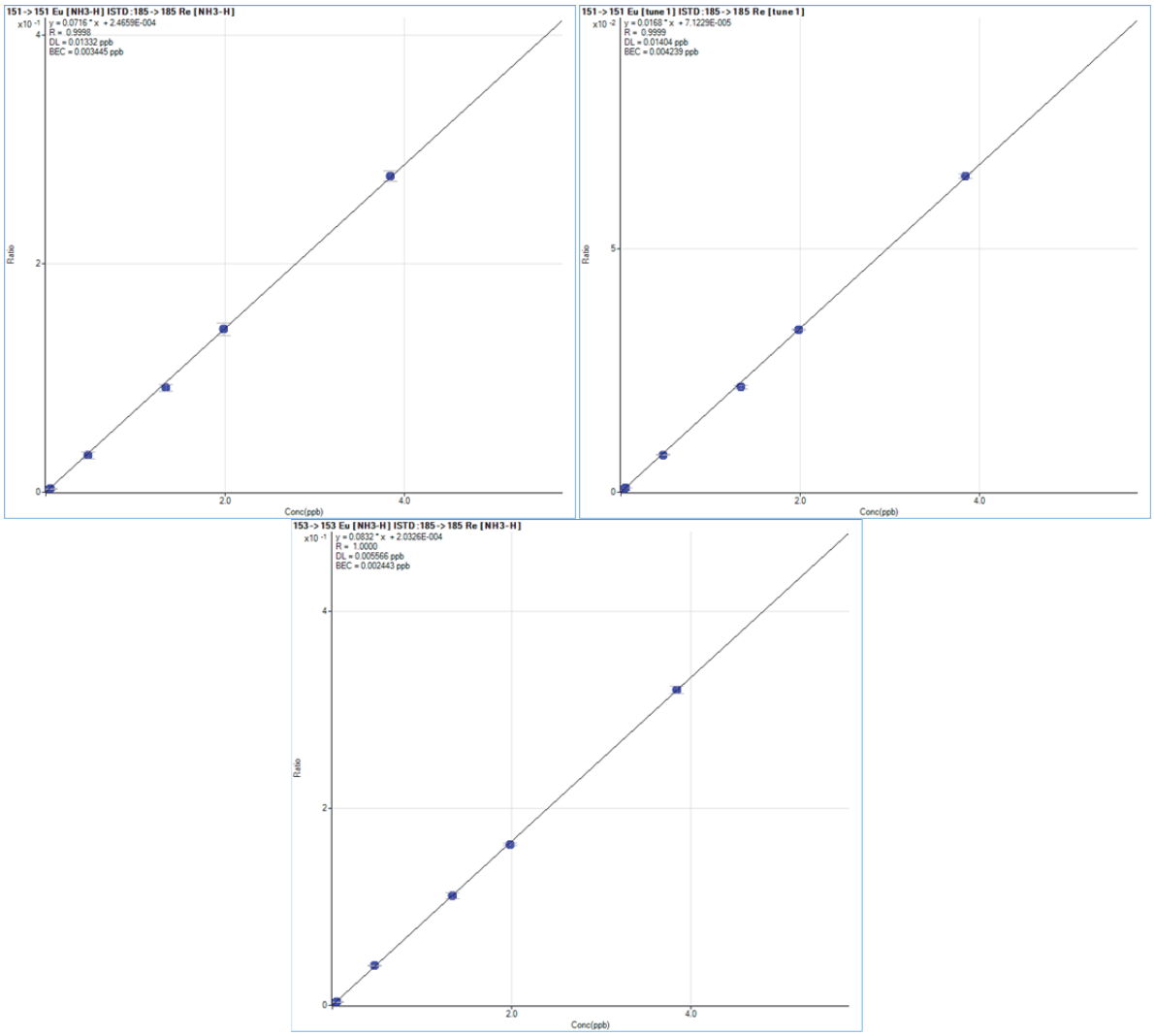

Figure 7.46: Matrix-matched calibration for gas modes under test for method validation

7.9.9 Results and discussion

7.9.9.1 Testing interference removal of BaO in no gas mode

The true isotopic compositions of ^{153}Eu and ^{151}Eu have always an accurate linear correlation. If the ratios are not altered by interferences caused by BaO then accurate linear correlation should exist and is expected between the mass fractions of ^{153}Eu and ^{151}Eu. Figure 7.47 shows a correlation of mass fractions of ^{153}Eu and ^{151}Eu experimentally determined for geological reference materials in no gas mode. The points are labelled 1, 2, 3… referring to each reference material. There does not seem to be any correlation of mass fraction of ^{153}Eu and ^{151}Eu for reference material with considerable amounts of Ba i.e. NKT-1, G-3 and MTA-1 etc. The more the concentration of Ba is, the more outwards are the points from correlation as shown in Figure 7.47 in no gas mode. This is not the case with point 8 and 9 referring MUH-1 and MRH-1, the mass fractions are not altered with BaO interference and there exists a good correlation. The mass fractions of Ba in MUH-1 and MTA-1 are 3.79 and 4.98 mg/kg which is very low concentration and hence has no effect on Eu isotopes even in no gas mode.

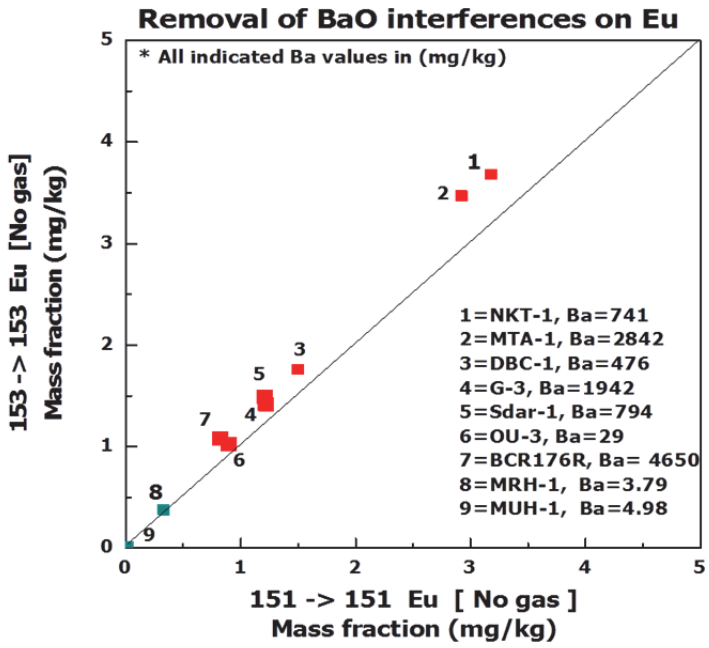

Figure 7.47: Correlation of mass fraction of ^{151}Eu and ^{153}Eu in no gas modes

7.9.9.2 Testing interference removal in He gas mode

Helium gas has been quite useful in regular single quad ICP-MS and has an important role in the removal of spectral interferences. He gas was also tested in BaO interference removal test on Eu. The switch time from no gas to He was kept 20 seconds so as to evacuate any remedies of previous gases and ions. The Figure 7.48 shows test results on reference material for removal of BaO interference on Eu isotopes. It can be observed that points for reference material with Ba contents are dispersed away from the line of correlation except for point 8 and 9 which refers to MUH-1 and MRH-1 with low Ba contents. Helium gas is also not good for BaO removal on Eu.

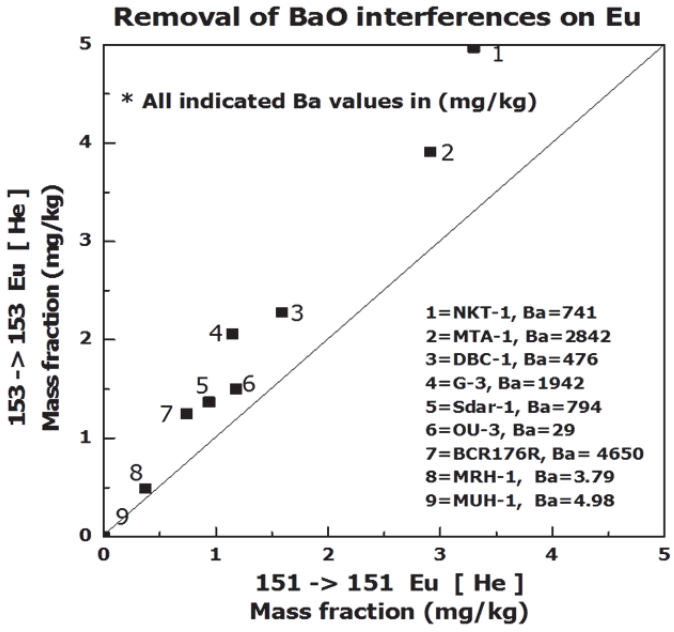

Figure 7.48: Correlation of mass fraction of ^{151}Eu and ^{153}Eu in He gas mode

7.9.9.3 Testing interference removal in H_2 gas mode

Initial tests with H_2 gas mode have revealed the hydride formation and incomplete interference removal of BaO. However, it was included in measurement for the purposes of

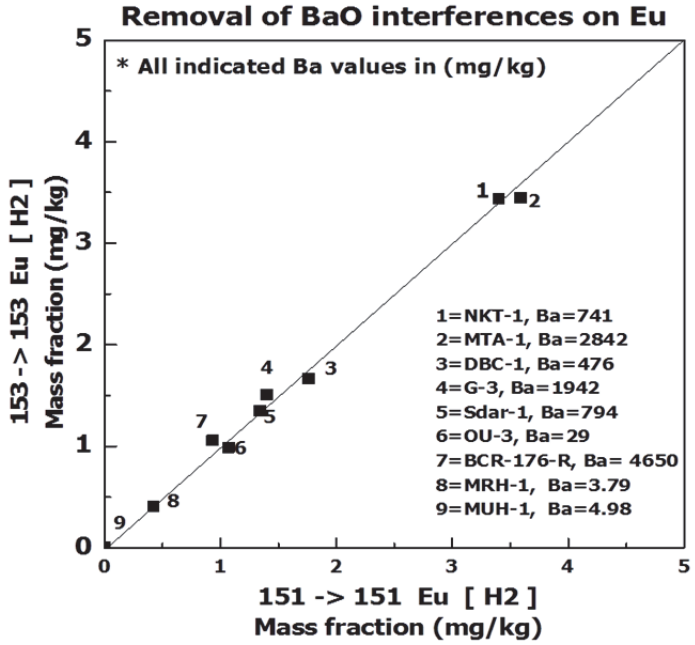

Figure 7.49: Correlation of mass fraction of ^{151}Eu and ^{153}Eu in H_2 gas mode

comparison with other gas modes. The results of this tests are shown Figure 7.50 which reflects that high Ba content are critical when Eu isotopes have to be measured using H_2 gas mode in reference material.

7.9.9.4 Testing interference removal in mass-shift O_2 gas mode

Initial tests of Ba reactivity with O_2 have demonstrated that if a mass-shift with O_2 gas is used, BaO interference can be avoided. Dealing with real matrices in reference material indicate that mass-shift with O_2 has also some problems regarding very high Ba contents as shown in Figure 7.50 and hypothesis is that some ionic species oxidise in plasma and enter the first quadrupole with m/z equivalent of 151, which are further oxidised while coming in contact with oxygen in collision/reaction cell. Point 2, 4 and 7 for reference materials MTA-1 (2842 mg/kg), G-3 (1942 mg/kg) and BCR-175-R (4650 mg/kg) still suffer BaO interference and do not lie on the line of correlation as shown in Figure 7.50. The reference materials with low Ba contents have no effect of oxide interferences of Ba and are located on the line of correlation as shown with points 8 (MRH-1 3.79 mg/kg) and 9 (MUH-1 4.98 mg/kg). The other reference material with points other than 2, 4 and 7, show that the interference has been removed and that is why a true correlation exist between the mass fractions of ^{151}Eu and ^{153}Eu.

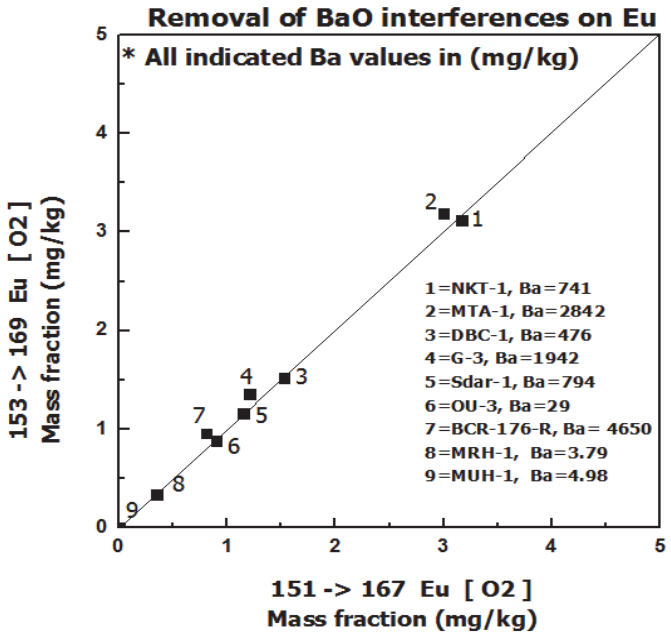

Figure 7.50: Correlation of mass fraction of ^{151}Eu and ^{153}Eu in O_2 gas mode

7.9.9.5 Testing interference removal in NH_3 gas mode (low, medium and high)

Initial testing on BaO removal on Eu isotopes has shown that ammonia gas is effective in minimising the BaO interference in comparison to other reactive gases as shown in section 17.5. The method was optimised with the best tune configuration of the instrument and ammonia gas was connected to the chamber with different flow rates. The flow rate low medium and high refer to 2, 3 and 5 ml/min of ammonia gas in helium gas. The switch time between the non-ammonia gas and ammonia gas was kept 25 seconds while the switch time amongst all ammonia modes was 5 seconds.

The results of the selected gas modes with on-mass ammonia gas modes are shown in Figure 7.51, Figure 7.52 and Figure 7.53. Although ammonia gas with a high flow rate of 5 ml/min has shown better results, other flow rates 2 and 3 ml/min were also chosen to compare the performance of BaO removal. A flow rate of 2 ml/min is not sufficient to make clusters of Ba and form $Ba(NH_3)_x$ as shown in Figure 7.51. But, with an increase in flow rate to 3 ml/min, the cluster formation of $Ba(NH_3)_x$ increased resulting in the shift of m/z of interference away from ^{151}Eu and ^{153}Eu isotopes. Figure 7.52 shows improvement in interference removal. To ensure removal of all oxides of Ba, the high flow rate has shown the best performance, as ^{151}Eu and ^{153}Eu isotopic mass fractions have an exact correlation as expected as shown in Figure 7.53. Therefore, a higher flow rate of ammonia i.e. is recommended in method validation and precise measurement of Eu in geological matrices.

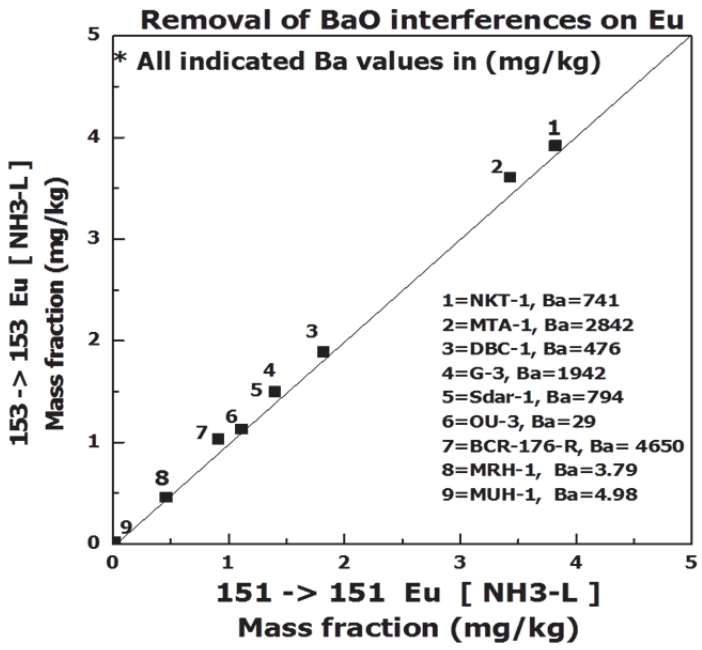

Figure 7.51: Correlation of mass fraction of ^{151}Eu and ^{153}Eu in NH_3-L gas mode

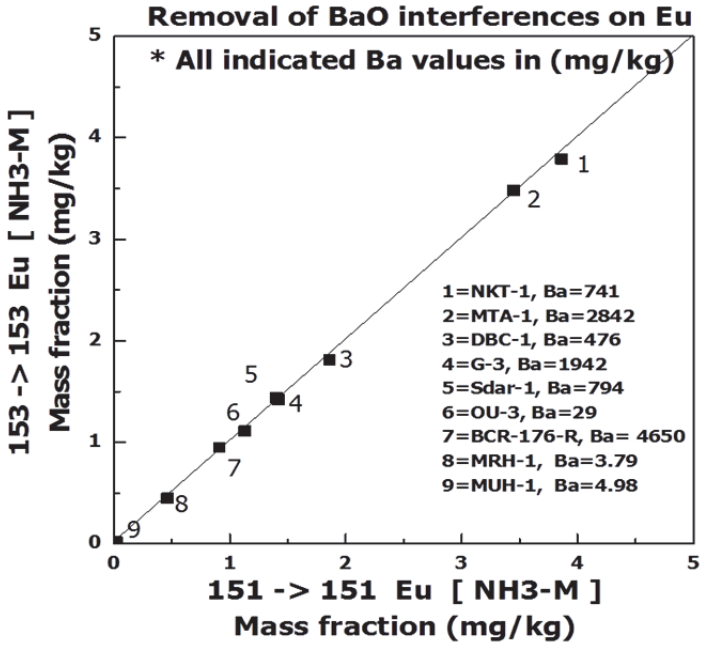

Figure 7.52: Correlation of mass fraction of ^{151}Eu and ^{153}Eu in NH_3-M gas mode

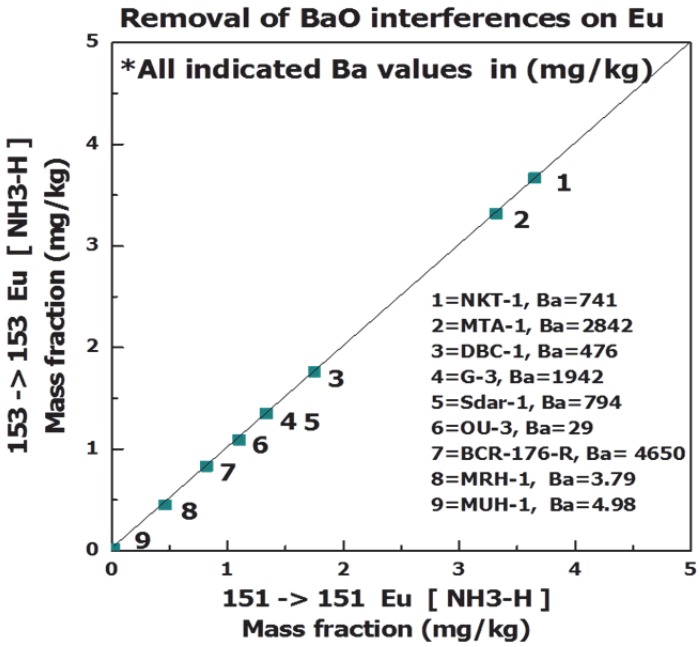

Figure 7.53: Correlation of mass fraction of ^{151}Eu and ^{153}Eu in NH_3-H gas mode

From the test results, it is shown that Ba interferences on Eu can remove with CRC technology without chromatographic separations and algebraic corrections.

Table 7.25: Measurement results of Eu in geological reference material

Results of measurement of Eu in geological reference material

	MRH-1		G-3		MTA-1		OU-3		DBC-1		NKT-1		BCR-176-R		SdAR-1		MUH-1	
Gas modes	mg/kg	RSD	mg/kg	RSD	mg/kg	RSD	mg/kg	RSD	mg/kg	RSD	mg/kg	RSD	mg/kg	RSD	mg/kg	RSD	mg/kg	RSD
Ref or certified value	0.47	2%	1.40	2%	3.36	10%	1.15	9%	1.77	3%	3.84	4%	0.87		1.34	2%	0.026	0%
151 -> 151 Eu [No Gas]	0.42	3%	1.54	2%	3.73	1%	1.15	3%	1.92	2%	4.06	2%	1.04	2%	1.56	2%	0.028	8%
151 -> 151 Eu [O2]	0.43	1%	1.52	1%	3.79	1%	1.15	1%	1.95	1%	4.04	1%	1.04	2%	1.47	2%	0.033	7%
151 -> 151 Eu [He]	0.42	7%	1.36	3%	3.37	3%	1.09	3%	1.85	2%	3.83	2%	0.86	3%	1.34	1%	0.022	7%
151 -> 151 Eu [H2]	0.43	1%	1.45	1%	3.54	1%	1.12	1%	1.86	0%	3.81	2%	0.99	3%	1.43	1%	0.029	4%
151 -> 151 Eu [NH3-M]	0.46	2%	1.42	2%	3.49	0%	1.15	1%	1.89	1%	3.95	2%	0.93	2%	1.45	2%	0.020	0%
151 -> 151 Eu [NH3-L]	0.47	1%	1.44	1%	3.56	1%	1.17	2%	1.92	0%	4.05	0%	0.97	2%	1.50	1%	0.020	5%
151 -> 151 Eu [NH3-H]	0.47	1%	1.38	2%	3.44	1%	1.15	2%	1.84	1%	3.87	0%	0.87	2%	1.42	2%	0.020	0%
151 -> 167 Eu [O2]	0.43	4%	1.37	2%	3.56	1%	1.10	3%	1.85	2%	3.76	2%	0.84	3%	1.29	4%	0.023	6%
153 -> 153 Eu [No Gas]	0.43	4%	1.67	1%	3.9	1%	1.14	2%	1.96	2%	4.11	3%	1.20	1%	1.58	1%	0.033	6%
153 -> 153 Eu [O2]	0.41	1%	1.67	1%	3.94	1%	1.09	1%	1.89	1%	3.89	0%	1.20	2%	1.45	2%	0.026	6%
153 -> 153 Eu [He]	0.47	10%	1.41	2%	3.64	4%	1.22	3%	1.98	2%	4.16	2%	1.00	3%	1.54	3%	0.035	8%
153 -> 153 Eu [H2]	0.44	2%	1.71	2%	3.96	1%	1.17	1%	2.01	1%	4.19	2%	1.30	3%	1.67	2%	0.010	5%
153 -> 153 Eu [NH3-M]	0.46	2%	1.47	1%	3.58	1%	1.15	1%	1.89	1%	3.96	0%	0.99	1%	1.49	2%	0.020	2%
153 -> 153 Eu [NH3-L]	0.46	0%	1.51	1%	3.63	1%	1.14	2%	1.92	1%	3.98	0%	1.05	1%	1.53	2%	0.020	10.0%
153 -> 153 Eu [NH3-H]	0.46	2%	1.38	1%	3.42	1%	1.14	1%	1.85	1%	3.87	1%	0.88	2%	1.44	1%	0.020	10.0%
153 -> 169 Eu [O2]	0.43	4%	1.44	2%	3.69	1%	1.19	2%	1.94	2%	3.98	1%	0.94	4%	1.43	2%	0.020	5%

7.10 Addressing the special case of removal of Zr interference on Sc

Interferences of $^{90}Zr^{2+}$ on $^{45}Sc^{+}$ were detected in zirconium rich reference materials e.g. OU-3 with 942.79 mg/kg Zr mass fractions. The study was conducted on interference removals of $^{90}Zr^{2+}$ on $^{45}Sc^{+}$, in several geological reference materials (RM), e.g. MRH, MUH-1, G-3, MTA, OU-3, DBC-1, NKT-1, SdAr-1, BCR-176-R (incineration ash) etc. The reference materials were digested with Na_2O_2 sintering and protocol is mentioned in chapter 5. The measurement of Sc in no gas mode always resulted in higher mass fractions than reference/certified values using regular single quad ICP-MS as shown in Figure 7.54. The reason for increased intensity of $^{45}Sc^{+}$ is due to increased $^{90}Zr^{2+}$ signals intensity that adds to $^{45}Sc^{+}$ intensity in no gas mode which leads to a false estimation of true concentrations of Sc. The study of interferences of $^{90}Zr^{2+}$ on $^{45}Sc^{+}$ was first reported in Bokhari and Meisel (2014a), Bokhari *et al.* (2015b).

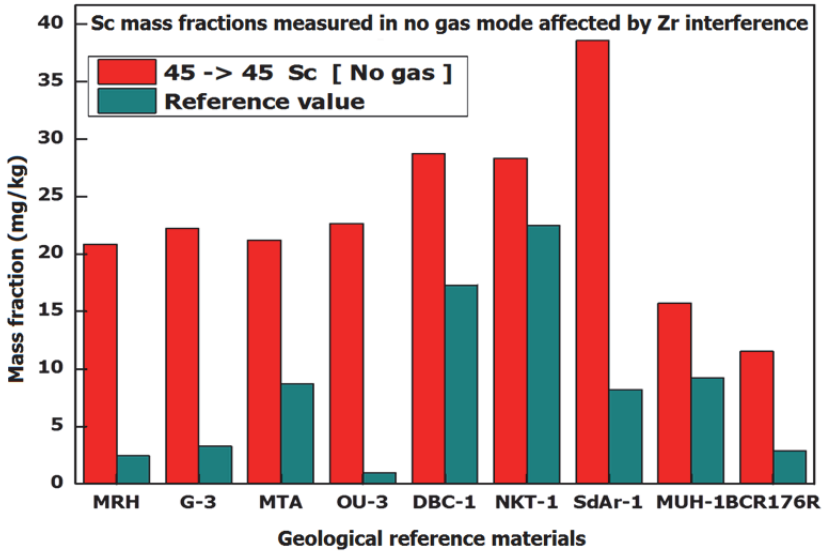

Figure 7.54: Interferences of Zr on Sc

7.10.1 Experimental

7.10.1.1 Initial testing with pure solution

The initial tests were performed on Sc and Zr pure solutions with 1:10 dilution separately i.e. 1 mg/kg solution of Sc and 10 mg/kg solution of Zr. The results of initial tests show that a 0.23% of interference is caused by 10 mg/kg mass fraction of Zr. This interference on Sc will multiplicate when a higher concentration of Zr is dealt with the real matrix or geological reference material e.g. MRH-1 has Zr mass fractions of 471 mg/kg. The increased concentration of Sc in MRH-1, when measured in no gas mode, is given in Figure 7.54 which is false when compared with certified value i.e. 21 vs 2.3 mg/kg. It became essential to control this interference using collision/reaction cell technology of the Agilent 8800 ICP-MS/MS.

7.10.1.2 Testing reactivity of Zr with cell gases

It was important to see the behaviour of the Zr interference inside collision/reaction cell with different test gases. The test gas that significantly decreased the Zr sensitivity was used in its removal on Sc analyte. The results of reactivity of Zr in CRC with different cell gases are given in Figure 7.55. The intensity of Zr increased with hydrogen gas and

decreased with the use of other gases i.e. Helium, Oxygen and ammonia gases. A higher flow rate of ammonia, i.e. 5 ml/min in helium gas has mostly decreased its intensity.

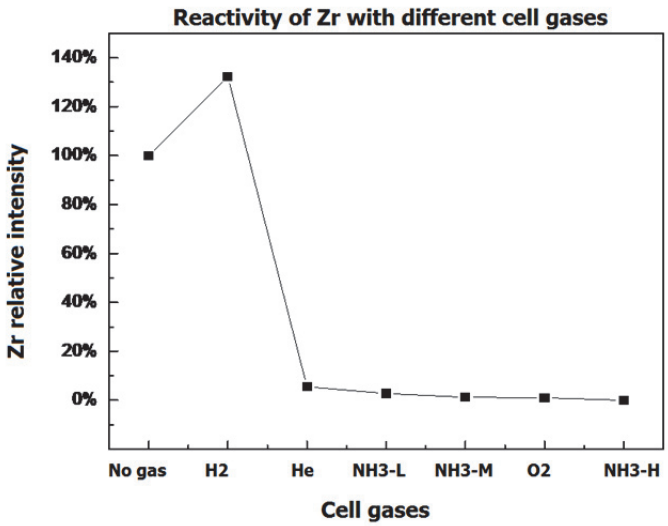

Figure 7.55: Tests of the reactivity of Zr with cell gases

This decrease in intensity on its mass-to-charge ratio of 90 means another product was being formed with ammonia or other gases. When Zr was tested for the type of product ions formed in oxygen gas with a flow rate of 0.7 ml/min, it had shown that zirconium is converted into ZrO^+, ZrO_2^+, ZrO_3^+ and ZrO_4^+. The loss in intensity in 90 -> 90 Zr [O2] was 0.04 % in on-mass Zr measurement. Thus oxygen gas is beneficial for the elimination of $^{45}Zr^{2+}$ interference on $^{45}Sc^+$. The results of the test are shown in Table 7.26.

Table 7.26: Behaviour of Zr in oxygen cell gas

Gas modes	Relative intensity of Zr
90 Zr [No Gas]	100%
90 -> 90 Zr [O2]	0.04%
90 -> 106 Zr [O2]	3.07%
90 -> 122 Zr [O2]	0.67%
90 -> 138 Zr [O2]	1.44%
90 -> 154 Zr [O2]	0.01%

The tests on the behaviour of Zr with ammonia gas revealed condensation products of zirconium and $Zr(NH_3)_5$ and $Zr(NH_3)_6$ were the main product and ammonia gas can also be used for elimination of zirconium interference. An on-mass measurement of Sc can be beneficial if Zr is reactive to oxygen and ammonia. But prior to test the method, product ions of Sc were also tested. The product ion of Sc based on its reactivity were chosen for the elimination of interference.

7.10.1.3 Scan of Sc product ions with relative intensities of Zr

Spectrum was scanned for the all possible product ions of scandium on Q2 using the mass-shift method with a view point of selection of the product ion with least Zr interferences. Following product ions were created with each gas modes and have their merits and demerits.

Product ions scan in H_2 gas

In hydrogen gas mode, none of the product ions removed the Zr interference on Sc completely. The underline mode had no intensities at all as shown in the Table 7.27.

Table 7.27: Effect of hydrogen gas in the reduction of Zr interference on Sc

Gas modes	Relative Sc intensities	Zr/Sc ratios
45 -> 45 Sc [tune 1]	100%	0.209%
45 -> 45 Sc [H2]	96%	0.172%
45 -> 46 Sc [H2]	0.12%	0.002%
45 -> 47 Sc [H2]	0%	0%

Product ions scan in O_2 gas

Only mass-shift mode **45 -> 61 Sc [O2]** was better than any other mode with good sensitivities as shown in the Table 7.28.

Table 7.28: Effect of oxygen gas in the reduction of Zr interference on Sc

Gas modes	Sc intensities	Zr/Sc intensities
45 -> 45 Sc [tune 1]	100%	0.210%
45 -> 61 Sc [O2]	91%	0.025%
45 -> 45 Sc [O2]	5%	0.051%
45 -> 77 Sc [O2]	1%	0%

Product ions scan in NH_3 gas

Several product ions of Sc were checked with ammonia gas modes with different flow rates i.e. 2, 3 and 5 ml/min in helium gas. These have been sorted for best intensities and least interferences as shown in Table 7.29. The only choice of the selection among ammonia gas mode was the 45 -> 130 Sc [NH3-M].

Table 7.29: Effect of ammonia gas in the reduction of Zr interference on Sc

Gas modes	Relative intensities of Sc	Zr/Sc ratios
45 -> 45 Sc [tune 1]	100.%	0.23%
45 -> 130 Sc [NH3-M]	5.0%	0.0022%
45 -> 130 Sc [NH3-L]	4.6%	0.0011%
45 -> 45 Sc [NH3-L]	1.9%	0.0006%
45 -> 147 Sc [NH3-M]	1.3%	0.0007%
45 -> 147 Sc [NH3-L]	1.26%	0.0004%
45 -> 45 Sc [NH3-M]	0.88%	0.0004%
45 -> 113 Sc [NH3-M]	0.69%	0.0003%
45 -> 130 Sc [NH3-H]	0.47%	0.0001%
45 -> 113 Sc [NH3-L]	0.41%	0.0001%
45 -> 147 Sc [NH3-H]	0.22%	0.0000%
45 -> 113 Sc [NH3-H]	0.05%	0.0000%
45 -> 96 Sc [NH3-M]	0.02%	0.0000%
45 -> 96 Sc [NH3-L]	0.016%	0.0000%
45 -> 45 Sc [NH3-H]	0.005%	0.0000%
45 -> 79 Sc [NH3-L]	0.004%	0.0000%
45 -> 62 Sc [NH3-L]	0.003%	0.0000%
45 -> 79 Sc [NH3-M]	0.002%	0.0000%
45 -> 62 Sc [NH3-M]	0.002%	0.0000%
45 -> 96 Sc [NH3-H]	0.001%	0.0000%
45 -> 62 Sc [NH3-H]	0%	0%
45 -> 79 Sc [NH3-H]	0%	0%

7.10.2 Method development for Sc measurement in geological reference material

Based on above testing on standard solutions of Sc and Zr, the capability of each product ion was evaluated and the best product ions were selected for interference removal studies on reference materials. The suggested gas modes and product ions were 45 -> 61 Sc [O2], 45 -> 45 Sc [NH3-L], 45 -> 130 Sc [NH3-M] or 45 -> 147 Sc [NH3-M] and on-mass He mode was added to see the effect on reference materials with less Zr contents.

7.10.2.1 Results and discussion

The chosen on-mass and mass-shift modes were applied for method validation on the reference materials. The zirconium mass fractions of the reference materials are given in Table 7.30 which can reflect the amount of zirconium interference on Sc. The details of certified/reference values can be found on geoanalyst.org.

Table 7.30: Certified/reference values of Zr mass fractions in reference materials

Reference materials	Zr reference value or *certified values
	mg/kg
NKT-1	292
*MTA-1	368
DBC-1	183
G-3	330
SdAR-1	352.8
OU-3	942
BCR-176-R	--
*MRH-1	471
MUH-1	--

The Zr contents of the reference material MRH-1 are 471 mg/kg. The results for MRH-1 are shown in Table 7.31 which indicates that all the nominated gas modes are good for Sc determination except He and no gas mode. The reference material MUH-1 has a less Zr mass fraction and Sc seems to be least affected and thus He is also better along with other gases. The Zr contents of the reference material G-3 are 330.5 mg/kg. The lower values determined with higher mass product ions are related with intensities but on-mass 45 -> 45 Sc [NH3-L] serves the purpose. The Zr contents of the reference material MTA-1 are 368 mg/kg. The mass fractions determined with suggested gas modes are in good agreement with reference value except no gas mode. OU-3 reference material has relatively higher Zr contents and lower Sc mass fraction. The lower mass fraction obtained for higher mass product ion can be due to loss in intensities in the product ion formation. In DBC-1, the results in He gas mode yield higher mass fractions than the reference value but suggested gas modes are better than helium and no gas mode. For reference material NKT-1, results with suggested gas modes are better than helium and no gas modes. BCR-176-R is the industrial incineration ash reference material with less Zr contents. All the mass fraction of Sc determined with suggested gas modes are good except the He and the no gas mode. The Zr contents of the reference material SdAR-1 are 352.8 mg/kg. Helium and no gas modes are not good but all other suggested gas modes yield results in accordance with reference values. From the test results and method validation on reference materials, it is evident that Sc can be measured without chromatographic separation using collision/reaction cell technology. The suggested gas modes are 45 -> 61 Sc [O2], 45 -> 45 Sc [NH3-L], 45 -> 130 Sc [NH3-M] or 45 -> 147 Sc [NH3-M].

Table 7.31: Table of results of Sc measurement in geological reference material

Mass fractions of Sc in geological reference material																		
Gas modes	**MRH-1**		**MUH-1**		**G-3**		**MTA-1**		**OU-3**		**DBC-1**		**NKT-1**		**BCR-176-R**		**SdAR-1**	
	mg/kg	RSD	mg/kg	RSD	mg/kg	RSD	mg/kg	RSD	mg/kg	RSD	mg/kg	RSD	mg/kg	RSD	mg/kg	RSD	mg/kg	RSD
Ref or certified Value	2.3	22%	9.0	4%	3.29	2%	8.6	7%	0.76		17.3	2%	22.5	2%	2.91		8.2	3%
45 -> 45 Sc [tune 1]	19	2%	13.2	7%	17.88	3%	16.17	6%	15.48	10%	18.56	3%	28.35	8%	6.66	1%	21.14	3%
45 -> 45 Sc [He]	5.2	10%	9.4	6%	5.95	13%	8.61	5%	5.57	4%	21.43	8%	27.08	11%	3.59	10%	13.74	12%
45 -> 45 Sc [NH3-L]	2.4	7%	8.6	8%	3.22	10%	8.1	5%	0.86	25%	15.56	3%	20.44	4%	2.88	8%	8.19	7%
45 -> 61 Sc [O2]	2.9	4%	9.6	2%	3.81	3%	8.56	6%	0.81	7%	17.17	2%	20.46	12%	2.51	5%	8.16	6%
45 -> 130 Sc [NH3-M]	2.2	4%	8.6	4%	2.6	3%	8.2	2%	0.52	13%	17.05	4%	19.77	2%	2.46	3%	8.24	1%
45 -> 147 Sc [NH3-M]	2.2	5%	9.0	2%	2.96	7%	8.16	4%	0.57	10%	17.0	2%	20.98	1%	2.4	6%	8.1	4%

7.11 Summary

In this chapter it is shown in particular, that the suppression of spectral interferences on the REE by using ion-molecule reactions in the collision/reaction cell can significantly improve elemental selectivity and accuracy in the ICP-MS/MS applications for the geological reference materials.

This chapter describes studies that were carried out in order to suppress spectral interferences on the REE under the influence of the cell gases in collision/reaction cell. It describes the chemical reactions that occur with the use of different reactive gases i.e. ammonia and oxygen in particular. The understanding of ion-molecule reaction, product ion with maximum intensities and efficiency towards interference removal was the foreground of this chapter.

The relative reactivities of NH_3 and O_2 gases with the interferences (oxides, hydroxides and hydrides are shown and the magnitude of interferences on rare earth elements is given details with initial testing of a standard solution of rare earth elements.

Chemistry of ion-molecule reactions has offered a wide variety of pathways for the separation of analyte ions from a given interference for a new method development. Two approaches have been discussed and applied in the elimination of the interferences i.e. on-mass and mass-shift methods in the reaction collision cell with the aid of a selective reactive gas. In an on-mass gas mode method, the elimination of the interference takes place by reactions that convert the interference into an ion of different mass, shifted away from the analyte of interest. In mass-shift gas mode method, an analyte ion is made to react with the reaction gas to shift its m/z to a non-interfered m/z for detection. The occurrence of these reactions is related to the thermodynamic properties of the ions and reaction gases. It can, in most cases, be estimated whether the reaction will occur in the CRC or not. Most of the current literature using collision reaction technology lack method validation on reference materials. This study has made use of optimised sample digestion method discussed in chapter 5 for sample preparation of reference materials and has validated the method with various reference materials

Initial testing with oxygen gas for interference removal capability, shows its excellent performance, but when it is applied in method validation to real matrices it is evident that use of O_2 leads to the formation of unidentified product ions, which cause additional interferences and reduce sensitivity for the analyte. This is the outlook of this study to further explore possibilities of using oxygen gas for reduction of interferences. However, the role of ammonia gas has been better than oxygen.

This study has described a new method for the determination of Sc in complex matrices with severe interferences of doubly charged ions of Zr. The method is capable of Sc determination even in industrial samples which is often a matrix full of all possible interferences i.e. BCR-176-R.

In the new methods developed in this study through ion-molecule reaction, different on-mass and mass-shift modes have been suggested in this chapter which can be applied for the routine determination of rare earth elements free from spectral interferences.

The results of the method on reference materials recommend the use of shaded gas modes/product ions with maximum integration times (Table 7.32), if whole-rock chemistry has to be performed during analysis. Use of oxygen gas in oxygen mass-shift mode was not satisfactory and it is not recommended.

Table 7.32 The recommended mode for measurement of REE and Sc

Analyte	m/z	Gas modes		
		Mass-shift O_2	Mass-shift NH_3	On-mass NH_3
La	139	139 -> 155 La [O2]	139 -> 224 La [NH3-M]	
Ce	140	140 -> 156 Ce [O2]	140 -> 225 Ce [NH3-M]	
Pr	141	141 -> 157 Pr [O2]		141 -> 141 Pr [NH3-M]
Nd	146	146 -> 162 Nd [O2]		146 -> 146 Nd [NH3-M]
Sm	147	147 -> 163 Sm [O2]		147 -> 147 Sm [NH3-L & M]
Eu	151	151 -> 167 Eu [O2]		151 -> 151 Eu [NH3-H]
Eu	153	153 -> 169 Eu [O2]		153 -> 153 Eu [NH3-H]
Gd	157	157 -> 173 Gd [O2]	157 -> 172 Gd [NH3-L]	
Tb	159	159 -> 175 Tb [O2]	159 -> 174 Tb [NH3-L]	
Dy	160	160-> 176 Dy [O2]		160-> 160 Dy [NH3-M]
Dy	163	163 -> 179 Dy [O2]		163 -> 163 Dy [NH3-M]
Ho	165	165 -> 181 Ho [O2]		165 -> 165 Ho [NH3-M]
Er	166	166 -> 182 Er [O2]		166 -> 166 Er [NH3-M]
Tm	169	169 -> 181 Tm [O2]		169 -> 169 Tm [NH3-M]
Yb	172	172 -> 188 Yb [O2]	172 -> 187 Yb [NH3-L]	
Lu	175	175 -> 191 Lu [O2]		175 -> 175 Lu [NH3-M]
Y	89	89 -> 105 Y [O2]	89 -> 157 Y [NH3-M]	
Sc	45		45 -> 130 Sc [NH3-M]	

Furthermore, significant signal suppression of analyte of trace concentration is of concern, which should be made a subject in further studies for spectral interference removals using ammonia gas.

8. Major and trace element chemistry in a collision/reaction cell

8.1 Introduction

Inductively coupled plasma mass spectrometry (ICP-MS) is the method of choice and most widely used technique for trace elemental analysis of industrial, geological, biological and environmental samples. It provides qualitative, semi-quantitative, quantitative elemental and isotopic ratio analysis of analytes in complex matrices. Other techniques i.e. ICP-AES, ICP-OES, or Flame-AA do not offer low detection limits and do not have simple spectra. Thus ICP-MS has preferences over several other techniques. Spectral interferences have been an issue in ICP-MS. A number of publications have described methods to reduce interferences with recent advances in technology. Interferences exist as spectral overlaps on the ions of interest from sample matrix or acids. These can also be isobaric or polyatomic. Polyatomic interferences are normally in the form of argides, oxides, hydroxides and dioxides. Spectral interferences have been addressed with two approaches i.e. high mass resolution and ion-molecule collision reaction chemistry in the collision/reaction cell. Ion-molecule reactions involve the use of appropriate reactive gas and determination of product ions free of spectral overlap. This may also lead to the formation of undesired product ions which are problematic for accurate analysis.

Several approaches have been reported to reduce the spectral overlap on analytes of interest. If the analyte is multi-isotopic, the ion signals of other isotopes with no overlaps are preferably measured. In many cases, it is the most abundant ion, that suffers from spectral overlaps of interferences. On the other hand, most of the monoisotopic elements are not interference free. This limits the approach of handling spectral overlaps (Jones 2007). Mathematical correction is another approach to deal with interferences for the accuracy of results, however, it only works when analyte signals over the overlapping ion signals are few (Date *et al.* 1987). Gases i.e. Xe, N_2, CH_4 and C_2H_6 have been reported to be added in argon flow to plasma for reduction of interferences but it did not improve much the signal to background ratios (Lam and Horlick 1990).

Analyte ions i.e. Ca^+ or K^+ with low ionisation energies were determined with cold plasma at lower temperatures for reduction of interferences with high ionisation energies i.e. Ar^+ and ArH^+ that increases the matrix effects more than being operated at conventional temperatures (Tanner 1995). Offline and online matrix separation using exchange chromatography have been used to remove interfering elements, however, that is time-consuming and not suitable for multi-elemental analysis (Ebdon *et al.* 1994).

$^{56}Fe^+$ was reported to be measured by ion-molecular reactions of ArO^+ with Xe to eliminate ArO^+ interference and Ar^{2+} was demonstrated to react with methane for $^{80}Se^+$ measurement by Rowan and Houk (1989). Ion-molecule reactions using O_2 gas provided higher reaction efficiency and improved detection limits (Douglas 1987). Ar^+ signals were lowered with a ICP-ion trap-MS by charge transfer reactions with water that was present in the trap (Barinaga *et al.* 1994).

Use of hydrogen gas for the elimination of Ar^+, N^+, O^+ and Cl^+ ions was demonstrated, oxygen gas was used for Sr^+ measurement by removal of Y^+ and Zr^+ interferences and methanol was used for removal of overlaps of $^{135}Ba^+$ and $^{139}Ba^+$ on $^{135}Cs^+$ and $^{139}Cs^+$ (Eiden *et al.* 1996). Turner *et al.* (1997) used helium gas to remove interferences by reactions/collision cell with ICP-MS linear r.f. device. Further status and development of ion-molecule reactions were described by Koppenaal *et al.* (2004). Koyanagi *et al.* (2009) contributed to the reaction chemistry of ion-molecular reactions. With the development of

ICP-DRC-MS, a new era of spectral interferences removal started using ion-molecule reactions (Jones 2007). Dr Bohme group introduced "ICP-Selected Ion Flight Tube-MS" instrument to measure ion-molecule reaction kinetics under thermal collision conditions (Koyanagi *et al.* 2000).

8.2 Aims of the chapter

The introduction of reaction collision cells into the field of analytical chemistry has revolutionised previous concepts of multi-stage analysis based on matrix separation with the anion and cation exchange chromatography etc. The analytical techniques that can perform rapid measurements in a short time are attractive to industrial, medicinal, geochemical and environmental science. With the invention of new technology by Agilent as 8800 ICP-MS/MS that is equipped with collision/reaction cell, the interferences on major and trace elements are being addressed.

We aim to address the background interferences in particular and interferences from the analytes from the geological matrices. Ion-molecule reactions have been explained in detail with its application to rare earth elements and platinum group elements in chapter 7 and 9. This section is related to the elements other than rare earth elements and PGE which involve major and trace elements. The salient aims of this chapter are as follows,

1. The goal of this chapter is to gain an understanding of ion-molecule reactions in a collision/reaction cell (CRC) for the perspective of resolving analyte ions from interferences by controlled chemical reactions in order to improve the ICP-MS measurement of elemental (analyte) ions.
2. To determine the influence of the cell gases i.e. ammonia and oxygen in collision/reaction cell (CRC in improving the performance of ICP-MS for the analysis of elements that suffer from polyatomic or isobaric interferences.
3. Investigation of instrumental background from gas blanks in different cell gases.
4. Investigation of solvent based interferences i.e. acids used in dilutions, on the background of the instrument in different cell gases.
5. Development of an analytical method for interference removal on Si, P, Ti, Cr, Mn, V, Fe, Cu, Zn, As, Sb and Pb etc. in geological reference materials.
6. To determine the reactivity of 46 analytes with ammonia and oxygen gases in collision/reaction cell.
7. To determine the product ions, an analyte may form with reaction to ammonia and oxygen gases.
8. Classification of the analytes on the basis of the product ions through ion-molecule reactions that an analyte can form in collision/reaction cell for determining the abundant product ion.
9. To provide the basis for future work for other elements by providing data on the product ions formed in collision/reaction cell in the presence of cell gases ammonia and oxygen.
10. Method validation with geological reference material.

8.3 Experimental

Single element standard solutions were prepared to 10 ng/ml final dilution with 1 % HNO_3. The details of ultra-pure water and acids used have been mentioned in chapter 5. Agilent 8800 ICP-MS/MS was used for analysis and instrument typical configurations are given in chapter 7.

8.4 Results and discussions

The gas flow rate of ammonia was selected as 3 ml/min and denoted as NH_3-M. The flow rate for oxygen gas was 0.3 ml/min. The instrument was tuned for best signal intensities and lowest background. The blanks were measured and subtracted from the reaction data of all the analytes. Gas modes used were no gas, on-mass ammonia, and several mass-shift for ammonia i.e. (M^+ +14), (M^++15), (M^++16), (M^++17), (M^++34), (M^++51), (M^++68), (M^++85) etc. The gas modes for oxygen gas were on-mass M^+ and mass-shift (M^++16). For some exceptional cases i.e. P higher oxides were also tested (M^+ +32), (M^++48), (M^++64). For W product ions were (M^++16), and (M^++32) etc.

8.4.1 Instrumental background interferences

Interferences caused solely by the plasma gas, entrained atmospheric gases and water are present regardless of whether a sample is being analysed or not (Date and Gray 1983, Evans and Giglio 1993). Houk *et al.* (1980) reported spectral overlaps in ICP-MS resulting from the plasma gas water and entrained air. The background ions from plasma, heavy noble gases at low concentrations and O, C, N and H, and impurities from cell gases may contribute to the instrumental background when no sample is run for analysis. Argon gas is the plasma gas and may carry impurities in it. The air entrained into the sampling zone in plasma from the atmosphere can also be the cause for instrumental background (Douglas and French 1988).

Thomas (2013) describes that in the argon plasma, spectral overlaps caused by argon ions and combinations of argon ions with other species are very common. The most abundant isotope of argon is at mass/z 40, which dramatically interferes with the most abundant isotope of calcium at mass/z 40, whereas the combination of argon and oxygen in an aqueous sample generates the $^{40}Ar^{16}O^+$ interference, which has a significant impact on the major isotope of Fe at mass 56 (Thomas 2013).

For the purpose of evaluation of the instrumental background and influence of the cell gases i.e. H_2, O_2, He and NH_3, the instrument was run on gas blank without the supply of solutions i.e. carrier solution and internal standard etc. Then gas blanks for reactive gases were run in the same batch. Three gas blanks were measured and ion signals were monitored for any interferences from plasma and air etc. The background for most of the elements is shown in Figure 8.1-Figure 8.5.

This can be observed that there is an abundance of $^{14}N^+$ and $^{12}C^+$ ions in the plasma. $^{23}Na^+$ ions might be due to the instrumental memory as sodium peroxide digested samples are routinely measured with this instrument. At m/z of $^{24}Mg^+$ and $^{12}C_2^+$, ions are formed which are reduced by cell gases He and ammonia significantly. The m/z of $^{27}Al^+$ is assumed to be overlapped by $^{12}C^{15}N^+$ and $H^{12}C^{14}N^+$ ions. He and ammonia reduce this background which is created by $^{12}C^{15}N^+$ and $H^{12}C^{14}N^+$ ions. The m/z of $^{28}Si^+$ is overlapped by $^{14}N_2^+$ and $^{12}C^{16}O^+$ and ammonia gas reduces these signals. The m/z of ^{37}Cl suffers from the overlap of $^{36}ArH^+$ which is eventually reduced with ammonia gas. The intensity of $^{36}Ar^+$ itself was observed in no gas, He, O_2 and hydrogen gases and it decreases significantly with ammonia gas. There are interferences at m/z of $^{31}P^+$ from $^{14}N^{16}OH^+$, $^{14}N^{17}O^+$, $^{13}C^{16}OH_2^+$, $^{13}C^{18}O^+$, or $^{15}N_2H^+$ and ammonia gas is effective in decreasing the effect of these interferences. $^{40}Ar^+$ and $^{36}ArH_4^+$ m/z of $^{40}Ca^+$ and $^{14}N_2O^+$ are seen at m/z of $^{44}Ca^+$ and best removal is observed with ammonia gas. At the m/z of $^{45}Sc^+$, $^{12}C^{16}O_2H^+$ and $^{14}N_2{}^{16}OH^+$ are assumed which are reduced with ammonia gas. At m/z of $^{48}Ti^+$, $^{12}C^{36}Ar^+$ and $^{14}N^{17}O_2^+$ are assumed and no intensity can be observed with helium and ammonia gases which are effective in removing these background interferences.

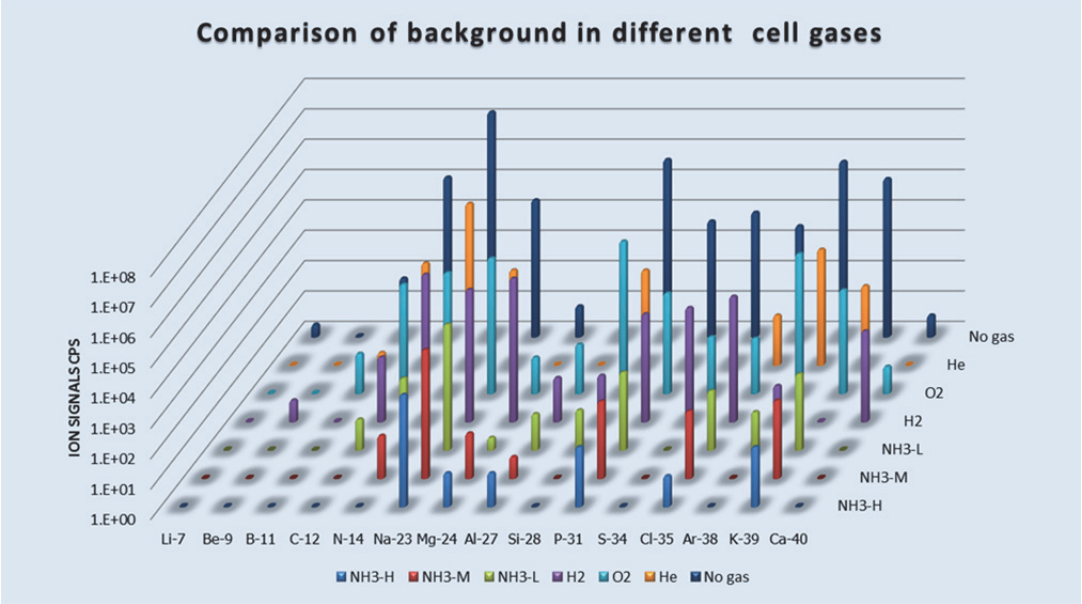

Figure 8.1: Influence of cell gases on instrumental background (Li - Ca)

At m/z of $^{55}Mn^+$, $^{40}Ar^{14}NH^+$, $^{40}Ar^{15}N^+$ and $^{38}Ar^{16}OH^+$are present. $^{40}Ar^{16}O^+$ and $^{40}Ar^{15}NH^+$ are present on $^{56}Fe^+$. At m/z of $^{63}Cu^+$ interferences from $^{40}Ar^{12}C^{14}NH^+$ are assumed. $^{40}Ar^{14}N^{12}O^+$, $^{40}Ar^{14}N_2^+$ and $^{40}Ar^{16}O_2^+$ are present at m/z of $^{68}Zn^+$. $^{40}Ar^{14}N^{16}O^+$ is present at $^{71}Ga^+$. $^{40}Ar^{16}O_2^+$ is present at $^{72}Ge^+$. $^{40}Ar_2^+$ is present at $^{80}Se^+$. $^{40}Ar_3^+$ is present at ^{120}Sn. Xe is heavy noble metal and is also seen in the spectrum. Some interferences at $^{197}Au^+$ and $^{205}Tl^+$ are also observed. All these plasma and air based interferences are effectively removed with ammonia gas. The overlap which is observed in no gas mode is from plasma-based interferences, while overlaps in cell gases might be due to impurities from the cell gases themselves. The efficiency of cell gases to remove these interferences is shown in Figure 8.1- Figure 8.5.

The elimination of argide interferences with ammonia has been exemplified by a simple reaction that occurs by charge transfer reaction. The ionisation potential of Ar^+ is 15.8 eV and for ammonia is 10.02 eV. The ionisation potential of ammonia is lower than Ar^+ that makes reaction extremely exothermic and fast (Tanner and Baranov 1999, Thomas 2013).

$$NH_3 + Ar^+ \longrightarrow NH_3^+ + Ar \qquad (A)$$

The reaction of ammonia with other elements for example Ca^+ with ionisation potential 6.1 eV is not possible because it is lower than 10.02 eV. This reaction (B) is endothermic (heat of formation is 4.05 eV) and will not occur in CRC. This can be applied to all other elements whose ionisation potential are lower than ammonia i.e. 10.02 eV (Jones 2007, Völlkopf *et al.* 1999).

$$NH_3 + Ca^+ \longrightarrow NH_3^+ + Ca \qquad (B)$$

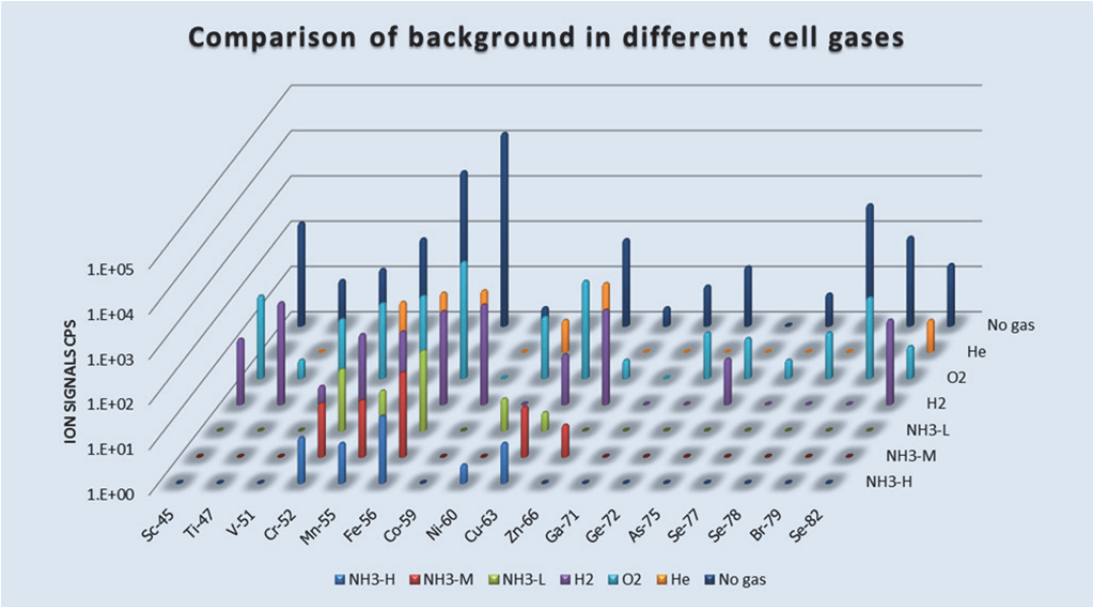

Figure 8.2: Influence of cell gases on instrumental background (Sc - Se)

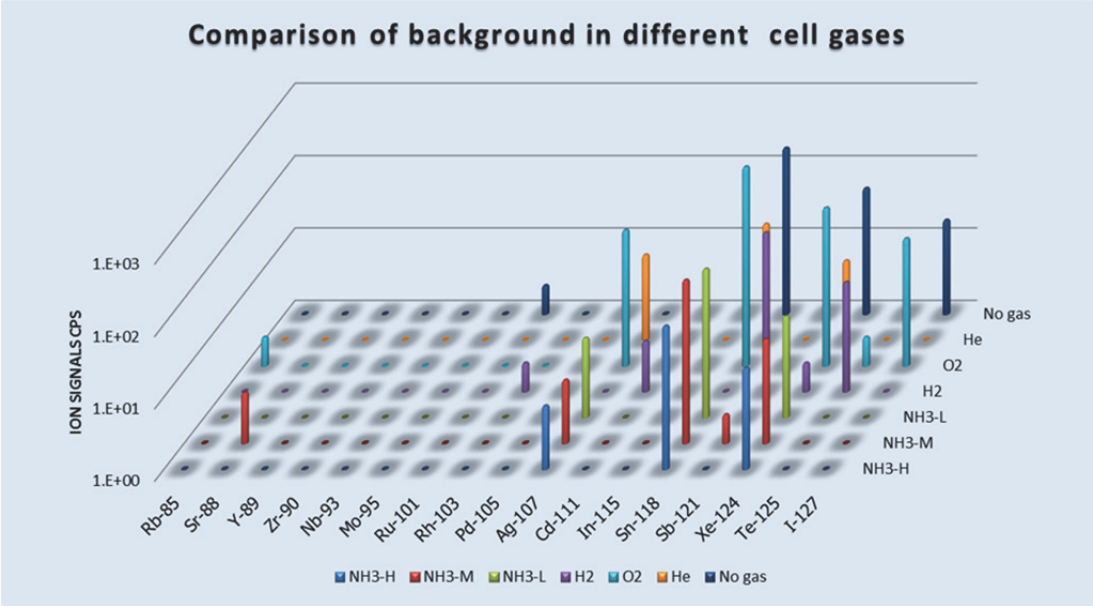

Figure 8.3: Influence of cell gases on instrumental background (Rb - I)

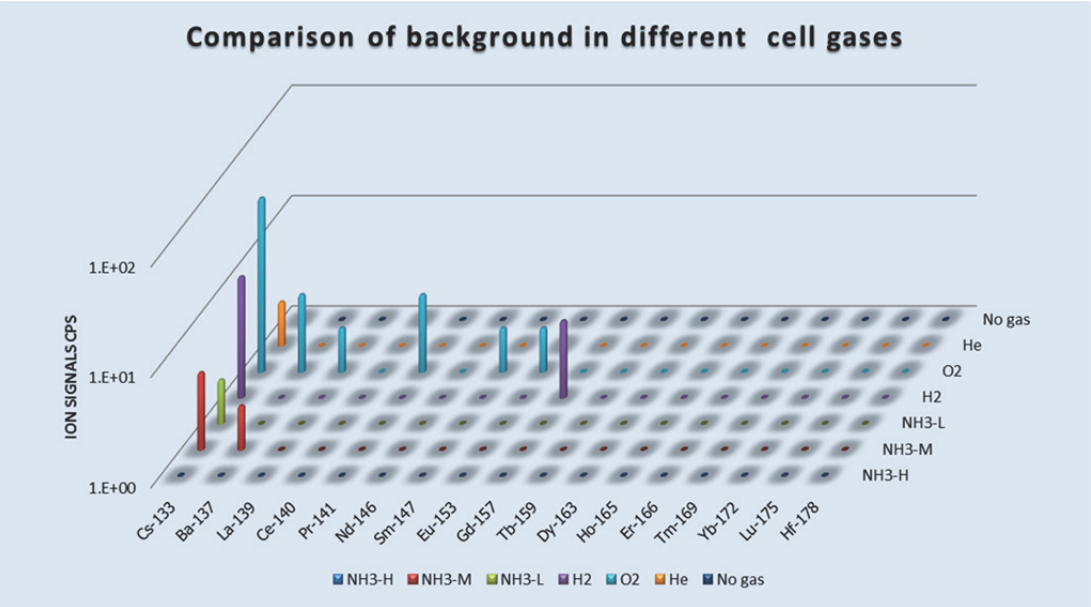

Figure 8.4: Influence of cell gases on instrumental background (Cs - Hf)

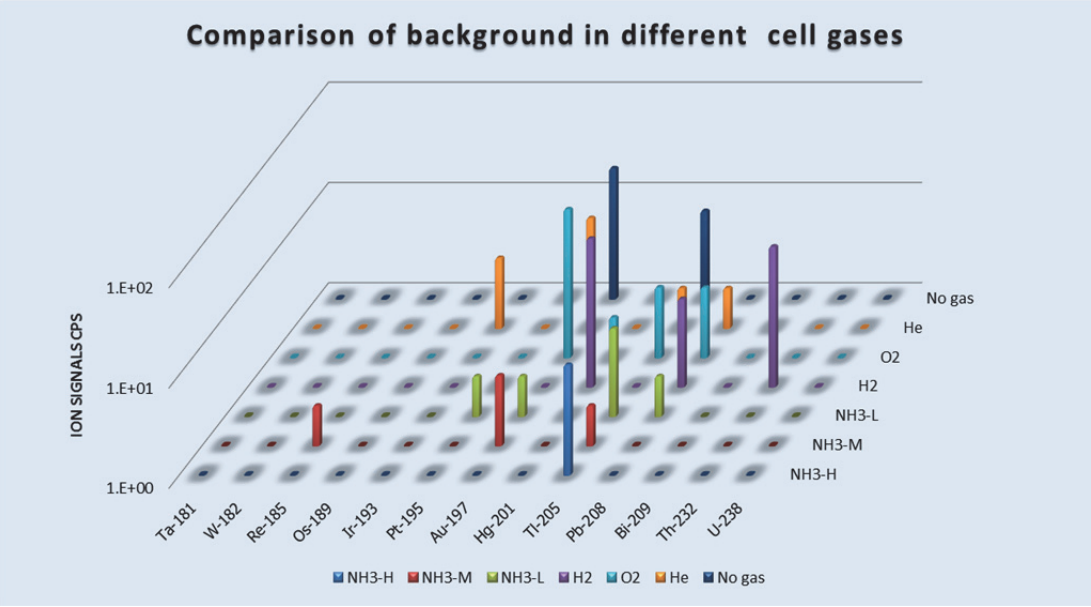

Figure 8.5: Influence of cell gases on instrumental background (Ta – U)

8.4.2 Background from aqueous acid based interferences

Ions that cause spectral overlaps can also arise from acids used in sample preparation procedures (Vaughan and Horlick 1986). When a sample is introduced into a ICP, polyatomic ions are produced at different rates from the elements present in the sample. With the use of acidified aqueous solution C, N and H concentrations are dramatically increased (Hattendorf 2002). A matrix of sodium chloride may generate $^{23}Na^{16}O^+$, $^{23}Na_2^+$, $^{23}Na^{40}Ar^+$, $^{23}Na^{35}Cl^+$, $^{35}Cl^{16}O^+$, $^{35}Cl^{16}OH^+$, $^{40}Ar^{35}Cl^+$, $^{35}Cl^{16}O_2^+$, $^{35}Cl_2^+$ etc. (Reed *et al.* 1994).

Thomas (2013) reports that argon can also form polyatomic interferences with elements found in the acids that are used to dissolve/digest the sample. For example, in a hydrochloric acid medium, $^{40}Ar^+$ combines with the most abundant chlorine isotope at 35 m/z to form $^{40}Ar^{35}Cl^+$, which interferes with the only isotope of arsenic at mass 75, while in

an organic solvent matrix, argon and carbon combine to form $^{40}Ar^{12}C^+$, which interferes with $^{52}Cr^+$, at the m/z of the most abundant isotope of chromium. According to Thomas (2013) matrix species may also combine with themselves to form polyatomic interferences. Sulphur may form $^{32}SO_2^+$ interference at $^{64}Zn^+$. $^{38}ArH^+$ may form at $^{39}K^+$ in water medium, $^{40}Ar^{16}O^+$ at $^{56}Fe^+$ in aqueous medium, $^{35}Cl^{16}O^+$ at ^{51}V in HCl medium, $^{40}Ar^{35}Cl^+$ at ^{75}As in HCl medium, $^{14}N^{14}N^+$ at ^{28}Si in HNO_3 medium, $^{14}N^{14}N^{16}O^+$ at $^{44}Ca^+$ in HNO_3 medium, $^{34}S^{18}O^+$ at $^{52}Cr^+$ in H_2SO_4 medium, $^{32}S^{16}O^{16}O^+$ at $^{64}Zn^+$ in H_2SO_4 medium etc. (Thomas 2013).

In order to investigate the background that acids i.e. HCl, HNO_3 and H_2SO_4 may generate polyatomic ions, several solutions of 0.1 mol/l HCl, 0.1 mol/l H_2SO_4 and 1 g/100 g HNO_3 were analysed in the presence of cell gases He, H_2, O_2 and NH_3 and in no gas modes. The corresponding interferences arising from the use of these acids and or plasma are shown in Figure 8.8 - Figure 8.20.

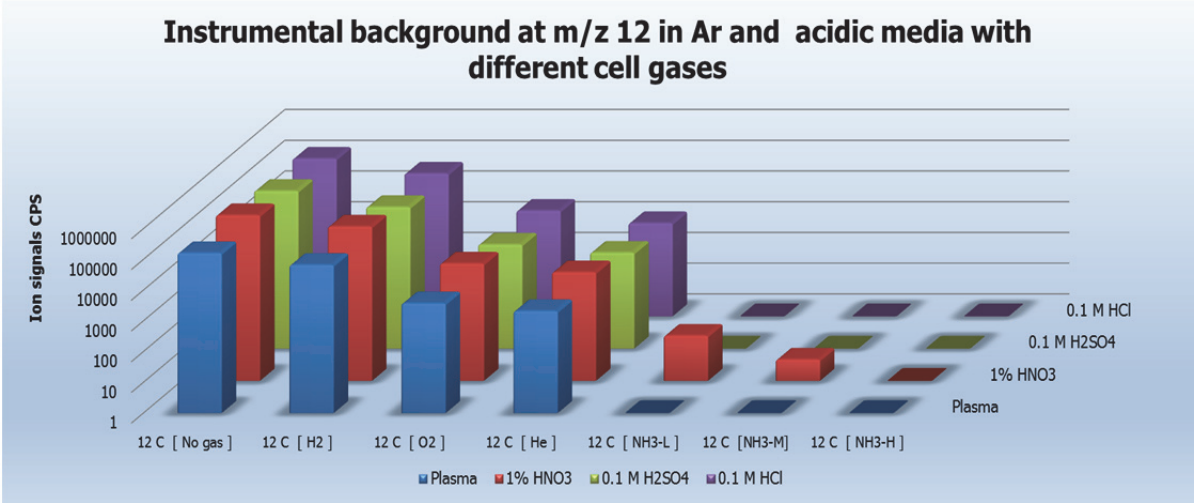

Figure 8.6: Reduction of background from C with CRC gases

Other interferences have been shown in gas blank section with reference to plasma-based interferences only. $^{12}C^+$ ions may originate from CO_2 entrained in plasma. C^+ ions may form polyatomic interferences by combining with other ions in plasma or by combing with itself. $^{12}C_2^+$ ion can overlap at m/z of $^{24}Mg^+$. $^{12}C^{16}O^+$ ion can overlap at m/z of $^{28}Si^+$ and $^{13}C^{18}O^+$ ions at $^{31}P^+$ as shown in Figure 8.8, $^{13}C^{16}O_2^+$ at $^{45}Sc^+$ as shown in Figure 8.14, $^{13}C^{35}Cl^+$ at ^{48}Ti, $^{38}Ar^{13}C^+$ at ^{51}V and ^{52}Cr as shown in Figure 8.15, $^{12}C^{35}Cl^{16}O^+$ at ^{63}Cu as shown in Figure 8.19 and $^{40}Ar^{12}C^{16}O^+$ at $^{68}Zn^+$ etc. Ammonia is potential gas that removes these interferences as shown in Figure 8.6. The source of nitride ions is both air and acids i.e. HNO_3. $^{14}N^{14}N^+$ ions may overlap at m/z of $^{28}Si^+$ in HNO_3 medium as shown in Figure 8.8. Other ions can also form e.g. $^{12}C^{15}N^+$ at $^{27}Al^+$. The removal of these ions is possible with ammonia gas as shown in Figure 8.7.

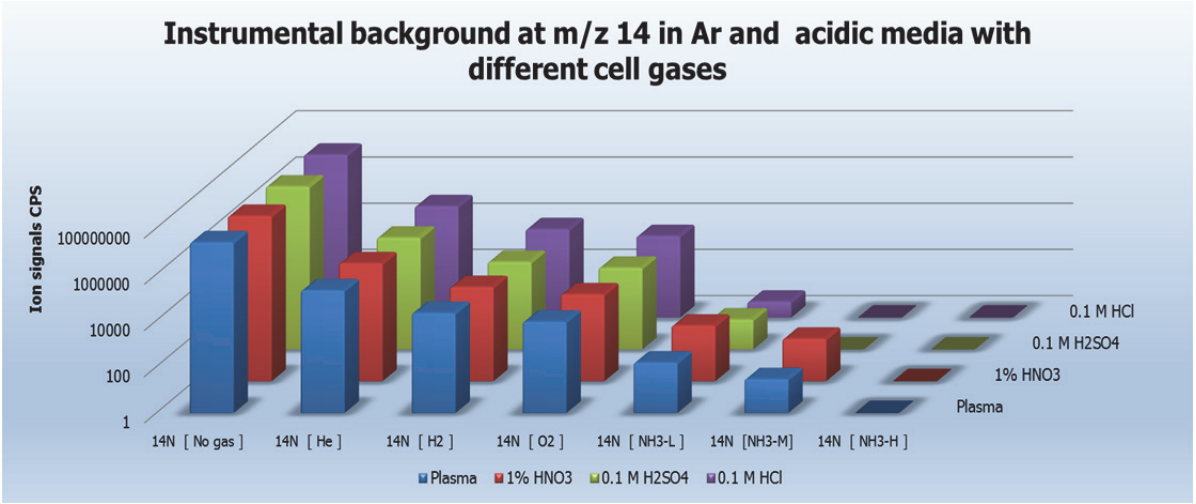

Figure 8.7: Reduction of background from N with CRC gases

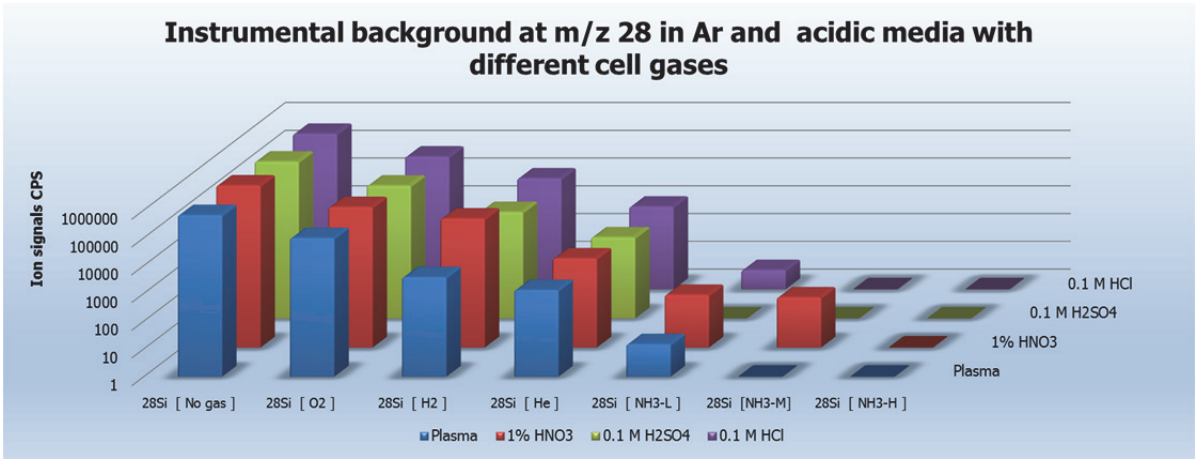

Figure 8.8: Reduction of background at Si with CRC gases

Background at m/z of $^{28}Si^{+}$ can be from $^{14}N_2^{+}$ and $^{12}C^{16}O^{+}$ ions and removal is possible with ammonia gas as shown in Figure 8.8.

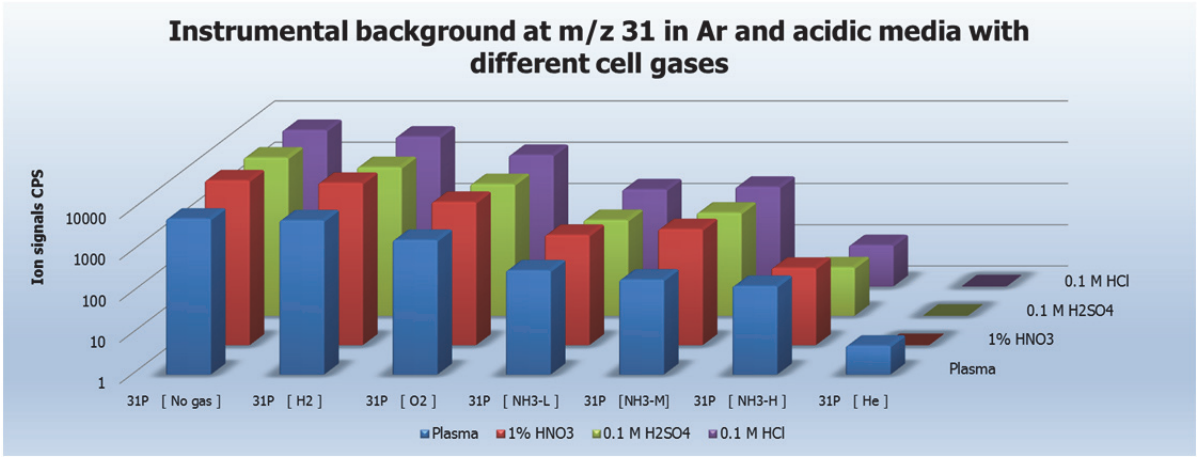

Figure 8.9: Reduction of background at P with CRC gases

The spectral overlap at $^{31}P^{+}$ can be from $^{12}N^{16}OH^{+}$, $^{15}N^{16}O^{+}$, $^{13}C^{17}OH^{+}$, $^{13}C^{18}O^{+}$ and $^{15}N_2H^{+}$ (Figure 8.9).

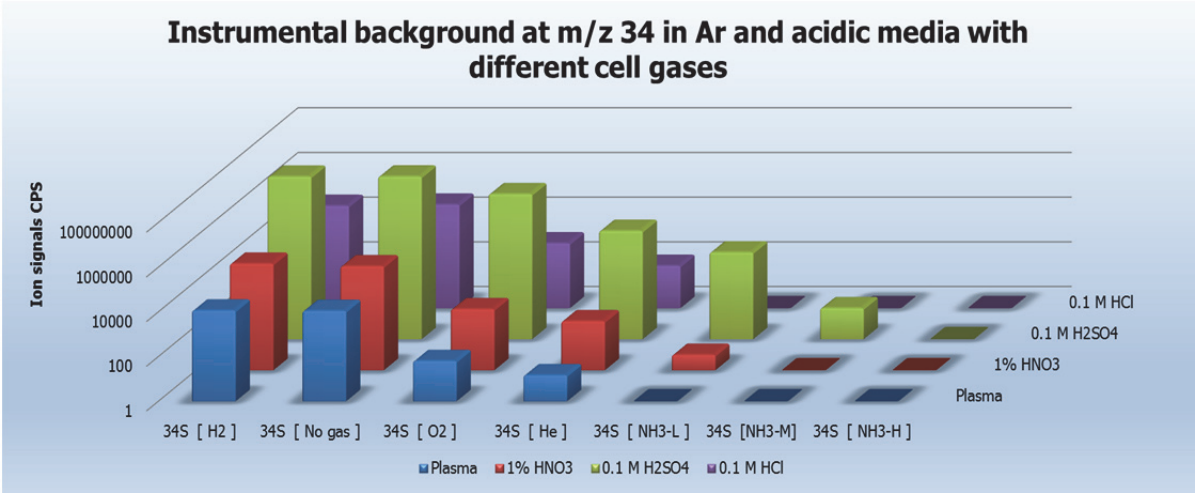

Figure 8.10: Reduction of background at S with CRC gases

In the absence of H_2SO_4 acidic media, the spectral overlap at m/z of $^{34}S^+$ can be from $^{17}O_2^+$, $^{15}N^{18}OH^+$ and $^{15}N^{17}OH_2^+$ etc. In the case of H_2SO_4 media, the main source of S is acid itself. However, a reduction in signals is possible with ammonia gas (Figure 8.10).

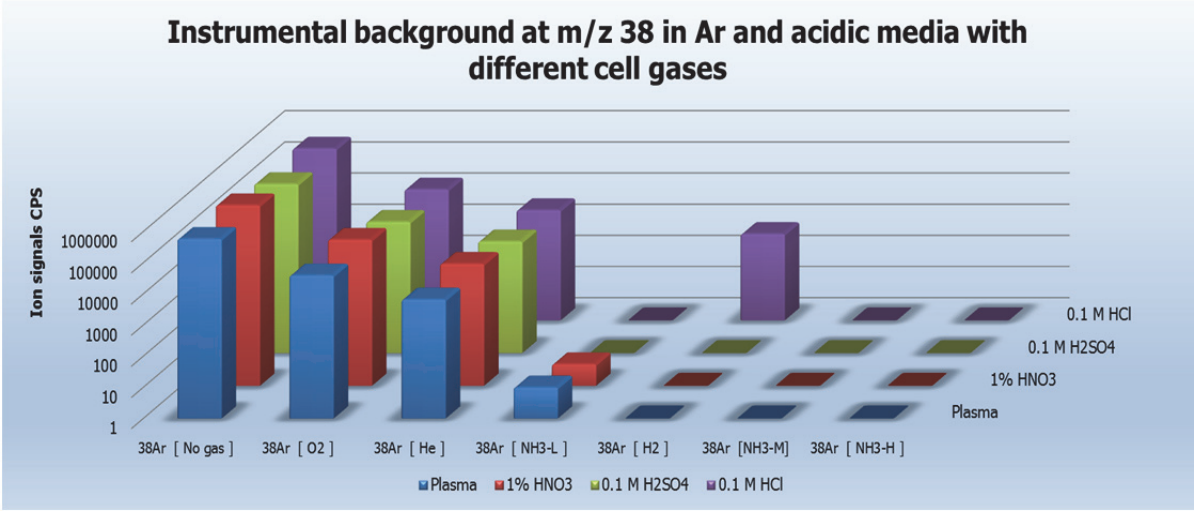

Figure 8.11: Reduction of background of Ar with CRC gases

The argide ions are shown to decrease with ammonia gas in comparison with other cell gases. It might react with O, Cl and S from acids and generate new overlap on other ions (Figure 8.11).

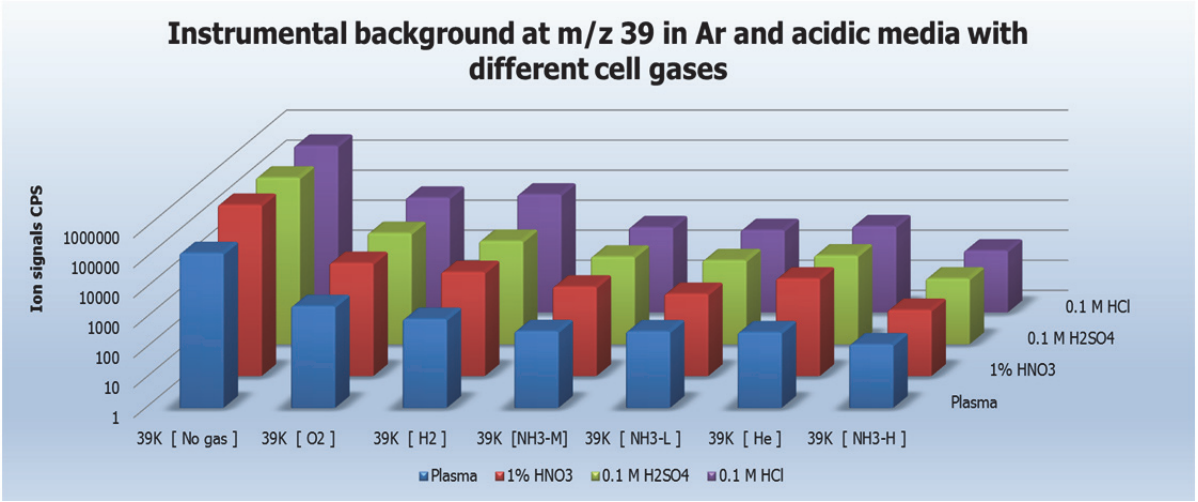

Figure 8.12: Reduction of background at K with CRC gases

The overlap at m/z of $^{39}K^+$ is expected from $^{38}ArH^+$ and $^{23}Na^{16}O^+$ etc. The overlap of these ions decreases with ammonia gas in comparison to other gases (Figure 8.12).

The overlap at $^{44}Ca^+$ is expected from $^{12}C^{16}O_2^+$, $^{12}C^{32}S^+$ and $^{14}N_2^{16}O^+$ etc. The overlap of these ions decreases with ammonia gas in comparison to other gases (Figure 8.13). The spectral overlap in the presence of H_2SO_4 is enhanced because it is a source of O and S.

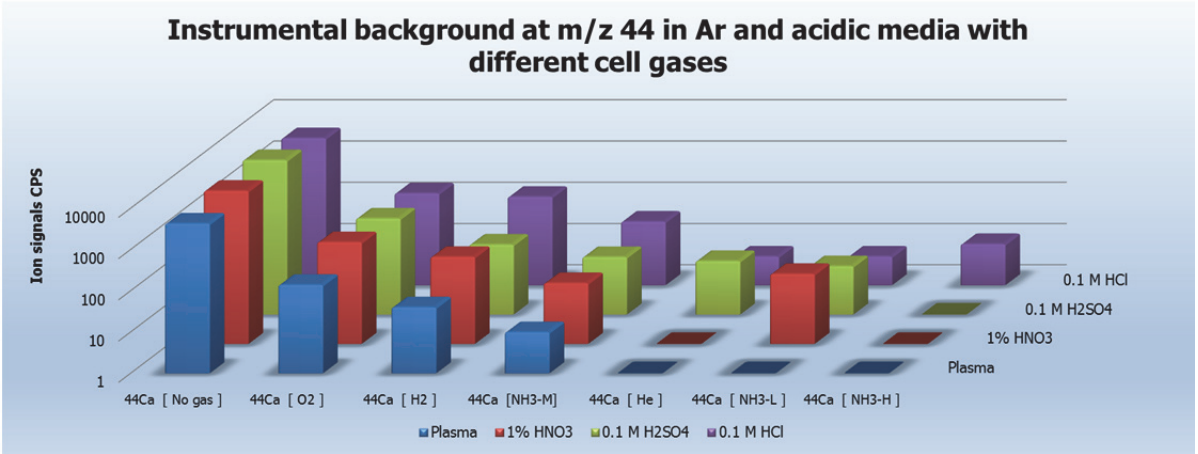

Figure 8.13: Reduction of background at Ca with CRC gases

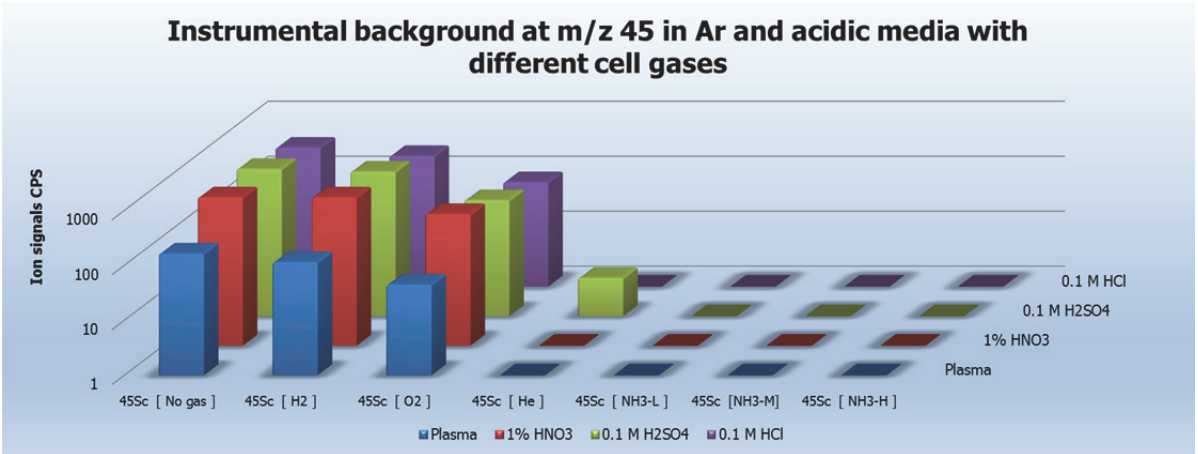

Figure 8.14: Reduction of background at Sc with CRC gases

The overlap at $^{45}Sc^{+}$ can be from $^{12}C^{16}O_2H^{+}$and $^{12}N_2{}^{16}OH^{+}$etc. The overlap of these ions decreases with ammonia gas in comparison to other gases (Figure 8.14).

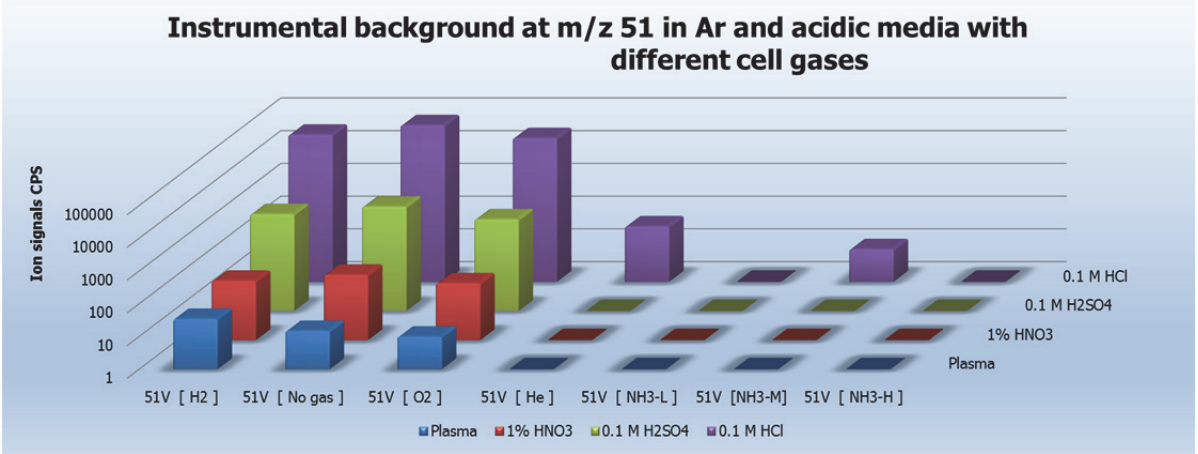

Figure 8.15: Reduction of background at V with CRC gases

The overlap at $^{51}V^{+}$ can be from $^{35}Cl^{16}O^{+}$, $^{37}Cl^{14}N^{+}$, $^{38}Ar^{13}C^{+}$, $^{40}Ar^{14}NH^{+}$ and $^{34}S^{16}OH^{+}$ etc. The overlap of these ions decreases with ammonia gas in comparison to other gases (Figure 8.15).

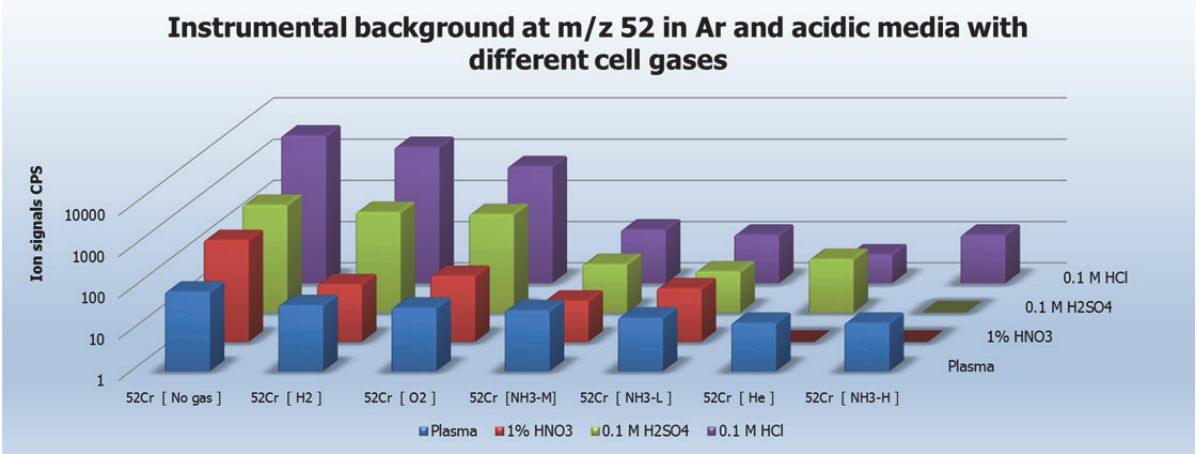

Figure 8.16: Reduction of background at Cr with CRC gases

The overlap at $^{52}Cr^{+}$ can be from $^{35}Cl^{16}OH^{+}$, $^{38}Ar^{14}N^{+}$, $^{36}Ar^{36}O^{+}$ and $^{40}Ar^{12}C^{+}$etc. The overlap of these ions decreases with ammonia gas in comparison to other gases (Figure 8.16). Chromium in acidic media of HCl and H_2SO_4 carry more intense overlaps due to $^{36}S^{16}O^{+}$ ion formation which originates from acids itself.

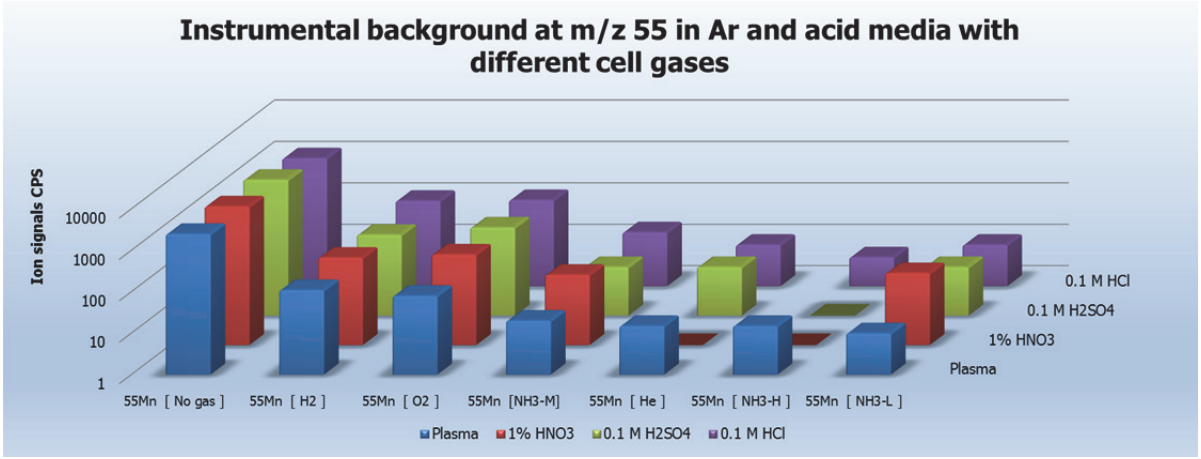

Figure 8.17: Reduction of background at Mn with CRC gases

The overlap at $^{55}Mn^{+}$ can be from $^{38}Ar^{17}O^{+}$, $^{23}Na^{32}S^{+}$, $^{37}Cl^{18}O^{+}$, $^{38}Ar^{16}OH^{+}$ and $^{40}Ar^{15}N^{+}$etc. The overlap of these ions decreases with ammonia gas in comparison to other gases (Figure 8.17).

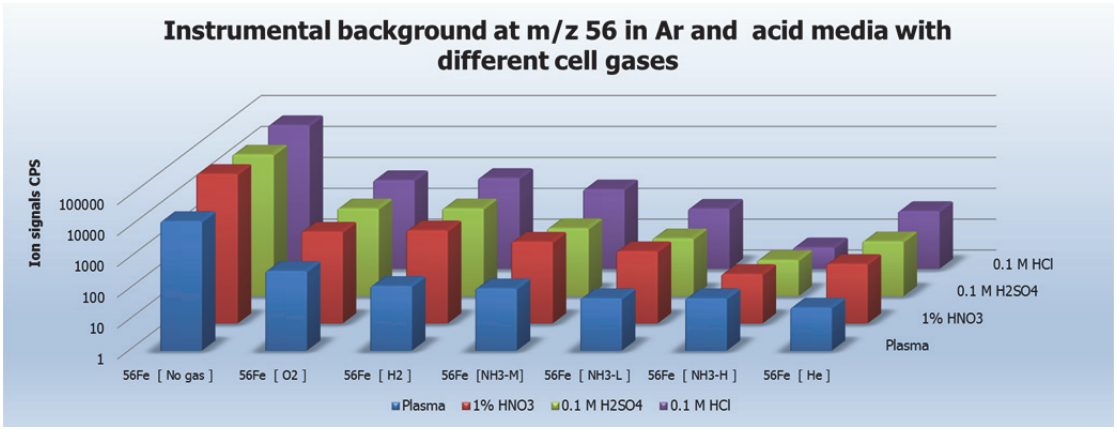

Figure 8.18: Reduction of background at Fe with CRC gases

The overlap at $^{56}Fe^{+}$ can be from $^{37}Cl^{18}OH^{+}$, $^{40}Ar^{15}NH^{+}$ and $^{40}Ar^{16}O^{+}$ etc. The overlap of these ions decreases with ammonia gas in comparison to other gases (Figure 8.18).

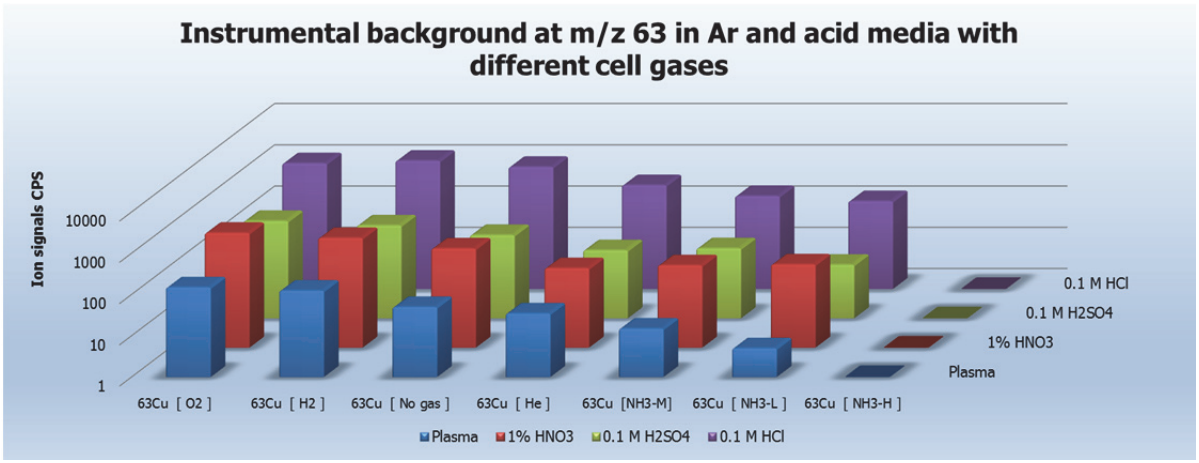

Figure 8.19: Reduction of background at Cu with CRC gases

The overlap at $^{63}Cu^{+}$ can be from $^{35}Cl^{14}N_2^{+}$, $^{36}Ar^{12}C^{14}NH^{+}$, $^{16}O^{12}C^{35}Cl^{+}$, $^{14}N^{12}C^{37}Cl^{+}$ and $^{36}Ar^{37}Cl^{+}$ etc. The overlap of these ions decreases with ammonia gas in comparison to other gases (Figure 8.19).

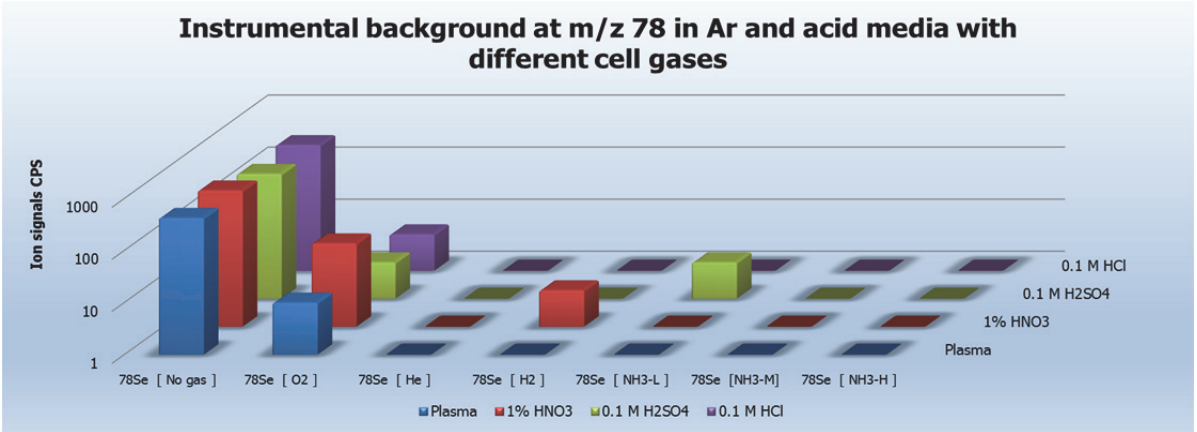

Figure 8.20: Reduction of background at Se with CRC gases

The overlap at $^{80}Se^{+}$ can be from $^{40}Ar_2^{+}$ etc. The overlap of these ions decreases with ammonia gas in comparison to other gases (Figure 8.20).

8.4.3 Product ions of 45 analytes in ammonia and oxygen gas

45 analytes were scanned to find their product ions relative to their intensity in no gas mode for interference removal purposes. The data for the relative intensity product ions to the intensity in no gas mode is given in Table 8.1.

Table 8.1: The relative intensity of the product ion in ammonia and oxygen gas

Product ion scan of analytes in NH_3 and O_2 gases											
Li		**Be**		**B**		**Na**		**Mg**		**Al**	
Gas modes	**R.I**	**Gas modes**	**R.I**	**Gas modes**	**R.I**	**Gas modes**	**R.I**	**Gas modes**	**R.I**	**Gas modes**	**R.I**
7->7Li[NoGas]	100%	9->9Be[NoGas]	100%	11->11B[NoGas]	100%	23->23Na[NoGas]	100%	24->24Mg[NoGas]	100%	27->27Al[NoGas]	100%
7->7Li[O2]	0.32%	9->9Be[O2]	3%	11->11B[O2]	10%	23->23Na[O2]	25%	24->24Mg[O2]	57%	27->27Al[O2]	40%
7->7Li[NH3M]	0.004%	9->25Be[O2]	0.40%	11->26B[NH3M]	0.00%	23->39Na[O2]		24->40Mg[O2]	6%	27->27Al[NH3M]	20%
7->22Li[NH3M]		9->9Be[NH3M]	0.02%	11->27B[O2]	0.70%	23->23Na[NH3M]	85%	24->24Mg[NH3M]	18%	27->42Al[NH3M]	
7->23Li[O2]		9->24Be[NH3M]		11->27B[NH3M]	0.0004%	23->38Na[NH3M]		24->39Mg[NH3M]		27->43Al[O2]	4%
7->23Li[NH3M]		9->25Be[NH3M]	0.004%	11->28B[NH3M]	0.0001%	23->39Na[NH3M]		24->40Mg[NH3M]	0.00%	27->43Al[NH3M]	0.00002%
7->24Li[NH3M]		9->26Be[NH3M]		11->45B[NH3M]		23->40Na[NH3M]	0.10%	24->41Mg[NH3M]	0.50%	27->44Al[NH3M]	0.47%
7->41Li[NH3M]	0.0001%	9->43Be[NH3M]		11->62B[NH3M]		23->57Na[NH3M]		24->58Mg[NH3M]	0.40%	27->61Al[NH3M]	0.11%
7->58Li[NH3M]	0.0004%	9->60Be[NH3M]	0.05%	11->79B[NH3M]		23->74Na[NH3M]		24->75Mg[NH3M]	0.90%	27->78Al[NH3M]	0.01%
7->75Li[NH3M]		9->77Be[NH3M]	0.64%	11->96B[NH3M]		23->91Na[NH3M]		24->92Mg[NH3M]	0.06%	27->95Al[NH3M]	0.01%
7->92Li[NH3M]		9->94Be[NH3M]						24->109Mg[NH3M]	0.00%	27->112Al[NH3M]	0.00%
Si		**P**		**S**		**K**		**Ca**		**Ti**	
28->28Si[NoGas]	100%	31->31P[NoGas]	100%	34->34S[Nogas]	100%	39->39K[NoGas]	100%	43->43Ca[NoGas]	100%	48->48Ti[NoGas]	100%
28->28Si[O2]	12%	31->31P[O2]	3%	34->34S[O2]	5%	39->39K[O2]	75%	43->43Ca[O2]	76%	48->48Ti[O2]	80%
28->28Si[NH3M]	0.004%	31->31P[NH3M]		34->34S[H2]	37%	39->39K[NH3M]	28%	43->43Ca[NH3M]	26%	48->48Ti[NH3M]	79%
28->43Si[NH3M]	0.0003%	31->46P[NH3M]	0.00%	34->34S[He]	0.20%	39->54K[NH3M]		43->58Ca[NH3M]		48->63Ti[NH3M]	2%
28->44Si[O2]	5%	31->47P[O2]	71%	34->35S[H2]	1%	39->55K[O2]		43->59Ca[O2]	6%	48->64Ti[O2]	20%
28->44Si[NH3M]	0.001%	31->47P[NH3M]		34->50S[O2]	14%	39->55K[NH3M]		43->59Ca[NH3M]	0.00%	48->64Ti[NH3M]	0.10%
28->45Si[NH3M]		31->48P[NH3M]		34->34S[NH3-M]		39->56K[NH3M]	0.19%	43->60Ca[NH3M]	0.40%	48->65Ti[NH3M]	1.20%
28->62Si[NH3M]		31->65P[NH3M]	0.004%	34->49S[NH3-M]		39->73K[NH3M]	0.02%	43->77Ca[NH3M]	0.20%	48->82Ti[NH3M]	0.70%
28->79Si[NH3M]		31->82P[NH3M]	0.0004%	34->50S[NH3-M]		39->90K[NH3M]	0.0002%	43->94Ca[NH3M]	0.20%	48->99Ti[NH3M]	0.80%
28->96Si[NH3M]		31->99P[NH3M]	0.00001%	34->51S[NH3-M]		39->107K[NH3M]		43->111Ca[NH3M]	0.30%	48->116Ti[NH3M]	3%

28->113Si[NH3M]		31->116P[NH3M]	0.0003%	34->68S[NH3-M]		39->124K[NH3M]	0.00004%	43->128Ca[NH3M]	0.20%	48->132Ti[NH3M]	35%
				34->85S[NH3-M]							
				34->102S[NH3-M]							
V		**Cr**		**Mn**		**Fe**		**Co**		**Cu**	
51->51V[NoGas]	100%	52->52Cr[NoGas]	100%	55->55Mn[NoGas]	100%	56->56Fe[NoGas]	100%	59->59Co[NoGas]	100%	63->63Cu[NoGas]	100%
51->51V[O2]	11%	52->52Cr[O2]	70%	55->55Mn[O2]	75%	56->56Fe[O2]	79.90%	59->59Co[O2]	79%	63->63Cu[O2]	88%
51->51V[NH3M]	4%	52->52Cr[NH3M]	27%	55->55Mn[NH3M]	25%	56->56Fe[NH3M]	15.50%	59->59Co[NH3M]	9%	63->63Cu[NH3M]	13%
51->66V[NH3M]	0.20%	52->68Cr[O2]	11%	55->70Mn[NH3M]	0.00%	56->90Fe[NH3M]	13.80%	59->74Co[NH3M]	0.00%	63->79Cu[O2]	0.19%
51->67V[O2]	82%	52->67Cr[NH3M]	0.0002%	55->71Mn[O2]	7%	56->72Fe[O2]	11.80%	59->75Co[O2]	10%	63->79Cu[NH3M]	0.00003%
51->67V[NH3M]	10.10%	52->68Cr[NH3M]	0.0004%	55->71Mn[NH3M]	0.00%	56->107Fe[NH3M]	3.70%	59->75Co[NH3M]	0.001%	63->80Cu[NH3M]	1%
51->68V[NH3M]	0.10%	52->69Cr[NH3M]	0.40%	55->72Mn[NH3M]	1%	56->73Fe[NH3M]	0.30%	59->76Co[NH3M]	0.30%	63->97Cu[NH3M]	5%
51->85V[NH3M]	0.10%	52->86Cr[NH3M]	7%	55->89Mn[NH3M]	2%	56->124Fe[NH3M]	0.02%	59->93Co[NH3M]	11.70%	63->114Cu[NH3M]	
51->102V[NH3M]	0.70%	52->103Cr[NH3M]	0.42%	55->106Mn[NH3M]	1%	56->72Fe[NH3M]	0.001%	59->110Co[NH3M]	7.00%		
51->119V[NH3M]	2%	52->120Cr[NH3M]	0.01%	55->123Mn[NH3M]	0.01%	56->141Fe[NH3M]	0.0002%	59->127Co[NH3M]	0.01%		
51->136V[NH3M]	2%	52->137Cr[NH3M]	0.001%	55->140Mn[NH3M]	0.001%	56->71Fe[NH3M]	0.00003%	59->144Co[NH3M]	0.0002%		
Ni		**Zn**		**Ga**		**Ge**		**As**		**Se**	
60->76Ni[O2]	4%	66->66Zn[NoGas]	100%	71->71Ga[NoGas]	100%	72->72Ge[NoGas]	100%	75->75As[NoGas]	100.00%	82->82Se[NoGas]	100%
60->60Ni[NoGas]	100%	66->66Zn[O2]	87%	71->71Ga[O2]	93%	72->72Ge[O2]	81%	75->91As[O2]	94.30%	80->80Se[O2]	21%
60->60Ni[O2]	94%	66->66Zn[NH3M]	23%	71->71Ga[NH3M]	45%	72->123Ge[NH3M]	13.00%	75->75As[O2]	9.90%	80->80Se[NH3M]	4%
60->111Ni[NH3M]	19%	66->100Zn[NH3M]	4%	71->86Ga[NH3M]		72->88Ge[O2]	9.50%	75->109As[NH3M]	0.60%	80->95Se[NH3M]	
60->60Ni[NH3M]	11%	66->117Zn[NH3M]	3%	71->87Ga[O2]	0.00%	72->88Ge[NH3M]	1.20%	75->75As[NH3M]	0.30%	80->96Se[O2]	1.20%
60->94Ni[NH3M]	4%	66->83Zn[NH3M]	2%	71->87Ga[NH3M]		72->106Ge[NH3M]	1.20%	75->91As[NH3M]	0.30%	80->96Se[NH3M]	
60->77Ni[NH3M]	0.34%	66->82Zn[O2]	0.60%	71->88Ga[NH3M]	1.69%	72->72Ge[NH3M]	1.10%	75->126As[NH3M]	0.20%	80->97Se[NH3M]	2.50%
60->128Ni[NH3M]	0.004%	66->134Zn[NH3M]	0.01%	71->105Ga[NH3M]	1.06%	72->140Ge[NH3M]	0.23%	75->92As[NH3M]	0.04%	80->114Se[NH3M]	0.002%
60->76Ni[NH3M]	0.0003%	66->151Zn[NH3M]	0.00%	71->122Ga[NH3M]	0.05%	72->89Ge[NH3M]	0.04%	75->92As[O2]	0.04%	80->131Se[NH3M]	
60->75Ni[NH3M]	0.0002%	66->82Zn[NH3M]	0.00%	71->139Ga[NH3M]		72->87Ge[NH3M]		75->90As[NH3M]	0.01%	80->148Se[NH3M]	
60->145Ni[NH3M]	0.00004%	66->81Zn[NH3M]	0.00%	71->156Ga[NH3M]		72->157Ge[NH3M]		75->143As[NH3M]	0.002%	80->165Se[NH3M]	
								75->160As[NH3M]	0.001%		

Rb		Se		Y		Te		Cs		Ba	
85->85Rb[NoGas]	99.10%	88->88Sr[O2]	100%	89->89Y[NoGas]	100%	125->125Te[NoGas]	100%	133->133Cs[NoGas]	100%	137->137Ba[NoGas]	100%
85->85Rb[O2]	100.00%	88->88Sr[NoGas]	104%	89->89Y[O2]	9%	126->126Te[O2]	92%	133->133Cs[O2]	98%	137->137Ba[O2]	98%
85->85Rb[NH3M]	57.60%	88->88Sr[NH3M]	53%	89->89Y[NH3M]	3%	126->126Te[NH3M]	98%	133->133Cs[NH3M]	97%	137->137Ba[NH3M]	60%
85->102Rb[NH3M]	0.30%	88->104Sr[O2]	0.00%	89->104Y[NH3M]	2%	126->141Te[NH3M]		133->148Cs[NH3M]		137->152Ba[NH3M]	0.00%
85->119Rb[NH3M]	0.02%	88->105Sr[NH3M]	5.30%	89->105Y[O2]	18%	126->142Te[O2]	20%	133->149Cs[O2]		137->153Ba[O2]	8%
85->100Rb[NH3M]		88->122Sr[NH3M]	0.04%	89->105Y[NH3M]		126->142Te[NH3M]	0.05%	133->149Cs[NH3M]	0.13%	137->153Ba[NH3M]	0.80%
85->101Rb[O2]		88->139Sr[NH3M]	0.70%	89->106Y[NH3M]		126->143Te[NH3M]	0.50%	133->150Cs[NH3M]	0.43%	137->154Ba[NH3M]	1.30%
85->101Rb[NH3M]		88->156Sr[NH3M]	0.30%	89->123Y[NH3M]		126->160Te[NH3M]		133->167Cs[NH3M]	0.04%	137->171Ba[NH3M]	0.50%
85->136Rb[NH3M]		88->104Sr[NH3M]	0.30%	89->140Y[NH3M]		126->177Te[NH3M]	0.10%	133->184Cs[NH3M]		137->188Ba[NH3M]	0.60%
85->153Rb[NH3M]		88->173Sr[NH3M]	0.08%	89->157Y[NH3M]	0.70%	126->194Te[NH3M]		133->201Cs[NH3M]	0.09%	137->205Ba[NH3M]	0.20%
85->170Rb[NH3M]		88->103Sr[NH3M]	0.02%	89->174Y[NH3M]		126->211Te[NH3M]		133->218Cs[NH3M]		137->222Ba[NH3M]	0.01%
				89->191Y[NH3M]	0.30%	126->228Te[NH3M]					
Zr		**Nb**		**Mo**		**Cd**		**In**		**Sb**	
90->90Zr[NoGas]	100%	93->93Nb[NoGas]	100.00%	95->95Mo[NoGas]	100%	110->110Cd[NoGas]	100%	115->115In[NoGas]	100%	121->121Sb[NoGas]	100%
90->90Zr[O2]	1.00%	93->93Nb[O2]	1.50%	95->95Mo[O2]	15%	110->110Cd[O2]	98%	115->115In[O2]	96%	121->121Sb[O2]	84%
90->90Zr[NH3M]	0.50%	93->93Nb[NH3M]	0.50%	95->95Mo[NH3M]	28%	110->110Cd[NH3M]	44%	115->115In[NH3M]	61%	121->121Sb[NH3M]	25%
90->105Zr[NH3M]	0.70%	93->108Nb[NH3M]	0.20%	95->110Mo[NH3M]	0.02%	110->125Cd[NH3M]		115->130In[NH3M]		121->136Sb[NH3M]	
90->106Zr[O2]	83%	93->109Nb[O2]	10.90%	95->111Mo[O2]	9%	110->126Cd[O2]	0.10%	115->131In[O2]	0.0001%	121->137Sb[O2]	26%
90->106Zr[NH3M]	0.04%	93->109Nb[NH3M]	0.004%	95->111Mo[NH3M]	0.01%	110->126Cd[NH3M]	0.00%	115->131In[NH3M]	0.00001%	121->137Sb[NH3M]	
90->107Zr[NH3M]	0.001%	93->110Nb[NH3M]	0.0004%	95->112Mo[NH3M]	0.50%	110->127Cd[NH3M]	2.40%	115->132In[NH3M]	0.74%	121->138Sb[NH3M]	18%
90->124Zr[NH3M]	0.001%	93->127Nb[NH3M]		95->129Mo[NH3M]	10%	110->144Cd[NH3M]	2.70%	115->149In[NH3M]	0.21%	121->155Sb[NH3M]	11%
90->141Zr[NH3M]	0.001%	93->144Nb[NH3M]		95->146Mo[NH3M]	0.10%	110->161Cd[NH3M]	0.90%	115->166In[NH3M]	0.004%	121->172Sb[NH3M]	1.00%
90->158Zr[NH3M]	0.10%	93->161Nb[NH3M]		95->163Mo[NH3M]	0.10%	110->178Cd[NH3M]	0.00%	115->183In[NH3M]	0.00001%	121->189Sb[NH3M]	
90->175Zr[NH3M]	1.80%	93->178Nb[NH3M]	0.003%	95->180Mo[NH3M]	0.02%	110->195Cd[NH3M]	0.00%	115->200In[NH3M]	0.0001%	121->206Sb[NH3M]	
90->192Zr[NH3M]	2.10%	93->195Nb[NH3M]	0.002%			110->212Cd[NH3M]	0.00%	115->217In[NH3M]	0.0001%		
Ta		**Hf**		**W**		**Re**		**Hg**		**Tl**	
181->181Ta[NoGas]	100%	178->178Hf[NoGas]	100%	182->182W[NoGas]	100%	185->185Re[NoGas]	100%	201->201Hg[NoGas]	100%	205->205Tl[NoGas]	100%

181->181Ta[O2]	0.09%	178->178Hf[O2]	0.13%	182->182W[O2]	0.16%	187->187Re[O2]	55%	198->198Hg[O2]	34%	205->205Tl[O2]	71%
181->196Ta[NH3M]	0.60%	178->178Hf[NH3M]	0.80%	182->197W[NH3M]	0.30%	187->202Re[NH3M]	0.30%	198->198Hg[NH3M]		205->205Tl[NH3M]	80%
181->197Ta[O2]	3.60%	178->193Hf[NH3M]	2.9%	182->198W[O2]	4.20%	187->203Re[O2]	12%	198->213Hg[NH3M]		205->220Tl[NH3M]	
181->197Ta[NH3M]	0.06%	178->194Hf[O2]	70%	182->198W[NH3M]	0.02%	187->203Re[NH3M]	0.03%	198->214Hg[O2]	18%	205->221Tl[O2]	
181->198Ta[NH3M]	0.0003%	178->194Hf[NH3M]	0.19%	182->199W[NH3M]		187->204Re[NH3M]	0.01%	198->214Hg[NH3M]		205->221Tl[NH3M]	0.00%
181->215Ta[NH3M]		178->195Hf[NH3M]	0.001%	182->214W[O2]	38%	187->221Re[NH3M]	0.001%	198->215Hg[NH3M]		205->222Tl[NH3M]	0.44%
181->232Ta[NH3M]		178->212Hf[NH3M]		182->216W[NH3M]		187->238Re[NH3M]	0.001%	198->232Hg[NH3M]		205->239Tl[NH3M]	0.09%
181->249Ta[NH3M]		178->229Hf[NH3M]	0.001%	182->233W[NH3M]		187->255Re[NH3M]		198->249Hg[NH3M]	0.09%	205->256Tl[NH3M]	0.001%
		178->246Hf[NH3M]	0.004%	182->250W[NH3M]							
Pb		**Bi**		**Th**		**U**					
208->208Pb[NoGas]	100%	209->209Bi[NoGas]	100%	232Th[Nogas]	100%	238U[Nogas]	100%				
208->208Pb[O2]	71%	209->209Bi[O2]	70.10%	232->248Th[O2]	15%	238->254U[O2]	0.10%				
208->208Pb[NH3M]	82%	209->224Bi[NH3M]	0.00%	232->232Th[O2]		238->238U[NH3M]	2.60%				
208->223Pb[NH3M]	0.0001%	209->225Bi[O2]	0.90%	232->247Th[NH3M]	0.0020%	238->253U[NH3M]	9.90%				
208->224Pb[O2]	0.24%	209->225Bi[NH3M]	0.03%	232->248Th[O2]	0.01%	238->254U[NH3M]	1.50%				
208->224Pb[NH3M]	0.0003%	209->226Bi[NH3M]	1.30%	232->248Th[NH3M]		238->255U[NH3M]	0.05%				
208->225Pb[NH3M]	1.18%	209->243Bi[NH3M]	0.30%	232->249Th[NH3M]							
208->242Pb[NH3M]	0.36%	209->260Bi[NH3M]	0.0001%								
208->259Pb[NH3M]	0.004%										

R.I is relative intensity

^{7}Li

Lithium is a lighter element and does not seem to react efficiently with ammonia gas due to collisional destabilisation energy and scattering losses. Hence no significant intensity was observed at on-mass and mass-shift product ions. A similar trend has been observed by Jones (2007) using ICP-DRC-MS. The ions less than 17 m/z were severely scattered because they are less than the mass of the reaction gas (NH_3). However, there were some intensities observed at mass-shifted product ions of MNH_3^+, $M(NH_3)_2^+$ and $M(NH_3)_3^+$. These type of addition are done through clustering reactions with ammonia. Li^+ does not oxidise in collision/reaction cell and no intensity was observed as LiO^+. It can be deduced that it would not make any interference on proceeding ions in spectra. The relative intensity of the Li^+ and product ions with ammonia and oxygen gas is given in Table 8.1.

^{9}Be

The chemical behaviour of $^{9}Be^+$ is similar to $^{7}Li^+$ with regards to its reaction with ammonia and oxygen gas. This is due to its smaller size and reaction with larger molecules. The only product ion observed was $Be(NH_3)_4^+$ at a flow rate of 3 ml/min. The clustering reaction is a suggested mechanism for the product ion. Other product ions (M+17, 34, 51) are expected at lower flow rates than 3 ml/min as observed by (Jones 2007) and Sugiyama and Kazumi (2014) at 1.5 ml/min in ICP-DRC-MS and Agilent 8800 ICP-MS/MS. Some intensity of Be-oxide formed was observed with oxygen gas that can be an interference on $^{25}Mg^+$.

^{11}B

Only fewer counts were observed due to scattering losses for the product ions of $^{11}B^+$ on reaction with ammonia gas at (M+17, 34, 68, 85). The reaction products of this kind are formed through clustering reactions. Oxide of $^{11}B^+$ was formed at m/z of 27 which is $^{27}Al^+$ and can pose an interference if it is present in higher concentration. No product ions were reported by Jones (2007) using ICP-DRC-MS.

^{23}Na

No product ions were observed except $NaNH_3^+$ as also reported by Sugiyama and Kazumi (2014). Other product ions (M+85, 136) were observed by Jones (2007) with ICP-DRC-MS at 0.25 ml/min flow rate of ammonia gas. $NaNH_3^+$ was also abundant product ion. No oxides were formed by reaction with oxygen gas or it needed a lower flow rate. The potential interferences from oxides of Na^+ are not expected.

^{24}Mg

Magnesium forms product ions as $MgNH_3^+$, $Mg(NH_3)_2^+$, $Mg(NH_3)_2^+$, $Mg(NH_3)_3^+$, $Mg(NH_3)_4^+$ and $Mg(NH_3)_5^+$. Other products ions were not tested. $Mg(NH_3)_3^+$ was the most abundant ion at given flow rate of ammonia. This confirms the experiments conducted by Jones (2007), Sugiyama and Kazumi (2014). The product ions of Mg are of the type $Mg(NH_3)_X$ and are formed by clustering reactions as described by Jones (2007). Magnesium is oxidised to MgO^+ at m/z 40 which can be interference on $^{40}Ca^+$.

^{27}Al

Aluminium tends to form $AlNH_3^+$, $Al(NH_3)_2^+$, $Al(NH_3)_3^+$, $Al(NH_3)_4^+$, and $Al(NH_3)_5^+$ product ions. The $AlNH_3^+$ is the most abundant ion and undergoes clustering reaction. $^{27}Al^+$

should not undergo charge transfer reactions with any of reaction gases tested (NH_3 and O_2) because the ionisation energy of $^{27}Al^+$ is lower than the reaction gases as mentioned in (Jones 2007). The oxides are formed at m/z of $^{43}Ca^+$. This can be a potential interference on $^{43}Ca^+$ in no gas mode.

^{28}Si

No product ions were observed in the reaction of $^{28}Si^+$ with ammonia gas just like studies of Jones (2007) with DRC and Sugiyama and Kazumi (2014) with CRC. Very less intensity of $^{28}Si^+$ ions was observed with on-mass-ammonia mode. The ionisation energy of Si is 8.15 eV, and that of ammonia is 10.02 eV, thus a charge transfer reaction cannot be attributed to this unreactive behaviour of $^{28}Si^+$. Product ions of $^{28}Si^+$ are formed on oxidation at m/z of $^{44}Ca^+$ and could pose an interference on $^{44}Ca^+$.

^{31}P

Phosphorus does not form any product ions (very less intensity) with ammonia gas similar to $^{28}Si^+$, $^{7}Li^+$ and $^{11}B^+$. The ionisation energy of P is 10.49 eV and is higher than ammonia 10.02 eV, hence a charge transfer reaction is expected because of exothermicity of reaction by (- 0.33 eV) as mentioned in (Jones 2007). The oxide product ion is formed at m/z of $^{48}Ti^+$ and can be an interference. The interferences from C^+ and N^+ based product ions are removed with mass-shift oxygen mode (Figure 8.21).

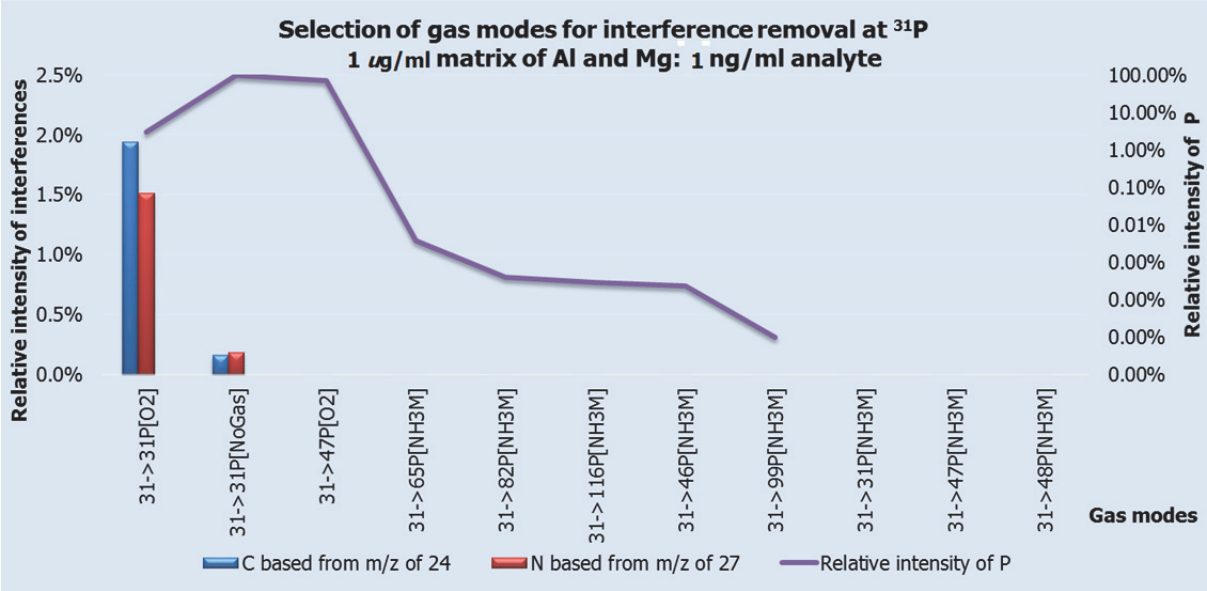

Figure 8.21: Relative intensity of product ions of P

^{32}S

It can be seen that $^{32}S^+$ ions are highly unstable in ammonia gas and no intensity is seen with ammonia in an on-mass mode in Table 8.1. All intensity which appears in the background is from $^{16}O_2^+$, $^{14}N^{16}O^+$, $^{15}N^{16}O^1H^+$ and $^{14}N^{16}OH_2^+$ has already been shown in the previous section of plasma backgrounds and with acid media. Charge transfer reaction can be assumed for $^{32}S^+$ on reaction with ammonia although no experimental data in the literature exist. The reaction of $^{32}S^+$ with oxygen is exothermic by -0.34 eV (Naoki 2013b). $^{32}S^+$ is also reported to form $^{32}S^+O^+$ in mass-shift oxygen mode (Naoki 2013b).

^{39}K

Three cluster products are formed by reaction with ammonia through clustering. The main abundant ion is KNH_3^+ also studied by Jones (2007). $^{39}K^+$ is not oxidised to $^{39}K^{16}O^+$ hence no interference is expected on m/z ^{55}Mn from ^{39}K. The interference $^{38}Ar^1H^+$ can be removed with on-mass measurement with ammonia gas.

^{43}Ca

Calcium undergoes clustering reaction with ammonia and up to five products ions of the type $Ca(NH_3)_x^+$ with the addition of m/z of (17, 34, 51, 68, 85) as also observed by (Jones 2007) and Sugiyama and Kazumi (2014). Calcium also undergoes oxidation reaction and form product ion at m/z of ^{59}Co. The interferences at m/z of ^{40}Ca by argide ions have been shown earlier to be removed by charge transfer reactions Figure 8.13.

^{48}Ti

The product ions of $^{48}Ti^+$ follow condensation reaction and form $TiNH^+$ type of ions with the elimination of hydrogen molecule. $TiNH_2(NH_3)_4^+$ is the most abundant ion tested. Glenn (2013c) has used $TiNH_2(NH_3)_4^+$ product ion for interference removal on Ti. Balcaen et, al. 2014 has used $Ti(NH_3)_6^+$ for the elimination of interferences in blood sample (Balcaen *et al.* 2014). Jones (2007) has also reported similar product ions. TiO^+ ions are formed on oxidation but in a mixture of elements, the product ion $^{48}Ti^{16}O^+$ do not remove interferences. Balcaen *et al.* (2014) do not confirm $^{48}Ti^{16}O^+$ as a product ion that can be used for interference removal.

^{51}V

Vanadium undergoes condensation reactions of the type VNH_2^+ which is also shown by Sugiyama and Kazumi (2014) and is the most abundant ion in CRC with ammonia gas. Vanadium is oxidised significantly at m/z of $^{67}Zn^+$ and can cause interferences on $^{67}Zn^+$ determination. Junichi (2013) has used on-mass measurement in ammonia gas for $^{51}V^+$ determination.

^{52}Cr

Chromium undergoes clustering reactions and forms product ions of the type $Cr(NH_3)_x^+$. The main product ion with the highest abundance was $Cr(NH_3)_2^+$ similar to the one reported in Jones (2007) with DRC and Sugiyama and Kazumi (2014) with CRC. The oxidation product of $^{52}Cr^+$ is $^{52}Cr^{16}O^+$ at m/z of $^{68}Zn^+$ and can be an interference on m/z of $^{68}Zn^+$ in the spectrum. The $^{36}Ar^{16}O^+$ and $^{35}Cl^{16}O^1H^+$ interferences are shown to be removed with all the product ions formed by $^{52}Cr^+$ with oxygen and ammonia. Junichi (2013) has recommended $^{52}Cr^{+16}O^+$ product ion for removal of $^{36}Ar^{16}O^+$ and $^{35}Cl^{16}O^1H^+$ interferences.

^{55}Mn

Chemistry of $^{55}Mn^+$ is analogous to $^{52}Cr^+$ in CRC as far as product ions with ammonia are concerned. The product ions are formed through clustering reactions with ammonia and the main product ion is $Mn(NH_3)_2^+$. The oxidation product is $^{55}Mn^{16}O^+$ at m/z of $^{71}Ga^+$ and can cause interference on $^{71}Ga^+$. The interferences on $^{55}Mn^+$ have been reported to be eliminated with helium gas modes (Yasuyuki and Kazumi 2013a).

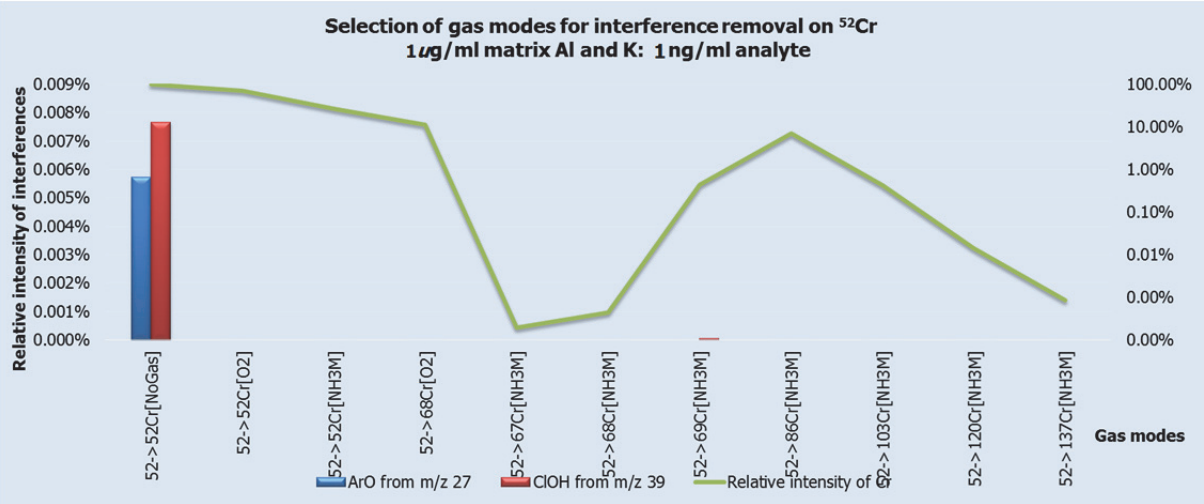

Figure 8.22: Minimisation of interferences on Cr

^{56}Fe

Iron forms $Fe(NH_3)_2$ as the main product ion through clustering reaction as cited in (Jones 2007) and Sugiyama and Kazumi (2014). The oxidation product of iron is $^{56}Fe^{16}O^+$ at m/z of ^{72}Ge and can cause interference on ^{72}Ge. The relative intensity of product ions with ammonia and oxygen gas is shown in Figure 8.23. The interferences of $^{40}Ar^{16}O^+$, $^{39}K^{14}N^1H_3$ and $^{40}Ca^{16}O^+$ on $^{56}Fe^+$ are shown to be removed with different product ions and $Fe(NH_3)_2^+$ is chosen because it still has sufficient intensity of 14% with $^{40}Ca^{16}O^+$ interference reduced to less than 0.093% from 3%.

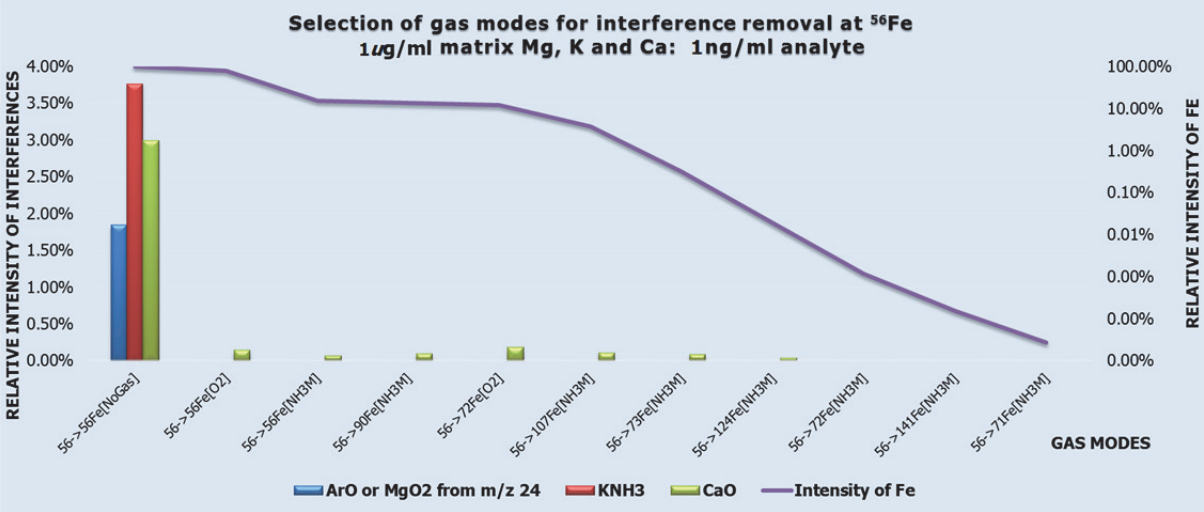

Figure 8.23: Minimisation of interferences on Fe

^{59}Co

The product ions of $^{59}Co^+$ are formed through clustering reactions. The main the product ion formed is $Co(NH_3)_2^+$ similar to studies of (Jones 2007) and Sugiyama and Kazumi (2014).The oxidation product ions $^{61}Co^{16}O^+$ interferes at m/z 75 of ^{75}As.

^{60}Ni

Nickel also forms product ions through clustering reactions with ammonia gas and the main abundant product ion is $Ni(NH_3)_3^+$ similar to studies of (Jones 2007) and Sugiyama and Kazumi (2014). The $^{60}NiO^+$ is formed through oxidation and can be an interference on $^{76}Ge^+$. The $^{44}Ca^{16}O^+$ interference is shown to be removed through $Ni(NH_3)_3^+$ cluster ions as shown in Figure 8.24.

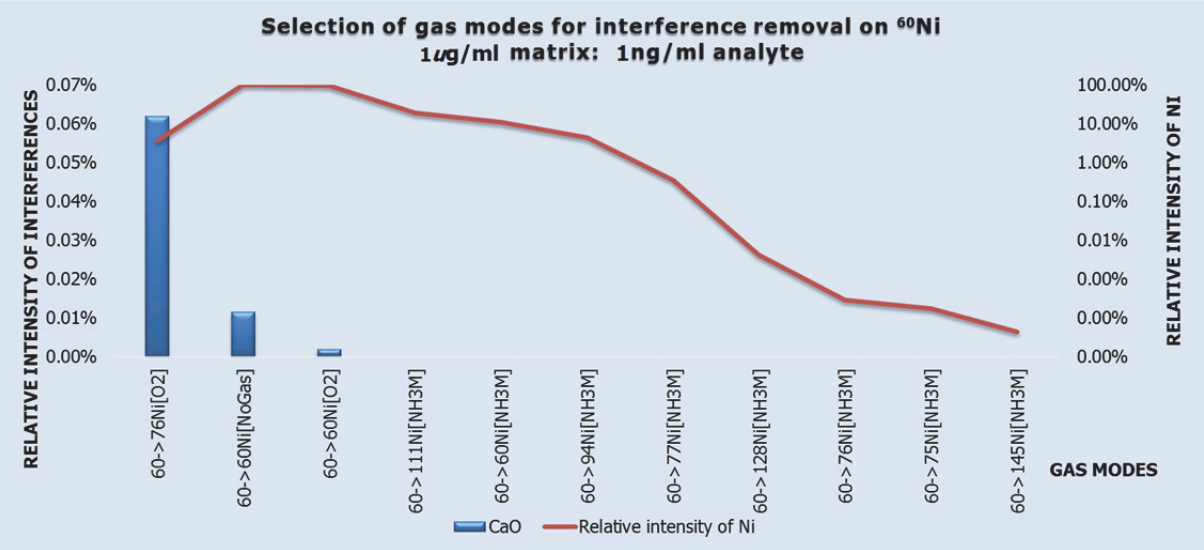

Figure 8.24: Minimisation of interferences of CaO on Ni

^{63}Cu

The main product ion of $^{63}Cu^+$ is $Cu(NH_3)_2^+$ formed through clustering reaction with ammonia gas as in studies of Jones (2007), Sugiyama and Kazumi (2014). The oxidation product is $^{63}Cu^{16}O^+$ at m/z of $^{79}Br^+$ was observed with minor intensities. Akio *et al.* (2013) have used helium gas mode for copper determination in semiconductor grade organometallic titanium complex. This study has used $Cu(NH_3)_2^+$ in the copper determination in geological reference materials and satisfactory results are obtained.

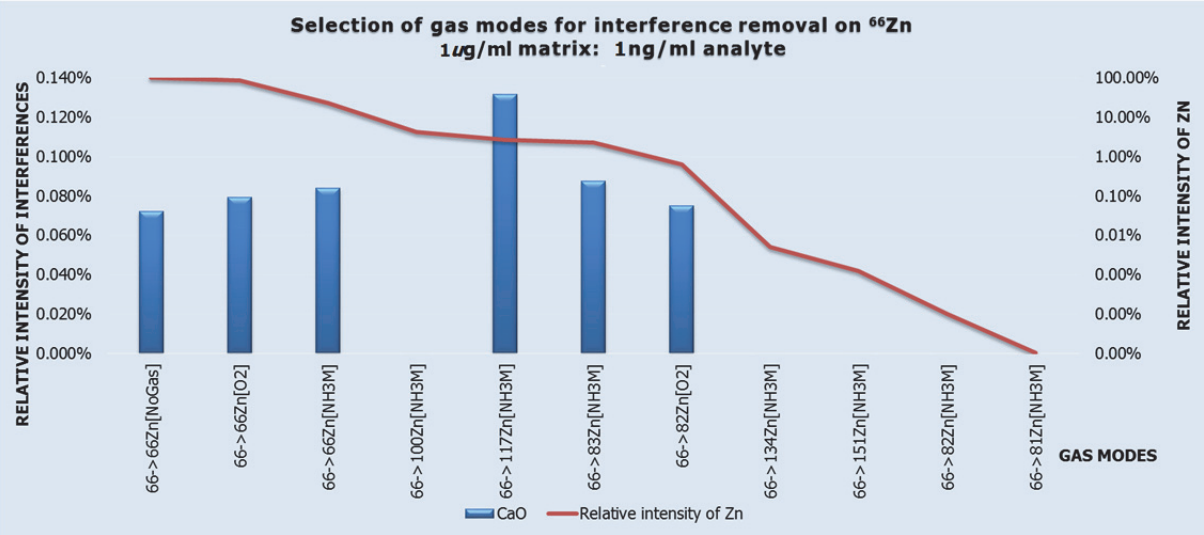

Figure 8.25: Minimisation of interferences of CaO on Zn

^{66}Zn

The product ions of $^{66}Zn^+$ are formed through clustering reaction with ammonia gas. $Zn(NH_3)_2^+$ are the abundant ions similar to the studies by Jones (2007), Sugiyama and Kazumi (2014). The oxides $^{66}ZnO^+$ formed on oxidation of Zn interfere at m/z of ^{82}Se and ^{82}Kr. The interference $^{40}Ca^{16}O^+$ ions on $^{66}Zn^+$ are removed through $Zn(NH_3)_2^+$ product ions as shown in Figure 8.25.

^{71}Ga

$Ga(NH_3)^+$ are the abundant ions formed through clustering reactions as in studies of Jones (2007), Sugiyama and Kazumi (2014). The oxidation product of $^{71}Ga^+$ is minor and fewer interferences are expected at $^{87}Rb^+$ and $^{87}Sr^+$.

^{72}Ge

$Ge(NH_3)_3^+$ are the most abundant ions formed and no intensity was observed as $Ge(NH)^+$. Some intensity was also observed as $Ge(NH_2)^+$. It should undergo condensation reactions as in studies of Jones (2007), Sugiyama and Kazumi (2014) but unlikely following this pattern, it has formed highest abundant ions at m/z of 123. The oxidation product of $^{72}Ge^+$ is at m/z of ^{88}Sr. The interferences of $^{56}Fe^{16}O^+$ and doubly charged ions of $^{144}Nd^+$ are reduced with $Ge(NH_2)^+$ ions as shown in Figure 8.26.

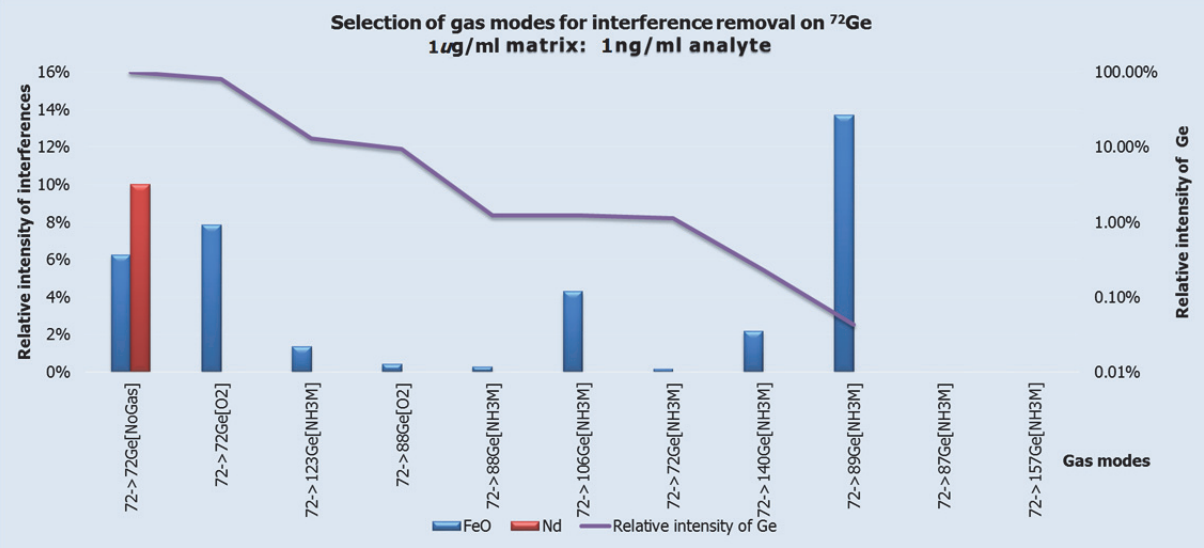

Figure 8.26: Minimisation of interferences on Ge

^{75}As

The product ions of $^{75}As^+$ undergo condensation reaction and form $As(NH_2)^+$ as the abundant ions, although the product ions formed, were very less because it is poorly ionised in plasma due to high IP 9.81 eV (Jones 2007). The oxide $^{75}As^{16}O^+$ is formed at m/z of $^{91}Zr^+$ and can be an interference for $^{91}Zr^+$. The doubly charged ions of $^{150}Nd^{2+}$ and $^{150}Sm^{2+}$ were removed using on-mass oxygen mode. Junichi (2013) has recommended $^{75}As^{16}O^+$ product ions to remove interferences on ^{75}As.

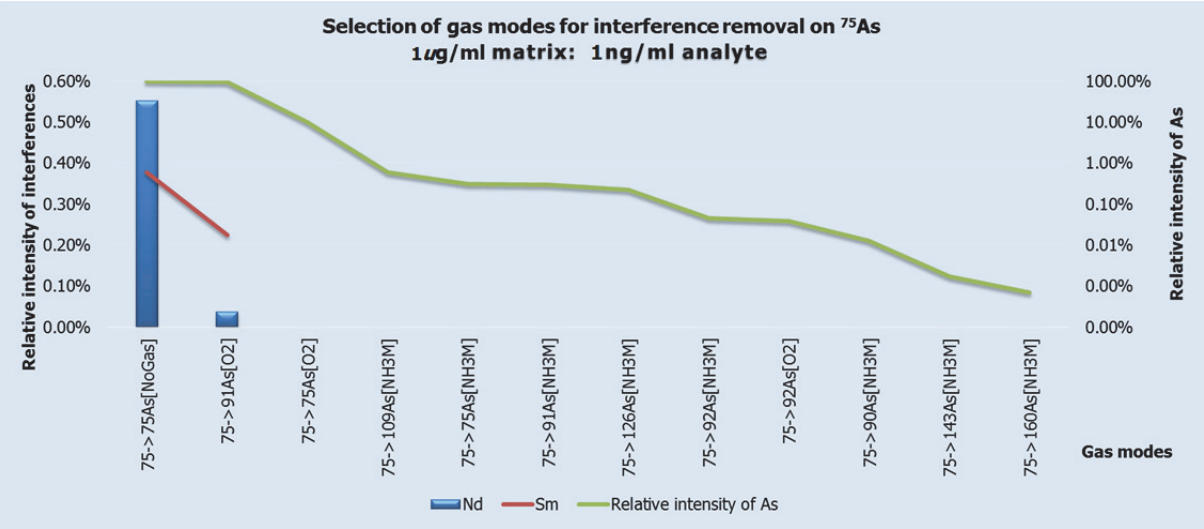

Figure 8.27: Minimisation of Nd and Sm interferences on As

^{80}Se

Ammonia can undergo slightly endothermic (~0.4 eV) charge transfer reactions with As^+ and Se^+ (Jones 2007). The Se^+ is poorly ionised just like As^+ due to high IP 9.75 eV (Naoki 2013a). We have observed abundant ions as $Se(NH_3)^+$ that suggests that it should undergo clustering reaction although, no other products were visible with ammonia gas. The oxidation product $^{80}Se^{16}O^+$ was very low yield due to endothermic reaction with oxygen (0.71 eV) (Glenn 2013b).

^{85}Rb

Two product ions of $^{85}Rb^+$ are formed through clustering reactions i.e. $Rb(NH_3)^+$, $Rb(NH_3)_2^+$ unlike studies of Jones (2007), Sugiyama and Kazumi (2014) as they do not report any product ions formed. Lavrov (2006) has observed one product ion $Rb(NH_3)^+$ as the main product ion in his study. The oxidation product $^{85}Rb^{16}O^+$ has not shown any intensity and is not oxidised as described in Sugiyama and Kazumi (2014). The interferences of $^{52}Cr^{16}O_2{}^1H^+$, $^{69}Ga^{16}O^+$ and $^{36}Ar^{16}O_3H^+$ are shown to be removed with $Rb(NH_3)^+$ product ions as shown in Figure 8.28.

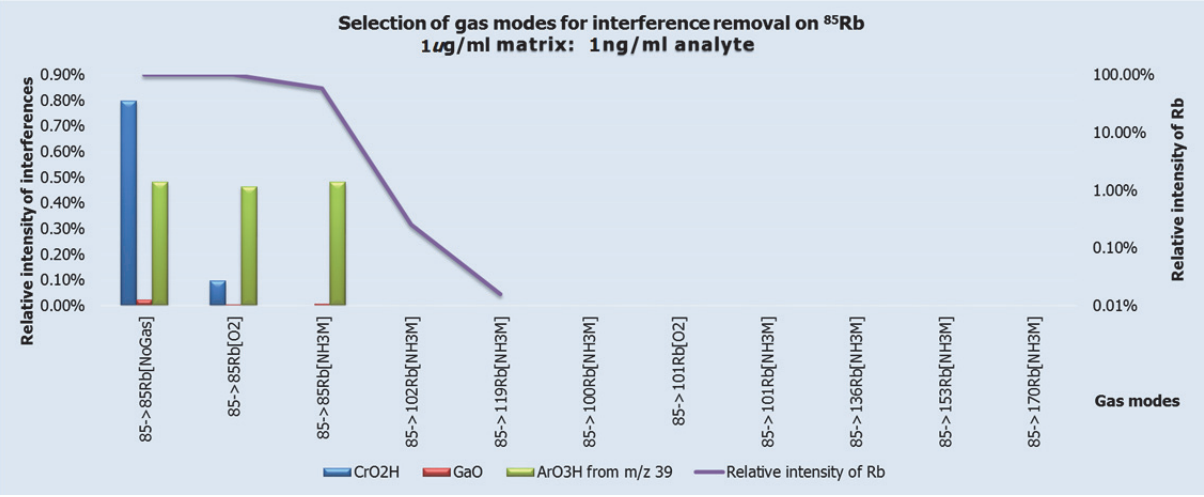

Figure 8.28: Minimisation of interferences on Rb

^{s88}Sr

The product ions of Sr^+ are formed through clustering reactions. $Sr(NH_3)^+$ is the main product ion formed. Just like studies of Jones (2007) up to 7 cluster products were observed, though with less intensity. The oxidation product $^{88}Sr^{16}O^+$ is formed at ^{104}Ru and ^{104}Pd. The interferences of $^{40}Ar^{16}O_3^+$ and $^{71}Ga^{16}O^1H^+$ are removed with $Sr(NH_3)^+$ product ion.

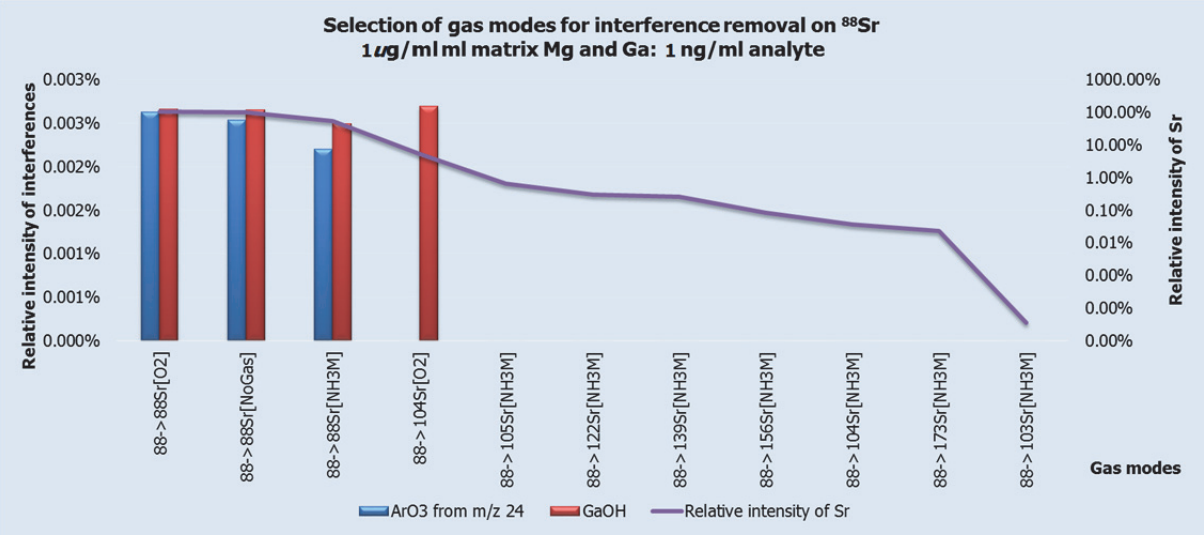

Figure 8.29: Relative intensity of product ions of Sr

Yasuyuki and Kazumi (2013b) has used $^{90}Sr^+$ on-mass measurement with O_2 + H_2 gases for interference removal of $^{90}Zr^+$.

^{90}Zr

The product ions of $^{90}Zr^+$ are formed through a condensation reaction. But $Zr(NH_3)_5^+$ and $Zr(NH_3)_6^+$ have shown with intensity more than $ZrNH^+$ product ion. $^{90}Zr^+$ ions are readily oxidised to high yield of $^{90}Zr^{+16}O^+$ causing an interference on $^{107}Ag^+$.

^{93}Nb

The product ions of $^{93}Nb^+$ are formed through condensation reactions. $NbNH^+$ is the main product ion formed although with very little intensity. A significant amount of $^{93}Nb^+$ is converted to $^{93}Nb^{16}O^+$ causing an interference on ^{109}Ag.

^{95}Mo

The product ions of Mo are formed through clustering reactions and $Mo(NH_3)_2^+$ is the main product ion. $^{95}Mo^+$ is oxidised to $^{95}Mo^{16}O^+$ causing interference on ^{111}Cd.

^{110}Cd

The product ions of $^{110}Cd^+$ are formed through clustering reactions and $Cd(NH_3)_2^+$ are the main product ions. The intensity of oxidation product of $^{110}Cd^+$ is less than 0.1% thus intensity of $^{110}Cd^+$ ions in on-mass oxygen mode is very high.

^{115}In

Three product ions of $^{115}In^+$ are formed through clustering reactions and $In(NH_3)_2^+$ are the main product ions similar to studies of Jones (2007). Indium is not oxidised in CRC with oxygen gas and intensity of $^{115}In^+$ ions in on-mass oxygen mode is very high.

^{121}Sb

Two product ions of $^{121}Sb^+$ are formed through clustering reactions and $Sb(NH_3)^+$ are the main product ions. Jones (2007) cites one product ion $Sb(NH_3)^+$ with DRC. $^{121}Sb^+$ is significantly oxidised in CRC with oxygen gas at m/z of $^{137}Ba^+$.

^{126}Te

Two product ions of $^{126}Te^+$ are formed through clustering reactions and $Te(NH_3)^+$ are the main product ions. Jones (2007) reports four product ion $Sb(NH_3)^+$ with DRC. Sugiyama and Kazumi (2014) has not reported any product ion with CRC. Tellurium is oxidised in CRC with oxygen gas at m/z of $^{142}Ce^+$.

^{133}Cs

Two product ions of $^{133}Cs^+$ are formed through clustering reactions i.e. $Cs(NH_3)^+$ $Cs(NH_3)_2^+$ and $Cs(NH_3)^+$. Jones (2007) cites three product ion $Sb(NH_3)^+$ with DRC. Sugiyama and Kazumi (2014) has not reported any product ion with CRC. $^{133}Cs^+$ is not oxidised in CRC with oxygen gas.

^{137}Ba

Barium forms minor product ion as $BaNH^+$ and major product ion as $Ba(NH_3)^+$ Four other product ions formed are through clustering reactions. Jones (2007) classifies $^{137}Ba^+$ product ions into clustering type. Barium is oxidised in CRC with oxygen gas at m/z of $^{153}Eu^+$ and is potential interference for $^{153}Eu^+$.

^{178}Hf

The product ions of $^{178}Hf^+$ are formed through condensation reactions and $Hf(NH)^+$ are the main product ion formed as in studies of (Jones 2007, Sugiyama and Kazumi 2014). Hafnium is significantly oxidised in CRC with oxygen gas (up to 69%) and ^{178}Hf intensity is lost in on-mass oxygen mode.

^{181}Ta

The product ions of $^{181}Ta^+$ are also formed through condensation reactions and $Ta(NH)^+$ are the main product ions formed as also in studies by Jones (2007), Sugiyama and Kazumi (2014). Tantalum is oxidised in CRC with oxygen gas at m/z of $^{197}Au^+$.

^{182}W

The product ions of W^+ are formed through clustering reactions and $W(NH)^+$ are the main product ions formed as in studies by Jones (2007), Sugiyama and Kazumi (2014). Tungsten is oxidised to $^{182}W^{16}O^+$ and $^{182}W^{16}O_2^+$. WO_2^+ ions are stable and abundant. The interferences of W^+ have been removed by converting $^{182}W^+$ into $^{182}W^{16}O_2^+$ in CRC with oxygen gas on Pt isotopes (Bokhari *et al.* 2015c). Xu and Diao (2008) has shown formation WO_3^+ with oxygen gas.

^{185}Re

The product ions of $^{185}Re^+$ are formed through condensation reactions and $Re(NH)^+$ are the main product ions formed as also in studies by Jones Jones (2007), Sugiyama and Kazumi (2014). Rhenium is significantly oxidised in CRC with oxygen gas up to 12% at m/z of $^{203}Tl^+$.

^{198}Hg

The chemistry of $^{198}Hg^+$ is very interesting regarding interference removal. No product ions of $^{198}Hg^+$ are formed due to charge transfer reaction with ammonia gas as also in studies by Jones (2007), Sugiyama and Kazumi (2014). $^{198}Hg^+$ interferences were removed from Pt isotopes on reaction with ammonia gas as described in Bokhari *et al.* (2015c). The IP of Hg is 10.43 eV and that of ammonia is 10.16 and the slightly endothermic reaction occurs (0.27 eV). This mode can also be applied in regular quad ICP-MS with ammonia gas for removal of Hg interference. The reaction shows the charge transfer reaction between ammonia and Hg^+.

$$Hg^+ + NH_3 \longrightarrow Hg + NH_3^+$$

Glenn (2013a) has used charge transfer reaction for removal Hg interference on Pb isotopes. Mercury is also oxidised in CRC with oxygen gas.

^{205}Tl

The product ions of $^{205}Tl^+$ are formed through clustering reactions and $Tl(NH_3)^+$ is the main product ion formed as also in studies of Jones (2007), Sugiyama and Kazumi (2014). Thallium is not oxidised in CRC with oxygen gas.

^{208}Pb

The product ions of $^{208}Pb^+$ are formed through clustering reactions and $Pb(NH_3)^+$ are the main product ions formed as also in studies of Jones (2007), Sugiyama and Kazumi (2014). Thallium is oxidised in CRC with oxygen gas at m/z of 224.

^{209}Bi

The product ions of $^{209}Bi^+$ are formed through clustering reactions and $Bi(NH_3)^+$ are the main product ions formed as also in studies of Jones (2007), Sugiyama and Kazumi (2014). Bismuth is oxidised in CRC with oxygen gas at m/z of 225.

^{232}Th

The product ions of $^{232}Th^+$ are formed through condensation reactions and $Th(NH)^+$ are the main product ions formed as also in studies of Jones (2007), Sugiyama and Kazumi (2014). Thorium is oxidised in CRC with oxygen gas at m/z of 248.

^{238}U

The product ions of $^{238}U^+$ are formed through condensation reactions and $U(NH)^+$ are the main product ions formed as also in studies of Jones (2007), Sugiyama and Kazumi (2014). Uranium is oxidised in CRC with oxygen gas at m/z of 253.

8.5 Method development for determination of major and trace elements in geological reference material

For the purpose of method validation of different gas modes in on-mass and mass-shift for the determination of major elements several geological reference materials i.e. ML-2 (Webb *et al.* 2012), GSM-1 (Flanagan 1986), OU-9 (Webb *et al.* 2008), NKT-1 (Webb *et al.* 2011), MTA-1 (Potts *et al.* 2015b), WG-1 (Potts *et al.* 2013), DBC-1, OKUM (Potts and Meisel 2015), MUH-1 (Potts and Meisel 2015) and OU-3 (Potts and Jean 2006) were digested with sodium peroxide sintering with 1:6 sample to sodium peroxide ratio. For matrix calibration 11 reference materials MUH-1, OU-3, OU-6 (Potts and Kane 2005), OU-9, BRP-1, BCR-2, SBC-1, NKT-1, SdAR-1, MRH-1 and along with procedural blank were also digested with the same method that was used for the preparation of reference materials. Indium, rhenium, bismuth beryllium and germanium, were selected as internal standard. The drift correction was made through linear regression. The measurement was made with no gas mode using single without MS/MS mode and for cell gases ammonia, oxygen, helium and hydrogen, MS/MS mode was used with the on-mass and mass-shift mode. Most of the elements were measured using ammonia and oxygen gas. The flow rates of ammonia gas were 3 ml/min denoted as NH3-M and for oxygen gas were 3 ml/min. One ml/min helium was added to the ammonia gas. The typical instrument configurations were the same as shown in section of PGE measurement.

8.5.1 Suggested method for the measurement

Based on the study of the product ions of all elements, testing of interferences a method is developed and can be used for routine analysis of major and trace element in geological reference materials. XRF is the non-destructive technique of choice for accurate analysis of major element which does not require recovery of elements through sample digestion methods, the suggested method can aid as a second method of choice for accurate determination of analytes. The gas modes and the product ions for each element are given in Table 8.2.

Table 8.2: Suggested method for routine analysis of major and trace elements

Gas modes/product ions	Gas modes/product ions
28 -> 44 Si [O2]	56 -> 90 Fe [NH3-M]
31 -> 47 P [O2]	63 -> 97 Cu [NH3-M]
48 -> 64 Ti [O2]	68 -> 100 Zn [NH3-M]
52 -> 68 Cr [O2]	75 -> 91 As [O2]
55 -> 71 Mn [O2]	121 -> 137 Sb [O2]
51 -> 51 V [NH3-M]	204 -> 204 Pb [NH3-M]

8.5.2 Blank, detection limit and BECs

The blank, detection limits and BECs of some elements are given in Table 8.3. (b) refers to the procedural blank. DL are the detection limits DL= (3 times the standard deviations of blank concentration/slope of the curve). BECs refer to background equivalent concentrations of the analytes BEC= (Blank concentrations/slope of the curve). R is the coefficient of linear regression obtained from the curve of matrix-matched calibrations with reference materials. The background equivalent concentrations were calculated by dividing procedural blank concentrations with a slope of the calibration curve. High blank values for elements e.g. Cu, Fe, Si, K, and V, in particular, represent a matrix effect of sodium ions. Sodium ions react with argide ions to form several interferences which then with a selection

of particular gas modes and product ions appear to reduce. Copper has false high blank, DL and BECs which is reduced with mass-shift ammonia mode. This shows the efficiency of the collision/reaction cell in reducing the background interferences in the instrument.

Table 8.3: Blanks, detection limits and BECs

Blanks, Detection limits and BECs								
Tune Step	**Scan Type**	**Q1**	**Q2**	**Name**	**R**	**b (blank)**	**DL**	**BEC**
						pg/ml	pg/ml	pg/ml
No gas	Single Quad		75	As	0.73	145	950	15016
Oxygen	MS/MS	75	91	As	0.99	38	83	281
No gas	Single Quad		52	Cr	1	204	534	11642
Oxygen	MS/MS	52	68	Cr	1	513	702	4236
No gas	Single Quad		63	Cu	0.08	22180	131981	865385
NH3-M	MS/MS	63	97	Cu	0.77	1.3	159.1	596.6
No gas	Single Quad		56	Fe	0.96	18677	6	117
NH3-M	MS/MS	56	90	Fe	0.99	42	1	8
No gas	Single Quad		39	K	0.96	28758	11	318
NH3-M	MS/MS	39	39	K	0.99	863	4	84
No gas	Single Quad		55	Mn	0.95	52	0	0
Oxygen	MS/MS	55	71	Mn	0.99	16	0	0
No gas	Single Quad		31	P	1	111	2	33
Oxygen	MS/MS	31	47	P	1	46	1	4
NH3-M	MS/MS	204	204	Pb	1	0	68	251
No gas	Single Quad		204	Pb	1	6	328	2297
No gas	Single Quad		121	Sb	1	0	74	210
NH3-M	MS/MS	121	121	Sb	1	0	80	142
Oxygen	MS/MS	121	137	Sb	1	0	58	98
No gas	Single Quad		28	Si	0.93	16330	38	510
No gas	Single Quad		48	Ti	0.98	17	0	3
Oxygen	MS/MS	48	64	Ti	0.98	278	0	1
No gas	Single Quad		51	V	0.95	948	3811	38350
NH3-M	MS/MS	51	51	V	1	0	94	314
Oxygen	MS/MS	51	67	V	0.99	298	71	308
No gas	Single Quad		66	Zn	0.89	153	1441	41226
NH3-M	MS/MS	66	100	Zn	0.94	3	620	591

8.5.3 Calibrations plots

The calibration plots were obtained using matrix-matched reference materials. The no gas mode and cell gas modes are both plotted to show the effect of the cell gas modes. The calibration plots for some elements are presented in Figure 8.30- Figure 8.45.

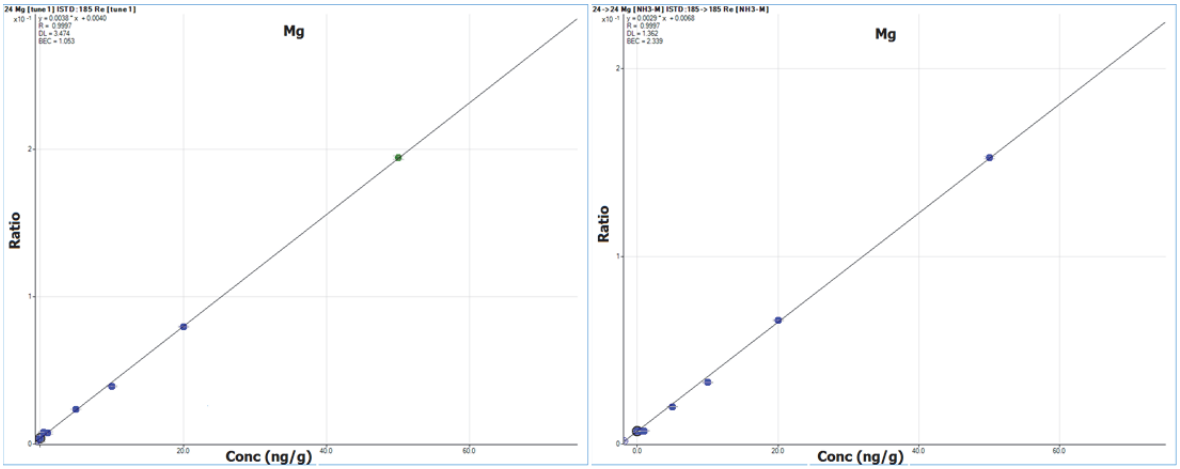

Figure 8.30: Calibration plots for Mg

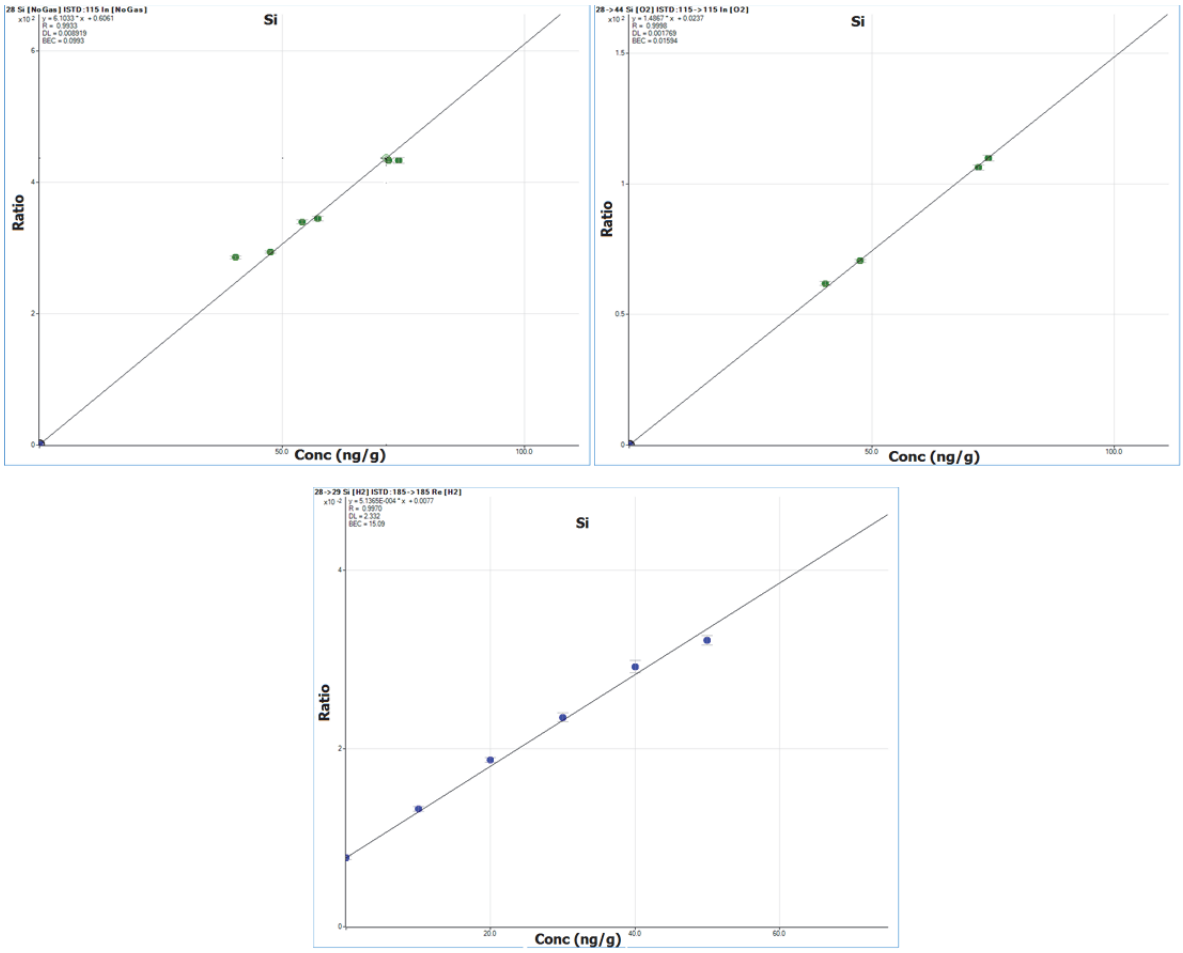

Figure 8.31: Calibration plots for Si

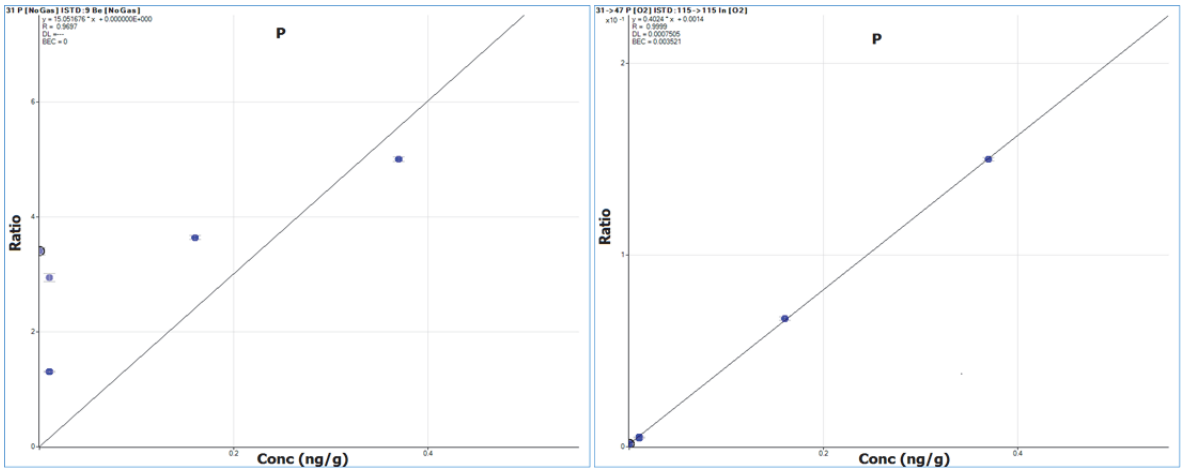

Figure 8.32: Calibration plots for P

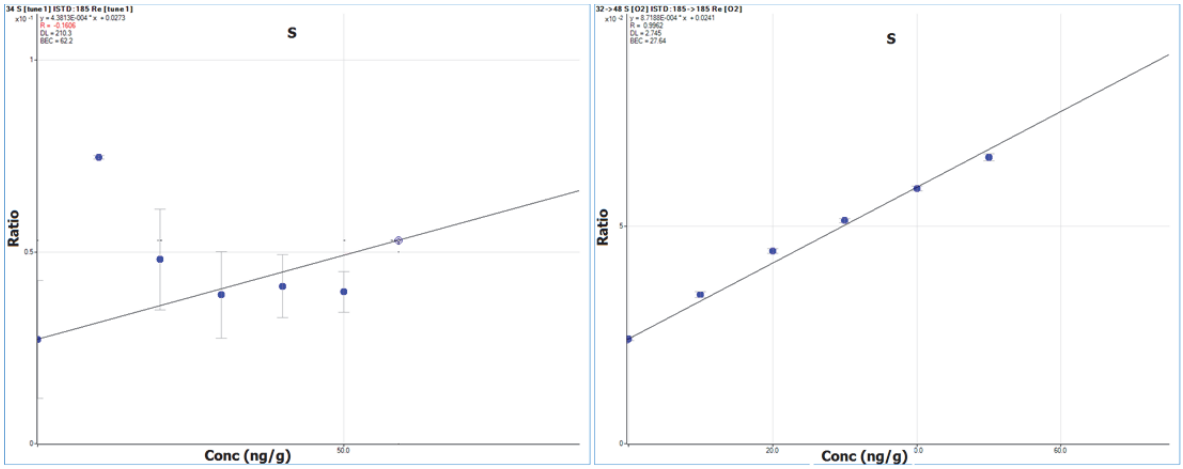

Figure 8.33: Calibration plots for S

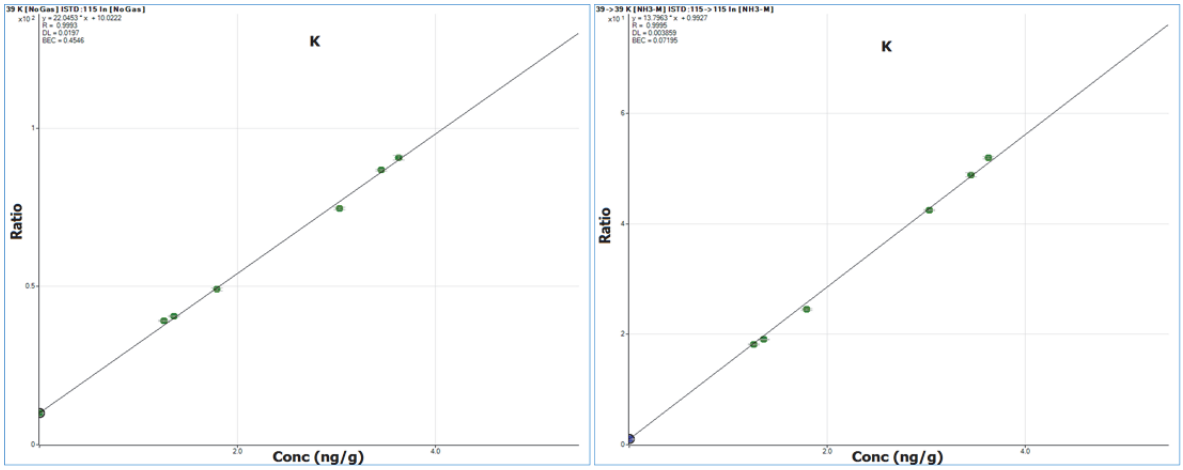

Figure 8.34: Calibration plots for K

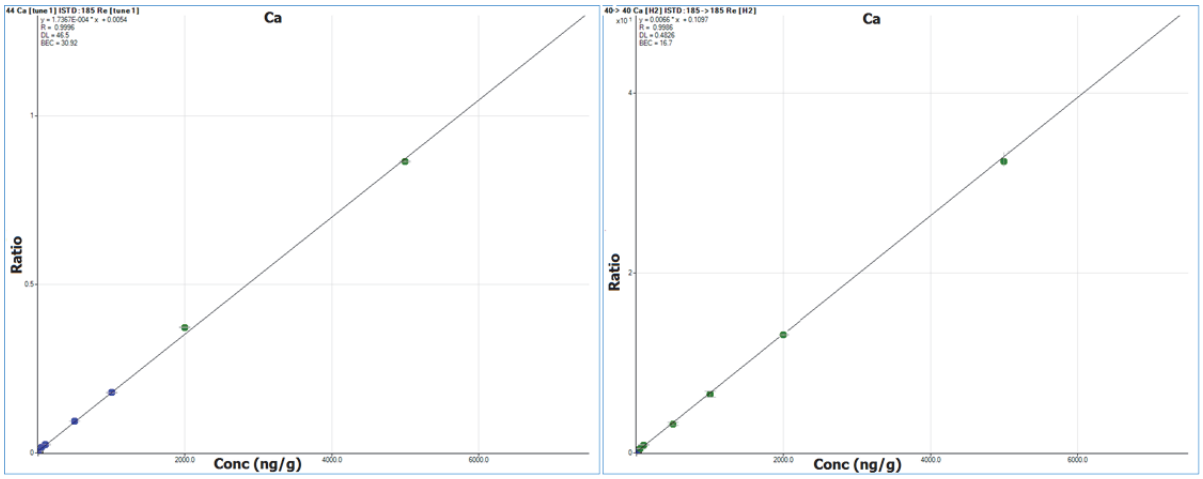

Figure 8.35: Calibration plots for Ca

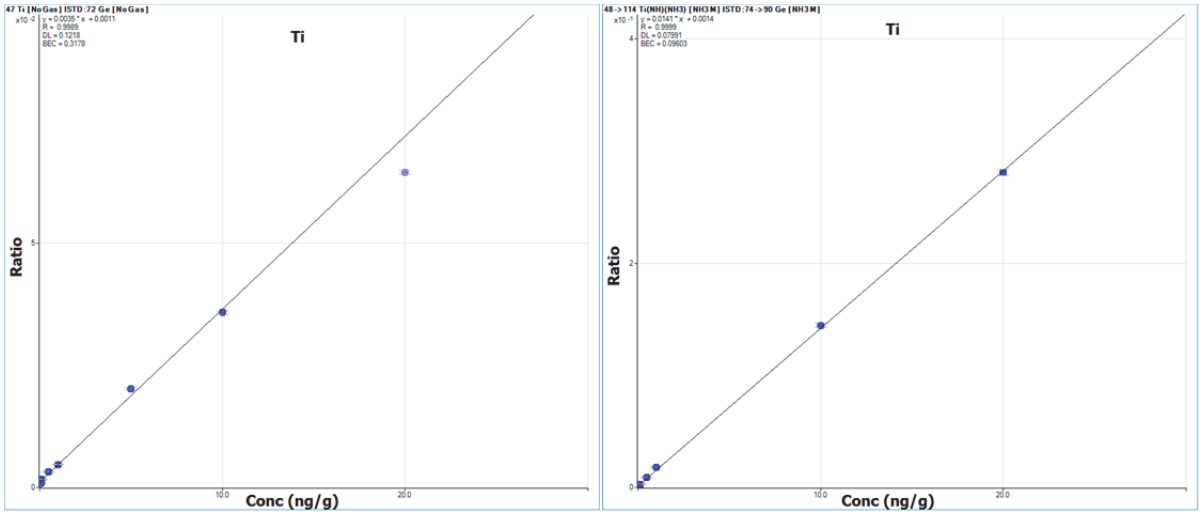

Figure 8.36: Calibration plots for Ti

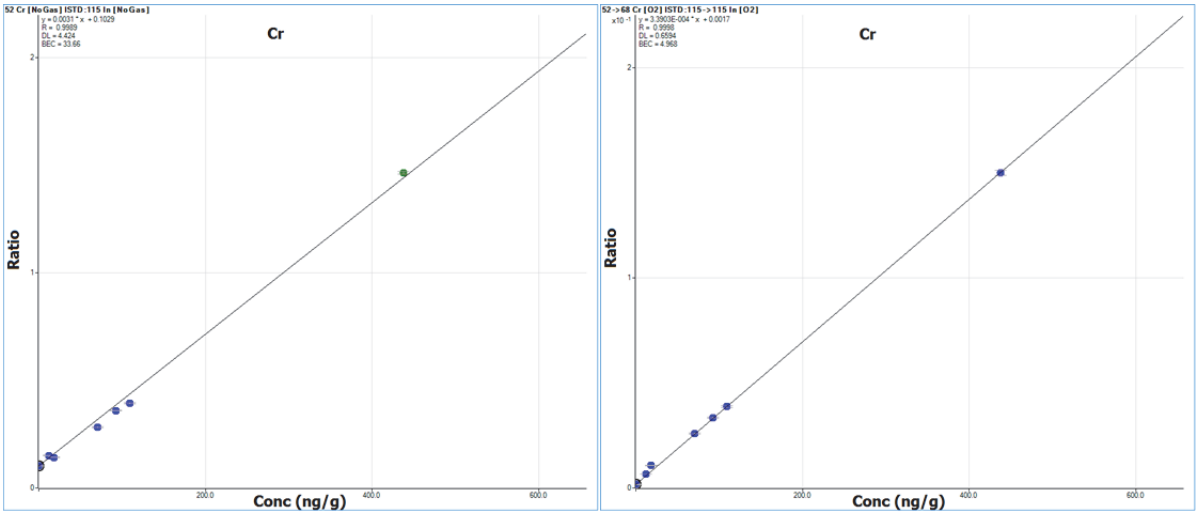

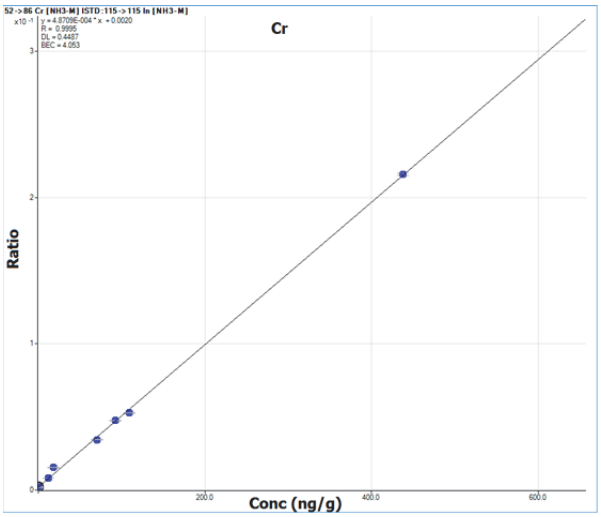

Figure 8.37: Calibration plots for Cr

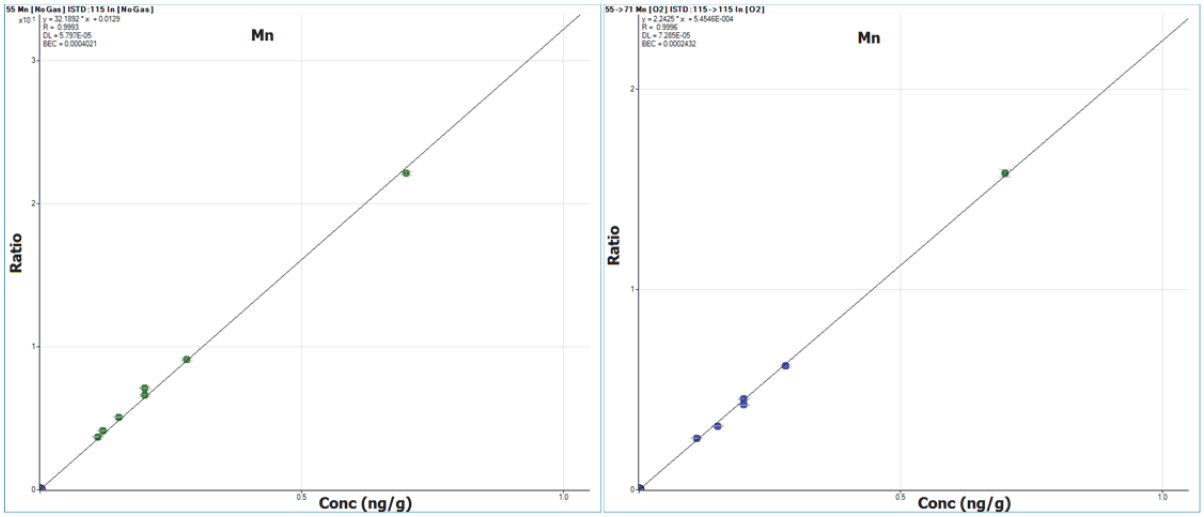

Figure 8.38: Calibration plots for Mn

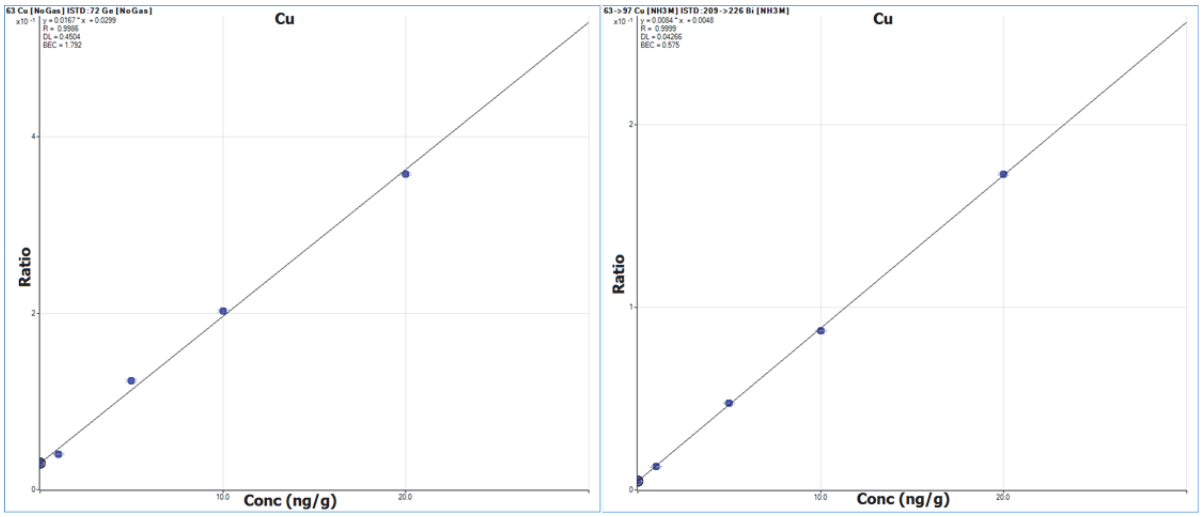

Figure 8.39: Calibration plots for Cu

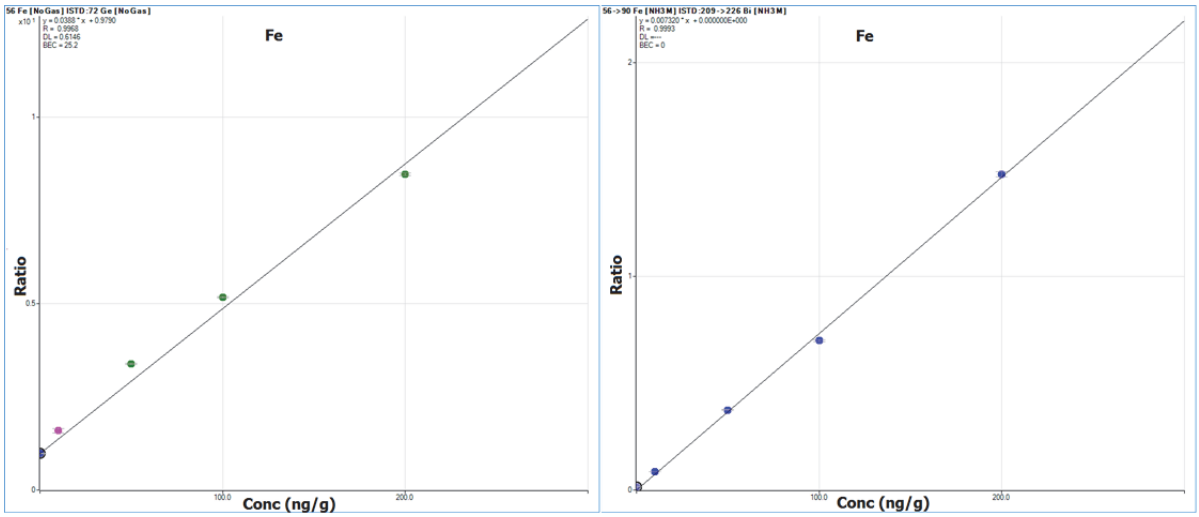

Figure 8.40: Calibration plots for Fe

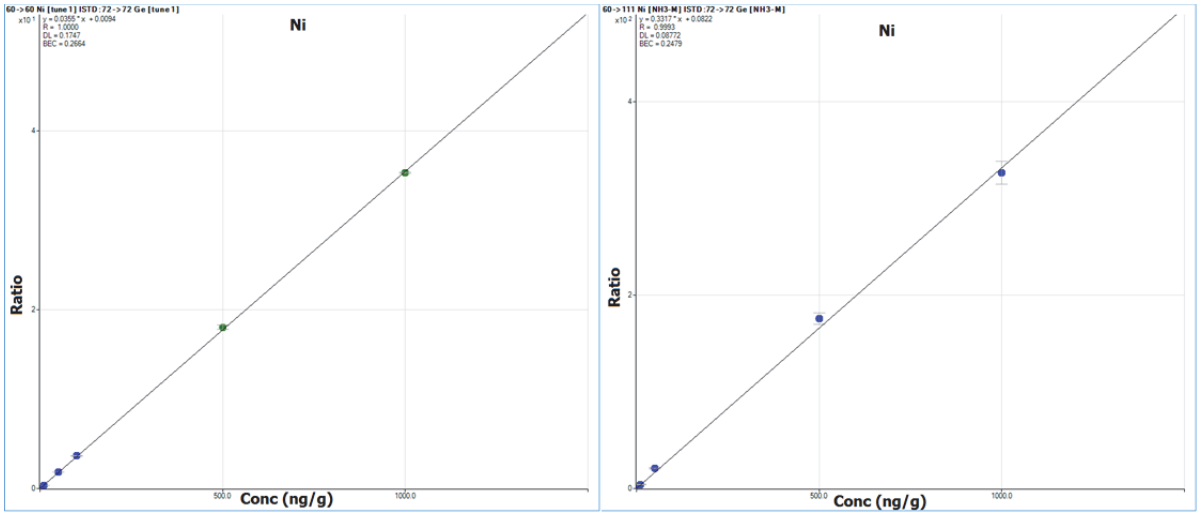

Figure 8.41: Calibration plots for Ni

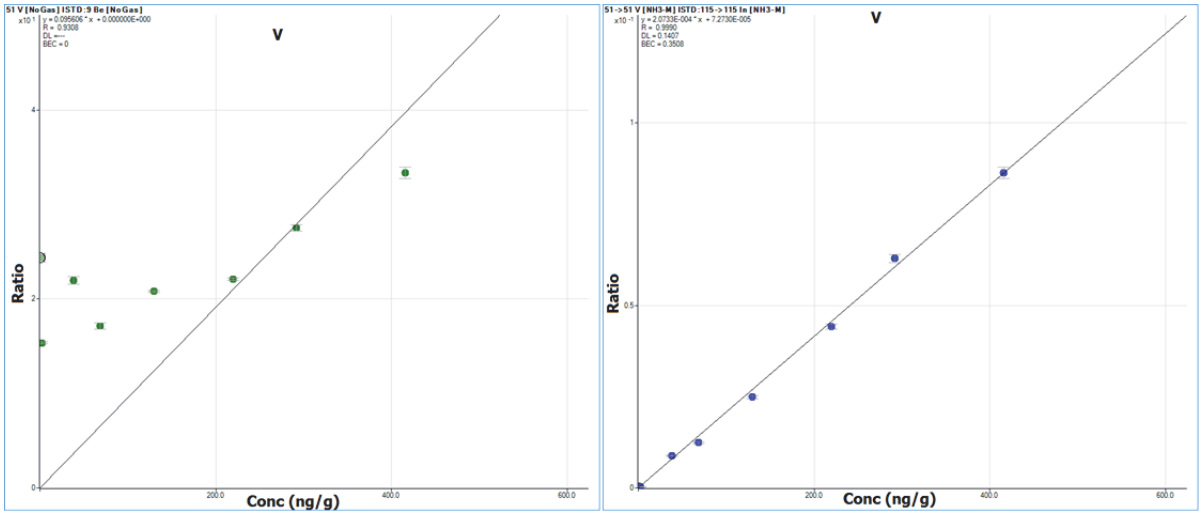

Figure 8.42: Calibration plots for V

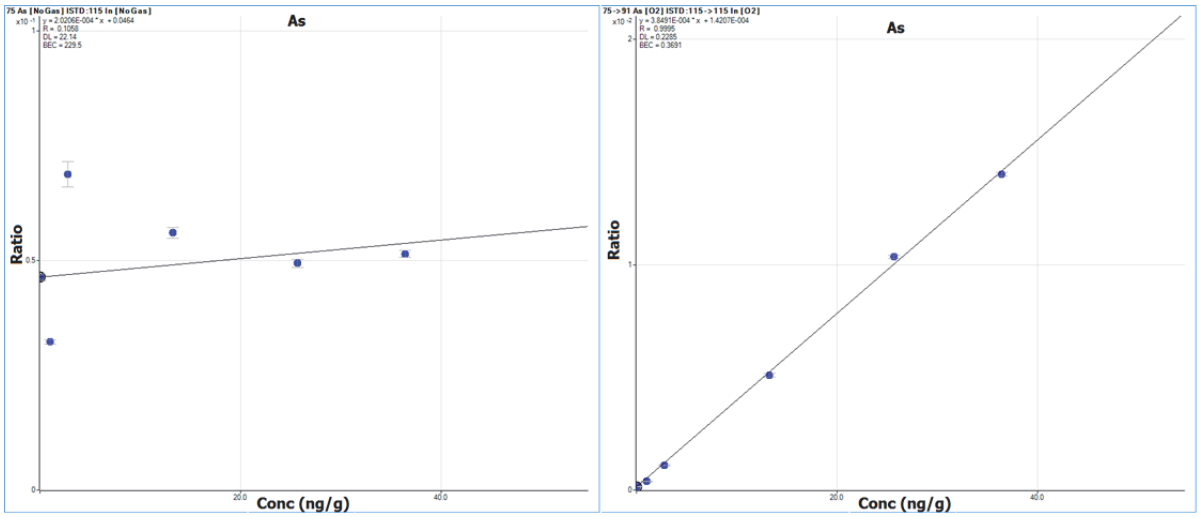

Figure 8.43: Calibration plots for As

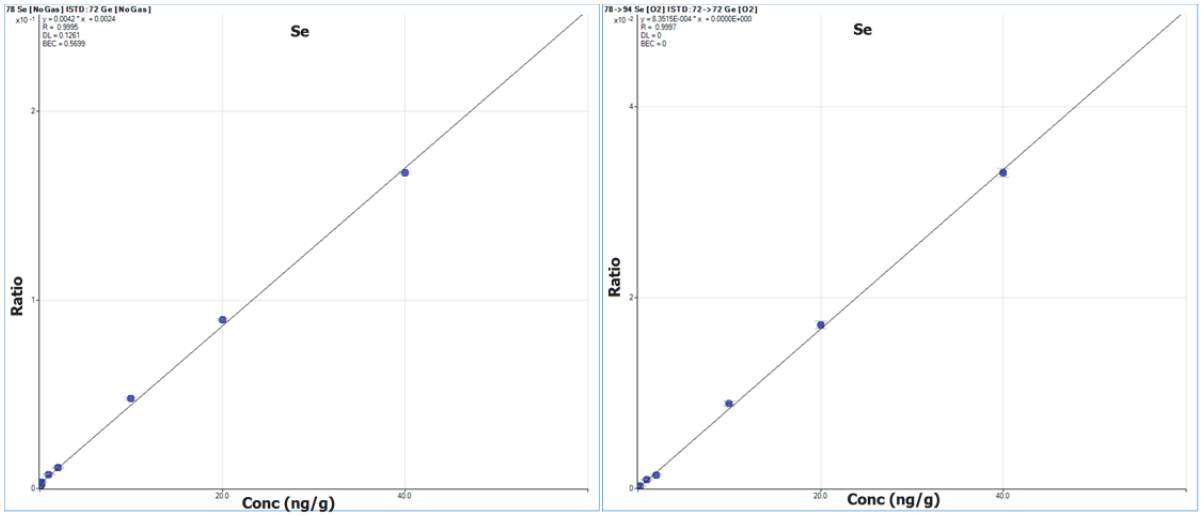

Figure 8.44: Calibration plots for Se

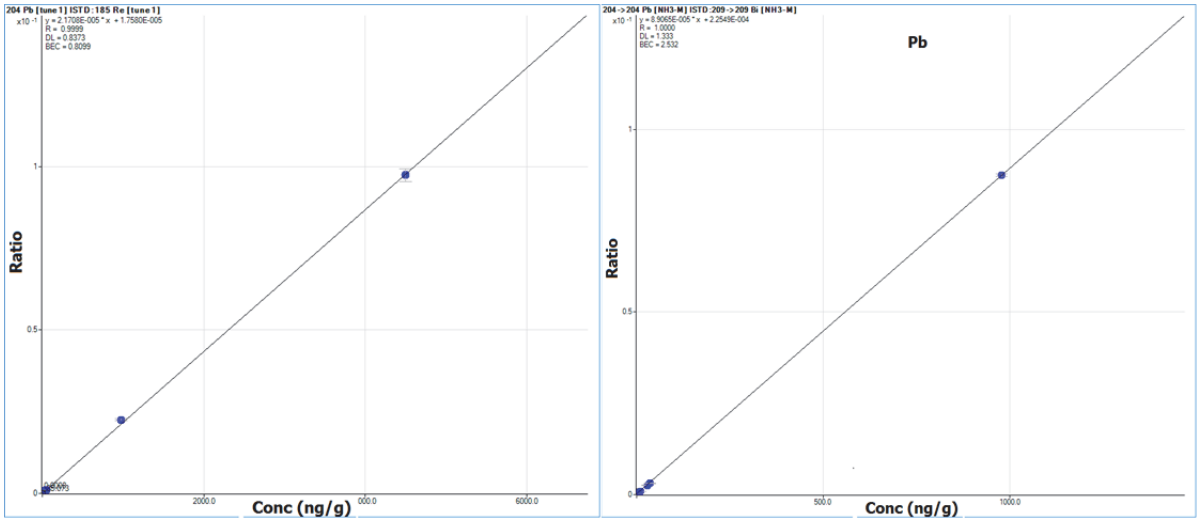

Figure 8.45: Calibration plots for Pb

8.5.4 Results

The results of critical elements namely Si, P, Ti, V, Cu, Fe, As, Sb, Zn, Mn, Cr and Pb are presented in Table 8.4. The data obtained through measurement of suggested method is in good agreement with reference values of the reference materials.

Table 8.4: Measurement of analytes mass fractions in geological reference material

Results of measurement of analytes in geological reference materials (mg/kg) n=4						
Si						
Reference Materials	**ML-2**	**GSM-1**	**OU-9**	**NKT-1**	**MTA-1**	**WG-1**
28 Si [No Gas]	3.06	45.31	91.44	45.12	65.21	57.34
Precision	1%	3%	1%	1%	4%	2%
28 -> 44 Si [O2]	2.81	45.16	78.89	39.21	60.51	53.67
Precision	4%	3%	1%	3%	4%	3%
Reference value	2.86	45.68	79.5	37.78	58.64*	53.23
Rel *u*	0.7%	0.1%	1.0%	0.2%	0.3%	0.1%
P						
Reference Material	**ML-2**	**GSM-1**	**OU-9**	**NKT-1**	**MTA-1**	**WG-1**
31 P [No Gas]	0.05	0.05	0.03	1.16	1.28	0.31
Precision	6%	7%	8%	4%	4%	4%
31 -> 47 P [O2]	0.044	0.036	0.028	0.921	1.07	0.297
Precision	5%	4%	7%	4%	5%	5%
Reference value	0.047	0.031	0.03	0.917	1.002*	0.291
Rel *u*	2%	3%	3%	0%	1%	1%
Ti						
Reference Material	**DBC-1**	**GSM-1**	**OU-9**	**NKT-1**	**MTA-1**	**WG-1**
48 Ti [No Gas]	1.6	1.46	0.059	4.35	1.52	1.85
Precision	5%	2%	3%	2%	4%	3%
48 -> 64 Ti [O2]	1.103	1.36	0.054	3.82	1.43	1.72
Precision	1%	2%	1%	2%	1%	2%
Reference value	1.123	1.38	0.057	3.84	1.40*	1.74
Rel *u*	6%	0%	4%	0%	1%	0%
V						
Reference Material	**ML-2**	**GSM-1**	**NKT-1**	**MTA-1**	**WG-1**	
51 V [No Gas]	11	625	330	148	171	
Precision	46%	4%	3%	6%	2%	
51 -> 51 V [NH3-M]	3.008	564	281	101	146	
Precision	5%	3%	4%	2%	3%	
Reference value	3.17	601	292	102*	155	
Rel *u*	13%	1%	1%	3%	1%	
Cr						

Reference Material	DBC-1	GSM-1	NKT-1	MTA-1		
52 Cr [No Gas]	124	14.91	525	47.41		
Precision	1%	17%	1%	4%		
52 -> 68 Cr [O2]	106	5.58	438	32.98		
Precision	1%	6%	4%	4%		
Reference value	105	5.6*	438	35*		
Rel *u*	2%		1%	6%		

Fe

Reference Material	ML-2	GSM-1	OU-9	NKT-1	MTA-1	WG-1
51 Fe [No Gas]	0.24	13.2	0.82	15.67	6.55	12.8
Precision	2%	1%	2%	1%	2%	2%
56 -> 90 Fe [NH3-M]	0.137	12.88	0.673	13.53	5.3	11.23
Precision	1%	1%	3%	3%	3%	3%
Reference value	0.14	13.21	0.74	13.29	5.91*	11.31
Rel *u*	2%	0.2%	2%	0%	1%	0%

Mn

Reference Material	ML-2	GSM-1	OU-9	NKT-1	MTA-1	WG-1
55 Mn [No Gas]	0.024	0.159	0.114	0.23	0.05	0.15
Precision	1%	2%	2%	1%	2%	3%
55 -> 71 Mn [O2]	0.022	0.155	0.102	0.2	0.047	0.143
Precision	5%	2%	1%	3%	4%	3%
Reference value	0.023	0.159	0.11	0.2	0.047*	0.143
Rel *u*	2%	0%	3%	1%	2%	0%

Cu

Reference Material	BRP-1	OKUM	MUH-1	OU-3		
63 Cu [No Gas]	90.84	55.29	62.02	55.18		
Precision	1%	38%	24%	34%		
63 -> 97 Cu [NH3-M]	48.74	46.67	61.46	3.64		
Precision	3%	9%	12%	12%		
Reference value	40.40*	43.50*	19.10*	3.3		
Rel *u*	12%	3%	6%	7%		

Zn

Reference Material	BRP-1	OKUM	MUH-1	OU-3		
68 Zn [No Gas]	161.1	75.5	54.1	143.2		
Precision	6%	10%	13%	2%		
68 -> 100 Zn [NH3-M]	76.4	64.0	43.9	150.0		
Precision	7%	7%	5%	4%		
Reference value	70.00*	61.20*	44.1	149.2		
Rel *u*	0.1%	0.1%	0.1%			

As

Reference Material	ML-2	GSM-1	OU-9	NKT-1	MTA-1	WG-1
75 As [No Gas]	25.3	16.0	11.6	16.7	20.9	16.2
Precision	29%	39%	9%	8%	16%	22%
75 -> 91 As [O2]	0.147	12.88	0.673	13.5	5.3	11.23

Precision	11%	1%	3%	3%	2%	3%
Reference value	0.14	13.21	0.74	13.29	5.91*	11.31
Rel *u*	2%	0%	2%		1%	0%

Sb

Reference Material	**DBC-1**	**GSM-1**	**OU-9**	**NKT-1**	**MTA-1**
121 Sb [No Gas]	3.31	1.91	8.77	0.59	9.33
Precision	10%	2%	3%	25%	3%
121 -> 137 Sb [O2]	2.59	1.86	7.43	0.13	8.43
Precision	0%	3%	6%	11%	2%
Reference value	2.81	1.83	7.67	0.12	8.50*
Rel *u*	5%	4%	6%	8%	13%

Pb

Reference Material	**DBC-1**	**GSM-1**	**NKT-1**	**MTA-1**	**WG-1**
204 Pb [No Gas]	59.4	12.3	2.6	38.8	3.7
Precision	16%	3%	6%	3%	6%
204 -> 204 Pb [NH3-M]	54	11	2.4	33	3.5
Precision	3%	3%	4%	3%	8%
Reference value	53.5	11	2.9	34.1*	3.4
Rel *u*	1%	2%	2%	4%	2%

*certified

Rel *u* is relative uncertainty

8.6 Summary

The study of all possible product ions of the analytes is essential in determining the extent to which a product ion can overlap on the other product ion while developing a method using collision/reaction cell. The products ions of the ion-molecule reactions of the majority of elements occurring in CRC with ammonia and oxygen gases were studied for removal of numerous interferences generated in the plasma. The identification of the product ions was feasible in ICP-MS/MS technique as it provided a quick scan of all the product ions on required m/z of the analytes. This study has provided information on possible product ions of most of the elements in the periodic table. The knowledge of the product ions has been used earlier in other section (chapter 7 and 9) for removal of interferences on rare earth elements and platinum group elements.

In this chapter, the role of ammonia, hydrogen, helium and oxygen gases in the collision/reaction cell is studied for reducing the background interferences from plasma and acids used for dilution and sample preparation (Figure 8.1- Figure 8.20). It is particularly shown that interferences such as argide ions, C^+, N^+, O^+, H^+, S^+, are reduced with the use of ammonia gas. The addition of H_2 in the cell also removes any residual $^{40}Ar^+$ that is formed even under cool plasma conditions (Figure 8.11).

The study of the behaviour of some analytes for examples Hg, S, Se, As and P which undergoes charge transfer reactions with ammonia, provides an application for removal of these interferences on other elements by the use of ammonia gas. For example, ^{204}Hg interference on ^{204}Pb can be removed using this behaviour of Hg. Mercury is neutralised by charge transfer reaction with ammonia, leaving ^{204}Pb interference free. On the other hand, S based interferences can be decreased using charge transfer reaction with ammonia gas.

Argide ions themselves react with ammonia through charge transfer reaction and interferences are removed.

The practical applicability of some suggested methods is compared with literature i.e. user guide of Agilent 8800 and has been tested and validated with reference material. It proves that collision/reaction cell technology is capable of replacing complex chromatographic separation methods of interference removal.

The on-mass and/or mass-shift mode with NH_3 and/or O_2 reaction gas provides reliable and consistent measurements of Si as 28 -> 44 Si [O2], P as 31 -> 47 P [O2], Ti as 48 -> 64 Ti [O2], Cr as 52 -> 68 Cr [O2], Cr as 55 -> 71 Mn [O2], V as 51 -> 51 V [NH3-M], Fe as 56 -> 90 Fe [NH3-M], Cu as 63 -> 97 Cu [NH3-M], Zn as 68 -> 100 Zn [NH3-M], As as 75 -> 91 As [O2], Sb as 121 -> 137 Sb [O2] and Pb as 204 -> 204 Pb [NH3-M] etc.

The outlook of the method is an improvement of elemental sensitivity for trace analysis. The data on product ions of the analytes studied can help develop other methods for interference removal on other analytes which are not presented in this study.

9. Method development for interference removal on platinum group elements-Ag-Au in geological materials

9.1 Introduction and background

Platinum group elements (PGE) are important industrial metals which are used in exhaust systems of vehicles, industrial catalysts and used in reducing the emission of gaseous pollutants, such as carbon monoxide, nitrogen oxides, and hydrocarbons (Bencs *et al.* 2003). The continuous emission of the PGE from the catalytic converters due to abrasion/ablation to the environment is a potential health risk to the human beings and animals (Palacios *et al.* 2000). Several studies report accumulation of PGE especially Pt, Pd and Rh along the roadside (Fritsche and Meisel 2004, Kalavrouziotis and Koukoulakis 2009, Schäfer and Puchelt 1998, Whiteley and Murray 2003). This factor emphasises the monitoring of the PGE concentrations continuously, for the estimation of future health risks to the environment. The monitoring of the PGE requires precise measurement procedures of high sensitivity and selectivity due to trace amounts of PGE and high matrix effects (Meisel and Moser 2004b).

For geochemical studies, the PGE mass fractions provide an insight into the petrogenesis and history of rocks. Scientific community wants to explore more and more natural and mineral deposits for meeting a huge PGE consumer demand in high-technology products. In recent years the recycling of the PGE has become an important topic in terms of both potential strategies for maintaining the supply and converting the previously disposable material into valuable renewable resources. Thus, reliable measurement procedures for PGE analysis are required to facilitate different fields of science.

Several sample digestion methods have been claimed for complete recovery of PGE from all kind of samples i.e. geological, environmental and industrial etc. An effective sample digestion method is a key factor for accurate determination of PGE contents. Details of the methods are discussed in the section of sample preparation (chapter 5) and elsewhere in introduction and backgrounds of all chapters of the thesis. These methods include acid digestions, fusion method with alkaline salts, fire assay methods e.g. NiS-fire assay (Savard *et al.* 2010), Pb fire assay etc. chlorination and fire assay, microwave acid digestion with Carius tubes and high-pressure-asher digestions (Meisel and Moser 2004b), aqua regia leaching, HF attacks etc. Sodium peroxide sintering has been used in the current study for sample digestion, which has been optimised earlier and discussed in the section of sample preparation (chapter 5). A pre-concentration step is normally required for PGE enrichment and removal of matrix from the samples. Pre-concentration can be achieved with exchange resins and co-precipitating agents i.e. Te/$SnCl_2$ etc. (Enzweiler and Potts 1995, Enzweiler *et al.* 1995).

The direct analysis of PGE is mostly applied to the environmental and industrial samples. For the direct analysis of PGE isotopes (i.e., without any previous pre-concentration, and/or separation of the analyte/matrix), only a few techniques are known which include inductively coupled plasma mass spectrometry (ICP-MS), adsorptive stripping voltammetry (ASV), and instrumental neutron activation analysis (INAA). However, these techniques are not effective due to spectral interferences on PGE isotope.

Platinum group elements are subject to a number of significant oxide-based interferences in ICP-MS analysis (Simpson *et al.* 2001). The removal of the oxide interferences would present a significant improvement in accuracy of ICP-MS method and detection power. These oxides result in interferences at 16, 32 and 48 atomic mass units

(m/z) above the parent ions (m/z), corresponding to MO^+, MO_2^+ or MO_3^+. The general consideration for interferences are normally only for MO^+ and literature describes several correction procedures for that. Oxide corrections methods rarely exceed more than 3-5%, thus for critical interferences of higher magnitudes on PGE isotopes, the mathematical and the statistical corrections offer no solution (Falkner and Edmond 1990, Sylvester and Eggins 1997).

Quadrupole ICP-MS (ICP-QMS) is commonly used for the quantification of PGE mass fractions i.e. environmental samples than the high-resolution (HR) sector-field ICP-SFMS. The ICP-QMS spectrometers possess a mean mass resolution of around 300 m/Δm, whereas the ICP-SFMS working under HR settings supplies with an enhanced selectivity (7500-11000 m/Δm) (Bencs *et al.* 2003).

Rauch *et al.* (2000) studied the interference effects on the determination of Pd, Pt and Rh in road dust and river sediment samples using ICP-SFMS with ultrasonic nebulisation (UN). For ^{103}Rh, both $^{206}Pb^{2+}$ and $^{40}Ar^{63}Cu^+$ were found to be the main interfering ions in LR (low resolution) mode, but they could be efficiently separated in the HR (high resolution) mode. The interferences from Zn in environmental samples as $^{36}Ar^{67}Zn^+$ can be removed by applying the HR mode. The interferences from $^{87}Sr^{16}O^+$ and $^{87}Rb^{16}O^+$ could not be removed, though. The apparent signal on $^{106}Pd^+$ due to interfering Cd^+ increased linearly with concentration. Both $^{105}Pd^+$ and $^{106}Pd^+$ were strongly interfered in low-resolution mode and most of the interferences were not removed by increasing the resolution. Cu and Rb were interferences on ^{106}Pd, due to the formation of $^{40}Ar^{65}Cu^1H^+$ and $^{87}Rb^{18}O^1H^+$, respectively. For ^{195}Pt, the HfO^+ was eliminated using high resolution, i.e. 10102 m/Δm (Bencs *et al.* 2003).

Petrucci *et al.* (2000) determined Pd, Pt and Rh in urine samples using SF-ICP-MS with UN. The effect of $^{87}Rb^{16}O^+$ and $^{87}Sr^{16}O^+$ on $^{103}Rh^+$ was minor but $^{63}Cu^{40}Ar^+$ and $^{67}Zn^{35}Cl^+$ were dominant due to higher concentration. $^{89}Y^{16}O^+$ was also reported on $^{105}Pd^+$.

Begerow *et al.* (1997) determined Pt, Pd and Ir with ICP-MS by UV photolysis of urine and blood. The interferences from Sr, Zr, Ru, and Cd on Pd isotopes were not removed using maximum resolution of spectrometer i.e. 7500 m/Δm. Pt and Ir did not suffer any interferences in blood and urine samples. The presence of $^{35}Cl^+$ interference on ^{105}Pd was also reported.

Gomez *et al.* (2000) studied the interference effects of $^{179}Hf^{16}O^+$ on the determination of $^{195}Pt^+$ and the effect of $^{206}Pb^{2+}$, $^{40}Ar^{63}Cu^+$, $^{87}Sr^{16}O^+$ and $^{87}Rb^{16}O^+$ on $^{103}Rh^+$ and also the effect of $^{89}Y^{16}O^+$, $^{40}Ar^{65}Cu^+$ and $^{36}Ar^{69}Ga^+$ on $^{105}Pd^+$ in airborne particulate matter by optimisation of the nebuliser gas flow rate and the plasma input power. The interferences were decreased by using high plasma power setting. Pb^{2+} interferences were decreased with lowering the plasma power setting.

Some authors have emphasised that alternative (e.g. He) or mixed (e.g. $Ar+N_2$) plasma gases have a potential for the reduction of spectral overlap problems in ICP-MS, a possibility which has not yet been utilised for the determination of PGE (Bencs *et al.* 2003, Montaser *et al.* 1992).

A commercial sector-field ICP-MS (ICP-SFMS) is capable of a mass resolution of up to 10 000, which is sufficient to resolve a number of spectral interferences on noble metal isotopes (Barefoot 2004). For instance, the required mass resolution to separate $^{103}Rh^+$ from $^{40}Ar^{63}Cu^+$ is 8040, $^{105}Pd^+$ from $^{40}Ar^{65}Cu^+$ requires 7300, and $^{188}Os^+$ from $^{172}Yb^{16}O^+$ requires 7700 (Bencs *et al.* 2003). There are also some interferences that need a higher mass resolution beyond the capability of ICP-SFMS; Resolution of 147 000 is needed to separate $^{103}Rh^+$ from $^{87}Rb^{16}O^+$ (Bencs *et al.* 2003) and 24 000 is needed to separate $^{107}Ag^+$ from $^{91}Zr^{16}O^+$ (Simpson *et al.* 2001).

Collision/reaction cell is a new technology patented by Agilent 8800 manufacturers has been used in the earlier section of rare earth element for the interference removal capacity. Some authors including our research group have contributed several conference papers on interference removal on rare earth elements and PGE and Ti etc. using collision/reaction cell technology (Balcaen *et al.* 2014, Bokhari *et al.* 2015a, Bokhari *et al.* 2015c, Bokhari *et al.* 2015d, Bokhari *et al.* 2015e, Sugiyama and Shikamori 2015, Suoranta *et al.* 2016).

9.2 Objectives of this chapter

In the absence of definitive methods for PGE determination, there is continuing interest in the development of new and effective measurement procedures for PGE analysis. Even most sensitive analytical techniques require matrix separation and concentration prior to the analysis. The main objective of this chapter is to develop a novel analytical method for accurate determination of platinum group elements in geological materials, which involve matrix separation using collision/reaction cell technology instead of complex chemical separations procedures.

An Agilent 8800 ICP-MS/MS apparatus with patented collision/reaction cell technology has been used in this study. An initial study is applied on reference material with high PGE mass fractions to meet the requirement of industries for method development which is sensitive, selective and offers a high mass resolution to deal with spectral interferences arising from the complex matrices. The literature using ICP-SF-MS and ICP-DRC-MS exists but with this new technology of collision/reaction cell of Agilent 8800 less work has been shown, although research from biological, environmental, geological, industrial fields are progressing steadily with this technology. Following were the salient features of this study,

1. To investigate the applicability and performance of collision/reaction cell for matrix separation and simultaneous recovery of PGE in terms of accurate mass fractions of geological reference material with good precision and selectivity.
2. The development of new analytical method with the systematic investigation of interference removal using reactive gases i.e. He, H_2, O_2 and ammonia gases in collision/reaction cell.
3. To develop a novel strategy for PGE quantification by finding an optimum product ion with no or least matrix elemental spectral overlap.
4. To evaluate the performance of collision/reaction cell and assessment of the magnitude of interference of relevant concentrations of matrix elements on given PGE concentration of analytes.
5. Assessment of two different acquisition modes i.e. on-mass and mass-shift mode for the gases that are used in reaction cell for suppression of signal intensities of matrix elements on PGE isotopes.
6. Evaluation of reactivity of matrix elements and PGE with reactive gases i.e. oxygen, hydrogen and ammonia etc.
7. To explore and provide the understanding for all the possible adduct ions of PGE and matrix elements with O_2 and NH_3 gas in reaction collision cell.
8. To propose gas modes/product ions for individual PGE analytes for removal of particular matrix interferences e.g. Hg removal on ^{198}Pt.
9. To optimise the gas flow rates for best product ions and stable signals for any suggested modes in the method development.
10. Testing the proposed method on the standard solution of PGE and matrix elements.
11. Method validation with reference materials and assessment of results.

9.3 Interferences on platinum elements group elements

Ruthenium occurs with seven isotopes in nature i.e. ^{96}Ru (5.54%), ^{98}Ru (1.87%), ^{99}Ru (12.76%), ^{100}Ru (12.60%), ^{101}Ru (17.06%), ^{102}Ru (31.55%) and ^{104}Ru (18.62%). For the purpose of direct and isotope dilution measurement, at least two isotopes are required and normally ^{99}Ru (12.76%), ^{101}Ru (17.06%) and ^{102}Ru (31.55%) are measured with ICP-MS. Common spectral interferences on ruthenium isotopes are hydrides of Mo, oxides of Rb and Sr, argides of Ni, chlorides of Zn and Cu as given in Table 9.1.

Rhodium is an only monoisotopic member of platinum group elements and suffers spectral interferences from oxides of Rb and Sr, argides of Cu, chlorides of Zn and doubly charged ions of lead as given in Table 9.1.

Palladium has six isotopes i.e. ^{102}Pd (1.02%), ^{104}Pd (11.14%), ^{105}Pd (22.23%), ^{105}Pd (27.33%), ^{106}Pd (26.46%) and ^{108}Pd (11.72%). The spectral interferences on Pd isotopes are the oxides of Y and Zr, hydroxides of Sr, Y and Zr, argides of Zn and chlorides of Zn and Cu and isobaric Cd interferences as given in Table 9.1.

Platinum is the most important element of platinum group elements. Platinum has six isotopes ^{190}Pt (0.014%), ^{192}Pt (0.782%), ^{194}Pt (32.97%), ^{195}Pt (33.83%), ^{196}Pt (25.24%) and ^{198}Pt (7.136%). The percent abundances are given in parenthesis along with relative atomic mass. The ^{194}Pt, ^{195}Pt, ^{196}Pt and ^{198}Pt are of the interest of the geological community and therefore interferences on only these isotopes will be discussed in this section. A list common interference on platinum isotopes is given Table 9.1. Interferences from Hf isotopes are mostly present on all isotopes of platinum except on $^{198}Pt^{+}$. Interferences from W and Hg are very severe on$^{196}Pt^{+}$ and $^{198}Pt^{+}$. Oxides of Hf and W, hydroxides of Hf and Ta, argides of Gd and Sm and isobaric interferences of Hg are shown in Table 9.1.

Iridium consists of two isotopes i.e. ^{191}Ir (37.3%) and ^{191}Ir (62.7%). The spectral interferences are the oxides of Lu and Hf, argides of Eu and Sm on iridium isotopes and are given in Table 9.1.

Gold exist as a monoisotopic element and the spectral interferences on Au are oxides of Ta, hydroxides of Hf and argides of Gd as given in Table 9.1.

Ag is not the member of platinum group elements but it is included in this study due to its economic importance and occurrence along with PGE. It has two isotopes i.e. ^{107}Ag (51.84%) and ^{109}Ag (48.16%). The spectral interferences on Ag are from oxides of Zr and Nb, hydroxides of Zr and argides of Zn as given in Table 9.1.

Osmium has seven isotopes i.e. ^{184}Os (0.02%), ^{186}Os (1.59%), ^{187}Os (1.96%), ^{188}Os (13.24%), ^{189}Os (16.15%), ^{190}Os (26.26%) and^{192}Os (40.72%). The interferences on osmium isotopes are from platinum, oxides of Yb, Lu, and Hf, hydroxides of Yb and Lu, hydrides of W, and argides of Sm and Nd as given in Table 9.1.

Table 9.1: Common spectral interferences on PGE isotopes + Ag and Au

Analyte	m/z	Abundance	Isobaric	MH^+	MO^+	MOH^+	MAr^+	MCl^+	Doubly charged
Ru	99	12.8		$^{98}Mo^{1}H^+$				$^{64}Zn\text{-}Ni^{35}Cl^+$	
	101	17.6		$^{100}Mo^{1}H^+$	$^{85}Rb^{16}O^+$		$^{61}Ni^{40}Ar^+$	$^{65}Cu^{35}Cl^+$	
	102	31.6	$^{102}Pd^+$		$^{86}Sr^{16}O^+$		$^{62}Ni^{40}Ar^+$	$^{67}Zn^{35}Cl^+$	
	104	18.6	$^{104}Pd^+$						
Rh	103	100.0			$^{87}SrO^+$,$^{87}RbO^+$		$^{63}Zn^{40}Ar^+$	$^{66}Zn^{35}Cl^+$	$^{206}Pb^{++}$
Pd	105	22.3			$^{89}YO^+$	$^{88}SrOH^+$		$^{65}Zn\text{-}Cu^{35}Cl^+$	
	106	27.3	$^{106}Cd^+$		$^{90}ZrO^+$	$^{89}YOH^+$	$^{66}Zn^{40}Ar^+$		
	108	26.5	$^{108}Cd^+$		$^{92}ZrO^+$, $^{92}MoO^+$	$^{91}ZrOH^+$	$^{68}Zn^{40}Ar^+$		
Ag	107	51.8			$^{91}ZrO^+$		$^{67}Zn^{40}Ar^+$		
	109	48.2			$^{93}NbO^+$	$^{92}ZrOH^+$			
Os	187	2.00	$^{187}Re^+$	$^{186}W^{1}H^+$	$^{171}YbO^+$,(Nd-ox)	$^{154}SmO^{1}HO^+$	$^{147}Sm^{40}Ar^+$		
	188	13.2			$^{172}YbO^+$	$^{171}YbO^{1}H^+$	$^{148}Sm\text{-}Nd^{40}Ar^+$		
	189	16.2			$^{172\text{-}173}YbO^+$				
	190	26.3	$^{190}Pt^+$		$^{174}YbO^+$	$^{173}YbO^{1}H^+$	$^{150}Sm\text{-}Nd^{40}Ar^+$		
	192	4.80	$^{192}Pt^+$		$^{176}Yb\text{-}Hf\text{-}LuO^+$	$^{175}LuO^{1}H^+$	$^{152}Sm^{40}Ar^+$		
Ir	191	37.3			$^{175}LuO^+$		$^{151}Eu^{40}Ar^+$		
	193	62.7			$^{177}HfO^+$		$^{153}Sm^{40}Ar^+$		
Pt	194	33.0			$^{176}HfO^+$		$^{154}Gd\text{-}Sm^{40}Ar^+$		
	195	33.8			$^{179}HfO^+$		$^{155}Gd^{40}Ar^+$		
	196	25.2	$^{196}Hg^+$		$^{180}HfO^+$		$^{156}Gd^{40}Ar^+$		
	198	7.2	$^{198}Hg^+$		$^{182}WO^+$	$^{181}TaOH^+$	$^{158}Gd^{40}Ar^+$		
Au	197	100.0			$^{181}TaO^+$	$^{180}HfOH^+$	$^{157}Gd^{40}Ar^+$		

9.4 Experimental

9.4.1 Reagents and materials

HCl 37 g/100g p.a., Roth, Karlsruhe, Germany was used as 0.1 mol/l in the preparation of PGE standard solution. HNO_3 65 g/100g p.a., Roth, Karlsruhe, Germany was used for the preparation of most of the matrix elements including Ag standard solution because Ag precipitates in HCl solution. An ultra-clear unit for ultra-pure water (Siemens water technologies) with conductivity: 0.055 µS/cm, TOC content: < 1 ng/g, (for diluting acids and samples) was used. Analytical reagent-grade sodium peroxide ACS, ISO Merck KGaA Darmstadt, Germany has been used for sample digestion. Glassy carbon crucibles (25 x 25 mm, HTW) were used for sample digestion. Single elements standard solution (1000 μg/l) of platinum group elements for initial testing of interferences were obtained from SPEX chemicals USA. The solutions were diluted to 1 ng/ml (final dilution) with 0.1 mol/l HCl. Solutions after preparation were stored in PP vials (50 ml, Sarstedt). Several geological reference materials for PGE (SARM-7, BIR-1, WMG-1 and PTC-1a and IMEP-11 (which is a catalytic converter RM) were digested with sodium peroxide sintering using 1:5 sample to sodium peroxide ratio for method validation. Single element pure PGE solutions were used for finding the effect of interferences establishing calibrations. 1 μg/g solutions of indium (In) and germanium (Ge) were used as internal standard to control the instrument drift during measurement. Indium was not used for ruthenium measurement because ^{115}In adds an interference to one of gas shift mode of Ruthenium i.e. $^{99}Ru^{16}O$.

Table 9.2: Instrument optimum tuning configurations

The instrument was tuned for best signal intensities with least oxide formation profile. The instrument configuration is given in Table 9.2.

Parameters	**No gas**	**O_2**	**NH_3**			**He**	**H_2**
Described in thesis as			**Low**	**Medium**	**High**		
Scan type	Single Quad	MS/MS	MS/MS	MS/MS	MS/MS	MS/MS	MS/MS
RF Power (W)	1550						
sample depth (mm)	8	5.6	6			5	5
Gas flow rate (ml/min)	-	0.3	2	3	5	2	2
He (ml/min)	-	-	1	1	1	2	2
Oxide formation CeO^+/Ce^+	1-1.03						
Doubly charged ions Ce^{++}	1-1.1						
Carrier gas flow rate (l/min)	variable-tuned for best signals						
Makeup gas flow rate (l/min)	variable-tuned for best signals						
Energy Discrimination (mV)	5	-7	-7			-7	-7
OctP Bias (V)	-8	-5				-5	-5
Q1 Bias (V)	0	-2	-2	-2	-3	-2	-2
Integration time (sec)	0.3	0.75				0.3	0.3
Replicates	4						

9.5 Experimental design for interference minimisation on PGE analytes

The detailed description of abundances of PGE isotopes and matrix elements that are expected to cause spectral interferences on PGE isotopes are shown in Table 9.1. These interferences are cited in literature have a long history of the efforts researchers have put together to eliminate with various techniques which have been discussed earlier. This chapter intends to address these interferences using collision/reaction cell technology. For a comprehensive study on interference removal on PGE analytes, detailed steps of procedure were outlined prior to the investigation of their elimination which involves following;

1. Determination of background equivalent concentration of matrix blank that causes an overlap over the background equivalent concentrations of the PGE analytes blanks, after listing the interferences that are expected and or cited in the literature.
2. Preparation of individual solutions of matrix elements and PGE analytes with concentrations resembling the crustal abundances.
3. Differentiation of the noise and signals on PGE analyte blank.
4. Running the matrix blank over the range of PGE analytes m/z in order to identify if the matrix creates any signal intensity on the given m/z of PGE analyte blank.
5. Numerical quantification of any BECs of matrix element of given PGE analyte blank by running a solution of PGE analyte of suitable concentration resembling crustal abundances.
6. Application of different cell gases for observation of any effect on the relative signal intensities of both matrix elements and PGE analytes.
7. Testing reactivity of the matrix elements and PGE analytes for planning method development.
8. Signal reduction of matrix elements with different flow rates of selected cell gases.
9. Determination of product ions in of matrix elements and PGE analytes.
10. Selection of product ions of PGE analytes with no spectral overlap of matrix elements.
11. Method development by selecting acquisition modes i.e. on-mass or mass-shift for the elimination of interferences, integration times, setting times and channels etc.
12. Method validation on PGE reference materials.

9.5.1 Determination of background equivalent concentrations (BECs) of matrix blank overlapping with BECs of PGE analyte blank

It is essential to determine the extent to which interferences cause an overlap on PGE spectrum or on BEC of the PGE analyte in ICP-MS/MS. In other words, exact quantification of the interferences is required for all PGE. For this purposes, 1 mg/l (final dilution 1 µg/ml) matrix blank solution of all the interferences were prepared and were tested with 1 ng/ml BECs of PGE analytes. To simplify the technical term, 1 µg/ml solution of each interfering species was run over the entire range of PGE's mass-to-charge (m/z) spectra for the determination of any background that an interference can create on PGE analytes. The intensities of pure PGE solutions of known concentrations were monitored. Several rinses with 0.1 mol/l HCl were made to clear any memory or noise to differentiate the BECs of the matrix elements. After that matrix blank was run on m/z of PGE analytes and BECs were determined. The BECs of the matrix blank of each interfering solution is shown in Table 9.3.

The BECs were measured/monitored in no gas mode using single quad configuration. Relative signal intensities of interferences were calculated in no gas mode. Relative signal intensity is the ratio of signal intensity of the matrix element to that of a PGE analyte. A

colour scheme has been added to help to understand the extent to which interferences are affecting the BECs of PGE analyte.

BECs >10 ng/g (critical interferences)

The most critical interferences are coded with the brown colour in Table 9.3 which range from BECs >10 ng/g i.e. $^{106\text{-}108}Cd^{+}$ on $^{106}Pd^{+}$ and $^{108}Pd^{+}$, $^{198}Hg^{+}$ and $^{+182}TaOH^{+}$ on $^{198}Pt^{+}$. The importance of chromatographic separation can be highlighted if such interferences are present in geological samples. A trace amount of Pd for example, less than a 1 ng/g if present in the geological sample with 10 ng/g Cd, would create a huge interference on Pd. The instrument will measure all Cd if no chromatographic separations have been made. Same is true for platinum when it is present in trace amount with a high mass fraction of Ta.

BECs =1-10 ng/g

Secondly, the critical interferences on PGE isotopes are highlighted with an orange colour that ranges from 1-10 ng/g BECs created by the matrix blank of the matrix interferences. These include polyatomic interferences i.e. oxides of Zr^{+} and Nb^{+} on Pd^{+} and Ag^{+} isotopes, oxides Y^{+}, Sr^{+} and Rb^{+} on Pd^{+} isotopes, $^{196}Hg^{+}$ on $^{196}Pt^{+}$, oxide $^{180}TaO^{+}$ on $^{196}Pt^{+}$, hydroxide of Ta^{+} on Au^{+}, Hf^{+} oxides and hydroxides on Os^{+}, Ir^{+}, Pt^{+} and Au^{+}, rare earth elements mainly on $^{99}Ru^{+}$, $^{191}Ir^{+}$ and Au^{+}.

BEC < 1 ng/g

Thirdly, the interferences ranging from BEC < 1 ng/g are highlighted with light yellow colour. Mostly argide interferences of Ni, Cu and Zn create BECs on Ru, Rh and Pd in a range 0.001 to 0.022 ng/g. Highest of the Mo interferences from this group observed was on $^{108}Pd^{+}$ i.e. 0.235 ng/g, TaO^{+} on $^{194}Pt^{+}$, $^{195}Pt^{+}$ i.e. 0.652 and 0.373 ng/g, some REE on $^{192}Os^{+}$ i.e. 0.172. The presence of such tremendous amounts of interferences makes PGE analysis impossible if separation techniques are not applied.

Table 9.3: BECs of matrix blank of interferences overlapping the BECs of the PGE analytes

BECS of 1 µg/ml matrix blank of interferences overlapping 1 ng/ml BECs of the PGE isotopes													
Analytes	**Ruthenium**				**Rhodium**	**Palladium**						**Silver**	
Interference	**^{99}Ru**	**^{101}Ru**	**^{102}Ru**	**^{104}Ru**	**^{103}Rh**	**^{102}Pd**	**^{104}Pd**	**^{105}Pd**	**^{106}Pd**	**^{108}Pd**	**^{110}Pd**	**^{107}Ag**	**^{109}Ag**
Cu		0.001			0.003	0.013		0.004					
Mo	0.003	0.005							0.005	0.235	0.293		
Nb													0.569
Ni	0.003	0.001	0.001			0.020							
Pb					0.001								
Pd			0.195	3.4									
Rb		0.0003			0.000								
Sr			0.0003		0.014	0.166	0.072	0.056					
Y								13.3	2.33				
Cd									36				
Zn	0.005		0.002		0.0005	0.033	0.042	0.002	0.009	0.006		0.003	
Zr									1.09	0.45	1.00	0.163	
Analytes	**Osmium**					**Iridium**		**Platinum**				**Gold**	
Interference	**^{187}Os**	**^{188}Os**	**^{189}Os**	**^{190}Os**	**^{192}Os**	**^{191}Ir**	**^{131}Ir**	**^{194}Pt**	**^{195}Pt**	**^{196}Pt**	**^{198}Pt**	**^{197}Au**	
Eu						0.013	0.004						
Gd								0.007	0.069	0.048		1.2	
Hf					0.559		2.0	8.6	12.4	35.0		2.0	
Hg										7.4	1353		
Lu					0.635	7.2							
Nd	0.095	0.002											
Pt				0.020	0.104								
Re	38876												
Sm	6.1	0.001		0.0003				0.025					
Ta											140	8.6	
W										12.1	82.0		
Yb	1.7	0.29	0.21	0.21	0.049								
Description		BEC >10 ng/g			BEC 1 - 10 ng/g			BEC < 1 ng/g					

9.6 Strategy for interference removal on platinum group elements

For utilising collision/reaction cell for effective removal of the interferences, a strategy was developed i.e. to use the reaction efficiency of analytes and interferences with cell gases for avoiding interferences. An analyte or interference that is more and or less reactive than each other can make the basis of their separation prior to making a spectrum on the detector of ICP-MS/MS. This planning makes the basis for the method development for interference elimination and can be divided into two categories;

Analyte more reactive than the interference to the cell gas

In the case when analyte ion is more reactive to the cell gas than the interference ion, a mass-shift method can be applied to the analyte. In the mass-shift method, the mass-to-charge ratio (m/z) of the analyte ion is shifted away from interference ion and the mass/charge of the product ion is detected free from the interference.

Interference more reactive to the cell gas than analyte

The other situation is when interference is more reactive to the cell gas than the analyte ion, then an on-mass method can be applied. In this case, the mass-to-charge ratio of the analyte ion is kept the same while interference species reacts with the cell gas and made to leave the collision/reaction cell because the second mass filter is set to the mass-to-charge ratio of the analyte ion only.

Analyte and interference both reactive to cell gas

A third situation which was often observed related with ion-molecule reaction chemistry in collision/reaction cell, when analyte and interference are both reactive to the cell gas. The only solution to this situation is to find the product ion of analyte ion or interference ion with no overlap in spectra. In some cases, the situation may suffer from reduction in signal intensities and then gas flow rate has to be optimised for better signals for measurement.

For the use of any method i.e. on-mass or mass-shift, it is essential to check the reaction efficiencies of the analyte ion and interference ions.

9.7 Testing reactivity of PGE and interferences with NH_3

It was important to see the behaviour/reactivity of platinum group elements with cell gases i.e. ammonia inside the collision/reaction cell prior to their use for any method validation step. The concentration of testing PGE solution was kept as low as possible i.e. 1 ng/ml so as to create a similar situation as that of real matrices. Most of the interfering species on platinum group elements are the rare earth elements and W, Hf, Nb, Ta, Zr, Rb, Sr, Y, Mo, Cd, Hg, Ni, Cu and Pb. The concentrations of the testing interferences were kept 1 µg/ml. The trends of reactivity of rare earth elements have also been established and presented in rare earth element interference removal section, however; the plots can be co-related in order to understand the validity of tests.

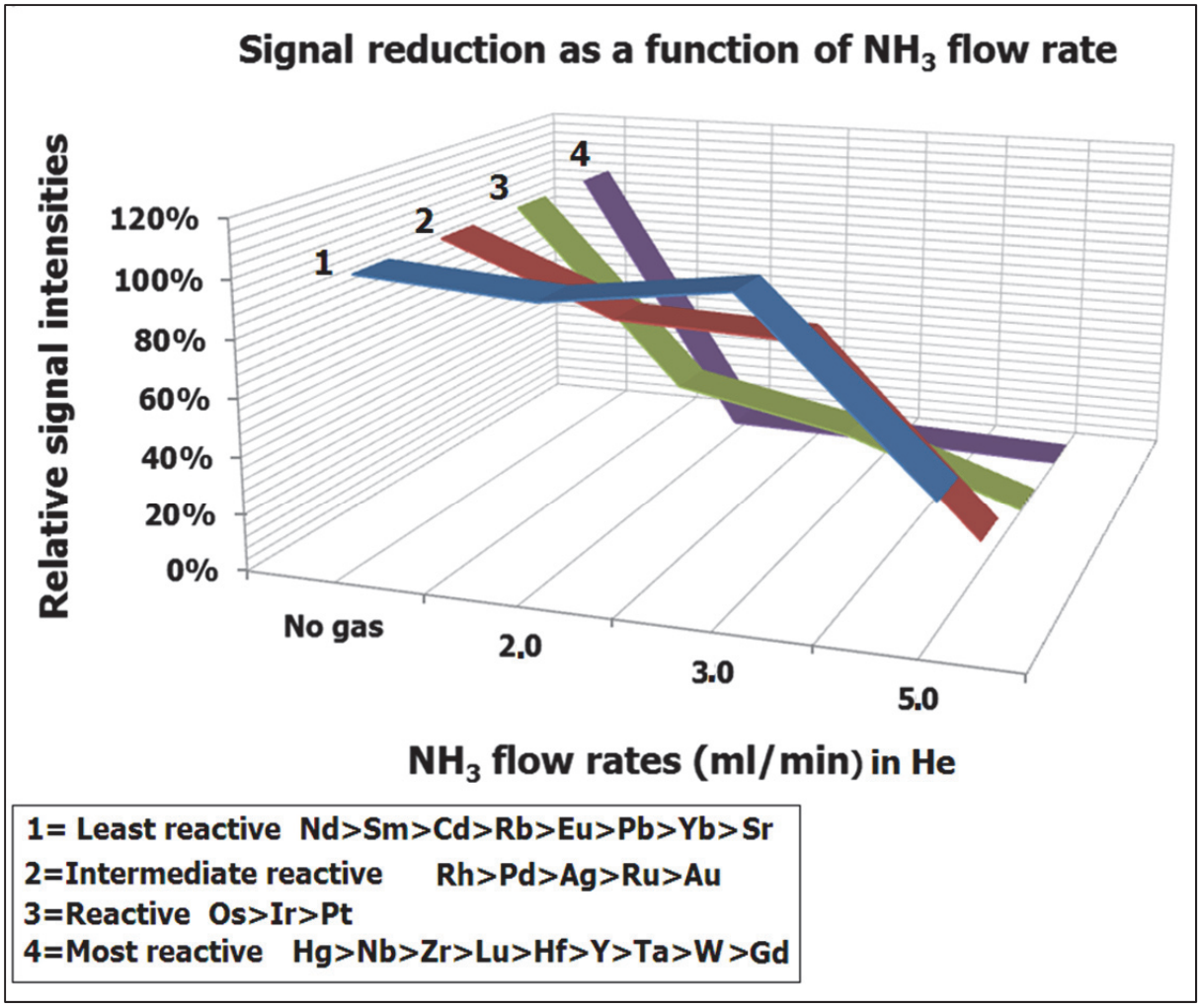

Figure 9.1: Reaction efficiencies of analytes and interferences

The reaction efficiencies of analytes and interference ions were determined with the on-mass method of measurement with different flow rates of ammonia gas in reaction collision cell of Agilent 8800 ICP-MS/MS. The intensities of both were measured in no gas mode and ammonia mode with different flow rates of ammonia. If the relative intensity of an analyte or interference has decreased relative to no gas mode, then that would reflect the formation of some product ion or collision. On the other hand, if relative intensity of an analyte or interference does not show the changes in intensity relative to no gas mode then it can be predicted that no product ion has formed. The signal reduction relative to no gas mode under similar conditions, i.e. concentration, flow rates of cell gas can give the order of the reaction efficiency. If the intensities of analytes and interferences are considered 100% relative to no gas mode, the reduction in signal intensity with flow rates of cell gas gives the extent to which an analyte or interferences has reacted.

This depends on ease of formation of product ions which in turn is related to thermodynamic properties of reaction between the analytes/interferences and cell gases. The reaction kinetics was not monitored using pathways or first order and second order reaction which are usually applied in chemical kinetics. The reaction efficiencies of PGE and interference ions are plotted in Figure 9.1. This makes the basis of classification of analytes and interferences into four groups. The reaction efficiencies described here are relative to analytes and interferences only.

a. Least reactive group
b. Intermediate reactive group
c. Reactive group
d. Most reactive group

9.7.1 Least reactive group

This group comprises of (on the basis signal reduction as a function of flow rate of ammonia gas) Nd>Sm>Cd>Rb>Eu>Pb>Yb>Sr etc. This include all interference ions that means if any of these interferences have an interference on any PGE isotopes it must be removed while using a mass-shift method for PGE. That requires the determination of product ion of PGE with a respective gas flow with appropriate intensities where no interference can be observed in its spectra.

9.7.2 Intermediate reactive group

This group consists of Rh>Pd>Ag>Ru>Au ions. If the interference from the least group of ions exists on an intermediate group of ions, a mass-shift method is hypothesised. This grouping of the PGE analytes based on reaction efficiencies is also affirmed from the publication of Bokhari *et al.* (2015c) and (Sugiyama *et al.* 2015b).

9.7.3 Reactive group

The reaction efficiencies of Os>Ir>Pt are highest among all PGE ions with ammonia gas on given flow rates of 2, 3 and 5 ml/min in collision/reaction cell. The interferences from the least reactive group should be removed with the mass-shift method in collision/reaction cell. Same reaction efficiencies have been stated in Bokhari *et al.* (2015c) and (Sugiyama *et al.* 2015b).

9.7.4 Most reactive group

This group of interferences are the most reactive interferences with ammonia gas in collision/reaction cell and consist of Hg>Nb>Zr>Lu>Hf>Y>Ta>W>Gd. If these most reactive interferences exist on PGE ions, then an on-mass method should be applicable for their removal.

9.8 Interference removal efficiency of cell gases

This section covers the aspect of reduction in BECs of interferences on each PGE isotope. The main focus here is to show the capability of the cell gases towards signal reduction on the mass-to-charge ratio of the given PGE isotope. The BECs created by each 1 µg/ml interferences on 1 ng/ml of PGE isotopes are shown in Table 7.2.

9.8.1 Signal reduction of interferences on Ru isotopes

^{99}Ru

The polyatomic interferences on $^{99}Ru^{+}$ caused by 1 µg/ml matrix of Zn^{+}, Ni^{+} and Mo^{+} are shown in Figure 9.2. The reduction in signal intensity is best achieved in ammonia cell gas. Ni^{+} and Mo^{+} form further hydrides when hydrogen gas is used and hence intensity is slightly increased with hydrogen gas. The decrease in intensity of these interferences suggests an on-mass ammonia measurement which needs to be further optimised. A

method for interference removal also demands one mode that can be applied to all interference removals.

^{101}Ru

The Figure 9.2 shows a significant decrease of false BECs created by $^{100}MoH^{+}$, $^{61}Ni^{40}Ar^{+}$, $^{65}Cu^{35}Cl^{+}$ and $^{85}Rb^{16}O^{+}$on $^{101}Ru^{+}$ isotope. The use of hydrogen and oxygen as a cell gas increases the BECs of Mo^{+}, Ni^{+}, Cu^{+} and Rb^{+} due to ease of formation of hydrides and oxides. Ammonia gases significantly decreases this background. Molybdenum interference shows a reduction in signal intensity but not completely at a lower flow rate of ammonia that suggests a mass-shift of ruthenium has to be found. The product ion that can be used to measure Ru will be discussed in proceeding sections.

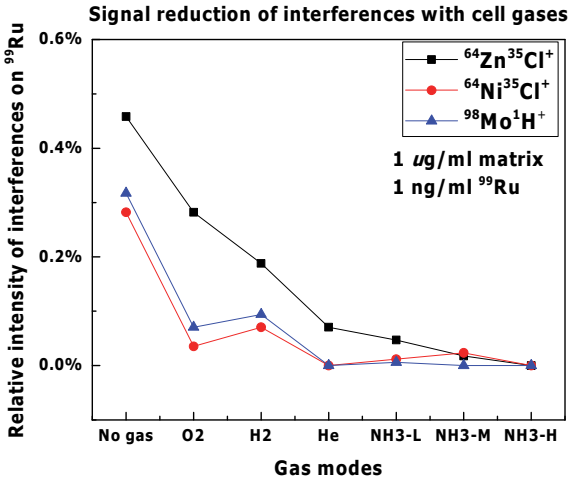

Figure 9.2: Signal reduction of interferences relative to no gas mode on $^{99}Ru^{+}$

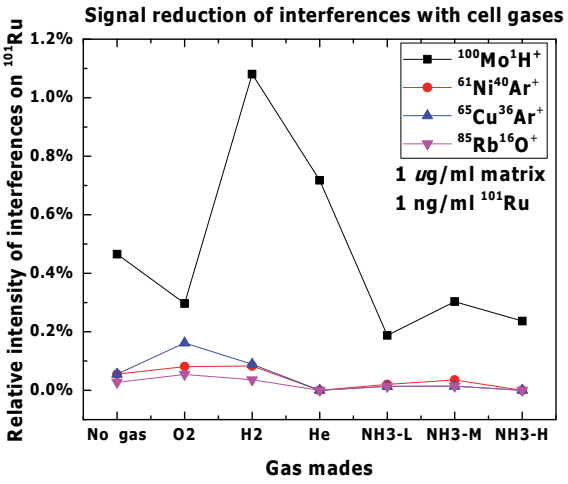

Figure 9.3: Signal reduction of interferences relative to no gas mode on $^{101}Ru^{+}$

^{104}Ru

Palladium is the main interference on $^{104}Ru^{+}$. The BECs of 10 ng/ml ^{104}Pd matrix on 1 ng/ml ^{104}Ru isotope is 3.44 ng/g. The Pd/Ru ratio and Pd intensity in each gas modes are shown in Figure 9.4. The Pd/Ru in oxygen gas increases due to a loss in intensity of

ruthenium, indicating that ruthenium is being oxidised to some oxide of ruthenium. So an oxide shift for ruthenium can be tried for removal of Pd, which will be discussed in later sections. The plot also suggests that at a higher flow rate of ammonia, the signal intensity of Pd is decreased. Palladium can be reacted with ammonia and ruthenium can be made interference free. Conversion of ruthenium to an oxide, or conversion of Pd to ammonia adduct can make the basis for interference removal. Overall, ammonia and oxygen are better for Pd removal.

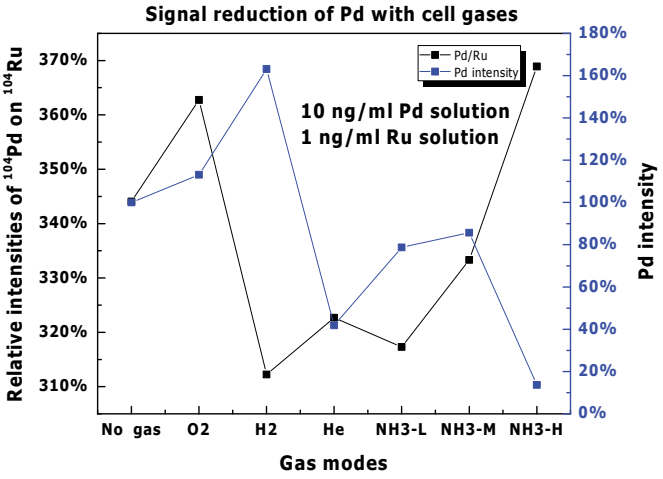

Figure 9.4: Signal reduction of $^{104}Pd^{+}$ relative to no gas mode on $^{104}Ru^{+}$

9.8.2 Signal reduction of interferences on mono-isotopic rhodium

The BECs created by 1 µg/ml matrix of Sr, Rb, Cu, Zn and Pb on 1 ng/ml $^{103}Rh^{+}$ as $^{87}SrO^{+}$, $^{87}RbO^{+}$, $^{63}Cu^{40}Ar^{+}$, $^{67}Zn^{36}Ar^{+}$ and $^{206}Pb^{2+}$ ranges from 0.001 to 0.002 ng/g. All the interferences are reduced significantly with higher flow rates of ammonia except $^{87}SrO^{+}$ which are making an adduct ions of $SrNH_2^{+}$ (Sr+16) with higher flow rates of ammonia gas as shown in Figure 9.5. It reduces to a little value only with flow rates of 3 ml/min of ammonia. This interference needs to be removed by mass-shift of Rh^{+} to a higher mass-to-charge ratio where Sr (adduct ion)$^{+}$ overlap is not existing. Use of helium gas can also be applied when pure solutions are concerned but results are critical when geological matrices are employed for interference removal. Minor interferences by $^{87}RbO^{+}$, $^{63}Cu^{40}Ar^{+}$, $^{67}Zn^{36}Ar^{+}$ and $^{206}Pb^{++}$ are shown to decrease with ammonia. An optimisation of flow rate of ammonia is needed in this regard. A mechanism of charge transfer reactions will be discussed for Pb^{++} removal in proceeding sections.

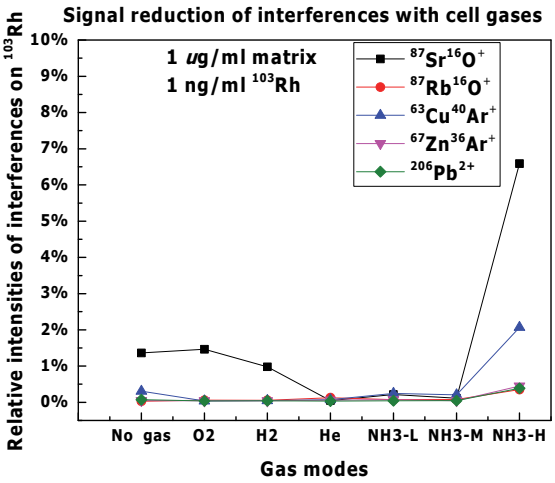

Figure 9.5: Signal reduction of interferences relative to no gas mode on $^{103}Rh^{+}$

9.8.1 Signal reduction of interferences on Ag isotopes

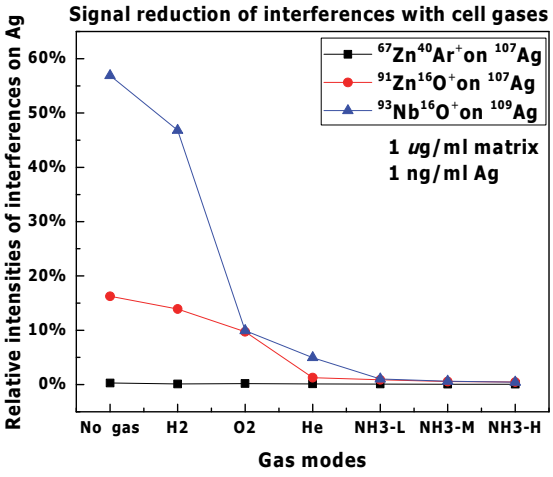

Figure 9.6: Signal reduction of interferences relative to no gas mode on $^{107}Ag^{+}$

The BECs of Zr and Nb matrix on Ag isotopes ranges from 0.163 to 0.6 ng/g while for Zn is 0.003 ng/g. Hydrogen and oxygen gases are not good for reducing the background from zinc argide, zirconium oxide and niobium oxide. However, Simpson *et al.* (2001) have converted ZrO^{+} interferences to multiple oxides i.e. ZrO_2^{+}, ZrO_2^{+}, ZrO_3^{+}, ZrO_4^{+}, ZrO_5^{+} and ZrO_6^{+} using 100 ng/ml matrix of Zr and Nb with 10 ng/ml Ag blank equivalent to crustal abundance. The matrix elements in this study are 1 µg/ml and Ag is 1 ng/ml. The effect of O_2 can then be better in interference removal if similar dilution factors are used as that of (Simpson *et al.* 2001). The tests with oxygen gas, however, will be applied to real geological samples that have the equivalent crustal abundances of matrix and analyte blank.

The intensity of ZrO^{+} increases in hydrogen gas due to the formation of hydrides ions. Ammonia and He are better in the elimination of these interferences as shown in Figure 9.6. BECs of 1 µg/ml Nb matrix are 0.6 ng/g on $^{109}Ag^{+}$. A gradual decrease in BECs is found with increasing flow rate of ammonia gas. Other gases i.e. oxygen and hydrogen gases do not seem to be promising for reduction of signal intensities of $^{93}Nb^{+}$ in the form of $^{93}NbO^{+}$ on $^{109}Ag^{+}$.

9.8.2 Signal reduction of interferences on Pd isotopes

^{105}Pd

A 1 µg/ml matrix blank of Y produces 13.3 ng/g BEC on 1 ng/ml of Pd. The use of cell gases oxygen and hydrogen increases this background due to the formation of oxides and hydride ions as shown in Figure 9.7. Helium and ammonia gases can reduce this background significantly. If ammonia and He are compared, then an optimised flow rate of ammonia would be suggested for $^{89}Y^{16}O^+$ removal if compared with He.

Sr^+, on the other hand, produces $^{88}Sr^{16}OH^+$ interference on ^{105}Pd. In comparison to other cell gases ammonia at a higher flow rate increases, conversion of Sr to another product ion and Pd turns free from interferences. The reactivity of Sr^+ with ammonia is more than Pd. An on-mass ammonia measurement of Pd can shift the Sr to Sr(ammonia)x^+ product ion. The flow rate of ammonia at which Sr can be fully eliminated will be discussed in proceeding sections. The efficiency of cell gases related to interference removal of $^{88}Sr^{16}OH^+$ is shown in Figure 9.8.

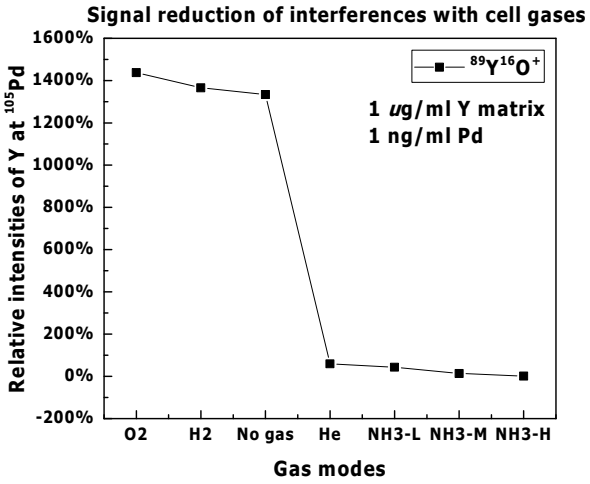

Figure 9.7: Signal reduction of $^{89}YO^+$ relative to no gas mode on $^{105}Pd^+$

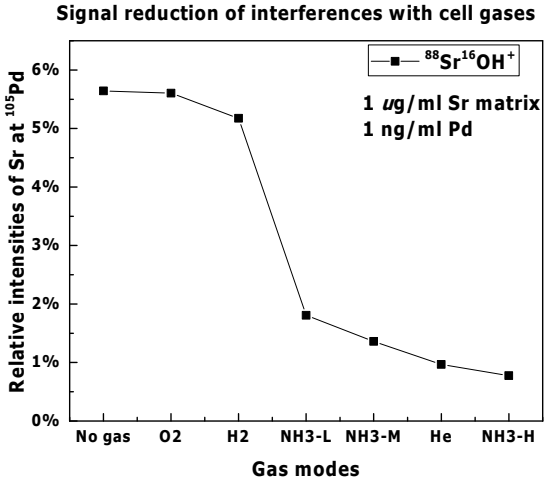

Figure 9.8: Signal reduction of $^{88}Sr^{16}OH^+$ relative to no gas mode on $^{105}Pd^+$

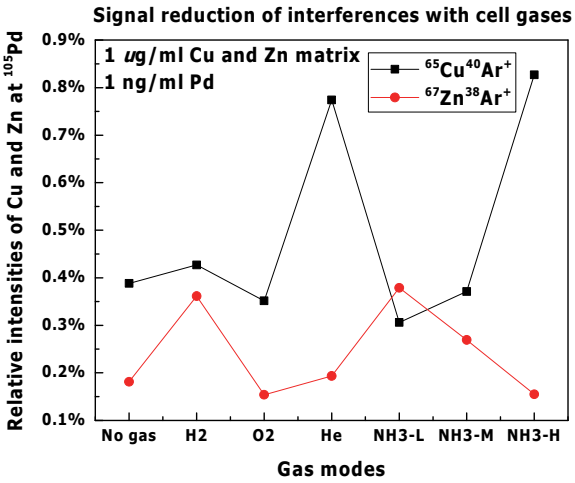

Figure 9.9: Signal reduction of argides of $^{65}CuAr^{+}$ and $^{67}Zn^{38}Ar^{+}$ relative to no gas mode on $^{105}Pd^{+}$

Argides of Zn are reduced with a higher flow rate of ammonia. Argides of Cu requires a mass-shift of Pd because the ratio of Cu to Zn is more, suggesting Pd has converted to another product ion while the intensity of Cu still persists on ^{105}Pd. Figure 9.9 shows the efficiencies of the cell gases for argide removal.

^{106}Pd

Zirconium and Y form oxides while Zn forms an argide at m/z 106. The oxides of Zr^{+} and hydroxides Y^{+} are critical interferences on ^{106}Pd $^{66}Zn^{40}Ar^{+}$ being minor. Hydrogen gas is not useful at all because of the formation of hydrides but ammonia gas is effective towards their reduction with suitable flow rates. The reduction in signal intensity of interferences is shown in Figure 9.10. $^{90}Zr^{16}O^{+}$ interference is not reduced with oxygen gas unlike studies by Simpson *et al.* (2001). This can be due to different matrix concentration and analyte blank (100 ng/ml matrix: 10 ng/ml analyte) compared to our study where concentrations as (1000 ng/ml matrix: 1 ng/ml analyte). The effect of Zr concentration is much larger in our study as compared to the one in (Simpson *et al.* 2001).

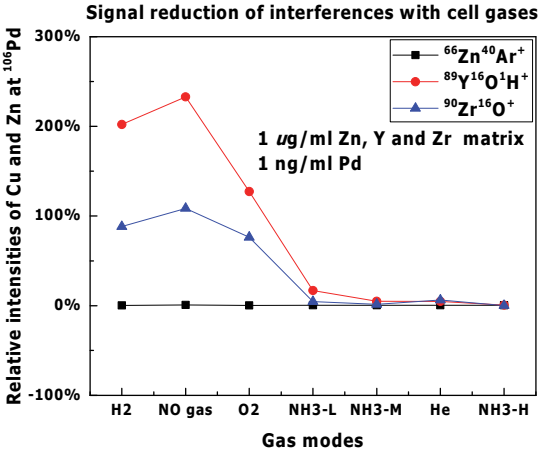

Figure 9.10: Signal reduction of $^{66}Zn^{40}Ar^{+}$, $^{89}Y^{16}OH^{+}$ and $^{90}Zr^{16}O^{+}$ relative to no gas mode on $^{106}Pd^{+}$

Cd^+ is the worse interference on Pd^+ isotopes mainly on $^{106}Pd^+$, $^{108}Pd^+$ and $^{110}Pd^+$. BECs of Cd^+ on $^{106}Pd^+$ is 36 ng/g. The Cd/Pd ratio increases with increasing flow rate of ammonia while the intensity of Cd^+ is lowered to around 20% suggesting that most of the Pd^+ have converted to a product ion at higher m/z.

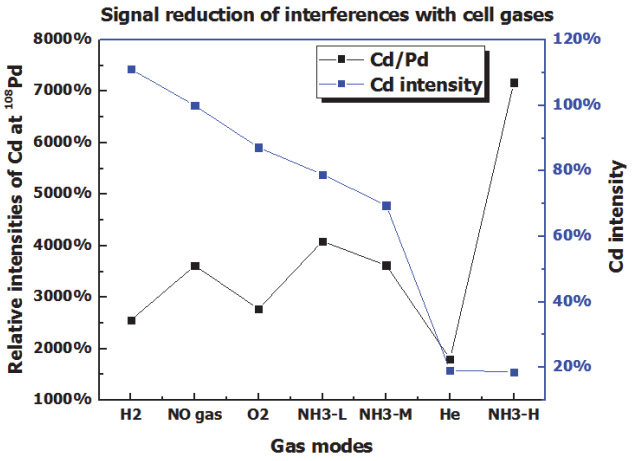

Figure 9.11: Signal reduction of isobaric $^{106}Cd^+$ interference relative to no gas mode on $^{106}Pd^+$

This can be beneficial in a way that a mass-shift of Pd^+ can eliminate the Cd interference. The efficiencies of gases for interference removal on $^{106}Pd^+$ are shown in Figure 9.11.

^{108}Pd

Oxides of Zr and Mo are the interferences formed at m/z of $^{108}Pd^+$. $^{68}Zn^{40}Ar^+$ has a minor interference on $^{108}Pd^+$. The $^{92}Zr^{16}O^+$, $^{92}Mo^{16}O^+$ and $^{68}Zn^{40}Ar^+$ interferences are reduced with ammonia cell gas in comparison to other gases. The efficiencies of the cell gases in reducing signal intensities of interferences are shown in Figure 9.12.

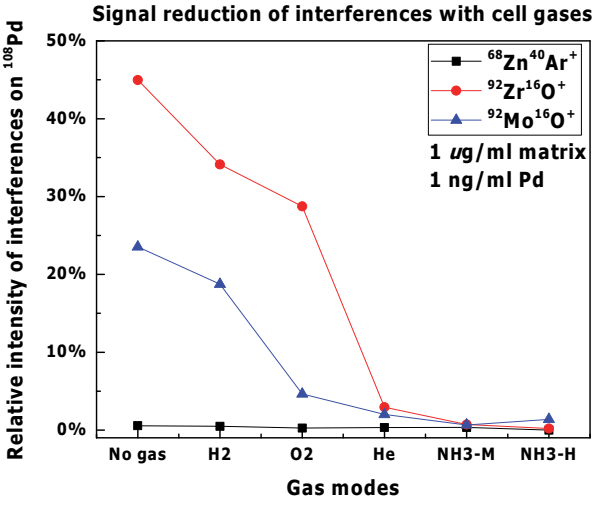

Figure 9.12: Signal reduction of $^{92}Zr^{16}O^+$, $^{92}Mo^{16}O^+$ and $^{68}Zn^{40}Ar^+$ interferences relative to no gas mode on $^{108}Pd^+$

9.8.1 Signal reduction of interferences on Pt isotopes

^{194}Pt, ^{195}Pt

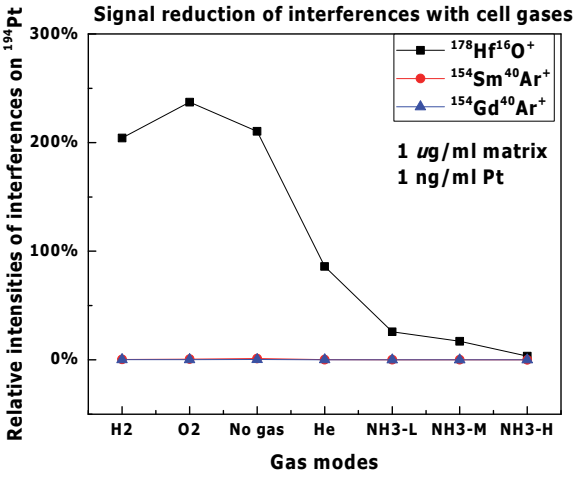

Figure 9.13: Signal reduction of $SmAr^+$, $GdAr^+$ and HfO^+ interferences relative to no gas mode on $^{194}Pt^+$

The isotope $^{194}Pt^+$ suffers critical interferences from $^{178}Hf^{16}O^+$ and minor interferences from argides of $^{154}Sm^+$ and $^{154}Gd^+$. Similarly, $^{195}Pt^+$ suffers from interferences of $^{179}Hf^{16}O^+$ and $^{155}Gd^{40}Ar^+$. Ammonia gas is effective in reducing the signal intensities of these interferences in comparison to other gases. Hafnium seems to react with ammonia and hence its ratio to Pt decreases with gradual increase in flow rate of ammonia. An on-mass measurement should suffice the $^{178\text{-}179}Hf^{16}O^+$ interferences removal. The trends in the removal of interference with cell gases are shown in Figure 9.13 and Figure 9.14.

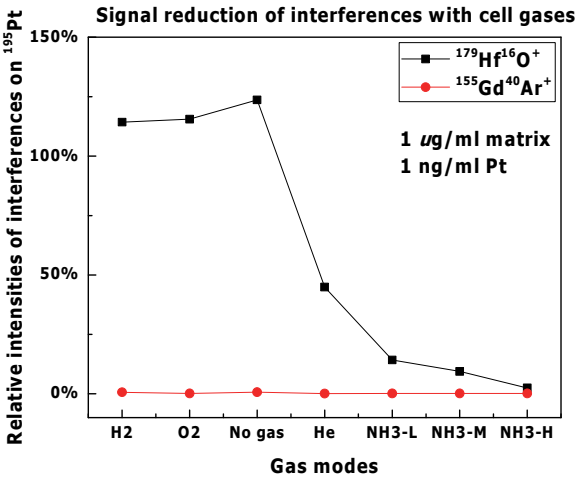

Figure 9.14: Signal reduction of $^{155}Gd^{40}Ar^+$ and $^{179}Hf^{16}O^+$ interferences relative to no gas mode on $^{195}Pt^+$

^{196}Pt, ^{198}Pt

The platinum isotope $^{196}Pt^+$ and $^{198}Pt^+$ suffers from common critical interferences from $^{196\text{-}198}Hg^+$ and $^{180\text{-}182}W^{16}O^+$. $^{156}Gd^{40}Ar^+$ and $^{180}Hf^{16}O^+$ interferences on $^{196}Pt^+$ show the similar

trend as discussed for interferences on $^{194}Pt^{+}$ and $^{195}Pt^{+}$. The behaviour of $^{196\text{-}198}Hg^{+}$ is interesting with ammonia, as it reacts with it more rapidly than platinum. This suggests that Hg interferences can be eliminated with on-mass ammonia measurement of Platinum isotopes.

^{180}W (0.21%) and ^{182}W (26.50%) show some reactivity towards oxygen cell gas as most of the $^{180}W^{16}O^{+}$ is wiped out to make other oxides of tungsten. $^{182}W^{16}O^{+}$ also tend to make an oxide and its intensity is decreased on $^{198}Pt^{+}$. This information can be useful for finding the product ion of W^{+} with oxygen gas. Besides oxygen gas, ammonia gas offers the best signal reduction of interferences as shown in Figure 9.15 and Figure 9.16.

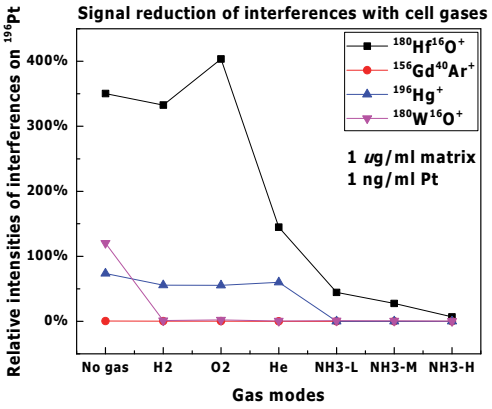

Figure 9.15: Signal reduction of $^{196}Hg^{+}$, $^{180}W^{16}O^{+}$, $^{156}Gd^{40}Ar^{+}$ and $^{180}Hf^{16}O^{+}$ and interferences relative to no gas mode on $^{196}Pt^{+}$

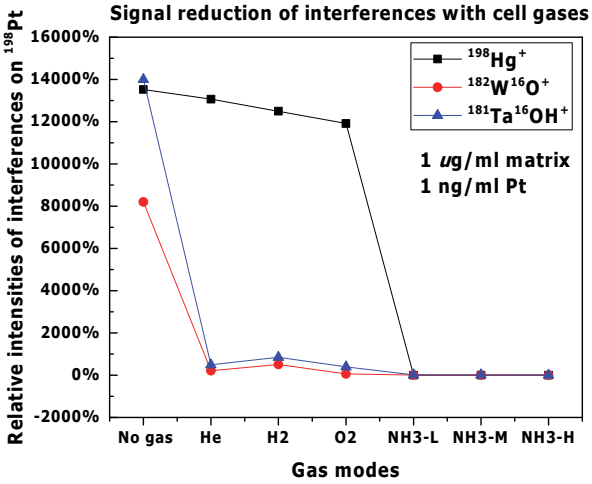

Figure 9.16: Signal reduction of $^{198}Hg^{+}$, $^{182}W^{16}O^{+}$and $^{181}Ta^{16}OH^{+}$ interferences relative to no gas mode on $^{198}Pt^{+}$

9.8.2 Signal reduction of interferences on Ir isotopes

The $^{175}Lu^{16}O^{+}$ and $^{177}Hf^{16}O^{+}$ are the major interferences on $^{191}Ir^{+}$ and $^{193}Ir^{+}$ respectively and $^{151\text{-}153}Eu^{40}Ar^{+}$ are the minor interferences on $^{191\text{-}193}Ir^{+}$ isotopes. Ammonia cell gas shows the maximum interference removal as compared to other gases. The interference removal efficiencies of the cell gases are shown in Figure 9.17.

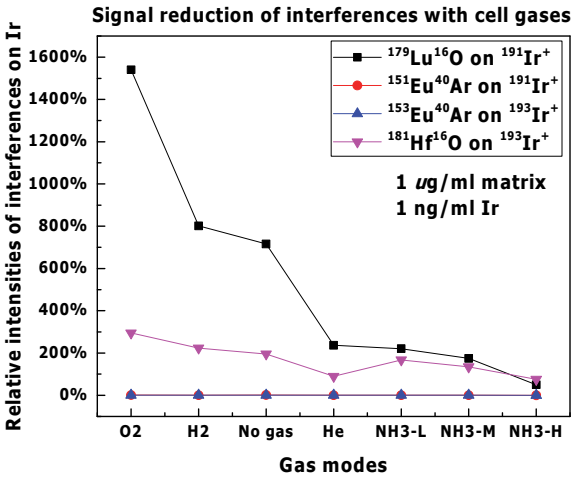

Figure 9.17: Signal reduction of $^{175}Lu^{16}O^+$ and $^{177}Hf^{16}O^+$ and $^{151\text{-}153}Eu^{40}Ar^+$ interferences relative to no gas mode on Ir isotopes

9.8.3 Signal reduction of interferences on Au

$^{181}Ta^{16}O^+$ is critical interference on gold. Other interferences are $^{157}Gd^{40}Ar^+$ and $^{180}Hf^{16}OH^+$. $^{181}Ta^{16}O^+$ interferences decrease with ammonia gas in comparison with other cell gases. $^{181}Ta^{16}O^+$ interference is not decreased unlike Simpson *et al.* (2001) which is probably due to a lower concentration of matrix elements. $^{180}Hf^{16}OH^+$ and $^{157}Gd^{40}Ar^+$ do not show any decrease with on-mass measurement with cell gases. $^{157}Gd^+$ makes an adduct ion with ammonia because the intensity of Gd increases with ammonia cell gas. For complete removal of $^{157}Gd^{40}Ar^+$ and $^{180}Hf^{16}OH^+$, another product of Pt^+ with mass-shift has to be determined.

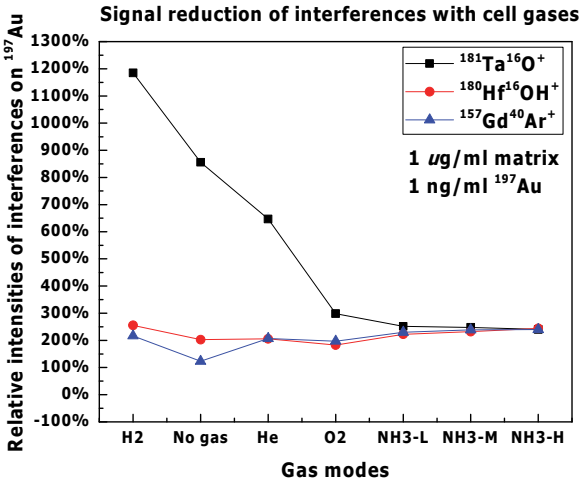

Figure 9.18: Signal reduction of $^{181}Ta^{16}O^+$, $^{157}Gd^{40}Ar^+$ and $^{180}Hf^{16}OH^+$interferences relative to no gas mode on $^{197}Au^+$

9.8.4 Signal reduction of interferences on Os isotopes

^{187}Os, ^{188}Os and ^{189}Os

$^{171\text{-}172}Yb^{16}O^{+}$ interferences on $^{187}Os^{+}$ and $^{188}Os^{+}$ are critical. Ammonia gas with high flow rate seems to reduce their intensity at m/z of ^{187}Os and ^{188}Os. Interferences from isotopes of Nd are generated on $^{187}Os^{+}$ (exact oxides are not known) however, NdOx interferences are reduced with oxygen gas. $^{154}Sm^{16}OH^{16}O^{+}$ interferences are not reduced at all with any cell gas. $^{148}Nd^{40}Ar^{+}$ and $^{148}Sm^{40}Ar^{+}$ interferences are minor on $^{188}Os^{+}$. $^{171\text{-}172}Yb^{16}O^{+}$ interferences on $^{189}Os^{+}$ have shown to decrease with ammonia and He gas. Its intensity increases with oxygen gas. The interference on $^{187}Os^{+}$, $^{188}Os^{+}$ and $^{189}Os^{+}$ are shown in Figure 9.19, Figure 9.20 and Figure 9.21.

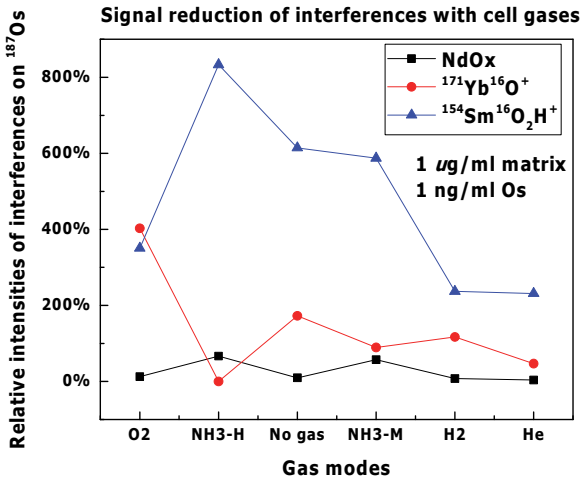

Figure 9.19: Signal reduction of NdOx, $^{154}Sm^{16}OH^{16}O^{+}$ and $^{171}Yb^{16}O^{+}$ interferences relative to no gas mode on $^{187}Os^{+}$

Rhenium-187 interference on $^{187}Os^{+}$ are significantly high as in Figure 9.20. At a higher flow rate of ammonia, the intensity of Os is decreased to a minimum ensuring formation of another product ion with ammonia. Rhenium does not show any complete removal with any cell gas. Therefore no further work was carried on rhenium removal in collision/reaction cell.

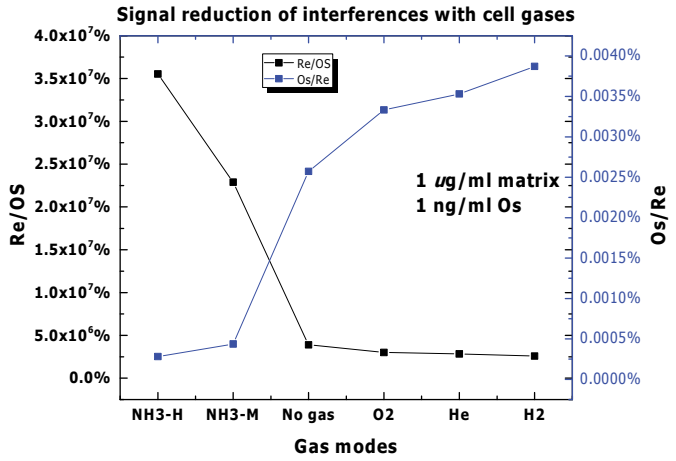

Figure 9.20: Signal reduction of $^{187}Re^{+}$ interferences relative to no gas mode on $^{187}Os^{+}$

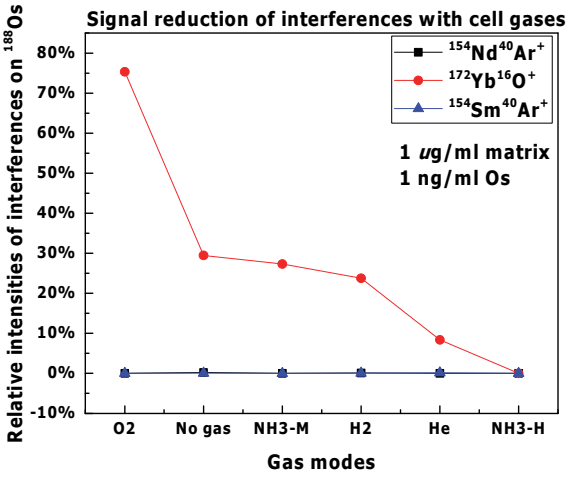

Figure 9.21: Signal reduction of $^{154}Nd^{40}Ar^{+}$, $^{154}Sm^{40}Ar^{+}$ and $^{172}Yb^{16}O^{+}$ interferences relative to no gas mode on $^{188}Os^{+}$

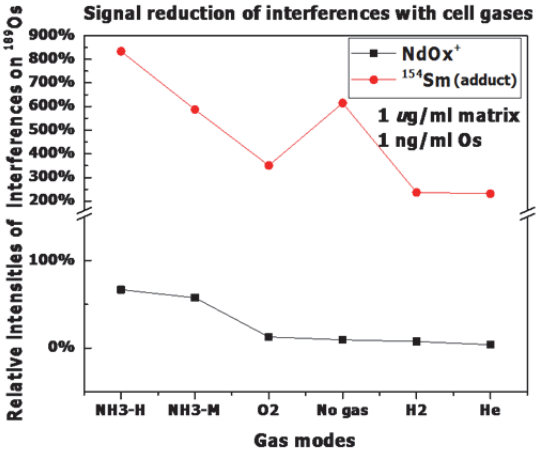

Figure 9.22: Signal reduction of $NdOx^{+}$ and $^{154}Sm(adduct)^{+}$ interferences relative to no gas mode on $^{189}Os^{+}$

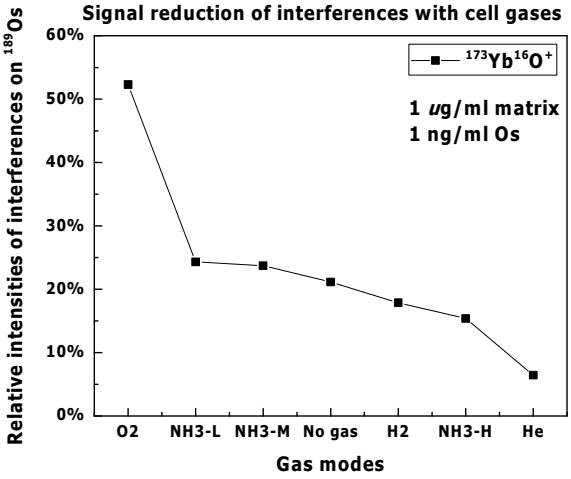

Figure 9.23: Signal reduction of $^{173}Yb^{16}O^{+}$ interferences relative to no gas mode on $^{189}Os^{+}$

^{190}Os and ^{192}Os

$^{174}Yb^{16}O^{+}$ interference on $^{190}Os^{+}$ and $^{192}Os^{+}$ can be decreased with a higher flow rate of ammonia. For $^{176}Lu^{16}O^{+}$, $^{176}Hf^{16}O^{+}$ and $^{190\text{-}192}Pt^{+}$ a mass-shift can be tested for interference removal. The efficiencies of cell gases towards interference removal are shown in Figure 9.24 and Figure 9.25.

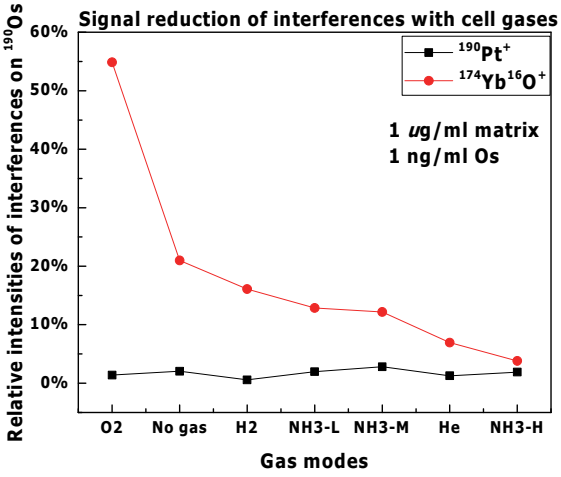

Figure 9.24: Signal reduction of $^{190}Pt^{+}$ and $^{174}Yb^{16}O^{+}$ interferences relative to no gas mode on $^{190}Os^{+}$

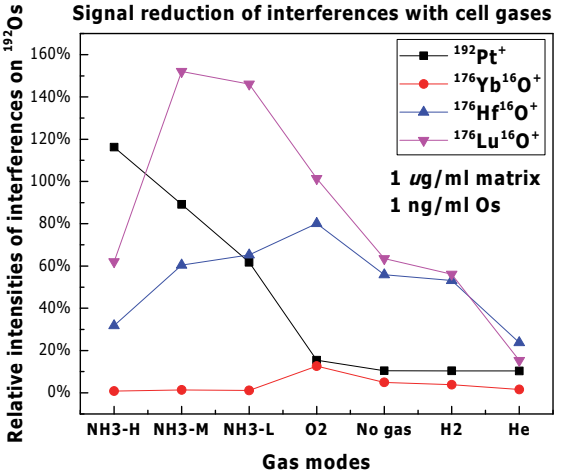

Figure 9.25: Signal reduction of $^{192}Pt^{+}$, $^{176}Yb^{16}O^{+}$, $^{176}Hf^{16}O^{+}$ and $^{176}Lu^{16}O^{+}$ interferences relative to no gas mode on $^{192}Os^{+}$

9.9 Method development for interference removal on PGE isotopes

So far the reactivity of critical interferences and PGE isotopes has been established and the signal reductions of interferences have been discussed. These two aspects studied are important in method development for interference removal on PGE isotopes. These are based on on-mass measurement of interferences and PGE isotopes with cell gases. Ammonia and in some cases oxygen have shown that any interference can be removed with few exceptions. As a next step, a mass-shift method is applied for interference removal on

PGE isotopes. It is important to find the product ions of PGE isotopes for application of mass-shift with ammonia or oxygen gas.

9.9.1 Signal intensities of PGE isotopes with ammonia gas

The signal intensities of PGE analytes if taken as 100% in no gas mode, then the relative signal intensities are shown to decrease with ammonia gas flow rates. For Ru, Rh, Ag, Pd and Au the decrease in intensity is less than Pt, Ir and Osmium in each flow rates i.e. 2, 3 and 5 ml/min. This decrease is related to ease of product ion formation. For a flow rate of ammonia at 2 ml/min Ru, Rh, Ag, Pd show a 20-40% decrease but at 5 ml/min it is up to 80-90% decrease in intensity. The ease of formation of product ion with ammonia gas seems higher for Pt, Ir and Os and lower for Ru, Rh, Ag, Pd and Au. This behaviour of PGE analytes is shown in Figure 9.26.

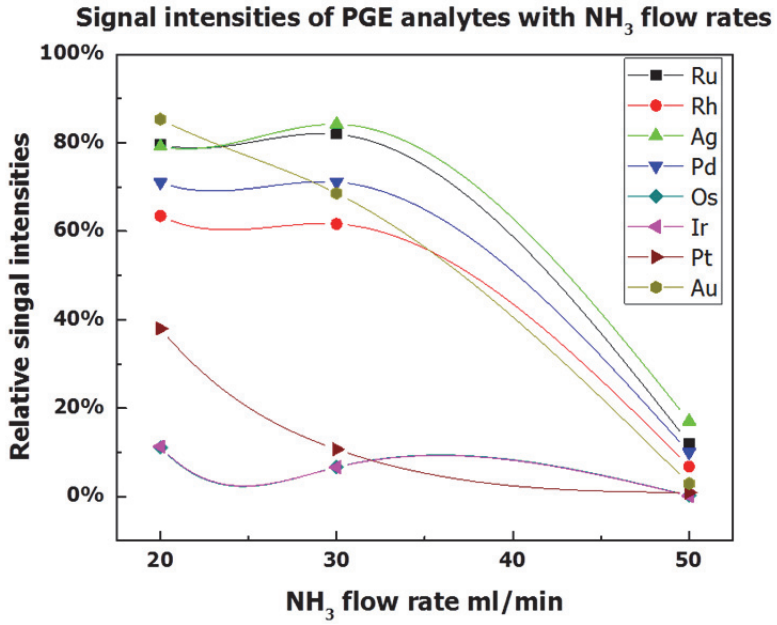

Figure 9.26: Signal intensities of PGE analytes with ammonia gas flow rates

9.9.1 Signal intensities of PGE analytes with oxygen gas

The relative intensities of PGE analytes in oxygen gas modes also differ to a varied extent. If 100% is the intensity of PGE analytes in no gas modes, then the relative intensity of Pt, Ag, Ru, Rh is higher than in no gas mode while for Pd, Os, Ir and Au is lower than in no gas mode as shown in Figure 9.27. The lowering down of the intensities is related to the formation of oxide product ions. These tendencies of PGE analytes can be useful for finding any product ion that can be free from interferences.

9.10 Product ions of PGE analyte in ammonia and oxygen gas

The product ions of PGE analytes were determined using 1 ng/ml solution of pure PGE standards separately. The maximum flow rate of ammonia can be 10 ml/min in mass hunter workstation of Agilent 8800. The initial testing with flow rates 2, 3, 5 ml/min are optimal flow rates where the drop in intensity is not worse as compared to higher flow rates.

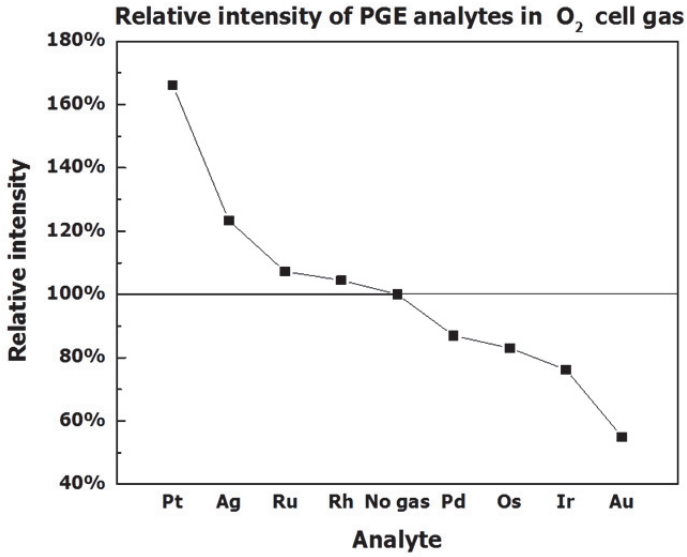

Figure 9.27: Signal intensities of PGE analytes with oxygen gas

9.10.1 Product ions of ruthenium in ammonia gas

The ruthenium product ions were determined with ammonia gas flow rates of 2, 3 and 5 ml/min. The main objective of finding these product ions was to explore a mass-shifted product of ruthenium where the overlap of interference does not exist. Beside these considerations, intensity of the product ion is an important factor that makes it measurable. Data for all product ions is presented which may be important for gas-phase reactions of ruthenium. Several product ions of ruthenium with ammonia gas were determined until 250 m/z on mass hunter workstation of Agilent 8800 ICP-MS/MS. These product ions were $Ru(NH3)_x^+$ where $_x$ is the number of ammonia molecules added to ruthenium ion. The addition of up to 5 ammonia molecules was observed while for $Ru(NH3)_6^+$ no intensity was observed but this may be due to weak bonding of the 6th ammonia molecule.

Observations from Gorelsky *et al.* (2001) of the sequential ligation of Ru^+ with ammonia for up to five molecules were seen to add to Ru^+ under SIFT conditions. Similar results have been reported by Favre (2008). Gorelsky *et al.* (2001) describe as the addition is presumed to occur by collisional rather than radiative association with He acting as the stabilising third body. From the SIFT experimental and theoretical calculations of Gorelsky *et al.* (2001), the gas-phase measurements of the kinetics for the sequential ligation of Ru^+ with ammonia at room temperature show an anomalous rise in the rate of addition of the fourth ammonia ligand as the rate of ligation is dependent on the free energy of ligation. The first addition has a large exothermicity (67.8 kcal/mol), and the next three sequential additions all have higher exothermicity. The addition of the second NH_3 is exothermic by 40.3 kcal/mol and the third and fourth additions are of comparable energies (35.4 and 29.8 kcal/mol). The addition of a fifth NH_3 molecule is very weakly exothermic (by 4.8 kcal/mol). The product ion 99 -> 167 Ru [NH3-L] presents the highest intensities of the ruthenium shift mode.

The mechanism of gas-phase reaction of Ru^+ takes place in three steps as suggested by Gorelsky *et al.* (2001).

1. The ligation of single ammonia molecule to ruthenium ion
   $Ru + NH_3 \longrightarrow Ru(NH_3)^+$ (A)

2. The collisional stabilisation of the adduct ion $Ru(NH3)_x^+$

$Ru\ (NH_3)^+ + NH_3 \longrightarrow (Ru\ (NH_3)_x^+)^*$ (B)

3. $(Ru\ (NH_3)^+)^* + He \longrightarrow (Ru\ (NH_3)_x^+) + He^*$ (C)

Reactions are expected to proceed through termolecular association where is He acting as a third body. The product ions of ruthenium are shown in Figure 9.28.

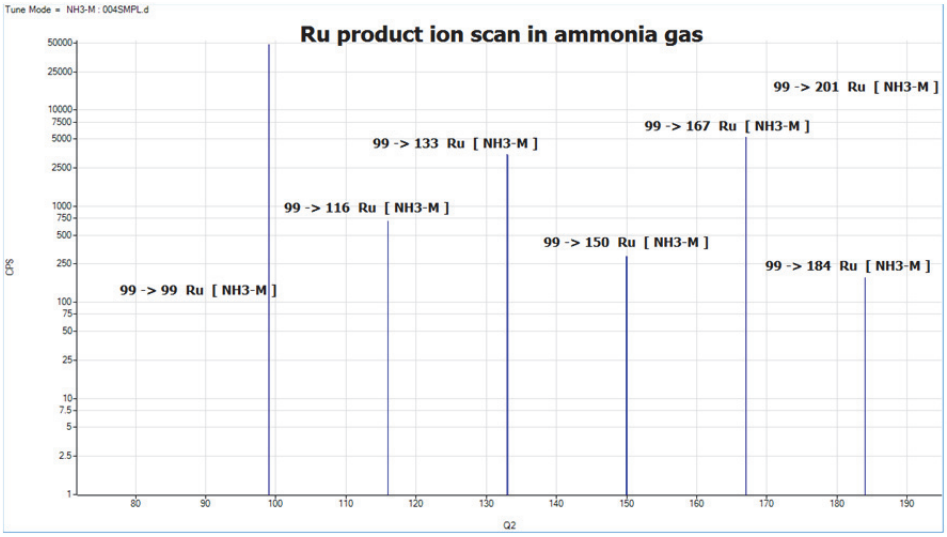

Figure 9.28: Ru product ion scan in ammonia gas

9.10.2 Product ions of rhodium in ammonia gas

Rhodium product ions were scanned with flow rates of ammonia i.e. 2, 3 and 5 ml/min. Rhodium undergoes clustering reactions with ammonia similar to ruthenium. The addition of up to 4 ammonia molecules was observed over the range of scanned masses. The product ion scan of Rh is given in Figure 9.29. Limited literature exists on Rh gas-phase reaction with ammonia. So far a publication of Cao *et al.* (2016) on gas-phase chemistry of rhodium carbonyl complexes has stated to form the addition of 4 CO groups to rhodium. The chemistry of this study of Rh ligation with ammonia seems analogous to CO chemistry. The intensities of 103 -> 171 Rh [NH3-M] were better as compared to other shifted mass products ion of Rh. Jones (2007) also reports the presence of same Rh and ammonia clusters in higher flow rates of ammonia. The presence of ammonia and its amount makes the basis of formation of the product besides thermochemical properties of the reaction of the analytes and ammonia. A sp3 hybridization according to Cao *et al.* (2016) is said to exist in $Rh(CO)_4$ complexes and similar can be applied for Rh ammonia complexes i.e. $Rh(NH_3)_4$.

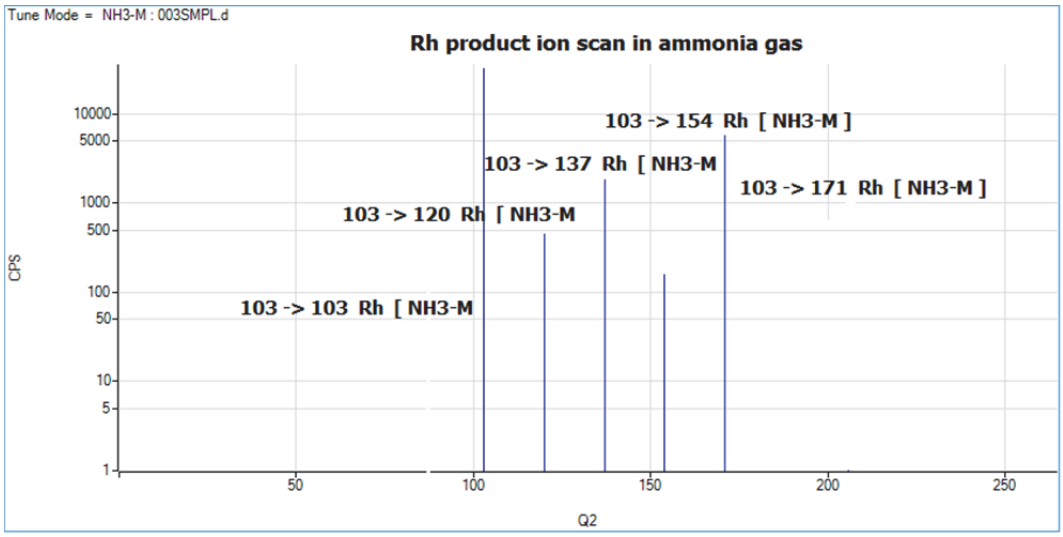

Figure 9.29: Rh product ion scan in ammonia gas

9.10.3 Product ions of Ag in ammonia gas

For Ag isotopes, addition of up to three ammonia molecules was observed over the ranges of scanned masses on Q2. The best intensities observed were for the ions of 107 -> 141 Ag [NH3-M] as shown in the Figure 9.30. The reaction of Ag^+ with NH_3 in the SIFT produced only the first three adducts, with no evidence of the fourth adduct even at high flow rates (Shoeib *et al.* 2000). This confirms the product ions of Ag^+ determined with a current study using collision/reaction cell technology of Agilent 8800. According to Shoeib *et al.* (2000), the molecular orbital calculations on ions $Ag(NH_3)^+$ and $Ag(NH_3)_2^+$ show that the binding enthalpies of these complexes are approximately large i.e. (40 kcal/mol), and the binding enthalpies of the $Ag(NH_3)_3^+$ are (15.1 kcal/mol). This relates to lower intensities of $Ag(NH_3)_3^+$ clusters.

Shoeib *et al.* (2000) have also detected the first three ions with electrospray experiments, but with only mono- and di-adducts being present in large amounts. They have described a forth adduct, with an additional NH_3 molecule providing solvation through hydrogen bonding.

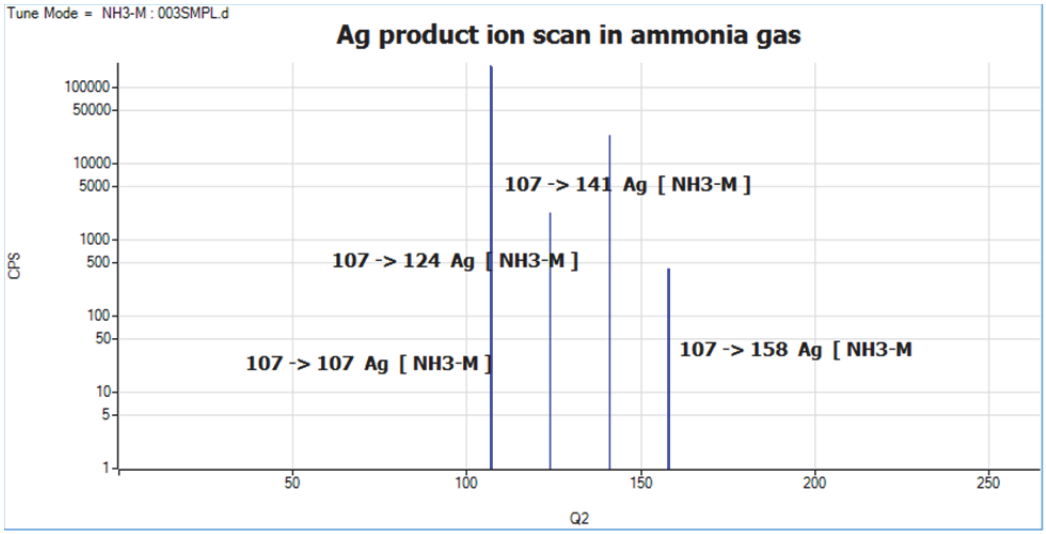

Figure 9.30: Ag product ion scan in ammonia gas

9.10.4 Product ions of Ir in ammonia gas

Ir has shown to form 191 -> 206 Ir [NH3-M], 191 -> 207 Ir [NH3-M] and 191 -> 225 Ir [NH3-M] products as shown in the Figure 9.31. These types of reactions are said to be condensation reactions by Jones (2007) and usually, follow the mechanism as given in equation

$$Ir^+ + NH_3 \longrightarrow Ir(NH_x)_y^+ \qquad (A)$$

The product ion 191 -> 206 Ir [NH3-M], 191 -> 207 Ir are $Ir(NH)^+$ and $Ir(NH_2)^+$. The addition of full ammonia takes place by clustering reaction as in 191 -> 225 Ir [NH3-M]. These reactions are analogous to reactions of La^+, Ce^+, Gd^+, Tb^+, Gd^+, Tb^+, Os^+ and Re^+ etc. The MNH^+ product ion i.e. $IrNH^+$ has always been the most abundant product ion taking place with hydrogen elimination and has been observed by other researchers as well Jones (2007), Koyanagi *et al.* (2009), Tanner *et al.* (2000). The ease of formation of MNH^+ is related to high exothermicity of reactions.

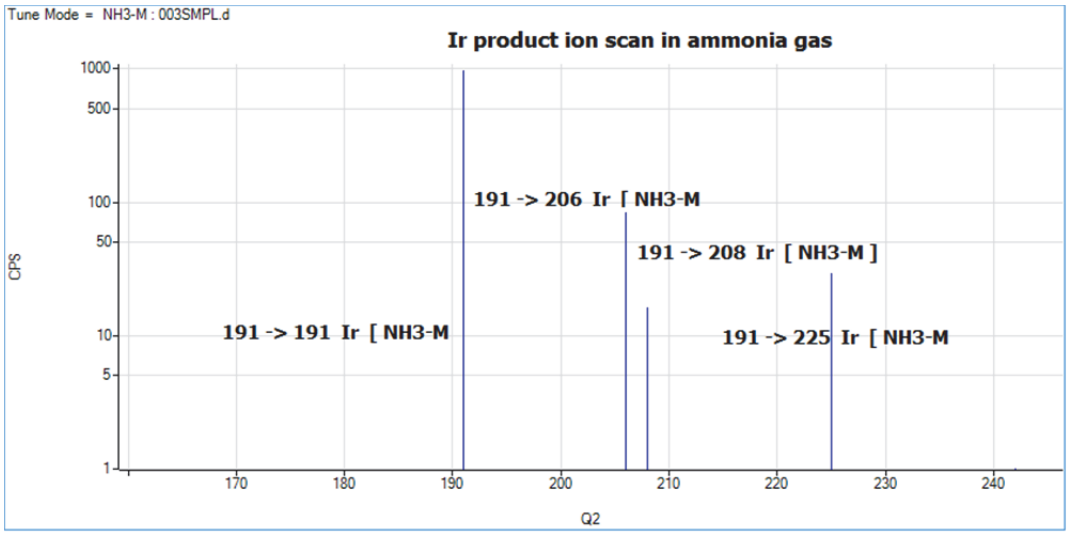

Figure 9.31: Ir product ion scan in ammonia gas

9.10.5 Product ions of Pd in ammonia gas

Several products of Pd were scanned for interference removal capacity i.e. 108 -> 123 Pd [NH3-L], 108 -> 125 Pd [NH3-L], 108 -> 142 Pd [NH3-L], 108 -> 159 Pd [NH3-L] and 108 -> 176 Pd [NH3-L]. The product ion 108 -> 159 Pd [NH3-L] was chosen for interference removal application. Pd appears to form $Pd(NH)^+$ beside addition reaction with ammonia. The product ions of Pd are shown in Figure 9.32.

9.10.6 Product ions of Pt in ammonia gas

Platinum scanned mass for shift modes were at 195 -> 212 Pt [NH3-M], 195 -> 227 Pt [NH3-M], 195 -> 229 Pt [NH3-M], 195 -> 246 Pt [NH3-M]. The signal intensities of 195 -> 229 Pt [NH3-M] were better than all other mass-shifted product ions. The product ions are shown in Figure 9.33.

9.10.7 Product ions of Au in ammonia gas

Gold mass-shifted product ion scanned were at 197 -> 214 Au [NH3-M], 197 -> 231 [NH3-M] and 197 -> 248 [NH3-M]. The signal intensities of 197 -> 231 Au [NH3-M]

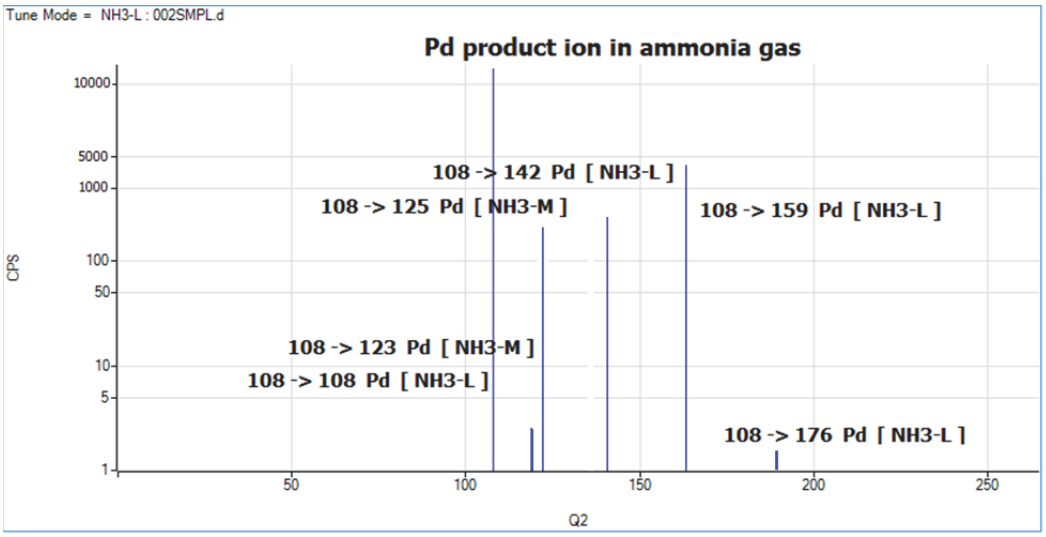

Figure 9.32: Pd product ion scan in ammonia gas

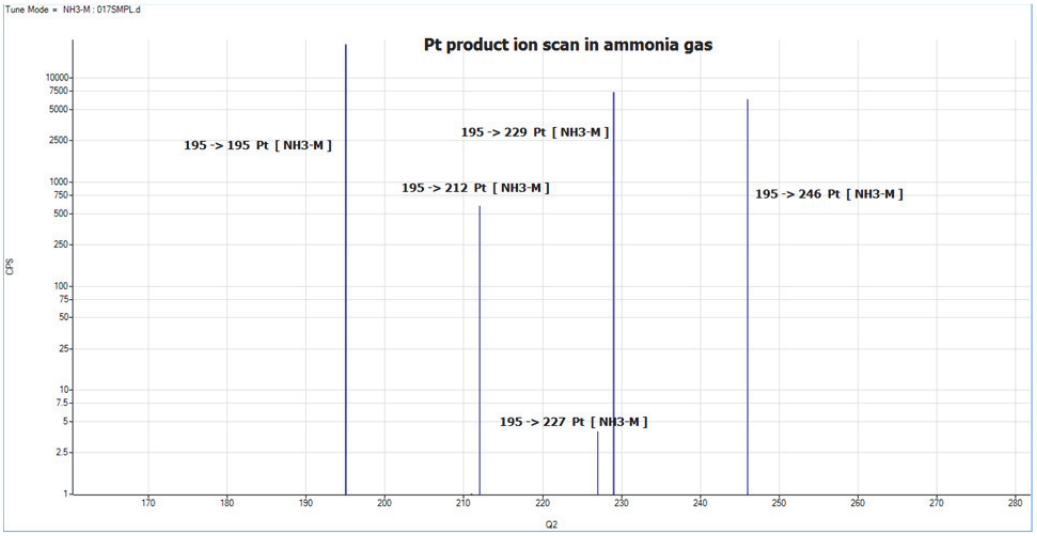

Figure 9.33: Pt product ion scan in ammonia gas

were better than all other mass-shifted product ions. Similar product ions are reported in Jones (2007) and Sugiyama and Shikamori (2015). The scanned product ions of Au are shown in Figure 9.34.

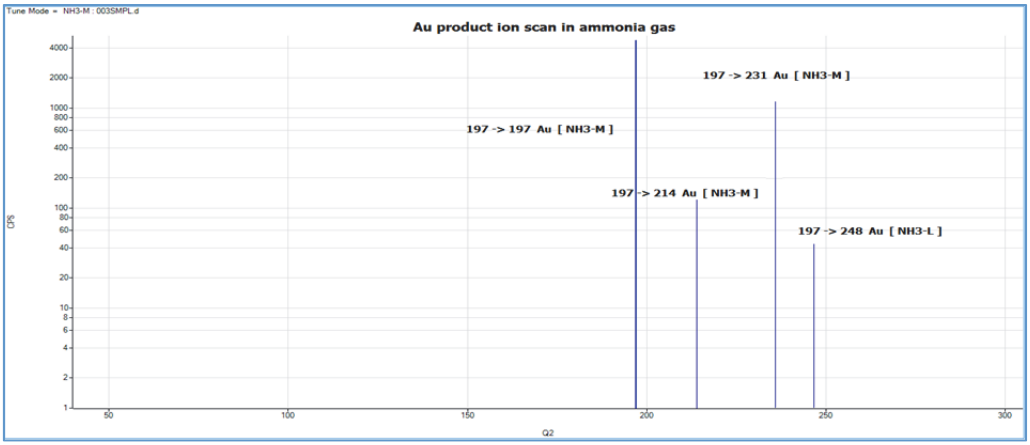

Figure 9.34: Au product ion scan in ammonia gas

9.10.8 Product ions of Os in ammonia gas

Os mass-shifted product ions scanned were at 192 -> 214 Os [NH3-L] and 192 -> 207 Os makes product ion of the type $Os(NH)^+$ product ions. The scan of product ions of Os is shown in Figure 9.34.

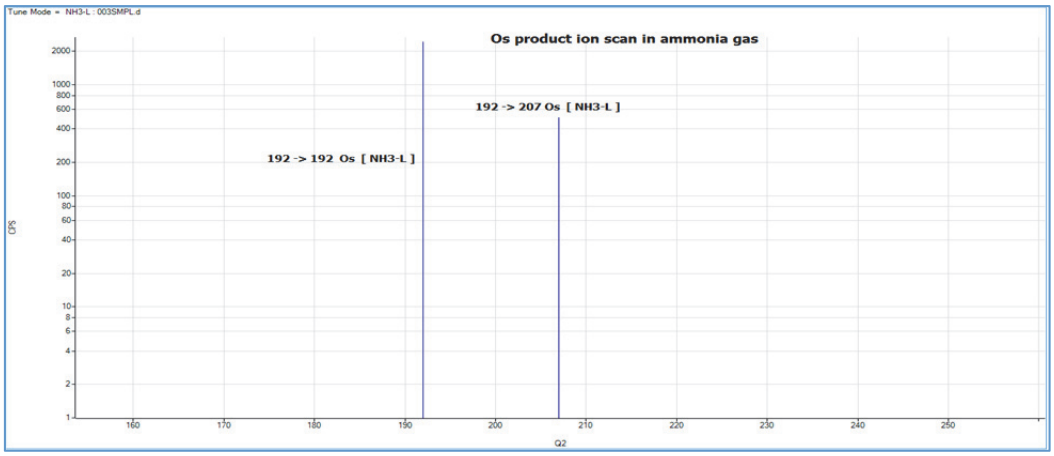

Figure 9.35: Os product ion scan in ammonia gas

9.10.9 Product ions of PGE analytes in oxygen gas

Douglas (1989) showed that ion-molecule reactions using O_2 provided high selectivity and reaction efficiency. If the background at the mass of the analyte-containing product ion is low, then even reactions with relatively low efficiency (10 to 25%) may be sufficient to dramatically improve detection limits.

The two products ions of ruthenium isotopes were tested with oxygen i.e. RuO^+ and RuO_2^+. RuO^+ oxide had better relative intensities than RuO_2^+. For Rh^+, RhO^+ and RhO_2^+ were tested and RhO_2^+ had no intensities indicating no formation. For Pt^+ only PtO^+ was identified with very low intensities. $^{191}IrO^+$ and $^{191}IrO_2^+$ were identified for Ir for which $^{191}IrO^+$ had better intensities than $^{191}IrO_2^+$. Au has also shown few counts for AuO^+ and AuO_2^+. Os had product ions up to four oxygen i.e. OsO^+, OsO_2^+, OsO_3^+ and OsO_4^+. The intensities of OsO_2^+ were better than all other oxides of Os.

9.11 Interference removal using on-mass and mass-shift method with oxygen and ammonia gas

The first step of the method development for interference removal was to gather experimentally the concrete information on the reactivity of PGE analytes and interferences, trends in signal reductions of interferences with ammonia gas and product ions of the PGE analytes with ammonia and oxygen gases. All these primary experiments provide sufficient information on interferences that can be removed with the on-mass or mass-shift method in reaction collision cell using oxygen and ammonia gases. As a second step matrix, blanks will be shown to reduce their BECs created on PGE analytes. Each PGE analyte will be discussed individually for any mass-shift or on-mass method for interference removal

9.11.1 Removal of interferences on Ruthenium isotopes

Interferences on ruthenium isotopes are $^{98}Mo^1H^+$, $^{100}Mo^1H^+$, $^{64}Zn^{35}Cl^+$, $^{85}Rb^{16}O^+$, $^{61}Ni^{40}Ar^+$, $^{65}Cu^{35}Cl^+$, $^{86}Sr^{16}O^+$, $^{62}Ni^{40}Ar^+$, $^{67}Zn^{35}Cl^+$, $^{102}Pd^+$ and $^{104}Pd^+$. Interference removal on ruthenium has already been presented in Bokhari *et al.* (2015e). According to Figure 9.36

and Figure 9.37 RuO^+ and $Ru(NH_3)_4^+$ for both ^{99}Ru and ^{101}Ru are best product ions to remove interferences. Other gas modes i.e. He and hydrogen gases are not good in interference removal capacity. Therefore, the suggested method for ruthenium measurement involves RuO^+ and $Ru(NH_3)_4^+$ product ions in mass-shift of ammonia and oxygen gas modes.

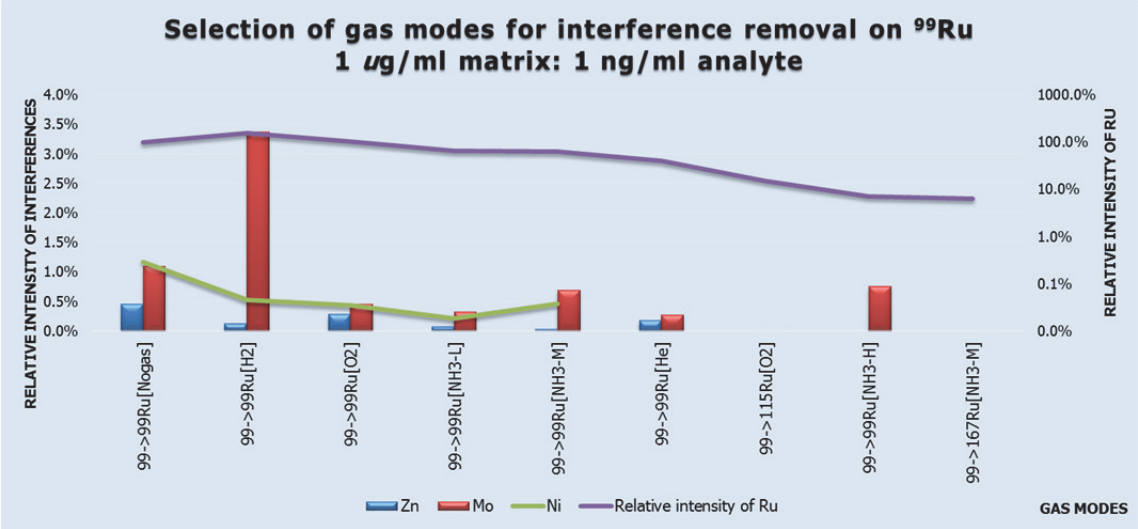

Figure 9.36: Selection of product ions for interference removal on ^{99}Ru

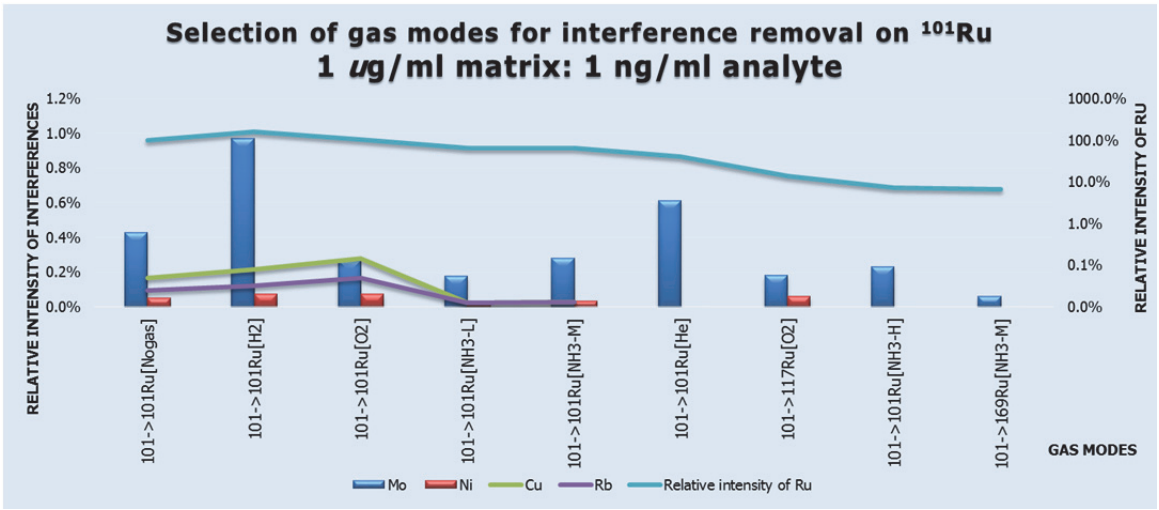

Figure 9.37: Selection of product ions for interference removal on ^{101}Ru

9.11.2 Pd interference on Ru and vice versa

Ruthenium has $^{102}Pd^+$ and $^{104}Pd^+$ interferences and palladium has $^{102}Ru^+$ and $^{104}Ru^+$. The percent abundance of ^{104}Pd (11.14) is less than ^{104}Ru (18.62), hence impact of ruthenium interference on palladium is larger than palladium interference on ruthenium. Figure 9.38 shows 29% interference of Pd on Ru and 344% interference of Ru on Pd when 1:1 ng/ml matrix and analytes are tested. The use of suggested method mentioned above for ruthenium can eliminate Pd interference and ruthenium interference on palladium can be removed with $Pd((NH_3)_3^+$ formation in gas-phase reactions in reaction collision cell. With oxygen shift mode of RuO^+, Pd left is decreased to 4% from 344%. This mode is good for separation of both Pd and Ru isotopes in analytical methods. With ammonia shift modes of $Ru(NH_3)_4^+$ and $Pd((NH_3)_3^+$, the interference from Ru and Pd can be minimised.

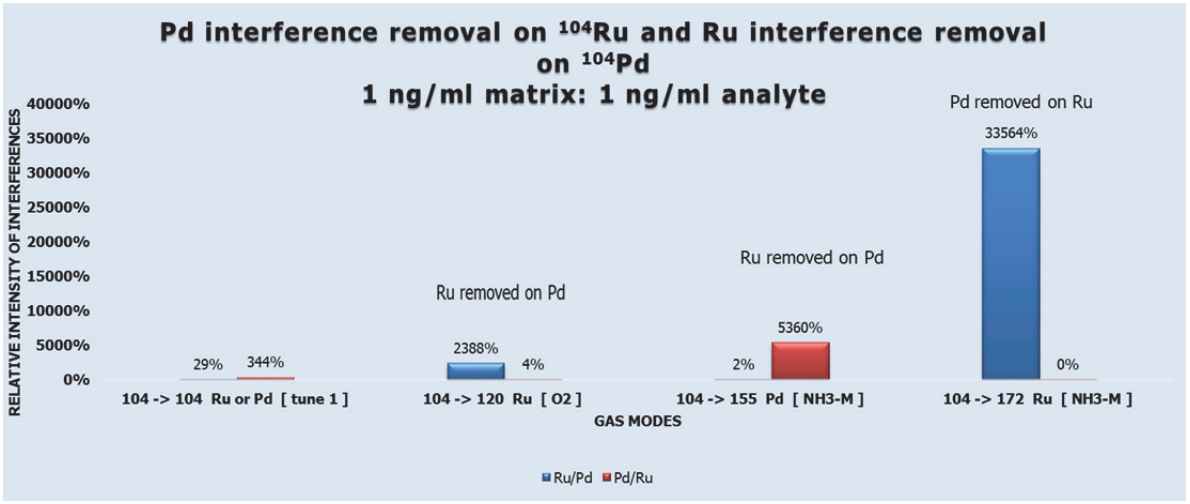

Figure 9.38: Removal of Ru and Pd interferences on each other

9.11.3 Removal of interferences on Rhodium

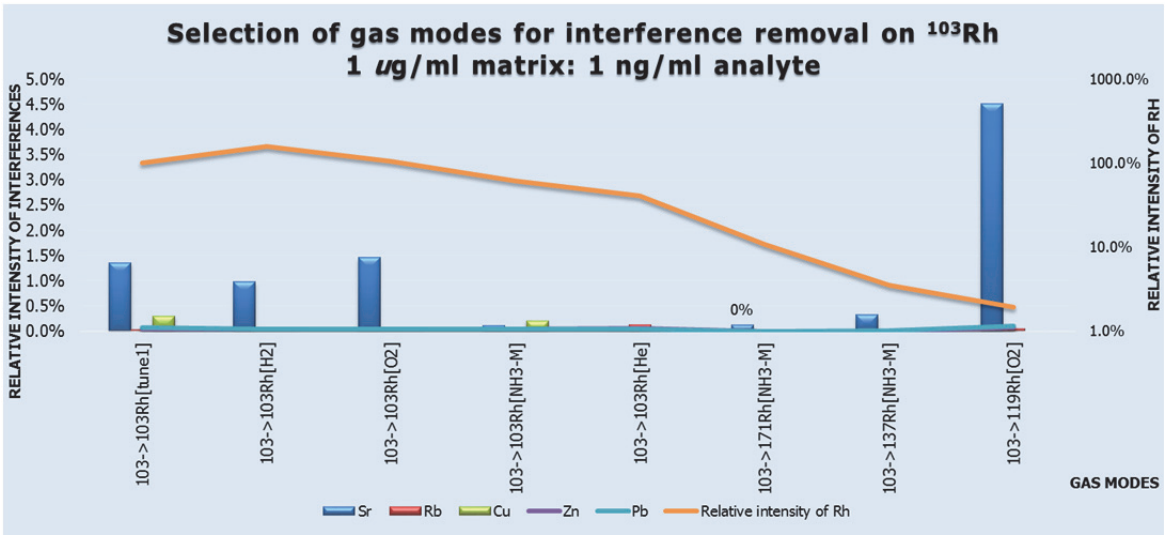

Figure 9.39: Selection of product ions for interference removal on Rh

It is evident from Figure 9.39 that Sr ($^{87}SrO^+$) is the main interference on rhodium in 1 µg/ml matrix. Hydrogen and oxygen gas modes are unable to reduce these interferences. On mass-ammonia, He, and mass-shift $Rh(NH_3)_4^+$ product ions minimise the interferences on rhodium. These modes will then be selected for measurement in geological materials. Pb^{2+} interference is removed by charge transfer reaction (Glenn 2013a, Takeo *et al.* 2010).

$$Pb^{++} + NH_3 \longrightarrow Pb^+ + NH_3^+ \quad 4.96eV \quad \text{Endothermic}$$

$$Rh^+ + NH_3 \longrightarrow Rh + NH_3^+ \quad -2.61eV \quad \text{Exothermic}$$

The transfer of charge from Pb^{++} is favoured due to endothermic nature while the transfer of charge from Rh is not possible due to exothermic nature. The ionisation potential for ammonia is 10.16 eV. If the ionisation energy of the gas is less than the ionisation energy of the atom or molecule that would be formed by the reaction, the charge transfer reaction is exothermic and likely to proceed. If the ionisation potential of the gas is greater than the ionisation energy of the atom or molecule that would be formed by the reaction, then the reaction is endothermic and not likely to proceed unless the ion kinetic energy is sufficiently high.

9.11.4 Selection of best product ions for Rh measurement

The merit for product ion selection for routine determination of any analyte in complex matrices is based on two factors i.e. the relative intensities of the product ion at optimised flow rate of cell gas and its position in the spectrum where no overlap of interferences exists (or have the least effect). The product ions scanned at Q2 for rhodium were $Rh(NH_3)^+$, $Rh(NH_3)_2^+$, $Rh(NH_3)_3^+$ and $Rh(NH_3)_4^+$. $Rh(NH_3)_5^+$ has shown the maximum removal of interferences as in Figure 9.39 and its intensities are (maximum) as shown relative to other product ions with ammonia in Figure 9.40. $Rh(NH_3)_4^+$ offers the best mass-shift mode with ammonia and therefore it is selected to be applied to real matrices i.e. geological materials.

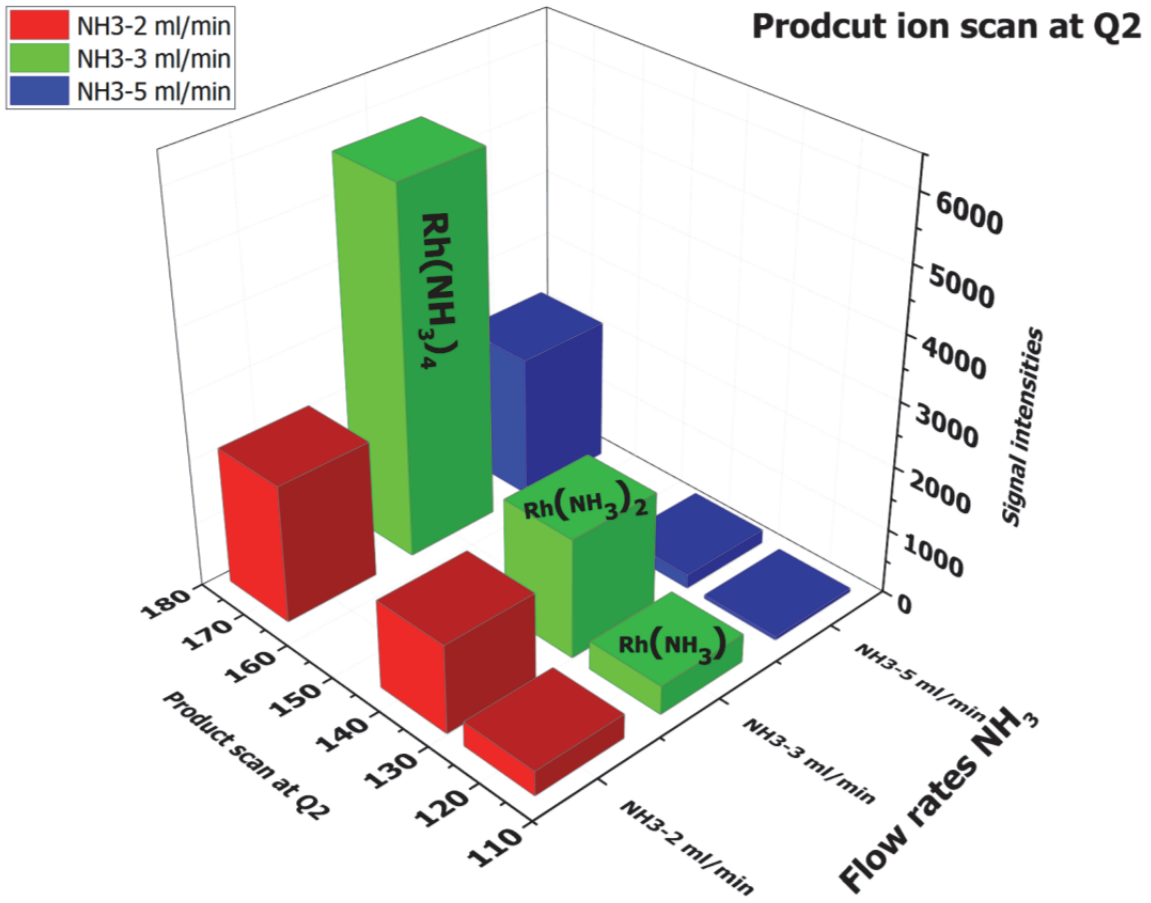

Figure 9.40: Comparison of intensities of product ions at Q2

9.11.5 Removal of interferences on Ag isotopes

The type of gases and product ions for interference removal on Ag isotopes are shown in Figure 9.41. $^{67}Zn^{40}Ar^+$ and $^{91}Zr^{16}O^+$ are the interferences on $^{107}Ag^+$ and $^{93}Nb^{16}O^+$ is the interference on $^{109}Ag^+$. $^{93}Nb^{16}O^+$ is shown with green bars and is only meant for ^{109}Ag shown in the plot. It is evident that hydrogen, helium and oxygen gas modes are unable to reduce the interferences in 1 µg/ml matrix. Only on-mass-ammonia, mass-shift $Ag(NH_3)_2^+$ product ion minimises the interferences on Ag isotopes. These modes will then be applied for measurement of Ag in geological materials.

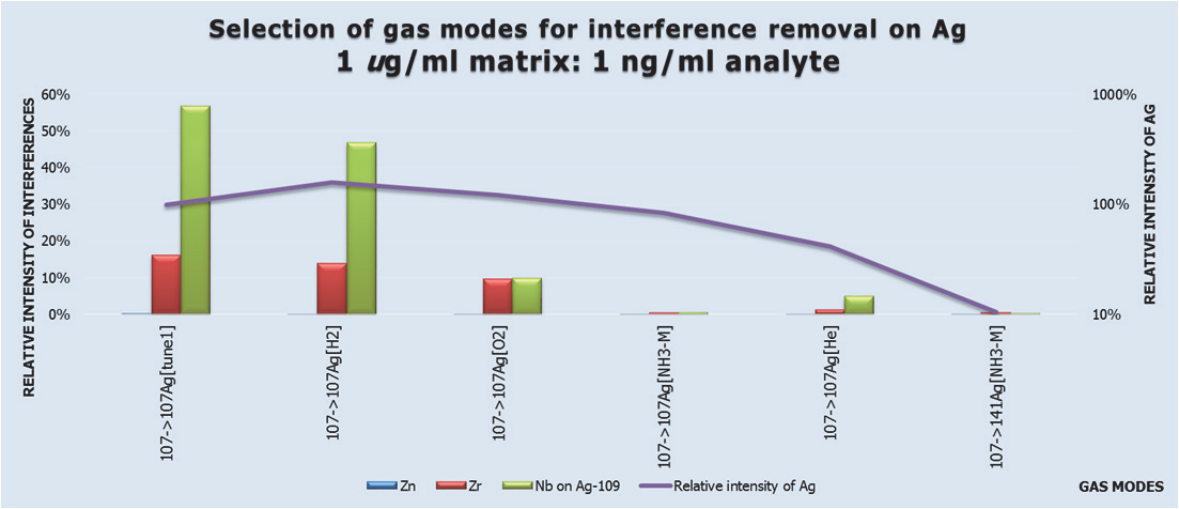

Figure 9.41: Selection of product ions for interference removal on Ag isotopes

9.11.6 Removal of interferences on Pd isotopes

The initial tests on Pd interferences show that $^{89}YO^+$ and $^{87\text{-}88}SrOH^+$ have interferences on ($^{104}Pd^+$, $^{105}Pd^+$), $^{104}Ru^+$ on ($^{104}Pd^+$), $ZnAr^+$ has slight interference on ($^{104}Pd^+$ and $^{106}Pd^+$), $NiAr^+$, $CuAr^+$ interferences are negligible, MoO^+ has severe interference on ($^{108}Pd^+$, $^{110}Pd^+$), ZrO^+ and Cd^+ has severe interferences on ($^{106}Pd^+$, $^{108}Pd^+$, $^{110}Pd^+$). In the same way $^{102}Ru^+$, $^{104}Ru^+$ is interfered by $^{102}Pd^+$and $^{104}Pd^+$.

The interferences from ruthenium isotopes on palladium have been mentioned in ruthenium section of interference removals. Hydrogen, oxygen and helium gases do not remove interferences except ammonia gas. Pd undergo clustering reactions with ammonia and creates the product ions at $Pd(NH_3)^+$, $Pd(NH_3)_2^+$, $Pd(NH_3)_3^+$, $Pd(NH_3)_4^+$ and $Pd(NH_3)_6^+$ at flow rates 2 and 3 ml/min which is also reported in Jones (2007) and Sugiyama and Kazumi (2014). The maximum removal of interferences was possible with $Pd(NH_3)_3^+$ cluster.

Y makes YNH^+, YNH_2^+, YNH_3^+, $YNH(NH_3)^+$, $YNH(NH_3)_2^+$, $YNH_2(NH_3)_2^+$, Y $(NH_3)_3^+$ $Y(NH)NH_3)_4^+$ and $Y(NH_3)_5^+$ product ions. The major product ions are YNH^+ and $Y(NH_3)_5^+$. The product ions of Y at $Pd(NH_3)_3$ are at minimum if compared on other Pd ammonia clusters. Thus Y interference can be considerably removed on Pd as shown in Figure 9.42-Figure 9.43. However, Y interference is not completely removed on a mass unit of 157 but on-mass Pd measurement is better than mass-shift.

Sr product ions scanned were $Sr(NH_2)^+$, $Sr(NH_3)^+$, $Sr(NH_3)_2^+$, $Sr(NH_3)_3^+$, $Sr(NH_3)_4^+$ and $Sr(NH_3)_5^+$. $Sr(NH_3)_4^+$ still have an interference of 0.08% on a mass unit of 156 in 1 µg/ml of Sr matrix. Cu and Zn argide interferences are minor and can be removed with on-mass ammonia and mass-shift $Pd(NH_3)_3$ modes.

Mo underdoes condensation reactions and forms $Mo(NH_3)^+$, $Mo(NH_3)_2^+$, $Mo(NH_3)_3^+$, $Mo(NH_3)_4^+$, $Mo(NH_3)_5^+$ and $Mo(NH_3)_6^+$ product ions. $Mo(NH_3)_2^+$ was the major product ion with highest intensities at a flow rate of 3 ml/min. There are no overlapping product ions of Mo at $Pd(NH_3)_3^+$, hence its removal is possible. Zr^+ undergoes condensation reactions and forms $ZrNH^+$ and $ZrNH_2^+$ as the major product ions. There is no overlap of any of Zr product ions on $Pd(NH_3)_3^+$ hence Zr interference can be easily removed.

Cd^+ undergoes clustering reaction with ammonia and forms $Cd(NH_3)^+$, $Cd(NH_3)_2^+$ and $Cd(NH_3)_3^+$. $Cd(NH_3)_2^+$ is the major product while intensity of $Cd(NH_3)_3^+$ is 0.08% hence ^{106}Cd

and $^{108}Cd^{+}$ will still have some intensity at $Pd(NH_3)_2^{+}$. The plots for interference removal are given in Figure 9.42-Figure 9.45.

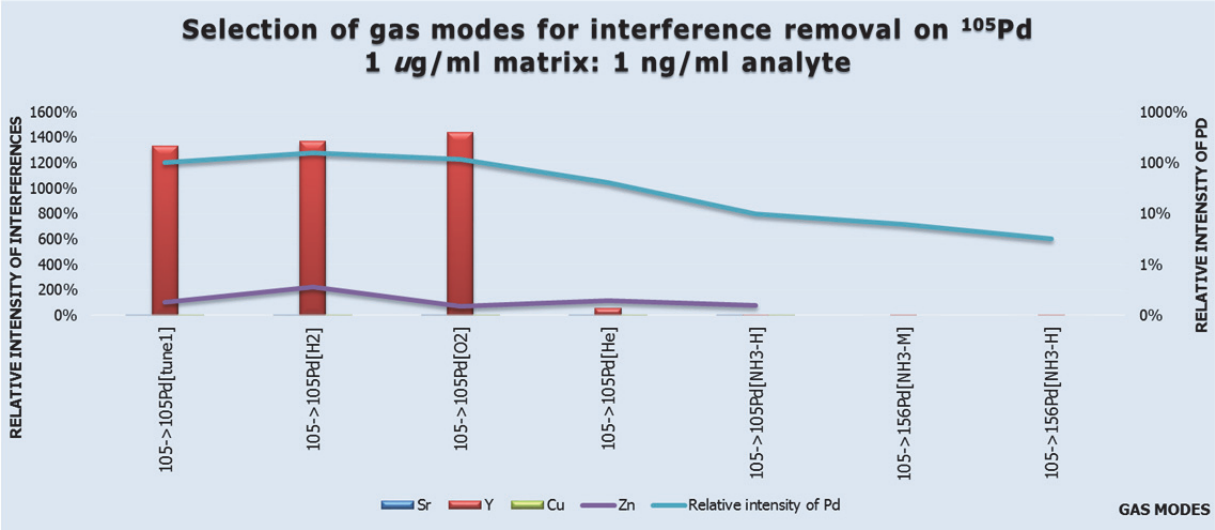

Figure 9.42: Selection of product ions for interference removal on ^{105}Pd

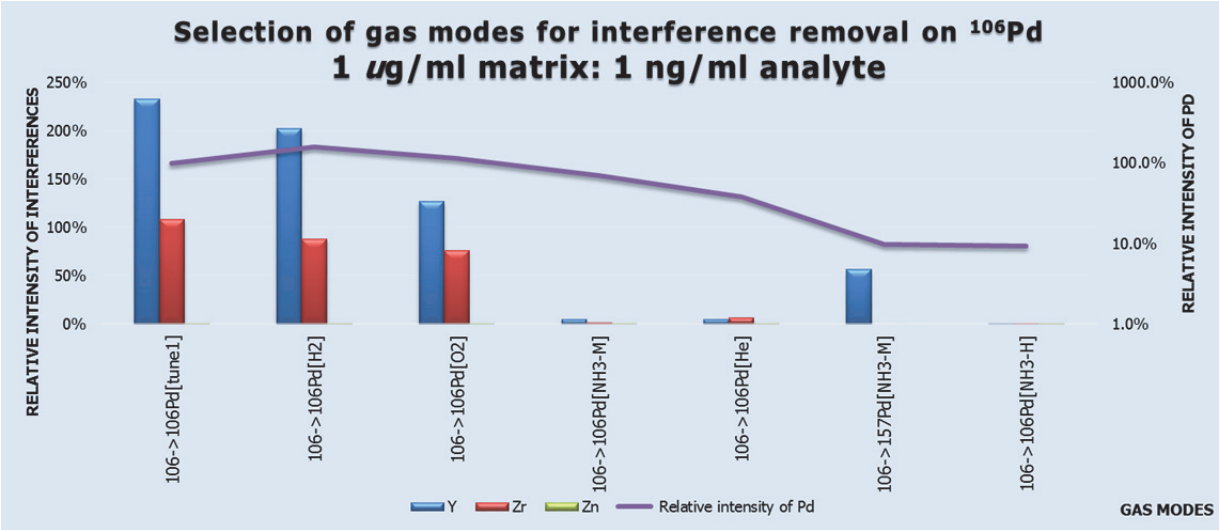

Figure 9.43: Selection of product ions for interference removal on ^{106}Pd

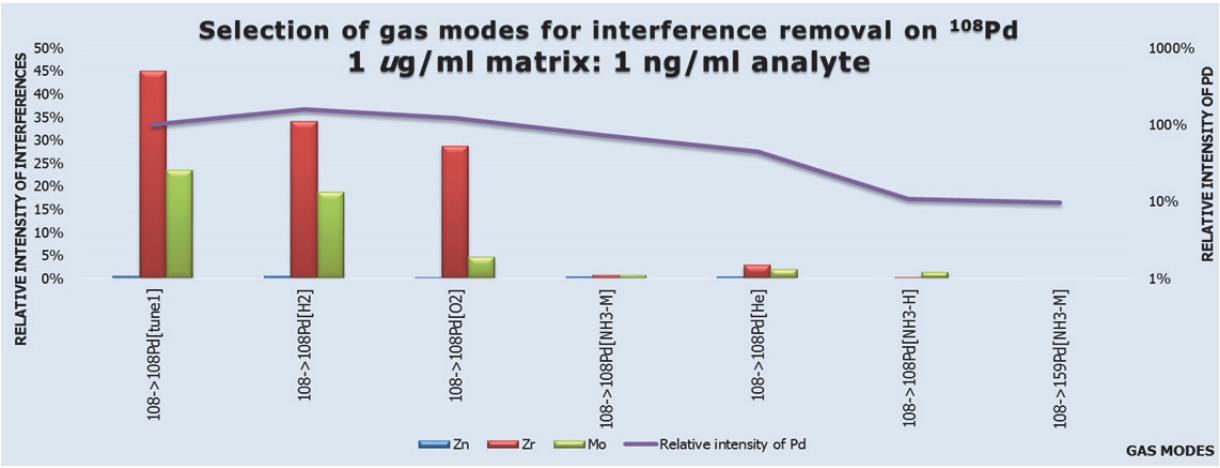

Figure 9.44: Selection of product ions for interference removal on ^{108}Pd

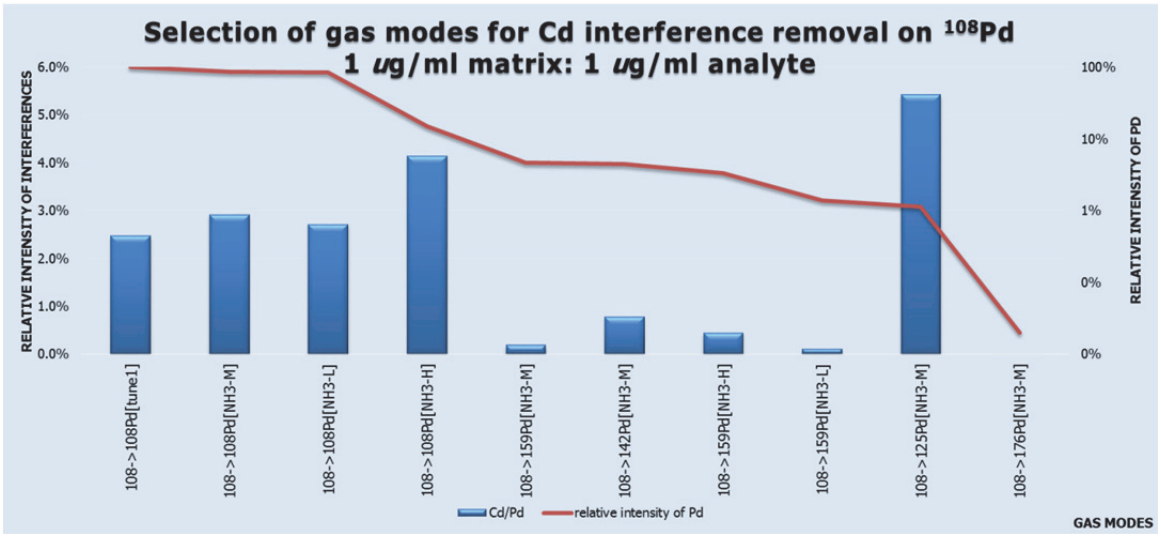

Figure 9.45: Selection of product ions for interference removal on ^{108}Pd

9.11.7 Removal of interferences on Pt isotopes

Hf and Gd interferences

$^{178,179,180}Hf^{16}O^{+}$ has severe interferences on $^{194,195,196}Pt^{+}$ isotopes and $^{178,179}Hf^{16}O^{1}H^{+}$ interfere $^{195,196}Pt^{+}$. $^{154,\ 155,\ 156,\ 158}Gd^{40}Ar^{+}$ interferences exist on $^{194}Pt^{+}$, $^{195}Pt^{+}$, $^{196}Pt^{+}$ and $^{198}Pt^{+}$. Hydrogen, oxygen and helium gases cannot remove Hf and Gd interferences. Ammonia shift-mode offer good interference removals. The product ion of Pt with least interferences are $Pt(NH_3)_2^{+}$. The major product ions of the Hf and Gd are $HfNH^{+}$ and $GdNH^{+}$ respectively with no overlap at mass unit 228, 229, 230 and 232 of $Pt(NH_3)_2^{+}$ shift modes. $Pt(NH_3)_2^{+}$ is a clustering product of ammonia and Pt. $HfNH^{+}$ and $GdNH^{+}$ are the condensation products which is also described in Jones (2007) and Lavrov (2006). $^{154}Sm^{40}Ar^{+}$ interferences on $^{194}Pt^{+}$ are minor and can be removed with $Pt(NH_3)_2$ mode. The interference removal efficiencies of each product ions are shown in Figure 9.46-Figure 9.49.

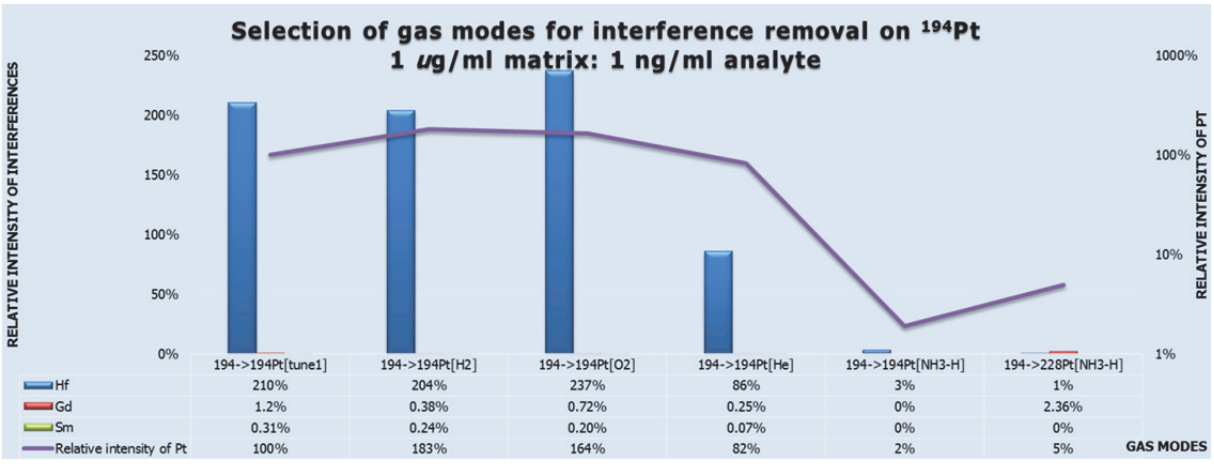

Figure 9.46: Selection of product ions for interference removal on ^{194}Pt

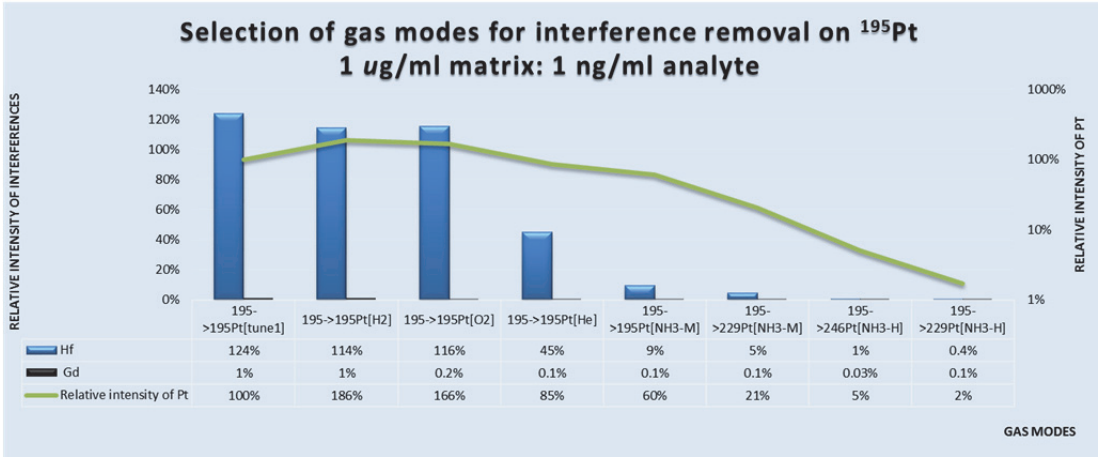

Figure 9.47: Selection of product ions for interference removal on ^{195}Pt

W interference on ^{196}Pt and ^{198}Pt and $^{181}Ta^{16}O^{1}H$ on ^{198}Pt

$^{180\text{-}182}WO^{+}$ has severe interference on $^{196}Pt^{+}$ and $^{198}Pt^{+}$. $^{181}Ta^{16}O^{1}H^{+}$ has severe interference on ^{198}Pt. For W major product ions were seen at $W(NH_3)_3^{+}$ and it does not make any product at mass-shift of 230 and 232. It can be removed with $Pt(NH_3)_2^{+}$ mode. On-mass measurement with oxygen can also be applied for W removal as W^{+} oxidises to make WO^{+}. WO^{+} is unstable product ion and changes to a stable product ion WO_2^{+} in oxygen gas stream. Ta makes $TaNH^{+}$ as major product ion and does not overlap with $Pt(NH_3)_2^{+}$. $Pt(NH_3)_2^{+}$ has also been reported in Sugiyama and Shikamori (2015) as well. The removal of interferences on $^{196,198}Pt$ is shown in Figure 9.48-Figure 9.49.

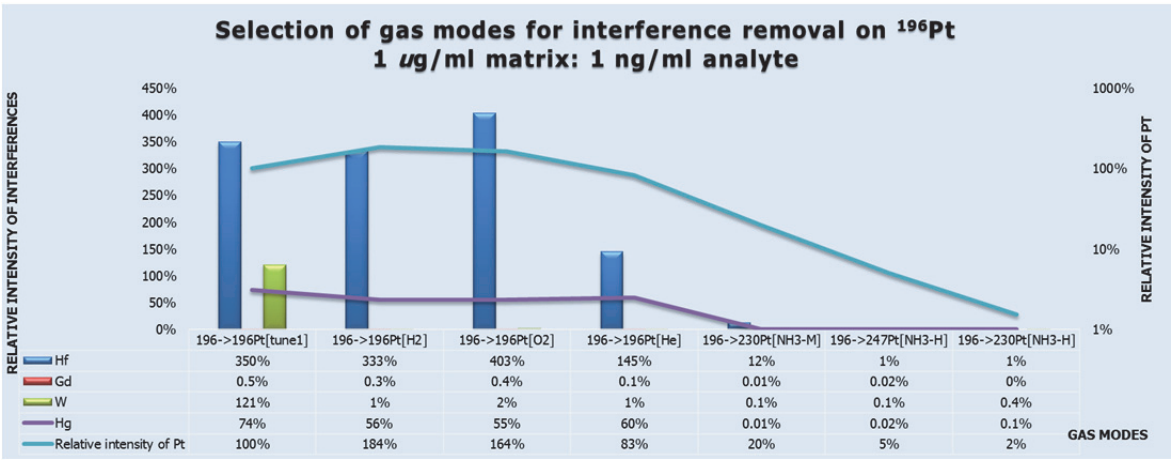

Figure 9.48: Selection of product ions for interference removal on ^{196}Pt

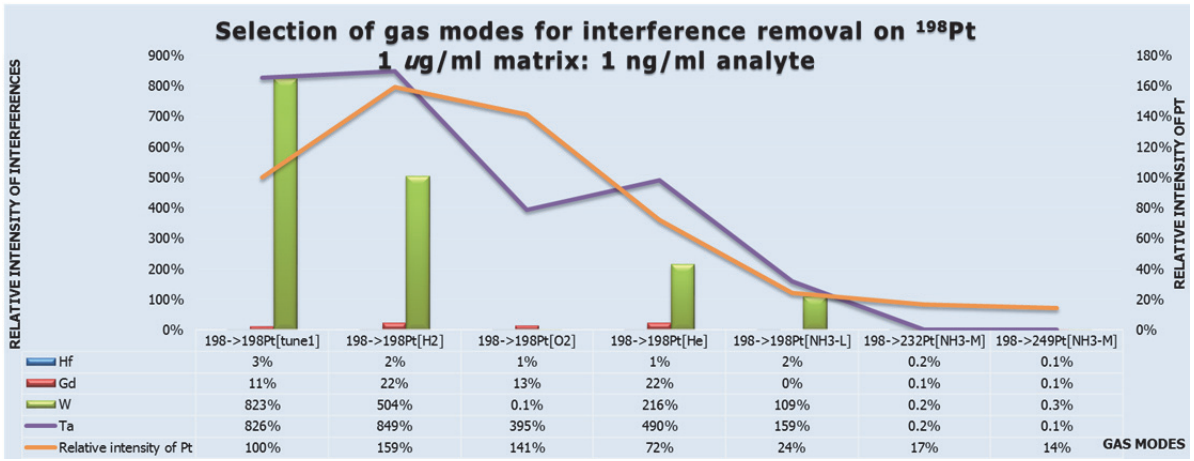

Figure 9.49: Selection of product ions for interference removal on ^{198}Pt

Hg interference on ^{196}Pt and ^{198}Pt

The product ions for Hg^+ were tested on m/z of 213, 214, 215, 232, 249 and no intensity was observed on any tested m/z unit. A similar phenomenon has been reported by Sugiyama and Kazumi (2014) for existence of any product ion using Agilent 8800 collision/reaction cell technology. Jones (2007) however, reports product ions at different flow rates and suggests a charge transfer reaction with ammonia. Glenn (2013a) reports removal of Hg interference on Pb^{2+} by charge transfer reaction. No intensity of Hg was observed at all the flow rates of ammonia i.e. 1-6 ml/min. The charge transfer reaction is exothermic and reaction is 100% efficient and is given as follows:

$$Hg^+ + NH_3 \longrightarrow Hg + NH_3^{+*}$$

The neutralised Hg becomes the leaving species from the collision/reaction cell and leaves the Pt as interference free. Therefore, Hg interference on ^{198}Pt can be fully removed with on-mass ammonia mode. The Hg removal on $^{196\text{-}198}$Pt is shown in Figure 9.49-Figure 9.50 in on-mass and mass-shift modes of ammonia. This mode and this type of reaction can be operated in single quad ICP-MS as well with ammonia gas.

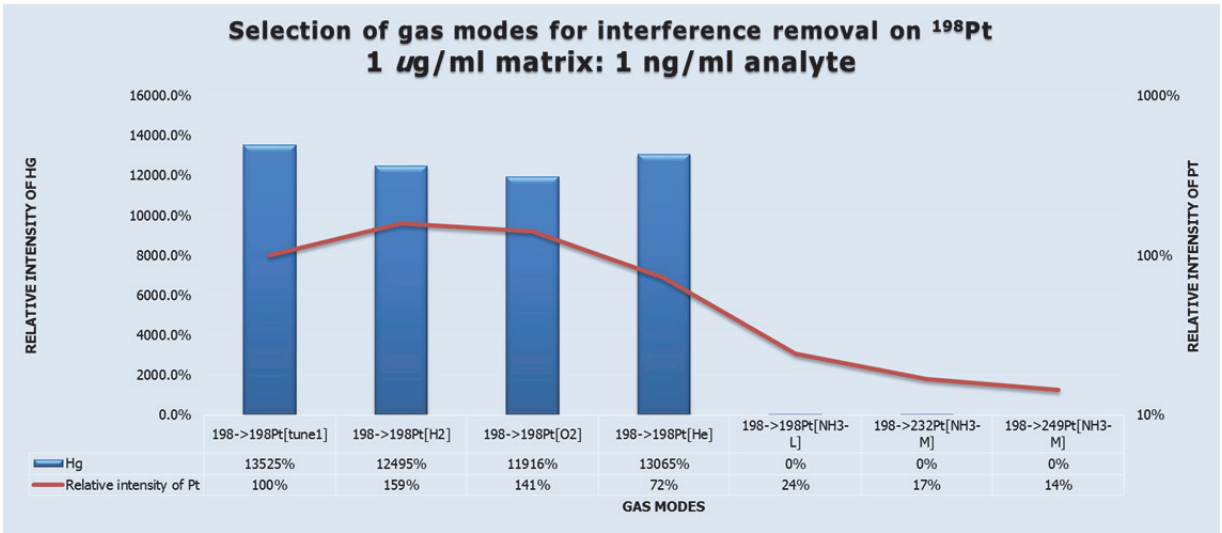

Figure 9.50: Selection of product ions for Hg removal on ^{198}Pt

9.11.8 Removal of interferences on Ir isotopes

$^{175}LuO^{+}$ and $^{151}Eu^{40}Ar^{+}$ are the interferences on $^{191}Ir^{+}$; $^{177}HfO^{+}$ is the interference on $^{193}Ir^{+}$. Hydrogen, oxygen and helium gases cannot remove these interferences. Best removal is only possible with $IrNH^{+}$ product ion. Flow rates of ammonia from 2 to 7 were tested for best signal intensities and only 2 ml/min was found to give intensities where interferences could be removed. Sugiyama and Shikamori (2015) also reports the same product ion $IrNH^{+}$ but at a different flow rate. The efficient product ions for removal of interferences are shown in Figure 9.51.

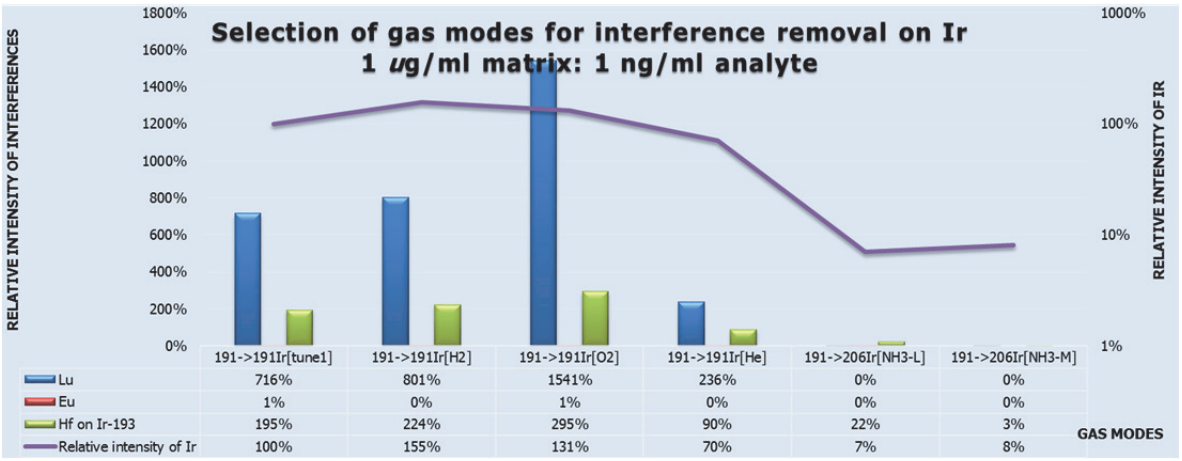

Figure 9.51: Selection of product ions for interference removal on Ir isotopes

9.11.9 Removal of interferences on Au

$^{181}TaO^{+}$, $^{180}HfOH^{+}$ and $^{157}Gd^{40}Ar^{+}$ are the interferences on Au^{+} and cannot be removed with hydrogen, oxygen and helium gases, but ammonia shift-mode can effectively remove these interferences. The product ion 197 -> 231 Au [NH3-L] has sufficient intensity of 17%. The clustering product of $Au(NH_3)_2^{+}$ has been observed by Jones (2007) using DRC, Lavrov (2006) using ICP-SIFT-MS instrument, Sugiyama and Shikamori (2015) using Agilent 8800 collision cell technology and Bokhari *et al.* (2015a) using Agilent 8800 collision cell technology. Sugiyama and Shikamori (2015) has mentioned product ion of gold for interference removal in the synthetic matrix. Diagrammatic presentation of a selection of product ions is given in Figure 9.52.

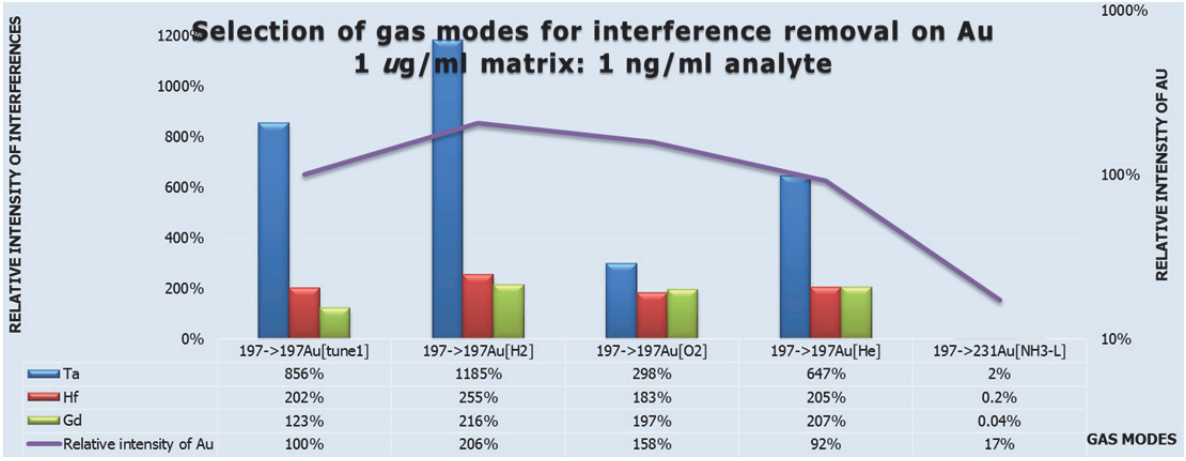

Figure 9.52: Selection of product ions for interference removal on Au

9.11.10 Removal of interferences on Os isotopes

Osmium is known for its volatile nature and rapidly oxidises to OsO_4 under oxidising conditions. OsO_4 is toxic. Osmium occurs in very low concentrations and suffers from matrix interferences. The wide application of the Re–Os isotope system is hampered by the complex chemistry that is necessary to isolate and purify osmium for Os isotopes ratio studies due to interferences. $^{171}YbO^+$, $^{147}Sm_2O_3^+$,$^{187}Re^+$,$^{186}W^1H^+$ and $^{147}Nd_2O_3^+$ are interferences on $^{187}Os^+$, $^{172}YbO^+$, $^{171}YbOH^+$, on $^{188}Os^+$, $^{173}YbO^+$ and $^{172}YbO^+$ on $^{189}Os^+$, $^{190}Pt^+$,$^{174}YbO^+$,$^{173}YbOH^+$, on $^{190}Os^+$, $^{192}Pt^+$,$^{176}YbO^+$,$^{176}Hf^{16}O^+$,$^{176}Lu^{16}O^+$ and $^{175}Lu^{16}O^1H^+$ on $^{192}Os^+$. A number of interferences from 1 µg/ml matrix on 1 ng/ml solution of Os is given in Figure 9.53. Rhenium and W are the severe interferences on Os isotopes. The study of interferences on osmium isotopes was presented in Bokhari *et al.* (2015d).

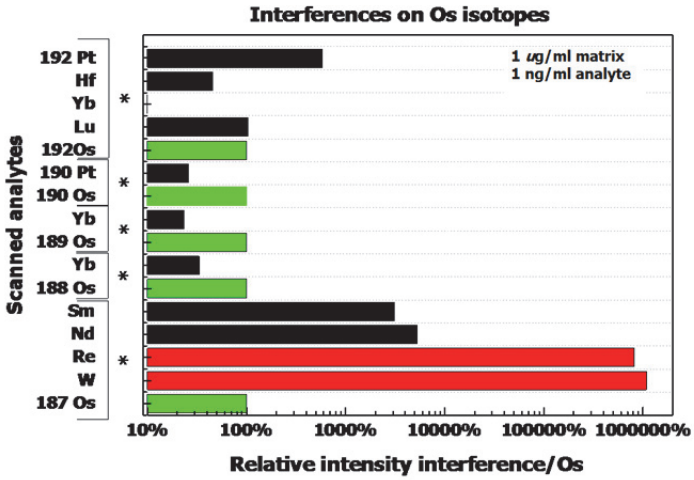

Figure 9.53: Quantity of interferences on Os isotopes

^{187}Os

$^{147}Sm^+$ and $^{147}Nd^+$ interferences can be decreased in mass-shift 187 -> 202 Os [NH_3-L], but at the cost of extreme loss in Os intensity. Os readily forms OsO_4 in nature. This volatile property of Os can be of use in collision/reaction cell to form oxides of Os. Osmium tends to make OsO^+, OsO_2^+, OsO_3^+ and OsO_4^+ in reaction collision cell also. This study presents this property of Os to be used in interference removal capacity. Yb intensity is considerably decreased with OsO_2 product ion. Sm and Nd tend to make further oxides in O_2 modes. Hydrogen gas is making hydrides of Os as well as Sm, Nd, and Yb and hence it is not good for interference removal. A further satisfactory removal of interferences is needed by optimising the flow rates of ammonia for better intensities of Os. The interference removal capability of each product ions is shown in Figure 9.54. The similar interferences on ^{188}Os and ^{189}Os also show the same patterns as in Figure 9.54.

W and Re interferences

For the purposes of interference removal of Re and W on Os, a product ion scan was made for both ions to see any decrease in intensities with the corresponding mass-shift with oxygen and ammonia gases. Re^+ undergo condensation reactions with the major product of $ReNH^+$ at flow rates of 2 ml/min. This is somewhat similar to Jones (2007) at a flow rate of 1 ml/min as shown in Figure 9.55. Jones (2007) reports identical species of rhenium using

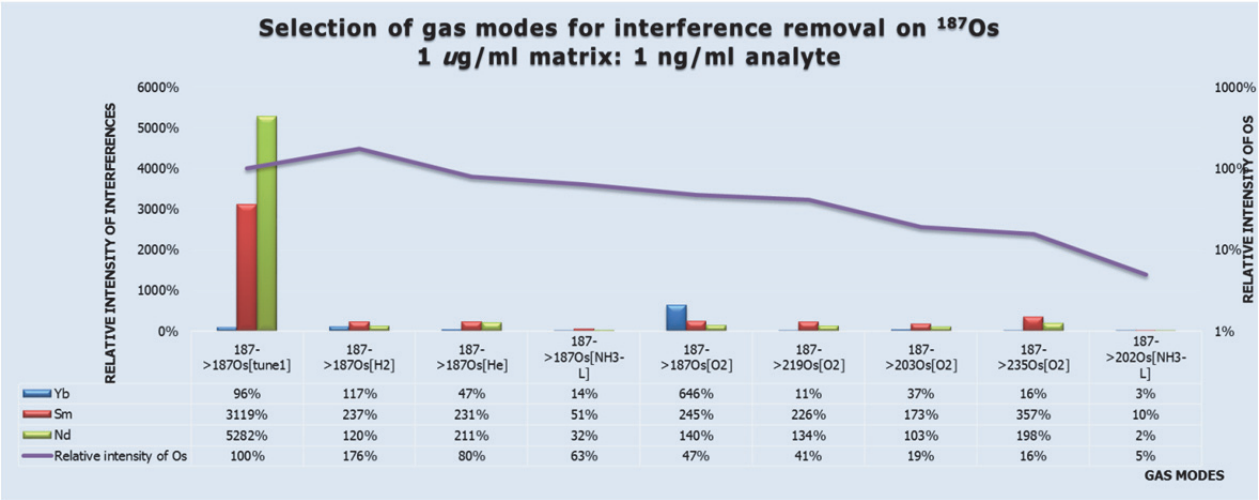

Figure 9.54: Selection of product ions for interference removal on ^{187}Os

ICP-DRC-MS instrument. However, no abundant $Re(NH_3)^+$ and $Re(NH_3)_3^+$ products were identified as reported in Lavrov (2006) using ICP-SIFT-MS instrument. For $^{182}W^+$ major product ion were seen at m/z 230 which is $W(NH_3)_3$, a higher mass unit more than 259 was not scanned for which no intensity was observed unlike (Jones 2007). Rhenium also forms oxides of the type ReO^+, ReO_2^+, ReO_3^+ and ReO_4^+ in reaction collision cell. The intensity of ReO^+ and ReO_2^+ were higher than ReO_3^+ and ReO_4^+. The use of O_2 gas in the elimination of interferences of $^{91}ZrO^+$ on $^{107}Ag^+$ has been shown in (Simpson *et al.* 2001) using collision/reaction cell (CRC) technology with ICP-MS. He converted ZrO^+ into ZrO_2^+ and ZrO_3^+ by reacting with oxygen gas. The use of O_2 has been evidenced by Guo *et al.* (2011) also. W forms oxides of the type WO^+, WO_2^+ and WO_3^+. The intensities of WO_2^+ were more than WO^+ as reported in Guo *et al.* (2011) where WO^+ drastically oxidises WO_2^+ and WO_3^+ in DRC instrument. Re and W under such circumstances cannot be separated from Os when both are forming identical product ions in reaction collision cell. Figure 9.56 shows a drastic decrease in intensities of Os in WH and Re removal at mass-shift ammonia and OsO_2^+ product ion.

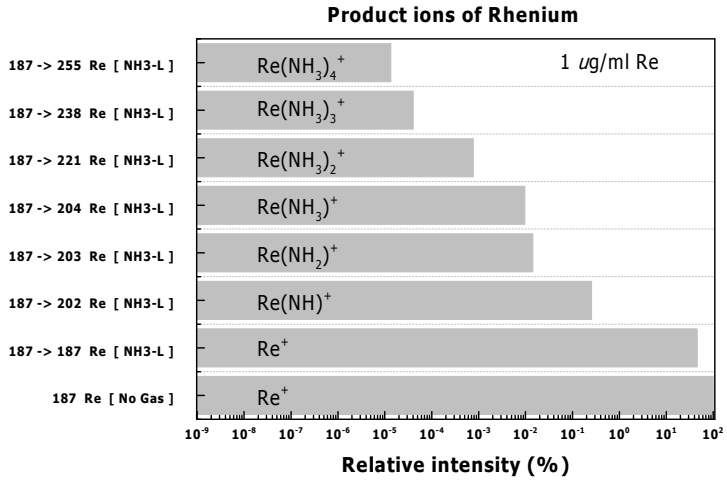

Figure 9.55: Scan of product ions of ^{187}Re

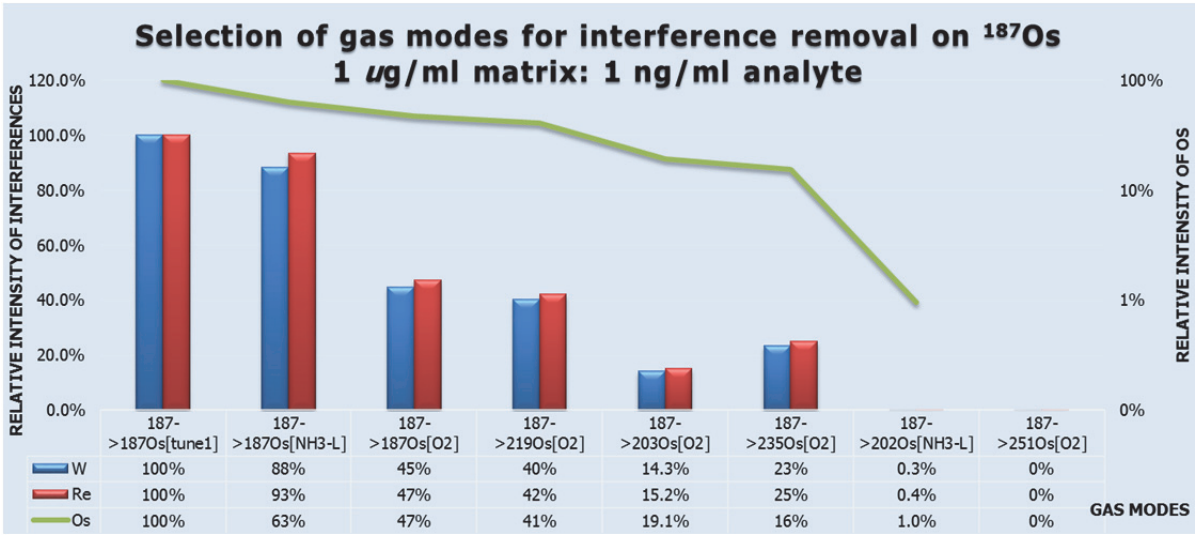

Figure 9.56: ^{186}WH and ^{187}Re removal possibilities on ^{187}Os

^{192}Os

Platinum interferences on $^{190}Os^{+}$ and $^{192}Os^{+}$ are reduced by using oxygen shift mode in oxygen gas by the formation of product ion OsO_2^{+}. Ammonia shift mode is also better but the loss of intensity of osmium is a question mark. The interference removal with oxygen and ammonia gas is shown in Figure 9.57. Lu is further oxidised in oxygen offering no practical removal in oxygen gas. Ammonia gas with shift-mode can decrease the interferences significantly. For Hf interference, oxygen mass-shift as OsO_2^{+} reduces the interference to less than 2% while relative intensity of Os^{+} is still 45% which offers a good removal of interference as shown in Figure 9.58.

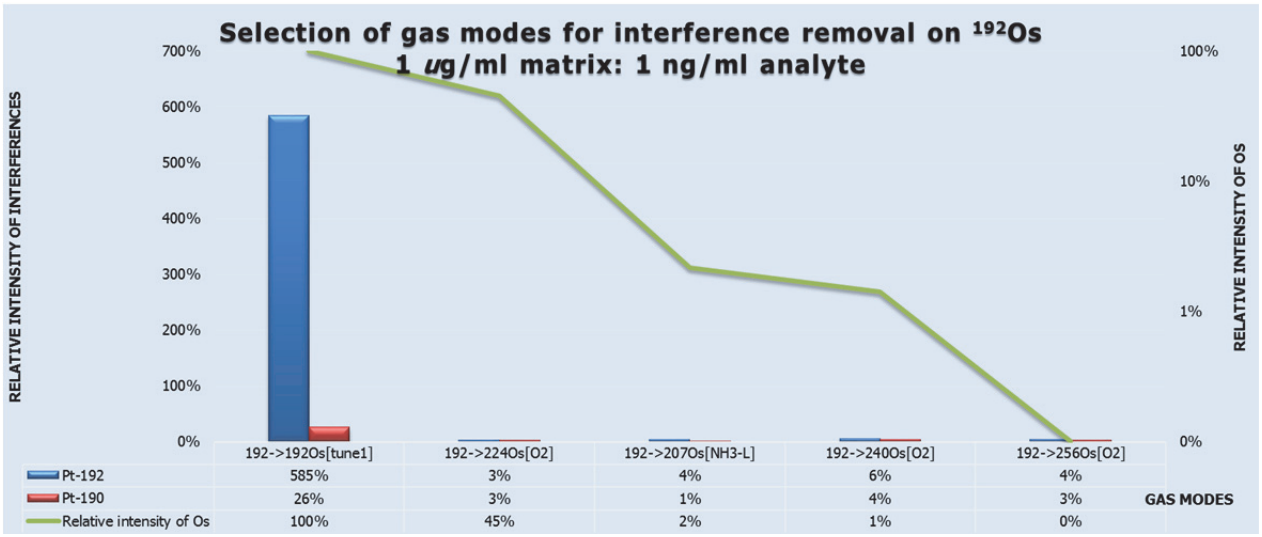

Figure 9.57: Selection of product ions for removal of Pt interference on Os isotopes

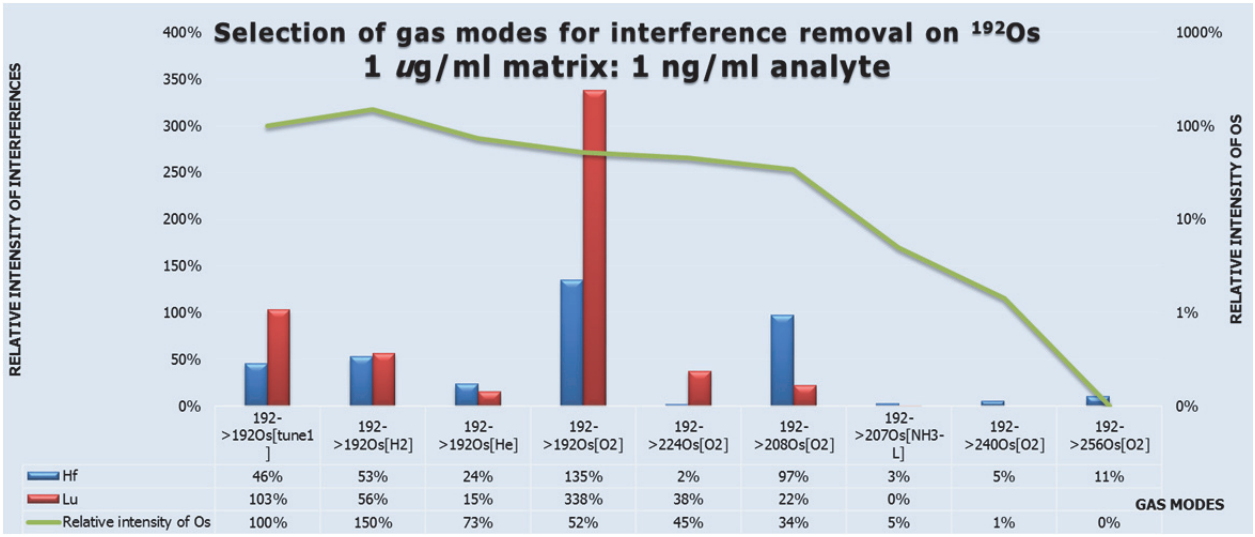

Figure 9.58: Selection of product ions for removal of Hf and Lu interference on Os isotopes

9.12 Optimised method and optimised gas flow rates for PGE determination.

After the thorough study of product ions in on-mass and mass-shift method, the best product ions were selected for interference removal on PGE-Ag isotopes and Au as shown in Table 9.4. The different colour scheme is used for different flow rates of gases. The method developed has already shown its capability for interference removal on PGE-Ag isotopes and Au in various plots. The method will now be validated by testing on reference material for platinum group elements.

9.13 Isotopic ratios of PGE-Ag

The natural isotopic ratio of PGE-Ag-Re was tested by preparing a solution of 1 ng/ml PGE and mixing with all interferences of 1 µg/ml solution. The PGE solution was prepared from 1 mg/l multi-element solution of PGE and matrix elements from Merck VI solution. The isotopic ratios were then determined with all suggested product ions studied earlier. The isotopic ratios are given in Figure 9.59-Figure 9.65. The isotopic ratios of the suggested modes are close to the natural isotopic ratios.

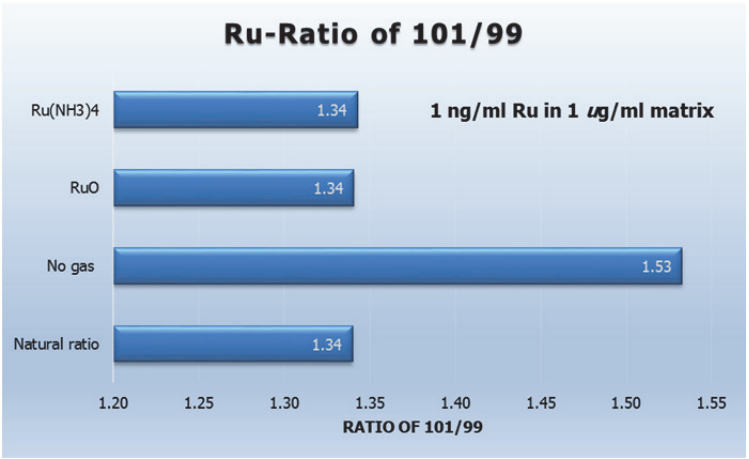

Figure 9.59: Isotopic ratio of ruthenium isotopes

Table 9.4 Optimised modes for PGE measurement

Interference	Ru	Rh	Ag	Pd	Os	Ir	Pt	Au
SrO	$Ru(NH_3)_4$	$Rh(NH_3)_4$		$Pd(NH_3)_3$				
RbO	$Ru(NH_3)_4$	$Rh(NH_3)_4$						
YO				Pd on mass				
ZrO			Ag On-Mass	Pd on mass				
NbO			Ag On-Mass					
MoH	$Ru(NH_3)_4$							
MoO				Pd on mass				
Cd				$Pd(NH_3)_3$				
HfO					$OsNH/OsO_2$	IrNH	$Pt(NH_3)_2$	$Au(NH_3)_2$
TaO							$Pt(NH_3)_2$	$Au(NH_3)_2$
NdO					OsNH			
SmO					OsNH			
GdAr								Au on mass NH_3
EuAr						IrNH		
LuO		$Rh(NH_3)_4$			$OsNH/OsO_2$	IrNH		
Pt					OsO_2			
Pd	RuO							
Pb^{++}		Rh on mass NH_3						
W							Pt-Pt $(WO_2)/Pt(NH_3)_2$	
Hg							Pt-On mass $NH_3/Pt(NH_3)_2$	
YbO					$OsNH/OsO_2$			

	Flow rate NH_3	NH3	3.0 (ml/min) M	O_2
NH3	2.0 (ml/min) L	NH3	5.0 (ml/min) H	2.0 (ml/min)

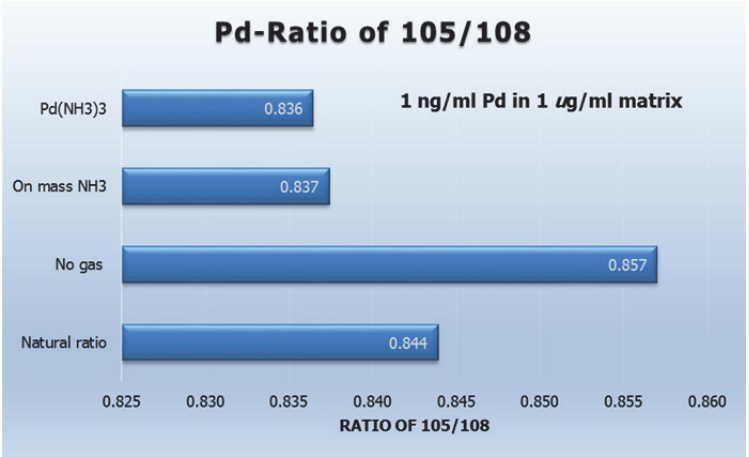

Figure 9.60: Isotopic ratio of Pd isotopes

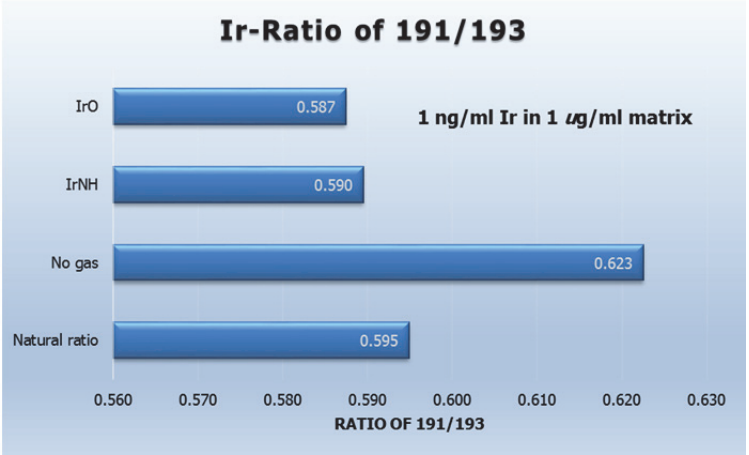

Figure 9.61: Isotopic ratio of Ir isotopes

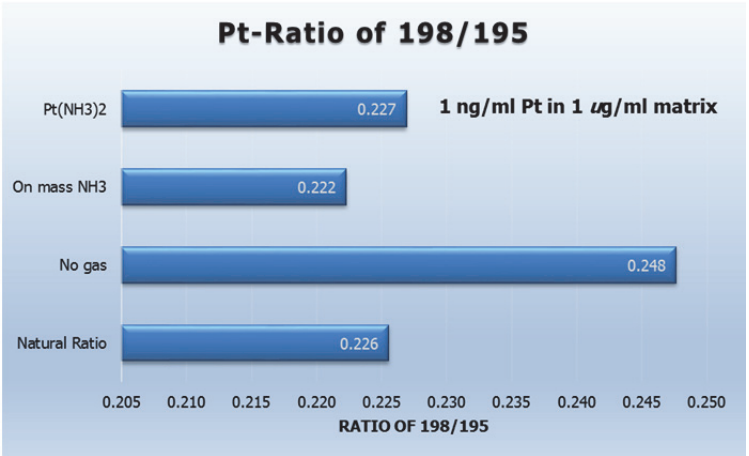

Figure 9.62: Isotopic ratio of Pt isotopes

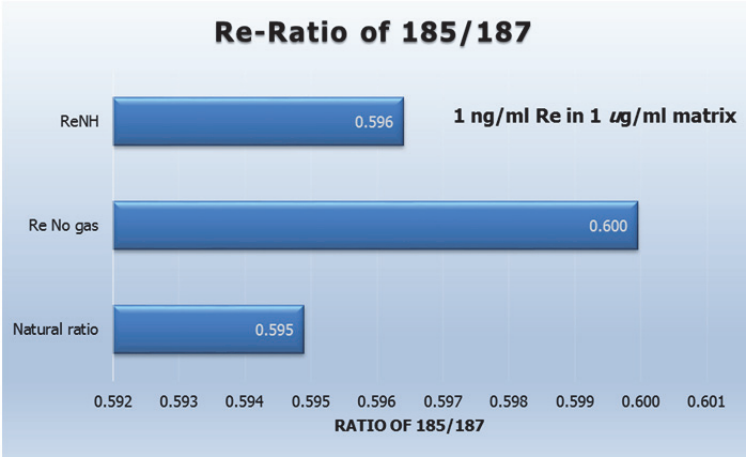

Figure 9.63: Isotopic ratio of Re isotopes

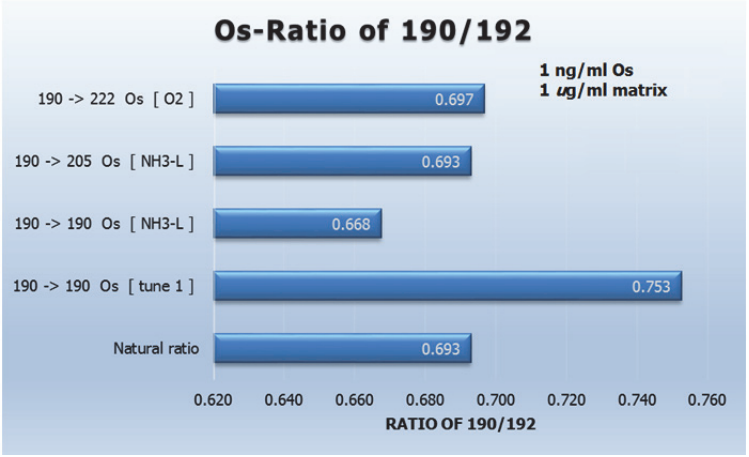

Figure 9.64: Isotopic ratio of Os isotopes

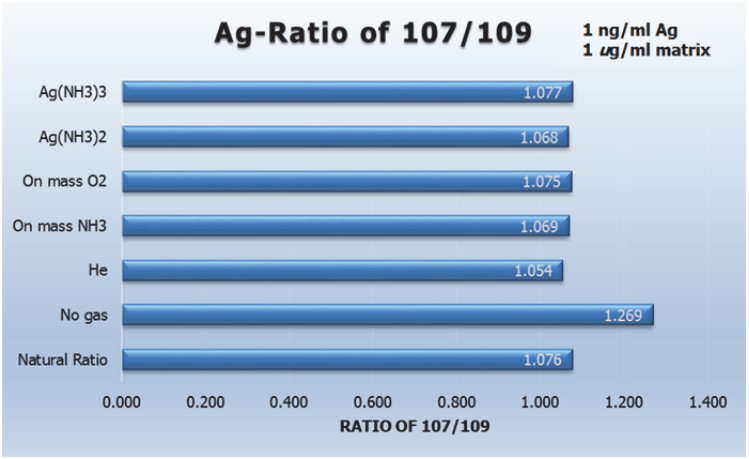

Figure 9.65: Isotopic ratio of Ag isotopes

9.14 Method validation

For the validation of the method developed for interference removal on platinum group elements and Ag isotopes several PGE reference materials were chosen i.e. PTC-1a, SARM-7, WMG-1 and IMEP-11, etc.

The PTC-1a reference material is copper-nickel sulphide concentrate with noble metals that originates from copper cliff Ontario Canada. It is a noble metal-bearing sulphide floatation concentrate of Sudbury ore. It is composed of chalcopyrite, pentlandite and pyrrhotite, with small amounts of quartz, feldspar, pyroxene, epidote, mica, pyrite and bravoite (CANMET 2012).

SARM-7 is a platinum ore reference material prepared by the council of mineral technology (MINTEK) South Africa. The material is a composite of samples from the Merensky reef in the Bushveld complex South Africa. The material is mainly consisting of felsphathic pyroxenite. Major constituents are pyroxene, olivine, serpentine, and plagioclase. Minor constituents are chromites, pentlandite, chalcopyrite, and pyrrhotite. The platinum minerals are mainly ferroplatinum, sperrylite, braggite, and moncheite (MINTEK 1975).

WMG-1 is mineralised gabbro with gold and PGE. The raw material for WMG-1 was obtained from the Wellgreen complex, Canada and was certified by a geological survey of Canada. The material mainly consists of pyroxene with prehnite, amphibole, chlorite and accessory magnetite, ilmenite and titanite. Mineralisation consists chiefly of chalcopyrite, pyrrhitite, pendlandite, violarite and altaite (GSC 2004).

IMEP-11 is a car exhaust catalyst material and was obtained from German car manufacturers. It was prepared at the MRM-unit at IRMM organized by the international measurement evaluation program (IMEP). The material is only certified for Pt, so only platinum data has been reproduced by current study for method validation with collision/reaction cell technology (Held *et al.* 1999).

The reference materials were digested with sodium peroxide sintering. The ratio of sample and sodium peroxide was kept 1:5 to keep the blanks as low as possible. PGE dissolve well in HCl, therefore, the calibration solutions were prepared in 0.1MHCl of different concentration ranging from 0 to 50 ng/g. (1 μg/g) solutions of germanium (Ge) and bismuth (Bi) were used as internal standard to control the instrument drift during measurement. Linear regression was used for drift correction. The instrument optimum tuning configurations are given in Table 9.2.

Table 9.5 Blanks, detection limits and BECs

Blanks, detection limits and BECs								
Tune Step	**Scan Type**	**Q1**	**Q2**	**Name**	**R**	**b (blank)**	**DL**	**BEC**
						pg/ml	pg/ml	pg/ml
No gas	Single Quad		197	Au	0.998	0.003	2	0
NH_3-L	MS/MS	197	197	Au	1.000	0.008	1	1
NH3-L	MS/MS	197	231	Au	1.000	0.004	1	0.5
No gas	Single Quad		191	Ir	0.998	0.023	4	1
No gas	Single Quad		193	Ir	0.998	0.009	1	0.3
NH_3-L	MS/MS	191	206	Ir	1.000	0.000	0	0
NH_3-L	MS/MS	193	208	Ir	1.000	0.000	0	0
No gas	Single Quad		105	Pd	1.000	0.126	33	22
NH_3-M	MS/MS	105	105	Pd	0.999	0.007	5	2
No gas	Single Quad		108	Pd	0.999	0.252	17	35

NH_3-M	MS/MS	108	108	Pd	0.999	0.051	57	11
NH_3-M	MS/MS	105	156	Pd	0.999	0.005	0.2	5
NH_3-M	MS/MS	108	159	Pd	0.999	0.001	6	1
No gas	Single Quad		195	Pt	0.999	0.026	4	3
NH_3-M	MS/MS	195	195	Pt	1.000	0.004	1	1
No gas	Single Quad		198	Pt	0.999	0.071	50	30
NH_3-M	MS/MS	198	198	Pt	1.000	0.002	10	3
NH_3-M	MS/MS	195	229	Pt	1.000	0.004	5	2
NH_3-M	MS/MS	198	232	Pt	1.000	0.002	22	5
No gas	Single Quad		185	Re	0.999	0.009	1	0.4
No gas	Single Quad		187	Re	0.998	0.018	1	0.5
NH_3-L	MS/MS	185	200	Re	1.000	0.000	0	0
NH_3-L	MS/MS	187	202	Re	1.000	0.000	0	0
No gas	Single Quad		103	Rh	0.999	0.199	2	5
O_2	MS/MS	103	103	Rh	0.999	0.167	0.2	3
NH_3-M	MS/MS	103	171	Rh	1.000	0.001	0.3	0.1
No gas	Single Quad		99	Ru	0.999	0.510	71	93
No gas	Single Quad		101	Ru	0.999	0.302	40	40
O_2	MS/MS	99	115	Ru	0.998	0.011	28	18
O_2	MS/MS	101	117	Ru	0.999	0.018	43	22
NH_3-M	MS/MS	99	167	Ru	1.000	0.012	11	11
NH_3-M	MS/MS	101	169	Ru	1.000	0.018	14	11
NH_3-H	MS/MS	107	107	Ag	0.998	0.302	40	40
NH_3-H	MS/MS	109	109	Ag	0.998	0.011	28	18

The blanks, detection limits and BECs are given in Table 9.5. (b) refers to the procedural blank. DL are the detection limits DL= (3 times the standard deviations of blank concentration/slope of the curve). BECs refer to background equivalent concentrations of the analytes BEC= (Blank concentrations/slope of the curve). R is the coefficient of linear regression obtained from the curve of matrix-matched calibrations with reference materials. The background equivalent concentrations were calculated by dividing procedural blank concentrations with a slope of the calibration curve. The blanks are determined from calibration blank, which are of the 0-10 pg/g range. The detection limits are determined after several rinses of 0.1 mol/l HCl and 1% HNO_3. The very low detection limits indicate the high sensitivity of the instrument. The BECs are also presenting a low budget for PGE and Ag, Au and Re in each product ions.

Table 9.6: PGE budget of procedural blank

PGE blanks of Na_2O_2 (pg/g)								
Ru	Rh	Pd	Pt	Ir	Re	Au	Os	Ag
22	<1	66	37	22	13	56	>1	100

The procedural blank with Na_2O_2 which is used as a flux in sample digestion is given in Table 9.6. The procedural blank involves sodium peroxide which is also used in sample preparation of samples as well in the ratio of 1:5 sample: sodium peroxide. The current data for PGE blanks is based on four blanks which were used in this measurement.

9.15 Calibrations

The multi stock PGE standard solution was used to establish calibration for the measurement of geological reference material in method suggested earlier. Several calibration points were achieved with solutions of concentration ranging from 0.1 ng/g to 50 ng/g. Ge, In and Re were used as internal standard for monitoring instrument drift and for plotting signal intensities of the analyte a function of intensities of the internal standard. The calibration plots for each suggested gas mode after the initial testing on the pure solution are given in this section for each PGE analyte. The functionality of each suggested gas mode can be seen from the calibration plot itself. A better precision calibration plot was obtained by setting greater integration time for analysis of the analytes. The calibration plots for each PGE are shown in Figure 9.66.

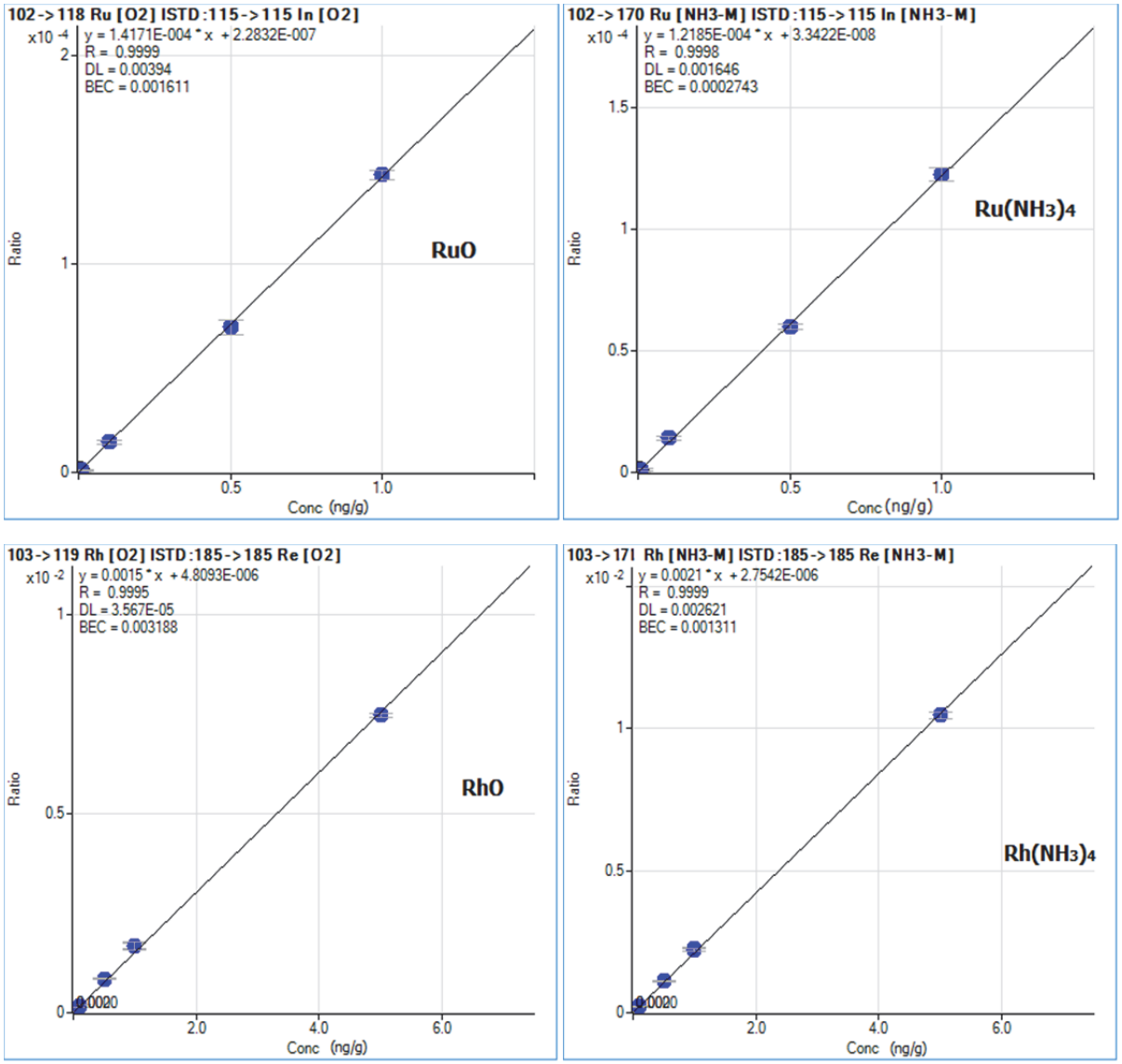

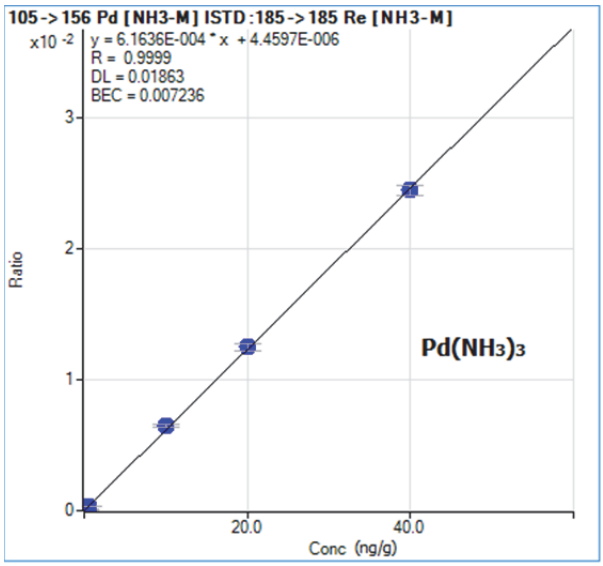
105->156 Pd [NH3-M] ISTD:185->185 Re [NH3-M]
x10 -2
y = 6.1636E-004 * x + 4.4597E-006
R = 0.9999
DL = 0.01863
BEC = 0.007236
Ratio
Conc (ng/g)
Pd(NH3)3

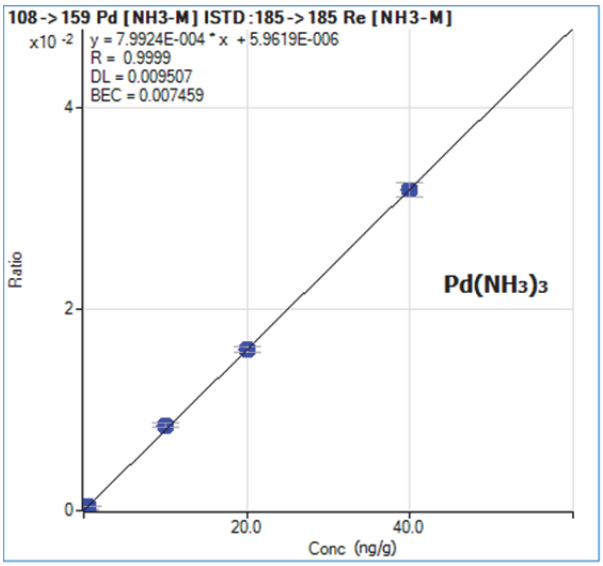
108->159 Pd [NH3-M] ISTD:185->185 Re [NH3-M]
x10 -2
y = 7.9924E-004 * x + 5.9619E-006
R = 0.9999
DL = 0.009507
BEC = 0.007459
Ratio
Conc (ng/g)
Pd(NH3)3

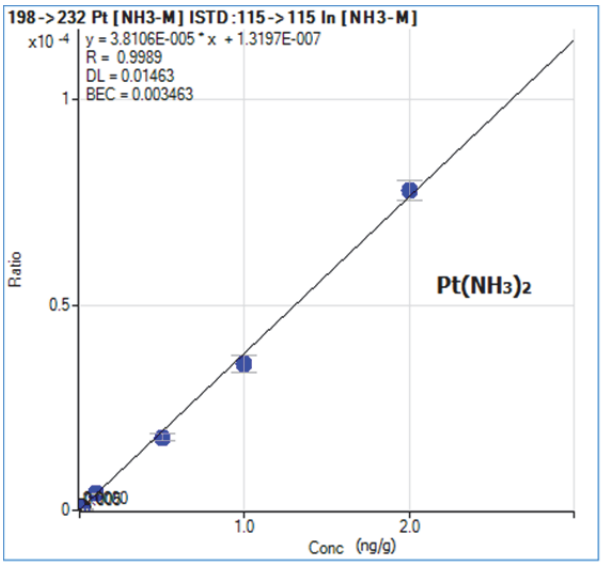
198->232 Pt [NH3-M] ISTD:115->115 In [NH3-M]
x10 -4
y = 3.8106E-005 * x + 1.3197E-007
R = 0.9989
DL = 0.01463
BEC = 0.003463
Ratio
Conc (ng/g)
Pt(NH3)2

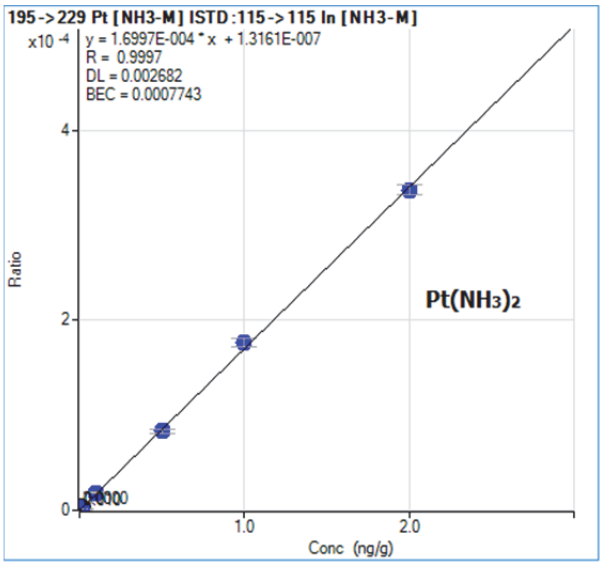
195->229 Pt [NH3-M] ISTD:115->115 In [NH3-M]
x10 -4
y = 1.6997E-004 * x + 1.3161E-007
R = 0.9997
DL = 0.002682
BEC = 0.0007743
Ratio
Conc (ng/g)
Pt(NH3)2

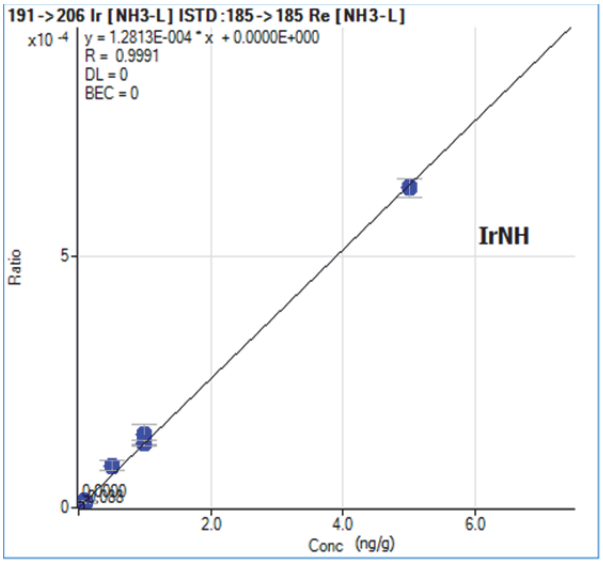
191->206 Ir [NH3-L] ISTD:185->185 Re [NH3-L]
x10 -4
y = 1.2813E-004 * x + 0.0000E+000
R = 0.9991
DL = 0
BEC = 0
Ratio
Conc (ng/g)
IrNH

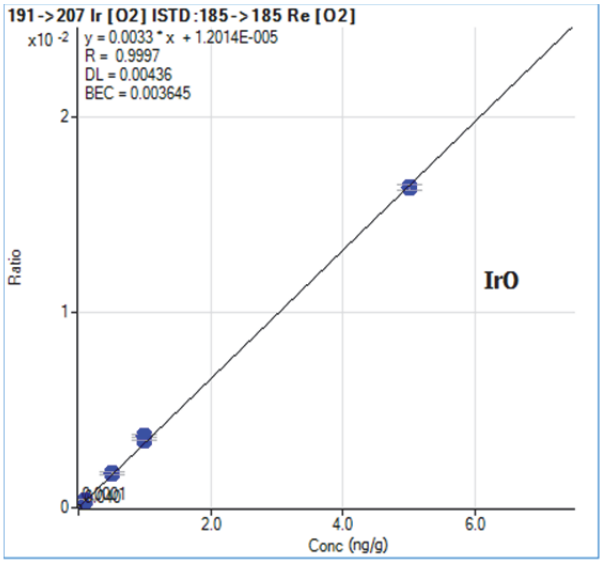
191->207 Ir [O2] ISTD:185->185 Re [O2]
x10 -2
y = 0.0033 * x + 1.2014E-005
R = 0.9997
DL = 0.00436
BEC = 0.003645
Ratio
Conc (ng/g)
IrO

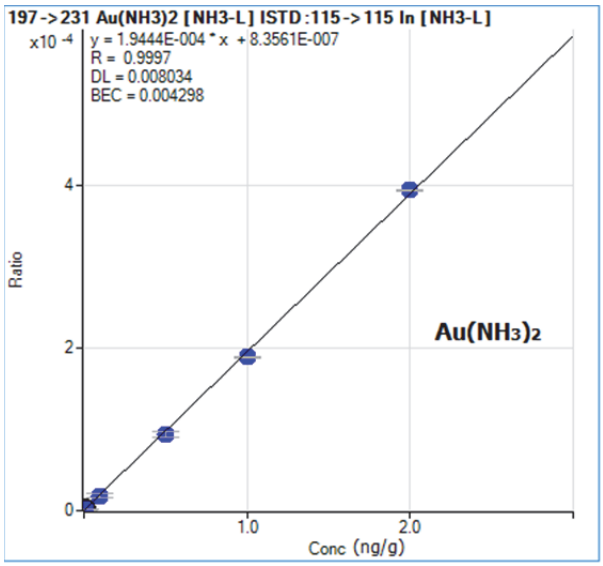

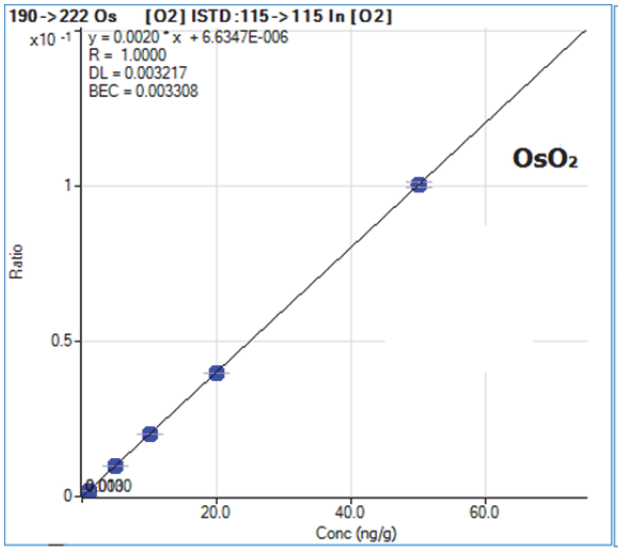

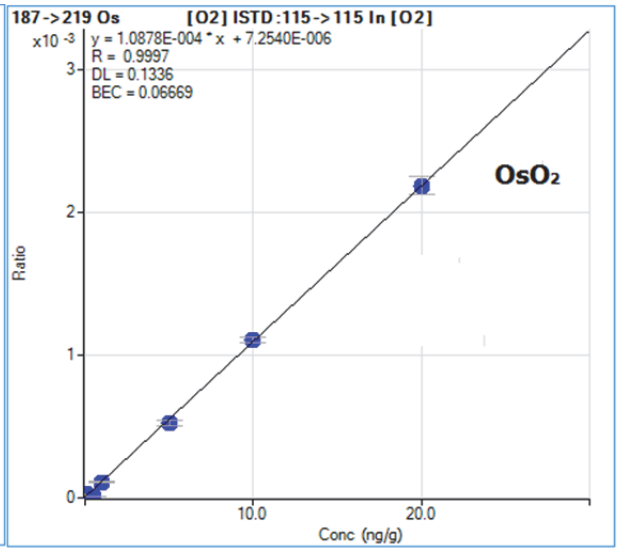

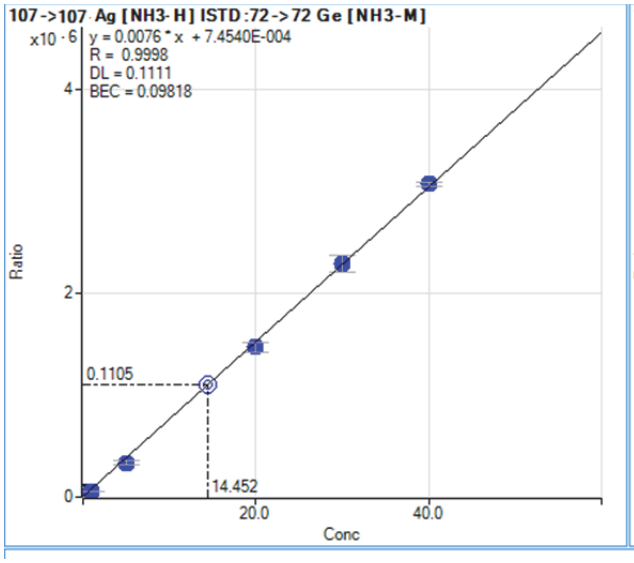

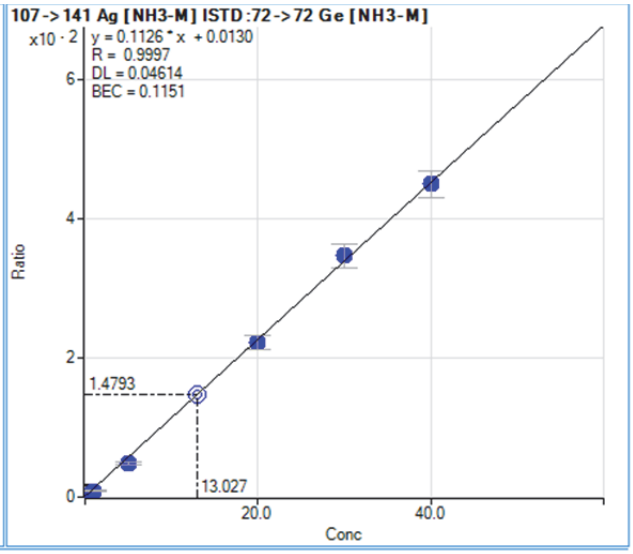

Figure 9.66: Calibration plots PGE-Ag-Au

9.16 Results and discussion

The results of the measurement in each gas mode with ammonia and oxygen in on-mass and mass-shift methods are given in Table 9.7.

RuO^+ and $Ru(NH_3)_4^+$ product ions were used in collision/reaction cell of Agilent 8800. The measurement using single quad mode results in high fractions of ruthenium as indicated in Table 9.7. The results of Ru determined with RuO^+ and $Ru(NH_3)_4^+$ suggested modes are in good agreement with the reference values. The precision of the measurement can be improved by setting longer integration times. The flow rates of ammonia are best between 2-3 ml/min.

Rhodium was measured as Rh^+ on-mass O_2, mass-shift RhO^+, mass-shift $Rh(NH_3)_4^+$. The interferences in the single quad in no gas modes results in Rh mass fraction into higher values, but measurement in suggested gas modes and product ions are better than in no gas modes. Results of the measurement lie close to the reference values. The best flow rates are between 2-3 ml/min of ammonia gas. The results are shown in Table 9.7.

Pd was measured in on-mass (NH_3-L) low flow rate of ammonia and cluster ion of shift-mode of ammonia $Pd(NH_3)_3^+$. The interferences, several order higher the magnitudes of the reference value may not be correct in case of very low Pd mass fraction for $Pd(NH_3)_3^+$. The best flow rates of ammonia are 2-3 ml/min. The results are shown in Table 9.7.

$Pt(NH_3)_2^+$ and on-mass ammonia mode are the best for Pt determination in reference material as shown in Table 9.7. Similar cluster ions of gold $Au(NH_3)_2^+$ can be applied for the measurement of gold in reference materials. The results lie in good agreement with certified values of RM. The flow rates of ammonia for platinum are 3 ml/min and for gold are 2 ml/min.

Iridium and Os were measured with $OsNH^+$ and $IrNH^+$ product ions. OsO_2 was also tested for its capability for interference removal. Results of one reference material are shown as the osmium loses are higher due to its volatility as OsO_4. The sample digested with sodium peroxide loses Os as OsO_4. As far as the capability of the method is concerned using $OsNH^+$ and OsO_2^+, it is shown provide good results. Iridium was also measured as IrO^+ and results, well in the determination of Ir in reference material. The flow rates were 2 ml min of ammonia. The results are shown in Table 9.7. For Ag, on-mass measurement with medium flow rates of ammonia serves the best. The product ions $Ag(NH_3)$ and $Ag(NH_3)_2$ also provide good results. Helium gas is better for ^{107}Ag but has higher RSDs. Simpson *et al.* (2001) used O_2 gas and our tests with oxygen gas affirm his tests as well. Although in our initial testing of standard solutions of 1 mg/l (matrix): 1ng/g (analyte) oxygen was not better. But when oxygen gas modes are applied with little higher flow rates 3ml/min than flow rates of 2.3 ml/min, the interferences from Ta, Zr and Nb are removed. Results are shown Table 9.7.

Table 9.7: Determination of PGE mass fractions in geological reference materials

Averages of mass fractions in geological reference materials								
Ruthenium (mg/kg) n=4								
	SARM-7		**PTC-1a**		**WMG-1**		**IMEP-11**	
	Determined	Precision	Determined	Precision	Determined	Precision	Determined	Precision
Reference value	0.43	13%	0.21	5%	0.035	15%		
^{99}Ru-No gas	0.448	2%	0.31	9%	0.157	21%		
^{99}RuO	0.427	1%	0.17	1%	0.044	24%		
$^{99}Ru(NH_3)_4$	0.43	1%	0.23	12%	0.062	14%		
^{101}Ru-No gas	0.54	3%	0.44	33%	0.157	5%		
^{101}RuO	0.43	1%	0.19	5%	0.060	19%		
$^{101}Ru(NH_3)_4$	0.45	3%	0.24	6%	0.065	6%		
Rhodium (mg/kg) n=4								
Reference Value	0.24	1%	0.33	18%	0.026	8%		
103 -> 103 Rh [No gas]	0.50	19%	1.27	27%	0.133	1%		
103 -> 103 Rh [O2]	0.21	2%	0.31	7%	0.021	6%		
103 -> 103 Rh [He]	0.21	6%	0.23	7%	0.019	12%		
103 -> 103 Rh [NH3-M]	0.21	9%	0.35	4%	0.014	4%		
103 -> 119 Rh [O2]	0.23	4%	0.17	2%	0.038	5%		
103 -> 171 Rh [NH3-M]	0.22	6%	0.35	1%	0.020	7%		
Palladium (mg/kg) n=4								
Reference Value	1.53	2.0%	4.481	3%	0.382	3%		
105 -> 105 Pd [No gas]	1.51	4.0%	5.661	32%	1.033	19%		
105 -> 105 Pd [NH3-M]	1.43	8.0%	4.492	4%	0.366	11%		
105 -> 156 Pd [NH3-L]	1.36	0.9%	4.876	4%	0.379	4%		

108 -> 108 Pd [No gas]	1.36	4.0%	5.189	21%	0.87	20%		
108 -> 108 Pd [NH3-M]	1.56	2.0%	5.094	4%	0.345	11%		
108 -> 159 Pd [NH3-L]	1.61	4.0%	4.782	3%	0.425	18%		
Platinum (mg/kg) n=4								
Reference value	3.74	1%	2.72	4%	0.73	5%	2190	17%
195 -> 195 Pt [No gas]	3.71	2%	2.14	5%	0.619	9%	2500	3%
195 -> 229 Pt [NH3-M]	3.83	9%	2.33	12%	0.67	21%	2067	10%
195 -> 246 Pt [NH3-M]	3.78	2%	2.47	5%	0.695	3%	2225	3%
198 -> 198 Pt or Hg [No gas]	3.83	3%	2.01	6%	0.658	3%	2310	4%
198 -> 198 Pt or Hg [O2]	3.48	0%	2.09	3%	0.68	5%	1901	1%
198 -> 198 Pt or Hg [NH3-M]	3.54	3%	2.19	6%	0.65	6%	1921	4%
198 -> 232 Hg [NH3-L]	3.56	4%	2.19	7%	0.672	6%	2017	5%
198 -> 249 Hg [NH3-M]	3.42	1%	2.45	4%	0.681	5%	2139	2%
Iridium (mg/kg) n=4								
Reference Value	0.07	16%	0.110	27%	0.0460	9%		
191 -> 191 Ir [No gas]	0.07	1%	0.088	2%	0.0500	0.2%		
191 -> 206 Ir [NH3-L]	0.08	3%	0.069	2%	0.0320	3%		
191 -> 207 Ir [O2]	0.06	1%	0.070	1%	0.0380	1%		
193 -> 193 Ir [No gas]	0.06	1%	0.078	2%	0.0510	1%		
193 -> 208 Ir [NH3-L]	0.08	2%	0.141	2%	0.0430	2%		
193 -> 209 Ir [O2]	0.07	2%	0.100	1%	0.0540	2%		
Gold (mg/kg) n=4								
Reference Value	0.31	5%	1.31	8%	0.11	10%		
197 -> 197 Au [No gas]	0.66	11%	1.70	23%	0.35	76%		
197 -> 197 Au [He]	0.30	9%	1.19	23%	0.34	17%		
197 -> 197 Au [NH3-L]	0.31	8%	1.29	22%	0.12	15%		
197 -> 231 Au(NH3)2 [NH3-L]	0.28	18%	1.04	2%	0.11	15%		

Silver (mg/kg) n =4				
	PTC-1a		WMG-1	
Product ions	Determined	Precision	Determined	Precision
Reference Value	56.0	3%	2.70	11%
107 -> 107 Ag [tune 1]	63.3	3%	4.38	4%
107 -> 107 Ag [O2]	56.8	6%	2.33	1%
107 -> 107 Ag [He]	56.1	4%	2.80	18%
107 -> 107 Ag [NH3-M]	58.7	1%	2.53	4%
107 -> 124 Ag [NH3-M]	60.4	15%	2.33	3%
107 -> 141 Ag [NH3-M]	58.7	2%	2.36	1%
109 -> 109 Ag [tune 1]	56.7	3%	4.24	5%
109 -> 109 Ag [O2]	55.9	6%	2.84	19%
109 -> 109 Ag [He]	53.0	18%	2.95	16%
109 -> 109 Ag [NH3-M]	59.2	1%	2.55	3%
109 -> 126 Ag [NH3-M]	59.1	1%	2.73	18%
109 -> 143 Ag [NH3-M]	58.5	2%	2.75	16%

Osmium (mg/kg) n=4		
	WMG-1	
Product ions	Determined	Precision
Reference Value	0.024	4%
189 -> 189 Os [No gas]	0.095	11%
189 -> 204 Os [NH3-L]	0.088	1%
189 -> 221 Os [O2]	0.032	4%

9.17 Summary

This study demonstrates the effectiveness of the MS/MS reaction cell using NH_3 and O_2 for the removal of spectral interferences on PGE analytes. This chapter has highlighted the analytical significance and magnitude of a number of oxide-based interferences on PGE isotopes in terms of background equivalent concentration created by matrix elements on PGE blank. A 1 µg/ml matrix solution of pure elements was used to investigate against 1 ng/ml solution of PGE isotopes. From the data on background equivalent concentration of matrix elements and generation of oxide species, their significance as a potential source of error can be predicted on crustal abundances. It has been shown that the collision/reaction cell is effective in removing oxide-based interferences through the use of reactive gases i.e. O_2 and ammonia etc.

This study shows the comparison of the gases for example helium, oxygen, hydrogen and ammonia in the signal reduction of matrix elements on each PGE isotope graphically. The oxygen and ammonia gases are far better than helium and hydrogen gases. The no gas mode is never good even under controlled lowest oxide i.e. CeO^+/ Ce^+.

Method developed was based on the reactions of PGE isotopes with ammonia and oxygen gases. The study of reactions of PGE isotopes was done in on-mass measurement with oxygen and ammonia gases. This study has shown that Ir and Os are most reactive PGE analytes to ammonia gas. The order of reactivity of PGE isotopes is Os>Ir>Pt>Rh>Pd>Ag>Ru>Au etc. This order matches with the natural existence of PGE isotopes e.g. Osmium and Iridium are mostly found together in nature and behave similarly. The reaction efficiencies of PGE analytes with oxygen gas show that Pt does not react efficiently with oxygen gas. The decrease in intensities of PGE analytes was observed for Pd, Os, Ir and Au, which ensures the formation of oxide product ions. Ru and Rh also undergo oxidation to make oxides.

It has been shown that the oxides of the matrix elements which are Nd, Sm, Cd, Rb, Eu, Pb, Sr show less reactivity with ammonia gas. On the other hand, Hg, Nb, Zr, Lu, Hf, Y, Ta, W and Gd show the most reactivity with ammonia gas. The reactivity of PGE is enveloped in between these two groups of matrix elements, which makes the basis of separation of matrix elements from PGE analytes inside collision/reaction cell.

This chapter has described the possible chemical reactions of PGE and matrix elements that occur with the use of different reactive gases i.e. ammonia and oxygen in particular. An understanding of the mechanism of the formation of the type of product ions was briefly discussed related to earlier studies using ICP-DRC-MS and SIFT etc.

Understanding of mechanism of ion-molecule formation of PGE analytes and matrix elements via clustering, addition, charge transfer or condensation reaction has offered two acquisition modes for their separation i.e. on-mass mode and mass-shift mode. Ammonia gas offered a variety of options for method development for matrix element separation. Oxygen gas also served to remove interferences e.g. RuO^+ formation removed interferences of Pd^+, IrO^+ has shown a reduction in interferences on Ir^+. Oxygen mass-shift mode successfully utilises volatile nature of Os to make abundant OsO_2^+ product ion. OsO_2^+ was used in the reduction of Yb^+ and Hf interferences on Os^+. From the given reactivities of the matrix elements and PGE analytes following product ions were suggested,

1. Ru as $Ru(NH_3)_4^+$ and RuO^+,
2. Rh as $Rh(NH_3)_4^+$ and on-mass ammonia,
3. Pd as $Pd(NH_3)_3^+$ and on-mass ammonia,
4. Ir as $IrNH^+$ and IrO^+,
5. Os as $OsNH^+$ and OsO_2^+,
6. Pt on-mass-ammonia and $Pt(NH_3)_2^+$,
7. Ag as on-mass ammonia,
8. Au as on-mass ammonia and $Au(NH_3)_2^+$.

The suitable flow rates of ammonia gas are given in Table 9.4.

With charge transfer reactions, in on-mass measurement of Pt and Rh in ammonia gas, Hg and Pb interferences can be effectively removed. Rhenium and W interferences on ^{187}Os are problematic because both make identical products ions in ammonia and oxygen gas.

The product ions of PGE formed through clustering reactions are $M(NH_3)_x^+$. These include $Pt(NH_3)_2^+$, $Pd(NH_3)_3^+$, $Au(NH_3)_2^+$, $Ru(NH_3)_4^+$, $Rh(NH_3)_4^+$ and $Ag(NH_3)_2^+$ etc. The product ions of PGE formed through condensation reactions are MNH^+ ($IrNH^+$, $OsNH^+$, and $ReNH^+$) etc.

The chapter provides data on determined values of mass fractions of PGE reference materials with suggested method. Method is validated and can be applied for PGE determination on similar reference material.

10. Method development for PGE determination with sintering and tellurium co-precipitation in geological reference material

10.1 Introduction and background

Alkali fusions provide an effective mean of dissolving highly refractory phases (Reisberg and Meisel 2002). The main advantage of alkali fusions is the effective dissolution of both refractory and sulphide mineral phases (Woodland 1999). Use of sodium peroxide + NaOH has been reported to be very effective for geological sample for PGE analysis (Chao and Sanzolone 1992, Corbett *et al.* 1974, Doleal and Povondra 1963, Enzweiler and Potts 1995, Enzweiler *et al.* 1995, Evans and Giglio 1993, Jarvis *et al.* 1997b, Jin and Zhu 2000, Markey *et al.* 1998, Qi *et al.* 2003, Seelye and Rafter 1950, Totland *et al.* 1995, Yi and Masuda 1996b). PGM are attacked by alkaline hydroxides in the presence of oxidising agents i.e. sodium peroxide or nitrates (Balcerzak 2002b). Sample mass with sodium peroxide fusion ranges from 0.5 to 2.0 g at temperatures higher than the melting temperature of sodium peroxide (Chao and Sanzolone 1992).

The Na-based fusions have been reported to be very rapid compared to the borate fusions as described in studies by Totland *et al.* (1995). Totland *et al*. (1995) describes that the flux melted in < 1 min and it was possible to assess the fluidity of the melt as well as the degree of digestion during the fusion. Sodium peroxide is very reactive. It causes a much higher rate of corrosion of crucibles used for fusion of silicate material and the rate of attack increases with temperature (Easton 1972). Nickel, iron and zirconium crucibles have been used in fusion experiments. Ni and Fe crucibles have short life while zirconium crucibles carry zirconium contaminations which are problematic for determination of Pt. Glassy carbon crucibles have been used for PGE dissolution by Enzweiler and Potts (1995) with fusion at higher temperatures. Zirconium crucibles have been used by Enzweiler *et al.* (1995). Corundum crucibles have been used by Jin and Zhu (2000), Qi *et al.* (2003). Qi (2007) has reported Zr and Hf interferences using sodium peroxide fusion with tellurium co-precipitation, which were corrected mathematically.

Jarvis et al. (1997b) combined alkali fusion with microwave-assisted acid digestions for determination of mass fractions of the Ru, Rh, Pd, Ir and Pt in geological samples. The pre-concentration was achieved by cation exchange chromatography. The detection limits were 1.3 ng/g for Rh to 11 ng/g for Pd using 1 g sample. The method used by Dai *et al.* (2001) for PGE determination utilises sodium peroxide fusion for 1.0 g sample digestion in graphite crucibles and combines anion-exchange chromatography for PGE pre-concentration. (Enzweiler *et al.* 1995) describe as they digests the 0.5 g geological samples with sodium peroxide fusion and describes higher detection limits (0.3–2.0 ng/g) for PGE determination. Totland *et al*. (1995b) improved the detection limits 0.03-0.22 ng/ml by combining microwave digestion with alkali fusion procedures for the determination of the PGE.

Jin and Zhu (2000) used alkali fusion-tellurium co-precipitation for dramatically reducing the detection limits below 10 pg/g. Qi (2007) have further improved the method by combining fusion-Te-co-precipitation and acid digestions by the use of corundum crucibles. He reported few zirconium and hafnium interferences which were mathematically corrected.

Fusion of sodium peroxide and sample are performed at a temperature above the melting temperature of the sodium peroxide. Contrary to the fusion, sintering is performed at lower temperatures below the melting point of sodium peroxide, allowing decomposition of the sample in series of solid state reactions (Richardson 2004). The sinter cake after heating can easily be transformed into a solution by dilute acids (3mol/l HCl). The PGE in

the solution can be accessed by further steps and for any pre-concentration techniques i.e. chromatographic separations, precipitation etc. or silica removal steps. The effectiveness of sinter procedure and fusion methods are comparable, but the degradation of the crucibles are significantly reduced in particular with sintering (Johnson and Maxwell 1981). NiS-FA method of PGE dissolution utilises larger samples masses and nugget effects are reduced, but lead to increased risk of procedural blanks (Sun and Sun 2005) and Savard *et al.* (2010). Acid dissolutions of PGE are often reported incomplete (Reisberg and Meisel 2002). Carius tube and high-pressure-asher digestions are complete but the use of HF is essential for release of PGE hosted in silicates phases (Meisel and Horan 2016). Studies using glassy carbon crucibles with alkali fusion-tellurium co-precipitation have been described in Enzweiler and Potts (1995). An earlier study using the same technique by (Richardson 2004) has determined detection limits i.e. Au 5.8 ng/g, Pt 6.4 ng/g, Pd 13 ng/g, Rh 1 ng/g, Ru 1.6 ng/g and Ir 0.7 ng/g. The durability of glassy carbon crucibles depends on the relative amount of sample, flux and the nature of flux used. A glassy carbon crucible can be used for 6 to 15 fusions due to brittle nature of crucibles that cause premature crucible failure (Qi 2007). Totland, Jarvis *et al*. (1995) used 4:1 mixture of sodium peroxide and sodium carbonate fusion that lasted 4-5 minutes, resulting in a hole in the base of carbon crucible. Only six fusions were possible with 2:1 ratio and 15-20 fusion were possible with 1:1 ratio until the crucible base cracks (Totland *et al.* 1995). Jin and Zhu (2000), after fusion of the sample with sodium peroxide, dries down the solution to remove insoluble SiO_2. In our method, the precipitates of SiO_2 are not discarded; rather upon dilution of the sample and addition of 1-2 ml concentrated HCl, a clear solution is formed. The removal of silicates may remove PGE associated within it.

10.1.1 Te co-precipitation (a pre-concentration technique)

Te has been reported for separation of PGE from complex matrices (Elson and Chatt 1983, Sandell and Neumayer 1951, Stockman 1983). In studies by Moloughney and Faye (1976) Te was added as carrier in tin fire assay charge. Shazali *et al.* (1988) described in his work for pre-concentration of precious metals by tellurium sulphide that (1) precious metals can be associated in nature with tellurium (2) precious metals can be beneficially co-precipitated from aqueous solutions with tellurium co-precipitation (3) an incomplete recovery of gold with NiS-fire assay motivated the research group to apply Te-PGE-sulphide fire assay. Tellurium co-precipitation is an effective pre-concentration technique for PGE. Tellurium (+2) is reduced to tellurium metal by $SnCl_2$ acting as reducing agent.

Tellurium co-precipitation has been reported by Savard *et al.* (2010), who combines it NiS (FA) for PGE mass fraction determination. In this chapter, pre-concentration with tellurium co-precipitation is combined with sodium peroxide sintering using glassy carbon crucibles instead of fusion. There is at least one study which combines Te-co-precipitation with sintering by (Richardson 2004) for PGE mass fraction determination.

10.2 Aims of the chapter

Sodium peroxide sintering is the routine method of sample digestion for major and trace elemental analysis at our research unit. It is observed that glassy carbon crucible last for more than 100 digestions if sintering (heating sample and flux below the melting point of sodium peroxide) is applied. It is aimed to improve and implement sodium peroxide based dissolution method for determination of PGE in geological materials by combination with tellurium co-precipitation. Sintering is a rapid method of sample digestions i.e. more than 20 samples can be prepared in a batch. Dissolution of PGE hosted in silicate phases can be performed easily without the use of HF as it was shown in (Bokhari and Meisel 2014b,

Bokhari and Meisel 2015b). Two new reference materials OKUM and MUH-1 have been mainly used in this study. The salient features of this study are as follows,

1. Method development with sodium peroxide sintering and combination with tellurium co-precipitation for PGE determination using isotope dilution.
2. Estimation of PGE contents in reagents i.e. Te, $SnCl_2$ and HCl.
3. Determination of rhodium and gold mass fractions using external calibration.
4. Purification of reagents prior to use in pre-concentration of PGE.
5. To minimise the steps for separation of Te-PGE precipitates i.e. using centrifugation instead of filtrations that may contribute to lowering down of PGE in the blanks.
6. To improve and strive for lowest procedural blanks by improving detection limits.
7. To provide data for new reference materials OKUM and MUH-1.
8. To apply collision/reaction cell technology in the measurement of monoisotopic rhodium and Au and where applicable for interference removals.

10.3 Experimental

10.3.1 Reagents and instrumentation

Analytical reagent-grade sodium peroxide ACS ISO Merck KGaA Darmstadt Germany has been used for sample digestion. Hydrochloric acid: 37 g/100 g p.a., Roth Karlsruhe, Germany was sub-boiled for experimental purposes. HNO_3: 65 g/100 g p.a., Roth Karlsruhe, Germany (sub-boiled). An ultra-clear unit for ultra-pure water (Siemens water technologies) with conductivity: 0.055 µS/cm, TOC content: < 1 ng/g, (for diluting acids and samples). Glassy carbon crucibles (25 x 25 mm HTW) were used for sample digestion. Hydrochloric acid was sub-boiled and further purified with tellurium precipitation. $SnCl_2$: 98-103% ASC, ISO was obtained from Merck KGaA Darmstadt Germany. Te powder: a 99,999% pure, 60 -mesh tellurium powder obtained from Alfa Aesar GmbH and Co Kg Karlsruhe Germany was used for co-precipitation. Agilent 8800 ICP-MS/MS was used for measurement of isotopic ratio through isotopic ratio analysis acquisition mode.

Measurements were performed in no gas mode as well as in ammonia and oxygen gas modes. The method developed earlier for PGE determination using collision/reaction cell was also applied in isotopic ratio analysis. The complete method details are found in method development for PGE using collision/reaction cell in chapter 9. The integration times were kept 0.75 seconds in no gas mode and 1 second when using cell gases. Total of 10 replicates were measured.

10.3.2 Preparation of reagents

Preparation of 1 mg/ml tellurium solution

250 mg of tellurium powder was weighed into a 100 ml beaker. 10 ml of aqua regia was added. The beaker was covered with a watch glass and heated at 50 °C to near dryness. The 1 or 2 ml of nearly dried residue was dissolved in 1 mol/l sub-boiled HCl. A clear solution of 1 mg/ml Te was obtained with a dilution of 250 ml.

Preparation and purification of $SnCl_2$ solution

A freshly prepared solution of approximately 20% $SnCl_2$ was used for PGE precipitation with tellurium. 50 g of $SnCl_2$ was weighed and taken into a volumetric flask. 250 ml of 6 mol/l sub-boiled HCl was added to it. The solution was heated to form a clear state. For removal of any PGE present in $SnCl_2$, already prepared solution of 1 mg/ml tellurium was

added until the appearance of black precipitates. The precipitates were removed by centrifugation. A total of three centrifugations step are enough to remove all the precipitates. The $SnCl_2$ solution was filtered in the end and stored in a conical flask. The removed precipitates were washed thrice to remove any residual $SnCl_2$. The precipitates were dried and dissolved in aqua regia and dried again. Finally, the PGE collected from $SnCl_2$ were dissolved 3 µl aqua regia and a PGE enriched spike was added to estimate the PGE contents. The final volume was kept 5 ml with a dilution of 0.1 mol/l HCl. The solution was kept in a sealed PFA vessel and heated to dissolve the contents.

Purification of concentrated HCl acid

To the 50 ml solution of concentrated hydrochloric acid, 2-5 ml of 1 mg/ml tellurium solution was added. A 20 % $SnCl_2$ solution was added until the appearance of blank precipitates. The solution was boiled and cooled to coagulate all the black precipitates. Heating was done under watch glass. The solution was centrifuged thrice to remove the black precipitates and finally filtered to collect purified HCl solution. This solution was further used in the preparation of samples and PGE precipitation with tellurium. The precipitates collected from HCl solution were rinsed and washed. These were collected and treated as in $SnCl_2$ purification step. An appropriate amount of spike was added and the solution was kept for analysis for the estimation of reagent blanks in HCl.

Sample preparation for geological reference material

Reference materials WGB-1, OKUM and MUH-1 were digested with sodium peroxide sintering. 0.5 g sample was taken and 2.5 g sodium peroxide was added. The sample was digested following the protocol developed in chapter 5. Heating of the sample and sodium peroxide was done at 480 °C for 2 hours instead of 30-45 minutes for complete digestion of the PGE contents. The final volume of the solution was kept 100 ml. PGE enriched spike was added to the solution and kept overnight for spike equilibration. If the precipitates of the silicates appear, these can be dissolved with addition 1-2 ml concentrated HCl and upon further dilution of the solution e.g. 150 ml solution instead of 100 ml. The solution volume can be adjusted to form a clear solution. In our experiments, clear solution with precipitates were observed on dilution from 100 ml to 200 ml. By discarding the silicates, we may lose PGE associated with it e.g. Ru and Re. The un-dissolved portion of sinter are the hydroxides and clear solution mostly contains silicates. PGE contents were estimated separately in un-dissolved and silicate portions. Silicate portion does carry PGE in it for which a quantitative estimate is described in sintering-anion exchange method in chapter 11 of the thesis. The flasks containing sinter solution were capped to avoid any losses of osmium and ruthenium.

The contents of the solution were transferred to 500 ml beaker and the solution was boiled. To the sinter solution, 1 mg/ml of tellurium solution was added until the appearance of blank precipitates. 20% $SnCl_2$ was added to the sinter solution until the appearance of black precipitates. The addition of 5-10 ml of 20% $SnCl_2$ was sufficient for the precipitate formation. The solution was heated at 90 °C overnight. Small magnet bars were added for stirring the solution on a hot magnetic plate. Then the solution was cooled down and coagulated black precipitates were collected after three centrifugation steps. The precipitates were rinsed, washed and dried. Small amounts of 3-5 µl aqua regia were added to dissolve the precipitates. Precipitates cannot be dissolved in 0.1 mol/l HCl alone. The final volume of the solution was kept 5 ml. The PFA vessels were placed in an ultrasonic bath, capped and heated for the dissolution of any un-dissolved particles.

Memory effect and cross contaminations

One biggest disadvantage of using same crucibles for digestion of the different matrices is the cross contamination and memory from the crucible. The glassy carbon crucibles must undergo proper cleaning procedures prior to use in next sample digestions. Heavy contaminations were observed for samples with trace PGE contents even after cleaning. Crucibles can be allocated for low content PGE samples and for high content PGE samples, which help to avoid contaminations. A normal cleaning procedure for crucibles was rinsing it with concentrated HCl and then the addition of few beads of NaOH and heating at 380°C for few minutes. The crucibles were then kept in deionized water overnight. The crucibles were washed properly and dried down before the digestion of new samples.

Instrument rinse/wash protocol

Jarvis *et al.* (1991) describes the importance of instrumental rinse during analysis and emphasises on extending the time for rinse to lower the instrumental backgrounds. In a routine analysis of PGE a few ng/g calibration standards of PGE are enough to create a memory in the tubing and in the spray chamber etc. Using 0.1 mol/l HCl solution does not show or remove the PGE sticking in the tubing or in the spray chamber. The instrument wash up protocol prior to every PGE analysis involved; cleaning of the cones (orifice and skimmer), rinsed with 0.5 mol/l HCl/HNO_3 solution until no background was observed. A dilute solution of 1 ng/g thiourea or 1 ng/g Te solution was also used for cleaning the tubing, probe and spray chamber. The background shows the removal of few thousands of counts of PGE which lowers down gradually after 10-12 rinses. A dilute solution of 2-MBT (2-mercaptobenzoothiazole) was also used for rinsing the instrument which helps in removing the memory from the tubing. Using a higher concentration of thiourea and 2-MBT (2-mercaptobenzoothiazole) may clog the nebuliser. The automated rinse of the probe was set to 120 seconds after every sample uptake.

Measurement sequence

Moser *et al.* (2003) have described a selection of a sequence of measurement steps that minimises the effects of corrections on the uncertainty of results. The measurement sequence for PGE analysis included instrument rinse protocol, background, rinse, standard solution measurement for estimation of mass bias correction, rinse, background and the measurement of the spiked sample. This sequence is repeated for every spiked sample. The PGE standard solution is measured in the beginning and at the end for keeping control on instrument drift and for mass bias corrections.

10.4 Spike preparation and calibration

Use of isotope dilution method requires an isotopically enriched PGE-spike that is added to the unknown sample for determination of isotopic ratios. The spike concentrations might change due to absorption or evaporation or under the storage conditions (Qi 2007). An ideal spike has freedom of isobaric and molecular interferences, highest enrichment of the isotope with low abundances in nature and minimum total uncertainties (Meisel *et al.* 2001a). A mixed isotopically enriched PGE-spike already available prepared by following the guidelines of Meisel *et al.* (2001a) was used in these experiment for PGE isotopic ratio calculations.

The enriched PGE-spike had ^{99}Ru, ^{108}Pd, ^{191}Ir, ^{185}Re, ^{198}Pt and ^{190}Os spiked isotopes. According to Meisel, *at al.* (2001), ^{190}Os is a common choice in N-TIMS, ^{108}Pd is preferred over ^{106}Pd (as ^{108}Cd concentrations are low in most of the geological materials + ^{108}Cd can

be separated through column chemistry) and ^{198}Pt is preferred over ^{194}Pt (as ^{198}Hg interference is corrected mathematically). Special care was taken to storing the spike in PFA vessels as storage in PP vessels degrades the Pd, Ru and Os concentrations. The spike was stored in 2 mol/l HCl for stability purposes.

Procedure of spike calibration

The mixed isotopically enriched PGE-spike was calibrated using single element standard PGE solution (High-Purity Standards, Charleston, SC, USA). The procedure is outlined below.

1. A 15 ml PFA vessel was washed and rinsed several times with ultra-pure water and dried.
2. The weight of the bottle was noted with high precision digital balance.
3. An appropriate volume of the spike was added and new weight was recorded.
4. A given PGE standard solution of a known concentration (1 ng/g) was added.
5. Final make up volume was kept 5 ml with 0.1 mol/HCl.
6. The solution was thoroughly mixed and was analysed with the Agilent 8800 ICP-MS/MS.

Isotopic ratios of the PGE isotopes were calculated using the isotope dilution method by given formula as in Moser *et al.* (2003).

$$K_x = \frac{R_y - R_B}{R_B - R_x} \cdot \frac{\sum R_{ix}}{\sum R_{iy}} \cdot \frac{m_y}{m_x} \cdot K_y \qquad (A)$$

Where K_x is the sample amount in mol/l

R_y is the isotope abundance ratio of the spike

R_x is the isotope abundance ratio of the sample

R_B is the isotopic ratio of the unknown sample

$\sum R_{iy}$ is the sum of the isotopic ratio of spike

$\sum R_{ix}$ is the sum of the isotopic ratio of sample

m_y is the mass of spike

m_x is the mass of the sample

K_y is the amount in mol/l of spike

The spike amount K_y has to be determined through spike calibration separately with a known amount of standard solution and thus equation can be rewritten as

$$K_y = \frac{R_x - R_B}{R_B - R_y} \cdot \frac{\sum R_{iy}}{\sum R_{ix}} \cdot \frac{m_x}{m_y} \cdot K_x \qquad (B)$$

K_x is the known amount of standard solution.

The isotopic mass fractions determined for 1 ng/g solution of PGE were the same as expected with no significant variations except Pd for which appropriate corrections were applied in calculations. The precision was determined with formula $\sqrt{(A)^2+(B)^2}$ where A and

B are the CPS RSDs of the isotopes. The spike was then used for further experiments. Spike calibration is shown in Table 10.1.

Table 10.1: Spike calibration for a 1 ng/g PGE standard solution

Spike calibration (ng/g)		
Ratio	Mass fractions	Precision
$^{102}Ru/^{99}Ru$	1.02	5%
$^{101}Ru/^{99}Ru$	1.09	5%
$^{105}Pd/^{108}Pd$	0.89	2%
$^{106}Pd/^{108}Pd$	0.88	6%
$^{191}Ir/^{193}Ir$	1.05	6%
$^{195}Pt/^{198}Pt$	0.97	7%
$^{194}Pt/^{198}Pt$	0.98	8%

Mass bias factor calculations of PGE isotopes

Heavier isotopes are transmitted more efficiently than lighter isotopes due to vacuum interface (nozzle effect) and ion lens system (space charge effect) in ICP-MS. This physical effect is said to be mass bias or mass discrimination effect (Alonso and Rodriguez-González 2013). This factor sums up in all the components of the mass spectrometer as there are ionisations, ion optics, mass separation and ion detection contribution to it (Nelms 2005). For the ions of the same energy, lighter mass ions will produce more secondary electrons when striking the first electrode of an electron multiplier detector than heavier mass ions (Nelms 2005). The heavier the ion, the longer time it spends in quadrupole fringing fields and the greater dispersions (Nelms 2005). For every isotopic PGE analysis with isotope dilution method, a standard solution of PGE was measured in the beginning and at the end to monitor instrumental transmission effect, which tends to bias in favour of heavier isotopes. For that reason, the isotopic ratios of the standard solution were always shifted away from the natural ratios. This uncertainty due to instrumental transmission effect was corrected through determination of mass bias factor.

Mass bias corrections factor (K) is determined by dividing natural ratio of the isotopes with the isotopic ratio determined in standard solution (Nelms 2005). This factor is divided with an isotopic ratio of the unknown sample. For routine analysis of PGE through isotope dilution method, 0.1 to 1 ng/g PGE standard solutions were measured because these concentrations ranges are similar to the concentration of geological samples. The mass bias correction using diluted PGE standard solution e.g. less than 100 ng/l PGE solution has shown more shift and larger mass bias correction as documented by Pearson and Woodland (2000).

For each measurement, the mass bias factor was determined and isotopic ratios were corrected for the best results possible. The calculation for a selected measurement for which mass bias corrections were made is shown in Table 10.2. For some PGE analysis method such as the cloud point extraction, thiourea extraction and even tellurium co-precipitation can be risky if instrument wash up protocol is not followed to eliminate the memory effect of PGE in the tubing of the instrument.

Table 10.2: Mass bias factor determination for one selected measurement

Mass bias correction factor for one measurement						
Isotopes	$^{99}Ru/^{101}Ru$	$^{105}Pd/^{108}Pd$	$^{185}Re/^{187}Re$	$^{191}Ir/^{193}Ir$	$^{189}Os/^{190}Os$	$^{195}Pt/^{198}Pt$
Natural ratio	0.748	0.844	0.597	0.595	0.571	4.723
Mean ratio	0.723	0.820	0.607	0.588	0.581	4.666
Mass bias correction	0.966	0.972	1.016	0.989	1.017	0.988

The degree of mass bias is calculated as (1-Mass bias correction factor)/2 (Ravizza and Pyle 1997). The trends for the degree of mass bias across PGE from lighter to heavier PGE are shown in Figure 10.1. PGE with lower atomic masses show a larger degree of mass bias than those of the heavier. The degree of mass bias for ruthenium is greater (1.7%) than Pd for the reasons of higher abundances of Pd than ruthenium.

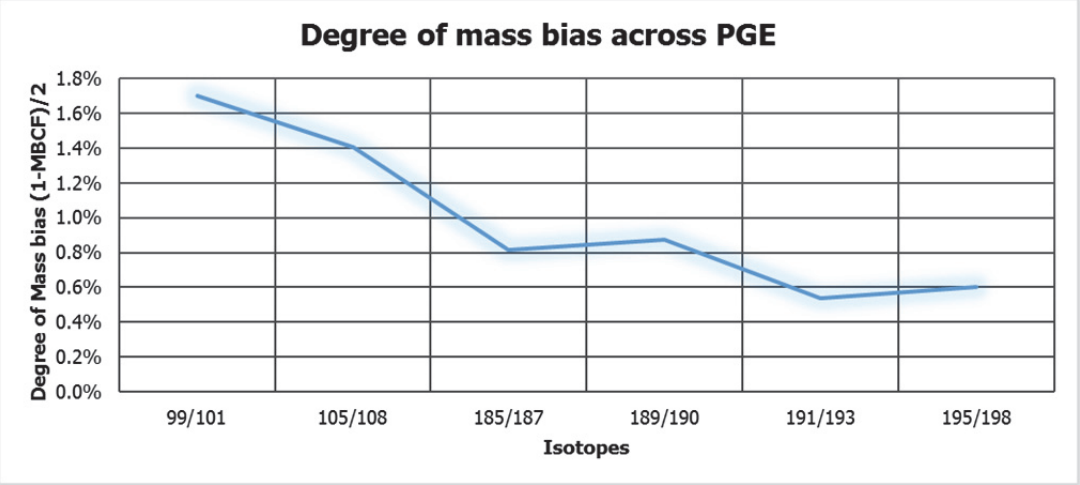

Figure 10.1: The degree of mass bias across the PGE

10.4.1 Acidic strength of the sinter solution and spike recovery test

The samples digested with sodium peroxide require the use of hydrochloric acid for the dissolution of un-dissolved hydroxides as described in the section of sintering optimisation (chapter 5). The acidic strength of the sinter solution is 1.45 mol/l with pH of 0.16. The recoveries of the PGE were evaluated for the real geological matrix samples with 1.45 mol/l acid concentrations through the pre-concentration method described above. Variable recoveries were achieved for all the PGE which are shown in the Table 10.3. The recoveries shown by Qi *et al.* (2004) using sodium peroxide fusion require higher acid concentrations. However, use of more hydrochloric acid was avoided for the risk of increasing blanks and dissolution of hydroxides was achievable with 1.45 mol/l acid concentrations. This also provides sufficient intensities for reliable results. Gold and Rh recoveries were monitored using external calibration with Ge as an internal standard. The recoveries Au and Rh in reference materials WGB-1, OKUM and MUH-1 were found to be within the certified range of reference materials that are presented in results in next sections.

Table 10.3: Spike recovery in real matrix samples with sinter solutions

Spike recovery in real matrix samples with sinter solutions	
Spike	Recovery
^{99}Ru	70-90%
^{108}Pd	50-70%
^{185}Re	60-70%
^{190}Os	20-30%
^{191}Ir	60-70%
^{198}Pt	70-90%

10.4.2 Tests on un-spiked digested with sintering and tellurium co-precipitation on OKUM reference material

The geological reference material OKUM was digested with sodium peroxide sintering following pre-concentration with tellurium co-precipitation. The sample was not spiked for finding the effect of interferences on PGE isotopes. The isotopic ratios of all the PGE isotopes are altered due to the interferences. The effect of interferences on ruthenium isotopes is very large as shown in the Figure 10.2. Isotopic ratios of Pd, Re, and Ir also affected. Fewer deviations are shown by isotopic ratios of platinum isotopes.

10.4.3 Spike equilibration in sinter solution

Isotope dilution method depends on the equilibrium of spike and sample and if these conditions are met the losses during sample preparation step can be tolerated (Woodland 1999). Spike equilibration in the case of fusion using sodium peroxide was possible with both before or after spiking (Qi 2007). Based on the literature Qi (2007) using a similar technique but fusion, we carried out sintering by using same chemical reagents and the addition of the spike was done after the sample digestion. Spiked samples were kept at ambient temperature for 5-6 hours. Spike dissolution required acidic media and the acid strength of the sample was sufficient for equilibration as seen from the recoveries of the PGE. Spike equilibration with sodium peroxide blank was problematic as sodium peroxide solution in the absence of any matrix provides oxidising conditions that were not suitable especially for ruthenium and osmium. The addition of 1 to 2 ml of concentrated hydrochloric acid solves the problem of spike equilibration for sodium peroxide blanks.

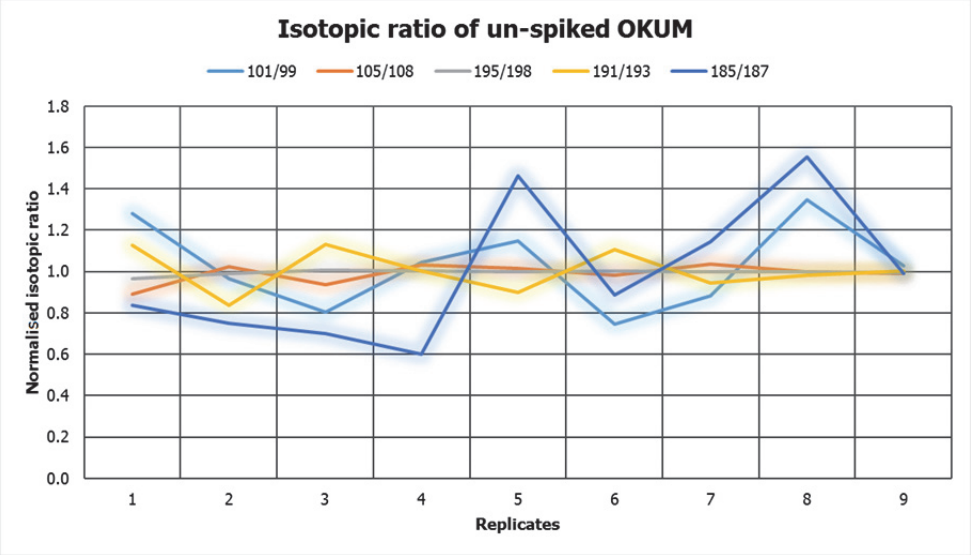

Figure 10.2: Interference effect on un-spiked OKUM sample

10.4.4 External calibration for Rh and Au

For the determination of monoisotopic Rh and Au, method of external calibration was selected using Ge and Bi as an internal standard. Qi (2007) has used Lu as an internal standard for sample digested with sodium peroxide fusion. We have found that $^{175}Lu^{16}O^{+}$ interference is generated in no gas mode on $^{191}Ir^{+}$ and when a higher concentration of Lu was used, it altered the isotopic ratio of $^{191}Ir/^{193}Ir$. Therefore, the use of Lu as an internal standard was avoided. Moreover, measurement of Rh was done in $Rh(NH_3)_4^{+}$ mass-shift mode and gold as $Au(NH_3)_2^{+}$ using collision/reaction cell technology of Agilent 8800. For the mass-shift mode using ammonia gas, Ge internal standard was measured as $GeNH_2^{+}$ and bismuth as $Bi(NH_3)^{+}$. The overall precision of intensity of Ge and Bi internal standards in no gas and mass-shift modes were less than 5%. The instrument rinse prior to the PGE analysis is very important. Rinse using 0.1 mol/l HCl or 1% HNO_3 does not show any significant instrumental memory. When the analysis is performed, the tellurium contents in the PGE solution may wipe out the PGE sticking to the tubing, causing an increase count rate of PGE isotopes. We have rinsed the instrument with 1 ng/g tellurium solution several times until no background was observed. Therefore, a diluted tellurium solution is recommended for clearing any background of PGE from the tubing.

10.4.5 Purification of HCl and $SnCl_2$

The main reagents that were used in sample digestion were 1 mg/ml Te solution, 20% $SnCl_2$, 2.40 g sodium peroxide and 1.45 mol/l hydrochloric acid. The addition of 2-5 ml of 1 mg/ml Te solution into the samples with 5-7 ml of 20% $SnCl_2$ was sufficient for precipitation of PGE. The 20% $SnCl_2$ solution was purified using tellurium co-precipitation, Hydrochloric acid was also purified with the same techniques. The PGE contents removed from un-purified $SnCl_2$ are shown below

PGE contents (pg) from un-purified $SnCl_2$						
Ru	Pd	Pt	Ir	Re	Rh	Au
15.7	88.6	23.0	22.9	13.1	90	120

The PGE mass fractions in $SnCl_2$ after purification were < 5-10 pg.

Te solution cannot be purified and PGE contents determined in 5 ml tellurium solution are given below.

PGE contents in Te (pg)						
Ru	Pd	Pt	Ir	Re	Rh	Au
85.9	356.2	40.7	41.7	18.0	45	35

Concentrated hydrochloric acid was purified with tellurium co-precipitation. The PGE contents removed from concentrated solution are

PGE contents in HCl (pg)						
Ru	Pd	Pt	Ir	Re	Rh	Au
84	35	610	29	584	50	90

The hydrochloric acid purified with tellurium co-precipitation had < 5-10 pg PGE contents.

10.4.6 PGE contents in procedural blanks

The reagents HCl and $SnCl_2$ were purified and were used in tellurium co-precipitation. It is assumed that any contribution for high procedural blanks must be from sodium peroxide and tellurium solution. Four replicates of sodium peroxide blanks were pre-concentrated with tellurium co-precipitation and the PGE contents are shown in the Table 10.4. The precisions were calculated with formula $\sqrt{(A)^2+(B)^2}$ where A and B are the Cps RSDs of the isotopes.

Table 10.4: PGE mass fractions in total procedural blanks

Mass fractions of PGE in procedural blank ng/g														
	Ru		Pd		Ir		Pt		Re		Rh		Au	
Sample	X	Precision	X	Precision	X	Precision	X	Precision	X	Precision	X	Precision	X	Precision
blank-01	0.45	15%	2.85	10%	0.40	7%	0.20	5%	1.1	6%	0.40	14%	0.25	7%
blank-02	0.35	17%	3.05	8%	0.30	10%	0.15	3%	1.0	7%	0.30	36%	0.15	10%
blank-03	0.35	16%	2.80	7%	0.30	11%	0.20	5%	2.1	3%	0.30	36%	0.15	11%
blank-04	0.25	8%	1.25	3%	0.50	4%	0.20	1%	1.1	10%	0.20	7%	0.35	4%
Mean	0.35	23%	2.49	33%	0.38	26%	0.19	13%	1.3	39%	0.30	27%	0.225	43%

Where x is the determined value.

10.4.7 Detection limits

The detection limits of PGE were found with 3 sigmas the standard deviations of the blanks concentrations. The detection limits have improved in comparison to the method of Richardson (2004). The detection limits of PGE with sintering-tellurium co-precipitation has not improved in comparison with other literature. Totland *et al.* (1995) has reported 0.03-

0.22 ng/ml with microwave and alkali fusion method. Jarvis *et al*. (1997b) have reported 1.3 ng/g for Rh and 11 ng/g for Pd. Enzweiler *et al.* (1995) have reported 0.4 ng/g for Ru, 1 ng/g for Pd, 0.3 ng/g for Ir and 2.0 ng/g for Pt. Qi (2007) has reported 0.045 ng/g for Ru, 0.024 ng/g for Rh, 0.230 ng/g for Pt, 0.02 ng/g for Ir 0.320 ng/g for Au. The detection limits of this work are shown below;

Detection limits (ng/g)						
Ru	Rh	Pd	Pt	Ir	Re	Au
0.24	0.24	2.50	0.08	0.23	1.51	0.29

10.5 Results and discussion

Three reference materials OKUM, MUH-1 and WGB-1 were digested with sodium peroxide sintering. The PGE contents were pre-concentrated with tellurium co-precipitation. Four replicates were digested and analysed with the Agilent 8800 ICP-MS/MS.

Reduction of interferences through sintering and tellurium co-precipitation

Chapter 9 covers the interference removal through collision/reaction cell and demonstrates the background created by interferences on PGE. These interferences have been already discussed in detail. The intensities of the interfering elements were monitored on the m/z of PGE isotopes during the measurement i.e. samples with co-precipitation and without co-precipitation. The relative intensities of the interferences were found to be significantly decreased after tellurium co-precipitation. Such intensities are shown in Table 10.5.

Table 10.5: The relative intensities of interferences in OKUM after sintering -Te-co-precipitation

Relative intensities of interferences after tellurium co-precipitation in OKUM			
Interference		PGE isotopes	Relative intensity
$^{85}Rb^+$	RbO^+	$^{101}Ru^+$	0.0204%
$^{88}Sr^+$	SrO^+	$^{104}Pd^+$	0.2287%
$^{89}Y^+$	YO^+	$^{105}Pd^+$	0.0125%
$^{90}Zr^+$	ZrO^+	$^{106}Pd^+$, $^{107}Ag^+$, $^{108}Pd^+$, $^{110}Pd^+$	0.00001%
$^{93}Nb^+$	NbO^+	$^{109}Ag^+$	0.22741%
$^{95}Mo^+$	MoO^+	$^{101}Ru^+$	0.06482%
$^{108}Cd^+$	Cd^+	$^{106}Pd^+$, $^{108}Pd^+$	0.15901%
$^{180}Hf^+$	HfO^+	$^{194}Pt^+$, $^{195}Pt^+$	0.00781%
$^{181}Ta^+$	TaO^+	$^{196}Pt^+$, $^{197}Au^+$	0.00332%
$^{198}W^+$	WO^+	$^{196}Pt^+$, $^{198}Pt^+$	0.02541%
$^{198}Hg^+$		$^{198}Pt^+$	0.06512%
$^{206}Pb^+$		$^{103}Rh^+$	0.01251%

No mathematical corrections were applied in determining the PGE mass fractions rather method developed with the collision/reaction cell described in chapter 9 was applied. Small interferences of $^{85}RbO^+$ (0.02%) on $^{101}Ru^+$ were removed using collision/reaction cell of the Agilent 8800. Ruthenium was measured as RuO^+ mass-shift mode in oxygen gas and as $Ru(NH_3)_4$ mass-shift mode in ammonia gas. Rhodium mass fraction was measured with on-mass ammonia and mass-shift ammonia $Rh(NH_3)_4^+$ mode to avoid the interferences of Pb^{2+}, $^{87}RbO^+$ and $^{87}SrO^+$. $^{89}YO^+$ is the main interference on $^{105}Pd^+$ and Pd^+ intensities were measured in $Pd(NH_3)_3^+$ mode to avoid (0.0125%) YO^+ interference. $^{96}ZrO^+$ had a little intensity in no gas mode at m/z of ^{106}Pd which was removed by measuring as $Pd(NH_3)_3^+$. Ag isotopes were not measured because of their precipitation as AgCl in hydrochloric acid. The interferences on Au^+ by TaO^+ were removed by measuring Au in ammonia gas as $Au(NH_3)_2^+$ and on-mass ammonia gold measurement. Hafnium and Hg interferences were significantly reduced with tellurium co-precipitation and minor intensities were removed by measuring Pt as $Pt(NH_3)_2^+$. Iridium measurement was problematic in the beginning due to the use of Lu as an internal standard for Rh measurement. When Lu was not used as internal standard, the results of Ir measurement were better even in no gas mode. The results of the measurement for OKUM, WGB-1 and MUH-1 are given in tables Table 10.6-Table 10.12.

10.5.1 PGE mass fractions determined in geological reference materials

Ruthenium

The mean value for OKUM is 4.37 ng/g with 12% precision and for MUH-1 is 7.68 ng/g with the precision of 14%. Ruthenium in WGB-1 was not determined due to high procedural blank. The bias from reference value for OKUM is 1% and for MUH-1 is 9%. The mean values, in case of MUH-1 determined with sintering-tellurium co-precipitation are slightly higher than preliminary ILC data. The precision was determined by formula $\sqrt{(A)^2+(B)^2}$ where A and B are the Cps RSDs of the isotopes. The precision of the measurement for OKUM is less than 6% and for MUH-1 is less than 14%. The data for ruthenium is given in Table 10.6.

Palladium

The mean value for Pd in OKUM is 10.1 ng/g with RSDs of 9% and for MUH-1 is 7.53 ng/g with 8% RSDs. The mean value of Pd in WGB-1 is 12.4 ng/g with 4% RSDs. The precision of the measurement of isotopic ratios was less than 10%. The bias from ILC value or reference value for Pd in OKUM is 11%, for MUH-1 is 14% and for WGB-1 is 11%. Pd data for reference materials is shown in Table 10.7.

Platinum

The data for OKUM shows platinum mass fractions as 12.3 ng/g with 3% RSDs, for MUH-1 9.70 ng/g with 17% RSDs and for WGB-1 as 6.10 ng/g with 15% RSDs. The biases from the ILC and or reference value are 11% for OKUM, 3% for MUH-1 and 1 % for WGB-1. The precision of the isotopic ratios is given in the Table 10.8.

Iridium

The mass fractions determined for iridium for reference materials are generally lower than the ILC or reference values i.e. 0.88 ng/g for OKUM, and 3.19 ng/g for MUH-1. The biases from the ILC values are 8%, and 7% for OKUM, and MUH-1 respectively. The data is shown in the Table 10.9.

Rhodium

The determined mass fraction of Rh for OKUM is 1.27 ng/g, for MUH-1 is 0.70 ng/g, for WGB-1 is 0.30 ng/g. The bias from the ILC or reference values for OKUM is 7%, for MUH-1 is 26% and for WGB-1 is 8%. The data for rhodium is shown in Table 10.10 - Table 10.12.

Gold

The reference data for Gold in MUH-1 is not available, but for OKUM and WGB-1 is compared with that of Savard *et. al* (2010). The mean value of OKUM is 1.20 ng/g with 15% bias from the reference value. For WGB-1 mean value is 1.27 ng/g with 1% bias from the reference value. The data for gold is shown in Table 10.10 - Table 10.12.

Table 10.6: Ruthenium mass fractions in OKUM and MUH-1

Ru mass fractions in geological reference material (ng/g)													
	OKUM-1	**OKUM-2**	**OKUM-3**	**OKUM-4**	**OKUM-5**	**MUH-1 a**	**MUH-1 b**	**MUH-1c**	**MUH-1d**	**MUH-1e**	**MUH-1f**	**MUH-1g**	**MUH-1h**
Determined	4.24	4.02	4.7	4.34	4.55	8.54	6.21	7.93	8.33	6.4	6.84	7.37	9.44
Precision	3%	6%	4%	3%	3%	7%	4%	3%	17%	3%	3%	2%	3%
*[1]Reference	4.33												
Precision	12%												
*[2]Mean	4.37								7.68				
Precision	6%								14%				
*[3]ILC value	4.48								7.06				
Rel *u*	5%								3%				

*[1]Savard *et al* (2010) *[2] This study *[3] ILC value (personal communication with Thomas Meisel)

Table 10.7: Palladium mass fractions in OKUM, WGB-1 and MUH-1

Pd mass fractions in geological reference material (ng/g)													
	OKUM-1	**OKUM-2**	**OKUM-3**	**OKUM-4**	**WGB-1a**	**WGB-1b**	**WGB-1c**	**WGB-1d**	**MUH-1 a**	**MUH-1 b**	**MUH-1c**	**MUH-1d**	**MUH-1e**
Determined	10.6	10.6	10.5	8.8	12.8	12.8	12.2	11.7	8.4	7.2	7.3	7.3	7.5
Precision	6%	9%	4%	3%	4%	4%	5%	4%	6%	4%	4%	3%	2%
*[1]Reference value	11.4				13.9								
Precision	7%				15%								
*[2]Mean	10.1				12.4				7.53				
Precision	9%				4%				8%				
*[3]ILC value	11.3								8.79				
Rel *u*	4%								10%				

*[1]Savard *et al* (2010) *[2] This study *[3] ILC value (personal communication with Thomas Meisel)

Table 10.8: Platinum mass fractions in OKUM, WGB-1 and MUH-1

Pt mass fractions in geological reference material (ng/g)													
	OKUM-1	**OKUM-2**	**OKUM-3**	**OKUM-4**	**WGB-1a**	**WGB-1b**	**WGB-1c**	**WGB-1d**	**MUH-1 a**	**MUH-1 b**	**MUH-1c**	**MUH-1d**	**MUH-1e**
Determined	12.4	12.8	11.9	12.1	5.9	5.9	6.8	6.1	9.0	9.6	12.1	8.2	11.7
Precision	4%	4%	4%	6%	10%	11%	9%	20%	6%	4%	6%	4%	3%
*[1]Reference	11				6.1								
Precision	5%				15%								
*[2]Mean	12.3				6.18				9.70				
Precision	3%				7%				17%				
*[3]ILC value	12.0								9.38				
Rel *u*	8%								19%				

*[1]Savard *et al* (2010) *[2] This study *[3] ILC value (personal communication with Thomas Meisel)

Table 10.9: Iridium mass fractions in OKUM and MUH-1

Ir mass fractions in geological reference material (ng/g)									
	OKUM-1	**OKUM-2**	**OKUM-3**	**OKUM-4**	**MUH-1 a**	**MUH-1 b**	**MUH-1c**	**MUH-1d**	**MUH-1e**
Determined	0.965	0.997	0.968	0.838	2.75	3.26	3.50	3.23	3.36
Precision	10%	7%	7%	9%	14%	21%	17%	25%	19%
*[1]Reference	1.00								
Precision	12%								
*[2]Mean	0.942				3.19				
Precision	11%				10%				
*[3]ILC value	0.957				3.44				
Rel *u*	6%				14%				

*[1]Savard *et al* (2010) *[2] This study*[3] ILC value (personal communication with Thomas Meisel)

Table 10.10: Rh and Au mass fractions in OKUM

	Rh (ng/g)		Au (ng/g)	
Sample	**Determined**	**Precision**	**Determined**	**Precision**
OKUM1	1.23	1.30%	1.20	9.50%
OKUM2	1.31	7.50%	1.07	7.90%
OKUM3	1.42	5.20%	1.30	8.10%
OKUM4	1.17	8.60%	1.24	6.10%
OKUM5	1.21	4.20%	1.20	5.20%
*[2]Mean	1.27	7%	1.20	7%
*[1]Reference	1.37	8%	1.41	40.2%
*[3]ILC value	1.43	20%		

*[1] Savard *et al* (2010) *[2] This study *[3] ILC value (personal communication with Thomas Meisel)

Table 10.11: Rh and Au mass fractions in MUH-1

	Rh (ng/g)		Au (ng/g)	
Sample	**Determined**	**Precision**	**Determined**	**Precision**
MUH-1a	0.65	2.60%	3.16	4.80%
MUH-1b	0.70	2.20%	2.96	3.90%
MUH-1c	0.61	5.90%	3.16	6.60%
MUH-1d	0.59	2.90%	3.76	2.10%
MUH-1e	0.67	4.20%	3.66	5.20%
MUH-1f	0.83	3.30%	3.46	6.30%
MUH-1g	0.73	2.80%	3.36	6.10%
MUH-1h	0.84	2.80%	3.76	5.10%
*[1]Mean	0.70	12%	3.41	9%
*[2]ILC value	0.951	114%		

*[1] This study *[2] ILC value (personal communication with Thomas Meisel)

Table 10.12: Rh and Au mass fractions in WGB-1

	Rh (ng/g)		Au (ng/g)	
Sample	**Determined**	**Precision**	**Determined**	**Precision**
WGB-1a	0.30	14%	1.17	9%
WGB-2a	0.29	11%	1.37	14%
WGB-3a	0.30	13%	1.27	15%

WGB-4a	0.29	15%	1.27	16%
*[2] Mean	0.30	7%	1.27	6%
*[1]Ref-value	0.32	66%	1.26	19.60%

*[1] Savard *et al.* (2010) *[2] This study

10.6 Summary

A Method using sodium peroxide sintering combined with tellurium co-precipitation isotope dilution mass spectrometry has been developed and improved for the determination of mass fractions of the PGE i.e. Ru, Rh, Pd, Pt, Ir and Au in geological reference materials after the reported method by Richardson (2004). Richardson (2004) has provided detection limits of PGE i.e. i.e. Au 5.8 ng/g, Pt 6.4 ng/g, Pd 13 ng/g, Rh 1 ng/g, Ru 1.6 ng/g, Ir 0.7 ng/g, whereas the detection limits of the method developed are Ru 0.24 ng/g, Rh 0.24 ng/g, Pd 2.50 ng/g, Pt 0.08 ng/g, Ir 0.23 ng/g and Au 0.29 ng/g.

The detection limits did not improve compared to the method of Qi (2007) using sodium peroxide fusion + acid digestion and tellurium co-precipitation in particular for Ru 0.045 ng/g, Pd 0.11 ng/g, Ir 0.02 ng/g, Rh 0.024 ng/g. The detection limits for Pt and Au of the developed method were better than Qi (2007). Therefore, there is further work require to lower the limit of detection by selection of appropriate chemicals i.e. Te powder, sodium peroxide etc.

We have reduced the number of steps for the method developed as;

1. Silica dissolution in more dilutions with the addition of 1 to 2 ml of concentrated HCl instead of its removal by drying or by use of HF.
2. The precipitates are collected by centrifugation instead of the requirement of more apparatus i.e. membrane filter paper, vacuum connected etc. flasks that may add to the procedural blanks as reported by Qi (2007).

Glassy carbon crucibles for sample digestion are still the best choice as around 100 digestions were performed using sintering that makes this method simple and inexpensive. Qi (2007) reported hafnium and zirconium contaminations from the material of corundum crucibles, which were mathematically corrected. Corundum crucibles need to be replaced after 10 fusions.

The experiments were performed in 25x25 mm glassy carbon crucibles. It is possible to acquire larger capacity sized carbon crucibles that can be used for sample sizes 2-10 g. Sintering-tellurium co-precipitation ID is a rapid, fast and reliable method of PGE dissolution that can be applied to complex matrices. This method is applied to PGE samples from the industrial and geological background for routine analysis.

This chapter describes the memory problems from the crucibles, possible contaminations from the tubing, spray chamber and suggests a cleaning procedure for removal of high background prior to PGE analysis.

The interferences were shown to reduce after tellurium co-precipitation, whereas collision/reaction cell of the Agilent 8800 was also applied for removal of small intensities of Sr, Rb and Pb etc.

The data for two new reference materials is presented for OKUM and MUH-1 which is being screened through the ILC.

11. Method development for Re and Ru mass fraction determination in BIR-1, TDB-1 and OKUM and a study of the low recovery of PGE with anion-exchange chromatography

11.1 Introduction and background

Due to low concentrations of the PGE, it is desirable to pre-concentrate the digests of the PGE samples to improve the sensitivity and precision of the measurement data. Anionic chromatographic separation of the PGE from the matrix elements have been widely used for geological samples. Studies using anionic separations indicate different and complex solution chemistry of PGE behaviour, which relates to the feasibility of the type of ions formed in solution after digestions. The mixed acid elution scheme has been reported for PGE elution from resins except Os (Rehkämper and Halliday 1997). PGE tend to form stable PGE anionic chloro-complexes upon addition of hydrochloric acid, which have a strong affinity to be retained in anion resins (Crocket *et al.* 1968, Enzweiler and Potts 1995, Korkisch 1989, Petrie and Morgan 1982). The chemistry of PGE retention on the columns is based on the valence states of the elements and ionic adherence of PGE-chloro-complexes with ammonium groups of the resins (Korkisch 1989). Iridium forms $IrCl_6^-$ which is strongly held by the resin, but $IrCl_5^-$, $IrCl_4^{2-}$ and hydroxyl-chloro complex of Ir are loosely held to the resin and require an oxidising agent to keep Ir in (+4) state (Yi and Masuda 1996a). Platinum has been reported to form hydroxy chloro-complexes which lower its affinity to be retained with anion resins, palladium has been suggested to form $Pd(OH)_2$, and gold as hydroxy chloro-complexes of gold (Enzweiler and Potts 1995). The PGE in hexachloro-PGE complexes are strongly held rather than triply charged complexes to the anion resin (Petrie and Morgan 1982). Different digestion techniques can be combined with anion-exchange resins depending upon low blanks, complete digestion and spike-sample equilibration. Acid digestions may not be complete for PGE minerals. NiS-fire assay yields poor recovery of rhenium and often suffer from the spike and sample losses. Aqua regia attacks cannot reach HSE in the silicate portion of rocks. HPA and Carius tube digestions require the use of HF for the complete release and recovery of rhenium and ruthenium in particular (Meisel and Horan 2016).

11.1.1 Aims of the chapter

Highly siderophile elements (HSEs: Re, Au, Ir, Os, Ru, Rh, Pt and Pd) and Pt-Re-Os isotope systems are important for the understanding of the formation and evolution of the Earth (Ishikawa *et al.* 2014). Highly siderophile elements are hosted in the silicate portions of rock (Ishikawa *et al.* 2014, Meisel *et al.* 2009, Meisel and Horan 2016). Current developments towards the use of acid digestions techniques have dominated the traditional flux fusion techniques because of lower blanks as in NiS-fire assay (Savard *et al.* 2010). Spike-sample equilibration problems, sample and or spike losses and poor recoveries of rhenium with NiS-FA are critical (Ishikawa *et al.* 2014, Ravizza and Pyle 1997, Shirai *et al.* 2003). The use of acid digestions for sample digestion may suffer nugget effects due to small test portion size and incomplete digestions due to the silicates and the acid-resistant phases (Dale *et al.* 2012, Ishikawa *et al.* 2014, Meisel *et al.* 2009, Meisel and Horan 2016). Studies by Dale *et al.* (2012) proves that de-silicification with HF, after dissolution using aqua regia in an HPA digestion, more efficiently extracted Ir, Ru, Pt, Pd and Re. For basaltic reference material TDB-1 and BIR-1, use of HF has shown the release of HSE particularly Re and Ru (Ishikawa *et al.* 2014) as can be seen in Figure 11.1. Use of HF has been objected by Day *et al.* (2015) as it may alter Re/Os and Pt/Os ratios for high-MgO basalts.

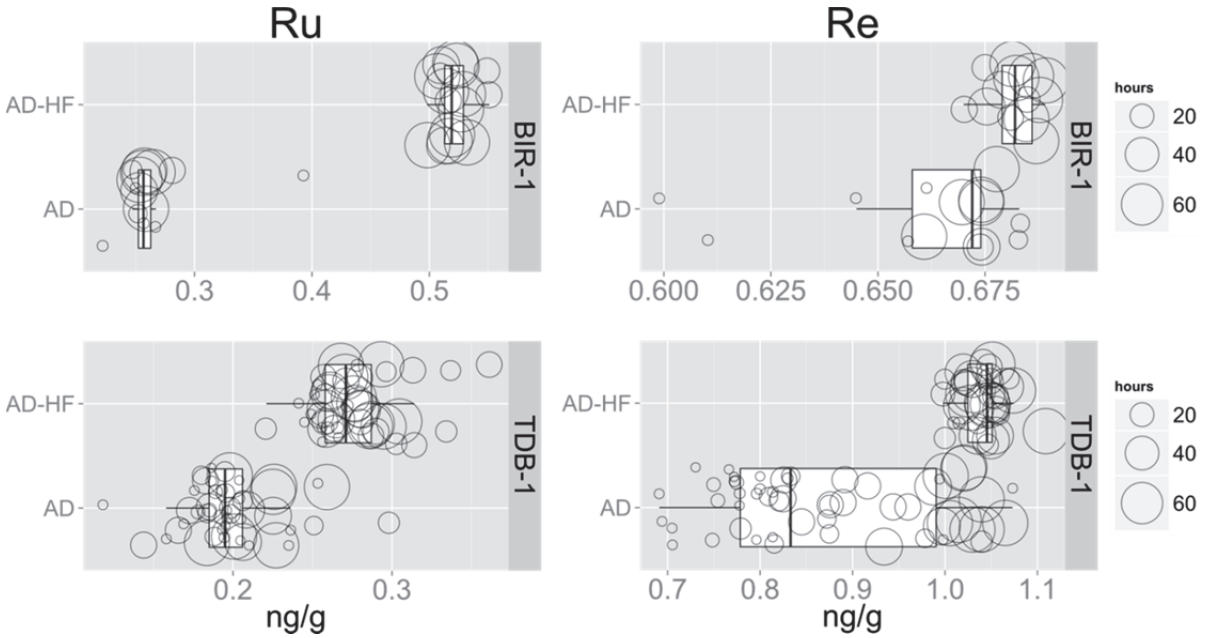

Figure 11.1: The yield of Re and Ru mass fractions in TDB-1 and BIR-1 using acid digestion (AD) (HCl-HNO_3) and acid digestion with HF (AD-HF). The source of the figure is (Meisel and Horan 2016).

In above Figure 11.1, the mass fractions for Re and Ru in TDB-1 and for BIR-1 obtained using HCl-HNO_3 digestion in Carius tubes and by HPA at temperatures between 240 and 320 °C are shown. The duration of the HCl-HNO_3 step is given by the size of the symbol. AD-HF refers to those methods that included HF treatment either prior or after HCl-HNO_3 digestion. For basalt TDB-1, these results show that the highest yield of Re can be achieved by treatment with HF or by digestion in HCl-HNO_3 for > 60 hours. Ru from TDB-1 is not fully liberated during HCl-HNO_3 digestions for > 60 hours but instead appears to require treatment with HF.

In particular, this study addresses the same reference material TDB-1 and BIR-1 which have been studied by Ishikawa *et al.* (2014) and apply sodium peroxide sintering for their digestions. It is also intended to evaluate, whether sodium peroxide sintering can help the release of rhenium and ruthenium from the silicate portions of the rocks by avoiding the use of HF, which is highly toxic and dangerous. Therefore, the major aims of the chapter are;

1. Method development with sodium peroxide sintering and combination with anion-exchange chromatography for the determination of rhenium and ruthenium mass fractions in TDB-1 and BIR-1 using isotope dilution mass spectrometry.
2. Testing retention and recoveries of PGE standard solutions and spike in real matrix with anion-exchange chromatography.
3. Evaluation of the low Pt, Pd, Rh, Au and Ir recoveries of with anion-exchange chromatography for samples digested with sodium peroxide sintering.
4. Study of the PGE contents in sinter phases i.e. residue and supernatant.

11.2 Instrumentation and reagents

The details of sodium peroxide, HCl, HNO_3, glassy carbon crucibles and ultra-pure has been described in previous chapters. Bio-Rad AG-1X8, 200-400 mesh were used for the anionic chromatographic pre-concentration of PGE. 2 ml columns with internal diameter of 7 mm, outlet diameter if 1.5 mm and 250 ml funnel was used for resin experiments. PFA vessel 10-15 ml capacity were used for collection of PGE eluates. The Agilent 8800 ICP-

MS/MS was used for measurement of isotopic ratio through isotopic ratio analysis acquisition mode. The measurements were performed in no gas, ammonia and oxygen gas modes. The method developed earlier for PGE determination using collision/reaction cell were also applied in isotopic ratio analysis. The complete method details are described in chapter 9. The integration times were kept 0.75 seconds per m/z in no gas mode and 1 second when using cell gases. A total of 10 replicates were measured.

11.3 Preparation of resin columns

11.3.1 Wash protocol

Some steps of resin preparation, wash and elution protocol were based on Reisberg and Meisel (2002). Bio-Rad AG-1X8 200-400 mesh resin was taken in a clean plastic bottle. Ultra-clean deionized water was added to the bottle. The bottle was shaken well and the resin was allowed to settle down. The water was decanted, which also removes finer resins particles that might be problematic during elution studies of PGE. This process was repeated twice or thrice. Then 6 mol/l HCl was added to the resin depending upon the its mass. Magnetic stirrer bars were added to the bottle and the bottle was placed on the magnetic plate overnight. The resin was allowed to settle and acid was decanted. Several rinses were made with ultra-pure water. 600 mg resin was taken and loaded on the column. Ultra-pure water was used for keeping the resin wet. The dried resin may from channels inside it that would affect the PGE and resin contact for the retention and the elution. A 250 ml funnel was connected to the column for letting the solution pass through the resin.

11.3.2 Column acid wash protocol and column blanks

The loaded column was rinsed with 3 ml of 0.8 mol/l HNO_3, followed by 10 ml of 8 mol/l HNO_3. Final rinse was made with 6 ml of 0.8 mol/l HNO_3. Final rinse with 5 ml of 8 mol/l HNO_3 was collected for column blanks and dried down for analysis. The dried contents were dissolved in 5 ml 0.1 mol/l HCl and solution was analysed with Agilent 8800 ICP-MS/MS for any intensities of PGE originally coming from the column contaminations. The instrument rinse was made to distinguish between instrumental background and that of column blank. No significant intensities were monitored after the wash protocol of the resin. PFA vessels which are used to collect the eluate were boiled in concentrated nitric acid for 180 minutes at 180 °C. Vessel blanks had no significant intensities. The columns were kept in 6 mol/l HCl overnight. These were thoroughly rinsed, washed and treated with ultrasonic bath prior to every use.

11.3.3 Acid blanks from HCl and HNO_3

5 ml of concentrated HCl and HNO_3 were taken in PFA-vials and the PGE-spike was added to them separately. The solutions were capped and kept for 30 minutes for the spike equilibration process. The solutions were dried and PGE were re-dissolved in 0.1 mol/l HCl. Solutions were treated with ultrasonic bath for 5 minutes for releasing the PGE into the solutions which might stick to the walls of vessels. The solutions were heated again and cooled to have an ambient temperature for the analysis. The PGE mass fractions in concentrated hydrochloric acid and nitric acid were less than 5 pg.

11.3.4 Sample loading

The sample solutions of reference materials which were digested with sintering were loaded on the columns. The samples were diluted to a larger volume (200-250 ml) to dissolve silicates. Clogging of the columns was observed when solutions were not diluted to

larger volumes. The flow rate of the solution through the column normally requires 7-10 hours. One disadvantage of larger dilutions of the sample solutions is the provision of hydroxy ligands to the chloro-complexes of the PGE, which have less affinity to be retained on the columns. This ensures complete rhenium recovery but other PGE are badly affected.

11.3.5 Elution scheme

After the whole of the solution has passed through the column, the anion-exchange resin was rinsed with 6 ml of 0.8 mol/l HNO_3, followed by an another rinse of 3 ml of 0.8 mol/l of HNO_3. This does not remove any PGE sticking to the resin, rather it clears the solution which is still present in the resin. The PGE were eluted using 4 ml of 8 mol/l HNO_3. Moreover, Re is more stable in HNO_3 media. The PGE were collected in PFA vessels. The vessels were kept on a hot plate at 110 °C for drying. The dried samples were dissolved in 5 ml of 0.1 mol/l HCl and were treated with ultrasonic bath to release any PGE sticking to the walls of the vessel. The vessels were heated to ensure dissolution of PGE in 0.1 mol/l HCl. The samples were analysed with the Agilent 8800 ICP-MS/MS in isotope ratio analysis acquisition mode.

11.3.6 Sample preparation of geological materials

The reference materials BIR-1, TDB-1 and OKUM were digested with sodium peroxide sintering. 0.5 g sample was taken and 2.5 g sodium peroxide was added. The sample was digested following the protocol developed in chapter 5. Heating of the sample and sodium peroxide was done at 480 °C for 2 hours instead of 30-45 minutes for complete digestion of the PGE contents. The final volume of the solution was kept 100 ml. A calibrated PGE enriched spike was added to the solutions and solutions were kept for some time for spike equilibration. The spike equilibration may not be obtained soon after its addition to the sample solutions. If the precipitates of the silicates appear, these can be dissolved with the addition 1-2 ml of concentrated HCl and upon further dilution of the solution e.g. 200 ml solution instead of 100 ml. The solution with the precipitates of the silicates may clog the column that makes it difficult for a solution to pass through the resin. The solution volume can be adjusted to form a clear solution by dilution and with the addition of 1-2 ml concentrated HCl. In our experiment clear solution with precipitates were observed by diluting from 100 ml to 200 ml. The solutions are loaded on the anion resin column for separation of matrix and pre-concentration of the PGE. A complete matrix removal process requires 7-10 hours.

11.3.7 Tests with standard solutions for uptake of the PGE

For the investigation of the retention of PGE on 500 mg Bio-Rad AG-1X8 200-400 mesh anion resin, a 50 ng standard solution of the PGE was mixed with a real matrix geological sample. The resin was washed with the protocol mentioned above. The PGE standard solution was loaded on the resin. The flow rate of the solution was controlled by connecting a stopper to the lower end of the column so as to bring maximum contact between PGE contents and the resin. The solution was collected and the PGE contents in the eluted solution were analysed. A similar aliquot of the sample containing the same concentration of PGE standard solution which was passed through the resin was measured to monitor the differences in the recovery and retention of the PGE in original solution and the solution passing the resin. The results of the measurement indicated that rhenium, osmium and gold were retained 90-100% by the resin. Palladium was retained 30%, Pt 70%, ruthenium 10% and rhodium 10%. The retention of ruthenium, palladium and rhodium were very less in comparison with other PGE contents. The reasons for lower retention by the resin are explained in coming sections.

11.3.8 Test of spike recovery with 0.5 g samples

The recovery of the spike was monitored in real geological samples after the elution. For evaluation of the recovery, a similar amount of the spike was analysed in parallel to the eluted sample solutions for finding the extent to which the spike has been recovered in real geological samples. The recoveries, in general, were low except rhenium, thus providing an ideal method for rhenium determination. The low recoveries of PGE have been reported by Enzweiler and Potts (1995) using the same experimental setup with sintering and fusion and slightly different elution scheme.

The recoveries of ruthenium were 20-30%. The solutions were diluted to 200-250 ml for dissolution of silicate precipitates, which had provided more hydroxy ligands upon dilution. $Ru(OH)_2Cl_2$ complexes might have formed and may not be retained by the resin as suggested by Enzweiler and Potts (1995). Palladium recovery was 60-70%. Silica was not removed and solutions upon dilution were clear. Then the argument of Pd precipitation with silica is not favourable. Pd-hydroxy complexes must have formed which were not retained by anion resin as also suggested by Enzweiler and Potts (1995). Platinum recovery was 40-50%. According to Enzweiler and Potts (1995), in alkaline solutions, Pt forms hydroxy chloro-complexes and substitution of chloro ligands for hydroxy ligands is not quantitative upon acidifying the solution with HCl. The anion resin is more preferential to retain chloro-complexes than the hydroxy complexes of the platinum.

Recovery of the rhenium was the highest 90-95%. Rhenium forms ReO_4^- and is strongly absorbed by the resin. It can be completely eluted with 3 mol/l HNO_3 (Morgan *et al.* 1991, Reisberg and Meisel 2002). Recovery of iridium was 30-40%. Iridium adsorption is possible when it is present in the form $IrCl_6^-$. It is easily reduced to the trivalent complexes which are not retained by the resin (Enzweiler and Potts 1995). The low recovery of osmium (10-20%) can be due to losses during heating steps of the sample preparation. The recovery of Au was 10-20% and that can be due to possible complexes of $[Au(OH)_3]^-$ or $[Au(OH)_4]^-$ which are not retained by the resin (Martin 1990). Rhodium with 10-20% recovery suggests that $RhCl_2^+$ species must have formed which are not retained by the resin as suggested in (Enzweiler and Potts 1995). The spike recoveries of PGE are shown in Table 10.3

Table 11.1: Spike recovery in all real matrix samples with sinter solutions

Spike recovery in real matrix samples with sinter solutions	
Spike	Recovery
^{99}Ru	20-30%
^{108}Pd	60-70%
^{185}Re	90-95%
^{190}Os	10-20%
^{191}Ir	30-40%
^{198}Pt	40-50%
^{197}Au	10-20%
^{103}Rh	10-20%

11.3.9 PGE contents in the residue and the supernatant of the sinter phases

To address the low recovery of PGE, the existing method was modified to determine the PGE contents of the geological samples. The sinter cake after the heating step in the oven was dissolved in 5 ml of deionized water. The spike was added at this stage. The suspension was centrifuged and two phases were obtained, i.e. residue and supernatant. The residue containing mostly un-dissolved hydroxides and supernatant containing silicates. These two phases were separated by centrifugation. The residue was dissolved in 15 ml of 3 mol/l HCl, while in supernatant which was already a clear solution and 2-3 ml concentrated HCl was added to it. The contents of the both phases were treated with resin separately. The analysis of isotopic ratios was performed and mass fraction data were summed for the individual mass fractions of PGE. The recovery of the PGE in sinter phases is shown in the Table 11.2.

Table 11.2: Recovery of the PGE in sinter phases in residue and supernatant

PGE recovery in sinter phases + resin						
Phases	Ru	Pt	Pd	Re	Ir	Os
R-1	6%	2%	25%	10%	14%	12%
R-2	8%	2%	20%	8%	11%	12%
R-3	7%	3%	31%	10%	17%	18%
R-4	12%	4%	35%	9%	15%	13%
S1	24%	37%	70%	98%	6%	4%
S2	26%	27%	69%	92%	9%	6%
S3	21%	23%	77%	92%	5%	2%
S4	19%	25%	73%	96%	5%	9%
R= residue S= supernatant						

From the study of the phases, it is shown that Ru, Pt, Pd and Re are more dispersed in silicate phases of the sinter, while Ir and osmium are more concentrated in the residue phases. Rhodium data show that it is more distributed in residual phase rather than in silicate phase. Gold contents were almost equally dispersed in both the phases of sinter. Overall chemistry of PGE is more complex in sinter solution due to a variety of complexes formed in solution. Reisberg and Meisel (2002) reported the chemical yield of rhenium up to 15% with alkali fusion, regardless of rhenium extraction technique. The rhenium yield obtained with sintering-anion exchange were 90-95% and anionic chromatographic extraction gives an ideal separation method for rhenium.

11.3.10 Re-PGE contents in procedural blanks

Five procedural blanks were prepared and loaded on anion resin for the determination of any PGE mass fractions. The blanks mainly consisted of sodium peroxide solution and hydrochloric acid, which were the same as used in the sample preparation. The eluates from the resin were measured for PGE isotopic ratios and mass fractions were calculated. The PGE contents (ng/g) are shown in Table 11.4. The precisions were calculated with the formula $\sqrt{(A)^2+(B)^2}$ where A and B are the Cps RSDs of the isotopes. The detection limits were calculated using 3 sigmas the standard deviations of the procedural blank concentrations.

11.3.11 Addressing discrepancies in Re data in RM TDB-1

Accurate $^{187}Re/^{188}Os$ and $^{187}Os/^{188}Os$ data in the geochronological and geochemical investigation of early Earth and subsequent evolution of silicate mantle are important for Re-Os isotope system. HPA acid digestions are complete for peridotites e.g. UB-N, but there have been observations that HNO_3/HCl acid attacks on basaltic material e.g. TDB-1 even with high temperature and pressure are not satisfactory for the complete extraction of Re (Meisel and Horan 2016). Only the addition of HF in combination with HPA proves to be effective (Dale *et al.* 2012, Ishikawa *et al.* 2014, Meisel *et al.* 2009). HF is hazardous, contact poison and causes MgF_2 precipitation. The lower recoveries of the rhenium in the initial work of Meisel and Moser (2004a) on TDB-1 were due to no use of HF on samples digested with HPA-ID. The recovery of rhenium improved with multi-wave digestion of samples using HF (Meisel *et al.* 2009). In the work of Ishikawa *et al.* (2014) with HPA-HF-HCl treatment on TDB-1 proved that HF is essential to release HSE from the silicate portions of rocks. Based on these observations a study on rhenium determination in geological reference material TDB-1 was conducted and presented in Goldschmidt 2014 Bokhari and Meisel (2014b). 500 mg test portions of TDB-1 were digested with Na_2O_2 sintering, spiked with PGE, pre-concentrated with anion-exchange column and measured with ICP-MS/MS. Data obtained with sintering shown 1.02 ng/g of Re with a precision of less than 1% which is in accordance with recent literature data Ishikawa *et al.* (2014). The data for Re is shown in Table 10.4 and its comparison with literature data is shown in Figure 11.2. Sintering method is safe, inexpensive and provides maximum yield of rhenium and does attack the silicate portions of the rock where HSE are hosted. A recent argument by Day *et al.* (2015) states that the use of HF which may alter the Re/Os and Pt/Os ratios. Thus, sintering-anionic exchange-ID provides a better way of determination of rhenium.

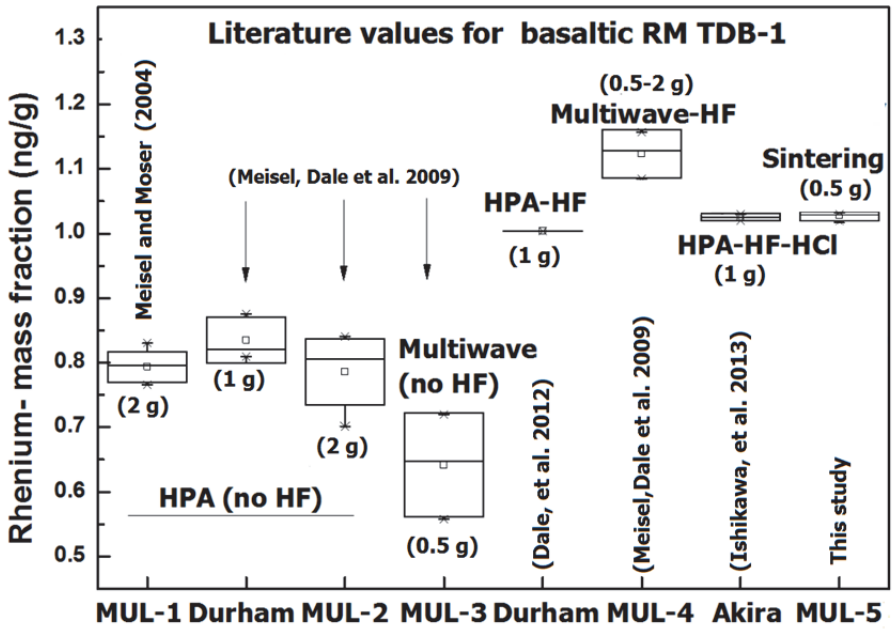

Figure 11.2: Re determination with sintering-anion exchange-ID and comparison with literature data

Table 11.3: Re mass fractions in geological reference material TDB-1

Re mass fractions in TDB-1 (ng/g)		
Sample	Determined	Precision
TDB-1a	1.08	1.4%
TDB-1b	1.10	1.3%
TDB-1c	1.10	1.0%
TDB-1d	1.09	1.8%
TDB-1e	1.10	1.5%
TDB-1f	1.09	1.7%
TDB-1g	1.10	1.4%
Mean	1.09	1.0%
Blank-corrected		

Table 11.4: Re-PGE mass fractions in procedural blanks

PGE mass fractions (ng/g) in procedural blanks																
Samples	Ru	Precision	Rh	Precision	Pd	Precision	Re	Precision	Pt	Precision	Ir	Precision	Au	Precision	Os	Precision
Blank-01	0.05	13%	0.40	8%	1.65	15%	0.15	3%	1.50	9%	0.19	7%	0.25	4%	0.30	4%
Blank-02	0.10	12%	0.30	8%	1.70	14%	0.05	2%	1.30	5%	0.09	10%	0.15	2%	0.30	13%
Blank-03	0.05	13%	0.30	8%	1.60	6%	0.20	4%	1.70	8%	0.09	11%	0.15	8%	0.10	7%
Blank-04	0.05	6%	0.20	7%	2.30	8%	0.20	4%	1.20	6%	0.29	4%	0.35	3%	0.25	7%
Blank-05	0.05	11%	0.45	14%	1.55	3%	0.38	3%	1.60	7%	0.13	26%	0.30	2%	0.25	10%
Mean	0.06		0.33		1.76		0.20		1.46		0.16		0.24		0.24	
Detection limits	0.07		0.29		0.92		0.36		0.62		0.25		0.27		0.25	

11.3.12 Addressing discrepancies in Ru data in RM BIR-1

Studies using BIR-1 as a reference for HSE and Re-Os isotope analysis are rare and only a few data are available. The literature on BIR-1 (Icelandic basalt ca. 48 g/100 g SiO_2) display poor reproducibilities of Ru and Ir indicating sample digestion problems for Ru and Ir relative to other PGE (Ishikawa *et al.* 2014, Meisel and Moser 2004b). BIR-1 replicates were digested with the main focus to determine ruthenium mass fraction. The method of supernatant and residue has been described earlier. The ruthenium contents in BIR-1 in replicates are shown in Table 10.12. The comparison of ruthenium values with literature data is shown in Figure 11.3. In the work of Bézos *et al.* (2005), Ishikawa *et al.* (2014), Meisel and Moser (2004b), it was shown that the recovery of ruthenium is affected if no HF is used with HPA/Carius tube digestions. The argument is that HF attacks the silicates sites where HSE are hosted. Similar to the study of rhenium, it is proved that sodium peroxide can be an alternative to avoid the use of HF. The values determined with sintering-anion exchange-ID are in good agreement with the existing literature data. Data for Pt, Pd, Re, Rh and Au were also determined through sintering-anion exchange-ID in the reference material BIR-1 as shown in Table 10.12. The data for PGE mass fractions is in good agreement with the literature values. The precision of the PGE data is less than 10%.

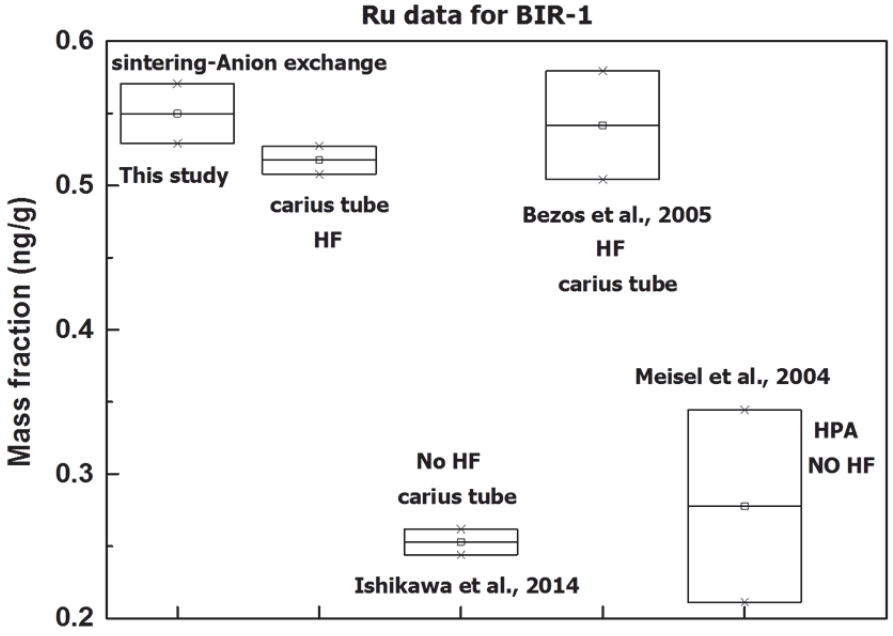

Figure 11.3: Ru mass fraction in BIR- 1 and its comparison with literature data

Table 11.5: PGE mass fractions (ng/g) in BIR-1 reference material

PGE mass fractions in BIR-1 (ng/g)					
Ruthenium					
	BIR-1	BIR-2	BIR-3	BIR-4	BIR-5
Determined	0.516	0.527	0.532	0.585	0.593
Precision	2%	2%	2%	4%	4%
Mean	0.551				
Precision	6%				
Meisel & Moser (2004)	0.278				

Akira *et al* (2013)	0.522
A. BÉZOS, *et al* (2005)	0.542

Palladium

	BIR-1	BIR-2	BIR-3	BIR-4	BIR-5
Determined	6.45	6.25	6.35	6.45	5.95
Precision	2%	2%	3%	3%	3%
Mean	6.29				
Precision	3%				
Meisel & Moser (2004)	6.11				
Akira *et al* (2013)	5.85				
A. BÉZOS, *et al* (2005)	6.33				

Platinum

	BIR-1	BIR-2	BIR-3	BIR-4	BIR-5
Determined	4.31	4.41	4.01	4.21	4.61
Precision	2%	3%	3%	3%	3%
Mean	4.31				
Precision	5%				
Meisel & Moser (2004)	4.3				
Akira *et al* (2013)	4.39				
A. BÉZOS, *et al* (2005)	4.56				

Rhenium

	BIR-1	BIR-2	BIR-3	BIR-4	BIR-5
Determined	0.606	0.621	0.647	0.611	0.618
Precision	2%	2%	3%	3%	3%
Mean	0.621				
Precision	3%				
Meisel & Moser (2004)	0.634				
Akira *et al* (2013)	0.684				

Rhodium

	BIR-1	BIR-2	BIR-3	BIR-4	BIR-5
Determined	0.321	0.381	0.397	0.366	0.318
Precision	3%	4%	2%	4%	3%
Mean	0.357				
Precision	10%				
Meisel & Moser (2004)	0.341				

Gold

	BIR-1	BIR-2	BIR-3	BIR-4	BIR-5
Determined	4.37	4.79	4.41	4.52	4.32
Precision	1%	2%	3%	3%	9%
Mean	4.482				

Precision	4%

11.3.13 PGE mass fractions in OKUM

OKUM is a new reference material that is included in this study for comparison of the PGE data with ILC data. The PGE contents determined for OKUM through the sintering-anion-exchange are in good agreement with literature/ILC data. The PGE mass fractions determined in OKUM are having a precision of less than 10%.

Table 11.6: PGE mass fractions in OKUM reference material

PGE mass fractions in OKUM (ng/g)					
Ruthenium					
	OKUM-1	OKUM-2	OKUM-3	OKUM-4	OKUM-5
Determined	4.26	5.53	4.55	4.83	5.4
Precision	2%	2%	2%	4%	4%
Mean	4.91				
Precision	11%				
ILC value	4.48				
Palladium					
	OKUM-1	OKUM-2	OKUM-3	OKUM-4	OKUM-5
Determined	12.4	12.5	12.7	12.3	12.7
Precision	2%	2%	3%	3%	3%
Mean	12.5				
Precision	2%				
ILC value	11.3				
Platinum					
	OKUM-1	OKUM-2	OKUM-3	OKUM-4	OKUM-5
Determined	11.81	10.41	13.02	11.57	11.25
Precision	2%	3%	3%	3%	3%
Mean	11.90				
Precision	8%				
ILC value	12.01				
Iridium					
	OKUM-1	OKUM-2	OKUM-3	OKUM-4	OKUM-5
Determined	0.79	0.81	0.73	0.79	1.08
Precision	2%	2%	3%	3%	3%
Mean	0.839				
Precision	17%				
ILC value	0.9572				

Rhodium					
	OKUM-1	OKUM-2	OKUM-3	OKUM-4	OKUM-5
Determined	1.476	1.34	1.397	1.366	1.318
Precision	3%	4%	2%	4%	3%
Mean	1.379				
Precision	4%				
ILC value	1.434				

Gold					
	OKUM-1	OKUM-2	OKUM-3	OKUM-4	OKUM-5
Determined	1.37	1.79	1.41	1.52	1.32
Precision	1%	2%	3%	3%	9%
Mean	1.48				
Precision	13%				
Savard *et. al* (2010)	1.33				

Osmium					
	OKUM-1	OKUM-2	OKUM-3	OKUM-4	OKUM-5
Determined	0.94	0.96	0.77	0.74	0.82
Precision	5%	18%	8%	4%	8%
Mean	0.80				
Precision	12%				
ILC value	0.84				

Rhenium					
	OKUM-1	OKUM-2	OKUM-3	OKUM-4	OKUM-5
Determined	0.405	0.48	0.421	0.488	0.452
Precision	2%	4%	7%	4%	4%
Mean	0.449				
Precision	8%				
ILC value	0.483				

11.4 Summary

In this chapter, the discrepancies in the Re and Ru mass fractions of TDB-1 and BIR-1 have been addressed through the development of a method based on sintering-anion-exchange chromatography. The existing methods using HPA and Carius tube digestions require the use of HF for attacking Re and Ru hosted in silicate portions of the rock. On the other hand, special care must be taken in handling HF as there is no excuse for mishandling HF which can lead to serious conditions in the case of unavailability of proper medical care.

This chapter provides an insight on the low recoveries of PGE using sinter-anion-exchange-ID due to the formation/presence of hydroxy chloro-complexes. They are not effectively retained on the resin, thus causing a low chemical yield. Rhenium recovery is 90-95%, while recovery of ruthenium did not improve. However, the isotope dilution method is

independent of chemical yields, thus enabling sintering-anion-exchange-ID to determine all PGE in geological samples.

An investigation of the extent to which PGE are present in two phases of sinter has been presented in this chapter. Based on the observations, it is shown that Rh, Ru, Re, Pt, Pd is mostly present in the supernatant and Ir and Os are present in the residue phase of sinter if the spike is added before centrifugation step. Gold is equally distributed in both the silicate and the residue phases of the sinter. Sintering-anion exchange method provides a slightly better detection limits but is not comparable with that of HPA and Carius tube digestion. The DL of the Ru is 0.06 ng/g, Pt is 0.62 ng/g, Pd is 0.92 ng/g, Re is 0.36 ng/g, Rh, 0.29 ng/g, Au is 0.27 ng/g, Ir is 0.25 ng/g and osmium is 0.25 ng/g. The detection limits were determined with 3 sigmas the standard deviations.

Further work is required to perform using larger sized glassy carbon crucibles for taking larger test portions for PGE mass fraction determination.

12. Novel method for ruthenium/osmium determination with sparging

12.1 Introduction and background

Ruthenium (Ru) and Osmium (Os) belong to the platinum group elements. Ru and Os were discovered in 1844 by K. Klaus and 1803 by S. Tennant. They were discovered independently in the residue left after the crude platinum was dissolved in aqua regia. The name ruthenium was kept after the Latin name of Russia (Ruthenia) and osmium after the Greek word of odour because of the characteristic and pungent smell of the volatile OsO_4 (Greenwood and Earnshaw 1997). Ruthenium and osmium are generally found in the metallic state with other platinum group elements and are hard, brittle and have poor oxidation resistance. The estimated abundance of Ru is 0.0001 mg/kg and 0.005 mg/kg in earth crustal rocks (Greenwood and Earnshaw 1997).

Ruthenium and Os are produced from the platinum concentrates, obtained as anode slimes from the electrolytic refinement of Ni. The aqua regia dissolves the Pt, Pd, and Au while Ru, Os, Ir and Rh are obtained in the form of powder or sponge consolidated by the powdered metallurgical techniques (Greenwood and Earnshaw 1997). The residue after the removal of Ag (with lead carbonate/HNO_3), Pt, Pd and Au (with aqua regia) is fused with sodium peroxide and leached with water after the removal of Rh and Ir. The solution contains $(RuO_4)^{2-}$ and $[(OsO_4\ (OH)]^{2-}$.

Ruthenium is mostly used in hard disks and in alloys with platinum for the jewellery and electrical contacts. It also has an increasing use in catalysis. Osmium is used in the production of very hard alloys, i.e. instrument pivots. It is used in the electronics industry for chip resistors and electrical contacts. Ruthenium oxide is used in the chemical industry to coat the anodes of the electrochemical cells for chlorine production. Ruthenium is also used in catalysts for ammonia and acetic acid production. Ruthenium compounds can be used in solar cells, which convert the light energy into electrical energy (Emsley 2011). Osmium is used to make very hard alloys, ball point ends and ends of the fountain pens etc.

Greenwood and Earnshaw (1997) reported the passage of chlorine gas through the solution containing volatile $(RuO_4)^{2-}$ and $[(OsO_4\ (OH)]^{2-}$ for the collection of ruthenium as H_3RuCl_6 solution in hydrochloric acid and $[(OsO_4\ (OH)]^{2-}$ in alcohol/NaOH. Both the solutions were treated with ammonium chloride, which forms the precipitates of $(NH_4)_3RuCl_6$ and $OsO_2(NH_4)_3Cl_2$ which on ignition in H_2 gas, form Ru and Os metal.

Ruthenium and osmium are unaffected by non-oxidising acids or aqua regia and are the most reactive with oxidising agents. Osmium, when present in finely divided form may also form OsO_4 (Greenwood and Earnshaw 1997). The lowest oxidation state of both is (+4) in the form of OsO_2 (yellowish brown solid) and RuO_2 (black solid). Osmium and Ru can attain (+8) oxidation state in the form of OsO_4 and RuO_4. Both the tetraoxides are volatile. The melting and boiling points for RuO_4 are 25°C and 40°C respectively. The melting and boiling for OsO_4 are 40°C and 130°C respectively. Osmium is converted to OsO_4 by concentrated nitric acid. The formation of RuO_4 requires stronger oxidising agent than for OsO_4 as concentrated nitric acid alone is not sufficient (Greenwood and Earnshaw 1997). The oxidising agent $KMnO_4$, KIO_4 or Cl_2 are required with acidified solutions.

Ruthenium occurs with seven isotopes in nature i.e. ^{96}Ru (5.54%), ^{98}Ru (1.87%), ^{99}Ru (12.76%), ^{100}Ru (12.60%), ^{101}Ru(17.06%), ^{102}Ru (31.55%) and ^{104}Ru (18.62%). ^{96}Ru and ^{98}Ru are produced via *p*-process, ^{100}Ru produced via *s*-process, ^{104}Ru produced via *r*-process and ^{99}Ru, ^{101}Ru and ^{102}Ru produced via *s* and *r*-processes (Fischer-Gödde *et al.*

2015). For the purposes of isotope dilution measurement at least two isotopes are required and normally ^{99}Ru (12.76%),^{101}Ru (17.06%) and ^{102}Ru (31.55%) are measured with the ICP-MS. The common spectral interferences on ruthenium isotopes are $^{98}Mo^{1}H^{+}$and $^{64}Zn^{35}Cl^{+}$ on $^{99}Ru^{+}$ and $^{100}Mo^{1}H^{+}$, $^{85}Rb^{16}O^{+}$, $^{61}Ni^{40}Ar^{+}$ and $^{65}Cu^{35}Cl^{+}$ on $^{101}Ru^{+}$ and $^{86}Sr^{16}O^{+}$, $^{62}Ni^{40}Ar$, $^{67}Zn^{35}Cl^{+}$ and $^{102}Pd^{+}$on $^{102}Ru^{+}$ and $^{104}Pd^{+}$ on $^{104}Ru^{+}$.

The precise determination of the ruthenium mass fractions in geochemical samples is important for determining the partitioning conditions between the silicate melts and the metal for an understanding of the geochemical evolutionary processes of the earth and the other planets. The isotopic studies of ruthenium are important for nuclear-physical interests i.e. ^{98}Tc- ^{98}Ru, and ^{99}Tc- ^{99}Ru decay systems for the early solar system chronology (Becker and Walker 2003) and for the geochemical detection of ^{100}Mo- ^{100}Ru double beta decay phenomenon (Poths and Rundberg 1990).

Understanding the origin of isotopic anomalies in materials may help to constrain the efficiency of mixing in the early solar system, and to access the nebular processes affecting the solid material contributing to the formation of planets testimonials and planets and to address these issues for ruthenium studies in the meteorites (Dauphas *et al.* 2002, Fischer-Gödde *et al.* 2015).

The study of Re-Os isotopic system is an important tool for the investigation of geological and Cosmo-chemical problems emerging from the differentiation of the meteorites to the variation of the Earth's climate. Several methods have been developed for the determination of osmium in different matrices. Osmium isotopic compositions were determined by electron bombardment of OsO_4 gas by Nier (1937). The gas source mass spectrometer was used for osmium determination in meteorites and molybdenites by Herr *et al.* (1961), Hirt *et al.* (1963). Accelerator mass spectrometer was used by Fehn *et al.* (1986). Secondary ion mass spectrometry technique (SIMS) was developed by Luck (1982). Resonance ionisation mass spectrometry (RIMS) technique was developed by Walker and Fassett (1986). Negative thermal ionisation method (NTIMS) used by (1991), Völkening *et al.* (1991). ICP-MS was employed by Dickin *et al.* (1988), Lichte *et al.* (1986), (Meisel *et al.* 2001a), Russ III *et al.* (1987). Magnetic-sector ICP-MS was used by Hassler *et al.* (2000). Laser ablation multi-collector-inductively coupled plasma mass spectrometry was used by Pearson *et al.* (2002).

The trace concentrations of Os in the Earth's mantle are sulphides, alloys and other trace phases, rather than by the major silicates. Reisberg and Meisel (2002) reported analytical difficulties for the osmium measurement due to the trace concentrations of Os, volatility of OsO_4, losses during the sample digestion with the classical techniques, nuggets of Os and the high ionisation potential is not suitable with positive TIMS analysis.

A review by Reisberg *et al.* (2002) describes that minimum quantities of Os required for isotopic analysis and improvement in precision over time have progressed with the innovation of the advanced instruments. The ICP-MS technique is rapid in comparison with single collector NTIMS measurements and the precision of ICP-MS analysis is significantly lower than that of NTIMS (ion yield ~ 0.08% for ICP-MS) (Schoenberg *et al.* 2000) up to 20% for NTIMS (Birck *et al.* 1997, Reisberg and Meisel 2002).

The sample digestion methods which can completely dissolve all the refractory contents of the sample are required. Several methods have been reported as in a review by Reisberg *et al.* (2002). Dissolution in reducing media (HBr, HCl-ethanol) can provide control on losses of OsO_4 but incomplete sample digestions are often reported. NiS-fire assay may offer complete sample digestion but have high blanks with losses of OsO_4. Carius tubes digestions are complete and have low blanks but accompanies danger of the explosions.

High-pressure-asher digestions are best suited for complete digestion and low blanks but suffer from expensive apparatus and huge maintenance costs (Meisel and Moser 2004b). Alkaline fusions offer complete sample digestions but high blanks and spike equilibration are problematic (Reisberg and Meisel 2002). The use of sodium peroxide is required for fusion or sintering methods. Fusion is acquired at higher temperatures than the melting point of the flux but sintering requires the heating below the melting point of the flux. Fusion is done in corundum crucibles Qi *et al.* (2004) but sintering can be done with carbon crucibles Meisel *et al.* (2002).

The method of sample digestion is sintering in this thesis. It is intended here now to determine the ruthenium and osmium mass fractions in the geological reference materials by the application of sintering for the sample digestion. This was done by the development of a new technique based on the principle of the sparging applied on sinter solutions. The sparging of ruthenium required volatilisation of ruthenium from the sinter solution and the essential details are given in next paragraphs.

12.1.1 Volatilisation of ruthenium

Ruthenium tetra-oxide is formed in the acidic solution by the strong oxidants and it begins to volatilise at 45 °C, which is complete at 110°C (Wyatt and Rickard 1961). In the study of ruthenium volatility, $Ru(NO)(NO_3)_3$ (in nitric acid solution) was oxidised to volatile RuO_4 and the reaction rate was increased when the acid concentrations were above 7.5 mol/l (Sasahira and Kawamura 1988). A study of the reaction of the elements with perchloric acid at 200 °C has also provided information on volatilisation of Os, Re and ruthenium into possible oxides (Hoffman and Lundell 1939). Gorsuch (1970) reported that during mineralisation, some elements Ru, Os, Re and Tc may volatilise under oxidising conditions. Meyer *et al.* (1970) have reported several oxidising agents for oxidation of ruthenium to RuO_4 i.e. Cl_2, $NaBrO_3$, $KBrO_3$, $KMnO_4$, KIO_4, $HClO_4$, $NaBiO_3$, CrO_3, $K_2Cr_2O_7$, $(NH_4)_2S_2O_8$, PbO_2 and $Ce(SO_4)_2$ etc.

For the ruthenium isotopic analysis with the ICP-MS, a chemical separation of matrix interferences i.e. Zr, Mo and Pd is required. Mo was reported to be a major interference in chemical analysis of ruthenium isotopes (Ly and Hidaka 2004). Based on volatilisation of ruthenium, it is aimed to sparge ruthenium and determine whether interferences are removed for quantification of Ru mass fractions. In this thesis, a new analytical method for the precise determination of the ruthenium isotopes with direct sparging into the ICP-MS is developed for geological reference materials. Osmium has also been measured which has already been developed and employed by Hassler *et al.* (2000), Meisel and Moser (2004b), Sen and Peucker-Ehrenbrink (2014).

12.2 Objectives of the chapter

A method is presented here for the rapid determination of Ru and Os isotopic compositions with isotope dilution in geological reference materials. The method is particularly applied to samples digested with sodium peroxide sintering. This method employs oxidation/volatilisation of ruthenium and osmium with $KMnO_4$ and transfer of RuO_4 and OsO_4 by an argon gas stream into the torch of ICP-MS for an analysis without the use of a nebuliser.

Following were the salient features of this study,

1. The volatilisation of Ru with different oxidising agents as Os sparging is already a state of the art for osmium determination.
2. Testing different acids with oxidising agents for optimisation of the method.

3. Testing different amounts of oxidising agent for maximum signal intensities for the isotopic ratio determination.
4. To determine the recovery of the ruthenium standard solution by sparging.
5. To acquire isotopic ratio for ruthenium and osmium.
6. To apply the method on real matrix.
7. Method validation with reference materials.

12.3 Experimental

12.3.1 Reagents and materials

Analytical reagent-grade sodium peroxide ACS, ISO Merck KGaA, Darmstadt, Germany has been used for the sample digestion. Hydrochloric acid 37 g/100 g p.a., Roth Karlsruhe, Germany was sub-boiled for experimental purposes. HNO_3 65 g/100 g p.a., Roth Karlsruhe, Germany (sub-boiled) was used in dilution and rinsing the instrument. An ultra-clear unit for ultra-pure water (Siemens water technologies) with conductivity: 0.055 µS/cm, TOC content: < 1 ng/g, was used for diluting acids and samples. Glassy carbon crucibles (25 x 25 mm HTW) were used for sample digestion. A PGE enriched spike containing ^{99}Ru and ^{190}Os was used for isotope dilution analysis. Single elements standard solution (1000 μg/l) of ruthenium for initial sparging was obtained from the SPEX Chemicals USA. The solutions were diluted to 1 ng/ml with 0.1 mol/l HCl. Special PFA-vials (Savillex, USA) are used for sparging. Solutions after preparation were stored in PP vials (50 ml, Sarstedt). The geological reference materials i.e. OKUM, MUH-1, WGB-1 and BRP-1 were digested with sodium peroxide sintering using 1:5 sample to sodium peroxide ratio for the method validation. No initial testing on osmium intensity was made, but osmium isotopes were measured when a solution containing ruthenium from real matrix was sparged. The Agilent 8800 ICP-MS/MS was used for isotope ratio analysis using manual acquisition mode by switching off the nebuliser in the remote setting of mass hunter workstation. The instrument was not tuned with tune solution, but the argon flow rate was adjusted for maximum signal intensities for ruthenium. However, the argon flow rate was kept around 1 ml/min.

12.3.2 Experimental design for ruthenium-osmium sparging

0.5-gram test portions of geological reference materials were digested with sodium peroxide sintering with 1:5 sample to the sodium peroxide ratio.

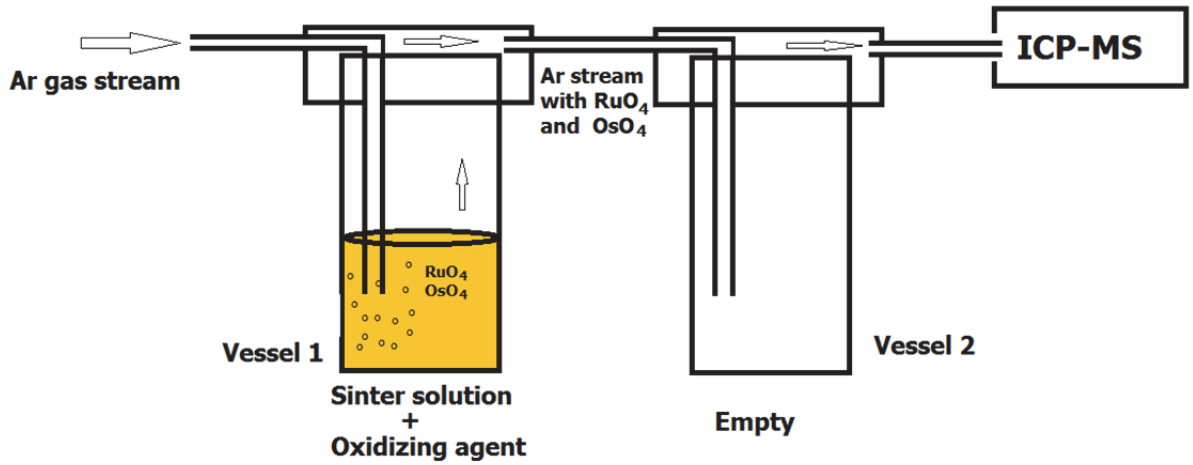

Figure 12.1: Experimental setup for ruthenium and osmium sparging

The makeup volume was kept 100 ml and a PGE enriched spike containing ^{99}Ru and ^{190}Os was added to the solution. The volumetric flask containing sinter solution was capped so as to avoid losses of OsO_4 and RuO_4.The solution was kept 2-3 hours at ambient temperature for spike equilibration, otherwise spike equilibration problems will arise. The losses of OsO_4 and RuO_4 has not been investigated during the sample preparation procedure as the isotope dilution method is independent of analyte losses during sample preparation procedures. The main operations of ruthenium sparging were similar as mentioned in Hassler *et al.* (2000) and Meisel *et al.* (2001a). 5 to 10 ml aliquots of the sample were taken in PFA vessels. The cap of the vessel had argon inlet and argon-OsO_4/RuO_4 outlet. To the solution containing ruthenium and osmium, an oxidising agent was added in small amounts i.e. 10-30 mg. The oxidising agents tested for ruthenium volatilisation are discussed in next sections. The solution was heated at 40 °C for one minute. Argon gas at a flow rate of 1 ml/min is connected with the argon inlet of the PFA vessel. The air was purged out for 30 seconds from the vessel to eliminate nitrous oxide and aerosols formed in it. The vessel was connected with another empty vessel for stabilisation of gas stream of Os and ruthenium signals. The empty PFA vessel is then connected to ICP-MS through glass connector (that replaces the nebuliser). The flow sheet diagram of ruthenium and osmium sparging is given in Figure 12.1. The integration time for isotopic ratio determination was kept 3 seconds per mass to acquire maximum precision. Gas blank, reagent blank and the procedural blank were tested for every batch of samples. The discussion on all the oxidising agents used in this study is given hereafter.

12.4 Initial sparging tests with different oxidising agents.

Volatilisation of ruthenium with $K_2S_2O_8$ powder in 0.1 mol/l HCl

A 10 ng standard solution of ruthenium was prepared in 0.1 mol/l HCl solution. A gas blank was run to identify any instrumental background on ruthenium isotopes. For initial testing, ^{99}Ru, ^{101}Ru, ^{102}Ru and ^{104}Ru were analysed along with osmium isotopes to control the sparging conditions. 10 mg powder of $K_2S_2O_8$ was added to the standard solution of ruthenium in PFA vessel and was heated at 40 ºC for one minute. The oxidation of RuO_4 occurs at a temperature of 40 ºC. The vessel was connected with argon plasma tubing to purge the trapped air for 30 seconds. The vessel was then connected with direct tubing of argon gas, which was immersed in the solution of ruthenium. A separate empty vessel was connected between a vessel containing the standard solution of ruthenium and the glass connector replacing the nebuliser. It traps any aerosol formed, preventing it from entering the ICP-MS/MS. The analysis was performed with no gas mode without MS/MS configurations at the mass hunter workstation of the Agilent 8800 with manual acquisition. An integration time of 3 seconds for 25 replicates was set for the isotope ratio analysis acquisition mode. Any ruthenium volatilised was introduced into a separate vessel and was then led to the instrument. For oxidising agent $K_2S_2O_8$, no ruthenium was mobilised through the solution as seen from the ion signals on the respective ruthenium isotopes. By increasing the concentration of the ruthenium solution of 100 ng and the addition of 20 mg $K_2S_2O_8$, ion signal appeared on ruthenium isotopes. An average of 4716 counts were observed at ^{99}Ru, 6519 counts at ^{101}Ru, 12365 counts at ^{102}Ru and 9128 counts at ^{104}Ru with 18% RSD. The intensity was far so less for trace analysis on given 100 ng ruthenium standard solution. The natural isotopic ratio of $^{99}Ru/^{101}Ru$ is 0.75, $^{99}Ru/^{102}Ru$ is 0.40, $^{99}Ru/^{104}Ru$ is 0.69. The determined isotopic ratio of volatilised ruthenium isotopes was 0.72, 0.38 and 0.52 respectively, which were not natural indicating presence of some interferences from the matrix elements. $K_2S_2O_8$ /H_2O_2 was tested for mobilisation of ruthenium and no intensity was observed with the addition of H_2O_2. The recovery with $K_2S_2O_8$ volatilisation of ruthenium was

too low beside incorrect ratios, therefore it was assumed $K_2S_2O_8$ is not a good oxidising agent for ruthenium volatilisation.

Volatilisation of ruthenium with $K_2Cr_2O_7$/ H_2SO_4 mixture

A mixture of $K_2Cr_2O_7/H_2SO_4$ was tested with a ruthenium standard solution. 1 ml of $K_2Cr_2O_7$/ H_2SO_4 was added to 10 ng ruthenium standard solution. The solution was sparged after following the protocol mentioned above. No significant volatilisation of ruthenium was observed, even with the addition of more amounts of 1 mol/l $K_2Cr_2O_7/H_2SO_4$ mixture or by increasing concentration of ruthenium solution.

Volatilisation of ruthenium with conc-$HClO_4$

The addition of concentrated $HClO_4$ in varying amounts to the ruthenium standard solution did not volatilise any ruthenium at the given experimental set up at 40 ºC.

Volatilisation of ruthenium with $KBrO_3$

The use of $KBrO_3$ powder was very effective in the ruthenium volatilisation. A 5 ng standard solution of ruthenium yielded 8629 cps at the first replicate. The drop in intensity of the ruthenium ions volatilised over 25 replicates is given in Figure 12.2. A similar check was made by increasing the concentration to 100 ng ruthenium standard solution that yielded 369067 counts at the first replicate and then the intensity dropped as shown in Figure 12.2. The isotopic ratios of the ruthenium isotopes determined for the ruthenium volatilised for 5 ng and 100 ng solutions with $KBrO_3$ are given in Figure 12.3 and Figure 12.4.

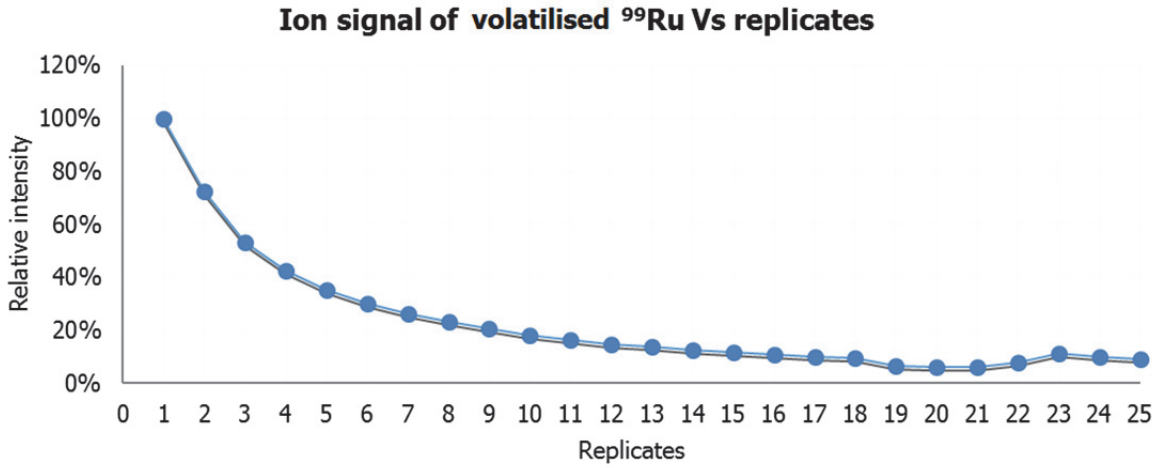

Figure 12.2: Drop in intensity of Ru ions with time

The isotopic ratio 99Ru/101Ru were most affected from matrix spectral overlap of bromide ions. However, isotopic ratios $^{99}Ru/^{102}Ru$, $^{99}Ru/^{104}Ru$ and $^{101}Ru/^{102}Ru$ were less interfered as shown in the Figure 12.3 and Figure 12.4. The isotopic ratios with a lower concentration solution i.e. 5 ng solution were more affected from interferences than the solution of the higher concentrations i.e. 100 ng.

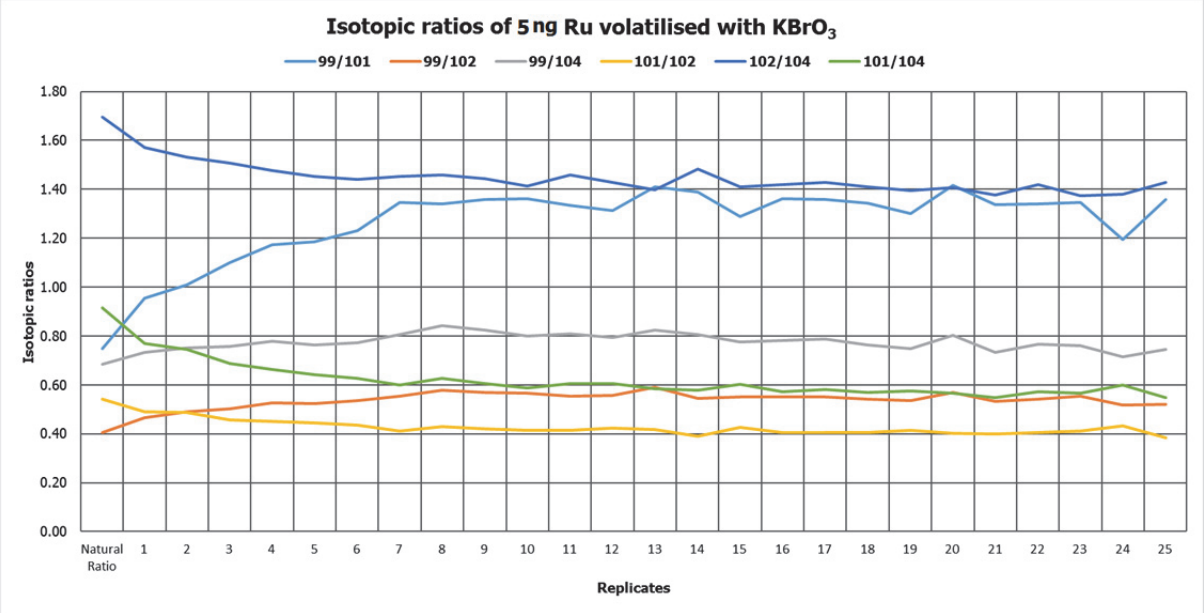

Figure 12.3: Isotopic ratios of ruthenium volatilised from 5 ng solution

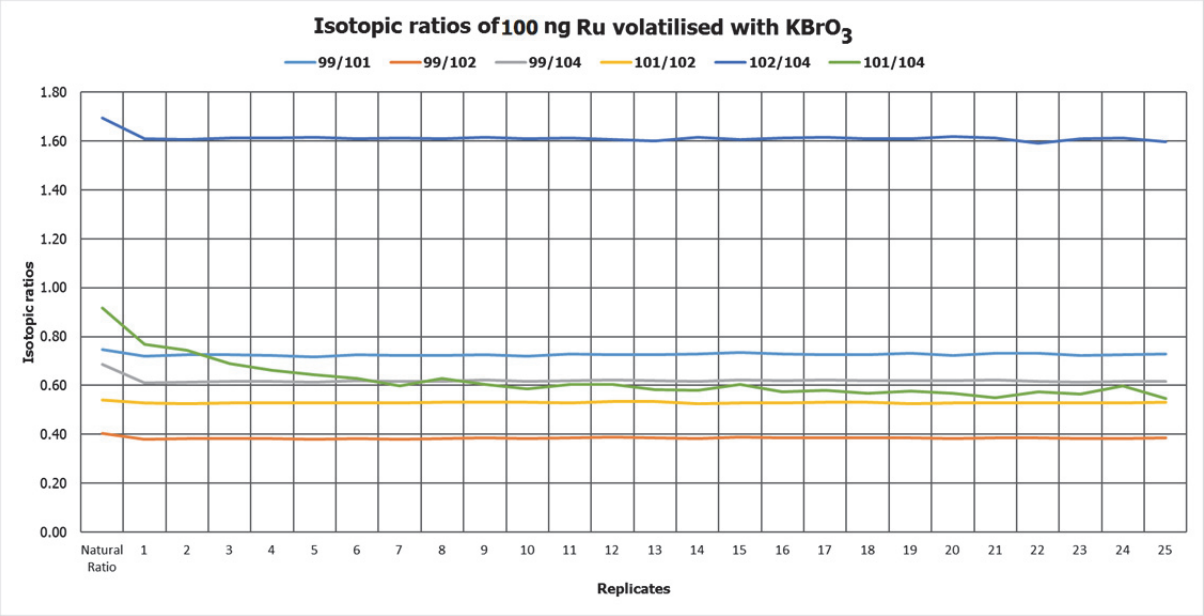

Figure 12.4: Isotopic ratios of ruthenium volatilised from 100 ng solution with $KBrO_3$

Reagent blanks with $KBrO_3$

The reagents used for the ruthenium volatilisation from the rutheium solution were $KBrO_3$ in 0.1 mol/HCl solution. The solution of HCl was used to prepare a standard solution of ruthenium. In the absence of ruthenium standard solution a high background was observed which is probably due to the formation of bromide ions as suggested by Raleigh (1935) in ruthenium distillation experiments. The reagent blank had the intensity at ^{99}Ru as 4558 Cps, at ^{101}Ru as 1727 CPS, at ^{102}Ru as 4142 Cps and at ^{104}Ru as 2939. However, the use of $KBrO_3$ in ruthenium distillation was useful and it will be discussed in distillation section.

12.4.1 Optimisation of $KBrO_3$ for ruthenium recovery

Effect of variable amounts of $KBrO_3$

The recovery of ruthenium from the standard solution depended on the amount of $KBrO_3$ used for volatilisation. Variable amounts of $KBrO_3$ were used to see the maximum recovery of ruthenium isotopes through volatilisation/mobilisation from the solution. 50-70 mg of $KBrO_3$ used, resulted in the maximum recovery of the ruthenium isotopes as shown in the Figure 12.5.

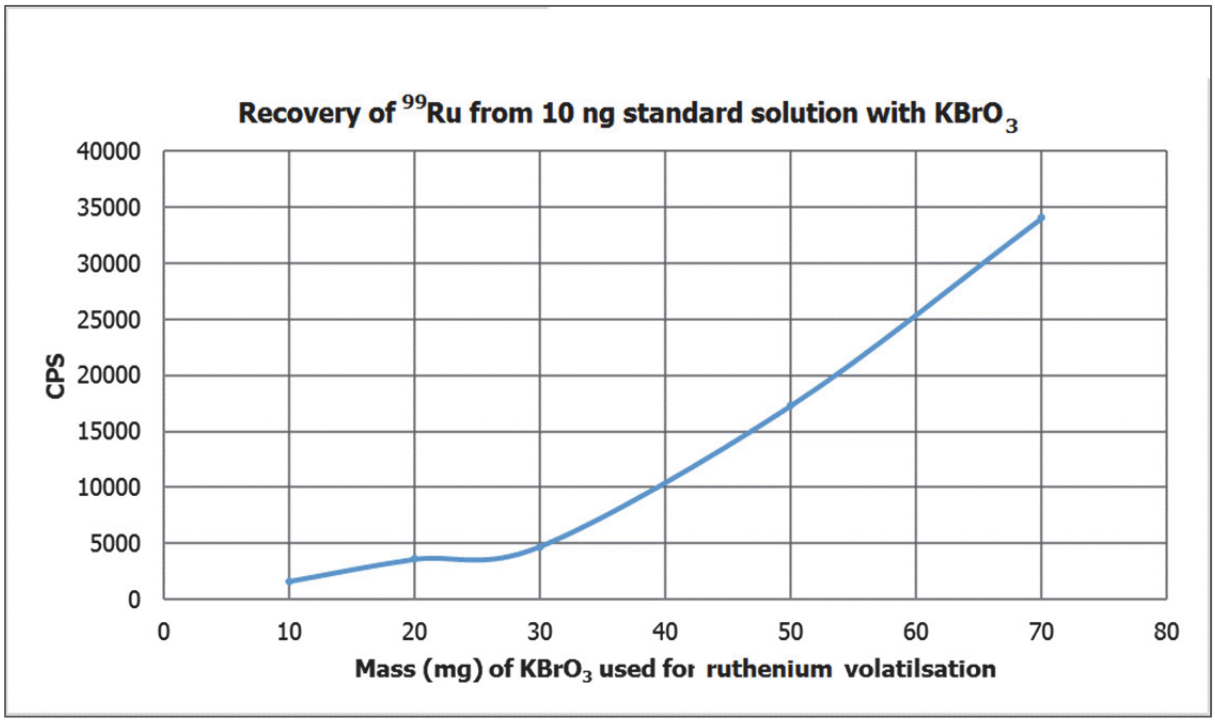

Figure 12.5: Effect of amount of $KBrO_3$ of ruthenium mobilised through the solution

Effect of nitric acid media

In order to optimise the sparging of ruthenium with $KBrO_3$, different amounts of $KBrO_3$ were tested with given standard solution of ruthenium and an improvement in intensity was observed. Further experiments were performed by the addition of 1 ml of concentrated nitric acid to the standard solution of ruthenium for its mobilisation to the instrument for analysis. As the presence of HCl in ruthenium mobilisation was objected by Raleigh (1935) during ruthenium distillation. Its presence causes a film of ruthenium dioxide to be formed on the walls of the apparatus unless care was taken to control the temperature during distillation (Raleigh 1935). The addition of nitric acid not only improved the intensity as well as the isotopic ratio and the precision. The average isotopic ratio determined for 20 replicates was 0.75 $^{99}Ru/^{101}$ Ru similar to natural ratio. The isotopic ratio of $^{99}Ru/^{102}Ru$ was not consistent as it suffered some spectral overlap from the matrix. The effect of the addition of nitric acid to a ruthenium standard solution is shown in Figure 12.6. The volatilisation of ruthenium without the addition of HNO_3 shows the highest intensity in the first replicates, which gradually decreased over the time span of the replicates (Figure 12.2). With the addition of nitric acid, intensity increases gradually and become constant and then decreases with time in further replicates.

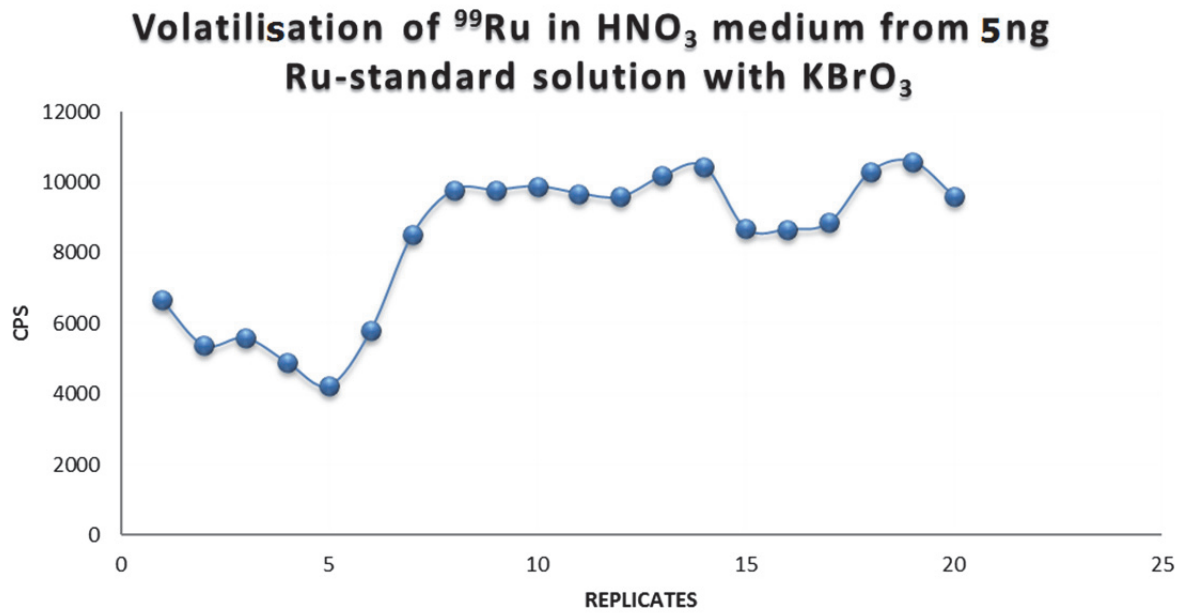

Figure 12.6: Volatilisation of ruthenium from 5 ng standard solution with $KBrO_3$

Volatilisation of ruthenium with $K_2Cr_2O_7$

Ruthenium did not volatilise from the solution upon addition of solid $K_2Cr_2O_7$ even with of HNO_3, H_2SO_4, H_2O_2 and HCl which were added separately in different experiments.

Volatilisation of ruthenium with solid Na_2O_2 in 0.1 mol/l HCl

The use of powdered sodium peroxide did not volatilise any ruthenium isotope from the solution except ^{102}Ru and ^{104}Ru. But the intensity of ^{102}Ru and ^{104}Ru isotopes was less than 3000 counts over 10 replicates. As sodium peroxide did not recover any ^{99}Ru isotopes it was assumed, this intensity may be from interference due to NaBr formation. Thus, no further work was carried on using sodium peroxide as an oxidising agent.

Volatilisation of ruthenium with $KMnO_4$

$KMnO_4$ is a strong oxidising agent and was tested for mobilisation of ruthenium from a solution into the ICP-MS through the direct sparging. A freshly prepared concentrated solution of $KMnO_4$ was initially tested for the ruthenium mobilisation from 10 ng ruthenium standard solution. Far better intensity of the ruthenium isotopes was observed compared to the use of $KBrO_3$ for the ruthenium volatilisation. The addition of H_2O_2 along with $KMnO_4$ solution decreased the intensity because it oxidised Mn^+ before it could oxidise any ruthenium. Then a test was performed by the addition 1 ml of concentrated H_2SO_4 with a few milligrams of solid $KMnO_4$, and the solution was heated at 40 °C. The highest intensities were initiated through ruthenium mobilisation in the ICP-MS spectrum. The addition of sulphuric acid with oxidising agent KMnO4 in solid state, proved to be excellent among all other oxidising agents that were tested so far. The comparison of intensities observed with use of solution $KMnO_4$ and solid $KMnO_4/H_2SO_4$ is shown in Figure 12.7.

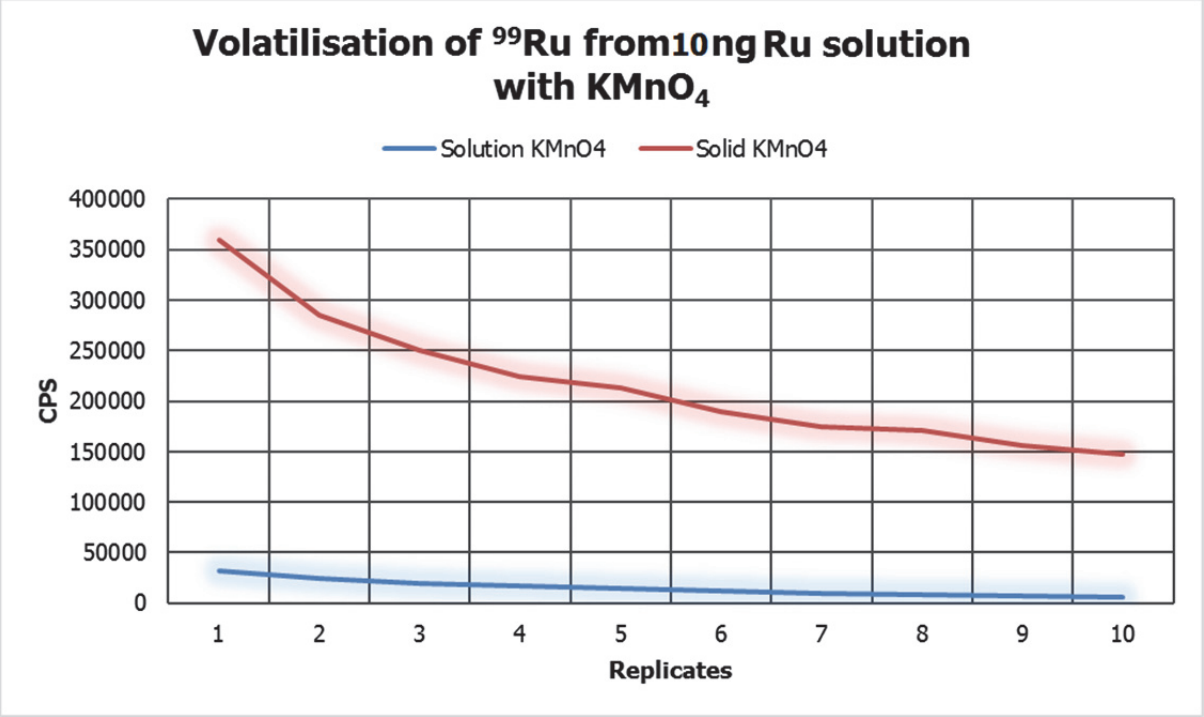

Figure 12.7: Volatilisation of ruthenium from 10 ng standard solution with $KMnO_4$

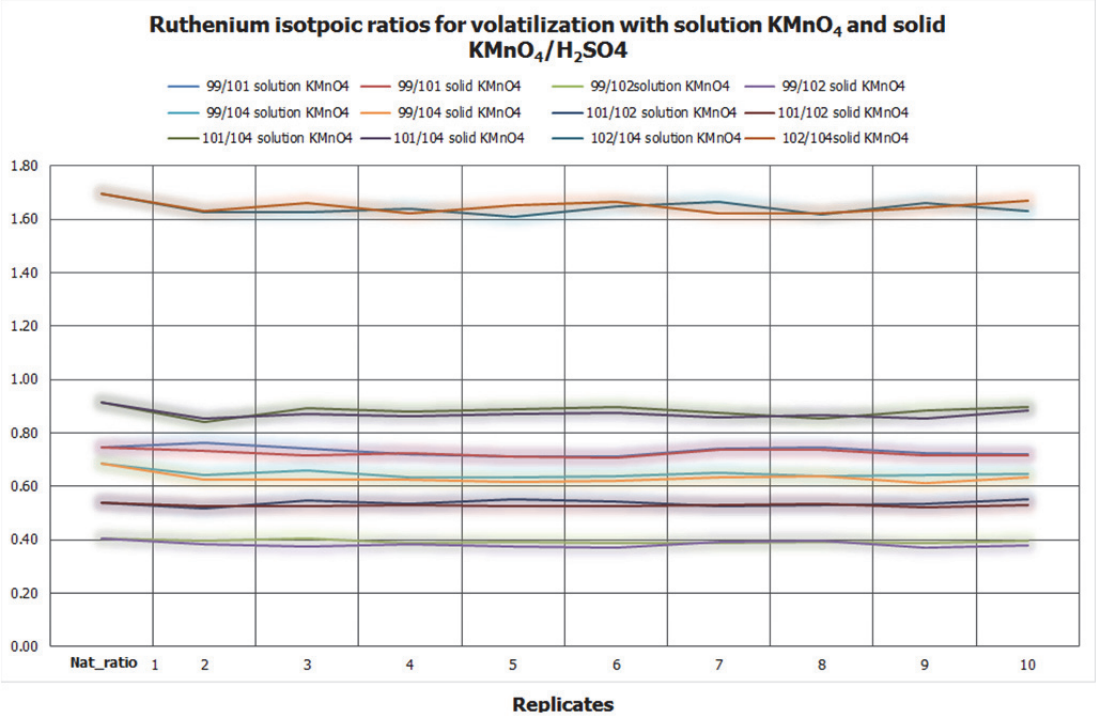

Figure 12.8: Comparison of isotopic ratios obtained with volatilisation of ruthenium with solution and solid $KMnO_4$

The average isotopic ratios of ruthenium isotopes with solution $KMnO_4$ and solid $KMnO_4/H_2SO_4$ are given in Figure 12.8. The isotopic ratios $^{102}Ru/^{104}Ru$, $^{101}Ru/^{104}Ru$, $^{99}Ru/^{102}Ru$ and $^{99}Ru/^{104}Ru$ were affected by matrix interferences while $^{99}Ru/^{101}Ru$ and $^{101}Ru/^{102}Ru$ were least affected as the determined isotopic ratios were closest to natural ratios.

12.5 Optimisation of ruthenium sparging conditions with $KMnO_4$

From the initial results of the experiments on sparging with $KMnO_4$, the addition of 1-2 ml concentrated H_2SO_4 followed by the addition of 20-30 mg of solid $KMnO_4$ was found to be effective for the ruthenium mobilisation. Ruthenium isotopes had significant intensities and the isotopic ratios were close to the natural isotopic ratios. Further experiments were performed for the optimisation of the method.

12.5.1 Gas blank for ruthenium isotopes

The gas blank was evaluated for the determination of any instrumental background due to Ar^+, C^+ and N^+ based interferences on ruthenium isotopes. No significant intensities of ruthenium isotopes were observed in the gas blank.

12.5.2 Reagent blanks

Two reagents were used for ruthenium sparging i.e. sulphuric acid and $KMnO_4$. 1 ml of sulphuric acid was added to the ruthenium standard solution followed by the addition of 20-30 mg of solid $KMnO_4$. It was shown before that the solid $KMnO_4$ yielded better intensities in comparison to the solution $KMnO_4$. Four tests were made for the determination of any blank for ruthenium isotopes, which might come from impurities of the reagents.

The blank from the averages of four reagent blanks for ruthenium isotopes is shown in Figure 12.9. The highest intensities in the range of 700-500 Cps were observed on ^{104}Ru and ^{102}Ru. The gas blank did not show such intensities and it was assumed from isotope ratio determinations which were variable in all the replicates that these intensities are from possible interferences present in the reagents used.

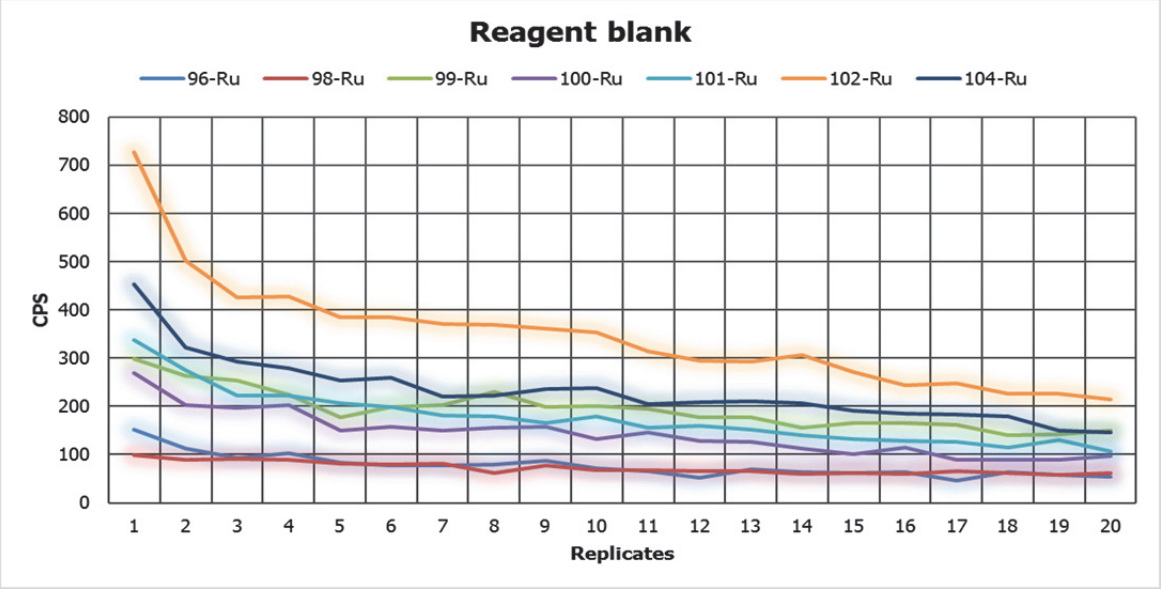

Figure 12.9: Evaluation of reagent blank for ruthenium isotopes

12.5.3 Intensities of mobilised ruthenium isotopes in the ICP-MS

10 ng standard solution of ruthenium upon sparging mobilised with $KMNO_4/H_2SO_4$ yielded 80-90% recovery if compared with solution measurement with ICP-MS/MS. The intensities are shown in Figure 12.10.

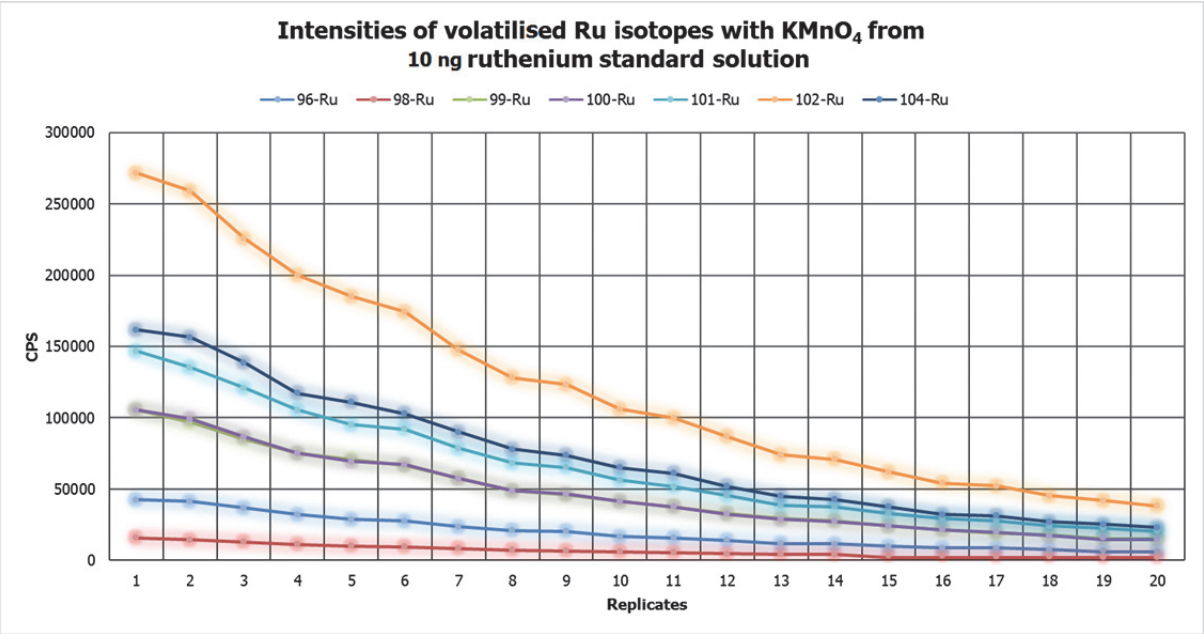

Figure 12.10: Intensities of ruthenium mobilised from 10 ng Ru-standard solution with KMnO4

12.5.4 Application of ruthenium sparging on an un-spiked real matrix

For testing, the method on real matrix a geological reference material, MUH-1 was selected. 0.5 g of MUH-1 was digested with sodium peroxide sintering with a final makeup volume of 100 ml. 5 ml of the solution was taken for sparging. 1 ml H_2SO_4 was added, followed by the addition of 10-30 mg solid $KMnO_4$. The solution was sparged and ratios of ruthenium isotopes were determined. The isotopic ratios are given in Figure 12.11. The isotopic ratio of first three replicates for all isotopes suffers the stabilisation effect and or nitrous oxides. These can be excluded while doing ratio analysis. The isotopic ratio of $^{99}Ru/^{101}Ru$, $^{99}Ru/^{102}Ru$ and $^{99}Ru/^{104}Ru$ were most affected and present volatilising of some matrix interferences. However, the isotopic ratios for $^{101}Ru/^{102}Ru$, $^{101}Ru/^{104}Ru$ and $^{102}Ru/^{104}Ru$ are close to the natural ratios. The box and whisker plot showing average isotopic ratios with deviations (the upper and lower values) are shown in Figure 12.12. The $^{102}Ru/^{104}Ru$ are the most precise isotopic ratios. The intensity of Mo was also monitored and it is assumed that Mo may also volatilise with $KMnO_4$.

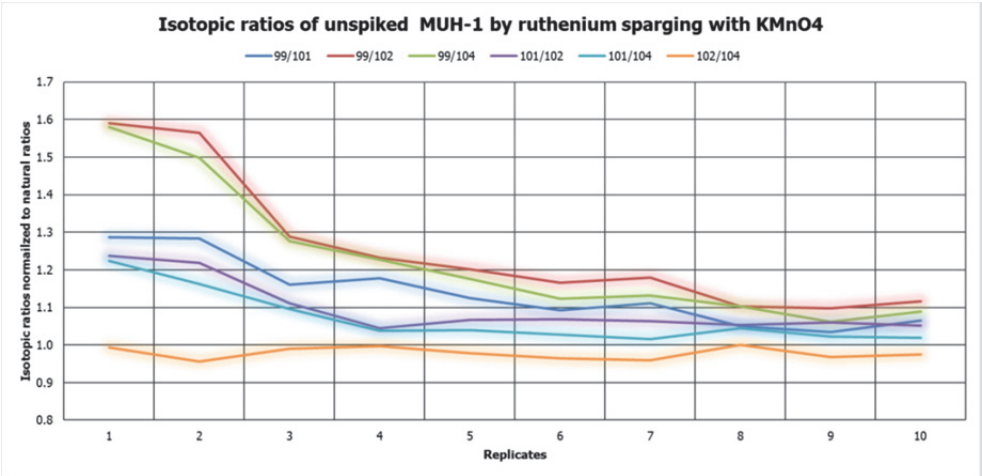

Figure 12.11: Isotopic ratios of un-spiked MUH-1 normalised to natural ratios

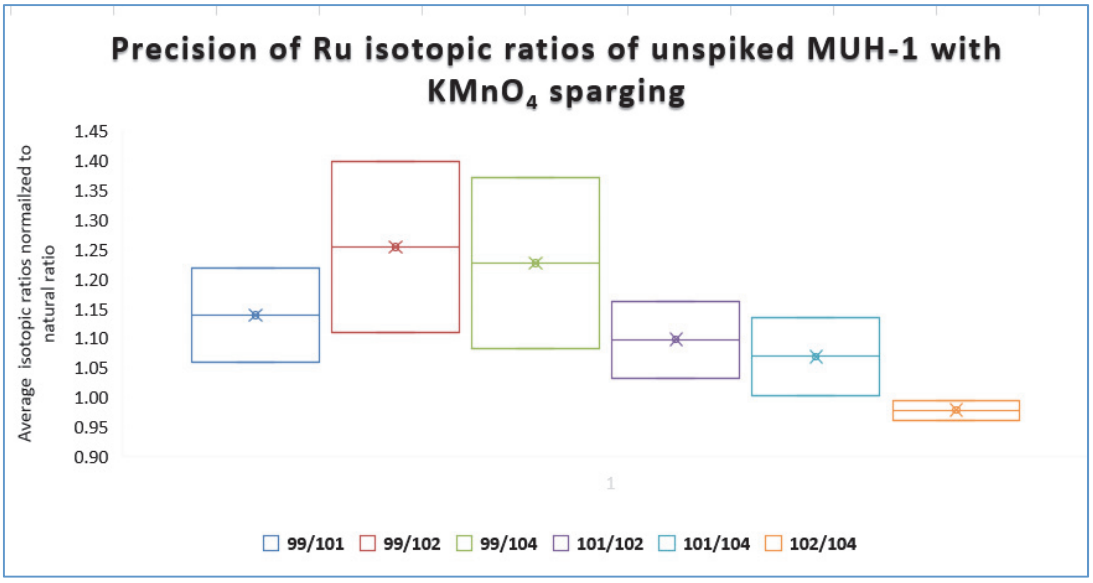

Figure 12.12: Box and whisker plot for mean isotopic ratios normalised to natural ratios

12.5.5 Application of ruthenium sparging on a spiked real matrix

Procedural blank and detection limits

Reagents, sodium peroxide (for sample digestion) $KMnO_4$ and H_2SO_4 (for sparging) were evaluated for the ruthenium mass fractions. The data presented in Table 12.1 is gas blank subtracted. The mass fractions of ruthenium in procedural blanks were determined with sparging and are relatively high. These high blanks are assumed to be from sodium peroxide as determined with the second method of PGE determination i.e. sintering-tellurium co-precipitation. The ruthenium contents in procedural blanks are shown in Table 12.1. The detection limits were calculated from the mass fraction of the blanks, which were determined with isotopic ratios of $^{96}Ru/^{99}Ru$, $^{101}Ru/^{99}Ru$, $^{102}Ru/^{99}Ru$ and $^{104}Ru/^{99}Ru$. The detection limits were determined with 3 sigmas the standard deviation of the five procedural blanks. The precision was determined by the relative standard deviations of the isotopic ratios of $^{96}Ru/^{99}Ru$, $^{101}Ru/^{99}Ru$, $^{102}Ru/^{99}Ru$ and $^{102}Ru/^{99}Ru$ for 20 replicates.

Table 12.1: Mass fraction of Ru and detection limits in procedural blanks

	Ruthenium blank ng/g							
	$^{96}Ru/^{99}Ru$		$^{101}Ru/^{99}Ru$		$^{102}Ru/^{99}Ru$		$^{104}Ru/^{99}Ru$	
Sample	Determined	Precision	Determined	Precision	Determined	Precision	Determined	Precision
Na_2O_2 blank-1	3.0	50%	0.9	50%	0.41	8%	0.8	58%
Na_2O_2 blank-2	1.6	59%	1.7	59%	0.47	9%	0.9	32%
Na_2O_2 blank-3	2.0	76%	2.1	76%	0.45	9%	0.9	40%
Na_2O_2 blank-4	1.5	70%	1.2	70%	0.40	8%	1.1	18%
Na_2O_2 blank-5	3.0	35%	2.8	35%	0.35	7%	1.9	23%
Mean Blank	2.2	33%	1.7	42%	0.41	11%	1.1	24%
Detection limits	2.2		2.2		0.14		1.4	

12.6 OKUM and MUH-1 geological reference material

For testing the sparging with spiked real samples, two reference material OKUM and MUH-1 were selected for which data is being compiled through inter-laboratory comparison. The OKUM literature data are available in Bokhari and Meisel (2015a), Qi *et al.* (2003), Savard *et al.* (2010).

Four samples of each RM were digested with sodium peroxide sintering with 1:5 sample to sodium peroxide ratio. PGE containing ^{99}Ru spike was added to the solutions of the samples. 5 ml aliquots of 100 ml/ 0.5 g were sparged following the protocol mentioned earlier. The ruthenium mass fractions were determined by the isotope dilution method. The mass fractions in ng/g of ruthenium in geological reference materials are given in Table 12.2. Each isotopic ratio used for the determination of the ruthenium mass fraction is discussed individually as below.

^{101}Ru/^{99}Ru

The mass fractions determined with ^{101}Ru/^{99}Ru for OKUM are shown in Table 12.2. Ruthenium contents determined with this ratio are higher than the literature value as in Savard *et al.* (2010). Higher concentrations of ruthenium are due to Mo interferences. These interferences are expected from Mo volatilisation as seen from the intensity of Mo observed with ruthenium isotopes. The ruthenium contents for MUH-1 are also higher with ^{101}Ru/^{99}Ru as compared to ILC data. On the average high precision of isotopic ratio is obtained for only some of the replicates. The precision of the mass fractions of OKUM is 5% and for MUH-1 is 14%.

^{102}Ru/^{99}Ru

The average mass fractions (blank subtracted) for OKUM determined with ^{102}Ru/^{99}Ru ratio are 3.71 ng/g which is lower than the literature value of 4.33 ng/g. The precision of the mass fraction is 3%. The blank-corrected mass fractions determined for MUH-1 are 9.20 ng/g as compared to ILC data. The precision of the mass fractions is 9%. For MUH-1, the mass fractions are slightly lower than the mass fraction determined with ^{101}Ru/^{99}Ru.The mass fractions determined are shown in Table 12.2.

^{104}Ru/^{99}Ru

Blank-corrected mass fractions determined with ^{104}Ru/^{99}Ru in OKUM is 4.22 ng/g with the precision of 6% and for MUH-1 is 9.69 with precision 9%. The results are shown in Table 12.2.

^{96}Ru/^{99}Ru

The ratios ^{96}Ru/^{99}Ru were also measured and mass fractions determined for OKUM and MUH-1 are 5.37 ng/g with 13% RSD and for MUH-1 are 6.13 ng/g with precision 21% as given in Table 12.2.

Table 12.2: Mass fractions of Ru determined with sparging with different ratios

Ru determination with sparging in geological reference material (ng/g)								
	$^{101}Ru/^{99}Ru$		$^{102}Ru/^{99}Ru$		$^{104}Ru/^{99}Ru$		$^{96}Ru/^{99}Ru$	
Sample	Determined	Precision	Determined	Precision	Determined	Precision	Determined	Precision
Reference value (OKUM)	4.30	12%	4.33	12%	4.33	12%	4.33	12%
OKUM-1	7.61	8%	3.84	9%	4.50	17%	4.84	14%
OKUM-2	7.51	55%	3.76	5%	4.00	17%	4.93	14%
OKUM-3	8.51	29%	3.61	17%	4.00	19%	5.36	13%
OKUM-4	8.21	27%	3.65	12%	4.38	20%	6.35	7%
OKUM Mean	7.96	5%	3.71	3%	4.22	6%	5.37	13%
ILC value (MUH-1)	7.06	24%	7.06	24%	7.08	24%	7.06	24%
MUH-1-a	8.51	7%	9.50	7%	10.03	7%	7.87	5%
MUH-1-b	9.01	6%	9.40	6%	10.05	6%	4.93	5%
MUH-1-c	7.21	10%	7.96	8%	8.42	8%	5.36	11%
MUH-1-d	9.41	6%	9.96	4%	10.26	5%	6.35	4%
MUH-1 Mean	8.54	14%	9.20	9%	9.69	9%	6.13	21%

12.6.1 Determination of ruthenium in MUH-1 by using collision/reaction cell

As seen from the above results, the MUH-1 mass fractions were higher than the expected value of 7.08 ng/g. Ruthenium mass fractions in MUH-1 were then determined using sparging and with the method developed with collision/reaction cell technology stated earlier in chapter 9. Ruthenium was determined as a RuO^+ product ion using oxygen as the cell gas. The mass fractions determined with isotopic ratio $^{101}Ru/^{99}Ru$ were improved to 6.03 ng/g with the precision of 14% which were lower than the ILC value of MUH-1. The results are shown in Table 12.3. The precision was determined by the relative standard deviations of the isotopic ratios of $^{101}Ru/^{99}Ru$ for 20 replicates.

Table 12.3: Mass fractions of Ru determined with sparging with ($^{101}Ru/^{99}Ru$)

Ru determination with sparging in geological reference material ($^{101}Ru/^{99}Ru$)		
Sample	Determined	Precision
ILC value	7.08	24%
MUH-1-a	5.80	15%
MUH-1-b	6.70	5%
MUH-1-c	4.63	43%
MUH-1-d	4.63	30%
MUH-1-e	6.97	6%
MUH-1-f	6.41	13%
MUH-1 Mean	6.03	14%

12.6.2 Estimation of osmium contents with $KMnO_4$ and $KBrO_3$ sparging in geological reference material

Recovery of ruthenium from sinter solution through sparging was the focus of this study. However, osmium intensity was also monitored with ruthenium isotopes. It will be an attractive method to determine both osmium and ruthenium from a sample which is completely digested with sodium peroxide sintering. Initial testing of the standard solution of osmium was not made for understanding the recovery of osmium through the solution. Also, a well-established method exists for osmium determination as in (Hassler *et al.* 2000). It was deduced in the beginning of the experiments that if ruthenium is volatilising from a real matrix, osmium will also be mobilised. PGE-spike contained both the ruthenium-99 and osmium-190 spikes. Therefore, when WGB-1 spiked with ^{190}Os and ^{99}Ru was volatilised with $KBrO_3$ and a quite a significant intensity was observed for osmium beside ruthenium. The plot for osmium intensity is given in Figure 12.13.

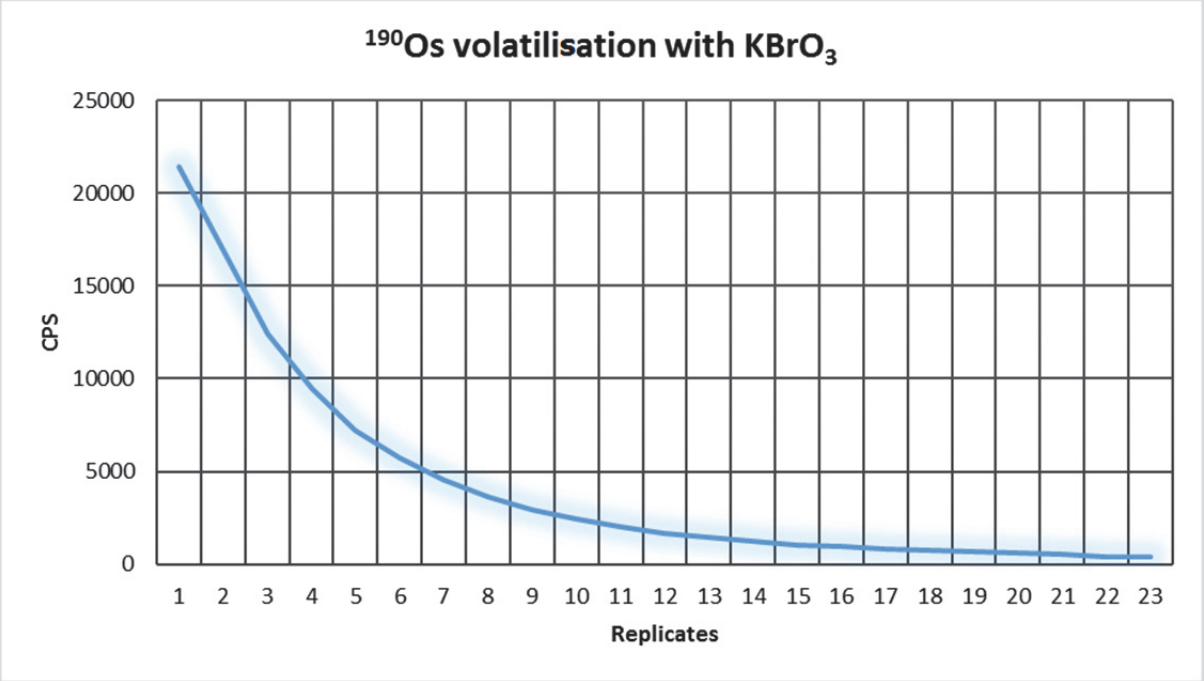

Figure 12.13: Os volatilisation with $KBrO_3$

Osmium intensity was also monitored with $KMnO_4$ sparging. A spiked solution of a 5 ml aliquot of MUH-1 was sparged with $KMnO_4$. A real estimate can be made on osmium lost during the sample preparation if the spike is added into the dry sample along with sodium peroxide following the digestion protocol from the beginning. A plot of the intensity observed is shown in Figure 12.14. Very low intensity as compared to the osmium sparging by Hassler *et al.* (2000) was observed because of open vessel digestion of the sample and small aliquot of the sample used. However, if samples which are digested with HPA ensuring complete digestion of ruthenium, both osmium and ruthenium can be determined in one run. A further work is though suggested to test samples with HPA digestion and sparging with $KMnO_4$.

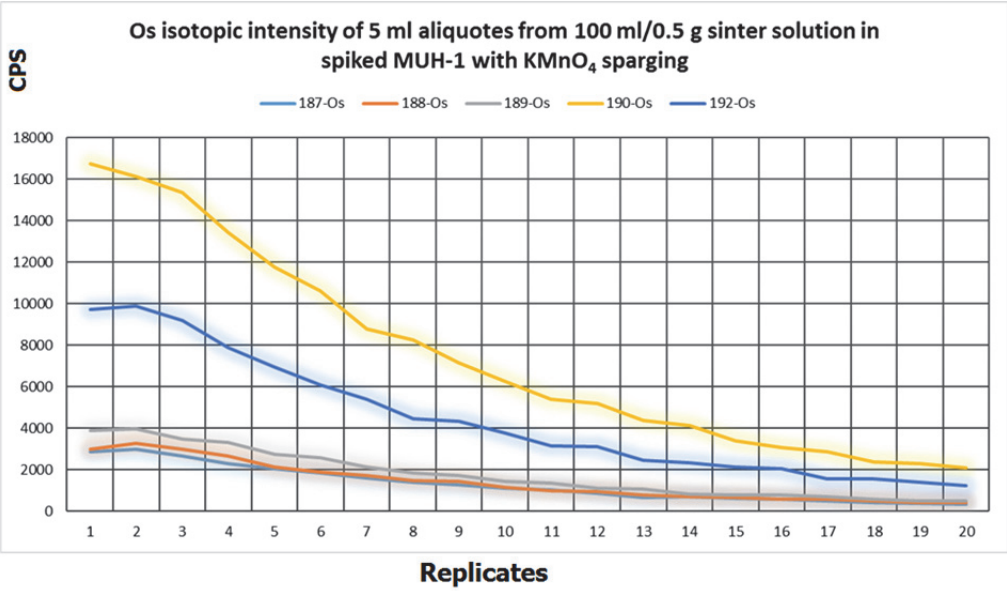

Figure 12.14: Osmium intensity in spike sinter solution of MUH-1

12.6.3 Determination of osmium mass fractions with $KMnO_4$ sparging

The reference material OKUM, MUH-1, BIR-1 and WGB-1 were evaluated for osmium contents through $^{190}Os/^{192}Os$ isotopic ratios. Mass fractions determined with the precision of isotopic ratios are given in Table 12.4. The mass fractions are corrected for the blanks. The mass fractions determined for MUH-1, OKUM and WGB-1 are in close agreement with literature data/ILC values. The detection limits determined with 3 sigmas the standard deviations were 0.18 ng/g for Os. The precision was determined by relative standard deviations of the isotopic ratios of $^{192}Os/^{190}Os$ for 20 replicates.

Table 12.4: Osmium mass fraction in geological reference materials

Os determination with sparging with $KMnO_4$ in geological reference materials (ng/g) $^{192}Os/^{190}Os$				
Samples	Determined	Precision	Reference value	Precision
Na_2O_2 blank-1	0.42	4%		
Na_2O_2 blank-2	0.32	3%		
Na_2O_2 blank-3	0.46	3%		
Na_2O_2 blank-4	0.42	4%		
Na_2O_2 blank-5	0.39	1%		
Na_2O_2 blank-6	0.31	1%		
Mean Blank	0.39	23%		
MUH-1 1	4.83	2%	4.1(ILC value)	
MUH-1 2	4.42	1%		
MUH-1 3	4.52	2%		
MUH-1 4	4.99	1%		
Mean MUH-1	4.69	6%		
WGB-1a	0.62	1%		

WGB-1b	0.40	1%	0.59 (Fritsche and Meisel 2004)	13%
WGB-1c	0.63	1%		
WGB-1d	0.61	1%		
Mean WGB-1	0.56	19%		
OKUM a	0.94	1%	0.98 (Savard, *et al*. 2010)	
OKUM b	0.76	2%	0.84 (ILC value)	
OKUM c	1.02	3%		
OKUM d	0.88	1%		
Mean OKUM	0.90	12%		

12.7 Summary

This chapter has provided an insight for the investigation of the possibilities of ruthenium sparging with different oxidising agents. Different oxidising agents have been tested for mobilisation of ruthenium from solution. It is particularly shown that ruthenium can be mobilised from the solution and argon gas-aided sparging can help in determining the ruthenium mass fractions with different isotopic ratios. Ruthenium mobilisation through distillation is not new but to our knowledge until today, sparging of ruthenium has not been tested with ICP-MS. This makes the basis of a novel analytical method for ruthenium determination with the sparging and the consequent determination of mass fractions in real matrices. This method is rapid and employs no chemical separation prior to analysis.

Ruthenium sparging with $KMnO_4$ ensures 80-90 % spike recovery in comparison to the intensity observed in solution measurement. Ruthenium sparging with $KMnO_4$ has been tested on 5-10 ml aliquots of sinter solution which follows open vessel digestion where losses of RuO_4 and OsO_4 cannot be retrieved. Better intensities can be obtained by taking more volume of solution for example, in volumetric flasks and by setting longer integration time for more precise measurement. However, if sample digestion is performed with sealed vessel as in the case of HPA and Carius tubes, this method can provide enhanced intensities of ruthenium isotopes and a better precision of the data. The interferences from volatilisation of other elements from the matrix still exist as seen on $^{99}Ru/^{101}Ru$ isotopic ratio. The possible interferences are from Mo volatilisation as deduced from its intensity that was also monitored. The isotopic ratios $^{102}Ru/^{104}Ru$ and $^{101}Ru/^{104}Ru$ are least affected. It is, therefore, suggested that, if a spike of ^{102}Ru or ^{104}Ru is added to the real matrix, accurate mass fractions of real samples can be determined. This study has also shown the use of collision/reaction cell for removal of interferences and for acquiring clean spectra in terms of isotopic ratios. The isotopic ratios $^{99}Ru/^{101}Ru$ of MUH-1 reference material were most affected by matrix interferences. Collision/reaction cell was used with oxygen gas in a mass-shift mode (RuO^+) for the determination of the isotopic ratio of $^{99}Ru/^{101}Ru$ of RM MUH-1. This provided satisfactory results of Ru mass fractions for MUH-1. Further work is required on ruthenium sparging for stabilisation of signal intensities of first replicates. This can be done by taking a large volume of sinter solution. Other closed sample digestion methods can also be applied where loss of ruthenium and osmium are minimized.

13. New method for ruthenium and osmium determination with distillation

13.1 Introduction and background

Separation of ruthenium from complex matrices was achieved by distillation of volatile tetroxide (RuO_4), in the presence of strong oxidants i.e. $HClO_4/H_2SO_4$, $NaBiO_3$, $K_2Cr_2O_7$, Cl_2 (in alkaline media) and $KMnO_4$ (Emeléus and Sharpe 1983). Volatile RuO_4 is absorbed in hydrochloric acid as described in many distillation separation procedures. In 1 to 2 mol/l solution of HCl, Ru (+8) changes to Ru (+6) as $RuO_2Cl_4^{2-}$ and then to (+4) as $RuOHCl_5^{2-}$ are formed. $RuCl_6^{2-}$ is formed in higher molarity HCl solutions of 6 to 10 mol/l (Balcerzak 2002a). The absorption of volatile RuO_4 in a hydrochloric acid solution containing ethanol reduces Ru (+8) complexes to Ru (+3) and $RuH_2OCl_5^{2-}$ is formed (Tikhonov *et al.* 1978). Ruthenium exists in nitric acid solutions as various nitroso nitrate complexes of Ru(+3), $[RuNO(NO_3)_n(H2O)_{5-n}]^{3-n}$ and $[RuNO(NO_3)_{5-n-m}OH_m(H_2O)_n]^{p-}$, or polymeric hydroxo nitrates of Ru (+4), $[Ru(OH)_x(H_2O)_{6-x}](NO_3)_{4-x}$ (Carron 2000). These nitroso nitrate complexes of ruthenium can easily undergo hydrolysis (Balcerzak 2002a). Hopp *et al.* (2016) has distilled ruthenium from geological samples digested with acid digestions using H_2SO_4/CrO_3 mixture in combination with cation exchange chromatography. Ly and Hidaka (2004) has used $K_2Cr_2O_7/H_3PO_4$ for ruthenium distillation in combination with acid digestion.

Different sample digestion procedure exists for ruthenium dissolution i.e. HF-aqua regia, alkaline fusion, aqua regia leaching, Carius Tube digestion, NiS-fire assay, Lithium tetraborate digestions, electrochemical anode dissolution, HF-HPA digestions (Balcerzak 2002a).

From the above-mentioned literature, it is evident that different ruthenium complexes exist in HCl and HNO_3 media. Sodium peroxide sintering is an effective technique for dissolution of refractory and acid-resistant phases of minerals. It is aimed here to release ruthenium into the solution with sodium peroxide sintering and develop new methods of distillation for ruthenium mass fraction determination. Therefore, it is the aim of this chapter to apply a distillation technique on sample digested with sodium peroxide sintering.

13.2 Objective of the chapter

Sodium peroxide sintering has been a method of choice for sample digestion of geological reference material in this thesis because it offers complete digestion and recovery of all the acid resistant and mineral phases. PGE hosted in silicate phases can be easily released with sodium peroxide attack instead of the use of HF aided digestions with Carius tubes and HPA (Meisel and Horan 2016). The main features of the chapter are as under;

1. Method development for mass fraction determination of ruthenium in geological reference materials through ruthenium distillation of sinter solution.
2. Investigation of Mo, Sr and Rb interferences on ruthenium isotopes.
3. Tests with liquid phosphoric acid/$K_2Cr_2O_7$ for ruthenium distillation.
4. Tests with condensed phosphoric acid/ $K_2Cr_2O_7$ for ruthenium distillation.
5. Development of new methods based on $KBrO_3$ distillation and the trap of ruthenium in chilled sulphuric acid vessels (micro-distillation of ruthenium) on samples digested with sodium peroxide sintering and HNO_3.
6. Exploring the possibilities of osmium determination through distillation.
7. Testing method on OKUM and MUH-1 geological reference materials.

13.3 Experimental

13.3.1 Reagents and materials

Liquid Phosphoric acid 99% and condensed phosphoric acid 99% from Sigma-Aldrich Switzerland were used as an oxidising agent. Potassium bromate $KBrO_3$ 99.8% from Sigma-Aldrich Switzerland was used as an oxidising agent. $K_2Cr_2O_7$ Potassium dichromate ACS reagent, ≥99.0% from Sigma-Aldrich Switzerland was used as an oxidising agent. Flat bottom PFA vessels of 10-15 ml capacity were used in distillation experiments. The rest of chemicals, sodium peroxide, ultra-pure water, HNO_3 and HCl etc. for which the specification has been mentioned in chapters 5, 7, 8 and 9.

13.3.2 Initial tests for ruthenium recovery through distillation with standard ruthenium solution with matrix interferences from Mo, Sr and Rb.

For initial testing of ruthenium distillation with phosphoric acid/$K_2Cr_2O_7$, 5.25 ng standard solution of ruthenium was taken in PFA vessels. Mo is the main interference on ruthenium spectra with Zr and Pd (Ly and Hidaka 2004). Therefore 5 µg solution of Mo, Sr and Rb was added to it to see the effect of interferences on isotopic ratio and ruthenium recovery. The ruthenium standard solution was prepared in 0.1 Mol/l HCl. The amounts of $K_2Cr_2O_7$ and concentrated phosphoric acid were modified from that of Ly and Hidaka (2004) which utilises 1 g $K_2Cr_2O_7$ and 15 g of condensed phosphoric acid with a large amount of sample in a conical flask. Distillation was applied on micro-scale for 5-10 ml solutions. Therefore, 1 g $K_2Cr_2O_7$ and 5 g concentrated phosphoric acid was added to the solution. Ly and Hidaka (2004) has used liquid and/or condensed phosphoric acid while in this study concentrated phosphoric acid was also evaluated for its use in distillation.

Argon gas was bubbled through the solution at the rate of 3 bubbles per seconds, so as to avoid the losses of volatilised RuO_4. Three trap solutions were connected with a vessel containing ruthenium solution. Trap solution contained 10 ml of 1:1 HCl/ethanol mixture. Mo is partially distilled with ruthenium if it is not bound with phosphoric acid (Emeléus and Sharpe 1983). Therefore, a trap of phosphoric acid was connected after the first vessel containing ruthenium solution with 5 µg matrix solution of Mo, Rb and Sr. The experimental design for ruthenium distillation is given in Figure 13.1.

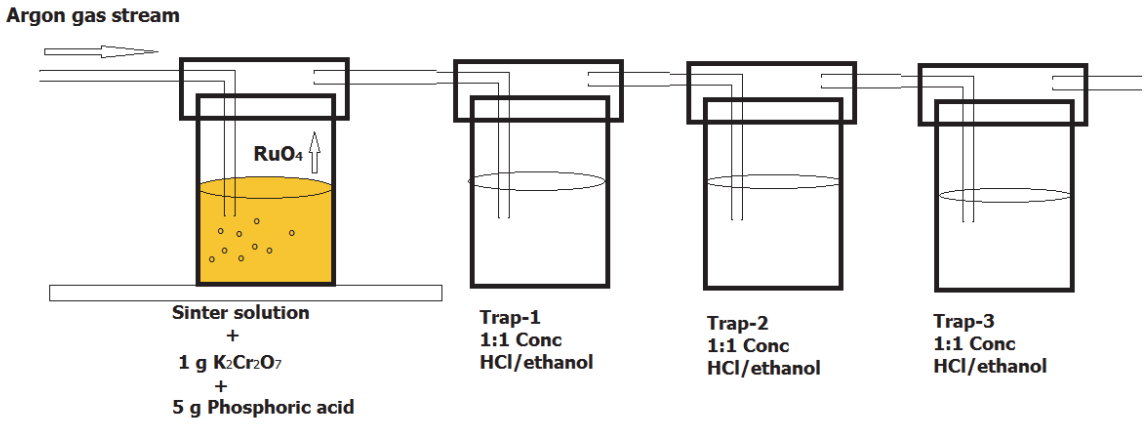

Figure 13.1: Experimental design for Ru distillation

The solution was heated at 180 °C for 40 minutes. Traps were collected and dried. The dried ruthenium from three traps was dissolved in 5 ml 0.1 mol/l HCl and was analysed with the Agilent 8800 ICP-MS/MS in no gas mode. The intensities of ruthenium recovered

after distillation were 7231 cps for 5.25 ng standard solution for ^{102}Ru as compared to Ly and Hidaka (2004) with 3000-3300 cps/ ppb. The isotopic ratios of ruthenium isotopes after mass bias corrections are given in Table 13.1. From the isotopic ratios it was observed that $^{99}Ru/^{101}Ru$, $^{99}Ru/^{102}Ru$ and $^{101}Ru/^{102}Ru$ were less affected as interferences were removed through the distillation step. The intensities of interferences were significantly reduced to less than 1%. Then the experiments were performed on real matrices digested with sodium peroxide sintering and the results of such experiments are given in the next section.

Table 13.1: The Isotopic ratio of ruthenium standard solution with 5 µg Mo, Sr, and Rb interferences.

Ru distillation with phosphoric acid/$K_2Cr_2O_7$		
Ratios	5.25 ng Ru + 5 µg matrix	Natural Ratio
$^{99}Ru/^{101}Ru$	0.75	0.75
$^{99}Ru/^{102}Ru$	0.41	0.40
$^{101}Ru/^{102}Ru$	0.54	0.54

13.3.3 Tests on un-spiked MUH-1 for ruthenium distillation

The method developed above was used for ruthenium determination in un-spiked MUH-1 sample. MUH-1 has 8.6 mg/kg Sr, 0.27 mg/kg Rb, and 1.5 mg/kg Mo. The signals of Sr, Rb, and Mo were also monitored during distillation of ruthenium. Rubidium did not volatilize as seen from its intensity, but Mo and Sr were mobilised although their intensities were reduced significantly. The intensities of interferences after distillation were reduced to 10.0% of Mo, 1.92% of Sr and 0.01% of Rb. The isotopic ratios of ruthenium 99/96, 99/98, 99/100 were most affected. The other ratios $^{99}Ru/^{101}Ru$ and $^{99}Ru/^{102}Ru$ were least affected. The isotopic ratios are given in Table 13.2. The average intensities of ruthenium isotopes were 20147, 27821, 52336 for ^{99}Ru, ^{101}Ru and ^{102}Ru with precision of less than 1.5%. Reagents used in the distillation of ruthenium were evaluated to have no background. On average 10-15 counts were observed for ^{99}Ru, ^{101}Ru and ^{102}Ru for reagent blanks of phosphoric acid/ $K_2Cr_2O_7$.

Table 13.2: Isotopic ratios of ruthenium isotopes after distillation normalised to natural ratios

Un-spiked MUH-1 (ratios normalised to natural ratios)	
Isotopes	Ratios
$^{99}Ru/^{96}Ru$	0.05
$^{99}Ru/^{98}Ru$	0.01
$^{99}Ru/^{100}Ru$	0.17
$^{99}Ru/^{101}Ru$	0.99
$^{99}Ru/^{102}Ru$	0.98
$^{99}Ru/^{104}Ru$	0.94
$^{101}Ru/^{102}Ru$	0.99
$^{102}Ru/^{104}Ru$	0.96

Four spiked solutions each of MUH-1 and OKUM were distilled for ruthenium contents with a protocol developed above. The intensity of ^{99}Ru spike was always lower than all other ruthenium isotopes. Experiments were then performed with condensed phosphoric acid and ruthenium spike recovered. It is therefore suggested that the use of concentrated phosphoric acid does not recover ^{99}Ru in sinter solution due to matrix effects on other ruthenium isotopes. Use of condensed phosphoric acid for ruthenium distillation was evaluated for ruthenium mass fractions in the reference materials.

13.3.4 Os determination through distillation with concentrated phosphoric acid

Osmium isotopic intensities were also monitored in distillation with concentrated phosphoric acid/$K_2Cr_2O_7$. Indispensable losses of OsO_4 occurred during the distillation process if sample preparation is ignored as seen from the intensities of the ^{190}Os spike. The mass fractions of osmium were calculated in the blanks, MUH-1 and OKUM reference materials and are given in Table 13.3. The average of four blanks yielded 0.30 ng/g Os. The detection limits were 0.18 ng/g calculated with 3 sigmas the standard deviations of the blank concentrations. The precision was determined from the relative standard deviations of the isotopic ratios of $^{192}Os/^{190}Os$ for 20 replicates.

Table 13.3: Os mass fractions determined in geological reference material through distillation

Results of Os (ng/g) with distillation ($^{192}Os/^{190}Os$)		
Samples	Determined	Precision
ILC value	4.12	
MUH-1 a	3.92	6%
MUH-1 b	4.03	4%
MUH-1 c	3.96	4%
MUH-1 d	4.64	8%
Mean MUH-1	4.14	12%
ILC value	0.94	
OKUM1	0.86	14%
OKUM2	1.16	6%
OKUM3	1.06	3%
Mean OKUM	1.02	15 %

13.3.5 Ruthenium distillation with condensed phosphoric acid/$K_2Cr_2O_7$

As the recovery of Ru isotopes was affected with the use of concentrated phosphoric acid. With the use of condensed phosphoric acid, Ru isotopes recovered and intensities were greatly enhanced. The ruthenium mass fractions determined in geological reference material are given in Table 13.4. The mass fractions of OKUM are in close agreement with literature value, whereas for MUH-1 are variating as compared to ILC data. The detection limits determined from four blanks were 0.12 ng/g (3 sigmas the standard deviations). The

precision was determined from the relative standard deviations of the isotopic ratios of $^{102}Ru/^{99}Ru$ for 20 replicates.

Table 13.4: Ru mass fractions determined in geological reference material through distillation with condensed phosphoric acid/ $K_2Cr_2O_7$ ($^{102}Ru/^{99}Ru$)

Results of Ru mass fractions (ng/g) ($^{102}Ru/^{99}Ru$)		
Samples	Determined	Precision
Na_2O_2-1	0.75	29%
Na_2O_2-2	0.90	20%
Na_2O_2-3	0.95	22%
Na_2O_2-4	0.95	19%
Mean blank	0.89	11%
ILC value (MUH-1)	7.08	23%
MUH-1 a	5.39	8%
MUH-1 b	3.59	17%
MUH-1 c	6.75	17%
MUH-1 d	4.26	1%
Mean MUH-1	5.00	24%
ILC value (OKUM)	4.33	12%
OKUM-1	3.19	9%
OKUM-2	4.16	18%
OKUM-3	5.35	17%
Mean OKUM	4.24	26%

13.3.6 Ruthenium distillation with $KBrO_3$ and chilled sulphuric acid trap

Another method for ruthenium distillation was developed in an effort to trap osmium together with ruthenium through distillation. As the heating arrangement in distillation was not suitable for volatile OsO_4. The trap of 1:1 conc. HCl/ethanol mixture for osmium capture was not effective as very little intensities were observed. To address this issue and to make the distillation process effective for both osmium and ruthenium determination, efforts were made for trapping both the analytes in thiourea. Intensities were better for both osmium and ruthenium, but the difficulties of drying, destroying organic matter and problems of extreme intensities with the use of thiourea from the tubing of instrument ICP-MS/MS make the measurement difficult. Therefore, use of thiourea as a trap for the ruthenium and osmium was not taken into further considerations.

A very useful conference abstract of Brauns (2004) was applied for osmium trap using micro-distillation with chilled sulphuric acid. Osmium was not captured through this method but enhanced intensities for ruthenium isotopes were observed which were better than using traps of 1:1 conc. HCl/ethanol. The use of chilled sulphuric acid for ruthenium trap do not exist in the literature for ruthenium to the best of the knowledge. The experimental setup for distillation with $KBrO_3$ and the chilled trap of sulphuric acid is similar to the one

described in Figure 13.1 with the only difference of use of small quantities of sulphuric acid. The diagrammatic setup for distillation is given as below.

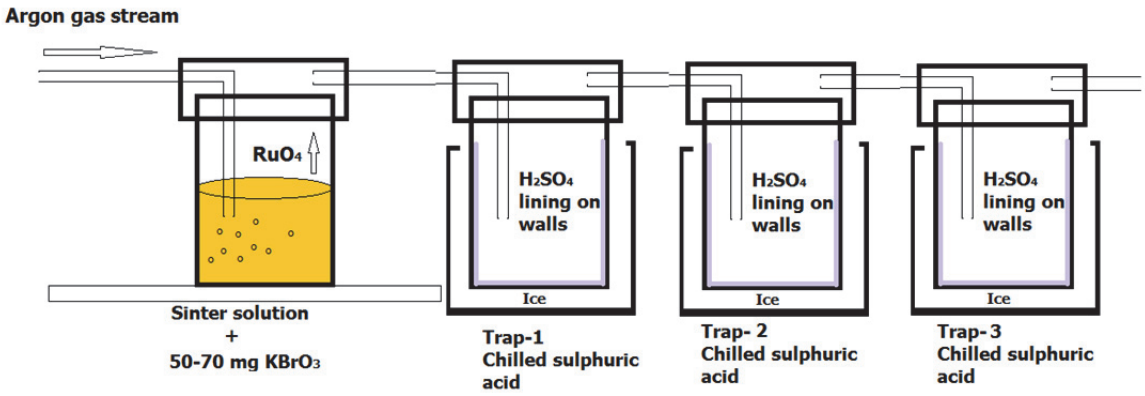

Figure 13.2: Experimental design for Ru distillation with $KBrO_3$ with chilled sulphuric acid traps.

Sulphuric was chilled in the freezer and a thin lining of the sulphuric acid was created with a plastic rod inside PFA vessels. PFA vessels were kept in a plastic bottle. The space between the PFA vessel and the plastic bottle was filled with water. It was kept in a freezer overnight. The ice layer between the PFA vessel and outer plastic bottle kept low the temperature of the trap for at least 30-40 minutes. 50-70 mg of $KBrO_3$ is added to the PFA vessel containing 5-10 ml of the sinter solution. The sinter solution was dissolved in HNO_3 instead of HCl for releasing ruthenium and for its volatilisation in the form of RuO_4. The reference material MUH-1, OKUM and procedural blanks were digested with sodium peroxide sintering and distilled with the $KBrO_3$/chilled sulphuric acid trap. The results of the experiments for mass fractions determination through the isotopic ratio of $^{101}Ru/^{99}Ru$ are given below in Table 13.5. The mass fractions for OKUM are in close agreement with literature values/ILC data. Other isotopic ratios $^{96}Ru/^{99}Ru$, $^{98}Ru/^{99}Ru$ and $^{100}Ru/^{99}Ru$ were affected by Mo interferences.

If a conical flask is used as in Ly and Hidaka (2004) for ruthenium distillation with condensed phosphoric acid/$K_2Cr_2O_7$, the interferences on ^{96}Ru, ^{98}Ru, ^{100}Ru might get eliminated. Distillation using small apparatus may suffer from aerosol transfer into the trap solution as suggested in Ly and Hidaka (2004) also. Therefore, further work is required using larger volume i.e. conical flask instead of small flat bottom PFA vessels with 10-15ml volume capacity. The high blanks are assumed to come from sodium peroxide itself. The detection limits determined from four blanks were 0.09 ng/g (3 sigmas the standard deviation). The precision was determined from the relative standard deviations of the isotopic ratios of $^{101}Ru/^{99}Ru$ for 20 replicates.

Table 13.5: Ru mass fractions determined in geological reference material through distillation with $KBrO_3$/Chilled sulphuric acid ($^{101}Ru/^{99}Ru$)

Results of Ru mass fractions (ng/g) ($^{101}Ru/^{99}Ru$)		
Samples	Determined	Precision
Na_2O_2-1	0.95	12%
Na_2O_2-2	0.95	21%
Na_2O_2-3	1.05	29%

Na_2O_2-4	0.95	20%
Mean blank	0.98	5%
ILC value (MUH-1)	7.08	23%
MUH-1 a	6.49	13%
MUH-1 b	5.18	33%
MUH-1 c	4.80	10%
MUH-1 d	5.89	23%
MeanMUH-1	5.59	12%
ILC value (OKUM)	4.33	12%
OKUM-1	3.25	6%
OKUM-2	3.08	10%
OKUM-3	3.29	8%
OKUM-4	3.25	8%
Mean OKUM	3.21	2%

Ruthenium distillation with perchloric acid and chilled trap of sulphuric acid

Perchloric acid was also tested for distillation of ruthenium, but it did not recover the Ru isotopes, therefore no further work was performed with perchloric acid.

13.4 Summary

Two methods have been developed for ruthenium distillation i.e. sodium peroxide sinter solutions with phosphoric acid/$K_2Cr_2O_7$ based on the method of Ly and Hidaka (2004) and sodium peroxide sinter solution with $KBrO_3$/chilled sulphuric acid trap based on the distillation method for osmium by Brauns (2004). Through the results obtained on MUH-1 and OKUM geological reference material digested with sodium peroxide sintering, it is shown that this method can be extended to a variety of geological material with high ruthenium mass fractions.

It is particularly shown that sodium peroxide digests can be applied for ruthenium determination without a pre-concentration step for ruthenium determination. The intensities of interferences after distillation were significantly reduced to 10.0% of Mo, 1.92% of Sr and 0.01% of Rb. The isotopic ratios $^{99}Ru/^{101}Ru$ and $^{99}Ru/^{102}Ru$ were less affected and thus were used in the ruthenium mass fractions determination. Osmium determination is not possible because of the open vessel digestion method and OsO_4 loss in drying step of traps. Distillation with phosphoric acid/$K_2Cr_2O_7$ shows some intensity of osmium isotopes, but $KBrO_3$/chilled sulphuric acid trap method did not provide any reasonable intensity for osmium.

Through this study, it is shown that Mo, Sr, and Rb interferences are significantly reduced, hence making $^{99}Ru/^{101}Ru$ and $^{99}Ru/^{102}Ru$ isotopes free for isotope ratio analysis with isotope dilution. Only the data for $^{99}Ru/^{102}Ru$ is shown in Table 13.4. Aerosol generation in small scale apparatus may be the cause of slight interferences on isotopic ratios $^{99}Ru/^{101}Ru$ and $^{99}Ru/^{102}Ru$.

The samples which are digested with sodium peroxide/HCl provide reducing conditions, restricting volatility of RuO_4 as observed with fewer intensities of ruthenium isotopes. The digests of sodium peroxide/HNO_3 have shown improved volatilisation of RuO_4 and hence the intensities of ruthenium isotopes.

The use of concentrated phosphoric acid does not recover the ruthenium isotopes. Using condensed phosphoric acid with $K_2Cr_2O_7$ dramatically improved the recovery of the isotopes.

The recovery of un-spiked ruthenium standard solution with the developed distillation methods was 90-95% as compared to solution measurement of a given strength of ruthenium solution. Further work can be performed by increasing the volume of the solution that would require larger vessels for distillation.

14. Evaluation of cloud point extraction with 2-MBT and thiourea complexing agents for PGE studies of the sinter solution

14.1 Introduction and background

The term cloud point extraction refers to the process of transferring a non-ionic surfactant from one liquid phase to another by heating. As the temperature of the solution rises, the surfactant molecules form micelles. If the temperature increases above the cloud point (CPT) the micelles become dehydrated and aggregate. This leads to macroscopic phase separation of the solution into a surfactant-rich phase and a solvent phase (Samaddar and Sen 2014, Silva *et al.* 2009, Tan *et al.* 2009).

Organic non-ionic surfactants exhibit a clouding phenomenon which forms the basis for the extraction technique for analytes (Li and Chen 2002). Surfactants contain both hydrophilic (water-loving) and hydrophobic (water repellent) group. The hydrophilic head consists of either polyether or polyhydroxy units. The hydrophobic tail/end forms aggregates called micelles. Surfactants are reported to solubilise different kind of solutes/analytes (Padrón Sanz *et al.* 2002). The non-ionic surfactants show a cloudy appearance at a well-defined temperature upon heating. When the temperature rises above the cloud point, the surfactant solution separates into two immiscible phases. One phase contains most of the surfactant and other contains mostly water (Silva *et al.* 2006). Micelles are formed in surfactant-rich phase. The phase rich in water forms less micelles. The density differences of the phases cause the separation (Nakagawa and Shinoda 1963). The solution becomes viscous/turbid by changing temperature, pH and salts due to the diminished solubility of surfactant water (Xie *et al.* 2010). When the solution is cooled down, the analytes are concentrated into the surfactant-rich phase due to the analyte-micelle interactions (Yu *et al.* 2015). Commonly used surfactant are tritons, igepals, tergitols, suronics, and plurafacs etc. (Maden 2010).

Triton family surfactants have been effectively used as a surfactant in cloud point extractions (Pytlakowska *et al.* 2013). Different complexing agents have been used depending upon the sample matrices i.e. 2-MBT (2-mercaptobenzoothiazole) by Niemelä *et al.* (2009), Simitchiev *et al.* (2008), Suoranta *et al.* (2015), DDTP (ammonium O, O-diethyl dithiophosphate) by Silva, Cerutti *et al*. (2006), DHBT (N,N-dihexyl-N'-benzoyl thiourea) by Meeravali and Jiang (2008), PAN (1-(2-Pyridylazo)-2-naphthol) by Mohammadi *et al.* (2011).

The pre-concentration of metal ions from aqueous samples with cloud point extraction was first reported by Watanabe and Tanaka (1978). The extraction of Cu(II) from water samples with CPE was reported by Fathi and Yaftian (2009). Nickel and Cu were determined in food and water samples with CPE by Şahin *et al.* (2010). CPE was reported for the extraction of cadmium (II), lead (II), palladium (II) and silver (I) from radiology waste, vegetable, blood and urine samples by Ghaedi *et al.* (2009). Noble metals were extracted in biological samples by electrothermal vaporisation inductively coupled plasma mass spectrometry and cloud point extraction by da Silva *et al.* (2001). The pre-concentration of ultra-trace amounts of gold prior to the determination by electrothermal atomic absorption spectrometry with CPE was used by Manzoori *et al.* (2007). PGE mass fractions in the abrasion of automotive catalytic converters were determined by Bencs *et al.* (2003). Microwave-assisted cloud point extraction of Rh, Pd and Pt with 2-mercaptobenzothiazole as the pre-concentration procedure for the pharmaceutical products was developed by Simitchiev *et al.* (2008). The determination of gold and palladium with CPE using ICP-OES was reported by Tavakoli *et al.* (2008). Platinum, Pd and Au using cloud point extraction in

geological and environmental samples was reported by Meeravali and Jiang (2008). The pre-concentration of palladium and lead with cloud point extraction in environmental samples by flow injection flame atomic absorption spectrometry was reported by Bakircioglu (2012). Cloud point pre-concentration of Pt and Pd prior to the capillary zone electrophoresis was described by Cerutti *et al.* (2005). Determination of Pt from coke samples by ICP-MS after microwave-assisted digestion and microwave-assisted cloud point extraction was reported by Niemelä *et al.* (2009). Cloud point extraction of platinum group elements and gold in environmental samples was reported by Suoranta *et al.* (2014). Determination of palladium, platinum, rhodium and ruthenium from catalytic materials using microwave-assisted leaching and cloud point extraction was reported by Suoranta *et al.* (2015).

14.1.1 Aims of the chapter

The trace PGE analysis is an analytical problem due to matrix/analyte interferences in ICP-MS analysis in geological materials. This issue of the matrix and spectral interferences is usually solved with chromatographic matrix separation and pre-concentration. The main objective of this chapter is to explore the possibilities of separation of interferences and pre-concentrations of PGE from sinter solution (samples digested with sodium peroxide sintering) using cloud point extraction with a surfactant i.e triton and the complexing agent 2-MBT and thiourea. The salient features of this chapter are;

1. Method development for removal of interferences with cloud point extraction of PGE in geological samples digested with sodium peroxide sintering with
    a. 2-MBT complexing agent in standard and sinter solutions.
    b. Thiourea complexing agent in standard and sinter solutions.
2. Evaluation of removal of interferences using thiourea or 2-MBT.
3. Application of isotope dilution method in spike recovery tests.

14.2 Instrumentation and reagents

Analytical reagent-grade sodium peroxide ACS, ISO Merck KGaA, Darmstadt, Germany has been used for sample digestion. Hydrochloric acid: 37% p.a., Roth Karlsruhe, Germany was sub-boiled for experimental purposes. HNO_3: 65% p.a., Roth Karlsruhe, Germany (sub-boiled) and was used in dilutions. Triton X-100 analytical grade from Sigma-Aldrich was used as a surfactant. 2-MBT, p.a., Merck, Darmstadt, Germany was used as a chelating agent. NH_3 25% from J.T.Baker was used for the preparation of 2-MBT (2-mercaptobenzoothiazole) solution. Thiourea ACS reagent, ≥99.0% was used for testing thiourea based CPE method. Multi element standard PGE solution 10 mg/l from SPEX chemicals USA was used for initial PGE recovery tests. Glassy carbon crucibles: (25 x 25 mm HTW) were used for sample digestion as discussed in chapter 5. Agilent 8800 ICP-MS/MS was used for the measurement of isotopic ratio through isotopic ratio analysis acquisition mode. Measurements were performed in no gas mode as well as using ammonia and oxygen gas modes. The complete method details are described in chapter 9. The integration times were kept 0.75 seconds in no gas mode and 1 second when using cell gases. In total, 10 replicates were measured.

14.2.1 Preparation of 2-MBT, thiourea, and triton for CPE

The preparation of chemicals 2-MBT (2-mercaptobenzoothiazole) and triton were based on the procedure of (Suoranta *et al.* 2014). For the preparation 10% triton, 2 grams of triton were taken in a 50 ml centrifugation vial (Sarstedt). Ultra-pure water was added to make the volume upto 20 ml. As triton does not dissolve easily, therefore vial was slowly shaken. The abrupt shaking of the liquid results into foaming in the vial. The mixing procedure took 1-2 hours to form a clear solution.

The preparation of 1% of 2-MBT (2-mercaptobenzoothiazole) was done by weighing 200 mg of 2-MBT (2-mercaptobenzoothiazole) in the 50 ml centrifugation vial (Sarstedt). 1.5 ml of 25% ammonia solution was added into it. The addition of ammonia was performed under the fume hood. The volume was made to 20 ml with ultra-pure water. The solution was thoroughly shaken until 2-MBT (2-mercaptobenzoothiazole) dissolved to form a clear solution. Similarly, 1 mol/l solution of thiourea was prepared in 2 mol/l HCl.

14.2.2 Initial tests for PGE recovery

For initial tests on the recovery of PGE with CPE using 2-MBT (2-mercaptobenzoothiazole) or thiourea, 1 ng/ml solution was prepared from the PGE standard solution in 20 ml of 0.1 mol/l HCl. To this solution, 2 ml of 10% triton was added, followed by the addition of 2 ml of 1% 2-MBT (2-mercaptobenzoothiazole) solution. The volume of the solution was made to 40 ml with ultra-pure water.

Similarly, 1 ng/ml PGE solution, 2 ml of 10% triton and 2 ml of 1 mol/l thiourea was taken in the second centrifugation vial. Its volume was made to 40 ml by addition of ultra-pure water. 2000 ml flat bottom flask was filled with water and bottles containing 2-MBT and thiourea were immersed in it. A thermometer was immersed in the flask for temperature readings. The flask was placed on a heating plate for heating at 90 °C for 2 hours. The temperature was maintained at 90 °C.

The clouds started to appear in the solution at above 60 °C. The separation of phases completely occurred when a distinct viscous phase formed at the base of the vials. The vials were taken out and placed in a refrigerator for cooling. First the solutions were cooled down to +5 °C, and then they were transferred to the freezer at -18 °C for at least 20 minutes. The aqueous phase of the solutions was decanted and PGE extracted in viscous form were rinsed with ultra-pure water. The viscous part containing the PGE was dissolved in 2 mol/l HCl. According to Suoranta, Niemelä et al. (2014), the extracted PGE can be dissolved in 20 ml of 1 mol/l HCl and analysis can be performed by ICP-MS. However, the PGE contents were dried in PFA vessels and organic matter was destroyed by the addition of small amounts of concentrated nitric acid. The PGE were re-dissolved in 0.1 mol/l HCl and analysed with ICP-MS/MS. The PGE recovery using triton and 2-MBT (2-mercaptobenzoothiazole) solution and using triton and thiourea combination are shown in Table 14.1.

Table 14.1: Recovery of 1 ng/ml PGE with 2-MBT and thiourea based CPE

Recovery of PGE with CPE		
	2-MBT/triton	**Thiourea/triton**
Analyte	Yield	Yield
Ru	80%	100%
Rh	54%	81%
Pd	90%	100%
Re	0.5%	12%
Ir	14%	100%
Pt	80%	100%
Au	82%	100%

The recovery of PGE from 2-MBT/triton and thiourea/triton was compared by measuring a solution of the same concentration initially taken in the bottles. As seen in Table 14.2 that the recovery of PGE in standard solution with cloud point extraction is better with thiourea than 2-MBT (2-mercaptobenzoothiazole). Rhenium is not recovered with both extraction procedures. Further tests were performed to evaluate the PGE recovery through CPE in sinter solutions.

14.2.3 Recovery of the PGE in sinter solutions using CPE with 2-MBT and thiourea

The procedure for recovery of PGE with cloud point extraction mentioned above was applied to real matrix samples which were digested with sodium peroxide sintering. A known amount of PGE enriched spike was added to the sinter solution and PGE were extracted using both 2-MBT (2-mercaptobenzoothiazole) and thiourea complexing agents with triton as a surfactant. The recoveries of PGE in sinter solution using CPE combined with 2-MBT (2-mercaptobenzoothiazole) and thiourea are shown in Table 14.2. The recoveries of the PGE-spike with both CPE extraction procedures using 2-MBT (2-mercaptobenzoothiazole) and thiourea were significantly lower. Thus, CPE method combined with sinter solutions do not provide a quantitative mean for mass fraction determination via isotope dilution method. The low recoveries of PGE using sinter solution might be due to the existence of hydroxy chloro- PGE complexes in solutions. The PGE extraction using microwave-assisted digestions with HCl or HNO_3 combined with CPE has been reported to yield quantitative recoveries (Suoranta *et al.* 2014).

Table 14.2: The recoveries of PGE in sinter solution using CPE with 2-MBT and thiourea

Recovery of spike based on isotope dilution in sinter solution		
Analyte	2-MBT	thiourea
Ru	4%	9%
Pd	40-60%	20%
Re	1%	4%
Pt	20-40 %	4%
Ir	8%	12%
Au	4%	4%
Rh	4%	4%
Os	4%	4%

14.2.4 Tests on PGE recovery for samples digested with a HPA

As sinter solution for geological reference materials did not make a good basis for a quantitative recovery of PGE-spike, experiments were also performed on sample digested with HPA with aqua regia. The recoveries of the PGE have been reported significant with aqua regia and CPE (Suoranta *et al.* 2014). The recoveries of the PGE using CPE for geological samples digested with HPA were improved and are given in Table 14.3. On average thiourea did not recover PGE better than 2-MBT. Ruthenium, Re and Ir yields were

low, but recoveries of Pd, Pt, Au and Rh were improved to about 80%. Osmium losses in HPA digestions were minimised and recovery was 60%.

Table 14.3: The recoveries of PGE in HPA digested samples using CPE with 2-MBT and thiourea

Recovery of the spike with CPE		
Analyte	2-MBT	thiourea
Ru	35%	15%
Pd	90%	20%
Re	15%	15%
Pt	80%	80%
Ir	10%	10%
Au	90%	10%
Rh	80%	40%
Os	60%	20%

14.2.5 Interferences removal with CPE in sinter and HPA digested solutions

The intensities of interfering elements after CPE extraction were monitored with both sample digestion types i.e. sinter solutions and HPA digestion. Real matrix samples were digested using sintering method and HPA digestion method. The intensities of the main interferences on PGE isotopes were measured. The interferences Rb, Sr, Y, Zr, Nb, Hf and Pb were not removed from both the sinter solutions and in solutions after HPA digestions. Other interferences Ta, Hg and Cd were low after CPE extractions of sinter solution and in solutions after HPA digestions.

Blanks

An estimate of reagent blanks used in the preparation of reagents and total procedure blanks was made for the sinter solutions. Same quantities of the reagents were taken which was used in the actual CPE procedure for the estimation of reagent blanks. Procedural blank was digested with sintering and only CPE with 2-MBT was applied. The PGE contents in reagents and total procedural blanks measured with isotope dilution method are shown in Table 14.4. Higher blanks are problematic, which are assumed to be driven from sodium peroxide used in sample digestion.

Table 14.4: PGE mass fractions (ng) in reagent and procedural blanks with CPE

CPE blanks with 2-MBT (ng)								
Sample	**Ru**	**Pd**	**Re**	**Ir**	**Pt**	**Os**	**Au**	**Rh**
NH_4OH blank	0.07	0.02	0.02	0.10	0.10	0.60	0.04	0.02
Triton blank	0.11	0.04	0.03	0.21	0.10	0.10	0.09	0.06

2-MBT blank	0.15	0.05	0.01	0.31	0.13	0.10	0.03	0.07
Procedural blank	0.95	0.90	0.15	1.87	1.02		0.32	0.32

14.2.6 Problems in analytical measurement using 2-MBT or thiourea based CPE

Care should be taken for PGE analysis with ICP-MS using 2-MBT (2-mercaptobenzoothiazole) or thiourea based CPE. These organic reagents, if not destroyed with concentrated nitric acid, they sweep the PGE sticking in the tubing and spray chamber of the instrument to the plasma. Rinsing of the probe and the tubing with 0.1 mol/l HCl did not show any background. But, once a dilute solution 2-MBT and thiourea bearing solutions were analysed, high intensities of PGE were observed. For cleaning purposes of the tubing and spray chamber, the instrument was turned off and the probe was inserted into a dilute solution of 2-MBT or thiourea with the appropriate speed of the peri-pump for 2-3 hours. This arrangement allows the solution to go through the probe, into the tubing and the spray chamber, but not the skimmer cones, etc. The tubing and spray chamber were then rinsed with 0.1 mol/l HCl and 1% HNO_3 and the intensity was observed again for any PGE instrumental background. No instrumental background for PGE was observed following the cleaning protocol above.

14.2.7 Determination of PGE mass fractions in OKUM and MUH-1 geological reference materials

The PGE mass fractions were evaluated in both the sinter solution and HPA digestions combined with CPE. The interferences removal was not successful in both kinds of digestion procedures combined with cloud point extraction. The PGE mass fractions for ruthenium, Ir, Re, Os, Au and Os were not reproducible and higher values were observed indicating that interferences were not removed. However, Pd and Pt values were better than all other PGE but these were not precise and reproducible and hence are not shown here.

14.2.8 Summary

The study in this chapter describes the possibilities of combining sinter solution with cloud point extraction using 2-MBT (2-mercaptobenzoothiazole) and thiourea for the extraction of PGE, removal of interferences and for the PGE mass fractions determination. It has been shown that cloud point extraction in sinter solutions leads to poor recoveries of PGE and incomplete interference removals. This behaviour of PGE in sinter solutions is because of the hydroxy chloro-complexes which are not bound efficiently with 2-MBT (2-mercaptobenzoothiazole) or thiourea based reagents. Thus, sintering combined with cloud point extraction does not provide a good basis for interference removals and subsequent PGE determinations. The recovery of the PGE was improved using samples digested with HPA digestions with aqua regia, which seems to provide only chloro-complexes for cloud point extraction. However, this method does not work with geological materials due to incomplete removal of interferences.

The combination of anion-exchange may help in removal of interferences after the PGE extraction with cloud point extraction for samples digested with high-pressure asher. Another possibility is the removal of interferences prior to cloud point extraction with cation exchange columns and then CPE can be performed.

15. Evaluation of Diphonix® and CL resins for PGE studies of sinter solutions

15.1 Introduction and background

Diphonix® Resin

Diphonix® an ion exchange resin (Triskem International) has been developed by members of the Separation Chemistry Group of the Chemistry Division of Argonne National Laboratory together with members of the University of Tennessee, Department of Chemistry (Chiariza *et al.* 1997). The resin is composed of geminally substituted diphosphonic acid groups chemically bonded to styrene-based polymer matrix and the strongly hydrophilic sulfonic acid group that provides high hydrophilicity for the fast kinetics of metal ions uptake from solutions (Chiariza *et al.* 1997). The resin has a dual mechanism because of diphosphonic acid groups and sulfonic acid group i.e. sulfonic acid group allows access of nonspecific ions into the polymeric network and diphosphonic acid groups is specific towards target metal ion (Horwitz *et al.* 1990). In near neutral solution, Diphonix® acts as selective or multivalent cation of various metals including Zn, Mn, Cr, U, Pb, Co, Ni, and Cu. Resin also removes Fe(III) ions, Cr, U, Po and certain other metals from strongly acidic solutions (Eichrom-resources//Eichrome.com).

Diphonix® resin has a strong affinity to retain actinides in tetra and hexavalent oxidation states and has been applied for the actinides pre-concentration/separation in waste treatment and environmental samples. Metal uptake studies have been applied to alkaline earth metal, transition metals and metal sorption in near neutral solution Chiarizia *et al.* (1995), Chiarizia *et al.* (1993), Horwitz *et al.* (1990). Zirconium and hafnium separations from each other have been achieved using Diphonix® resin in an effort to minimise the hafnium contents in nuclear studies by Smolik and Jakóbik-Kolon (2009), Smolik *et al.* (2009). Chromium (III) separation has been achieved using Diphonix® resin from electroplating effluents and regeneration studies with 1 mol/l NaOH and 0.33 mol/l H_2O_2 by Fernandes *et al.* (2007). Elution of actinides from Diphonix® has been carried out using Hydroxy Ethylidene Diphosphonic Acid (HEDPA) by Kim *et al.* (2000). An eluting mixture of 1 mol/l NaOH and 1 mol/l H_2O_2 has been used for the elution of 90% uranium from the resin by Turner *et al.* (2015). The efficient strip of the divalent metal ions from the Diphonix® resin has been performed with 1 mol/l H_2SO_4 and for Fe (III) with 1 mol/l HEDPA by Chiarizia *et al.* (1993).

CL resin

CL resin from Triskem International is a new anion resin which has been reported to be utilised in the separation of halides and chlorides and is selective for Ag, Au and Pd (Triskem product sheet). The specificity of CL resin provided was 100-150 mesh size with a density of 0.37 g/ml. A method for separation of chorides and iodides has been described using CL resin in Zulauf *et al.* (2010). Only data available from the manufacturer's product sheets states that Ag and Pd have the highest distribution coefficient on CL resin whereas, Cd, Ce, Co, Cu, Fe, Mn, Ni and Zn have distribution coefficient from 1 to 25. The extraction media have been reported to be 1 mol/l H_2SO_4. Other eluting agents reported for halides were KSCN and NH_4SCN etc.

The main aim of this chapter is to explore the possibilities, whether Diphonix® and CL resin can be used for the separation of the matrix elements or combination of the both resins can be applied together with sodium peroxide sintering for PGE studies.

15.1.1 Aims of the chapter

The trace PGE analysis is an analytical problem due to matrix interferences in geological materials. PGE analysis in geological material requires matrix separation and pre-concentration of PGE. The main purpose of this study was to explore the possibilities of separation of interferences i.e. Cu, Ni, Zn, Rb, Sr, Y, Zr, Nb, Mo, Cd, REE, Hg, W, Ta and Pb etc. from the sinter solutions (samples digested with sodium peroxide sintering) using Diphonix® a cation resin and CL an anion resin for PGE studies. The salient features of this chapter are;

1. Method development for removal of interferences by using Diphonix® resin in sinter solutions of geological materials.
2. Method development for removal of interferences by using CL resin in sinter solutions of geological materials.
3. Evaluation of the possibilities of the combination of Diphonix® and CL resin with sinter solutions for accurate analysis of PGE isotopes through isotope dilution.
4. Tests with standard PGE solutions and real matrix samples on Diphonix® and CL resins.
5. Evaluation of the blanks obtained by treating samples with Diphonix® and CL resins.
6. Tests on Ag-loaded CL resin for improving the chemical recovery of the PGE isotopes.

15.2 Material and reagents

Diphonix® a cation resin 100-200 mesh and CL an anion resin 100-150 resin were tested for retention evaluation of the PGE and the separation of the matrix elements. 250 ml conical flask were used for cleaning the resin prior to use. 20 ml polypropylene + polyethene columns with internal diameter of 15 mm, outlet diameter 1.5 mm and 250 ml funnels were used for Diphonix®. 2 ml polypropylene + polyethene columns with internal diameter of 7 mm, outlet internal diameter 1.5 mm and funnel of 25 ml capacity with an internal diameter of 25 mm were used for CL resin. Fritz sizes were 20 μm. Plastic racks were used for holding the columns. Flow rate regulation valves were used for controlling the required flow rates in the columns. Columns and accessories were obtained from Triskm International. The specification of sodium peroxide, hydrochloric acid, HNO_3, glassy carbon crucibles, PFA-vials, and ICP-MS/MS have already been described in the previous chapters.

15.3 Preparation of resin columns

15.3.1 Wash protocol for resins

Different amounts 1-8 g of moist Diphonix® resin were taken in conical flasks. For stripping of the possible contaminations, the protocol of Fernandes *et al.* (2007) was used for stripping the metal ions using a mixture of 1 mol/l NaOH and 0.33 mol/l H_2O_2. A magnetic bar was placed in each flask and the resin was stirred on a magnetic plate for three hours. The resin was washed with deionised water several times and kept in 1 mol/l H_2SO_4 for the activation of its functional group. The resin was loaded on the 20 ml columns and rinsed with deionised water. The resin on the column was kept under wet conditions to avoid resin gaps and cracks which would hinder the metal ions uptake and their elutions.

Different amounts of CL resin 100, 200, 300, 400 and 500 mg were taken in 50 ml centrifugation vials. 1 mol/l H_2SO_4 was added in each vial with a 7 mm magnetic strip for

stirring at least 3 hours on magnetic plate. The resins were loaded on the column and rinsed with deionized water. The resins were kept under wet conditions.

PFA-vials and columns cleaning

The columns were kept in 6 mol/l HCl overnight, thoroughly rinsed and washed, and were treated with ultrasonic both prior to every use. PFA vessels which are used to collect the eluates were boiled in concentrated nitric acid for 180 minutes at 180 °C.

15.3.2 Tests on standard solutions for removal of matrix elements on Diphonix® resin (100-200 mesh)

For the evaluation of retention ability of Diphonix® cation resin, a 50 ng solution of Re-PGE was mixed with a real matrix SdAR-1 reference material that was digested with the sodium peroxide sintering. 50 ng PGE + matrix solutions were added to each flask containing 1-8 g Diphonix® resin. The pH of the solution was 0.8 which was checked with pH meter. A magnetic bar was added to each flask and solution was stirred (500 rpm) on the magnetic plate left to 70 °C for 5-6 hours for bringing PGE + matrix analytes in contact with Diphonix® resin. The contents containing Diphonix® resin and PGE+matrix were loaded onto the column. The flow rate was adjusted to 5-10 drop/min with a valve connected to the outlet of the column. The solution was collected in PFA-vials and dried at 110 °C on hot plate. The dried contents were re-dissolved in 0.1 mol/l HCl and were analysed with the Agilent 8800 ICP-MS/MS. The retention of the metal ions by amounts of Diphonix® below 8 g was not satisfactory. Only 8 g Diphonix® provided maximum uptake of ions. The results of the retention of metal ions on Diphonix® resin are given in the Table 15.1.

Table 15.1: Retention of metal ions with 8 g Diphonix® from sinter solutions

Retention of analytes from sinter solution pH (0.8) by 8 g Diphonix®							
Element	Retention	Element	Retention	Element	Retention	Element	Retention
Li	50%	Zn	0%	In	50%	Tm	96%
Be	50%	Ga	70%	Sn	0%	Yb	96%
B	50%	Ge	80%	Sb	50%	Lu	96%
Mg	50%	AS	50%	Te	70%	Hf	96%
Al	90%	Se	0%	Cs	30%	Ta	30%
K	0%	Rb	30%	Ba	60%	W	80%
Ca	50%	Sr	50%	La	96%	Re	20%
Sc	0%	Y	98%	Ce	96%	Os	0%
Ti	98%	Zr	98%	Pr	96%	Ir	0%
V	60%	Nb	98%	Nd	96%	Pt	20%
Cr	70%	Mo	75%	Sm	96%	Au	5%
Mn	50%	Ru	75%	Eu	80%	Hg	0%
Fe	99%	Rh	90%	Gd	96%	Tl	40%
Cu	90%	Pd	50%	Tb	96%	Pb	15%
Co	50%	Ag	0%	Dy	96%	Bi	80%
Ni	0%	Cd	0%	Ho	96%	Th	70%
Cu	50%			Er	96%	U	98%

From the viewpoint of PGE studies, it was expected that PGE should not be retained on the resin except matrix elements. But ruthenium is also retained (75%) on Diphonix®, indicating that ruthenium exists as positive complexes in sinter solutions. This factor explains the low retention on anion-exchange columns. It is deduced that ruthenium also exists as positive ion complexes in the sinter solutions. Rhodium is 90% adsorbed on Diphonix®, and suffers its chemical recovery. Pd, Re, Pt and Au are 50%, 20%, 20% and 5% adsorbed respectively on Diphonix® while Ir and Os are not retained.

From the results of this test, it can be seen that Cu is 50% retained by the resin and will still cause interferences on ^{101}Ru, ^{103}Rh, ^{102}Pd and ^{105}Pd. Mo is 75% retained and will cause interferences on ^{99}Ru, ^{101}Ru, ^{106}Pd, ^{108}Pd and ^{110}Pd. Zn is not retained and hence PGE isotopes ^{99}Ru, ^{102}Ru, ^{103}Rh, ^{102}Pd, ^{104}Pd, ^{105}Pd ^{106}Pd, ^{108}Pd and ^{107}Ag will be interfered. Rb is 30% retained and ^{101}Ru and ^{103}Rh will still have interferences. Sr is 50% retained and PGE isotopes ^{102}Ru, ^{103}Rh, ^{102}Pd, ^{104}Pd and ^{105}Pd will be interfered. Zr, Nb and Y are 98 % retained, thus interferences on Pd and Ag isotopes will be minimised. Cd is not retained and will be the cause of interferences on Pd isotopes. REE are 98% retained which is beneficial for the most of the PGE isotopes. Mercury is not retained; thus Pt isotopes will be heavily interfered. Lu, Yb, and Hf are 96% retained and Os, Ir and Pt isotopes will be less suffered by interferences. Ta is only 30% retained and will be an interference on Pt and Au. W is 80% retained and there will be interferences on Pt isotopes. Pb is only 15% retained and Rh will be mostly suffering from doubly charged species in the ICP-MS spectrum.

Advantages and disadvantages of Diphonix®

From the above tests following can be considered as an advantage of Diphonix®

1. Almost all rare earth elements are retained from the sinter solutions (up to 96% except Eu 80%).
2. Cu, Fe, Y, Zr, Nb and Hf are retained (up to 96-98%), which are the main interferences on Pd, Ag and Pt.

The following are the negative points about Diphonix® resin in sinter solution.

1. PGE are also retained in significant amounts from the sinter solution i.e. Ru 75%, Rh 90% and Pd 50%. This does not provide an ideal situation for PGE analysis as the recovery might be too low.
2. Ag, Cd and Hg from sinter solutions are not retained from sinter solution. This demands to combine anion resin for the elimination of such ions coming from cation resins.

As the focus of this study was on sinter solutions that offer complete sample digestions, but this combination cannot be extended to good PGE analysis. Other methods of digestions may offer suitability of usage of Diphonix® for matrix removal in PGE analysis.

15.3.3 Tests on standard solutions for removal of matrix elements on AG50Wx8 cation resin (100-200 mesh)

AG50Wx8 cation resin is a well-tested resin and had been used for matrix removal in several studies. The results of Diphonix® were compared with AG50Wx8 cation applied to sinter solution. Several amounts of AG50Wx8 cation resin (100-200 mesh) were tested for 50 ng solution of PGE + matrix elements in sinter solutions. Only 32 grams of AG50Wx8 cation resin provided satisfactory results. Whereas only 8 g Diphonix® was sufficient for matrix elimination of most of the ions. The results of the removal of matrix elements from the sinter solution are given in Table 15.2.

Table 15.2: Retention of matrix elements with 32 g AG50Wx8 cation resin from sinter solution pH (0.8)

Results of retention of analytes on 32 g AG50Wx8 cation resin							
Element	Retention	Element	Retention	Element	Retention	Element	Retention
Li	70%	Zn	68%	In	85%	Tm	100%
Be	80%	Ga	100%	Sn	40%	Yb	100%
B	80%	Ge	80%	Sb	20%	Lu	100%
Mg	99%	AS	50%	Te	70%	Hf	97%
Al	0%	Se	30%	Cs	50%	Ta	80%
K	70%	Rb	70%	Ba	100%	W	40%
Ca	99%	Sr	100%	La	100%	Re	40%
Sc	0%	Y	100%	Ce	99%	Os	0%
Ti	97%	Zr	99%	Pr	99%	Ir	3%
V	85%	Nb	50%	Nd	100%	Pt	7%
Cr	70%	Mo	80%	Sm	99%	Au	70%
Mn	99%	Ru	80%	Eu	99%	Hg	0%
Fe	100%	Rh	80%	Gd	99%	Tl	90%
Co	99%	Pd	90%	Tb	98%	Pb	95%
Ni	92%	Ag	0%	Dy	100%	Bi	75%
Cu	88%	Cd	80%	Ho	100%	Th	90%
				Er	100%	U	98%

From the results of retention of analytes from sinter solution with AG50Wx8 cation resin, it can be seen that matrix elements Fe, Cu, Ni, Co, Sr, Zr, Y, Ba, REE, Hf, Ta, Pb and Tl are effectively removed from the sinter solutions. Mercury is not retained at all, W is only 40% retained, Ta is 80% retained, Rb is 70% retained, Nb is 50% retained and Cd is 80% retained. The PGE analytes are also retained in significant amounts specially Ru (80%), Rh (80%), and Pd (90%). Thus sinter solutions do not provide a good basis for PGE resin chromatography. Meisel and Moser (2004a) has however, used HPA digested solutions for complete removal of matrix elements.

15.3.4 Tests on standard solution + sinter solution for uptake of PGE on CL and AG1X8 resin

CL resin has been used for separation for chlorides and halides. It has selectivity for Ag and Pd. Tests were conducted to combine CL resin with the sinter solution for the separation/pre-concentration of PGE from matrix elements. For these purposes, initial tests were performed with standard solution + sinter solution to see the retention ability of the resin for PGE. 600 mg CL resin was taken in 50 ml centrifugation vials and 1mol/l sulphuric acid was added. For the activation of the resin, stirring was done with the aid of magnetic bars placed in the resin. The resin was placed on a magnetic plate and stirring was done for 3 hours. The resin was loaded into the column. The resin was treated with deionized water several times. A 50 ng PGE standard solution + sinter solution was prepared and loaded on the resin. The flow rate of solution passing through the CL resin so as to bring maximum contact between metal ions and resin. The solution was collected and dried at 110 °C on hot

plate. Dried components were re-dissolved in 0.1 mol/l HCl and analysed with the Agilent 8800 ICP-MS/MS.

Similar experiments were performed on AG1X8 anion resin for the comparison of the results. AG1X8 anion was used in combination with a sintering solution. Wash protocol for the rinse was the same as mentioned in the sintering-anion section of the thesis (chapter 11). A similar amount of the resin as that of CL resin was taken and PGE + sinter solution was passed through the resin. The solution was collected in PFA vessel, dried, re-dissolved in 0.1 mol/l HCl and analysed with the Agilent 8800 ICP-MS/MS. The results of the retention ability of the both the resins are shown in Table 15.3.

Table 15.3: Retention of PGE+ sinter solution on CL and AG1X8 resins

Results of retention on resins

Analyte	Retention on CL resin	Retention on AG1X8
Ag	99%	98%
Au	98%	99%
Ir	17%	38%
Os	90%	95%
Pd	59%	50%
Pt	78%	73%
Re	34%	100%
Ru	14%	22%
Rh	10%	20%
Cd	39%	66%
Eu	18%	13%
Gd	18%	14%
Hf	54%	39%
Hg	71%	92%
Mo	10%	0%
Nb	62%	47%
Nd	17%	12%
Sm	16%	13%
Ta	62%	71%
W	3%	85%
Y	16%	12%
Zr	55%	40%

Ag and Au were 98-99% absorbed on both the resin. Os retention on both the resin was more than 90 %. Iridium was 17 % retained on CL resin, and 38% on AG1X8 resin. Retention of the Pd was 59 % on CL resin and 50 % on AG1X8 resin. Platinum retention on both the resins were comparable 73-78%. Re retention was 100% on AG1X8 resin and 34 % on CL resin. The retention of the Ru and Rh was low in both the resins 10-22%. In an ideal situation, the matrix elements should not be retained on anion resins. The matrix

elements e.g. Cd 39%, Eu and Gd 18%, Hf 54%, Hg 71%, Mo 10%, Nb 62%, Nd and Sm 60-17%, Ta 62%, W 3%, Y 16% and Zr 55% were also retained on CL resin. Hg, Ta and W retained on AG1X8 were ranging from 72-91%.

15.3.5 Elution tests on CL resin

Further tests were performed for the elution of PGE metal ions from the resin. No significant elution of PGE ions was possible with a 1 mol/l solution of NH_4SCN. Elution of PGE ions with 1 mol/l solution of KSCN was significant, but it also eluted the matrix elements. When 1 mol/l solution of thiourea was used for the elution, it eluted all matrix elements except Zr, Gd, Hf, Nb, Ta, Nb, Nd and Sm etc. PGE ions were significantly eluted except the Rh and Ru 3-4%. High procedural blanks were obtained that restricted further work on the resin. The results of the elution studies are presented in Table 15.4.

Table 15.4: Elution of PGE from CL resin

50 ng PGE solution+ 1 mg/l matrix elements on 500 mg CL resin					
Analyte	Retention	Elution with 1 mol/l KSCN	Elution with 1 mol/l thiourea	Overall yield (KSCN)	Overall yield (Thiourea)
Ag	99%	8%	100%	8%	99%
Au	98%	24%	100%	24%	98%
Ir	17%	100%	52%	17%	9%
Pd	59%	50%	50%	30%	30%
Pt	78%	12%	100%	9%	78%
Re	34%	100%	100%	34%	34%
Os	90%	3%	48%	3%	43%
Rh	10%	100%	1%	10%	0.1%
Ru	14%	100%	4%	14%	1%
Cd	39%	100%	100%	39%	39%
Eu	18%	100%	100%	18%	18%
Gd	18%	100%	0%	18%	0%
Hf	54%	55%	0%	30%	0%
Hg	71%	100%	100%	71%	71%
Mo	10%	100%	100%	10%	10%
Nb	62%	54%	5%	33%	3%
Nd	17%	100%	0%	17%	0%
Sm	16%	100%	1%	16%	0.1%
Ta	62%	59%	3%	37%	2%
W	3%	100%	100%	3%	3%
Y	16%	100%	100%	16%	16%
Zr	55%	58%	3%	32%	2%

15.3.6 Tests on Ag-loaded CL resin

Silver has been reported to be added to the fusion mixture of NiS either as metallic silver or in the form of silver nitrate solution because it acts as a carrier for gold, palladium

and platinum (Juvonen *et al.* 1994). The manufacturer has recommended the use of silver loaded CL resin for halides (Triskem product sheet).

A similar test was performed for PGE retention on CL resin loaded with Ag. For that purposes, 1 mg/l solution of Ag was prepared and was added to the resin. Resin with $AgNO_3$ solution was poured into the centrifugation vials and 1 mol/l sulphuric acid was added. The solution was placed on the magnetic plate with a magnetic bar in the vials for 3 hours stirring. The resin with Ag was loaded onto the column and rinsed with deionized water several times. Finally, 50 ng standard PGE solution + sinter solution was loaded onto the column. The flow rate of the standard PGE solution + sinter solution was adjusted to 5-10 drops per minute by connecting a valve with column outlet. The solution was collected and dried in PFA vessels. The dried solution was re-dissolved in 0.1 mol/l HCl for the determination of PGE amounts retained on the Ag-loaded resins through the contents determined in the solution. PGE retained on the Ag-loaded resin are shown in the Table 15.5. PGE were then eluted with 0.5 mol/l thiourea prepared in 2 mol/l HCl. The eluate was collected in PFA vessel and dried at 110 °C on hot plate. Thiourea eluate needed to be treated for the destruction of organic matter. For that purposes, 100-500 µl concentrated HNO_3 was added while heating. This also leads to loss of osmium contents and therefore it is not presented in the results. After the destruction of organic matter, dried PGE contents were re-dissolved in 0.1 mol/l HCl and were analysed with the Agilent 8800 ICP-MS/MS. The results of the elution study are shown in Table 15.5. From the results, it can be seen that Ru, Rh and Ir retention significantly improved by loading Ag on the resin. However, Ru, Rh, Ir, Pt and Au were not eluted to expected yields. Only Pd and Re were 100% eluted. The elution from Ag-loaded resin was itself a problem and other eluting agents are needed to be tested.

Table 15.5: Retention and elution study of PGE with 0.5 mol/l thiourea

Results of retention and elution on 600 mg Ag-loaded CL resin

Analyte	retention	elution	Overall yield
Ru	48%	7%	3.4%
Rh	52%	1%	0.5%
Pd	97%	100%	97%
Re	100%	100%	100%
Ir	59%	20%	12%
Pt	95%	39%	37%
Au	100%	15%	15%

15.4 Summary

This chapter has provided an insight on initial tests in brief for PGE retention and elution studies using two resins i.e. Diphonix® cation exchange resin and CL resin (Triskem international) from the sinter solution. Retention abilities of the two resins have been compared with two old resins AG50Wx8 cation resin and Ag1X8 an anion resin. The Diphonix® cation exchange resin provides an excellent capability for the retention of the metal ions from sinter solution especially rare earth elements. Only 8 g in moist form was shown to be sufficient for satisfactory removal of matrix ions, while 32 g moist AG50Wx8 cation needed to provide satisfactory metal ion retention. The PGE metal ions are also

retained on the resin, especially Ru, Rh and Pd and chemistry of sinter solution are more complex than expected. It is, however, suggested to further carry on experimental tests for matrix removal for samples digested with acid digestions i.e. Carius tube, HPA etc. As the online matrix removal using digestion method with HPA by Meisel and Moser (2004a) has already shown complete removal of matrix elements using cation AG50Wx8 resin.

The retention abilities of CL resin were evaluated in this chapter in comparison with AG1X8 100-200 mesh anion resin from sinter solution. CL resin also provides excellent retention abilities from standard PGE solution + sinter solutions, especially for Ag, Pd, Os, Au and Pt. The retention abilities of Ru, Rh, Ir and Re were low because of the solution chemistry of the ions in sinter solutions. The retention of Ru, Rh, Ir and Re were dramatically improved by loading Ag on the resin. The elution of the PGE was quantitative for only Re and Pd with thiourea, while the recoveries of other PGE were not satisfactory. This suggests the need of other eluting agents for elution of PGE from silver loaded resin.

Further investigation of PGE retention and elution needs to be performed using CL resin with other sample digestion methods.

16. Summary and conclusion

An improved and optimised method for sample digestion that provides the basis for whole-rock chemistry evaluation is presented in this thesis. Throughout this study sodium peroxide sintering is used for the sample preparation and evaluated for the elemental mass fraction determination in geological reference materials. The results obtained are precise and satisfactory. The method can be used for routine and quality control purposes. Following new measurement procedures have been developed:

1. A method for the accurate determination of the rare earth elements using collision/reaction cell.
2. A method for the accurate determination of PGE, Au and Ag using collision/reaction cell.
3. A rapid analytical method for the determination of ruthenium and osmium mass fractions through sparging combined with an isotope dilution method.
4. Methods for the determination of ruthenium and osmium mass fractions through distillation combined with an isotope dilution method.

The optimisation of sample digestion method is shown in chapter 5. Sodium peroxide sintering combined with the ICP-MS is a rapid and reliable analytical method for the method validation and homogeneity testing of reference materials. The supernatant and the residue are the essential components of the sinter solutions. The supernatant cannot be discarded when the whole-rock chemistry of the analyte is required. The effect of the amount of sodium peroxide on complete sample digestion and recovery of the analyte has been shown and at least a 1:5 sample to sodium peroxide ratio is needed for digestion of refractory minerals. 120 minutes at 480 °C are required to decompose the refractory phases in the rocks. The stability of sinter solution has been studied and it is shown that sample solutions can be used after the several months of their preparation for materials low in zircon contents. Zircon-rich samples may suffer precipitation of zircon etc. over time. The SiO_2 can be accurately measured with the ICP-MS if the supernatant is not discarded. The optimised method has been combined with different techniques for PGE determination in this thesis.

The method validation of sodium peroxide sintering and homogeneity of the three reference materials MTA-1, MRH-1 and G-3 is described in chapter 6. The importance of consideration of several influencing quantities that may affect the homogeneity of a reference material is described. For the determination of the effect of only test portion size on the homogeneity, the influencing quantities i.e. purity of reagents, calibration, tune condition, the sample to sodium peroxide ratio, incomplete digestions, replicate measurements and nugget effects need to be minimised. Test portion size is important in determining the homogeneity of the reference material. Smaller test portions e.g. 50 mg show larger variance in RSDs and shows heterogeneity of most the analytes, especially in rock types which contain the refractory mineral zircon. The minimum test portion size for homogeneity testing in RM trachyandesite MTA-1 and RM granite G-3 is 300 mg and for RM rhyolite MRH-1 is 100 mg. This assures the acceptable precision of less than 3% with 1:6 sample: Na_2O_2 ratio.

The suppression of the spectral interferences on the rare earth elements by using ion-molecule reactions in a collision/reaction cell can significantly improve elemental selectivity and accuracy in ICP-MS/MS applications in geological reference materials. The relative reactivities of interferences with NH_3 and O_2 gases (oxide, hydroxides and hydrides) has been shown in chapter 7. The ion-molecule reactions of rare earth elements with oxygen and ammonia gas and their product ions have been discussed thoroughly. Initial testing with oxygen gas for the removal of interference shows its excellent performance, but when

applied to real matrices, the use of O_2 leads to the formation of unidentified product ions, which cause additional interferences and reduce the sensitivity of the analytes. The optimised gas modes and product ions suggested after a thorough study which can be applied for routine analysis are given below;

1. 139 -> 224 La [NH3-M]	10. 160-> 160 Dy [NH3-M]
2. 140 -> 225 Ce [NH3-M]	11. 163 -> 163 Dy [NH3-M]
3. 141 -> 141 Pr [NH3-M]	12. 165 -> 165 Ho [NH3-M]
4. 146 -> 146 Nd [NH3-M]	13. 166 -> 166 Er [NH3-M]
5. 147 -> 147 Sm [NH3-L & M]	14. 169 -> 169 Tm [NH3-M]
6. 151 -> 151 Eu [NH3-H]	15. 172 -> 187 Yb [NH3-L]
7. 153 -> 153 Eu [NH3-H]	16. 89 -> 157 Y [NH3-M]
8. 157 -> 172 Gd [NH3-L]	17. 175 -> 175 Lu [NH3-M]
9. 159 -> 174 Tb [NH3-L]	18. 45 -> 130 Sc [NH3-M]

L= Low, M=Medium, H= High (flow rates of ammonia)

The product ions through ion-molecule reactions of 45 analytes in the collision/reaction cell with ammonia and oxygen gases were studied for removal of numerous interferences generated in the plasma. A scan of all the product ions on m/z of the analytes is possible in few seconds with ICP-MS/MS using reactive gases in collision/reaction cell. The role of ammonia, hydrogen, helium and oxygen gases in the collision/reaction cell is studied for reducing the background interferences from plasma and acids used in dilutions and sample preparations (Figure 8.1- Figure 8.20). The argide ions, C^+, N^+, O^+, H^+, S^+, are reduced with the use of ammonia gas. The addition of H_2 in the cell also removes any residual $^{40}Ar^+$ ions formed(Figure 8.11). Some analytes e.g. Hg, S, Se, As and P undergo charge transfer reactions with ammonia gas.

These reactions can be applied for the removal of interferences of such elements on other elements by the use of ammonia gas. For example, $^{204}Hg^+$ interference on $^{204}Pb^+$ can be removed with charge transfer reaction. Mercury is neutralised by charge transfer reaction with ammonia gas, thus leaving Pb free from interference. Similarly, S based interferences can be decreased using charge transfer reaction with ammonia gas. Argide ions also react with ammonia through charge transfer reaction with ammonia gas and argide interferences are removed. The on-mass and/or mass-shift modes with NH_3 and/or O_2 reaction gas provides reliable and consistent measurements of Si as 28 -> 44 Si [O2], P as 31 -> 47 P [O2], Ti as 48 -> 64 Ti [O2], Cr as 52 -> 68 Cr [O2], Cr as 55 -> 71 Mn [O2], V as 51 -> 51 V [NH3-M], Fe as 56 -> 90 Fe [NH3-M], Cu as 63 -> 97 Cu [NH3-M], Zn as 68 -> 100 Zn [NH3-M], As as 75 -> 91 As [O2], Sb as 121 -> 137 Sb [O2], Pb as 204 -> 204 Pb [NH3-M] etc.

The effectiveness of the collision/reaction cell using NH_3 and O_2 gases for the removal of spectral interferences on PGE analytes is shown in chapter 9. A new method for interference free determination of PGE mass fractions is developed. It can be demonstrated that the collision/reaction cell is effective in removal of oxide interferences through the use of reactive gases i.e. O_2 and ammonia etc. A thorough study has been conducted in the determination of BECs on PGE analytes from the interferences. The reaction behaviour of PGE isotopes was studied by on-mass measurement with oxygen and ammonia gases. The order of reactivity of PGE isotopes is Os>Ir>Pt>Rh>Pd>Ag>Ru>Au etc. The reaction efficiencies of PGE analytes with oxygen gas were also tested which shows that Pt does not react efficiently with oxygen gas. The decrease in intensities of PGE analytes was observed for Pd, Os, Ir and Au, which relates to the formation of other product ions. Ruthenium and Rh also undergo oxidation to make oxides. The oxides matrix elements which are Nd, Sm,

Cd, Rb, Eu, Pb and Sr show less reactivity with ammonia gas and Hg, Nb, Zr, Lu, Hf, Y, Ta, W and Gd show the highest reactivity with ammonia gas. This behaviour of PGE and interferences has been used to develop a new method for the determination of PGE mass fractions. The ion-molecule reactions of PGE analytes and matrix elements via clustering, addition, charge transfer or condensation reaction has offered two acquisition modes for their separation i.e. on-mass mode and mass-shift mode. Ammonia and oxygen gases have offered a variety of options for interference removals on PGE isotopes.

The product ion of RuO has no overlap of Pd interferences. Oxygen mass-shift mode successfully utilises volatile nature of Os to make an abundant OsO_2 product ion. OsO_2 was used in the reduction of Yb and Hf interferences on Os. The following product ions can be used in routine determination of PGE in geological reference materials;

1. Ru as $Ru(NH_3)_4^+$ and RuO
2. Rh as $Rh(NH_3)_4^+$ and on-mass ammonia
3. Pd as $Pd(NH_3)_3^+$ and on-mass ammonia
4. Ir as $IrNH^+$ and IrO^+
5. Os as $OsNH^+$ and OsO_2^+
6. Pt on-mass-ammonia and $Pt(NH_3)_2^+$
7. Ag as on-mass ammonia
8. Au as on-mass ammonia and $Au(NH_3)_2^+$

The suitable flow rates of ammonia gas are given in Table 9.4. The useful product ions for the quantification of PGE formed through clustering reactions are $M(NH_3)_x^+$ and include ($Pt(NH_3)_2^+$, $Pd(NH_3)_3^+$, $Au(NH_3)_2^+$, $Ru(NH_3)_4^+$, $Rh(NH_3)_4^+$ and $Ag(NH_3)_2^+$, etc. The product ions of PGE formed through condensation reactions are MNH^+ ($IrNH^+$, $OsNH^+$ and $ReNH^+$) etc.

Two important reactions as charge transfer reactions for Hg and Pb removal has been discussed which shows the success of the method for on-mass measurement of Pt in and Rh in ammonia gas. Rhenium and W interference on ^{187}Os are problematic because both make identical product ions in ammonia and oxygen gas.

A method using sodium peroxide sintering in combination with tellurium co-precipitation isotope dilution mass spectrometry has been developed. The method has been improved for the determination of PGE mass fractions i.e. Ru, Rh, Pd, Pt, Ir and Au in geological reference materials after the reported method by Richardson (2004). Richardson (2004) has provided detection limits of PGE i.e. Au 5.8 ng/g, Pt 6.4 ng/g, Pd 13 ng/g, Rh 1 ng/g, Ru 1.6 ng/g, Ir 0.7 ng/g, whereas the detection limits of the method developed are Ru 0.24 ng/g, Rh 0.24 ng/g, Pd 2.50 ng/g, Pt 0.08 ng/g, Ir 0.23 ng/g, Au 0.29 ng/g. The detection limits did not improve compared to the method of Qi (2007) using sodium peroxide fusion and tellurium co-precipitation in particular for Ru 0.045 ng/g, Pd 0.11 ng/g, Ir 0.02 ng/g, Rh 0.024 ng/g. Therefore, there is further work require to lower the limit of detection by selection of appropriate chemicals i.e. Te powder, sodium peroxide etc. Two modifications have been applied to the method of Qi (2007). Silicates are dissolved with the addition of 1 to 2 ml concentrated HCl and dilution to larger volume instead of removal by drying or by use of HF. The precipitate is collected by centrifugation instead of the requirement of more apparatus i.e. membrane filter paper, vacuum connected etc. flasks that may add to the procedural blanks as predicted by Qi (2007). Qi (2007) reported hafnium and zirconium contaminations from the material of corundum crucibles which were mathematically corrected. Corundum crucibles need to be replaced after 10 fusions. Glassy carbon crucibles can be used for around 100 digestions using sintering making this method simple and inexpensive. The larger size crucibles are required for testing larger test portions to reduce the effect of inhomogenously distributed nuggets. The manufacturers can prepare such large capacity glassy carbon crucibles. Sintering-tellurium co-precipitation ID is a rapid, fast and reliable method of PGE dissolution that can be applied to complex matrices. This

method is applied for routine analysis of PGE samples from the industrial and geological background.

Through the development of a method based on sintering-anion-exchange chromatography, the discrepancies in the Re and Ru mass fractions of TDB-1 and BIR-1 have been addressed which were pointed out in literature as discussed in chapter 12. HPA and Carius tube digestions require the use of HF for attacking Re and Ru hosted in silicate portions of the rock. The use of HF if mishandled can lead to serious conditions including deaths. Thus, sodium peroxide sintering has been applied for ruthenium and rhenium mass fractions determination combined with anion-exchange chromatography, which abolishes the use of HF by accurate quantification. The lower recoveries of PGE in sinter solution have to do with the chemistry of PGE ions, however, rhenium recovery is 90-95% but recoveries of ruthenium did not improve. Based on the observations, it is shown that Rh, Ru, Re, Pt, Pd is mostly presented in the supernatant and Ir and Os are present in the residue phase of sinter. Gold is equally distributed in both the supernatant and residue phases of the sinter.

The possibilities of ruthenium sparging with different oxidising agents have been tested for mobilisation of ruthenium from the sinter solution. From the tests, it is shown that ruthenium can be mobilised from the solution with the use of appropriate oxidising agents in argon gas-aided sparging. This method is applied in combination of isotope dilution mass spectrometry for the ruthenium mass fractions determination. Ruthenium mobilisation through distillation is not new but to our knowledge until today, sparging of ruthenium has not been tested with the ICP-MS. The novel analytical method for ruthenium determination with sparging and subsequent determination of mass fractions in real matrices is rapid and employs no chemical separation prior to the analysis. Ruthenium sparging with $KMnO_4$ ensures 80-90 % spike recovery. The losses of RuO_4 and OsO_4 during open vessel digestions with glassy carbon crucibles and sparging in small 15 ml PFA vessels cannot be estimated as spike was added after sintering. Closed vessels digestions i.e. HPA, larger sparging vessels and longer integration time for the measurement of isotopic ratios can help in improving the precision of the data. Other analytes are also volatilised during sparging for example Mo which causes interferences on $^{99}Ru/^{101}Ru$. The isotopic ratios $^{102}Ru/^{104}Ru$ and $^{101}Ru/^{104}Ru$ are least affected. It is, therefore, suggested that, if a spike of ^{102}Ru or ^{104}Ru is added to the real matrix, accurate mass fractions of real samples can be determined. As palladium did not volatilise thus, ^{102}Ru or ^{104}Ru spikes can be an ideal solution for ruthenium sparging. The isotopic ratios $^{99}Ru/^{101}Ru$ in case of MUH-1 reference material were most affected by matrix interferences of Mo. The isotopic ratios $^{99}Ru/^{101}Ru$ of MUH-1 reference material, were determined using a collision/reaction cell in MS/MS mass-shift mode (RuO) using oxygen gas which improved the accuracy of the results. Further work is required for the optimisation of signal intensity for the first replicates, stabilisation of signals by the use of large volumes of the solutions, application of the method on sample digested with other techniques and trap of RuO_4 in HCl for solution measurement etc.

Two methods have been developed for the ruthenium distillation i.e. (a) sodium peroxide sinter solutions distilled with phosphoric acid/$K_2Cr_2O_7$ based on the method of Ly and Hidaka (2004) (b) sodium peroxide sinter solutions distilled with $KBrO_3$/chilled sulphuric acid trap based on micro-distillation method for osmium of Brauns (2004). Osmium determination was difficult with these methods. High temperature in open vessel digestions of sintering may volatilise OsO_4. Further loses were expected in drying step of the trap solutions. Distillation with phosphoric acid/$K_2Cr_2O_7$ has shown some intensity of osmium isotopes but $KBrO_3$/chilled sulphuric acid trap method did not provide any reasonable intensity for osmium quantification. Mo, Sr, and Rb interferences were quantitatively reduced and $^{99}Ru/^{101}Ru$ and $^{99}Ru/^{102}Ru$ isotopic ratios were least affected due to such interferences. Aerosol generation in a small scale apparatus might have induced slight

interferences on $^{99}Ru/^{101}Ru$ and $^{99}Ru/^{102}Ru$. The samples which were digested with sodium peroxide/HCl provided reducing conditions which restricted the volatility of RuO_4 as very less intensities of ruthenium isotopes were observed. The solutions obtained from sodium peroxide/HNO_3 digestion have shown improved volatilisation of RuO_4 as intensities of ruthenium isotopes were enhanced. More work on the reference materials is required using more volume of the solution in a larger apparatus i.e. conical flasks etc. which will quantitatively improve the precision and accuracy of the technique. Sodium peroxide digests can be applied for ruthenium determination without pre-concentration step for ruthenium determination. The blanks were high due to sodium peroxide itself. Through the results obtained on MUH-1 and OKUM geological reference material digested with sodium peroxide sintering, it is shown that this method can be extended to a variety of geological material for ruthenium mass fraction determination.

The combination of sinter solution with cloud point extraction using 2-MBT (2-mercaptobenzoothiazole) and or thiourea for the extraction of PGE and removal of interferences leads to poor recoveries of PGE and incomplete interference removals. This is due to the chemistry of PGE in sinter solutions related to the existence of hydroxyl-chloro complexes which are not chelated efficiently with 2-MBT (2-mercaptobenzoothiazole) or thiourea based reagents. Thus sinter solutions combined with cloud point extraction does not provide a good basis for interference removals and subsequent PGE determinations. The recoveries of the PGE were improved by using a solution prepared with high-pressure asher digestions which seem to produce only chloro-complexes in solution for which 2-MBT (2-mercaptobenzoothiazole) or thiourea complexing agents have better affinities. However, the method is not suitable for geological materials with complex matrices and interferences. The combination of anion-exchange may help in the removal of interferences after the PGE extraction with CPE if samples are digested with high-pressure asher. The removal of interferences prior to cloud point extraction with cation exchange columns can also be tested.

Capabilities of retention of metal ions from the sinter solution with two new CL and Diphonix® resins have been shown and compared with two resins AG50Wx8 (cation resin) and AG1X8 (an anion resin). Diphonix® cation exchange resin has retained almost all the rare earth elements from the matrix of sodium peroxide solutions. Only 8 g in moist form was shown to be sufficient for satisfactory removal of matrix ions, while 32 g moist AG50Wx8 cation resin needed to provide satisfactory metal ions retention. The disadvantage which is more related to the sintering solution is that the PGE ions are also retained on the resin, thus making it unsuitable for PGE studies. The PGE metals ions retained on the resin were Ru, Rh and Pd due to their complex chemistry. However, other methods of sample digestion are needed to be tested for PGE studies on Diphonix® resin. CL resin also provides excellent metal ions uptake from the standard solution PGE solution + sinter solutions, especially for Ag, Pd, Os, Au and Pt. The uptake of Ru, Rh, Ir and Re were low. The retention of Ru, Rh, Ir and Re were dramatically improved by loading Ag on the resin. The elution of the PGE was only quantitative for Re and Pd with thiourea, while the recoveries of other PGE were not satisfactory. Other eluting agents are required to be tested for PGE elution from the resin.

This study has combined sodium peroxide sintering with various techniques and has developed new measurement procedures for the major, REE and platinum group elements including ruthenium with sparging and distillation. These methods can be applied for the routine determination of mass fractions of major, REE and platinum group elements.

References

Agilent-Notes. (2012)
Agilent 8800 Triple Quadrupole ICP-MS: Understanding oxygen reaction mode in ICP-MS/MS. **2012, 5991-1708EN,** 1-8.

Akio H., Toshiya S. and Katsuo M. (2013)
Ultra trace copper analysis in a semiconductor grade organometallic titanium complex **Agilent Notes,** p57.

Alonso J.I.G. and Rodriguez-González P. (2013)
Isotope dilution mass spectrometry. **Royal Society of Chemistry (United Kingdom),** 453 pp.

Amr M., Al-Saad K. and Helal A. (2010)
Ultra-trace measurements of 210 Pb in natural occurring radioactive materials by ICP-MS **Nuclear Instruments and Methods in Physics Research Section A: Accelerators, Spectrometers, Detectors and Associated Equipment, 615,** 237-241.

Anders E. and Ebihara M. (1982)
Solar-system abundances of the elements **Geochimica et Cosmochimica Acta, 46,** 2363-2380.

Anders E. and Grevesse N. (1989)
Abundances of the elements: Meteoritic and solar **Geochimica et Cosmochimica Acta, 53,** 197-214.

Ardini F., Soggia F., Rugi F., Udisti R. and Grotti M. (2010)
Conversion of rare earth elements to molecular oxide ions in a dynamic reaction cell and consequences on their determination by inductively coupled plasma mass spectrometry **Journal of Analytical Atomic Spectrometry, 25,** 1588-1597.

Aries S., Valladon M., Polvé M. and Dupré B. (2000)
A routine method for oxide and hydroxide interference corrections in ICP-MS chemical analysis of environmental and geological samples **Geostandards and Geoanalytical Research, 24,** 19-31.

Armentrout P.B. (2004)
Fundamentals of ion-molecule chemistry **Journal of Analytical Atomic Spectrometry, 19,** 571-580.

Aspinall H.C. (2012)
Properties of the elements, in chemistry of the f-block elements. **Gordon and Breach Science Publishers,** 10-21.

Bakircioglu D. (2012)
Cloud point extraction for the preconcentration of palladium and lead in environmental samples and determination by flow injection flame atomic absorption spectrometry **Environmental Science and Pollution Research, 19,** 2428-2437.

Balaram V. (2005)

Recent developments in analytical techniques for characterization of ultra pure materials—An overview **Bulletin of Materials Science, 28,** 345-348.

Balcaen L., Bolea-Fernandez E., Resano M. and Vanhaecke F. (2014)
Accurate determination of ultra-trace levels of Ti in blood serum using ICP-MS/MS **Anal Chim Acta, 809,** 1-8.

Balcaen L., Moens L. and Vanhaecke F. (2010)
Determination of isotope ratios of metals (and metalloids) by means of inductively coupled plasma-mass spectrometry for provenancing purposes—A review **Spectrochimica Acta Part B: Atomic Spectroscopy, 65,** 769-786.

Balcerzak M. (2002a)
Analytical methods for the determination of ruthenium: the state of the art **Critical Reviews in Analytical Chemistry, 32,** 181-226.

Balcerzak M. (2002b)
Sample digestion methods for the determination of traces of precious metals by spectrometric techniques **Analytical sciences, 18,** 737-750.

Ballhaus C., Bockrath C., Wohlgemuth-Ueberwasser C., Laurenz V. and Berndt J. (2006)
Fractionation of the noble metals by physical processes **Contributions to Mineralogy and Petrology, 152,** 667-684.

Barefoot R. (2004)
Determination of platinum group elements and gold in geological materials: a review of recent magnetic sector and laser ablation applications **Analytica Chimica Acta, 509,** 119-125.

Barinaga C.J., Koppenaal D.W. and McLuckey S.A. (1994)
Ion-trap mass spectrometry with an inductively coupled plasma source **Rapid Communications in Mass Spectrometry, 8,** 71-76.

Barnes S.-J., Naldrett A. and Gorton M. (1985)
The origin of the fractionation of platinum-group elements in terrestrial magmas **Chemical Geology, 53,** 303-323.

Bayon G., Barrat J.A., Etoubleau J., Benoit M., Bollinger C. and Révillon S. (2009)
Determination of rare earth elements, Sc, Y, Zr, Ba, Hf and Th in geological samples by ICP-MS after Tm addition and alkaline fusion **Geostandards and Geoanalytical Research, 33,** 51-62.

Bea F. (1996)
Controls on the trace element composition of crustal melts **Geological Society of America Special Papers, 315,** 33-41.

Becker H. and Walker R.J. (2003)
In search of extant Tc in the early solar system: 98 Ru and 99 Ru abundances in iron meteorites and chondrites **Chemical Geology, 196,** 43-56.

Begerow J., Turfeld M. and Dunemann L. (1997)

Determination of physiological palladium, platinum, iridium and gold levels in human blood using double focusing magnetic sector field inductively coupled plasma mass spectrometry **Journal of Analytical Atomic Spectrometry, 12,** 1095-1098.

Bencs L., Ravindra K. and Van Grieken R. (2003)
Methods for the determination of platinum group elements originating from the abrasion of automotive catalytic converters **Spectrochimica Acta Part B: Atomic Spectroscopy, 58,** 1723-1755.

Bezerra M.d.A., Arruda M.A.Z. and Ferreira S.L.C. (2005)
Cloud point extraction as a procedure of separation and pre-concentration for metal determination using spectroanalytical techniques: a review **Applied Spectroscopy Reviews, 40,** 269-299.

Bézos A., Lorand J.P., Humler E. and Gros M. (2005)
Platinum-group element systematics in Mid-Oceanic Ridge basaltic glasses from the Pacific, Atlantic, and Indian Oceans **Geochimica et Cosmochimica Acta, 69,** 2613-2627.

Birck J.L., Barman M.R. and Capmas F. (1997)
Re-Os isotopic measurements at the femtomole Level in natural samples **Geostandards newsletter, 21,** 19-27.

Bokhari S. and Meisel T. (2014a)
Accurate determination of Sc and Eu in Zr- and Ba-rich matrix in geological reference materials with ICP-MS **(ChemCYS 2014-Chemistry Conference for Young Scientists 2014., At Blakenberge, Belgium)**.

Bokhari S. and Meisel T. (2014b)
Accurate rhenium determination in basaltic geological reference material **Minerological Magazines Goldschmidt abstract, 765,** 233.

Bokhari S. and Meisel T. (2015a)
Data for Ru, Pd, Ir au and Rh for OKUM reference material with sintering-Te-coprecipitation **http://www.euroanalysis2015.com/book/**.

Bokhari S. and Meisel T. (2015b)
Method development for PGE determination in reference material BIR-1 **Mineralogical Magazine Goldschmidt abstract** 331.

Bokhari S., Meisel T. and Christoph W. (2015a)
Interference removals on Palladium and Gold with ICP-QQQ-MS in platinum group elements reference materials. **http://www.ewcps2015.org**.

Bokhari S., Meisel T. and Christoph W. (2015b)
Interference removals on Sc and Eu in Zr and Ba-rich matrix in geological reference material with ICP-QQQ-MS.
http://www.hzg.de/mw/icpms_anwendertreffen2014/index.html.de.

Bokhari S., Meisel T. and Christoph W. (2015c)
Removal of interferences on platinum in platinum group elements PGE reference materials RM. **2015.geoanalysis.info/documents/abstract_volume_geoanalysis2015.pdf**.

Bokhari S., Meisel T. and Christoph W. (2015d)
Study of interferences on Os isotopes **Book of abstract ASAC 2015 Innsbruck.**

Bokhari S., Meisel T. and Walkner C. (2015e)
Interference removals on Pd, Ru and Au with ICP-QQQ-MS in PGE RM. **EGU General Assembly Conference Abstracts,** 13473.

Bouberlová-Kosinová L. (1970)
Beitrag zur Theorie der Platin-, Palladium-und Goldsorption an Aktivkohle **Collection of Czechoslovak Chemical Communications, 35,** 1464-1472.

Boynton W.V. (1985)
Chapter 3. Cosmochemistry of the rare earth elements: Meteorite studies, In Rare Earth Element Geochemistry **Elsevier, Amsterdam,** 115-1522 pp.

Brauns C.M. (2004)
Applying new ideas for the distillation of osmium. **Goldschmidt 2004. Pergamon Press (Copenhagen),** A320-A320.

Bulman R.A. (2003)
Metabolism and toxicity of the lanthanides **Metal Ions in Biological Systems, 40,** 683.

Campbell M.L. (1999)
Temperature dependent rate constants for the reactions of gas phase lanthanides with N2O **Journal of Chemical Physics, 111,** 562-566.

CANMET (2012)
certificate of analysis:PTC-1a
https://www.nrcan.gc.ca/sites/www.nrcan.gc.ca/.../PTC-1a-eng.pdf.

Cao S., Wang Y., Qin Z., Fan F., Haba H., Komori Y., Wu X., Tan C. and Zhang X. (2016)
Gas-phase chemistry of ruthenium and rhodium carbonyl complexes **Physical Chemistry Chemical Physics, 18,** 119-125.

Cao X., Yin M. and Wang X. (2001)
Elimination of the spectral interference from polyatomic ions with rare earth elements in inductively coupled plasma mass spectrometry by combining algebraic correction with chromatographic separation **Spectrochimica Acta Part B: Atomic Spectroscopy, 56,** 431-441.

Capobianco C.J., Hervig R.L. and Drake M.J. (1994)
Experiments on crystal/liquid partitioning of Ru, Rh and Pd for magnetite and hematite solid solutions crystallized from silicate melt **Chemical Geology, 113,** 23-43.

Carron V. (2000)
ÉTUDE DU MÉCANISME D'OXYDATION DES FORMES DISSOUTES DU RUTHÉNIUM DANS LES SOLUTIONS D'ACIDE NITRIQUE- APPLICATION À L'ÉLIMINATION DU RUTHÉNIUM DES SOLUTIONS DE DISSOLUTION DES COMBUSTIBLES NUCLÉAIRES IRRADIÉS. **Université de Grenoble (Grenoble)**.

Cerutti S., Silva M.F., Gásquez J.A., Olsina R.A. and Martínez L.D. (2005)

Cloud point preconcentration prior to capillary zone electrophoresis: simultaneous determination of platinum and palladium at trace levels **Electrophoresis, 26,** 3500-3506.

Chao T.T. and Sanzolone R.F. (1992)
Decomposition techniques **Journal of Geochemical Exploration, 44,** 65-106.

Cheatham M.M., Sangrey W.F. and White W.M. (1993)
Sources of error in external calibration ICP-MS analysis of geological samples and an improved non-linear drift correction procedure **Spectrochimica Acta Part B: Atomic Spectroscopy, 48,** 487-506.

Cheng P., Koyanagi G.K. and Bohme D.K. (2006)
Gas-phase reactions of atomic lanthanide cations with D2O: room-temperature kinetics and periodicity in reactivity **ChemPhysChem, 7,** 1813-1819.

Chiariza R., Horwitz E., Alexandrators S. and Gula M. (1997)
Diphonix® resin: a review of its properties and applications **Separation Science and Technology, 32,** 1-35.

Chiarizia R., Ferraro J., Horwitz E. and D'Arcy K. (1995)
Uptake of metal ions by a new chelating ion-exchange resin. VII. Alkaline earth cations **Solvent Extraction and Ion Exchange, 13,** 1063-1082.

Chiarizia R., Horwitz E., Gatrone R., Alexandratos S., Trochimczuk A. and Crick D. (1993)
Uptake of metal ions by a new chelating ion-exchange resin. Part 2: Acid dependencies of transition and post-transition metal ions **Solvent Extraction and Ion Exchange, 11,** 967-985.

Claiborne L.L., Miller C.F., Walker B.A., Wooden J.L., Mazdab F.K. and Bea F. (2006)
Tracking magmatic processes through Zr/Hf ratios in rocks and Hf and Ti zoning in zircons: An example from the Spirit Mountain batholith, Nevada **Mineralogical Magazine, 70,** 517-543.

Coplen T.B. B.J.K., De Bievre P., Ding T.,, Holden N.E. H.J.A., Krouse H.R., Lamberty A.,, Peiser H.S. R.K., Rieder S.E., Rosman K.J.R.,, Roth E. T.P.D.P., Vocke R.D. and and (2002) X.Y.K. (2003)
Isotope-abundance variations of selected elements (IUPAC Technical Report). **Chemistry International - Newsmagazine for IUPAC,** 22.

Corbett J.A., Godbeer W.C. and Watson N.C. (1974)
The application of sodium peroxide sintering techniques to the analysis of minerals and rocks by atomic absorption spectroscopy **Australas. Inst. Mining Met. Proc.,** 51-54.

Cornehl H.H., Wesendrup R., Diefenbach M. and Schwarz H. (1997)
A comparative study of oxo-ligand effects in the gas-phase chemistry of atomic lanthanide and actinide cations **Chemistry-A European Journal, 3,** 1083-1090.

Cotta A.J.B. and Enzweiler J. (2012)
Classical and new procedures of whole rock dissolution for trace element determination by ICP-MS **Geostandards and Geoanalytical Research, 36,** 27-50.

Cotta A.J.B., Enzweiler J., Wilson S.A., Pérez C.A., Nardy A.J.R. and Larizzatti J.H. (2007)
Homogeneity of the geochemical reference material BRP-1 (Paraná Basin Basalt) and assessment of minimum mass **Geostandards and Geoanalytical Research, 31,** 379-393.

Cotton F.A., Wilkinson G., Murillo G., Bochmann M. and Rabinovich D. (2000)
Advanced Inorganic Chemistry **Journal of Chemical Education, 77,** 311.

Creaser R., Papanastassiou D. and Wasserburg G. (1991)
Negative thermal ion mass spectrometry of osmium, rhenium and iridium **Geochimica et Cosmochimica Acta, 55,** 397-401.

Cremer M. and Schlocker J. (1976)
Lithium borate decomposition of rocks, minerals, and ores **American Mineralogist, 61,** 318-321.

Crock J., Arbogast B. and Lamothe P. (1999)
Laboratory methods for the analysis of environmental samples **Reviews in Economic Geology, 6,** 264-287.

Crock J.G., Lichte F.E. and Wildeman T.R. (1984)
The group separation of the rare-earth elements and yttrium from geologic materials by cation-exchange chromatography **Chemical Geology, 45,** 149-163.

Crocket J., Keays R. and Hsieh S. (1968)
Determination of some precious metals by neutron activation analysis **Journal of Radioanalytical and Nuclear Chemistry, 1,** 487-507.

da Silva M.A.M., Frescura V.L.A., Aguilera F.J.N. and Curtius A.J. (1998)
Determination of Ag and Au in geological samples by flame atomic absorption spectrometry after cloud point extraction **Journal of Analytical Atomic Spectrometry, 13,** 1369-1373.

da Silva M.A.M., Frescura V.L.A. and Curtius A.J. (2001)
Determination of noble metals in biological samples by electrothermal vaporization inductively coupled plasma mass spectrometry, following cloud point extraction **Spectrochimica Acta Part B: Atomic Spectroscopy, 56,** 1941-1949.

Dai X., Koeberl C. and Fröschl H. (2001)
Determination of platinum group elements in impact breccias using neutron activation analysis and ultrasonic nebulization inductively coupled plasma mass spectrometry after anion exchange preconcentration **Analytica Chimica Acta, 436,** 79-85.

Dale C.W., Macpherson C.G., Pearson D.G., Hammond S.J. and Arculus R.J. (2012)
Inter-element fractionation of highly siderophile elements in the Tonga Arc due to flux melting of a depleted source **Geochimica et Cosmochimica Acta, 89,** 202-225.

Date A.R., Cheung Y.Y. and Stuart M.E. (1987)
The influence of polyatomic ion interferences in analysis by inductively coupled plasma source mass spectrometry (ICP-MS) **Spectrochimica Acta Part B: Atomic Spectroscopy, 42,** 3-20.

Date A.R. and Gray A.L. (1983)
Progress in plasma source mass spectrometry **Spectrochimica Acta Part B: Atomic Spectroscopy, 38,** 29-37.

Dauphas N., Marty B. and Reisberg L. (2002)
Molybdenum nucleosynthetic dichotomy revealed in primitive meteorites **The Astrophysical Journal Letters, 569,** L139.

Day J., Waters C.L., Schaefer B.F., Walker R.J. and Turner S. (2015)
Use of hydrofluoric acid desilicification in the determination of highly siderophile element abundances and Re-Pt-Os isotope systematics in mafic-ultramaficrocks **Geostandards and Geoanalytical Research, 03,** 49-64.

de Madinabeitia S.G., Lorda M.S. and Ibarguchi J.G. (2008)
Simultaneous determination of major to ultratrace elements in geological samples by fusion-dissolution and inductively coupled plasma mass spectrometry techniques **Analytica Chimica Acta, 625,** 117-130.

Dickin A.P., McNutt R.H. and McAndrew J.I. (1988)
Osmium isotope analysis by inductively coupled plasma mass spectrometry **Journal of Analytical Atomic Spectrometry, 3,** 337-342.

Dinnin J.I. (1959)
Rapid analysis of chromite and chrome ore. **Bulletin(Washington),** 31-68.

Djingova R. and Ivanova J. (2002)
Determination of rare earth elements in soils and sediments by inductively coupled plasma atomic emission spectrometry after cation-exchange separation **Talanta, 57,** 821-829.

Doleal J. and Povondra P. (1963)
Decomposition techniques in inorganic analysis. **Iliffe Books Ltd, London** 224 pp.

Douglas D. and French J. (1988)
Gas dynamics of the inductively coupled plasma mass spectrometry interface **Journal of Analytical Atomic Spectrometry, 3,** 743-747.

Douglas D.J. (1987)
Method and apparatus having RF biasing for sampling a plasma into a vacuum chamber. **4,682,026 Google Patents**.

Dulski P. (2001)
Reference materials for geochemical studies: new analytical data by ICP-MS and critical discussion of reference values **Geostandards Newsletter, 25,** 87-125.

Dybczyński R.S., Czerska E., Danko B., Kulisa K. and Samczyński Z. (2010)
Comparison of performance of INAA, RNAA and ion chromatography for the determination of individual lanthanides **Applied Radiation and Isotopes, 68,** 23-27.

Easton A. (1972)
Chemical analysis of silicate rocks. **Elsevier (London, UK, Amsterdam),** 264 pp.

Ebdon L., Ford M.J., Hutton R.C. and Hill S.J. (1994)
Evaluation of ethene addition to the nebulizer gas in inductively coupled plasma-mass spectrometry for the removal of matrix-, solvent-, and support-gas-derived polyatomic ion interferences **Applied Spectroscopy, 48,** 507-516.

Eggins S., Woodhead J., Kinsley L., Mortimer G., Sylvester P., McCulloch M., Hergt J. and Handler M. (1997)
A simple method for the precise determination of more than 40 trace elements in geological samples by ICP-MS using enriched isotope internal standardisation **Chemical Geology, 134,** 311-326.

Eiden G.C., Barinaga C.J. and Koppenaal D.W. (1996)
Communication. Selective removal of plasma matrix ions in plasma source mass spectrometry **J. Anal. At. Spectrom., 11,** 317-322.

Ellison S. and Williams A. (2013)
Eurachem/CITAC guide: quantifying uncertainty in analytical measurement, (2012), ISBN: 978-0-948926-30-3.

Elson C. and Chatt A. (1983)
Determination of gold in silicate rocks and ores by coprecipitation with tellurium and neutron activation—γ-spectrometry **Analytica Chimica Acta, 155,** 305-310.

Emeléus H.J. and Sharpe A.G. (1983)
Advances in inorganic chemistry and radiochemistry. **Academic Press (London)**.

Emsley J. (2011)
Nature's building blocks: an AZ guide to the elements. **Oxford University Press (London),** 720 pp.

Enzweiler J. and Potts P.J. (1995)
The separation of platinum, palladium and gold from silicate rocks by the anion exchange separation of chloro complexes after a sodium peroxide fusion: an investigation of low recoveries **Talanta, 42,** 1411-1418.

Enzweiler J., Potts P.J. and Jarvis K.E. (1995)
Determination of platinum, palladium, ruthenium and iridium in geological samples by isotope dilution inductively coupled plasma mass spectrometry using a sodium peroxide fusion and tellurium coprecipitation **Analyst, 120,** 1391-1396.

Evan C.H. (1997)
Episodes from the History of the Rare Earth Elements. **Springer (London),** 268 pp.

Evans E.H. and Giglio J.J. (1993)
Interferences in inductively coupled plasma mass spectrometry. A review **Journal of Analytical Atomic Spectrometry, 8,** 1-18.

Evensen N., Hamilton P.J. and O'nions R. (1978)
Rare-earth abundances in chondritic meteorites **Geochimica et Cosmochimica Acta, 42,** 1199-1212.

Falkner K.K. and Edmond J.M. (1990)

Determination of gold at femtomolar levels in natural waters by flow-injection inductively coupled plasma quadrupole mass spectrometry **Analytical Chemistry, 62,** 1477-1481.

Fan J. and Kerrich R. (1997a)
Geochemical characteristics of aluminium depleted and undepleted komatiites and HREE-enriched low-Ti tholeiites, western Abitibi greenstone belt: A heterogeneous mantle plume-convergent margin environment **Geochimica et Cosmochimica Acta,** 4723-4744.

Fan J. and Kerrich R. (1997b)
Geochemical characteristics of aluminum depleted and undepleted komatiites and HREE-enriched low-Ti tholeiites, western Abitibi greenstone belt: A heterogeneous mantle plume-convergent margin environment **Geochimica et Cosmochimica Acta, 61,** 4723-4744.

Fathi S. and Yaftian M. (2009)
Cloud point extraction and flame atomic absorption spectrometry determination of trace amounts of copper (II) ions in water samples **Journal of Colloid and Interface Science, 334,** 167-170.

Favre G. (2008)
Etude des réactions" ions-molécules" en phase gazeuse dans les dispositifs de collision réaction: Application à la résolution directe des interférences spectroscopiques en ICP-MS. **Université d'Evry-Val d'Essonne ('Essonne)**.

Fehn U., Teng R., Elmore D. and Kubik P. (1986)
Isotopic composition of osmium in terrestrial samples determined by accelerator mass spectrometry **Nature, 323,** 707-710.

Feldman C. (1983)
Behavior of traces of refractory minerals in the lithium metaborate fusion-acid dissolution procedure **Analytical Chemistry, 55,** 2451-2453.

Fernandes S., Cavaco S., Quina M. and Ferreira L. (2007)
Selective separation of chromium (III) from electroplating effluents by ion-exchange processes. **Proceedings of European Congress of Chemical Engineering(Copenhagen)**.

Finch R.J. and Hanchar J.M. (2003)
Structure and chemistry of zircon and zircon-group minerals **Reviews in Mineralogy and Geochemistry, 53,** 1-25.

Fischer-Gödde M., Burkhardt C., Kruijer T.S. and Kleine T. (2015)
Ru isotope heterogeneity in the solar protoplanetary disk **Geochimica et Cosmochimica Acta, 168,** 151-171.

Flanagan F.J. (1986)
Rock reference samples, San Marcos Gabbro, GSM-1 and Lakeview Mountain Tonalite, TLM-1 **Geostandards Newsletter, 10,** 111-120.

Fleet M.E. and Wu T.-W. (1993)
Volatile transport of platinum-group elements in sulfide-chloride assemblages at 1000 C **Geochimica et Cosmochimica Acta, 57,** 3519-3531.

Fritsche J. and Meisel T. (2004)
Determination of anthropogenic input of Ru, Rh, Pd, Re, Os, Ir and Pt in soils along Austrian motorways by isotope dilution ICP-MS **Science of the Total Environment, 325,** 145-154.

Funari V., Bokhari S., Vigliotti L., Meisel T. and Braga R. (2016)
The rare earth elements in municipal solid waste incinerators ash and promising tools for their prospecting **Journal of Hazardous Materials, 301,** 471-479.

Funari V., Braga R., Bokhari S., Dinelli E. and Meisel T. (2015)
Solid residues from Italian municipal solid waste incinerators: A source for "critical" raw materials **Waste Management, 45,** 206-216.

Gambogi J. (2015)
Rare earths in mineral commodity summaries 2015 **U.S. Department of the Interior U.S. Geological Survey,** 199.

Gao S., Ling W., Qiu Y., Lian Z., Hartmann G. and Simon K. (1999)
Contrasting geochemical and Sm-Nd isotopic compositions of Archean metasediments from the Kongling high-grade terrain of the Yangtze craton: Evidence for cratonic evolution and redistribution of REE during crustal anatexis **Geochimica et Cosmochimica Acta, 63,** 2071-2088.

Geelhoed B. and Glass H.-J. (2001)
A new model for sampling of particulate materials and determination of the minimum sample size **Geostandards Newsletter, 25,** 325-332.

Ghaedi M., Shokrollahi A., Niknam K., Niknam E., Najibi A. and Soylak M. (2009)
Cloud point extraction and flame atomic absorption spectrometric determination of cadmium (II), lead (II), palladium (II) and silver (I) in environmental samples **Journal of Hazardous Materials, 168,** 1022-1027.

Gibson J.K. (2003)
Role of atomic electronics in f-element bond formation: bond energies of lanthanide and actinide oxide molecules **The Journal of Physical Chemistry A, 107,** 7891-7899.

Glenn w. (2013a)
Lead isotope analysis: Removal of 204Hg isobaric interference on 204Pb using ICP-QQQ MS/MS reaction cell **Agilent notes,** p63.

Glenn W. (2013b)
Measurement of selenium in clinical samples in the presence of gadolinium-based magnetic resonance imaging contrasting agents **Agilent Notes,** p81.

Glenn W. (2013c)
Measurement of titanium in clinical samples: Possible application to monitoring patients with joint replacements **Agilent Notes,** p77.

Gomez M., Gomez M. and Palacios M. (2000)
Control of interferences in the determination of Pt, Pd and Rh in airborne particulate matter by inductively coupled plasma mass spectrometry **Analytica Chimica Acta, 404,** 285-294.

Gorelsky S.I., Lavrov V.V., Koyanagi G.K., Hopkinson A.C. and Bohme D.K. (2001)

Effect of spin-surface crossing on the kinetics of sequential ligation of Ru+ with ammonia in the gas phase at room temperature **The Journal of Physical Chemistry A, 105,** 9410-9414.

Gorsuch T. (1970)
The destruction of organic matter: International series of monographs in analytical chemistry. **Pregamon Press (London),** 456 pp.

Gray A.L. (1986)
Mass spectrometry with an inductively coupled plasma as an ion source: the influence on ultratrace analysis of background and matrix response **Spectrochimica Acta Part B: Atomic Spectroscopy, 41,** 151-167.

Greenwood N.N. and Earnshaw A. (1997)
Iron, Ruthenium and Osmium. **In: Earnshaw A. (ed), Chemistry of the Elements. Butterworth-Heinemann (Oxford),** 1070-1112.

Gross M.L. and Caprioli R.M. (2003)
The Encyclopedia of Mass Spectrometry: Hyphenated methods. **Elsevier Science Limited (London),** 1068 pp.

GSC (2004)
Certificate of analysis:WMG-1
https://www.nrcan.gc.ca/sites/www.nrcan.gc.ca/.../wmg-1a-eng.pdf.

Gschneidner K.A., Eyring L. and Lander G.H. (2002)
Handbook on the physics and chemistry of rare earths. **Elsevier (London),** 456 - 470 pp.

Guo W., Hu S., Wang X., Zhang J., Jin L., Zhu Z. and Zhang H. (2011)
Application of ion molecule reaction to eliminate WO interference on mercury determination in soil and sediment samples by ICP-MS **Journal of Analytical Atomic Spectrometry, 26,** 1198-1203.

Gupta J.S. (1981)
Determination of yttrium and rare-earth elements in rocks by graphite-furnace atomic-absorption spectrometry **Talanta, 28,** 31-36.

Hall G. and Pelchat J. (1994)
Analysis of geological materials for Au, Pt and Pd at Low ppb Levels by fire Assay-ICP mass spectrometry **Chemical Geology, 115,** 61-72.

Hall G.E.M. and Plant J.A. (1992)
Analytical errors in the determination of high field strength elements and their implications in tectonic interpretation studies **Chem. Geol., 95,** 141-156.

Haskin L., Haskin M., Frey F. and Wildeman T. (1968)
Relative and absolute terrestrial abundances of the rare earths **Origin and Distribution of the Elements, 1,** 889-911.

Hassler D.R., Peucker-Ehrenbrink B. and Ravizza G.E. (2000)
Rapid determination of Os isotopic composition by sparging OsO 4 into a magnetic-sector ICP-MS **Chemical Geology, 166,** 1-14.

Hattendorf B. (2002)
Ion molecule reactions for the suppression of spectral interferences in elemental analysis by inductively coupled plasma mass spectrometry. **Diss., Naturwissenschaften ETH Zürich, Nr. 14926, 2003 (Zurich),** 163.

Heinrichs H. and Herrmann A.G. (2011)
Praktikum Der Analytischen Geochemie. **Springer London, Limited,** 68 pp.

Held A., Van Nevel L., Poulsen E. and Taylor P. (1999)
IMEP-11 Metals in car exhaust catalyst **Report to Participants, Geel**.

Henderson P. (2013)
Rare earth element geochemistry. **Elsevier (New York),** 501 pp.

Herr W., Hoffmeister W., Hirt B., Geiss J. and Houtermans F. (1961)
Versuch zur datierung von eisenmeteoriten nach der rhenium-osmium-methode **Zeitschrift für Naturforschung A, 16,** 1053-1058.

Hirt B., Herr W. and Hoffmeister W. (1963)
Age determinations by the rhenium-osmium method **Radioactive Dating,** 35-43.

Hoffman J.I. and Lundell G. (1939)
Volatilization of metallic compounds from solutions in perchloric or sulfuric acid **J. Research Natl. Bur. Standards, 22,** 465.

Hopp T., Fischer-Godde M. and Kleine T. (2016)
Ruthenium stable isotope measurements by double spike MC-ICPMS **Journal of Analytical Atomic Spectrometry, 31,** 1515-1526.

Horwitz E.P., Diamond H., Gatrone R., Nash K.L. and Rickert P. (1990)
TUCS: A new class of aqueous complexing agents for use in solvent extraction processes. **Argonne National Lab. (IL (USA))**.

Hoskin P.W. and Schaltegger U. (2003)
The composition of zircon and igneous and metamorphic petrogenesis **Reviews in Mineralogy and Geochemistry, 53,** 27-62.

Houk R. and Praphairaksit N. (2001)
Dissociation of polyatomic ions in the inductively coupled plasma **Spectrochimica Acta Part B: Atomic Spectroscopy, 56,** 1069-1096.

Houk R.S., Fassel V.A., Flesch G.D., Svec H.J., Gray A.L. and Taylor C.E. (1980)
Inductively coupled argon plasma as an ion source for mass spectrometric determination of trace elements **Analytical Chemistry, 52,** 2283-2289.

Hu Z., Gao S., Liu Y., Hu S., Zhao L., Li Y. and Wang Q. (2010)
NH4F assisted high pressure digestion of geological samples for multi-element analysis by ICP-MS **Journal of Analytical Atomic Spectrometry, 25,** 408-413.

Huang C.-H. (2011)

Rare earth coordination chemistry: Fundamentals and applications. **John Wiley & Sons (London),** 566 pp.

Inagaki K. and Haraguchi H. (2000)
Determination of rare earth elements in human blood serum by inductively coupled plasma mass spectrometry after chelating resin preconcentration **Analyst, 125,** 191-196.

Ingamells C. and Switzer P. (1973)
A proposed sampling constant for use in geochemical analysis **Talanta, 20,** 547-568.

Ingamells C.O. (1973)
Sampling for chemical analysis **Analytical Chemistry, 53,** 924a-938a.

Ingamells C.O. and Pitard F.F. (1986)
Applied geochemical analysis **John Wiley & Sons,** 733p.

Ishikawa A., Senda R., Suzuki K., Dale C.W. and Meisel T. (2014)
Re-evaluating digestion methods for highly siderophile element and 187 Os isotope analysis: Evidence from geological reference materials **Chemical Geology, 384,** 27-46.

Ishikawa T., Sugimoto K. and Nagaishi K. (2003)
Determination of rare-earth elements in rock samples by an improved high-performance ion chromatography **Geochemical Journal, 37,** 671-680.

Isnard H., Aubert M., Blanchet P., Brennetot R., Chartier F., Geertsen V. and Manuguerra F. (2006)
Determination of 90 Sr/238 U ratio by double isotope dilution inductively coupled plasma mass spectrometer with multiple collection in spent nuclear fuel samples with in situ 90 Sr/90 Zr separation in a collision-reaction cell **Spectrochimica Acta Part B: Atomic Spectroscopy, 61,** 150-156.

Jarvis I., M. Totland M. and Jarvis K.E. (1997a)
Assessment of Dowex 1-x 8-based anion-exchange procedures for the separation and determination of ruthenium, rhodium, palladium, iridium, platinum and gold in geological samples by inductively coupled plasma mass spectrometry **Analyst, 122,** 19-26.

Jarvis I., Totland M.M. and Jarvis K.E. (1997b)
Determination of the platinum-group elements in geological materials by ICP-MS using microwave digestion, alkali fusion and cation-exchange chromatography **Chemical Geology, 143,** 27-42.

Jarvis K.E. (1989)
Determination of rare earth elements in geological samples by inductively coupled plasma mass spectrometry **Journal of Analytical Atomic Spectrometry, 4,** 563-570.

Jarvis K.E., Gray A.L. and Houk R.S. (1991)
Handbook of inductively coupled plasma mass spectrometry. **Blackie; Chapman and Hall (New York),** 380 pp.

Jeffery P.G. (1975)
Chemical methods of rock analysis. **Pergamon Press Ltd. (London),** 30p pp.

Jin X. and Zhu H. (2000)
Determination of platinum group elements and gold in geological samples with ICP-MS using sodium peroxide fusion and tellurium co-precipitation **Journal of Analytical Atomic Spectrometry, 15,** 747-751.

Johnson W.M. and Maxwell J.A. (1981)
Rock and mineral analysis. **John Wiley & Sons (London),** 489 pp.

Jones D.M.R. (2007)
A study of ion-moleucle reactions in a dynamic reaction cell to improve elemental analysis with inductively coupled plasma-mass spectrometry. **The Ohio State University (Ohio United states),** 583.

Juane S., Xiang-Cheng Z., Dong Y. and Wu W.-m. (2015)
Routine determination of trace rare earth elements in high purity Nd2O3 using the Agilent 8800 ICP-QQQ **Agilent Notes,** 1-5.

Junichi T. (2013)
Direct determination of V, Cr, Ge and As in highpurity 20% hydrochloric acid **Agilent Notes,** p12.

Juvonen R., Kallio E. and Lakomaa T. (1994)
Determination of precious metals in rocks by inductively coupled plasma mass spectrometry using nickel sulfide concentration. Comparison with other pre-treatment methods **Analyst, 119,** 617-621.

Juvonen R., Lakomaa T. and Soikkeli L. (2002)
Determination of gold and the platinum group elements in geological samples by ICP-MS after nickel sulphide fire assay: difficulties encountered with different types of geological samples **Talanta, 58,** 595-603.

Kalavrouziotis I. and Koukoulakis P. (2009)
The environmental impact of the platinum group elements (Pt, Pd, Rh) emitted by the automobile catalyst converters **Water, Air, and Soil Pollution, 196,** 393-402.

Kane J.S. (1997a)
Homogeneity of reference materials **Analyst, 122,** 1289-1292.

Kane J.S. (2002)
Fitness-for-purpose of reference material reference values in relation to traceability of measurement, as illustrated by USGS BCR-1, NIST SRM 610 and IAEA NBS28 **Geostandards Newsletter, 26,** 7-29.

Kane J.S. (2005)
Report of the International Association of Geoanalysts on the Certification of Penrhyn Slate, OU-6 **Geostandards and Geoanalytical Research, 29,** 237-239.

Kane J.S. and Potts P.J. (2007)
ISO Best practices in reference material certification and use in geoanalysis **Geostandards and Geoanalytical Research, 31,** 361-378.

Kane J.S., Potts P.J., Meisel T. and Wiedenbeck M. (2007)

International Association of Geoanalysts' protocol for the certification of geological and environmental reference materials: A supplement **Geostandards and Geoanalytical Research, 31,** 285-288.

Kane J.S., Potts P.J., Wiedenbeck M., Carignan J. and Wilson S. (2003)
International association of geoanalysts'protocol for the certification of geological and environmental reference materials **Geostandards Newsletter, 27,** 227-244.

Kane J.S. and Xu Z. (1993)
Implications of sampling statistics in using slurry introduction fro atomic absorption spectrometric analysis of geochemical reference samples **Geological Survey of Canada Bulletin, 451,** 95-104.

Kawabata K., Kishi Y., Kawaguchi O., Watanabe Y. and Inoue Y. (1991)
Determination of rare-earth elements by inductively coupled plasma mass spectrometry with ion chromatography **Analytical Chemistry, 63,** 2137-2140.

Kempenaers L., Vincze L. and Janssens K. (2000)
The use of synchrotron micro-XRF for characterization of the micro-heterogeneity of heavy metals in low-Z reference materials **Spectrochimica Acta Part B: Atomic Spectroscopy, 55,** 651-669.

Kim G., Burnett W.C. and Horwitz E.P. (2000)
Efficient preconcentration and separation of actinide elements from large soil and sediment samples **Analytical Chemistry, 72,** 4882-4887.

Koppenaal D.W., Eiden G.C. and Barinaga C.J. (2004)
Collision and reaction cells in atomic mass spectrometry: development, status, and applications **Journal of Analytical Atomic Spectrometry, 19,** 561-570.

Korkisch J. (1989)
Handbook of ion exchange resins, Vol. V. **CRC Press Inc (Boca Raton, Florida),** 56.

Korotev R.L. (1996)
A self-consistent compilation of elemental concentration data for 93 geochemical reference samples **Geostandards Newsletter, 20,** 217-245.

Koyanagi G.K., Baranov V.I., Tanner S.D. and Bohme D.K. (2000)
An inductively coupled plasma/selected-ion flow tube mass spectrometric study of the chemical resolution of isobaric interferences Presented at the 2000 Winter Conference on Plasma Spectrochemistry, Fort Lauderdale, FL, USA, January 10–15, 2000 **Journal of Analytical Atomic Spectrometry, 15,** 1207-1210.

Koyanagi G.K. and Bohme D.K. (2001)
Oxidation reactions of lanthanide cations with N2O and O2: Periodicities in reactivity **The Journal of Physical Chemistry A, 105,** 8964-8968.

Koyanagi G.K., Cheng P. and Bohme D.K. (2009)
Gas-phase reactions of atomic lanthanide cations with ammonia: room-temperature kinetics and periodicity in reactivity **The Journal of Physical Chemistry A, 114,** 241-246.

Kumar M. (1994)

Recent trends in chromatographic procedures for separation and determination of rare earth elements. A review **Analyst, 119,** 2013-2024.

Lam J. and Horlick G. (1990)
A comparison of argon and mixed gas plasmas for inductively coupled plasma-mass spectrometry **Spectrochimica Acta Part B: Atomic Spectroscopy, 45,** 1313-1325.

Lang P.F. and Smith B.C. (2010)
Ionization energies of lanthanides **Journal of Chemical Education, 87,** 875-881.

Lapakko K. (2002)
Metal mine rock and waste characterizationtools an overview **IIED WBCSD Great Britan,** 14p.

Laul J. (1979)
Neutron activation analysis of geological materials **Atomic Energy Review 17,** 603-695.

Lavrov V. (2006)
Gas-phase Chemistry of ICP Atomic Ions with Selected Molecules. **York University (Canada)**.

Le Fèvre B. and Pin C. (2002)
Determination of Zr, Hf, Th and U by Isotope Dilution and Inductively Coupled Plasma-Quadrupole Mass Spectrometry After Concomitant Separation Using Extraction Chromatography **Geostandards Newsletter, 26,** 161-170.

Letcher T.M. and Scott J.L. (2012)
Rare earths, in materials for a sustainable future **The Royal Society of Chemistry,** 60-89.

Li B., Zhang Y. and Yin M. (1997)
Determination of trace amounts of rare earth elements in high-purity cerium oxide by inductively coupled plasma mass spectrometry after separation by solvent extraction **Analyst, 122,** 543-547.

Li J.-L. and Chen B.-H. (2002)
Solubilization of model polycyclic aromatic hydrocarbons by nonionic surfactants **Chemical Engineering Science, 57,** 2825-2835.

Li X. and Ebihara M. (2003)
Determination of all platinum-group elements in mantle derived xenoliths by neutron activation analysis with NiS fire-assay preconcentration **Journal of Radioanalytical and Nuclear Chemistry, 255,** 131-135.

Lias S.G. (1988)
Gas-phase ion and neutral thermochemistry. **American Chemical Society and the American Institute of Physics for the National Bureau of Standards (United states),** 861 pp.

Lichte F.E., Meier A.L. and Crock J.G. (1987)
Determination of the rare-earth elements in geological materials by inductively coupled plasma mass spectrometry **Analytical Chemistry, 59,** 1150-1157.

Lichte F.E., Wilson S.M., Brooks R.R., Reeves R.D., Holzbecher J. and Ryan D.E. (1986)
New method for the measurement of osmium isotopes applied to a New Zealand Cretaceous/Tertiary boundary shale **Nature, 322,** 816-717.

Linge K.L. and Jarvis K.E. (2009)
Quadrupole ICP-MS: Introduction to instrumentation, measurement techniques and analytical capabilities **Geostandards and Geoanalytical Research, 33,** 445-467.

Lipin B.R., McKay G.A. and Boynton W.V. (1989)
Geochemistry and mineralogy of rare earth elements. **Mineralogical Society of America Washington,** 348 pp.

Locht R., Leyh B., Denzer W., Hagenow G. and Baumgärtel H. (1991)
The photoionization of ammonia revisited. The vibrational autoionization of NH 3 and its three isotopomers in the 10–12 eV photon energy range **Chemical Physics, 155,** 407-422.

Long K.R., Van Gosen B.S., Foley N.K. and Cordier D. (2012)
The principal rare earth elements deposits of the United States: a summary of domestic deposits and a global perspective. **Springer (New York),** 131-155 pp.

Longerich H.P., Jenner G.A., Fryer B.J. and Jackson S.E. (1990)
Inductively coupled plasma-mass spectrometric analysis of geological samples: A critical evaluation based on case studies **Chemical Geology, 83,** 105-118.

Luck J.-M. (1982)
Géochimie du rhénium-osmium: Méthode et applications. **Université de Paris VII (Paris)**.

Ly C.V. and Hidaka H. (2004)
Determination of ruthenium contents in terrestrial minerals by isotope dilution mass spectrometry after preconcentration via distillation **Geochemical Journal, 38,** 485-490.

Maden M. (2010)
Spectrofluorimetric determination of organic and inorganic selenium in vitamin supplements after cloud point extraction. **Turkey. Middle East Technical University**.

Madsen F.A., Rose M.C. and Cee R. (1995)
Review of quartz analytical methodologies: present and future needs [**Applied Occupational and Environmental Hygiene, 10,** 991-1002.

Makishima A., Kobayashi K. and Nakamura E. (2002)
Determination of chromium, nickel, copper and zinc in milligram samples of geological materials using isotope dilution high resolution inductively coupled plasma-mass spectrometry **Geostandards Newsletter, 26,** 41-51.

Makishima A. and Nakamura E. (2001)
Determination of total sulfur at microgram per gram levels in geological materials by oxidation of sulfur into sulfate with in situ generation of bromine using isotope dilution high-resolution ICPMS **Analytical Chemistry, 73,** 2547-2553.

Manzoori J.L., Abdolmohammad-Zadeh H. and Amjadi M. (2007)

Simplified cloud point extraction for the preconcentration of ultra-trace amounts of gold prior to determination by electrothermal atomic absorption spectrometry **Microchimica Acta, 159,** 71-78.

Markey R., Stein H. and Morgan J.W. (1998)
Highly precise Re-Os dating for molybdenite using alkaline fusion and NTIMS **Talanta, 45,** 935-946.

Martin C.E. (1990)
Rhenium-osmium isotope geochemistry of the mantle. **Department of Geology. Yale University (United States),** 563.

Martin W.C., Zalubas R. and Hagan L. (1978)
Atomic energy levels-the rare earth elements.(the spectra of lanthanum, cerium, praseodymium, neodymium, promethium, samarium, europium, gadolinium, terbium, dysprosium, holmium, erbium, thulium, ytterbium, and lutetium).[66 atoms and ions]. **Manchester Coll. of Science and Technology (UK). Dept. of Chemistry (Manchester),** 36.

Masuda A., Nakamura N. and Tanaka T. (1973)
Fine structures of mutually normalized rare-earth patterns of chondrites **Geochimica et Cosmochimica Acta, 37,** 239-248.

Mattiuzz M. and Markowicz A. (2000)
A modified approach to homogeniety testing at microscale **Advances in X-ray Analysis,, Vol.42,** 74-82.

McDonough W.F. and Sun S.-S. (1995)
The composition of the Earth **Chemical geology, 120,** 223-253.

Meeravali N.N. and Jiang S.-J. (2008)
Interference free ultra trace determination of Pt, Pd and Au in geological and environmental samples by inductively coupled plasma quadrupole mass spectrometry after a cloud point extraction **Journal of Analytical Atomic Spectrometry, 23,** 854-860.

Meier A. (1980)
Flameless atomic-absorption determination of gold in geological materials **Journal of Geochemical Exploration, 13,** 77-85.

Meisel T., Dale C., Pearson D. and Sergeev D. (2009)
Complete sample digestions for accurate isotope measurements? The Re-Os isotope system under scrutiny **Geochimica et Cosmochimica Acta Supplement, 73,** 867.

Meisel T., Fellner N. and Moser J. (2003)
A simple procedure for the determination of platinum group elements and rhenium (Ru, Rh, Pd, Re, Os, Ir and Pt) using ID-ICP-MS with an inexpensive on-line matrix separation in geological and environmental materials **Journal of Analytical Atomic Spectrometry, 18,** 720-726.

Meisel T. and Horan M.F. (2016)
Analytical methods for the highly siderophile elements. **Reviews in Mineralogy and Geochemistry. Mineralogical Society of America (United States),** 89-106.

Meisel T. and Kane J.S. (2011)
The future demand for geological reference materials **Accreditation and Quality Assurance, 16,** 407-414.

Meisel T. and Moser J. (2004a)
Platinum-group element and rhenium concentrations in low abundance reference materials **Geostandards and Geoanalytical Research, 28,** 233-250.

Meisel T. and Moser J. (2004b)
Reference materials for geochemical PGE analysis: new analytical data for Ru, Rh, Pd, Os, ir, Pt and Re by isotope dilution ICP-MS in 11 geological reference materials **Chemical Geology, 208,** 319-338.

Meisel T., Moser J., Fellner N., Wegscheider W. and Schoenberg R. (2001a)
Simplified method for the determination of Ru, Pd, Re, Os, Ir and Pt in chromitites and other geological materials by isotope dilution ICP-MS and acid digestion **Analyst, 126,** 322-328.

Meisel T., Moser J. and Wegscheider W. (2001b)
Recognizing heterogeneous distribution of platinum group elements (PGE) in geological materials by means of the Re–Os isotope system **Fresenius' Journal of Analytical Chemistry, 370,** 566-572.

Meisel T., Schöner N., Paliulionyte V. and Kahr E. (2002)
Determination of rare earth elements, Y, Th, Zr, Hf, Nb and Ta in geological reference materials G-2, G-3, SCo-1 and WGB-1 by sodium peroxide sintering and inductively coupled plasma-mass spectrometry **Geostandards Newsletter, 26,** 53-61.

Meyer R., Kotwoski A., Becke-Goehring M. and Busch-Beck K. (1970)
Gmelins handbuch der Anorganischen Chemie. Silber, Teil A2, Verlag Chemie. **Weinheim (Leipzig-Berlin),** p124-128.

Miller C.F. and Mittlefehldt D.W. (1982)
Depletion of light rare-earth elements in felsic magmas **Geology, 10,** 129-133.

MINTEK (1975)
certificate of analysis:SARM-7 **www.mintek.co.za/wp-content/uploads/2011/10/SARM-7.pdf**.

Mohammadi S.Z., Afzali D. and Pourtalebi D. (2011)
Flame atomic absorption spectrometric determination of trace amounts of palladium, gold and nickel after cloud point extraction **Journal of Analytical Chemistry, 66,** 620-625.

Moloughney P. and Faye G. (1976)
A rapid fire-assay/atomic-absorption method for the determination of platinum, palladium and gold in ores and concentrates: A modification of the tin-collection scheme **Talanta, 23,** 377-381.

Montaser A., Ohls K. and Golightly D. (1992)
Inductively coupled plasmas in gases other than argon. **Inductively Coupled Plasmas in Analytical Atomic Spectrometry. VCH (New York),** 490.

Moreira E.G., Vasconcellos M.B.A., Catharino M.G.M., Maihara V.A. and Saiki M. (2012)
Applying INAA to the homogeneity study of a Perna perna mussel reference material **Journal of Radioanalytical and Nuclear Chemistry, 291,** 107-111.

Morgan J., Golightly D. and Dorrzapf A. (1991)
Methods for the separation of rhenium, osmium and molybdenum applicable to isotope geochemistry **Talanta, 38,** 259-265.

Moser J., Wegscheider W., Meisel T. and Fellner N. (2003)
An uncertainty budget for trace analysis by isotope-dilution ICP-MS with proper consideration of correlation **Analytical and Bioanalytical Chemistry, 377,** 97-110.

Münker C. (1998)
Nb/Ta fractionation in a Cambrian arc/back arc system, New Zealand: source constraints and application of refined ICPMS techniques **Chemical Geology, 144,** 23-45.

Murad E. and Hildenbrand D. (1980)
Dissociation energies of GdO, HoO, ErO, TmO, and LuO; correlation of results for the lanthanide monoxide series **The Journal of Chemical Physics, 73,** 4005-4011.

Nakagawa T. and Shinoda K. (1963)
Colloidal Surfactants **Isemura Academic, New York**.

Nakamura N. (1974)
Determination of REE, Ba, Fe, Mg, Na and K in carbonaceous and ordinary chondrites **Geochimica et Cosmochimica Acta, 38,** 757-775.

Naoki S. (2013a)
The accurate measurement of selenium in reference materials using online isotope dilution **Agilent Notes,** p22.

Naoki S. (2013b)
Analysis of sulfur, phosphorus, silicon and chlorine in N-methyl-2-pyrrolidone **Agilent Notes,** p16.

Navarro M.S., Andrade S., Ulbrich H., Gomes C.B. and Girardi V.A.V. (2008)
The direct determination of rare earth elements in basaltic and related rocks using icp-ms: testing the efficiency of microwave oven sample decomposition procedures **Geostandards and Geoanalytical Research, 32,** 167-180.

Nelms S. (2005)
ICP mass spectrometry handbook. **Blackwell Publishing (Oxford),** 485 pp.

Niemelä M., Huttunen S.M., Gornostayev S.S. and Perämäki P. (2009)
Determination of Pt from coke samples by ICP-MS after microwave assisted digestion and microwave assisted cloud point extraction **Microchimica Acta, 166,** 255-260.

Nier A.O. (1937)
The Isotopic Constitution of Osmium **Physical Review, 52,** 885-885.

O'Hara K.D. (2001)

A pseudotachylyte geothermometer **Journal of Structural Geology, 23,** 1345-1357.

Olivares J.A. and Houk R. (1985)
Ion sampling for inductively coupled plasma mass spectrometry **Analytical Chemistry, 57,** 2674-2679.

Padrón Sanz C., Sosa Ferrera Z. and Santana Rodríguez J.J. (2002)
Extraction and preconcentration of polychlorinated dibenzo-p-dioxins using the cloud-point methodology: Application to their determination in water samples by high-performance liquid chromatography **Analytica Chimica Acta, 470,** 205-214.

Palacios M.A., Gómez M., Moldovan M. and Gómez B. (2000)
Assessment of environmental contamination risk by Pt, Rh and Pd from automobile catalyst **Microchemical Journal, 67,** 105-113.

Paliulionyte V., Meisel T., Ramminger P. and Kettisch P. (2006)
High pressure asher digestion and an isotope dilution-ICP-MS method for the determination of platinum-group element concentrations in chromitite reference materials CHR-Bkg, GAN Pt-1 and HHH **Geostandards and Geoanalytical Research, 30,** 87-96.

Palme H. (1988)
Chemical abundances in meteorites. **Cosmic Chemistry. Springer (London),** 28-51.

Panteeva S., Gladkochoub D., Donskaya T., Markova V. and Sandimirova G. (2003)
Determination of 24 trace elements in felsic rocks by inductively coupled plasma mass spectrometry after lithium metaborate fusion **Spectrochimica Acta Part B: Atomic Spectroscopy, 58,** 341-350.

Parry S., Asif M. and Sinclair I. (1988)
Radiochemical fire-assay for determination of the platinum group elements **Journal of Radioanalytical and Nuclear Chemistry, 123,** 593-606.

Pauwels J., Lamberty A. and Schimmel H. (1998)
Homogeneity testing of reference materials **Accreditation and Quality Assurance: Journal for Quality, Comparability and Reliability in Chemical Measurement, 3,** 51-55.

Peach C. and Mathez E. (1996)
Constraints on the formation of platinum-group element deposits in igneous rocks **Economic Geology, 91,** 439-450.

Pearson D. and Woodland S. (2000)
Solvent extraction/anion exchange separation and determination of PGEs (Os, Ir, Pt, Pd, Ru) and Re–Os isotopes in geological samples by isotope dilution ICP-MS **Chemical Geology, 165,** 87-107.

Pearson N.J., Alard O., Griffin W.L., Jackson S.E. and O'Reilly S.Y. (2002)
In situ measurement of Re-Os isotopes in mantle sulfides by laser ablation multicollector-inductively coupled plasma mass spectrometry: analytical methods and preliminary results **Geochimica et Cosmochimica Acta, 66,** 1037-1050.

Pedreira W., Sarkis J., Rodrigues C., Tomiyoshi I., da Silva Queiroz C. and Abrao A. (2002)
Determination of trace amounts of rare earth elements in high pure lanthanum oxide by sector field inductively coupled plasma mass spectrometry (HR ICP–MS) and high-performance liquid chromatography (HPLC) techniques **Journal of Alloys and Compounds, 344,** 17-20.

Peräniemi S., Parkkinen J., Smolander K., Mustalahti H. and Ahlgren M. (1992)
Determination of gold in ore samples by EDXRF after thiourea leaching and adsorption on activated charcoal **Fresenius' Journal of Analytical Chemistry, 343,** 292-296.

Peter W.C., Micheal T., Potts P.J. and Wilson S. (2012)
GeoPT31- an international proficiency test for analytical geochemistry laboratories-report on rpound 31 (modified river sediment,SdAR-1) **http://www.geoanalyst.org/**.

Petrie R. and Morgan J. (1982)
Anion-exchange separation of Pt and Pd using perchloric and hydrochloric acid solutions **Journal of Radioanalytical Chemistry, 74,** 15-23.

Petrucci F., Bocca B., Alimonti A. and Caroli S. (2000)
Determination of Pd, Pt and Rh in airborne particulate and road dust by high-resolution ICP-MS: a preliminary investigation of the emission from automotive catalysts in the urban area of RomePresented at the 2000 Winter Conference on Plasma Spectrochemistry, Fort Lauderdale, FL, USA, January 10–15, 2000 **Journal of Analytical Atomic Spectrometry, 15,** 525-528.

Poths H. and Rundberg R. (1990)
Double beta decay of 100 Mo: a geochemical approach. **Seventh international conference on geochronology, cosmochronology and isotope geology**.

Potts P.J. (1987a)
Concepts in analytical chemistry: In Handbook of silicate rock analysis. **Blackie, Glasgow and London (Glasgow and London),** 1-42 pp.

Potts P.J. (1987b)
Inductively coupled plasma-mass spectrometry. In: Handbook of Silicate Rock Analysis. **Blackie (Glasgow and London),** 622 pp.

Potts P.J. (1987c)
Inductively coupled plasma-mass spectrometry. In: Handbook of Silicate Rock Analysis**, Blackie, Glasgow,** 575-586.

Potts P.J. (1992)
A handbook of silicate rock analysis. **Blackie, Glasgow and London,** 610.

Potts P.J. and Jean S.k. (2006)
Certificate of analysis OU-3 **Geostandards and Geoanalytical Research, 29,** 233-236.

Potts P.J. and Kane J.S. (2005)
International association of geoanalysts certificate of analysis: Certified Reference Material OU-6 (Penrhyn Slate) **Geostandards and Geoanalytical Research, 29,** 233-236.

Potts P.J. and Meisel T. (2015)
Certificate of analysis IAG MUH-1 **http://www.iageo.com/index.php/certified-reference-materials/14-products/39-okum-products.html**.

Potts P.J., Meisel T. and Norov T. (2015a)
Certificate of analysis MRH-1 **International Association of Geoanalysits: Unpublished report**.

Potts P.J., Thomas M. and Norov T. (2015b)
Certificate of analysis IAG/CGL 019 MTA-1 Trachyandesite **http://www.geoanalyst.org/**.

Potts P.J., Thompson M., Webb P.C. and Webbe E. (2013)
GeoPT32 - An international proficiency test for analytical geochemistry laboratories — report on round 32 (woodstock basalt, WG-1) **http://www.geoanalyst.org**.

Pourmand A., Dauphas N. and Ireland T.J. (2012)
A novel extraction chromatography and MC-ICP-MS technique for rapid analysis of REE, Sc and Y: Revising CI-chondrite and Post-Archean Australian Shale (PAAS) abundances **Chemical Geology, 291,** 38-54.

Pretorius W., Weis D., Williams G., Hanano D., Kieffer B. and Scoates J. (2006)
Complete trace elemental characterisation of granitoid (USGS G-2, GSP-2) reference materials by high resolution inductively coupled plasma-mass spectrometry **Geostandards and Geoanalytical Research, 30,** 39-54.

Pytlakowska K., Kozik V. and Dabioch M. (2013)
Complex-forming organic ligands in cloud-point extraction of metal ions: a review **Talanta, 110,** 202-228.

Qi L. (2007)
Determination of trace platinum group elements in geological samples: application to Emeishan flood basalts in SWChina. **The univeristy of Hong Kong (Hong Kong),** 237.

Qi L., Gregoire D.C., Zhou M.-F. and Malpas J. (2003)
Determination of Pt, Pd, Ru and Ir in geological samples by ID-ICP-MS using sodium peroxide fusion and Te co-precipitation **Geochemical Journal, 37,** 557-565.

Qi L., Zhou M.-F. and Wang C.Y. (2004)
Determination of low concentrations of platinum group elements in geological samples by ID-ICP-MS **Journal of Analytical Atomic Spectrometry, 19,** 1335-1339.

Raleigh G. (1935)
A method for the separation of ruthenium from platinum, palladium, rhodium, and iridium **U.S. Department of Commerce, Bureau of Standards Part of Bureau of Standards Journal of Research, , 12,** 12-23.

Ramsey M. (1997)
Measurement uncertainty arising from sampling: implications for the objectives of geoanalysis **Analyst, 122,** 1255-1260.

Rauch S., Motelica-Heino M., Morrison G.M. and Donard O.F. (2000)

Critical assessment of platinum group element determination in road and urban river sediments using ultrasonic nebulisation and high resolution ICP-MS **Journal of Analytical Atomic Spectrometry, 15,** 329-334.

Ravizza G. and Pyle D. (1997)
PGE and Os isotopic analyses of single sample aliquots with NiS fire assay preconcentration **Chemical Geology, 141,** 251-268.

Reed N.M., Cairns R.O., Hutton R.C. and Takaku Y. (1994)
Characterization of polyatomic ion interferences in inductively coupled plasma mass spectrometry using a high resolution mass spectrometer **Journal of Analytical Atomic Spectrometry, 9,** 881-896.

Rehkämper M. and Halliday A. (1997)
Development and application of new iondashexchange techniques for the separation of the platinum group and other siderophile elements from geological samples **Talanta, 44,** 663-672.

Reisberg L. and Meisel T. (2002)
The Re-Os isotopic system: A review of analytical techniques **Geostandards Newsletter, 26,** 249-267.

Revel G. and Ayrault S. (2000)
Comparative use of INAA and ICP-MS methods for environmental studies **Journal of Radioanalytical and Nuclear Chemistry, 244,** 73-80.

Révillon S. and Hureau-Mazaudier D. (2009)
Improvements in digestion protocols for trace element and isotope determinations in stream and lake sediment reference materials (JSd-1, JSd-2, JSd-3, JLk-1 and LKSD-1) **Geostandards and Geoanalytical Research, 33,** 397-413.

Richardson T. (2004)
A Semi-quantitative Method for the Rapid Determination of Gold, Platinum, Palladium and Rhodium in Geological Materials Using a Small Sample Mass. **Laurentian University (Ontario Canada),** 117.

Robinson P., Higgins N.C. and Jenner G.A. (1986)
Determination of rare-earth elements, yttrium and scandium in rocks by anion exchange X-ray fluorescence technique **Chemical Geology, 55,** 121-137.

Robinson P., Townsend A.T., Yu Z. and Münker C. (1999)
Determination of scandium, yttrium and rare earth elements in rocks by high resolution inductively coupled plasma-mass spectrometry **Geostandards Newsletter, 23,** 31-46.

Rodgers K. (1972)
The decomposition and analysis of chrome spinel. A survey of some published techniques **Mineralogical Magazine, 38,** 882-840.

Ross J.R. and Keays R.R. (1979)
Precious metals in volcanic-type nickel sulfide deposits in Western Australia. I. Relationship with the composition of the ores and their host rocks **Can. Mineral, 17,** 417-435.

Rossbach M., Ostapczuk P. and Emons H. (1998)
Microhomogeneity of candidate reference materials: Comparison of solid sampling Zeeman-AAS with INAA **Fresenius' Journal of Analytical Chemistry, 360,** 380-383.

Rowan J.T. and Houk R. (1989)
Attenuation of polyatomic ion interferences in inductively coupled plasma mass spectrometry by gas-phase collisions **Applied Spectroscopy, 43,** 976-980.

Russ III G.P., Bazan J.M. and Date A.R. (1987)
Osmium isotopic ratio measurements by inductively coupled plasma source mass spectrometry **Analytical Chemistry, 59,** 984-989.

S. Kane J. (2001)
The use of refrence material:A tutorial **Geostandards and Geoanalytical Research, 25,** 7-22.

Şahin Ç.A., Efeçınar M. and Şatıroğlu N. (2010)
Combination of cloud point extraction and flame atomic absorption spectrometry for preconcentration and determination of nickel and manganese ions in water and food samples **Journal of Hazardous Materials, 176,** 672-677.

Samaddar P. and Sen K. (2014)
Cloud point extraction: A sustainable method of elemental preconcentration and speciation **Journal of Industrial and Engineering Chemistry, 20,** 1209-1219.

Sandell E. and Neumayer J. (1951)
Photometric determination of traces of silver **Analytical Chemistry, 23,** 1863-1865.

Sasahira A. and Kawamura F. (1988)
Formation rate of ruthenium tetroxide during nitric acid distillation **Journal of Nuclear Science and Technology, 25,** 603-606.

Savard D., Barnes S.-J. and Meisel T. (2010)
Comparison between Nickel-Sulfur Fire Assay Te Co-precipitation and Isotope Dilution with High-Pressure Asher Acid Digestion for the Determination of Platinum-Group Elements, Rhenium and Gold **Geostandards and Geoanalytical Research, 34,** 281-291.

Sawka W.N. and Chappell B.W. (1988)
Fractionation of uranium, thorium and rare earth elements in a vertically zoned granodiorite: Implications for heat production distributions in the Sierra Nevada batholith, California, USA **Geochimica et Cosmochimica acta, 52,** 1131-1143.

Schäfer J. and Puchelt H. (1998)
Platinum-Group-Metals (PGM) emitted from automobile catalytic converters and their distribution in roadside soils **Journal of Geochemical Exploration, 64,** 307-314.

Schoenberg R., Nägler T.F. and Kramers J.D. (2000)
Precise Os isotope ratio and Re–Os isotope dilution measurements down to the picogram level using multicollector inductively coupled plasma mass spectrometry **International Journal of Mass Spectrometry, 197,** 85-94.

Seelye F.T. and Rafter T.A. (1950)

Low-temperature decomposition of rocks, ores and minerals by sodium peroxide using platinum vessels **Nature, 166,** 317.

Sen I.S. and Peucker-Ehrenbrink B. (2014)
Determination of osmium concentrations and 187Os/188Os of crude oils and source rocks by coupling high-pressure, high temperature digestion with sparging OsO4 into a multicollector Inductively Coupled Plasma Mass Spectrometer **Analytical Chemistry, 86,** 2982-2988.

Sengupta S., Acharyya S. and De Smeth J. (1996)
Geochemical characteristics of the Abor volcanic rocks, NE Himalaya, India: nature and early Eocene magmatism **Journal of the Geological Society, 153,** 695-704.

Shabani M., Akagi T., Shimizu H. and Masuda A. (1990)
Rapid and accurate determination of sub-parts per trillion lanthanides and yttrium in seawater by development of solvent extraction and back extraction using inductively coupled plasma mass spectrometry **Anal. Chem, 62,** 2709.

Shazali I., Van't Dack L. and Gijbels R. (1988)
Preconcentration of precious metals by tellurium sulphide fire-assay followed by instrumental neutron activation analysis. **In: Prichard H.M., Potts P.J., Bowles J.F.W. and Cribb S.J. (eds), Geo-Platinum 87. Springer Netherlands (Dordrecht),** 29-42.

Shirai N., Nishino T., Li X., Amakawa H. and Ebihara M. (2003)
Precise determination of PGE in a GSJ reference sample JP-1 by ID-ICPMS after nickel sulfide fire assay preconcentration **Geochemical Journal, 37,** 531-536.

Shirdashtzadeh N., Torabi G., Meisel T., Arai S., Bokhari S.N.H., Samadi R. and Gazel E. (2014)
Origin and evolution of metamorphosed mantle peridotites of Darreh Deh (Nain Ophiolite, Central Iran): Implications for the Eastern Neo-Tethys evolution **Neues Jahrbuch für Geologie und Paläontologie-Abhandlungen, 273,** 89-120.

Shirey S.B. and Walker R.J. (1995)
Carius tube digestion for low-blank rhenium-osmium analysis **Analytical Chemistry, 67,** 2136-2141.

Shirey S.B. and Walker R.J. (1998)
The Re-Os isotope system in cosmochemistry and high-temperature geochemistry **Annual Review of Earth and Planetary Sciences, 26,** 423-500.

Shoeib T., Milburn R.K., Koyanagi G.K., Lavrov V.V., Bohme D.K., Siu K.M. and Hopkinson A.C. (2000)
A study of complexes Mg (NH3) n+· and Ag (NH 3)n+, where n= 1–8: competition between direct coordination and solvation through hydrogen bonding **International Journal of Mass Spectrometry, 201,** 87-100.

Sialer E.J.M. (2010)
Development of an analytical method for determination of rare earth elements in rock samples by HPIC-ICP-MS. **General and Analytical Chemistry. Montanuniversitate (Leoben),** 120.

Silva M.F., Cerutti E.S. and Martinez L.D. (2006)

Coupling cloud point extraction to instrumental detection systems for metal analysis **Microchimica Acta, 155,** 349-364.

Silva S.G., Oliveira P.V., Nobrega J.A. and Rocha F.R.P. (2009)
Cloud point extraction to avoid interferences by structured background on nickel determination in plant materials by FAAS **Analytical Methods, 1,** 68-70.

Simitchiev K., Stefanova V., Kmetov V., Andreev G., Kovachev N. and Canals A. (2008)
Microwave-assisted cloud point extraction of Rh, Pd and Pt with 2-mercaptobenzothiazole as preconcentration procedure prior to ICP-MS analysis of pharmaceutical products **Journal of Analytical Atomic Spectrometry, 23,** 717-726.

Simpson L.A., Thomsen M., Alloway B.J. and Parker A. (2001)
A dynamic reaction cell (DRC) solution to oxide-based interferences in inductively coupled plasma mass spectrometry (ICP-MS) analysis of the noble metals **Journal of Analytical Atomic Spectrometry, 16,** 1375-1380.

Smolik M. and Jakóbik-Kolon A. (2009)
Determination of microamounts of hafnium in zirconium using inductively coupled plasma atomic emission spectrometry and inductively coupled plasma mass spectrometry during their separation by ion exchange on diphonix chelating resin **Analytical Chemistry, 81,** 2685-2687.

Smolik M., Jakobik-Kolon A. and Porański M. (2009)
Separation of zirconium and hafnium using Diphonix® chelating ion-exchange resin **Hydrometallurgy, 95,** 350-353.

Stockman H. (1983)
Neutron activation determination of noble metals in rocks: a rapid radiochemical separation based on tellurium coprecipitation **Journal of Radioanalytical Chemistry, 78,** 307-317.

Sugiyama N. and Kazumi N. (2014)
Reaction data for 70 elements using O2,NH3 and H2 gases with the Agilent 8800 Triple Quadrupole ICP-MS **www.agilent.com** **Publication number: 5991-4585EN,** 7.

Sugiyama N. and Shikamori Y. (2015)
Removal of spectral interferences on noble metal elements using MS/MS reaction cell mode of a triple quadrupole ICP-MS **Journal of Analytical Atomic Spectrometry, 30,** 2481-2487.

Sugiyama N., Woods,Glenn (2012)
Removal of hydride ion interferences (MH+) on Rare Earth Elements using the Agilent 8800 Triple Quadrupole ICP-MS **Agilent 8800 icp-qqq application handbook,** 8.

Sulcek Z. and Povondra P. (1989)
Methods of decomposition in inorganic analysis. **CRC Press (Boca Raton, FL.),** 325 pp.

Sun Y. and Sun M. (2005)
Nickel sulfide fire assay improved for pre-concentration of platinum group elements in geological samples: a practical means of ultra-trace analysis combined with inductively coupled plasma-mass spectrometry **Analyst, 130,** 664-669.

Suominen M., Kontas E. and Niskavaara H. (2004)
Comparison of silver and gold inquarting in the fire assay determination of palladium/platinum and rhodium in geological samples **Geostandards and Geoanalytical Research, 28,** 131-136.

Suoranta T., Bokhari S., Meisel T., Niemelä M. and Perämäki P. (2016)
Elimination of interferences in the determination of palladium, platinum and rhodium mass fractions in moss samples using ICP-MS/MS **Geostandards and Geoanalytical Research**.

Suoranta T., Niemelä M. and Perämäki P. (2014)
Cloud point extraction of platinum group elements and gold: elimination of nitric acid-related problems with sulphamic acid **Analytical Methods, 6,** 9321-9327.

Suoranta T., Zugazua O., Niemelä M. and Perämäki P. (2015)
Recovery of palladium, platinum, rhodium and ruthenium from catalyst materials using microwave-assisted leaching and cloud point extraction **Hydrometallurgy, 154,** 56-62.

Sylvester P.J. and Eggins S.M. (1997)
Analysis of Re, Au, Pd, Pt and Rh in NISTglass certified reference materials and natural basalt glasses by laser ablation ICP-MS **Geostandards Newsletter, 21,** 215-229.

Taicheng D., Hangting C. and Xianjin Z. (2002)
Determination of rare and rare earth elements in soils and sediments by ICP-MS using Ti(OH)4 – Fe(OH)3 co-precipitation preconcentration **Journal of Analytical Atomic Spectrometry, 17,** 410-413.

Takeo K., Noriyuki Y., Jun K., Hironori Y. and Takashi K. (2010)
New reaction cell ICP-MS with improved ion optics arrangement and vacuum system **https://www.agilent.com/.../applications/5990-9755EN_8800_ICPQQQ**.

Tan Z.-q., Liu J.-f., Liu R., Yin Y.-g. and Jiang G.-b. (2009)
Visual and colorimetric detection of Hg2+ by cloud point extraction with functionalized gold nanoparticles as a probe **Chemical Communications,** 7030-7032.

Tanner S.D. (1995)
Characterization of ionization and matrix suppression in inductively coupled 'cold'plasma mass spectrometry **J. Anal. At. Spectrom., 10,** 905-921.

Tanner S.D. and Baranov V.I. (1999)
Theory, design, and operation of a dynamic reaction cell for ICP-MS **Atomic Spectroscopy, 20,** 45-52.

Tanner S.D., Baranov V.I. and Bandura D.R. (2002)
Reaction cells and collision cells for ICP-MS: a tutorial review **Spectrochimica Acta Part B: Atomic Spectroscopy, 57,** 1361-1452.

Tanner S.D., Baranov V.I. and Vollkopf U. (2000)
A dynamic reaction cell for inductively coupled plasma mass spectrometry (ICP-DRC-MS) **Journal of Analytical Atomic Spectrometry, 15,** 1261-1269.

Tavakoli L., Yamini Y., Ebrahimzadeh H., Nezhadali A., Shariati S. and Nourmohammadian F. (2008)
Development of cloud point extraction for simultaneous extraction and determination of gold and palladium using ICP-OES **Journal of Hazardous Materials, 152,** 737-743.

Taylor S.R. and McLennan S.M. (1985)
The continental crust: its composition and evolution **Blackwell, Oxford.,** 312.

Taylor V., Toms A. and Longerich H. (2002)
Acid digestion of geological and environmental samples using open-vessel focused microwave digestion **Analytical and Bioanalytical Chemistry, 372,** 360-365.

Thomas R. (2013)
Practical guide to ICP-MS: a tutorial for beginners. **CRC press (New York),** 339 pp.

Thompson M. and Wood R. (1993)
International harmonized protocol for proficiency testing of (chemical) analytical laboratories **Pure & Applied Chemistry, 65,** 2123-2144.

Tikhonov I., Bodnya V. and Alimarin I. (1978)
Spectrophotometric investigation of products of RuO4 reduction in HCl solutions **Vestn. Mosk. Univ., Ser. II. Khim, 19-4,** 463-466.

Tonietto G.B., Godoy J.M., Oliveira A.C. and de Souza M.V. (2010)
Simultaneous speciation of arsenic (As (III), MMA, DMA, and As (V)) and selenium (Se (IV), Se (VI), and SeCN−) in petroleum refinery aqueous streams **Analytical and Bioanalytical Chemistry, 397,** 1755-1761.

Topp N.E. (1965)
The chemistry of the rare-earth elements. **Elsevier Pub. Co. (Amsterdam New York),** 164 pp.

Totland M., Jarvis I. and Jarvis K.E. (1992)
An assessment of dissolution techniques for the analysis of geological samples by plasma spectrometry **Chemical Geology, 95,** 35-62.

Totland M.M., Jarvis I. and Jarvis K.E. (1995)
Microwave digestion and alkali fusion procedures for the determination of the platinum-group elements and gold in geological materials by ICP-MS **Chemical Geology, 124,** 21-36.

Turner, P.J. and Holland (1997)
Plasma ource mass spectrometry: Developments and applications,
The Royal Society of Chemistry, p 28.

Turner G.S., Mills G.A., Burnett J.L., Amos S. and Fones G.R. (2015)
Evaluation of diffusive gradients in thin-films using a Diphonix® resin for monitoring dissolved uranium in natural waters **Analytica Chimica Acta, 854,** 78-85.

Van der Veen A.M.H., Linsinger T., Schimmel H., Lamberty A. and Pauwels J. (2001)

Uncertainty calculations in the certification of reference materials 4. Characterisation and certification **Accreditation and Quality Assurance, 6,** 290-294.

Van Loon J.A. (1980)
Analytical atomic absorption spectroscopy: selected methods. **Academic Press Inc (Ontario Canada),** 94 pp.

Van Loon J.C. and Barefoot R. (1991)
Determination of the precious metals: selected instrumental methods. **John Wiley & Son Ltd (London),** 268 pp.

Vaughan M. and Horlick G. (1990)
Effect of sampler and skimmer orifice size on analyte and analyte oxide signals in inductively coupled plasma-mass spectrometry **Spectrochimica Acta Part B: Atomic Spectroscopy, 45,** 1289-1299.

Vaughan M.A. and Horlick G. (1986)
Oxide, hydroxide, and doubly charged analyte species in inductively coupled plasma/mass spectrometry **Applied Spectroscopy, 40,** 434-445.

Verma S.P. and Santoyo E. (2007)
High-performance liquid and ion chromatography: separation and quantification analytical techniques for rare earth elements **Geostandards and Geoanalytical Research, 31,** 161-184.

Vlašánková R., Otruba V., Bendl J., Fišera M. and Kanický V. (1999)
Preconcentration of platinum group metals on modified silicagel and their determination by inductively coupled plasma atomic emission spectrometry and inductively coupled plasma mass spectrometry in airborne particulates **Talanta, 48,** 839-846.

Völkening J., Walczyk T. and Heumann K.G. (1991)
Osmium isotope ratio determinations by negative thermal ionization mass spectrometry **International Journal of Mass Spectrometry and Ion Processes, 105,** 147-159.

Völlkopf U., Baranov V. and Tanner S.D. (1999)
ICP-MS multielement analysis at sub-ppt levels applying new instrumental design concepts **Royal Society of Chemistry, 241,** 63-79.

Wakita H., Rey P. and Schmitt R. (1971)
Abundances of the 14 rare-earth elements and 12 other trace elements in Apollo 12 samples: five igneous and one breccia rocks and four soils. **Lunar and Planetary Science Conference Proceedings,** 1319.

Walker R.J. and Fassett J.D. (1986)
Isotopic measurement of subananogram quantities of rhenium and osmium by resonance ionization mass spectrometry **Analytical Chemistry, 58,** 2923-2927.

Walsh J., Buckley F. and Barker J. (1981)
The simultaneous determination of the rare-earth elements in rocks using inductively coupled plasma source spectrometry **Chemical Geology, 33,** 141-153.

Wasson J. and Kallemeyn G. (1988)

Compositions of chondrites **Philosophical Transactions of the Royal Society of London A: Mathematical, Physical and Engineering Sciences, 325,** 535-544.

Watanabe H. and Tanaka H. (1978)
A non-ionic surfactant as a new solvent for liquid—liquid extraction of zinc (II) with 1-(2-pyridylazo)-2-naphthol **Talanta, 25,** 585-589.

Webb P., Thompson M., Potts P., Batjargal B. and Long D. (2012)
GeoPT30 — An international proficiency test for analytical geochemistry laboratories — Report on round 30 (syenite, CG-2) and 30a (limestone, ml-2) **http://www.geoanalyst.org/**.

Webb P.C., Thompson M., Potts P.J., Watson J.S. and Kriete C. (2008)
GeoPT23-An international proficiency test for analytical geochemistry laboratories-report on round 23 (separation lake pegmatite, OU-9) and 23a (manganese nodule, FEMN-1) **http://www.geoanalyst.org/**.

Webb P.C., Thompson M., Potts P.J. and Wilson S.A. (2011)
GeoPT29 – An international proficiency test for analytical geochemistry laboratories – report on round 29 (nephelinite, NKT-1**, 30**.

Whiteley J. and Murray F. (2003)
Anthropogenic platinum group element (Pt, Pd and Rh) concentrations in road dusts and roadside soils from Perth, Western Australia **Science of the Total Environment, 317,** 121-135.

Willbold M. and Jochum K.P. (2005)
Multi-element isotope dilution sector field ICP-MSs: A precise technique for the analysis of geological materials and its application to geological reference materials **Geostandards and Geoanalytical Research, 29,** 63-82.

Woodland S.J. (1999)
Development ICP-MS isotope dilution preconcentration techniques for determination of platinum group elements in volcanic rocks. **Durham University (Durham)**.

Wyatt E.I. and Rickard R.R. (1961)
The radiochemistry of ruthenium. **National Academies of science (Washington USA),** 78 pp.

Xie S., Paau M.C., Li C.F., Xiao D. and Choi M.M. (2010)
Separation and preconcentration of persistent organic pollutants by cloud point extraction **Journal of Chromatography A, 1217,** 2306-2317.

Xu S. and Diao L. (2008)
Study of tungsten oxidation in O2⁄H2⁄N2 downstream plasma **Journal of Vacuum Science & Technology A, 26,** 360-364.

Yasuyuki S. and Kazumi N. (2013a)
Determination of sulfur, phosphorus and manganese in high purity iron **Agilent Notes,** p49.

Yasuyuki S. and Kazumi N. (2013b)

Feasibility study on the analysis of radioisotopes: Sr-90 and Cs-137 **Agilent Notes,** 70.

Yi Y.V. and Masuda, Akimasa (1996a)
Isotopic Homogenization of Iridium for High Sensitivity Determination by Isotope Dilution Inductively Coupled Plasma Mass Spectrometry **Analytical Sciences, 12,** 7-12.

Yi Y.V. and Masuda A. (1996b)
Simultaneous determination of ruthenium, palladium, iridium, and platinum at ultratrace levels by isotope dilution inductively coupled plasma mass spectrometry in geological samples **Analytical Chemistry, 68,** 1444-1450.

Yokoyama T., Makishima A. and Nakamura E. (1999)
Evaluation of the coprecipitation of incompatible trace elements with fluoride during silicate rock dissolution by acid digestion **Chemical Geology, 157,** 175-187.

Yu S., Zhou X. and Liu J. (2015)
Separation and determination of silver nanoparticles. **Silver Nanoparticles in the Environment. Springer (London),** 9-42.

Yu Z., Robinson P. and McGoldrick P. (2001)
An evaluation of methods for the chemical decomposition of geological materials for trace element determination using ICP-MS **Geostandards Newsletter, 25,** 199-217.

Zhang X., Yi Y., Liu Y., Li X., Liu J., Jiang Y. and Su Y. (2006)
Direct determination of rare earth impurities in high purity erbium oxide dissolved in nitric acid by inductively coupled plasma mass spectrometry **Analytica Chimica Acta, 555,** 57-62.

Zulauf A., Happel S., Mokili M.B., Bombard A. and Jungclas H. (2010)
Characterization of an extraction chromatographic resin for the separation and determination of 36Cl and 129I **Journal of Radioanalytical and Nuclear Chemistry, 286,** 539-546.

Zuleger E. and Erzinger J. (1988)
Determination of the REE and Y in silicate materials with ICP-AES **Fresenius Journal of Analytical Chemistry, 332,** 140-143.